Reconstructing lost plates of the Panthalassa Ocean

Lydian Boschman

Reconstructing lost plates of the Panthalassa Ocean

Reconstructie van verdwenen platen van de Panthalassa Oceaan

(met een samenvatting in het Nederlands)

Proefschrift

Promotoren:

Prof. dr. D. J. J. van Hinsbergen
Prof. dr. W. Spakman

Contents

INTRODUCTION

Serpentinite matrix mélange - Cedros Island, Mexico

Compared to continental lithosphere, which was generated through many cycles of partial melting and fractional crystallization of the mantle since the early days of the Earth, oceanic lithosphere has a limited lifespan at the Earth's surface. Oceanic lithosphere is continuously generated at mid-ocean ridges, cools down, becomes denser than the sub-lithospheric mantle, and is eventually consumed in subduction zones. As a result, the total of oceanic lithosphere was repeatedly renewed throughout the history of the Earth, and modern oceanic crust is almost nowhere older than ~200 Ma (Müller et al., 2008a). This implies that the lithosphere that was underlying ancestral oceans, such as the Paleo- and Neo-Tethys Oceans that once separated Gondwana from Laurasia, or the Panthalassa Ocean surrounding Pangea during its culmination in late Paleozoic – early Mesozoic times, has (almost) all been lost to subduction. As a result, deep-time plate tectonic reconstructions rely primarily on geological, paleontological and paleomagnetic data from the continents. Such reconstructions portray the distribution of plates that host continents through geological time, but generally lack (or include only conceptual) plate motions and -geometry in the oceanic domains. This thesis attempts to develop approaches and collect data to improve deep-time global plate kinematic reconstructions through quantitative restoration of lost oceanic plates.

The Panthalassa Ocean (from the Greek παν (all) and θάλασσα (sea)), covered approximately half of the globe during the culmination of Pangea ("all-Earth")(Wegener, 1915). Since then, it decreased in size due to area gain in the Atlantic and Indian oceans breaking up the supercontinent. The present-day descendant of the Panthalassa, the Pacific Ocean, is mainly occupied by the Pacific Plate, which originated in Jurassic time and increased in size since then. The overall area loss of the Panthalassa Ocean, combined with the continuous growth of the Pacific Plate led to the subduction of the surrounding oceanic plates that were underlying the Panthalassa Ocean in Mesozoic and older times. Nonetheless, even though these Panthalassa plates are no longer at the Earth's surface, their formation and demise left an imprint in and on the Earth and these records allow the reconstruction of plate motions from indirect sources of data.

Despite the challenges and uncertainties that come with it, reconstructing the tectonic history of the Panthalassa Ocean is worthwhile, because accurate deep-time plate tectonic reconstruction of all (and sometimes especially oceanic) plates, play a crucial role in many other areas of Earth scientific and biological science. In geodynamics, plate kinematics derived from global plate tectonic reconstructions are for example used to model whole-Earth mantle convection in relation to supercontinent cycles (e.g. Zhong et al., 2007), to calculate net lithosphere rotation (Torsvik et al., 2010b), or to calculate True Polar Wander (TPW; the motions of the Earth's crust and mantle relative to the spin axis (Steinberger & Torsvik, 2008; Torsvik et al., 2012)). The uncertainties in, or even absence of, plate motions in the oceanic domains in the current state-of-the-art global plate reconstructions limit these geodynamic studies, especially for deep geological times.

Other fields of research, especially those involving the evolution of ocean systems on geological timescales, whether it be from for example a marine biological, climatological, sedimentological, or geochemical perspective, rely for their data on exposures of remnants of ancient oceans. To develop an understanding of the full range of Mesozoic open ocean conditions, exposures in the accretionary belts around the Pacific Ocean are key, because throughout the Mesozoic, the Panthalassa Ocean was the only oceanic domain stretching from pole to pole. Other marine domains were restricted to equatorial latitudes (Pangea's internal Paleo- and Neo-Tethys Oceans) or consisted of shallow seas (e.g. the Paratethys Sea). However, even though the rock record of the circum-Pacific accretionary belts provides a large archive with information on (changes in) Mesozoic marine conditions and environments, remnants are often displaced relative to their original geological context (e.g. radiolarian chert sequences forming hills on the Japanese Islands) and paleolatitude. Without knowledge on plate motions and paleolatitudes, this archive cannot be used to its full potential.

Reconstructing the Panthalassa Ocean starts with defining the location and tectonic nature of its boundaries. Determining the location of these boundaries through time relies first on detailed kinematic reconstructions of the Indo-Atlantic plate system (and hence, the position of the continents surrounding Panthalassa during the culmination and break-up of Pangea), and second, on reconstruction of Pangea's (and post-Pangea's) external trenches relative to those continents. Relative trench-continent distances may vary significantly as a result of overriding plate extension (creating fore- or back-arc basins) or shortening (forming Cordillera-type orogens), thereby reducing or enlarging the extent of the Panthalassa Ocean. The first aspect, reconstructing the Indo-Atlantic plate system, is relatively straightforward (e.g. Müller et al., 2016; Seton et al., 2012). It follows conventional plate reconstruction methods based on marine magnetic anomaly and fracture zone data, recording the age, rate, and direction of relative plate motion between two plates separated by a spreading ridge. The second aspect requires the restoration of complex crustal deformation at subduction plate boundary zones, which is considerably more challenging.

In 2013, at the beginning of this research, recent developments in (free) plate reconstruction software (Boyden et al., 2011) opened new opportunities for reconstructing complex plate boundary regions, whereby relative plate motions between tectonic blocks or terranes are mathematically described by sets of Euler poles. At that time, only a few of such reconstructions were available (e.g. Ross & Scotese, 1988; van Hinsbergen, 2010; van Hinsbergen et al., 2011a; van Hinsbergen & Schmid, 2012), and generally, regional plate reconstructions were presented in literature as a series of drawings illustrating the location of different tectonics terranes through time (e.g. Hall, 2002; McQuarrie & Wernicke, 2005; Pindell & Kennan, 2009; Stampfli & Borel, 2002). In contrast to ocean basin reconstructions based on marine geophysical data, reconstructions of plate boundary deformation cannot be based on a single type of data, but may result from integration

of quantitative data such as crustal shortening/extension estimates, estimates on the direction and amount of motion along strike-slip faults, and paleomagnetic data, as well as more qualitative data such as magmatic geochemistry or paleontology. Because of this, the results depend highly on the choices made during the reconstruction process and vary considerably from author to author. With the increase in accessibility of reconstruction software and the opening of a new avenue of reconstructing complex geological regions thus arose the need for standardization of reconstruction methods. A key aspect of this thesis is the development of a reconstruction protocol (presented in Chapter 2 and further expanded in subsequent chapters) that defines how a limited selection of data types that quantitatively constrain plate motions is used, layer by layer, in order of decreasing certainty. Following this protocol results in reproducible reconstructions that are independent of qualitative datasets, and the reconstructions can therefore be tested against such datasets, or used as input or boundary conditions for studies in e.g. paleontology, paleoclimate, or magmatic geochemistry. This reconstruction protocol is rooted in the "rules of plate tectonics" (e.g. Cox and Hart, 1986) that define when reconstructions are kinematically feasible; for instance, relative motions between two tectonic blocks or terranes must be accommodated by a (discrete or diffuse) plate boundary, plate boundaries end in triple junctions, and no gaps or overlaps may be present in a reconstruction without geological evidence for shortening or extension, respectively. By employing this protocol, reconstructions become transparent, reproducible and globally compatible, and are straightforwardly adjustable when new data become available. As part of this thesis, as well as in side projects associated with this thesis, my colleagues, students and I developed Cenozoic reconstructions of circum-Pacific regions, thereby reversing overriding plate deformation and restoring the circum-Panthalassa trenches back towards their pre-Cenozoic location. These reconstructions include the Caribbean region (Chapter 2; Molina Garza et al., 2017), the Andes (Schepers et al., 2017), the Scotia Sea region (van Hinsbergen et al, submitted), the Southwest Pacific (van de Lagemaat et al., 2018a) and the Northwest Pacific (Vaes et al, submitted).

The next step in reconstructing the Panthalassa Ocean is to use all available data from oceanic lithosphere that did not (yet) subduct. The modern Pacific Ocean is underlain by a plate system including the Pacific, Juan de Fuca, Cocos, Nazca and Antarctic plates that are separated by spreading ridges and contain marine magnetic anomalies and fracture zones/transform faults recording their spreading history. By restoring past plate motions from these spreading records, these modern plates become smaller as the young history of oceanic lithosphere formation is reversed (Wright et al., 2016). At 83 Ma, only the central part of the Pacific Plate is left, and all other modern plates have disappeared. Moreover, Pacific-Antarctic spreading is fully reversed, implying that the Pacific Plate is no longer connected to the Indo-Atlantic plate system by a passive margin, but instead, the Panthalassa was likely entirely surrounded by active margins.

The oldest part of the Pacific Plate contains magnetic lineations in three orientations (the Japanese, Hawaiian and Phoenix lineations (Larson & Chase, 1972)) that constrain relative plate motions of three conceptual plates conjugate to the Pacific (Izanagi in the northeast, Farallon in the northeast and Phoenix in the south) back to ~190 Ma. Since 190 Ma, a four-plate system is thus reconstructed including relative plate motions, plate boundary geometry, and lithospheric ages of the Pacific, Izanagi, Farallon and Phoenix plates (hereafter referred to as the Panthalassa plate system). However, due to the lost Pacific-Antarctic connection, relative plate motions between the Panthalassa and Indo-Atlantic plate systems are not directly constrained. Some constraint on these relative motions comes from geological evidence of millions of years of subduction in the circum-Panthalassa trenches of for example Japan (Maruyama et al., 1997) and New Zealand (Mortimer, 2004), but otherwise, relative Panthalassa - Indo-Atlantic plate motion can only be estimated using absolute plate motion models, either from paleomagnetic data, or by placing both systems in mantle reference frames (e.g. Doubrovine et al., 2012; van der Meer et al., 2010; Wessel & Kroenke, 2008). Such mantle reference frames may be used as first-order connection between the Panthalassa and Indo-Atlantic plate systems back to 140 Ma. Prior to 140 Ma, this mantle-connection is lost, and prior to 190 Ma, even the relative plate motions within the Panthalassa plate system are unknown.

The third and final step in reconstructing the Panthalassa Ocean involves the use of data from fully subducted lithosphere. This includes paleomagnetic and stratigraphic data from 'Ocean Plate Stratigraphy' materials (Isozaki et al., 1990) that were scraped of during subduction and are now exposed in the circum-Panthalassa accretionary complexes. OPS sequences consist of magmatic basement, pelagic (cherts and carbonates), hemipelagic, and trench-fill sediments that represent rocks accumulated on an oceanic plate on its journey from a mid-ocean ridge to a trench. Second, seismic tomographic images reveal the locations of subducted material in the mantle that may be correlated to reconstructed intra-oceanic or continental margin subduction zones, thereby constraining the position of these subduction zones relative to the mantle (van der Meer et al., 2012).

Throughout this thesis, I use and integrate a (selected) set of different data types that contain quantitative information on the direction, rate, and timing of either relative or absolute plate motion. I intend to be transparent about my assumptions, methods and reconstruction choices, and attempted to identify and explain the uncertainties in every step in our reconstruction. The thesis develops step by step a reconstruction approach and a plate kinematic reconstruction of Panthalassa Ocean, as follows:

Chapter 1: exploring the limits of marine magnetic anomaly and fracture zone data of the Pacific Plate

Marine geophysical data from the oldest part of the Pacific Plate enable the reconstruction of the Izanagi, Farallon and Phoenix plates since 190 Ma. In Chapter 1, we explore the possibilities of interpreting plate kinematic configurations and evolution prior to the onset

of Pacific Plate formation based on this data set, and discuss possibilities to link the birth of the Pacific Plate to modern mantle structure.

Chapter 2: Panthalassa plate motions from preserved lithosphere

Chapter 2 presents a kinematic reconstruction of the Caribbean region. The lithosphere underlying the Caribbean Sea is interpreted to be a Jurassic remnant of the Farallon Plate that escaped subduction because of inception of westward subduction of North and South American ('Proto-Caribbean') oceanic lithosphere below the Caribbean lithosphere since the Early Cretaceous. The Caribbean Plate thus represents a unique fragment of old Panthalassa lithosphere. Since ~100 Ma, the Caribbean Plate has been surrounded by subduction zones and transform plate boundaries, and ~90 Ma eruption of a large igneous province covered the original oceanic basement. We develop a reconstruction protocol for restoring plates devoid of marine magnetic anomaly data, and reverse the plate tectonic history of the Caribbean Plate relative to the Americas.

Chapters 3-4: reconstructing Farallon-North America plate boundary evolution since the Triassic

Late Cretaceous to recent arc magmatic provinces in Baja California and mainland Mexico have been linked to continuous eastward subduction of the Farallon (and since ~23 Ma, Cocos) Plate below the western continental margin. The tectonic origin of older (Triassic – Lower Cretaceous) records of subduction of the Guerrero terrane and Baja California (arc magmatic rocks, fore-arc deposits, accretionary complexes, supra-subduction zone ophiolite), however, have been subject of debate. Geological evidence unequivocally demonstrates that in pre-Cretaceous times, these terranes were separated from the North American continent by an oceanic basin. Some authors consider these terranes to be exotic to North America, formed above a westward-dipping intra-oceanic subduction zone within the eastern Panthalassa ocean, and accreted upon full subduction of the intermediate ocean basin, whereas others consider them to have formed at the continental margin whereby overriding plate deformation (and the existence of temporal fore- and back-arc basins) resulted in the complex geology. This controversy has far-reaching implications for the tectonic history of the eastern Panthalassa Ocean. In chapters 3 and 4, we present new paleomagnetic data from the Lower Cretaceous Guerrero arc and the Upper Triassic Vizcaíno ophiolite and overlying Jurassic sediments of Baja California. We use these data to evaluate whether the western Mexican arc and ophiolite terranes have a latitudinal plate motion history equal to, or different from that of the North American Plate, which we use as an indicator of an overriding plate versus an independent (intra-Panthalassa) origin. In the light of these data, we interpret the longest slab on Earth – the Cocos slab – in terms of a long-term connection of the Indo-Atlantic and Panthalassa plate systems.

Chapter 5: linking Caribbean lithosphere to the Farallon Plate

Where Chapter 2 restored the Caribbean Plate relative to the American continents and Chapters 3 and 4 provided constraints on relative motions between the Farallon Plate and North America, Chapter 5 explores how to reconstruct the Caribbean Plate within the eastern Panthalassa Ocean, prior to any connection to the Americas. Chapter 5 presents paleomagnetic data from Jurassic and Cretaceous rocks of the Nicoya Peninsula of western Costa Rica, including basalts related to several pulses of mantle-plume magmatism. From these data, we establish paleolatitude estimates of the Caribbean lithosphere within the Panthalassa Ocean. We develop an approach to estimate relative motions between the Panthalassa and Indo-Atlantic systems prior to 83 Ma through the use of mantle reference frames of each system. We test the different options for this this connection from different mantle frames by placing the global plate circuits in a paleomagnetic reference frame, and testing the reconstructions against kinematic feasibility, our new paleomagenetic data, and connections of the plume-related volcanics of Nicoya to the Pacific LLSVP.

Chapter 6: diving deeper into the Panthalassa Ocean from analysis of the accretionary records of Hokkaido

In Chapter 6, we shift focus to the northwestern Panthalassa, and analyze sequences of Ocean Plate Stratigraphy exposed in the accretionary complexes of Hokkaido, Japan, which contain remnants of a Jurassic intra-oceanic island arc (the Oku-Niikappu Complex) that went extinct ~145 Ma. First, we analyze the pattern of marine magnetic anomalies of the Pacific Plate to evaluate whether it holds clues on Pacific-Izanagi spreading in relation to intra-oceanic Oku-Niikappu subduction. Second, we evaluate the age of the subducting lithosphere at the Hokkaido margin through time, and whether there are significant changes coeval with Oku-Niikappu accretion that may shed light on the intra-oceanic subduction evolution. Third, we attach the OPS remnants to the reconstructed Izanagi plate, and test our reconstruction of Izanagi Plate and intra-oceanic subduction evolution against new (sparse) paleomagnetic data, and evaluate a previously proposed connection to lower mantle slabs.

Chapter 7: bringing it all together: integrating absolute plate motions with paleomagnetic data from accreted materials from Mexico, Costa Rica, New Zealand and Japan derived from the Farallon, Phoenix and Izanagi plates.

Chapter 7 starts with the reconstruction of the Panthalassa plate system, which contains both absolute (in a mantle reference frame) and relative plate motions of the Pacific, Izanagi, Farallon and Phoenix plates back until 140 Ma, only relative plate motions of these plates until 190 Ma, and no plate motions (nor plate boundaries) before that time. We present new paleomagnetic data from accreted OPS rocks exposed in the accretionary complexes and tectonic mélanges of Cedros Island (Baja California, Mexico), the Santa Elena Peninsula (Costa Rica), the North Island of New Zealand, and Japan, yielding plate motions of the Farallon, Phoenix and Izanagi plates, respectively. We supplement this dataset with previously published paleomagnetic data from the same regions. We

develop a reconstruction of 140-260 Ma Izanagi, Farallon and Phoenix plate motions that satisfies paleomagnetic constraints and is consistent with constraints from upper plate deformation and accretion in Japan, Mexico and New Zealand. This chapter explores the possibility of developing reconstructions of oceanic plates in absence of constraints other than paleomagnetism and develops a method that may be applied to any other ancient lost ocean.

Many analyses in this thesis are prone to high degrees of uncertainty, rely on debatable assumptions, and may by some readers be considered speculative. This was anticipated from the start of the project, and the answer to my own doubts and to comments from outsiders concerning these issues has throughout the years always been 'Yes, I know, but we are trying it anyway'. Four years of trying it anyway led to the collection of more than a thousand remagnetized paleomagnetic samples and many dead ends, but also, it placed a few of the pieces of the Panthalassa puzzle in their place. I hope that this thesis will be the starting point from which many other researchers dare to dive in and enjoy the tectonics of lost oceans that existed in deep geological time.
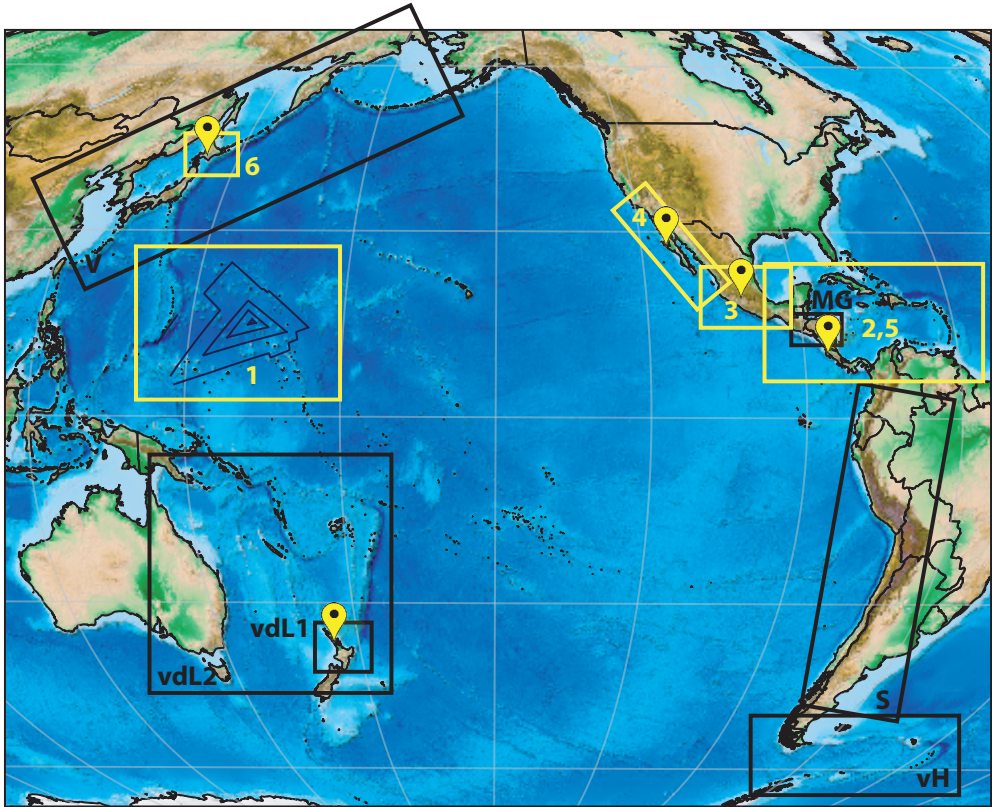
Figure 1. Sampling locations (pins), study areas involved in the chapters in this thesis (in yellow) and study areas of various side projects (in black). V: Vaes et al. (submitted), vdL1: van de Lagemaat et al. (2018a), vdL2: van de Lagemaat et al. (2018b), MG: Molina Garza et al. (2018), S: Schepers et al. (2017), vH: van Hinsbergen et al. (submitted).

1

On the enigmatic birth of the Pacific Plate within the Panthalassa Ocean

Pillow basalts - Murciélago Islands, Costa Rica

Abstract

The oceanic Pacific Plate started forming in Early Jurassic time within the vast Panthalassa Ocean that surrounded the supercontinent Pangea, and contains the oldest lithosphere that can directly constrain the geodynamic history of the circum-Pangean Earth. We show that the geometry of the oldest marine magnetic anomalies of the Pacific Plate attests to a unique plate kinematic event that sparked the plate's birth at virtually a point location, surrounded by the Izanagi, Farallon, and Phoenix plates. We reconstruct the unstable triple junction that caused the plate reorganization, which led to the birth of the Pacific Plate, and present a model of the plate tectonic configuration that preconditioned this event. We show that a stable but migrating triple junction involving the gradual cessation of intra-oceanic Panthalassa subduction culminated in the formation of an unstable transform-transform-transform triple junction. The consequent plate boundary reorganization resulted in the formation of a stable triangular three-ridge system from which the nascent Pacific Plate expanded. We link the birth of the Pacific Plate to the regional termination of intra-Panthalassa subduction. Remnants thereof have been identified in the deep lower mantle of which the locations may provide paleolongitudinal control on the absolute location of the early Pacific Plate. Our results constitute an essential step in unraveling the plate tectonic evolution of "Thalassa Incognita" that comprises the comprehensive Panthalassa Ocean surrounding Pangea.

1. Introduction

Oceanic spreading records are the primary source of data in making global plate reconstructions. Because the oldest seafloor currently present on the Earth dates back to ~200 million years ago (Ma), building models of plate tectonic before 200 Ma requires a different approach and relies on data from the continents. As a result, continent motion in global plate reconstructions for times before 200 Ma (e.g. Domeier & Torsvik, 2014; Stampfli & Borel, 2002) is well constrained, but the now-subducted oceanic plates in those models are conceptual and inevitably speculative.

The Panthalassa Ocean (Wegener, 1915) was the comprehensive oceanic domain surrounding the supercontinent Pangea in Late Paleozoic and Early Mesozoic times. This vast water mass must have been underlain by multiple oceanic tectonic plates, comparable to the Pacific Ocean today (Engebretson et al., 1985; Seton et al., 2012; Wright et al., 2016). Because the Panthalassa Ocean was completely surrounded by subduction zones, none of its plates was connected to a continent by an oceanic spreading record, and the majority of the plates have been lost to subduction. As a result, reconstructing Panthalassa's plate tectonic evolution has proved to be a challenge. However, attempting this reconstruction is worthwhile because the motion of Panthalassa's surface plates may provide the only direct kinematic constraint that we can obtain to assess the style of mantle dynamics in the presence of a supercontinent and particularly may help resolve how Pangea was formed and eventually broke up (e.g. Conrad et al., 2013). The starting point for a Panthalassa reconstruction is a full kinematic restoration of the plates underlying the present-day

Pacific Ocean, on the basis of their marine magnetic anomalies. The oldest lithosphere present in the Pacific domain is the oldest part of the Pacific Plate (the "Pacific triangle") and is of Early Jurassic age (Müller et al., 2008a, 2008b; Seton et al., 2012; Tominaga et al., 2015), setting the limit of this reconstruction at ~190 Ma. However, we show here that this piece of lithosphere also contains clues on the plate boundary configuration of the "pre-Pacific" plates of the Panthalassa Ocean and can take us an essential step further back in time.

The Pacific triangle is located just east of the Marianas Trench (Fig. 1) and contains magnetic anomalies in three orientations: the northeast trending Japanese, northwest-trending Hawaiian, and east-trending Phoenix lineations (Larson & Chase, 1972). The geometry of the triangle that is formed by these sets of anomalies (Fig. 1) implies that the Pacific Plate (PAC) grew as a result of ocean spreading at three ridges that must have separated the Pacific Plate from three conceptual preexisting oceanic plates. These plates are known as the Izanagi (IZA), Farallon (FAR), and Phoenix (PHO) plates to the northwest, northeast, and south, respectively. Except for some relics of the Farallon Plate, these plates have been lost to subduction. Mirroring the Japanese, Hawaiian, and
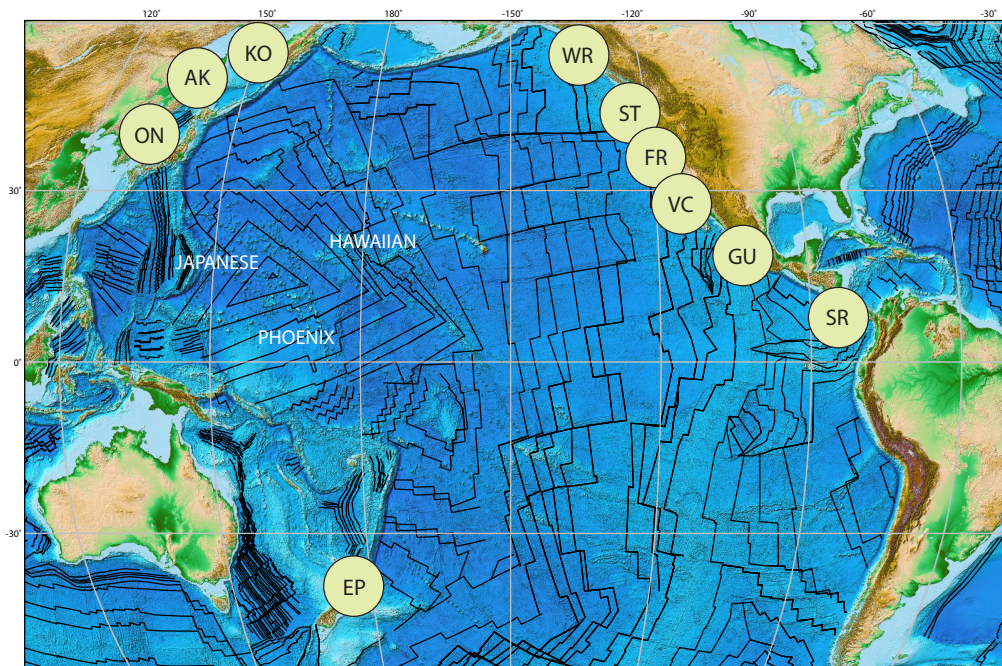
Figure 1: Isochrons of the Pacific Plate based on marine magnetic anomaly data, including the Japanese, Hawaiian and Phoenix sets (from Seton et al. (2012)) and accretionary intra-Panthalassa subduction complexes. KO: Kolyma-Omolon, AK: Anadyr-Koryak, ON: Oku-Niikappu, EP: New Zealand's Eastern Province, WR: Wrangellia, ST: Stikinia, FR: Franciscan accretionary complex, VC: Vizcaíno-Cedros region of Baja California, GU: Guerrero, SR: Santa Rosa Accretionary Complex.

Phoenix lineations at conceptual ridges with Izanagi, Farallon, and Phoenix allows for reconstructing a plate boundary evolution of the nascent stages of the Pacific Plate in the Early Jurassic, showing that the Pacific Plate originated virtually at a point. This is a very unusual tectonic event because all other modern plates formed as a result of breakup of a predecessor by rifting and subsequent mid-ocean ridge formation within the continental or oceanic lithosphere. For example, the African Plate became a separate plate as a result of the breakup of Pangea, whereby the current plate obtained its final plate boundary by the formation of the South Atlantic mid-ocean ridge upon the separation of Africa from South America (Gaina et al., 2013; Torsvik et al., 2009). This not only holds true for plates containing continental crust, but also for purely oceanic plates. For example, the oceanic Juan de Fuca, Cocos, and Nazca plates of the eastern Pacific region formed as a result of the breakup of the former Farallon Plate (McKenzie & Morgan, 1969; Menard, 1978). Thus, all of these plates contain or contained crust that is older than the formation of at least one of its plate boundaries. However, the center of the Pacific triangle contains crust that is no older than the formation of the ridges that created it. This point of birth of the Pacific Plate represents the triple junction between the Farallon, Izanagi, and Phoenix plates (Engebretson et al., 1985) and is generally portrayed as a ridge-ridge-ridge (RRR) triple junction, at which the Pacific microplate formed ~190 Ma as a result of the triple junction falling apart into three new RRR triple junctions (Hilde et al., 1977; Seton et al., 2012). However, an RRR triple junction is stable (Cox & Hart, 1986; McKenzie & Morgan, 1969; Patriat & Courtillot, 1984), and there is no reason for this triple junction to spontaneously fall apart. Present day RRR triple junctions (for example, in the South Atlantic, Indian, and Pacific Oceans) have been stable for tens of millions of years, or even more than 100 million years (Müller et al., 2008a; Seton et al., 2012). Oceanic plate boundary reorganization is instead expected when existing plate boundaries are obstructed (for example, by collision) or cease to exist (for example, because of ridge subduction), or when an unstable triple junction forms (Cox & Hart, 1986). With the Pacific Plate originating from a triple junction, we therefore explore how it may have originated from an unstable triple junction between the Izanagi, Farallon, and Phoenix plates, and discuss how reconstructing this is relevant for deciphering the plate tectonic evolution of the Panthalassa Ocean.

2. Results

The orientations of the Pacific triangle magnetic anomalies allow construction of the relative motions between IZA-PAC, FAR-PAC, and PHO-PAC, and, indirectly, of IZA-FAR-PHO motions. The relative motion diagram (Fig. 2) shows that, since 190 Ma, IZA-FAR, FAR-PHO, and PHO-IZA were diverging; thus, their plate boundaries, as well as the triple junction at which the Pacific Plate was born, must have consisted of a combination of only ridges (R) or transform faults (F). The orientation of these ridges and transform faults can be inferred from the relative motion diagram (Fig. 2). RRR, RRF, and RFF triple junctions are all stable, and these three can alternate through time (Kleinrock & Morgan, 1988; Viso et al., 2005). However, the fourth option, an FFF triple junction, is unstable and
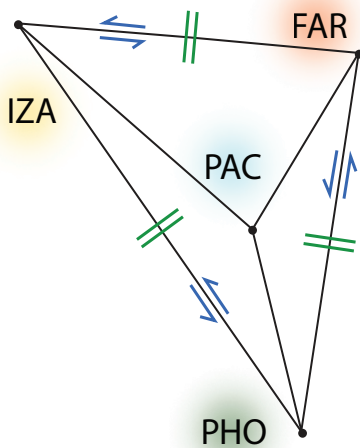
Figure 2: Relative motion diagram of the PAC-IZA-FAR-PHO plate system. The sense of motion of transform segments (in blue) and the orientation of ridges (in green) of the conceptual IZA-FAR, FAR-PHO, and PHO-IZA plate boundaries.

has the property of opening a triangular "gap" in its center immediately after its formation (Fig. 3B). Consequently, ridges form at which new oceanic crust is accreted, which then fills this gap, and a new plate is born at this now stable plate boundary configuration (Fig. 3C). This plate system predicts the ridges and their geometry that generated the Jurassic triangular magnetic anomalies of the Pacific Plate observed on the seafloor.

By definition, an unstable triple junction can only exist temporarily (McKenzie & Morgan, 1969) as a transitional plate boundary configuration between one stable situation and the next. The nature of the IZA-FAR-PHO triple junction before the birth of the Pacific Plate can be constructed using the basic rules of plate tectonics, assuming no change in relative plate motion in the IZA-FAR-PHO system before and after the birth of the Pacific Plate occurred. To end up in the unstable FFF triple junction, two plate boundaries must have been transform faults that remained unchanged, whereas the third plate boundary must have been kinked, resulting in a transform plate boundary on one side of the kink and an oblique subduction zone (trench (T)) on the other (Fig. 3A). The resulting transform-transform-trench (FFT) triple junction is stable but migrates along the trench toward the kink. During triple junction migration, the length of the subduction zone segment reduces diachronously, and when the triple junction arrives at the kink, an unstable FFF triple junction is generated at which the Pacific Plate starts forming (Cox & Hart, 1986). On the basis of the marine magnetic anomaly data of the Pacific triangle, it is impossible to determine which plate boundary contained the subduction segment and which plate was in the overriding plate position. As a result, three different but geometrically similar plate boundary configurations are possible. Figure 3A shows the scenario in which the Farallon Plate is subducted below the Izanagi Plate, resulting in a subduction segment that is oriented north-northwest–south-southeast.

Figure 3: Three-step evolution of the FAR-PHO-IZA plate system and birth of the Pacific Plate. A) Pre–190Ma. B) ~190 Ma. C) Post–190Ma.

3. Discussion

Current plate motion models of the Pacific Plate (e.g. Wright et al., 2016) show that it can be incorporated into the global plate circuit until 83 Ma. This age marks the onset of spreading in the Antarctic-Pacific ridge, and the record of this spreading allows for constraining the motion of the Pacific Plate relative to the global plate circuit in great detail. Before 83 Ma, the Pacific Plate and the oceanic plates from which it was separated by spreading ridges were entirely surrounded by subduction zones, isolating it from the global plate circuit. The best available constraint on Pacific Plate motion before 83 Ma is provided by a fixed hotspot reference frame for the Pacific Plate (Wessel & Kroenke, 2008), which goes back to 145 Ma. This hotspot frame provides the position of the Pacific Plate with respect to the mantle. There is currently no control on either relative (to the global plate circuit) or absolute Pacific Plate motion before this time.

Our reconstruction infers an essential role for subduction and subduction termination in the formation of the unstable triple junction that sparked the birth of the Pacific Plate. Remnants of such Early Jurassic subduction can be found with deep-earth seismology. Seismic tomography (Amaru, 2007; French & Romanowicz, 2014; Grand et al., 1997; Lu & Grand, 2016; Ritsema et al., 2011) and seismic waveform analysis (He & Wen, 2009; Kaneshima & Helffrich, 2010) of deep mantle structure below the present Pacific Ocean show two major high-velocity anomaly zones that have been interpreted as remnants of slabs belonging to two large-scale intra-Panthalassa subduction systems that are oriented north-northwest–south-southeast: a central system ("Telkhinia" subduction system) and a "fringing" subduction system, closer to the present American continents (Sigloch & Mihalynuk, 2013; van der Meer et al., 2012). The depth of these anomalies suggests that intra-oceanic subduction occurred during and before the time window in which the Pacific Plate originated. Furthermore, the modern circum-Pacific accretionary prisms of Japan, Siberia, New Zealand, and western North and Central America contain accretionary subduction complexes (Fig. 1), including Lower to Middle Mesozoic ocean floor rocks that are scraped off downgoing Panthalassa plates, as well as intra-oceanic volcanic arcs that went extinct up to tens of millions of years before accretion into the fold-thrust belts where they currently reside (Nokleberg, 2000; Sigloch & Mihalynuk, 2013; Ueda & Miyashita, 2005; van der Meer et al., 2012). The arc remnants of the North American margin have previously been linked to the fringing subduction system (Sigloch & Mihalynuk, 2013; van der Meer et al., 2012), whereas the remnants of the northwest Pacific appear to have traveled farther and are related to the Telkhinia subduction system (van der Meer et al., 2012).

Our reconstruction links the birth of the Pacific Plate to the termination of an intra-Panthalassa subduction system, which may correlate either to the Telkhinia or to the fringing subduction system. Figure 4 shows the motion path of the Pacific Plate relative to the mantle in 5-My steps. The motion path is based on the model of Wright et al. (2016), placed in a slab-fitted mantle reference frame (van der Meer et al., 2010) for 0 to
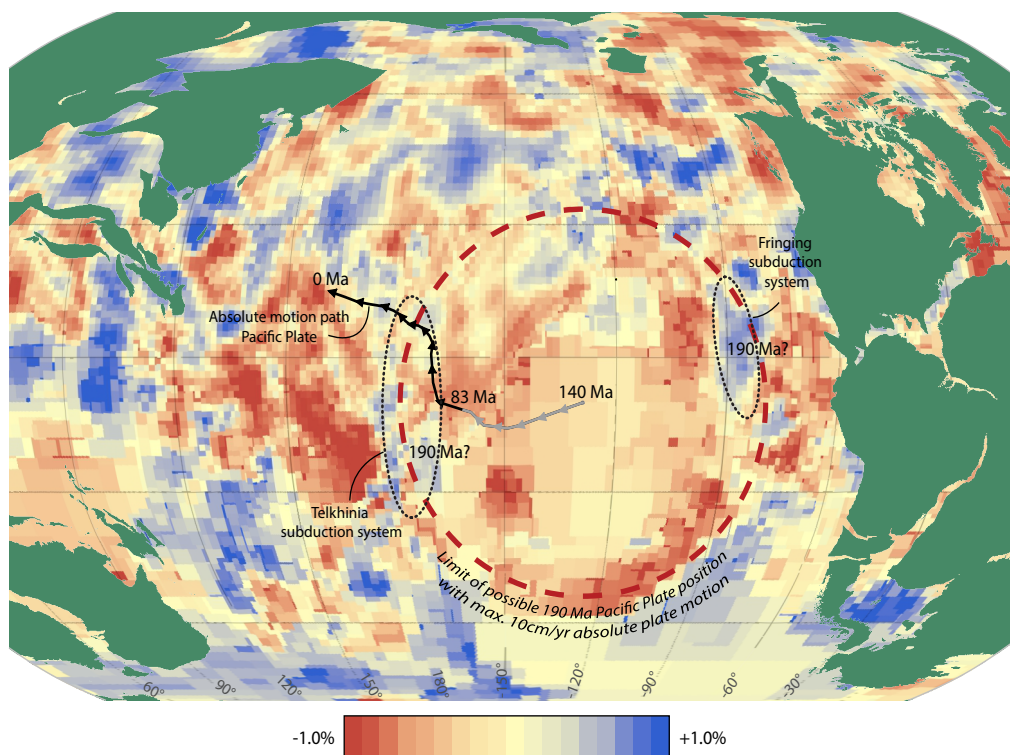
Figure 4: Absolute plate motion path of the Pacific Plate. The black line is based on the model of Wright et al. (2016) incorporated in the mantle reference frame of van der Meer et al. (2010); the gray line is based on the fixed Pacific hotspot frame from Wessel and Kroenke (2008). Red and blue background colors represent the 2480-km depth slice of the UU-P07 tomographic model.

83 Ma (in black), and in the Pacific hotspot WK08-A model (Wessel & Kroenke, 2008) for 83 to 140 Ma (in gray). The motion path shows an unrealistic jump between 85 and 80 Ma, illustrating the uncertainties in both the slab and fixed Pacific hotspot frames, but the trend in both frames shows an overall westward motion since 140 Ma. Figure 4 also shows the position of the continents at 190 Ma (Müller et al., 2016) and a 2480 km depth tomography slice from the UU-P07 tomographic model (Amaru, 2007), interpreted to show slabs that subducted in the Early Jurassic (van der Meer et al., 2012).

Using a maximum absolute plate motion velocity of 10 cm/year as reasonable upper bound (Zahirovic et al., 2015), the 190-Ma position of the Pacific Plate should lie within a circle with a radius of 5000 km centered around its 140 Ma position (Fig. 4). Both the fringing and the Telkhinia subduction systems are present within the limits of this circle, and therefore, deep mantle anomalies of both could be linked to the reconstructed subduction segment. A comparison of alternative tomographic models (French & Romanowicz, 2014; Lu & Grand, 2016; Ritsema et al., 2011) with the UU-P07 model shows that the

anomalies related to the fringing subduction system are a common feature in all four models. The equatorial part of this system, located within the dotted black line in Figure 4, was previously detected in seismological (Hutko et al., 2006; Kito et al., 2007; Thomas et al., 2004) and tomographic (van der Hilst et al., 2007) studies and was named the Trans-Americas slab by van der Meer et al. (2010). The Telkhinia system, a prominent positive anomaly in the UU-P07 model, is less evident in the other tomographic models. However, the other models do show a weakly positive or subdued negative anomaly, interpreted to reflect the effect of a sinking slab into the anomalously hot Pacific large low shear wave velocity province (van der Meer et al., 2012).

If the Pacific Plate started forming as a result of cessation of a part of the fringing subduction system, the absolute Pacific Plate motion would have been more or less continuously westward since 190 Ma. The second scenario, whereby the Pacific Plate originated at the Telkhinia subduction system, would require an abrupt absolute plate motion change around 140 Ma. Although not impossible, this second scenario depends on a less simple tectonic model and is therefore not favored. To further discriminate between the two possible scenarios, relative motions of the Panthalassa plates with respect to the surrounding continents, or absolute plate motion rates of the Izanagi and Farallon plates, play an essential role. To investigate those, paleolatitudinal motions can be inferred from paleomagnetic and faunal analysis on the Panthalassa rocks in the geological records of the circum-Pacific margins (e.g. Kodama et al., 2007; Oda & Suzuki, 2000; Tarduno et al., 1986), and paleolongitudinal motion can be inferred from linking paleolatitudinally constrained intra-oceanic volcanic arcs to deep mantle structure (Grand et al., 1997; Viso et al., 2005).

4. Conclusion

Our analysis shows that it is possible to develop a data-informed plate model of the IZA-FAR-PHO system before the birth of the Pacific Plate using the philosophies and techniques from the early days of plate tectonic reconstructions. Including the Izanagi, Farallon, and Phoenix plates into a global plate reconstruction requires control on absolute plate motions, which can be inferred from combining this surface model with seismology. The analysis presented here provides a key to unlocking the plate kinematic history of the plates that once occupied the "Thalassa Incognita," which comprises the comprehensive Panthalassa Ocean surrounding Pangea.

5. Materials and Methods

Our reconstruction of relative motions between the Pacific, Farallon, Izanagi, and Phoenix plates was inferred from isochrons (Wright et al., 2016), on the basis of marine magnetic anomaly data. The absolute motion path of the Pacific Plate (tracking the center of the Pacific triangle) was plotted in the context of a global plate reconstruction (Müller et al., 2016), using the GPlates plate reconstruction software (www.gplates.org; Boyden et al., 2011)). The global reconstruction was placed in a slab-fitted mantle reference frame (van

der Meer et al., 2010); for the time period between 140 and 83 Ma, the Pacific Plate was placed in a Pacific fixed hotspot frame (Wessel & Kroenke, 2008), Figures 1 and 4 were produced using GPlates.

2

Kinematic reconstruction of the Caribbean region since the Early Jurassic

Sunset at a Caribbean beach - Playa Hermosa, Costa Rica

Abstract

The Caribbean oceanic crust was formed west of the North and South American continents, probably from Late Jurassic through Early Cretaceous time. Its subsequent evolution has resulted from a complex tectonic history governed by the interplay of the North American, South American and (Paleo-)Pacific plates. During its entire tectonic evolution, the Caribbean Plate was largely surrounded by subduction and transform boundaries, and the oceanic crust has been overlain by the Caribbean Large Igneous Province (CLIP) since ~90Ma. The consequent absence of passive margins and measurable marine magnetic anomalies hampers a quantitative integration into the global circuit of plate motions. Here, we present an updated, quantitatively described kinematic reconstruction of the Caribbean region back to 200 Ma, integrated into the global plate circuit, and implemented with GPlates free software. Our reconstruction includes description of the tectonic units in terms of Euler poles and finite rotation angles. Our analysis of Caribbean tectonic evolution incorporates an extensive literature review. To constrain the Caribbean Plate motion between the American continents, we use a novel approach that takes structural geological observations rather than marine magnetic anomalies as prime input, and uses regionally extensive metamorphic and magmatic phenomena such as the Great Arc of the Caribbean, the CLIP and the Caribbean high-pressure belt as correlation markers. The resulting model restores the Caribbean Plate back along the Cayman Trough and major strike-slip faults in Guatemala, offshore Nicaragua, offshore Belize and along the Northern Andes towards its position of origin, west of the North and South American continents in Early Cretaceous time. We provide the paleomagnetic reference frame for the Caribbean region by rotating the Global Apparent Polar Wander Path into coordinates of the Caribbean plate interior, Cuba, and the Chortis Block. We conclude that formation of the Caribbean Plate, west of the North and South Americas, as a result of Panthalassa/Pacific spreading leads to a much simpler plate kinematic scenario than Proto-Caribbean/Atlantic spreading. Placing our reconstruction in the most recent mantle reference frames shows that the CLIP originated 2000–3000 km east of the modern Galápagos hotspot, and may not have been derived from the corresponding mantle plume. Finally, our reconstruction suggests that most if not all modern subduction zones surrounding the Caribbean Plate initiated at transform faults, two of these (along the southern Mexican and NW South American margins) evolved diachronously as a result of migrating trench–trench–transform triple junctions.

1. Introduction

Kinematic reconstruction of regional tectonic evolution comprises translation of qualitative geological data into a quantitative model, describing the relative motions of plates and regional tectonic units. Ideally, the reconstruction is quantified by sets of Euler poles and corresponding finite rotation angles. This has become normal practice in the global reconstruction of continents and continental fragments through geological time (e.g. Besse & Courtillot, 2002; Doubrovine et al., 2012; Müller et al., 2008a; Seton et al., 2012; Torsvik et al., 2008, 2012)), but regional examples are still few (e.g. van Hinsbergen

et al., 2011a, 2014; van Hinsbergen & Schmid, 2012). Generally, regional tectonic reconstructions compile relative motions through time, but when being linked to the global plate circuit of plate motions using a mantle reference frame, they become key input for the assessment of how lithospheric evolution is coupled to underlying mantle processes and mantle structure (Spakman & Hall, 2010).

In the present paper, we aim to develop this kind of kinematically quantified tectonic evolution model of the Caribbean region since ~200 Ma, tied to the North and South American plates. This model can be incorporated in a current or future global plate circuit of choice of either relative of absolute motion. There is currently no generally accepted global plate circuit, but through time the differences in relative plate motions among the models proposed have become gradually smaller (e.g. Doubrovine et al., 2012; Gordon & Jurdy, 1986; Müller et al., 2008a; Seton et al., 2012; Torsvik et al., 2008, 2012). In this study, we incorporate our plate model into the South America-Africa and North America-Africa frame of the global plate circuit of Torsvik et al. (2012).

The Caribbean Plate is a largely oceanic tectonic plate (3500 km E-W by 1000 km N-S), bounded by convergent margins in the east (Lesser Antilles subduction zone), west (Central American subduction zone), and along the northeastern margin of South America (South Caribbean Deformed Belt), and strike-slip-dominated boundaries in the north and southeast, accommodating a relative westward movement of the Americas with respect to the Caribbean Plate (Pindell & Barrett, 1990; Wilson, 1966). Marine magnetic anomalies and fracture zones are usually key in reconstructing past plate motions, providing a direct indication of the position of passive margins back in time. However, only sparse evidence exists of marine magnetic anomalies within the Caribbean Plate (Ghosh et al., 1984) and ages of the anomalies are unconstrained. In conjunction with the either strike-slip dominated or convergent nature of the plate boundaries and the consequent absence of passive margins, it has proved challenging to reconstruct the movement of the Caribbean Plate relative to its surrounding plates back in time. In modern global plate reconstructions (e.g. Seton et al., 2012), the Caribbean region is included using the Euler poles provided in the seminal paper of Ross and Scotese (1988). Based on the reconstruction of Pindell and Barrett (1990), Ross and Scotese (1988) provided poles for a large number of tectonic elements in the Caribbean region, placed in context of the history of seafloor spreading in the Central and South Atlantic (based on poles of Klitgord and Schouten (1986)), magnetic anomalies of the Cayman Trough (using Rosencrantz et al. (1988), Rosencrantz and Sclater (1986), and various geological studies predating 1988.

Since Ross and Scotese (1988), further progress in understanding Caribbean kinematics has been made owing to increase of the geological database, as well as major leaps forward in our understanding of the fundamental behavior and geological expression of subduction zone evolution. Incorporation of these new data and concepts into plate

Figure 1: Geographic map of the Caribbean region. Countries: C, Cuba; H, Haïti; DR, Dominican Republic; FG, French Guyana; Sur, Suriname; Guy, Guyana; E, Ecuador; P, Panamá; ES, El Salvador; Guat, Guatemala; B, Belize; IM, Isla Margarita.

tectonic models of the Caribbean has been compiled in the form of qualitative tectonic reconstructions by e.g. Burke (1988), Pindell et al. (1988); Pindell et al. (1998), Pindell and Barrett (1990), Meschede and Frisch (1998), Müller et al. (1999), Kerr et al. (2003), Pindell and Kennan (2009) and Kennan and Pindell (2009) and generally published in the form of time-sequences of paleogeographic maps. No kinematic parameters in terms of Euler pole rotations are available which renders these reconstructions less useful for quantitative approaches of linking driving mantle processes to tectonic evolution of the region. Van Benthem et al. (2013) discussed the possible links between Caribbean tectonic evolution and remnants of more than 100 Myr of subduction, now detected in the upper and lower mantle. To step forward from this analysis and allow for a quantitative assessment of the coupling between Caribbean tectonic evolution, driving processes and mantle structure (as a memory of past processes), a kinematically quantified reconstruction of the region will be key for testing first order evolution hypotheses using geodynamic modeling of crust–mantle evolution.

To this end and for incorporation of 25 years of geological observations and research of the region since Ross and Scotese (1988), we aim to construct a kinematically quantified reconstruction of Caribbean region evolution since the Early Jurassic using the state-of-the-art of global plate reconstructions for casting the regional reconstruction in a global plate motion frame. We use the freely available software package GPlates (www.gplates.org; Boyden et al., 2011) as the versatile platform for converting geological data and interpretations into Euler poles and finite rotations.

The organization of our paper is as follows. We first provide a research philosophy and approach, and a description of the main geological features used for regional correlation. Then, we review the structural geology of the Caribbean region, as well as the geology of units that can serve for correlation across major fault zones key geological features of the Caribbean region to obtain kinematic constraints as basis for our reconstruction, starting with the Caribbean plate interior, and then in a clockwise journey across the region from Central America, over Cuba to the Lesser Antilles, and via the Leeward Antilles to the northern Andes. We provide this fairly extensive geological review for two reasons: firstly, to help demonstrate the relationship between Caribbean Plate movements and geology, and thus to show where our reconstruction is based on, and secondly, because it has been many years since local works around the Caribbean have been synthesized into a coherent model. Next, we will provide a restoration of the Caribbean from the Present back in time and present selected time-slices from the continuous reconstruction. Finally, the resulting reconstruction will be used to evaluate the origin of the lithosphere of the Caribbean Plate, the origin of the Caribbean Large Igneous Province, the initiation of subduction zones, and the role of absolute plate motions in the evolution of the Caribbean region.

2. Approach

In reconstructing past plate motions, oceanic magnetic anomalies are the most robust data source. In an extensional setting, crustal material has little opportunity to disappear from the rock record, and extensional geological records are most complete at the end of the tectonic event. Conversely, the geological record of convergent plate boundaries are the most incomplete at the end of the tectonic event, and in the most extreme case, crust may entirely subduct without leaving a rock record at all. In addition, compression normally emerges rocks, which may disappear from the geological record belt by erosion. Reconstructed amounts of shortening will consequently be minimum estimates of the amount of convergence accommodated in the shortened zone and therefore, extensional records are preferred. To illustrate this, Europe-Africa motion can be determined by shortening records from the Alps, providing a minimum estimate of convergence. However, combining North and Central Atlantic ocean spreading reconstructions that quantify the movement of Europe relative to North America and the movement of North America relative to Africa, respectively, will provide a much more accurate estimate (e.g. Dercourt et al., 1986; Dewey et al., 1989; van Hinsbergen et al., 2014; van Hinsbergen & Schmid, 2012).

For the Caribbean Plate, the only oceanic extensional records that can be used in a quantitative sense are the magnetic anomalies in the Cayman Trough, an oceanic pull-apart basin on the Caribbean-North American plate boundary, where the Swan Island and Oriente faults accommodate left-lateral transform motion (Fig. 1). The Cayman Trough provides kinematic data for the Caribbean Plate with respect to the Cuban segment, formerly part of the Caribbean Plate but welded to the North American Plate since the Paleogene collision of the Caribbean Plate with the Bahamas borderlands (Pindell and

Barrett, 1990). Before opening of the Cayman Trough (i.e., prior to an estimated 49.4 Ma; Leroy et al., 2000), other data sources are needed to reconstruct relative plate motions, such as major strike-slip fault displacements, continental extensional or shortening estimates, paleomagnetism (indicating rotations and paleolatitudes of plates or plate fragments), plate boundary volcanism and metamorphic belts, and obducted ophiolites indicating former intra-oceanic subduction zones.

The boundary conditions for our Caribbean reconstruction are provided by the relative movements between the North American and African plates, and the South American and African plates using poles from Central and South Atlantic ocean reconstructions of Torsvik et al. (2012) using the timescale of Gradstein et al. (2004)(with the exception of the age of M0, where we adopt a 120.8 Ma age following He et al. (2008)). Figure 2 shows the resulting relative motion of South America relative to North America. These movements constrain the opening evolution of the Proto-Caribbean Ocean (i.e. the westward continuation of the Central Atlantic Ocean) between the Americas during Jurassic break-up of Pangea (Dickinson & Coney, 1980; Pindell, 1985).

The starting point of our reconstruction is the present-day situation. For the last 49.4 Myr, the motion of the Caribbean Plate relative to the Cuban segment is constrained by oceanic spreading in the Cayman Trough. The first step in reconstructing is therefore reversing the oceanic Cayman extension, recorded by magnetic anomalies (Leroy et al., 2000). Prior to opening of the Cayman Trough and before welding of the Cuban segment to North America, reconstruction requires less straightforward data and becomes more difficult and uncertain. Some types of data are considered to constrain motion more precise than others. We therefore composed an interpretation hierarchy of data types, arranged from higher to lower degree of certainty (Table 1). After interpretations from extensional records from the Atlantic and Cayman Trough we first consider interpretations from continental transform and strike-slip records. The precise amount of fault displacement may not be known in cases, but the presence of strike-slip faults provides hard constraints on the orientation and sense of relative motion. Thirdly, we consider continental extension. Even though continental extension is more difficult to reconstruct than oceanic spreading, it provides a maximum geological record at the end of deformation. Subsequently, continental collisional records provide constraints on the age and nature of collision. In collision zones, crustal material can (and frequently will) disappear by subduction, but remnants of the preceding situation can be preserved in the form of ophiolites, high-pressure (HP) metamorphic rocks, syn-kinematic sedimentary basins, or thin- or thick-skinned fold-thrust belts. We then consider interpretations based on volcanic data. Here, we particularly focus on ages of magmatism (e.g. oceanic island arc rocks), to infer the presence of a convergent plate boundary for that period. The geochemical literature of the Caribbean contains a large number of models invoking major geodynamic events such as subduction polarity reversals or slab break-off episodes, and complex subduction zone configurations (e.g. Hastie et al., 2013; Kerr et al., 1999; Meschede & Frisch, 1998;
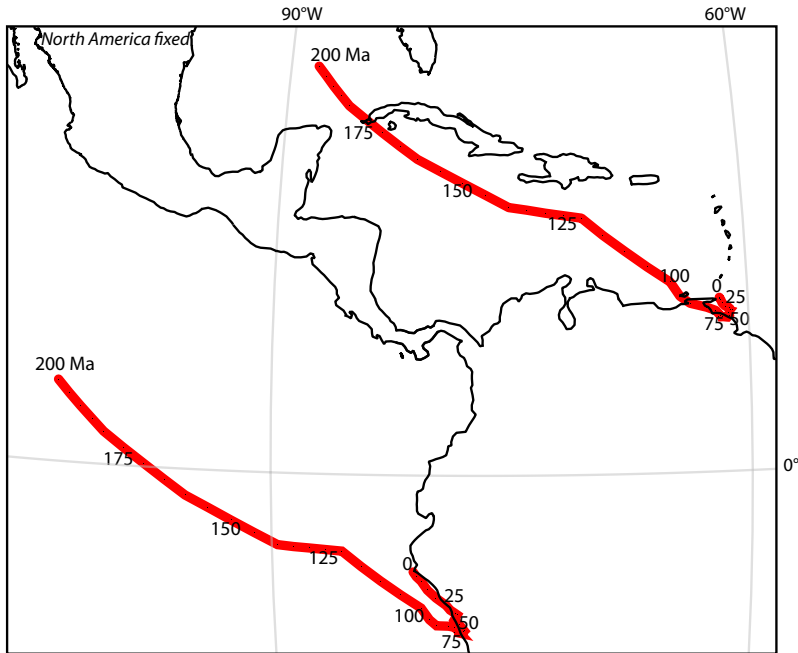
Figure 2: 200–0 Ma motion paths for two locations on the South American continent, relative to a stable North America, based on the plate circuit of Torsvik et al. (2012). 3D Globe projection. The distance between two black dots represents 5 million years.

Neill et al., 2011). Such interpretations are not a priori followed here, but rather, our reconstruction may serve as an independent kinematic basis to evaluate the kinematic feasibility of such scenarios. The before last category is the existence of geological and geophysically imaged features like magnetic boundaries, basement ages or comparable stratigraphic sections as potential correlation tools across tectonic boundaries. Finally, we use paleomagnetic data. Paleomagnetic data are normally high-quality quantitative constraints in kinematic reconstructions, but in the Caribbean area, only few data are available, and not always of the quantity and quality that passes modern quality criteria. Furthermore, paleomagnetic results from the northern and southern plate boundary zones often represent local strike-slip rotations, instead of large scale block rotations (MacDonald et al., 1996; MacDonald, 1980; Mann & Burke, 1984b).

Our hierarchy is chosen such that the uncertainty of kinematic interpretations based on these increases with every next step. This ranking allowed us to choose between contradicting interpretations. We stress, however, that this hierarchy is used to choose between preferred interpretations of certain data sets: we have not discarded data. Our reconstruction is at every step tested against the basic concepts of plate tectonics (Cox & Hart, 1986). We took the following, conservative assumptions: (1) A tectonic terrane/

block is rigid, unless there is evidence for the contrary. (2) A tectonic terrane can only move independently relative to the major plates if it is bordered by plate boundaries and conversely: if two blocks have different movements, there must be a plate boundary in between. (3) Triple junctions are stable, or, for a short period of time, unstable and transforming, or falling apart into two stable triple junctions. (4) Without evidence for a subduction polarity reversal and a straightforward kinematic evolution of such a reversal, the direction of subduction is assumed to remain the same. These assumptions ensure that a tectonic terrane will always be part of one of the large tectonic plates (the North or South American, Caribbean or Pacific plate), unless there is evidence for microplate motion and ensure that we always reconstruct the most simple plate kinematic scenario, within the restrictions provided by the geological data.

These assumptions provide a test for the geological and paleomagnetic interpretations and limit the amount of contradicting reconstruction scenarios. When geological interpretations were clearly inconsistent with the basic rules of plate tectonics, we refuted these interpretations in order to keep the reconstruction kinematically consistent. The final plate-tectonic model is supported by as many geological data and interpretations as possible, but the 'rules of plate tectonics' are considered to be superior to regional interpretations and scenarios based on individual tectonic terranes.

We used the freely available software package GPlates to make the reconstruction. The surface of the Caribbean Plate is divided into undeformable polygons, reconstructed using a reconstruction tree starting with North America (except for the NW Andes, which are reconstructed relative to South America). When reconstructing back in time, the polygons may overlap (indicating extension) or drift apart (indicating shortening). GPlates

Data type	Application	Reference
Oceanic extensional records	Atlantic; Cayman Trough	Torsvik et al. (2012); Leroy et al. (2000)
Transform and strike-slip records	Motagua; Cuba; Andes	Burkart (1983, 1994); Rosencrantz (1990), Cruz-Orosa et al. (2012a); Kerr et al. (1998), Trenkamp et al. (2002)
Continental extensional records	Nicaragua	Phipps Morgan et al. (2008)
Continental collisional records	Siuna-Chortis; Great Arc-Yucatan; Cuba-Bahamas; Great Arc-South American continent	Venable (1994), Rogers et al. (2007); Pindell and Kennan (2009), Ratschbacher et al. (2009), Martens et al. (2012), Solari et al. (2013); Meyerhoff and Hatten (1968), Knipper and Cabrera (1974), Pardo (1975), Iturralde-Vinent et al. (2008); e.g. Kennan and Pindell (2009)
Volcanism	Subduction related (Great Arc of Caribbean; Lesser Antilles Arc; Central American Arc)	e.g. Stanek et al. (2009); Briden et al. (1979); Denyer et al. (2006), Buchs et al. (2010)
	Oceanic plateau material (CLIP)	e.g. Sinton et al. (1998)
Matching basement types/ magnetic boundaries etc.	Chortis-Western Mexico	Rogers et al. (2007)
Paleomagnetism	Cuba; Chortis; Aruba and Bonaire; Tobago; Puerto Rico	Tait et al. (2009); Molina Garza et al. (2012); Stearns et al. (1982) ; Burmester et al. (1996) ; Reid et al. (1991)

Table 1: The reconstruction of the Caribbean region is made using a hierarchy of data types, in decreasing order of certainty. Where interpretations based on different data types are mutually exclusive, this hierarchy is used to select the preferred interpretation.
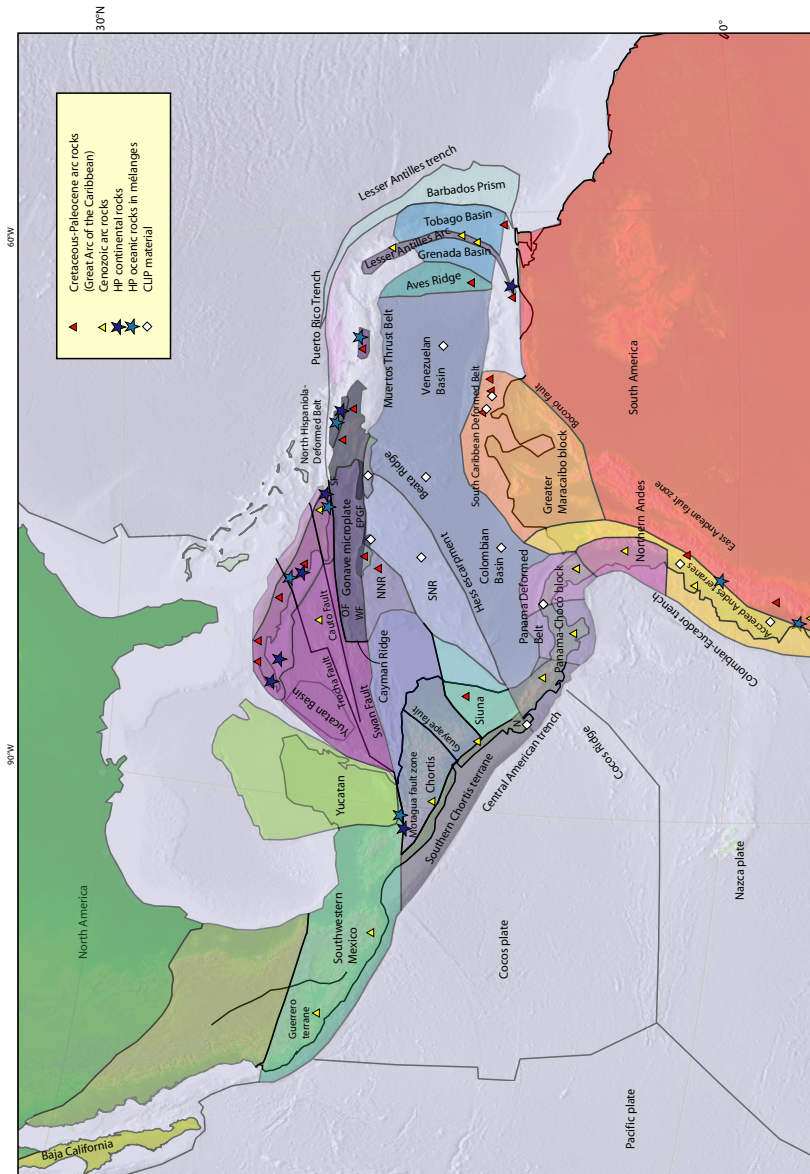
Figure 3: Tectonic map of the Caribbean region, showing the tectonic blocks as described in Section 3 and locations of arc material (from Iturralde-Vinent et al., 2008; Krebs et al., 2008; Buchs et al., 2010), HP rocks (from García-Casco et al., 2006, 2008a; Iturralde-Vinent et al., 2008; Krebs et al., 2008) and CLIP material (from Geldmacher et al., 2003; Buchs et al., 2010; Lewis et al., 2011). Tectonic features: OF, Oriente Fault; WF, Walton Fault; SF, Septentrional Fault; EPGF, Enriquillo–Plantain Garden Fault; NNR, North Nicaraguan Rise; SNR, South Nicaraguan Rise; N, Nicoya Peninsula.

interpolates motion of polygons with constant rates between constrained situations, leading to a visualization and mathematical description of continuous plate motion.

3. Previous work and correlation concepts

In previous studies of the Caribbean region, several ideas and concepts were developed that may form a useful basis for correlation in our reconstruction, and which will be used in the subsequent review of geological data. These concern Burke's (1988) 'Great Arc of the Caribbean', García-Casco et al.'s (2008a) 'Caribeana continental promontory' and the Caribbean Large Igneous Province (CLIP).

3.1. Great Arc of the Caribbean

Volcanic arc material is present along the perimeter of most of the present-day Caribbean Plate (e.g. in Central America, on the Greater Antilles (Cuba, Jamaica, Hispaniola and Puerto Rico), on the Aves ridge and the Lesser Antilles and in the Northern Andes; Fig. 1, 3). Mann and Burke (1984) and (Speed, 1985) were the first to suggest that there may be a coherence between different arc segments, based on similarities in age and composition between arc material on the Greater Antilles, the Aves ridge-Lesser Antilles Arc system and the Netherlands Antilles, in contradiction with the then prevailing concept of independent island arcs developed in different times at different places. Burke (1988) introduced the term 'Great Arc of the Caribbean', being a volcanic arc that developed at the subduction plate boundary between the future Caribbean Plate and the Proto-Caribbean Ocean (that was part of the North and South American plates and connected to the Central Atlantic Ocean) and that migrated towards the east relative to the Americas. As the Great Arc entered the Atlantic realm, the northern segment collided progressively from west to east with Yucatan and the Bahamas platform, leaving arc material behind in Guatemala and on the islands of Cuba, Hispaniola, Jamaica and Puerto Rico. The central segment, the present-day Aves ridge, remained in this concept an active subduction system while the southern segment collided with the northwestern margin of South America, leaving tectonic slivers of arc material behind in Ecuador and Colombia. Subsequent transform motion transported fragments of Great Arc material to Venezuela, the Leeward Antilles and Tobago (Burke, 1988; Fig. 3). Our reconstruction tests this hypothesis and, in addition to other sources of information, uses fragments of the Great Arc as kinematic markers of (particularly strike-slip) displacements.

3.2. Caribeana continental promontory

Arc material of the Great Arc of the Caribbean is found on the Greater Antilles to intrude in and overlie ophiolitic complexes, which in turn overlie accretionary wedges of deformed sediments, all related to Proto-Caribbean subduction and subsequent collision of the Caribbean Plate with the Yucatan and Bahamas borderlands. Joyce (1983) and Wadge et al. (1984) found evidence for a fourth element in the subduction complexes, defined by García-Casco et al. (2008a) as the continental 'Caribeana' terrane. Caribeana is described as 'a conceptual paleogeographic domain characterized by Mesozoic sedimentary piles that

occupied a portion of the Proto-Caribbean oceanic domain' (García-Casco et al., 2008a). The rocks of Caribeana are HP–LT metamorphic (up to eclogite facies) metasedimentary and -volcanic rocks found in thrust piles with a metamorphic grade decreasing within every next tectonic unit (e.g. in the Sierra de Escambray on Cuba). These rocks are found in, form west to east, the Cangre, Pinos, Escambray, Asunción (on Cuba) and Samaná (on Hispaniola) terranes (Figs. 3 and 4). Geophysical data and samples dredged from the ocean floor also provide evidence of metasedimentary complexes offshore eastern Yucatan and offshore eastern Hispaniola, northern Puerto Rico and the northeastern Virgin Islands (East Yucatan terrane and Puerto Rico Trench terrane) (García-Casco et al., 2008a). Although these rocks were previously interpreted to have been derived from the Bahamas borderlands, the accretionary prism of Cuba demonstrates that the Caribeana rocks of Cuba were underthrusted by oceanic sedimentary rocks between ~60 and ~45 Ma before collision of the Caribbean Plate, overlying arc and accreted Caribeana fragments with North America (García-Casco et al., 2008a; Iturralde-Vinent et al., 2008; van Hinsbergen et al., 2009). Caribeana is thus envisaged as a NW-SE elongated submarine domain with (stretched) continental basement, likely positioned as a promontory of the southeastern Yucatan block. We will use the Caribeana HP belt as correlation marker in our reconstruction, in tandem with the Great Arc of the Caribbean.

3.3. Caribbean Large Igneous Province (CLIP)

The majority of the oceanic crust of the Caribbean Plate is anomalously thick (15–20 km), as measured by seismic refraction studies (Burke et al., 1978). Exceptions are the Cayman Trough and the Yucatan, Grenada and Tobago Basins (Fig. 1, 3). Deep sea drilling (DSDP and ODP) into this thick crust showed that the ocean floor consists of basaltic rocks, mainly tuffs and fine-grained intrusives, interbedded with roughly 80 Ma pelagic sediments (Donnelly et al., 1973). Based on these results, Donnelly et al. (1973) proposed that a large basalt flooding event occurred in the Late Cretaceous. This flood basalt formed a major oceanic plateau, now known as the Caribbean Large Igneous Province (CLIP) (Burke, 1988; Burke et al., 1978; Saunders et al., 1996). The same material as found in drill cores from the Venezuelan and Colombian basins and the Beata Ridge has also been found on-land (e.g. on Hispaniola, Costa Rica, Panama, and in the Northern Andes, see Figure 3). Radiometric dating of DSDP and ODP drill samples and of samples from Haiti, Curaçao and Western Colombia suggests that the massive basalt flooding happened between 91 and 88 Ma (Hauff et al., 2000; Hoernle et al., 2002; Kerr et al., 1997; Révillon et al., 2000; Sinton et al., 1997, 1998). This short-lived magmatic event has often been attributed to the plume-head stage of the Galápagos hotspot (e.g. Duncan, 1984; Hill, 1993). Hoernle et al. (2004), however, propose a 70 Myr (139-69) history for the CLIP, but the deviating ages are found in multiple different oceanic igneous structures, accumulated on the western boundary of the Caribbean Plate during the subduction of the Farallon Plate. An example is the magmatic rock suite of the Nicoya Peninsula of western Costa Rica, containing fragments of plateau basalt and hotspot volcanoes of ages ranging between 139 and 111 Ma (Hoernle et al., 2004). In our study, these and equivalent rocks

of deviating age are not considered to be part of the Caribbean Large Igneous Province, but as accreted fragments of Panthalassa/Pacific crust. The total area of the CLIP is ~6*10⁵ km2, but since part of the plateau was thrusted onto the South American margin of Colombia and Ecuador, the plateau may originally have been more than twice this size (Burke, 1988). CLIP material is used in the reconstruction as a correlation marker for the interior of the Caribbean Plate.
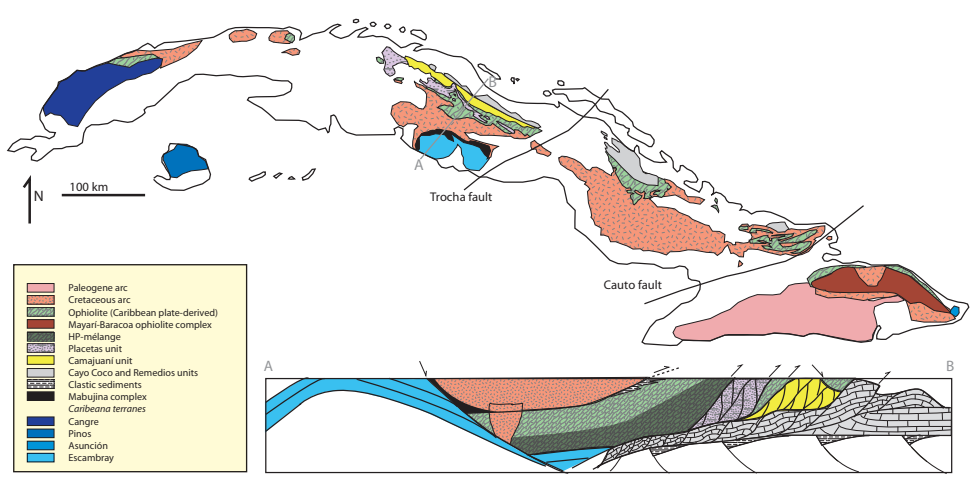
Figure 4: Map and cross section of Cuba displaying the major geological units. Based on García-Casco et al. (2001), Iturralde-Vinent et al. (2008), and Lázaro et al. (2013).

4. Review

The following section provides a review of the geological data of the Caribbean region that can be used for kinematic restoration. A summary of the temporal and spatial constraints on key geological markers is given in Figure 5. The most important quantitative constraints on fault displacements provided in the literature, inferred by us in the review below, applied in the reconstruction for optimal fits, and predicted by the final model is given in Table 2. Geological rock units are described per area from old to young, and from bottom to top. The review starts with the interior of the Caribbean Plate, and subsequently describes the plate boundaries clockwise, starting with Central America, the Motagua fault zone, the Cayman Trough and the Cuban segment in the north, followed by the eastern subduction system, the southern transform boundary and finalizing with the Northern Andes. In addition to the geological data, paleomagnetic data and seismic tomographic constraints on mantle structure (relevant for the subduction systems) is described.

4.1. Caribbean Sea floor

The Caribbean Sea floor contains several basins and highs with various basement types. From northwest to southeast, it contains the North and South Nicaraguan Rise, Colombian Basin, Beata Ridge, and the Venezuelan Basin (Fig. 3). Other basins and highs formed within the Caribbean Plate - the Yucatan Basin, Cayman Trough, Aves Ridge, Grenada Basin, Lesser Antilles Arc and Tobago Basin - will be described later. The boundary between the Nicaraguan Rise and the Colombian Basin is a major fault scarp, the Hess escarpment, which has been interpreted as inactive since the Late Cretaceous, except for the southwestern part that has been active in recent times (Bowland, 1993; Case et al., 1990; Mauffret & Leroy, 1997). The Colombian Basin, Beata Ridge, and Venezuelan Basin are underlain by oceanic plateau crust, interpreted as part of the CLIP (Donnelly et al., 1973). Despite the presence of the CLIP, some magnetic anomalies were identified by Ghosh et al. (1984) on the ocean floor in the eastern basins, which they interpreted as typically spreading-related, although their age remains uncertain. These anomalies are currently NE-SW trending. The original orientation of the anomalies is not known, as

Figure 5: Overview of temporal constraints on geological phenomena used for regional correlation per area. For references, see text.

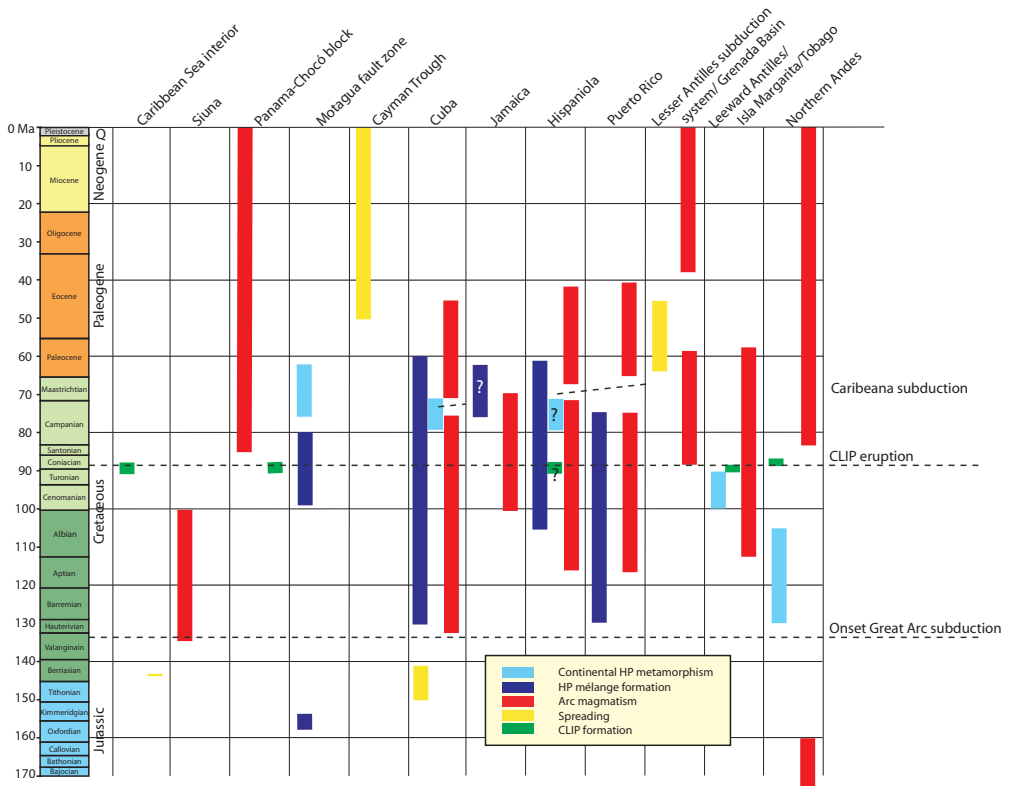| Structure	Displacement	Age range	Reference
Displacement estimates from literature			
Puerto Rico rotation	25°ccw rotation	11-4 Ma	Reid et al., 1991
Maracaibo block versus South America	250 km right-lateral slip	11-0 Ma	Ross and Scotese, 1988
Chortis Block	insignificant rotation	17-0 Ma	Molina-Garza et al., 2012
Western Panama-South America motion	1000 km NE-SW convergence	35-0 Ma	Montes et al., 2012
Tobago, Aruba and Bonaire	90°cw rotation	65-0 Ma	Burmester et al., 1996; Stearns et al., 1986
Panama Deformed Belt	250 km NE-SW convergence	35-0 Ma	Montes et al., 2012
Cayman trough	900 km	49.4-0 Ma	Leroy et al., 2000
Displacement estimates based on geological correlation (see text)			
Nicaraguan Basin extension	100 km E-W extension	15-0 Ma	
Nicaraguan forearc	4°ccw rotation	15-0 Ma	
Nicaraguan forearc-Chortis motion	150 km right-lateral slip	15-0 Ma	
Chortis block	32°ccw rotation	largely 38-33 Ma	
Muertos Trench convergence	30 km N-S shortening	40-0 Ma	
La Trocha fault Cuba	20 km left-lateral slip	44-40 Ma	
Cauto fault Cuba	15 km left-lateral slip	40-38 Ma	
Septentrional Fault Hispaniola	500 km left-lateral slip	50-0 Ma	
Puerto Rico Trench	300 km left-lateral slip	40-0 Ma	
Cuba-Yucatan slip along Belize margin	900 km left-lateral slip	70-45 Ma	
Subduction erosion Cuba	140 km	70-45 Ma	
Tobago/Grenada basin extension	75 km E-W extension	55-40 Ma	
Mayari-Baracoa ophiolite emplacement	≤135 km N-S convergence	75-70 Ma	
Mayari-Baracoa back-arc extension	≤135 km N-S extension	80-75 Ma	
Chortis-Jamaica and North Nicaraguan Rise motion	550 km left-lateral slip	85-70 Ma	
Displacement estimates to optimize fits (see text)			
Siuna-Chortis-North Nicar. Rise and the South Nicar. Rise	300 km left-lateral slip	50-38 Ma	
Siuna-Chortis-North Nicar. Rise and the South Nicar. Rise	100 km right-lateral slip	38-32 Ma	
Hess Escarpment	150 km right-lateral slip	50-30 Ma	
Caribbean plate rotation vs North America	7°ccw rotation	50-0 Ma	
Cuban segment-Caribbean plate interior displacement	400 km left-lateral slip	70-50 Ma	
Caribbean plate rotation vs North America	17°ccw rotation	70-50 Ma	
Siuna-Chortis-North Nicar. Rise and the South Nicar. Rise	600 km left-lateral slip	70-50 Ma	
Nicaraguan Rise/offshore Chortis Block extension	100 km N-S extension	75-70 Ma	
Caribbean plate rotation vs North America	9°ccw rotation	100-70 Ma	
Caribbean-North America motion	900 km left-lateral motion	135-100 Ma	
Caribbean plate rotation vs North America	5°ccw rotation	135-100 Ma	
Model predictions			
Caribbean-South America strike-slip	1000 km right-lateral slip	50-0 Ma	
SCDB subduction (eastern Venezuela)	250 km	50-0 Ma	
SCDB subduction (Colombia)	800 km	50-0 Ma	
Caribbean-South American motion; transform component	700 km right-lateral slip	70-50 Ma	
Caribbean-South American motion; subduction component	500 km convergence	70-50 Ma	
Caribbean-South American motion; transform component	1300 km right-lateral slip	100-70 Ma	
Caribbean-South American motion; subduction component	200 km convergence	100-70 Ma	
Pre-drift extension in Proto-Caribbean basin	300-400 km	200-170 Ma	

Table 2: Quantitative constraints mentioned in the text on fault displacements, shortening, extension and rotation in the Caribbean region (1) provided in the literature; (2) inferred in this paper through correlation of geological units; (3) applied in our reconstruction along structures without direct geological constraints to yield an optimal fit and (4) predicted by the final model.

a result of the unknown ages, and rotations of the Caribbean Plate following spreading. Therefore, the probable orientation of the spreading ridge and, perpendicular to that, the direction of paleo-spreading cannot be determined accurately. The oceanic basement of La Désirade Island in the Lesser Antilles, formed in a back-arc supra-subduction setting, has a 143.74 ± 0.33 Ma U-Pb age (Mattinson et al., 2008; Neill et al., 2010), suggesting that ocean spreading continued at least until the latest Jurassic. There is no evidence for spreading within the Caribbean Plate since the emplacement of the CLIP basalts (except for the Grenada Basin in the far east and the Yucatan Basin and Cayman Trough in the north), so ages of CLIP material in the Venezuelan and Colombian Basins provide a minimum age for sea-floor spreading. Since ~91-88 Ma, the Caribbean plate interior has not been increasing in size anymore and has only been reduced by subduction below South America.

The Nicaraguan Rise floors the Caribbean Sea between the Hess escarpment and the Cayman Trough and covers an area of ~4*105 km2. The North Nicaraguan Rise consists of thinned continental crust with correlative outcrops in northern Central America and calc-alkaline Upper Cretaceous–Paleocene island arc rocks (Arden, 1975; Lewis & Draper, 1990; Lewis et al., 2011; Perfit & Heezen, 1978). The South Nicaraguan Rise is composed of thick oceanic plateau crust similar to the Venezuelan and Colombian Basins and is interpreted as CLIP material (Case et al., 1990; Mauffret & Leroy, 1997).

The role of the Nicaraguan Rise in tectonic reconstructions of the Caribbean region is controversial. Some reconstructions show 500–700 km of Eocene-Oligocene convergence between the Nicaraguan Rise and north Hispaniola (Müller et al., 1999; Sykes et al., 1982) based on paleomagnetic data suggesting as much as ~8° of latitudinal convergence between south and north Hispaniola (Van Fossen & Channell, 1988). Pindell and Barrett (1990) and Pindell et al. (2012) suggested that the Nicaraguan Rise and Jamaica formed a contiguous island arc, below which several hundred kilometers of Proto-Caribbean lithosphere subducted in the Late Cretaceous. Lewis et al. (2011) postulated that an extension of the South Nicaraguan Rise was subducting below the North Nicaraguan Rise and caused Late Cretaceous magmatism in the North Nicaraguan Rise. In contrast, Mann et al. (2007) suggested strike-slip as the main process to bring the Nicaragua Rise and southern Hispaniola in place. Recently, van Benthem et al. (2013) found no evidence for Nicaraguan Rise subduction in seismic tomographic images of underlying mantle structure, confirming the model of Mann et al. (2007).

Recent GPS observations indicate that the Caribbean plate interior is not rigid, but internally deforming with 1-3 mm/yr. A two plate model best explains the data, but the plate boundary is unknown. Relative motions between the western and eastern Caribbean Plate are suggested to be accommodated in the Nicaraguan Rise or Beata Ridge (Mattioli et al., 2014).

In summary, the Caribbean Sea can be divided into two parts: oceanic crust formed before emplacement of the CLIP (South Nicaraguan Rise, Colombian and Venezuelan Basins and Beata Ridge) and locally, crust formed by extension after emplacement of the CLIP (Yucatan Basin, Cayman Trough, Grenada and Tobago Basins). Paleo-spreading directions in modern orientations were NW-SE, and limited age constraints suggest that spreading occurred at least in late Jurassic time.

4.2. Central America

The western boundary of the Caribbean Plate is the Central America Trench, accommodating eastward subduction of the Cocos Plate and before the Miocene the Farallon Plate (Barckhausen et al., 2008), below the Caribbean Plate. The Central American land bridge can be divided into several tectonic blocks, from north to south including: the Chortis Block, the Southern Chortis terrane, the Siuna block and the Panama–Chocó block (Fig. 3).

The Chortis Block (southern Guatemala, Honduras and northern Nicaragua) exposes crystalline Paleozoic and older continental basement that was probably part of the North American continent prior to the Cenozoic. The block is bounded by the Motagua left-lateral strike-slip fault zone to the north and a geological basement transition interpreted as a former passive margin (Rogers et al., 2007) to the south and west. A major tectonic feature within the Chortis Block is the Guayape fault system, which is currently inactive (DeMets et al., 2007), but which acted as a strike-slip fault system in the Cretaceous–Miocene (Finch & Ritchie, 1991). A two-stage model was proposed by Finch and Ritchie (1991), with more than 50 km sinistral strike-slip displacement probably related to Cenozoic sinistral movement along the Motagua fault zone followed by a dextral phase of smaller displacement. The area south of the Guayape fault (named Eastern Chortis by Rogers et al. (2007)), is interpreted as an extended continental margin of the Chortis Block, formed when it was still part of the North American Plate during the Jurassic opening of the Proto-Caribbean ocean (Rogers et al., 2007). James (2006) interpreted the Guayape fault as an Upper Jurassic normal fault associated with rifting.

The area to the southwest of the Chortis Block is the Southern Chortis terrane (southwestern Guatemala, Honduras, Nicaragua and El Salvador). As inferred from geochemistry of Quaternary lavas (Carr et al., 2004), the Southern Chortis terrane probably has no (pre-)Paleozoic basement. One single known exposure of basement contains metavolcanic amphibolite of unknown age (Markey, 1995). The Southern Chortis terrane is interpreted as an accreted island arc (Rogers et al., 2007), similar in nature to parts of the Guerrero island arc composite terrane that fringes the continental basement of western Mexico to the northwest. The Guerrero terrane accreted to western Mexico in the Cretaceous (Centeno-García et al., 2011; Tardy et al., 1994). The age of accretion of the Southern Chortis terrane to the Chortis Block is uncertain. Because the Southern Chortis

terrane is not directly relevant for reconstruction of the Caribbean Plate, and the timing of accretion is unknown, we kept it fixed to the Chortis Block.

The sinistral movement along the Motagua fault system indicates an eastward movement of the Chortis Block with respect to the Yucatan block (Fig. 1, 3). It was suggested that the Chortis Block was located along the southwestern margin of Mexico prior to its eastward displacement (e.g. Dengo, 1985; Pindell & Barrett, 1990; Ross & Scotese, 1988). Tectonic models (e.g. Pindell & Barrett, 1990; Ross & Scotese, 1988) incorporate this interpretation and suggest that the Chortis Block was transferred from the North American to the Caribbean Plate by the formation of the Motagua fault. Rogers et al. (2007) summarized arguments for this scenario and suggested that the Chortis-Southern Chortis terrane boundary corresponds to the west Mexican continental basement-Guerrero terrane boundary. This correlation provides an estimate of displacement of the Chortis Block relative to North America of ~1000 km since formation of the Motagua fault. Because of the absence of evidence for convergence between southern Mexico and the Chortis Block during displacement and because the southern Mexican margin is oriented WNW-ESE, the motion of Chortis towards the E-W striking Motagua fault zone would require a counterclockwise rotation of the Chortis Block (Rogers et al., 2007). Paleomagnetic data from Miocene volcanics in western Honduras (17-14 Ma) show no significant rotation of these volcanics and constrain any rotation to pre-Middle Miocene (Molina Garza et al., 2012).

South of the Chortis composite terrane is the Siuna block, composed of volcanics, serpentinized peridotite and associated ultramafic cumulates, and carbonate-rich sediments. The Siuna block is interpreted as a Lower Cretaceous island arc, probably part of the Great Arc of the Caribbean, developed on ocean floor and accreted to (thrusted over) the Chortis Block in the Late Cretaceous (Rogers et al., 2007; Venable, 1994).

The southern part of Central America, between the Siuna block and the South American continent, is known as the Panama-Chocó block and contains the countries Panama and Costa Rica. Boundaries of this block are the Panama Deformed Belt in the northeast, the Central American trench in the west (where the Cocos Plate, Cocos Ridge and Nazca Plate are subducting), a diffuse thrust belt in the Cordillera Central of Costa Rica in the northwest, and the suture with the South American continent in the southeast (Buchs et al., 2010). The bulk of the Panama-Costa Rica land bridge is composed of upper Campanian-Neogene volcanic arc rocks (Buchs et al., 2010; Denyer et al., 2006; Montes et al., 2012) underlain by oceanic plateau crust, as suggested by geochemical characteristics of recent magmas (Feigenson et al., 2004; Gazel et al., 2009). Ar-Ar ages of oceanic plateau fragments range from 139 to 71 Ma (Sinton et al., 1997; Hoernle et al., 2002, 2004). Middle Turonian-Santonian and Coniacian-Santonian ages of radiolarites intercalated with arc-derived volcanic material from the Nicoya Peninsula of Costa Rica indicate that the volcanic arc has been active since at least the Santonian (Bandini et al., 2008).

Geochemical data suggest that at ~75 Ma, a protoarc formed (represented by dikes and lava flows of the Azuero Protoarc Group with a geochemistry similar to CLIP material). In the Maastrichtian, the arc system matured (Buchs et al., 2010; Lissinna et al., 2006; Wegner et al., 2010). Formation of a protoarc indicates subduction initiation, formation of a western Caribbean plate boundary and therefore separation of the Farallon and Caribbean plates (Pindell and Kennan, 2009). Pindell and Kennan (2009) proposed an age of 80-88 Ma for subduction initiation, considering that a slab needs several million years to reach depths where melt can be generated. The Pacific margin of Costa Rica and Panama is characterized by accreted fragments of Upper Triassic to Middle Miocene radiolarites and volcanic rocks from seamounts derived from the far interior of the Farallon/Cocos Plate (Baumgartner et al., 2008; Denyer et al., 2006; Feigenson et al., 2004). Prior to collision with the South American continent, the Panama-Chocó block formed a straight volcanic arc, that started to segment into the western, central, eastern and Greater Panama blocks during Late Eocene-Early Oligocene times (~28-38 Ma, (Cardona et al., 2012; Farris et al., 2011). Segmentation and deformation was achieved by vertical axis rotation of the individual blocks and local folding and faulting (Montes et al., 2012; Rockwell et al., 2010). In our reconstruction, we follow the model of Montes et al. (2012) for the Panama-Chocó block.

Finally, the western margin of Central America, including the Southern Chortis terrane is presently moving as a fore-arc sliver relative to the Caribbean Plate (Ranero et al., 2000; Von Huene et al., 1980). This fore-arc sliver contains the Nicaraguan Basin, where extension was recorded in basins filled by volcanics ranging in age from 25 Ma to Recent (Molina Garza et al., 2012; Phipps Morgan et al., 2008). Phipps Morgan et al. (2008) interpreted these volcanics as recording 100 km of E-W extension in the last 15 Myr. GPS studies show that the eastern part of the Chortis Block (eastern Honduras and Nicaragua) is currently moving with the same eastward velocity and direction relative to North America as the interior of the Caribbean Plate. The westernmost part of the Chortis Block, on the other hand, is moving with a slightly lower eastward relative velocity, resulting in arc-normal extension (DeMets et al., 2007). Furthermore, DeMets (2001) shows that the fore-arc sliver is transported northwestward relative to the Caribbean Plate. Slip directions of earthquakes on the boundary between the fore-arc sliver and the Chortis Block are deflected 10° clockwise from the plate convergence direction, indicating partitioning of oblique Cocos-Caribbean plate convergence (DeMets, 2001; LaFemina et al., 2009). LaFemina et al. (2009) suggested that the collision of the Cocos Ridge contributes to the northwestward motion of the fore-arc sliver. The buoyant, thickened crust of the Cocos Ridge acts as an indenter (Gardner et al., 2013) and arc-parallel fore-arc motion, as well as relative (north)eastward motion of the Panama-Chocó block represents tectonic escape (Kobayashi et al., 2014). Phipps Morgan et al. (2008) noticed that the Motagua fault zone at present does not crosscut the Central American fore-arc and does not continue towards the Central American trench. With plate rigidity, the south Mexican trench-Central American trench-Motagua transform triple junction should move eastward along

the Motagua transform. Phipps Morgan et al. (2008) suggested that the extension in the Nicaraguan Basin and the northwestward motion of the fore-arc sliver are the result of the stationary position of this triple junction due to a strong, undeforming Cocos Plate. The triple junction is unstable (see Fig. 2b, c of Phipps Morgan et al. (2008)) and because the Cocos Plate is not tearing, the eastward movement of the Caribbean Plate relative to North America is not accommodated in the Cocos Plate, but by internal deformation in the two overriding plates. This deformation is manifested in transpressional structures in the North American Plate (Guzmán-Speziale, 2010) and extension and fore-arc motion in the Caribbean Plate ("zipper" process, Authemayou et al. (2011)).

In summary, the Central American land bridge consists of three types of crust: continental (Chortis terrane), volcanic arc upon regular oceanic crust (Siuna block, southern Chortis terrane) and volcanic arc upon oceanic plateau crust (Panama-Chocó block). Subduction initiation of the Farallon Plate below the Caribbean Plate in the Panama-Chocó Block occurred ~88-80 Ma. Caribbean-North American plate motion culminated in thrusting of the Caribbean Plate over the southern Chortis margin in late Cretaceous time, and since the Cenozoic formation of the Motagua fault zone, the Chortis Block moved eastwards over ~1000 km towards its modern position.

4.3. Motagua fault zone

The northern boundary of the modern Caribbean Plate is a left lateral transform boundary that extends from western Guatemala to the Lesser Antilles subduction zone (Fig. 3). The western part of the plate boundary consists of a continental arcuate strike-slip fault system in central Guatemala and the oceanic Cayman Trough. This intra-continental fault system separates the North American Yucatan block (southern Mexico, Belize and northern Guatemala, also referred to as the Maya block) in the north from the continental Chortis Block in the south, which at present belongs to the Caribbean Plate (see above). The Motagua fault zone exposes a complex amalgamation relict ocean floor, metamorphic complexes, and volcanics, in roughly west-east trending belts, separated by faults and shear zones (Ratschbacher et al., 2009; Fig. 6). The four main features in the fault zone are, from north to south, the Polochic fault, the Baja Verapaz shear zone (a 5-10 km wide greenschist facies mylonite zone), the Motagua fault and the Jocotán fault (Ortega-Obregon et al., 2008; Ratschbacher et al., 2009).

The basement of the Yucatan block is exposed in the Santa Rosa Group north of the Polochic fault and in the Rabinal complex between the Polochic fault and the Baja Verapaz shear zone. The Santa Rosa Group contains Paleozoic sediments and locally some felsic intrusions. The Rabinal complex contains Lower Paleozoic, low-grade volcaniclastic rocks and granitoids (Ratschbacher et al., 2009; Solari et al., 2013). Metamorphism of the Rabinal Granite is dated at 70.1 ± 0.6 Ma (40Ar-39Ar white mica age, Solari et al., 2013). There is no obvious difference in Paleozoic lithostratigraphy and magmatism between the
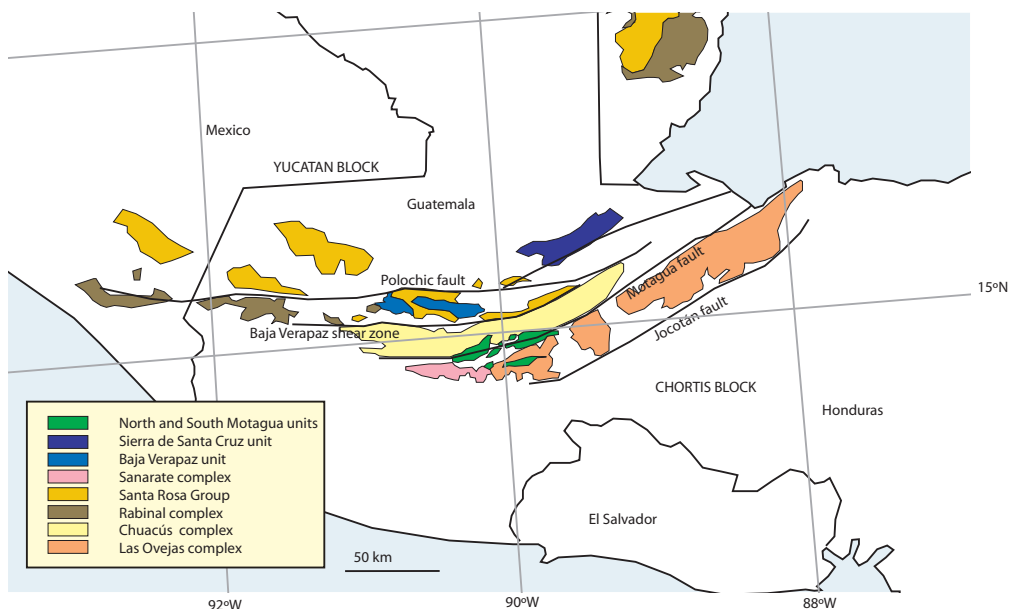
Figure 6: Basement geology of the Motagua fault zone. Based on Ratschbacher et al. (2009).

Santa Rosa Group and the Rabinal complex (Ortega-Gutiérrez et al., 2007; Ratschbacher et al., 2009).

South of the Motagua fault, two metamorphic complexes are defined that are interpreted as the basement of the Chortis Block: the Sanarate complex in the west and the Las Ovejas complex in the east (Ratschbacher et al., 2009). The Sanarate complex contains Jurassic metapelites and the Las Ovejas complex is characterized by Precambrian-Paleozoic volcaniclastic rocks that have undergone Cenozoic amphibolite facies metamorphism (Ratschbacher et al., 2009).

Between the Baja Verapaz shear zone and the Motagua fault to the south, the Chuacús complex is exposed, containing Paleozoic-Triassic, high-grade metamorphic volcano-sedimentary rocks and granitoids. The Chuacús complex has been interpreted as a part of the Yucatan block (Dengo, 1969; Donnelly et al., 1990; Ratschbacher et al., 2009), or as the separate Jacalteco terrane accreted to the Yucatan block by shearing along the Baja Verapaz shear zone (Ortega-Gutiérrez et al., 2007; Ortega-Obregon et al., 2008; Solari et al., 2011). (Ultra-)high pressure metamorphism in the Chuacús complex has been dated at ~76-62 Ma (U-Pb, Rb-Sr and Ar-Ar cooling ages of white mica and amphibole; Ratschbacher et al., (2009); and references therein; Martens et al. (2012)). The Baja Verapaz shear zone is a 5-10 km wide, south dipping shear zone, thrusting (with a minor sinistral strike-slip component) the Chuacús complex onto pre-Silurian low-grade metasedimentary rocks of the Yucatan block (Ratschbacher et al., 2009). Shearing in the Baja Verapaz shear zone

is simultaneous with metamorphism in the Chuacús complex, dated by 74-66 Ma white micas from sheared shales (K–Ar dating, Ortega-Obregón et al., 2008) and ~70 Ma white micas in mylonite gneiss (Ratschbacher et al., 2009).

The metamorphism in the Rabinal Granite and the Chuacús complex, and shearing in the Baja Verapaz shear zone is interpreted to result from Campanian-Maastrichtian oblique collision of the Great Arc of the Caribbean thrusting over the southern margin of the Yucatan block. During collision, continental material of the Yucatan promontory entered the subduction zone and was subjected to HP metamorphism (Martens et al., 2012; Pindell & Kennan, 2009; Ratschbacher et al., 2009; Solari et al., 2013).

Overlying the Yucatan block are two northward-emplaced harzburgite-dominated ophiolitic nappes of the El Tambor complex: the Sierra de Santa Cruz unit in the east, north of the Polochic fault and the Baja Verapaz unit south of the Polochic fault (Giunta et al., 2002a; Solari et al., 2013). These units comprise serpentinized harzburgites, layered gabbros, dolerites and scarce basalts with island-arc affinity (Giunta et al., 2002a; Ratschbacher et al., 2009). The Baja Verapaz unit overlies the Chuacús complex and the Sierra de Santa Cruz unit overlies Maastrichtian-Danian turbidite fan successions of the Sepur Formation (Beccaluva, 1995; Giunta et al., 2002a; Wilson, 1974). This formation is interpreted to have formed in a foreland basin and is the youngest unit involved in deformation produced by thrusting of nappes. The arrest of convergence between the ophiolite units and the Yucatan peninsula is therefore constrained by the age of the Maastrichtian-Danian Sepur Formation (Martens et al., 2012; Solari et al., 2013). Also part of the El Tambor complex are the North and South Motagua units, north and south of the Motagua fault. The North and South Motagua units contain HP-LT serpentinite-matrix mélanges (Harlow et al., 2004) and ophiolitic sheets of MORB-type geochemical affinity (Beccaluva, 1995; Giunta et al., 2002a). The North Motagua unit overlies the Chuacús complex of the Yucatan block and the South Motagua unit overlies the Chortis Block. These units are unconformably overlain by Eocene continental molasses of the Subinal Formation (Giunta et al., 2002a). Ar-Ar cooling ages from blueschist blocks within the serpentinites are 77-65 Ma for the northern, and 124-113 Ma (Harlow et al., 2004) to 144-132 Ma (Brueckner et al., 2009) for the southern mélange. U-Pb zircon dating of jadeitites, phengite jadeitites and mica-albite rocks provided ages of ~98-80 Ma and ~154-158 Ma for the North and South Motagua unit mélanges, respectively. These ages are interpreted to represent the age of crystallization of the rocks during active subduction (Flores et al., 2013). The mélange units are either interpreted to have formed in two subduction-collision events (one in the Late Jurassic-Early Cretaceous and the other in the Late Cretaceous), followed by juxtaposition through eastward movement of the Chortis Block along the Motagua fault zone (e.g. Harlow et al., 2004), an interpretation we will follow in our restoration. Alternatively, these data have been interpreted to reflect a long-lasting single subduction event (e.g. Brueckner et al., 2009). According to the latter authors, exhumation of the southern mélange in the Early Cretaceous caused them to be unaffected by later

events, whereas the northern mélange was reworked, or accreted below the southern, in a Late Cretaceous subduction event.

The youngest part of the history of the Motagua fault zone is the formation of a sinistral brittle strike-slip duplex with several restraining and releasing bends, displacing the Chortis Block relative to the Yucatan block (Giunta et al., 2002a). Burkart (1994) proposed that the Jocotán fault was active from 20 Ma to 10 Ma, the Polochic fault from 10 Ma to 3 Ma, and the Motagua fault from 3 Ma to present, the latter being the present-day plate boundary. Despite attempts to quantify the displacement along the faults (e.g. Burkart, 1983; Donnelly et al., 1990), there is no estimate of cumulative offset by direct correlation across the fault segments. We will therefore use the correlation of the western continental margin of Chortis to the western continental margin of Mexico as proposed by Rogers et al. (2007). The present displacement rate along the Motagua fault zone is ~21 mm/year (DeMets et al., 2007).

In summary, the plate boundary zone between the Yucatan and Chortis Block records events starting with HP metamorphism between 158 and 124 Ma in the South Motagua unit as a result of subduction of oceanic crust connected to the Chortis Block below southwestern Mexico. HP metamorphism in the North Motagua unit indicates subduction of oceanic crust with an opposite polarity underneath the Great Arc since the early Late Cretaceous until ~70 Ma, when an ophiolite and overlying arc (represented by the North Nicaraguan Rise and Jamaica (see below)) collided with southern Yucatan. This oblique collision resulted in a phase of sinistral shearing in the Baja Verapaz shear zone and burial and HP-LT metamorphism of the Yucatan passive margin (i.e. the Chuacús complex). Left-lateral strike-slip faulting in the Cenozoic moved the Chortis Block to the east and positioned the North and South Motagua units adjacent to each other. The short-lived character of the arc systems in the Motagua fault zone indicates that they are not part of the Great Arc of the Caribbean, which is located further south (Siuna block).

4.4. Cayman Trough

The Cayman Trough is an oceanic pull-apart basin that formed along the eastward extension of the Motagua fault zone. It is a rectangular depression on the transform plate boundary between the Caribbean Plate and the Cuban segment, currently part of the North American Plate, extending from the Belize margin to Jamaica. The trough is underlain by oceanic crust accreted along an ~110 km long N-S trending spreading center (CAYTROUGH, 1979). The northern and southern boundaries of the trough are the Oriente and Swan Island faults, respectively. Holcombe et al. (1973) were the first to provide evidence for seafloor spreading in the Cayman Trough and MacDonald and Holcombe (1978) identified magnetic anomalies. Although identification of the anomalies was problematic and based on models, Leroy et al. (2000) re-interpreted the anomalies to reflect A1 (0.8 Ma), A3a (6.3 Ma), A5 (11.0 Ma), A6 (19.7 Ma), A8 (26.2 Ma), A13 (33.7 Ma), A20 (42.8 Ma) and A22 (49.4 Ma) and suggested an age of 49.4 Ma for onset

of opening of the trough. Early (?) Paleocene-Early Eocene rifting preceded formation of oceanic crust (Mann & Burke, 1990).We follow the interpretations of Leroy et al. (2000) and assume constant, symmetric spreading between the anomalies. The Cayman Trough is frequently assumed to reflect Caribbean-North American plate motion, but a note of caution is relevant here: in the first few Myr of opening of the Cayman Trough, the Cuban segment still moved with respect to the North American Plate (until collision with the Bahamas platform, ~45 Ma, see below). Furthermore, the eastern half of the Cayman Trough is part of the Gonave block, which slightly moves relative to the Caribbean Plate along the Walton-Enriquillo-Plantain Garden fault system (see Section 4.7). It is thus more accurate to state that the Cayman Trough records Cuban segment-Gonave block motion.

4.5. Cuban segment

The Cuban segment consists of the Yucatan basin and the island of Cuba, which exposes a lower North America/Proto-Caribbean-derived fold-thrust belt overlain by a Caribbean Plate-derived ophiolite and volcanic arc sequence. The Yucatan basin is an oceanic basin bounded by the Cayman Trough to the south, the Yucatan peninsula to the west and Cuba to the north (Rosencrantz, 1990). It can be divided into two segments; a western deep basin and the eastern two-thirds including the topographically heterogeneous domains of the Cayman rise. The western basin is a NNE-SSW striking rectangular deep underlain by oceanic crust that formed during the Paleocene to Middle Eocene and is interpreted as a large, currently inactive pull-apart basin that formed as a result of left-lateral transform motion of the Cuban segment along the Belize margin (Rosencrantz, 1990). The Cayman rise contains volcanic arc material, probably resting upon oceanic crust of pre-Cenozoic age (Rosencrantz, 1990). Cuba is a fold-thrust belt, composed of rock sections of pre-Jurassic to Eocene age that developed as a result of convergence between the North American and Caribbean plates in Mesozoic and Cenozoic times (Iturralde-Vinent, 1988, 1994, 1996; Iturralde-Vinent et al., 2008).

To the west, the Cuban fold-thrust belt rests upon Neoproterozoic basement of the Yucatan borderlands overlain by Paleogene clastic successions, and to the north and east on the Bahamas carbonate platform (Fig. 4), which is underlain by ~200 Ma Central Atlantic Magmatic Province (CAMP)-related volcanic rocks (Iturralde-Vinent, 1994, 1998, 2006; Renne et al., 1989; Somin & Millán, 1981). Thrust slices tectonically imbricating the North American borderlands and the Proto-Caribbean basin underlie, or are incorporated in, Cretaceous-Paleocene serpentinite-matrix subduction mélanges (García-Casco et al., 2002, 2006; Iturralde-Vinent, 1994, 1998; Iturralde-Vinent et al., 2008; Kerr et al., 1999; van Hinsbergen et al., 2009). These thrust slices comprise four tectonostratigraphic units, from north to south including the Cayo Coco, Remedios, Camajuaní and Placetas units (Ducloz & Vuagnat, 1962; Hatten et al., 1988; Khudoley, 1967; Meyerhoff & Hatten, 1968, 1974). The Cayo Coco and Remedios units consist of evaporates and carbonate rocks. The Camajuaní and Placetas units contain calcareous and siliceous rocks that are interpreted as deposits from the basin between the Bahamas carbonate platform and

Caribeana (Díaz et al., 1997; Ducloz & Vuagnat, 1962; Meyerhoff & Hatten, 1968, 1974; Pszczkowski & Myczyski, 2003). Collision of the Caribbean Plate with the Bahamas and Yucatan borderlands started in the latest Paleocene to ~45 Ma (Bralower & Iturralde-Vinent, 1997; Gordon et al., 1997; Knipper & Cabrera, 1974; Meyerhoff & Hatten, 1968; Pardo, 1975), as shown by biostratigraphy of foreland basin deposits and was finalized by the early Late Eocene as shown by shallow marine deposits unconformably overlying the thrusted sequences (~40-35 Ma; Iturralde-Vinent et al., 2008). Folding in the Bahamas foreland continued until the Miocene (Masaferro et al., 2002). Overthrusting the thrust slices mentioned above is an ophiolite-arc terrane, outcropping south of the continental margin units (Draper & Barros, 1994; Hatten et al., 1958; Iturralde-Vinent, 1997; Pardo, 1975); Fig. 4). It contains, from north to south, an ophiolite belt, a volcanic–sedimentary complex, a plutonic complex, and the up to amphibolite-facies metamorphic Mabujina complex. The age of formation of the oceanic lithosphere of the ophiolites, containing harzburgites and other elements of the PENROSE ophiolite suite, is constrained to Late Jurassic by Tithonian (145-152 Ma) radiolarites (Fonseca et al., 1985; Iturralde-Vinent, 1994, 1996; Iturralde-Vinent & Marí-Morales, 1988; Lewis et al., 2006; Llanes et al., 1998). Ages of the igneous rocks range from 160 to 50 Ma of which only the Late Jurassic to Early Cretaceous dates are considered to represent formation of oceanic lithosphere (see review by Iturralde-Vinent et al. (1996)). The ophiolitic complexes are geochemically fingerprinted to supra-subduction environments (García-Casco et al., 2006). Island Arc Tholeiite (IAT) to MORB signatures are found in the basaltic rocks from the Cajálbana ophiolite (western Cuba), metamorphosed in an Early Cretaceous (130 Ma) volcanic arc environment (García-Casco et al., 2001). Boninitic rocks of unknown age (Fonseca et al., 1989; Kerr et al., 1999) and calc-alkaline signatures are found in the northern ophiolite belt towards the paleo-forearc (Andó et al., 1996; García-Casco et al., 2001).

The northern part of the ophiolite is separated from the underlying thin-skinned fold-thrust belt by a 1.5 km thick serpentinite-matrix mélange with HP metamorphic (eclogite, amphibolite, greenschist), plutonic, ultramafic, as well as non-metamorphic sedimentary rocks (Bush & Shcherbakova, 1986; García-Casco et al., 2006; MacGillavry, 1937; Millán, 1996; Somin & Millán, 1981; van Hinsbergen et al., 2009). K-Ar and U-Pb zircon ages from samples in HP-LT rocks range from ~130 to 60 Ma, suggesting that subduction started not later than in the Early Cretaceous (García-Casco et al., 2006; Iturralde-Vinent et al., 1996; Lázaro et al., 2009; Rojas-Agramonte et al., 2010; Somin & Millán, 1981; Somin et al., 1992). Aptian amphibolite blocks from eastern Cuba record anomalously high geothermal conditions (~700 °C and 14 to 15 kbar) and counterclockwise PTt-paths, suggesting that these blocks originated from very young subducted oceanic lithosphere (Blanco-Quintero et al., 2010; García-Casco et al., 2008b). Therefore, García-Casco et al. (2008b) and Blanco-Quintero et al. (2010) suggested the presence of a trench-trench-ridge triple junction, situated north of Eastern Cuba around 120 Ma. On top of the northern ophiolite is a >3 km thick volcanic-sedimentary and plutonic complex that is interpreted to belong to the Great Arc of the Caribbean (Burke, 1988; Cruz-Orosa et al., 2012b).

U-Pb ages date arc magmatism to have lasted from at least 133 to 80 Ma (see review by Rojas-Agramonte et al. (2011); Stanek et al., 2009). Arc magmatism terminated in the late Campanian in west-central Cuba, but continued in east Cuba into the Paleogene (García-Casco et al., 2001, 2008a, 2008b). The volcanic arc of Cuba is located only ~20 km to the south of the suture zone and the Late Cretaceous fore-arc, typically 166 ± 60 km wide (Gill, 2012), is largely missing. Van Hinsbergen et al. (2009) concluded that this is the consequence of subduction erosion of the fore-arc after the Late Cretaceous to Paleocene arrest of the arc exposed on Cuba, and before the final collision of the ophiolite with the Bahamas platform in the Middle Eocene. This tectonic erosion of the Cretaceous fore-arc may explain the absence of post-Campanian arc-related rocks on Cuba, as this arc may have shifted southwards into the Yucatan Basin during subduction erosion. In eastern Cuba (Fig. 4), Cretaceous volcanic arc rocks assigned to the Great Arc (the Purial metavolcanics) have been metamorphosed at blueschist facies (Boiteau et al., 1972; Somin & Millán, 1981) and are overlain by the Upper Cretaceous (Santonian) Mayarí-Baracoa ophiolite, which is associated with an underlying metamorphic sole (Güira de Jauco Amphibolite Complex; Lázaro et al., 2013). The sole formed sometime in de Late Cretaceous dated by K-Ar ages of 72 ± 3 and 58 ± 4 Ma (Somin & Millán, 1981). Peak pressures recorded in the sole are 8.5-8.7 kbar (ca. 30 km depth; Lázaro et al., 2013). Nonmetamorphic arc rocks from this area contain geochemical evidence for two distinct slab components (Marchesi et al., 2007). Lázaro et al. (2013) interpreted this sequence as evidence that subduction in eastern Cuba jumped, probably locally, from below the Great Arc into the overriding plate, towards a Campanian back-arc spreading ridge, to allow for the formation of the metamorphic sole below the Mayarí-Baracoa ophiolite and subduction-related metamorphism of the Purial complex. Subduction initiation here occurred in the late Campanian (modeled as 75 Ma) and buried the original arc below back-arc ocean floor. In several places on Cuba, underlying the ophiolites and volcanic arc complexes are metasedimentary and meta-volcanic rocks probably derived from continental crust, exposed in the Cangre, Isla de Iuventud, Sierra de Escambray and Asunción complexes (García-Casco et al., 2001, 2006, 2008a). The Escambray complex in central Cuba contains three thrust slices of metacarbonates and quartz-mica schists with tectonic slivers of metagabbro, greenschist and serpentinite (Millán & Somin, 1985; Somin & Millán, 1981; Stanek et al., 2006). The upper thrust slice is eclogite-facies metamorphic, the middle reaches blueschist metamorphism and the lower thrust slice is lowest-grade at greenschist metamorphic. This downward decrease in metamorphic grade is interpreted as the result of stacking of HP metamorphic thrust slices in a subduction channel during an episode of continental subduction (García-Casco et al., 2008a; Millán, 1997; Stanek et al., 2006). The metamorphic peak occurred during the latest Campanian (García-Casco et al., 2006, 2008a; Schneider et al., 2004; Stanek et al., 2006). After 70 Ma, exhumation started and HP metamorphic rocks reached the surface at about 45 Ma (Kantchev, 1978). The Escambray complex is imbricated north and south by the HT arc-related Mabujina-complex (Cruz-Orosa et al., 2012b) and its final exhumation is thought to have occurred in a metamorphic core-complex (García-Casco et al., 2008a; Pindell et al., 2005). These HP

metamorphic, continent-derived metasediments are interpreted to belong to Caribeana, which underthrusted the ophiolites ~75-70 Ma ago - simultaneously with the Chuacús complex in Guatemala, see Section 4.3, well before the final suturing of the ophiolite with North America in the Eocene (García-Casco et al., 2008a).

Finally, Cuba and the Yucatan Basin are cut by large-scale strike-slip faults, the two largest being the La Trocha and Cauto faults (Fig. 4). Being poorly exposed, the amount and nature of displacement on these faults remain poorly constrained. Rosencrantz (1990) suggested that the La Trocha fault acted as a sinistral strike-slip fault with an offset of less than 50 km. Uppermost Cretaceous sediments are cut by the La Trocha fault and syntectonic sedimentation (>1200 m of growth strata), indicating a component of normal fault motion, occurring between the Paleocene and Eocene (Cruz-Orosa et al., 2012a). A model has been proposed (Mann, 1997; Mann & Burke, 1990; Mann et al., 1995; Pindell & Barrett, 1990; Pindell et al., 2005), showing a gradual change in motion of the Caribbean Plate, with Cuba at its leading edge, with respect to the North American Plate during collision with the Bahamas borderlands: the Caribbean Plate escaped towards a free face in the Atlantic ocean. During this process, the Caribbean-North American relative plate motion changed from NNE to E, and the plate boundary jumped stepwise from the Belize margin (west-Yucatan deep) and the subduction zone north of Cuba, to the Cauto fault and subsequently the La Trocha fault, to eventually the Oriente fault north of the Cayman Trough, leaving the Cuban segment welded to the American Plate. These regional changes are recorded in the nature and structure of the La Trocha fault. The La Trocha fault evolved from a left-lateral strike-slip fault during shortening in the Cuban orogen to a post-welding normal fault (Cruz-Orosa et al., 2012a).

Paleomagnetic data from a small section of Cretaceous volcanic and sedimentary rocks in central Cuba show a counterclockwise rotation with respect to the North American Plate of 43 ± 16° since the mid-Cretaceous (Renne et al., 1991) to ~70-80° between 120 and 90-45 Ma (Tait et al., 2009). These latter authors suggested a local, strike-slip related origin for these rotations.

In summary, the Cuban segment plays a crucial role in the geological history of the Caribbean region. The Cuban orogen records tectonic events starting with the onset of formation of oceanic crust in the Proto-Caribbean Ocean since ~160 Ma, followed by the establishment of a subduction zone below the oceanic Caribbean lithosphere at or before ~130 Ma. Subduction of the Proto-Caribbean oceanic crust led to the formation of the Great Arc of the Caribbean in the Early Cretaceous. In the Campanian, the Caribeana promontory reached the subduction zone. This first led to a short-lived jump of subduction to a previously opened back-arc basin and led to burial and blueschist metamorphism of Great Arc rocks below the Mayarí-Baracoa ophiolite in eastern Cuba. Ongoing Caribbean-North America convergence subsequently resulted in HP metamorphism in Caribeana-derived units with an ~70 Ma peak. Ongoing SSW-ward

subduction led to a subduction transform fault along the margin of Belize, in which a releasing bend formed the western Yucatan pull-apart basin. This basin opened until the collision of the Cuban ophiolite with North America and the Bahamas platform ~45 Ma ago. Following Caribeana subduction and accretion, and prior to Eocene collision, the Placetas and Camajuani complexes were accreted from subducting Proto-Caribbean lithosphere or extended North American continental crust, followed by underthrusting of the Cayo Coco and Remedios complexes. After arrest of the Cuban arc in the late Cretaceous and before Eocene collision, the bulk (~100-200 km) of the Cretaceous fore-arc was removed from the Cuban ophiolite by subduction erosion. Collision was associated with a change in relative motion of Caribbean Plate versus North America from NNE to E, stepwise accommodated along the increasingly more easterly trending Cauto and La Trocha faults, transferring the plate boundary towards the Cayman Trough, leaving the Cuban segment welded to the North American Plate.

4.6. Jamaica
The island of Jamaica is located between the Yucatan Basin in the north and the Caribbean Sea in the south (Figs. 1, 3). Jamaica's basement consists of Lower Cretaceous to Paleocene volcanic and plutonic arc-related rocks with a similar composition as those found on the North Nicaraguan rise, and metamorphic rocks (Abbott et al., 1999; Hastie & Kerr, 2010; Lewis et al., 2011; Mitchell, 2006). The metamorphic rocks are mainly schists (Westphalia Schist and Mt. Hibernia Schist) and serpentinites (Abbott et al., 1996, 1999, 2003). Trace element geochemistry of the Westphalia Schist is consistent with an island arc setting (West et al., 2014). The blueschist facies Mt. Hibernia Schist (cropping out east of the Blue Mountain Fault, on the eastern side of the island) has CLIP-related geochemistry and has been exhumed in Maastrichtian times, suggesting Late Cretaceous (~75 Ma) subduction of CLIP material. The HP rocks are overlain by upper Maastrichtian sediments (McFarlane, 1977; Mitchell, 2006; Robinson, 1994; West et al., 2014). Jamaica formed as a restraining bend between the Wagwater and Blue Mountain transpressional faults. These NW-striking faults are interpreted as transpressional stepovers in the left-lateral strike-slip system of the Walton fault, an eastward propagation of the Swan Island fault to the east of the Cayman spreading center, and the Plantain Garden fault of Hispaniola. Uplift of the island started in the Late Miocene (Mann et al., 2007). Jamaica can thus be regarded as an exposed portion of the North Nicaraguan rise. Tectonic reconstructions (e.g. Ross and Scotese, 1988; Pindell and Kennan, 2009) locate the island of Jamaica adjacent to the 1southern margin of Yucatan between ~70 and ~50 Ma after restoring the opening of the Cayman Trough, matching the blueschists on Jamaica with the blueschists of the Rabinal and the Chuacús Complexes and forming a link between the Great Arc rocks of Siuna and Cuba. Prior to ~70 Ma, the island was part of the active Great Arc.

4.7. Hispaniola
The island of Hispaniola is divided into the countries Haiti in the west and the Dominican Republic in the east. It is located on the transform plate boundary between the North

American and Caribbean plates. Hispaniola can be divided into two tectonic domains, separated by the Enriquillo-Plantain Garden fault: the northern two-thirds and the southern one-third. The northern two-thirds of the island contain metasedimentary rocks, interpreted as accreted continental material from the Bahamas carbonate platform overlain by an ophiolitic complex and associated arc intrusives and overlying Lower Cretaceous to Middle Eocene volcanic arc rocks. Between the accreted Bahamas platform rocks and the ophiolite is a serpentinite-matrix mélange with HP rocks (blueschists and eclogites) (Escuder-Viruete et al., 2006, 2013; Krebs et al., 2008, 2011). The ophiolitic rocks (dated at 136.4 ± 0.32 Ma, U-Pb age of Escuder-Viruete et al. (2011a) and serpentinite-matrix mélanges can be found on the northernmost part of the island, north of the Septentrional fault in e.g. the Río San Juan and Puerto Plata complexes (Draper & Lewis, 1991; Draper & Nagle, 1991; Escuder-Viruete et al., 2013). These complexes are ~50 km apart and are essentially the same but displaced by a strike-slip fault (Krebs et al., 2008). Blocks in the mélange recorded peak metamorphism at different times, ranging from 103.6 ± 2.7 Ma dated from an eclogite, 80.3 ± 1.1 Ma from an omphacite blueschist and 62.1 ± 1.4 Ma for a jadeite blueschist (Lu-Hf and Rb-Sr ages; Krebs et al., 2008). Krebs et al. (2008) interpreted the subduction zone forming these HP blocks as active between ~130 and ~55 Ma. The mélange contains blocks originating from both the upper (Caribbean) and downgoing (Proto-Caribbean Ocean) plate. This suggests that subduction erosion took place at the base of the Caribbean Plate in the Late Cretaceous (Escuder-Viruete et al., 2011a). On the Samaná Peninsula, east of the Río de San Juan complex, the HP metamorphic Samaná terrane is exposed (Escuder-Viruete et al., 2011b, 2011c). This is a more coherent unit interpreted as part of Caribeana (García-Casco et al., 2008a).

In the Cordillera Central, south of the Septentrional fault, and overlying the mélange, ophiolitic and Cretaceous-Eocene metamorphic, plutonic and island-arc volcanic rocks (Tireo formation), as well as covering non-metamorphic rocks are found (Escuder-Viruete et al., 2006, 2013; Kesler et al., 1991). Escuder-Viruete et al. (2006) showed that subduction below the oceanic lithosphere from which the ophiolites were derived started shortly before 116 Ma, indicated by a volcanic complex with three units: boninites and LREE depleted IAT volcanics at the bottom, an intermediate unit dated 116 Ma, and normal IAT volcanics at the top. The non-metamorphic rocks are interpreted to have deposited in a fore-arc basin (Escuder-Viruete et al., 2013). Upper Campanian-Maastrichtian non-volcanic sediments are locally overlying the Tireo formation, and volcanics from this period are missing (García-Casco et al., 2008a; Lewis et al., 1991). This hiatus was interpreted by García-Casco et al. (2008a) to reflect a period of inactivity of the Great Arc during underthrusting of Caribeana (Samaná terrane), but it may also be the result of younger strike-slip motions, transporting bodies of arc material eastwards, leading to gaps and duplications (K. Burke, 2013, personal communication).

Volcanic arc rocks and associated sediments are regionally angularly unconformably covered by Upper Eocene to Recent sediments that post-date island arc magmatism

(Dolan et al., 1998; Krebs et al., 2008; Mann et al., 1991). Collision of the volcanic complex of Hispaniola with the Bahamas borderlands is dated at Middle-Late Eocene (Cribb et al., 1989; de Zoeten & Mann, 1991; Vila et al., 1987) and is documented by this angular unconformity separating folded Upper Paleocene-Lower Eocene sediments from an Upper Eocene basal conglomerate (de Zoeten and Mann, 1991). The southern one-third of the island, on the other hand, exposes flood basalts, interpreted as CLIP material (Mann et al., 1991; Maurrasse et al., 1979; Sen et al., 1988).

Eocene-Recent North American-Caribbean transpressional plate motion is accommodated by plate boundary-perpendicular motion in the offshore North Hispaniola Deformed Belt, north of the island and strike-slip motion, localized along seismically active faults: the Septentrional fault in the north (i.e. an eastward extension of the Oriente fault), and the Enriquillo-Plantain Garden and Los Pozos faults in the south (Hayes et al., 2010; Mann et al., 1984, 1991; Pindell & Barrett, 1990; Prentice et al., 2010). The western part of Hispaniola is part of the Gonave block, bounded by the Cayman spreading center in the west, the Oriente-Septentrional fault system in the north, the Walton-Enriquillo-Plantain Garden fault system in the south and NS-oriented thrust faults in Hispaniola in the east (Fig. 3). The western part of Hispaniola is moving faster to the east with respect to North America than the eastern part of Hispaniola and is uplifting as a result of this differential motion (DeMets & Wiggins-Grandison, 2007; Mann et al., 1995).

In summary, Hispaniola contains a segment of the Great Arc of the Caribbean, active from before 116 Ma until collision with the North American continental margin in the Middle-Late Eocene (with a hiatus in the upper Campanian-Maastrichtian). The interruption in volcanic activity is attributed to the collision of Hispaniola with the Samaná terrane of Caribeana, simultaneously, or slightly later than the underthrusting of the Escambray terrane in Cuba. Eocene-recent strike-slip faulting moved Hispaniola eastward with respect to the Cuban segment, whereby left-lateral strike-slip was partitioned over two fault systems: the Oriente-Septentrional fault system in the north and the Walton-Enriquillo-Plantain Garden fault system in the south. The latter fault system juxtaposed oceanic Caribbean crust overlain by CLIP lavas against Great Arc of the Caribbean-equivalent rocks of central Hispaniola.

4.8. Puerto Rico

Puerto Rico lies east of Hispaniola and exposes Cretaceous-Eocene island arc rocks associated with southwest dipping subduction, underlain by a serpentinite-matrix mélange (Bermeja complex), containing blocks of serpentinized peridotite, altered basalt, amphibolite and chert (Larue, 1991; Schellekens, 1991, and references therein; Jolly et al., 2008; Laó-Dávila et al., 2012). K-Ar whole rock ages of the amphibolite blocks range between ~130 and 75 Ma (Bandini et al., 2011a, and references therein). Radiolarian chert date the 'Mariquita Chert Formation' of the Bermeja complex at lower Middle Jurassic to lower Upper Cretaceous (upper Bajocian-lower Callovian to upper lower Albian-lower

Middle Cenomanian; Bandini et al., 2011), reflecting the minimum age of the oceanic crust that subducted below the arc of Puerto Rico. The serpentinites have been emplaced by thrusting in two events: in Maastrichtian-Paleocene and Late Eocene-Early Oligocene times (Laó-Dávila et al., 2012).

The record of arc magmatism contains an Upper Cretaceous-Danian hiatus (~75–65 Ma) (García-Casco et al., 2008a; Jolly et al., 1998), roughly equivalent to the hiatus on Hispaniola. García-Casco et al. (2008a) suspected that this may also be an expression of the collision of the Caribbean Plate with Caribeana, although HP-LT metamorphic rocks that underwent late Cretaceous metamorphism have only been found offshore Puerto Rico (Puerto Rico Trench terrane; García-Casco et al. 2008a), and not on the island itself. Final arrest of arc magmatism was in the Eocene (Jolly et al., 1998). The volcanic arc rocks are overlain by Eocene-Pliocene sediments, including sandstones, shales and limestones, deposited in both shallow and deep water (Larue, 1991). An angular unconformity between strongly folded, deep-marine middle Eocene rocks and gently folded middle-upper Oligocene shallow marine and nearshore rocks indicate a tectonic event in the Upper Eocene, simultaneously with cessation of the volcanic arc (Dolan et al., 1991; Mann et al., 2005). This unconformity is interpreted to date the collision of Puerto Rico with the Bahamas (Dolan et al., 1991). Paleomagnetic data from this Oligocene and younger series showed that the island underwent an ~25° counterclockwise rotation between upper Miocene (~11 Ma) and Pliocene (~4 Ma) times (Reid et al., 1991), interpreted by Mann et al. (2002) as the result of oblique collision with the Bahamas borderlands, and GPS data confirm the absence of active rotation (Jansma et al., 2000), which we adopt in our reconstruction.

The Puerto Rico trench, north of the island, lies along the eastward extension of the North Hispaniola Deformed Belt and curves southward towards the East, to connect with the Lesser Antilles trench. A south-dipping slab can be traced to a depth of 240 km underneath Puerto Rico (van Benthem et al., 2013). The area is a zone of transition between transform motion along the northern plate boundary and convergent motion along the eastern plate boundary of the Caribbean Plate, resulting in a curved slab that can be traced to below eastern Hispaniola (van Benthem et al., 2013). Focal mechanisms record almost pure strike-slip motion, indicating very strong obliquity of subduction (Dillon et al., 1996; Dolan et al., 1998; McCann & Sykes, 1984; Molnar & Sykes, 1969). This highly oblique convergence may explain the absence of active arc magmatism above the Puerto Rico slab; dehydration melting and magmatism already occurred earlier beneath the Lesser Antilles Arc, before the slab arrived underneath Puerto Rico farther to the west (Calais et al., 1992; van Benthem et al., 2013). Relative westward motion of the slab edge below Hispaniola results in surface deformation (Benthem et al., 2014).

South of the island of Puerto Rico, the Muertos Thrust Belt is located and a north-dipping seismic zone can be traced to 100 km depth (van Benthem et al., 2013), associated with

underthrusting of the Caribbean oceanic interior in the Muertos Trough (Byrne et al., 1985; Dillon et al., 1996; Dolan et al., 1998). The Muertos Thrust Belt is interpreted as a back thrust response to the oblique Bahamas collision and subduction in the Puerto Rico trench (Mann et al., 2002). In the footwall of the thrust belt, beneath the basal detachment, Lower Miocene and older sedimentary rocks are found. Younger sediments are incorporated into the thrust belt itself, which is active today (ten Brink et al., 2009). Thrusting is thought to have started in the Late Miocene (Mann et al., 2002). The relative plate velocity between Puerto Rico and the Caribbean Plate is very small (~1 mm/yr, GPS measurements, Jansma et al., 2000). Northwestern Puerto Rico is tectonically separated from the eastern part of Hispaniola by the N–S Mona rift, opening with ~5 mm/yr (Hippolyte et al., 2005; Jansma et al., 2000).

In summary, the island of Puerto Rico exposes rocks ascribed to the Great Arc of the Caribbean, which formed until Late Eocene collision of the Caribbean Plate with the Bahamas platform. Interruption of arc volcanism indicates that Puerto Rico may have collided with a part of Caribeana. Since collision with the North American Plate, highly oblique convergence between the North American and Caribbean plates has led to underthrusting of North American lithosphere in the Puerto Rico trench and Caribbean lithosphere in the Muertos Trough below Puerto Rico.

4.9. Eastern Caribbean subduction system: Lesser Antilles Arc

The eastern part of the Caribbean Plate consist of a series of N-S trending bathymetric zones including, from west to east, the Aves ridge, the Grenada Basin, the Lesser Antilles Arc, the Tobago Basin and the Barbados Accretionary Prism (Fig. 1, 3). The Lesser Antilles Arc is the active volcanic arc associated with westward subduction of Atlantic oceanic lithosphere below the Caribbean Plate. Tomographic images indicate at least 1100 km of subduction (van Benthem et al., 2013; van der Hilst, 1990). Ages of arc volcanism range from 38 Ma to present (K-Ar, Briden et al., 1979). The Barbados prism is an accretionary prism that formed along the Lesser Antilles subduction zone between the Early Eocene and the present (Speed & Larue, 1982). The prism is exposed on the island of Barbados. The southern half of the prism is extraordinarily large due to favorable conditions for accretionary buildup: sediment that constitute the southern half of the prism were supplied by the Orinoco River that runs through Colombia and Venezuela and flows out into the Atlantic Ocean close to Trinidad and Tobago. Since formation of the Orinoco river delta, a large amount of sediment is scraped off the downgoing Atlantic oceanic lithosphere and accreted to the Caribbean Plate (Speed and Larue, 1982).

The Aves ridge is a remnant island arc, interpreted to have been part of the Great Arc of the Caribbean (Bird et al., 1993; Burke, 1988). The ridge contains granodiorite, diabase, porphyritic basalt and metabasalt (Fox & Heezen, 1975; Neill et al., 2011) and has a similar seismic velocity structure and crustal thickness as the Lesser Antilles Arc (Christeson et al., 2008). The arc was active in at least the Late Cretaceous and Paleocene (Bouysse, 1988;

Fox & Heezen, 1975; Pinet et al., 1985) indicated by ages of dredged and drilled volcanic rocks ranging from 88 to 59 Ma (Neill et al., 2011). No CLIP material has been reported from the Aves ridge.

The Grenada basin is an oceanic basin of which the origin is debated. Different models for basin opening have been proposed, as outlined by Bird et al. (1993), Bird et al. (1999) and Aitken et al. (2011). These models vary in spreading direction (east-west (e.g. Bird et al., 1999; Tomblin, 1975), north-south (e.g. Pindell and Barrett, 1990) or northeast-southwest (e.g. Bouysse, 1988)), but all consider the Grenada Basin to be a back-arc basin. In the models of Bouysse (1988) and Pindell and Barrett (1990), the Grenada Basin formed as a result of right-lateral shear between the Great Arc and the South American continent. Aitken et al. (2011) proposed a different model of evolution of the Lesser Antilles subduction system based on seismic, well and onshore geological data. The basement of the Grenada and Tobago basins, on both sides of the active Lesser Antilles Arc, is considered to be the extended oceanic fore-arc of the Aves Ridge, widened (in E-W direction) in the Paleocene-Middle Eocene. Due to roll-back of the Proto-Caribbean downgoing slab, volcanism ceased in the Aves ridge and migrated to the Lesser Antilles Arc, dividing the former fore-arc into two basins, the Grenada and Tobago Basins. We adopt this hypothesis in our reconstruction.

4.10. Trinidad, Tobago, Isla Margarita and the Leeward Antilles

The Leeward Antilles (Aruba, Curaçao, Bonaire, Las Aves, Los Roques, La Orchilla, La Blanquilla, Los Hermanos and Los Testigos), Isla Margarita (West Indies) and Trinidad and Tobago are located in the Caribbean Sea off the coast of Venezuela, near the Caribbean-South American plate boundary (Fig. 1). The island of Trinidad exposes a continental basement, Cretaceous mafic volcanic rocks and Mesozoic and younger sediments and is cut by right-lateral strike-slip fault systems accommodating Caribbean-South American motion. The sediments bear evidence for Jurassic extension - probably related to the opening of the Atlantic Ocean - and Miocene compression and dextral wrenching, leading to low-grade metamorphism on the northern part of the island (Donovan, 1994; Frey et al., 1988; Neill et al., 2014; Pindell & Kennan, 2009; Saunders, 1974). The volcanics document the opening of the Proto-Caribbean Ocean at 135.0 ± 7.3 Ma (crystallization age of a mafic volcanic rock, Neill et al., 2014). Trinidad is considered to be part of the South American continent, with Neogene deformation being related to right-lateral dextral wrenching between South America and the Caribbean Plate (Pindell and Kennan, 2009).

The island of Tobago, on the other hand, contains three different types of oceanic island arc rocks, exposed in roughly north-south belts; the North Coast Schist, the Tobago Volcanic Group and the Tobago Pluton. The southern part of the island is covered by Pliocene to recent sediments (Neill et al., 2012; Snoke et al., 2001a). The Volcanic Group and Pluton are of Albian age (~110 to 103 Ma based on faunal and Ar-Ar hornblende dating; (Sharp &

Snoke, 1988; Snoke et al., 1990; Snoke & Noble, 2001) and were formed by partial melting of MORB-crust (Neill et al., 2013). The North Coast Schist contains meta-igneous and metasedimentary greenschist and amphibolite facies metamorphic rocks. Greenschist rocks of the Palatuvier Formation have a U-Pb age of 128.7 ± 0.2 Ma (Neill et al., 2012). Greenschist facies metamorphism is interpreted to be regional, and related to an episode between ~129 and 110 Ma of dextral shearing, whereas amphibolite facies metamorphism is interpreted to relate to contact metamorphism associated with intrusion of the Tobago pluton (Neill et al., 2012; Snoke et al., 2001b). Magmatism and metamorphism on Tobago is considered to be part of the Great Arc of the Caribbean (Burke, 1988).

Isla Margarita exposes Paleozoic-Mesozoic metamorphic rocks of both continental (metapelites, marbles, gneisses) and oceanic (metabasalts, carbonaceous schists) character (Maresch, 1975; Maresch et al., 2009). The island contains two eclogite facies metamorphic complexes, structurally overlain by greenschist facies rocks. The age of metamorphism is constrained by the age of the protolith of the youngest HP unit (the Guayacán gneiss, crystallization at ~116-106 Ma, U-Pb age) and the intrusion of the El Salado Metagranite (island arc affinity, ~86 Ma), which intrudes the HP units and has not been subjected to HP metamorphism itself. Peak metamorphism probably occurred between 100 and 90 Ma (Maresch et al., 2009). The HP rocks are interpreted to have formed in a subduction zone at a depth of 50 km. Juxtaposition of the greenschist units happened upon exhumation, after 80 Ma (Maresch et al., 2009). Maresch et al. (2009) interpreted the Isla Margarita HP rocks to be derived from the NW South American continental margin upon Cretaceous collision with the Caribbean Plate, after which they were translated to their current position by right-lateral wrenching between the Caribbean and South American plates.

Aruba, Curaçao, La Blanquilla and Gran Roque of the Los Roques contain magmatic rocks that are geochemically very similar to the island arc rocks from the southern Aves Ridge (Neill et al., 2011). Granodiorites and tonalites of La Blanquilla are dated at 75.5 ± 0.9 Ma and 58.7 ± 0.5 Ma respectively, the Aruba batholith at 88.6 ± 0.5 Ma (U-Pb ages of van der Lelij et al. (2010) and Wright and Wyld (2011)) and dikes of diorite on Curaçao at 86.2 ± 1.1 Ma (Wright & Wyld, 2011). Bonaire contains island arc rocks with ages of 94.6 ± 1.4 Ma, 98.2 ± 0.6 Ma and ~112 Ma (Thompson et al., 2004; Wright & Wyld, 2011). These rocks are interpreted to have formed above a depleted mantle (Wright & Wyld, 2011). No CLIP material has been found on La Blanquilla and Bonaire (Neill et al., 2011). On Aruba, Curaçao and Gran Roque however, gabbros and dolerites of CLIP affinity are present (Giunta et al., 2002b). CLIP material of the Curaçao Lava Formation has been dated by Sinton et al. (1998) at 88.6 ± 0.5 Ma (Ar-Ar), CLIP material of the mafic Aruba Lava Formation at ~90 Ma (White et al., 1999). The Leeward Antilles area has been subjected to shortening by inversion of normal faults and right-lateral strike-slip faulting related to collision with the South American continent and subsequent segmentation in extensional basins by a phase of oblique normal faulting (Escalona & Mann, 2011). Paleomagnetic data from arc volcanics suggest a clockwise rotation of Tobago, Aruba and Bonaire of 90°

since the Late Cretaceous with respect to a stable South America (Burmester et al., 1996; Stearns et al., 1982).

In summary, the Leeward Antilles and Tobago are interpreted as fragments of the Great Arc of the Caribbean on the former leading edge of the Caribbean Plate, which has been in oblique collision with the northern margin of South America for most of the Cenozoic (Escalona & Mann, 2011; Neill et al., 2012; Snoke et al., 2001b). The present day position of the Leeward Antilles (500-600 km west of the southern tip of the Aves Ridge) may be the result of Cenozoic dextral shearing of the Caribbean Plate along the South American margin, slowing down the motion of the Leeward Antilles. Tobago, on the other hand, is currently located ~350 km east of the southern tip of the Aves Ridge and became further separated upon opening of the Grenada and Tobago basins in the former fore-arc of the Aves ridge. Isla Margarita is interpreted as a fragment of the northwestern South American margin that was metamorphosed when the Great Arc of the Caribbean collided and the South American continental margin underthrusted ~100-90 Ma ago. This fragment was accreted to the Caribbean Plate, intruded by arc magmas and displaced eastwards along the South American margin towards its present position (Maresch et al., 2009).

4.11. Northern Andes

The Northern Andes (northwesternmost Peru, western Ecuador, western Colombia and the northwestern corner of Venezuela) is a complex tectonic region of intense deformation. It is bounded by the Colombian-Ecuador trench in the west, the Panama-Chocó block in the northwest, the South Caribbean Deformed Belt in the north and a major fault system in the east, including the East Andean fault zone and the Boconó fault (Egbue & Kellogg, 2010; Kellogg & Vega, 1995; Pennington, 1981)(Fig. 3). The Northern Andes and the Panama-Chocó block together accommodate the strain associated with the triple junction between the Nazca, South American and Caribbean plates (Cortés & Angelier, 2005).

The Northern Andes can be divided into two basement provinces: a continental eastern province and a western province composed of thrusted fragments of continental and oceanic crust, including island arc volcanics and associated sedimentary rocks and slivers of oceanic plateau basalts (Cortés & Angelier, 2005; Kennan & Pindell, 2009; Kerr et al., 2003)(Fig. 7). The eastern province contains Neoproterozoic gneisses and schists, and unmetamorphosed to low-grade metamorphic Paleozoic sediments (Restrepo-Pace, 1992; Restrepo-Pace et al., 1997) intruded by plutons ranging in age from ~241 to 80 Ma and overlain by a thinCretaceous sedimentary cover (González, 2001; Litherland et al., 1994; Montes et al., 2010; Noble et al., 1997; Villagómez et al., 2008, 2011). The continental basement is interpreted as the former southern passive margin of the Proto-Caribbean Ocean, conjugate to the southeastern Chortis margin. The plutons are interpreted as part of a broad volcanic arc, related to eastward dipping subduction below the South American continent.

The western province can be subdivided into three belts. The easternmost belt of the western province exposes high to intermediate pressure metamorphic rocks (blueschists, amphibolites and eclogites), Paleozoic and Mesozoic schists and amphibolites and Lower Cretaceous metatuffs, pillow basalts and volcaniclastic sediments (Kennan & Pindell, 2009). Geochemical data from the volcanics suggest a tholeiitic to andesitic island-arc or back-arc origin with some influence of underlying continental crust, and magmatism took place between ~180 and 145 Ma (Nivia et al., 2006; Villagómez et al., 2011). All volcanic rocks of this belt are classified by Kennan and Pindell (2009) as sheared and accreted fragments on the Trans-American Arc and its successor, the Great Arc of the Caribbean. K-Ar, Lu-Hf and Ar-Ar ages of the metamorphic rocks of 133-126, 120-110 and 68-61 Ma and whole rock K-Ar ages of mafic HP/LT rocks of 125 ± 15, 110 ± 10 and 120 ± 5 Ma reflect peak metamorphism and onset of cooling, and suggest an exhumation event starting in the Early Cretaceous (Bustamante et al., 2011; John et al., 2010; Maya-Sánchez, 2001; Maya-Sánchez & Vásquez-Arroyave, 2001; McCourt et al., 1984). The trace element signatures of the 133–126 Ma rocks provide evidence for subducted seamounts and MORB-crust (John et al., 2010). The 120-110 Ma rocks have a continental origin and
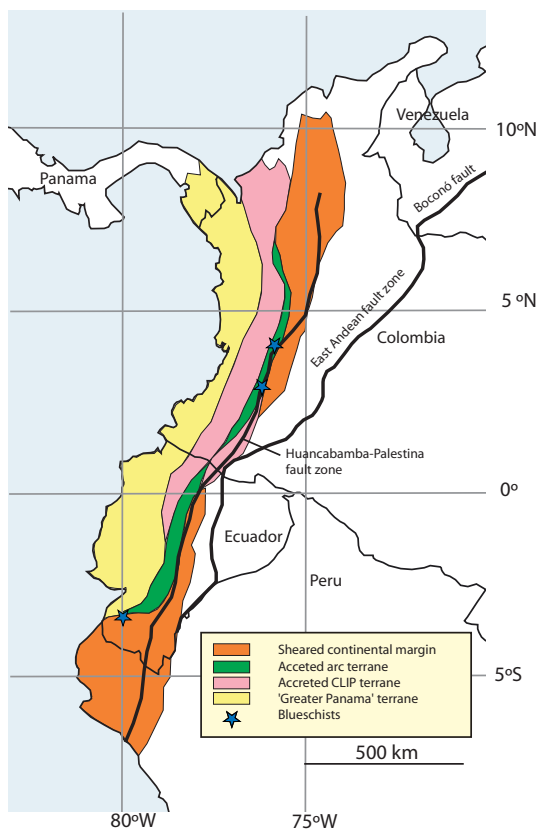

Figure 7: Tectonic terrane map of the Northern Andes. Based on Kennan and Pindell (2009).

are interpreted to result from subduction of the continental margin of South America during collision with, and underthrusting below the Great Arc (Kennan & Pindell, 2009), following subduction of oceanic South American Plate. The 67-61 Ma rocks have been interpreted by Bustamante et al. (2011) as part of a tectonic mélange, related to a younger accretion event.

The central belt comprises slivers of oceanic plateau basalts and associated ultramafic rocks and sediments. The plateau basalts are dated between ~100 and 87 Ma and geochemistry indicates an intra-oceanic plateau origin interpreted as related to the CLIP (Vallejo et al., 2006; Villagómez et al., 2011). The basalts are thrusted over, as well as imbricated against the western margin of the South American continent (Kerr et al., 1997). This suggests that the South American continent was originally in a downgoing plate position relative to the Caribbean Plate after the formation of the CLIP, followed by a subduction polarity reversal and underthrusting of the Caribbean Plate below South America, as seen today. In the northwestern part of the northern Andes, intrusive rocks of 54-59 Ma (U-Pb zircon ages, (Bayona et al., 2012) are found. This period of magmatism is thought to be related to oblique and shallow subduction of the edge of the CLIP, following arc-continent collision (Bayona et al., 2012; Cardona et al., 2011). The westernmost belt of the Northern Andes contains Santonian-Campanian boninites, tholeiites and calc-alkaline basalts of an intra-oceanic island arc origin, underlain by oceanic plateau basalts, and covered by Paleogene and younger fore-arc basin sediments (Borrero et al., 2012; Kennan & Pindell, 2009). Kennan and Pindell (2009) propose that these rocks were formed above a northeast dipping subduction zone at the trailing edge of the Caribbean Plate, as a result of subduction of the Farallon Plate. The Santonian-Campanian age of the boninites indicate an age shortly post-dating the onset of subduction (e.g. Stern et al., 2012). This westernmost terrane is interpreted as an extension of the Panama-Chocó block (or 'Greater Panama') that subducted beneath the South American continent until the collision of the present-day Panama-Chocó arc with Colombia in the Late Miocene-Pliocene (Coates et al., 2004; Duque-Caro, 1990; Kennan & Pindell, 2009). Kennan and Pindell (2009) suggested that the buoyant upper crustal parts of the lithosphere were scraped off the downgoing plate and accreted to the South American overriding plate, while their original lower crustal and mantle underpinnings subducted. The present-day Panama-Chocó block behaves as a rigid indenter and is thought to be the main reason for the Andean compressional phase in Colombia (Taboada et al., 2000; Trenkamp et al., 2002; Vargas & Mann, 2013). Ongoing Panama-Chocó-South America convergence is estimated by GPS measurements at 25 mm/yr (Trenkamp et al., 2002). Cenozoic subduction of the Caribbean Plate below the South American continent and the Panama-Chocó block led to the formation of the Panama Deformed Belt and the South Caribbean Deformed Belt (Kennan & Pindell, 2009; van Benthem et al., 2013). Subduction in the South Caribbean Deformed Belt initiated diachronously from west to east in Middle- Eocene to Late Neogene times. Before subduction initiation, in Late Cretaceous-Miocene times, the belt

acted as a back thrust associated with subduction of the South American Plate below the Great Arc (Kroehler et al., 2011).

Within the eastern province, the Huancabamba-Palestina fault zone is exposed, which can be traced more or less continuously from northern Peru to northern Colombia. This anastomosing fault zone records brittle, dextral strike-slip motion. The southern part of the fault zone has been active throughout the Late Cretaceous and Paleogene, the northern part is still active today (Kennan & Pindell, 2009). The amount of Cretaceous to Eocene offset of the fault zone has been estimated at ~300 km (Kennan & Pindell, 2009). The boundary between the eastern and central belt in the western province is the Romeral suture, which recorded significant dextral strike-slip fault movement since the Cretaceous (Kennan & Pindell, 2009; Kerr et al., 1998; Trenkamp et al., 2002). There is no cumulative estimate of dextral strike-slip displacement in the Northern Andes from the Cretaceous to present day. GPS data shows that the Maracaibo block of northern Colombia and northwestern Venezuela (the fault bounded crustal feature defined by the Maracaibo, Oca and Santa Marta fault zones, Mann and Burke, 1984) is currently moving to the northeast with respect to a stable South America with 6 mm/yr. This movement is interpreted as northeastward tectonic escape following the collision between the South American continent and the Panama-Chocó block (Freymueller et al., 1993; Kellogg & Vega, 1995; Mann & Burke, 1984a; Trenkamp et al., 2002). Note that the "Greater Maracaibo" block defined in Figure 3 also includes areas west of the Santa Marta fault and north of the Oca fault.

In summary, the geology and geometry of the Northern Andes is the result of a series of events starting with eastward subduction of the Farallon Plate below the west coast of South America in pre-late Jurassic time, when South America was still part of Pangea. During the break-up of Pangea, the Northern Andes became a passive margin bordering the South American continent from the Proto-Caribbean Ocean. Since the Early Cretaceous onset of subduction below the Caribbean Plate and the associated volcanism in the Great Arc of the Caribbean, the Caribbean Plate moved with an easterly direction relative to South America, consuming Proto-Caribbean ocean floor. Ages of continental metamorphic HP/LT rocks date the onset of collision of the Caribbean Plate and Great Arc with the passive margin of South America in the Early Cretaceous. After collision, westward subduction ceased and the leading edge of the Caribbean Plate moved dextrally alongside the South American continent towards the northeast, accommodated along major strike-slip faults. Ongoing convergence between the Caribbean Plate and the South American margin with its accreted terranes led to the formation of an eastward dipping subduction zone in the Maastrichtian, accretion of plateau basalts and resulting progressive westward back-stepping of the subduction zone (Kerr et al., 1997; Millward et al., 1984; Vallejo et al., 2006). Since the Eocene, Panama arc crust has been indenting Colombia, resulting in the accretion of the upper crustal parts of the extension of the Panama-Chocó block, collision of the present day Panama-Chocó block in the Late

Miocene-Pliocene (Kennan & Pindell, 2009) and escape tectonics in Colombia and Venezuela.

5. Reconstruction

We now integrate the constraints described above and summarized in Figure 5 and Table 2, and the first-order kinematic interpretations per sub-region into a kinematic restoration of the Caribbean Plate relative to the Americas, starting in the present and presented backward in time. Per time interval, the motions of plates or plate fragments are described forwards, as this is easier to comprehend. All figures are shown in a North America-fixed frame just as all motions (except for the NW South American terranes) are described relative to a fixed North America. The hierarchy of interpretations indicated in Table 1 is retained here in the order in which the constraints for the reconstruction are used.

5.1. 50 Ma-present
5.1.1. Caribbean-North American plate boundary evolution: the Motagua-Cayman-Oriente fault system and the Cuban segment

The youngest part of the reconstruction, between 50 Ma and the present, is primarily based on oceanic extension recorded in the Cayman Trough that currently forms the Caribbean-North American plate boundary (Leroy et al., 2000). The Cayman Trough recorded ~900 km of sinistral motion between the Caribbean Plate and the Cuban segment since the estimated 49.4 Ma (Leroy et al., 2000). As a consequence, reversing the oceanic spreading in the Cayman Trough displaces the Caribbean Plate ~900 km to the west with respect to the Cuban segment, which since the early Late Eocene was firmly welded to the North American Plate.

To the west, the Cayman Trough connects to the Motagua fault zone, which since the incorporation of the Chortis Block to the Caribbean Plate must have accommodated Caribbean-North American (Yucatan) plate motion (Burkart, 1994; DeMets et al., 2007). Following the interpretation of Rogers et al. (2007), we reconstructed the Chortis Block to move along the southern margin of Mexico in the Early Eocene. Due to the difference in orientation between the Motagua fault zone (~E-W trending) and the margin of southern Mexico (NW-SE trending), this restoration requires a counterclockwise rotation of Chortis relative to North America. We reconstructed a 32° counterclockwise rotation between ~50 Ma and the present. The bulk of this rotation is reconstructed between ~38 and 33 Ma, when Chortis passed the bend in the margin of southwestern Mexico, corresponding with a phase of the largest rotation (~1.7°/Myr). After 17 Ma, the rotation is negligible, consistent with paleomagnetic constraints from Molina Garza et al. (2012) that could not demonstrate significant rotation of volcanics of the Chortis Block in western Honduras since this time.

The island of Hispaniola is dissected by multiple left-lateral strike-slip faults, accommodating the Caribbean-North American plate motion. The southern part of

Hispaniola contains CLIP material and no faults are documented separating it from the Caribbean plate interior. Therefore, we kept the southern 'CLIP' part of Hispaniola fixed to the Caribbean plate interior. The cumulative displacement of the strike-slip faults and the North Hispaniola Deformed Belt must be equal to the amount of spreading in the Cayman trench, but how this displacement is partitioned is not directly geologically constrained. We therefore align the tectonostratigraphy of Hispaniola, with Caribeana-related terranes and Lower Cretaceous to Middle Eocene arc material, with their equivalents of southeastern Cuba (following suggestions in (Rojas-Agramonte et al., 2005, 2008). As a result, we partition the Caribbean-North American motion with ~550 km displacement on the North Hispaniola Deformed Belt, accommodating relative motion between southern Cuba and northern Hispaniola and aligning the tectonostratigraphies of Hispaniola and southeastern Cuba at ~50 Ma, and the remaining ~350 km on the Enriquillo-Plantain Garden/Los Pozos fault, separating northern (Great Arc material) and southern (CLIP material) Hispaniola, similar to tectonic reconstructions of the area of Calais and De Lépinay (1995) and Rojas-Agramonte et al. (2005, 2008).

The island of Puerto Rico contains Cretaceous-Eocene volcanics, interpreted as Great Arc rocks (Jolly et al., 1998). We restored ~300 km displacement between Puerto Rico and Hispaniola, accommodated by strike-slip motion in the Puerto Rico Trench (McCann & Sykes, 1984; Molnar & Sykes, 1969), to locate Puerto Rico adjacent to eastern Hispaniola at 50 Ma, following Ross and Scotese (1988).We reconstructed ~30 km Neogene convergence between the Caribbean Plate and Puerto Rico, representing underthrusting of the Caribbean Plate in the Muertos Trough (Byrne et al., 1985; Dillon et al., 1996; Dolan et al., 1998) and restore a 25° counterclockwise rotation between 11 and 4 Ma following Reid et al. (1991).

The island of Jamaica and the North Nicaraguan Rise, containing Great Arc rocks (Abbott et al., 1999; Lewis et al., 2011), are currently not aligned with the arc rocks of the other Great Antilles. Because Jamaica and the North Nicaraguan Rise are located south of the main strike-slip boundary between the Caribbean Plate and the Cuban segment, we restored them as part of the Caribbean Plate since 50 Ma, which results in restoring Jamaica to southern Yucatan at 50 Ma. Cooling ages of the Chuacús complex (~70 Ma) coincide with the age of cessation of arc magmatism on Jamaica. This is consistent with collision of the Great Arc with southern Yucatan resulting in the end of subduction and exhumation of HP rocks, currently exposed in Guatemala.

Collision of the Caribbean Plate and leading Cuban segment with the Bahamas platform started in the latest Paleocene to ~45 Ma and was finalized by early Late Eocene (Bralower and Iturralde-Vinent, 1997; Iturralde-Vinent et al., 2008). The collision was associated with a gradual change in Caribbean plate motion from NNE-wards along the Belize margin transform to eastwards along the Cayman Trough, accommodated along progressively more easterly oriented left-lateral strike-slip faults (e.g. Mann et al., 1995).

We reconstructed the final collision of western Cuba at 45 Ma and reconstructed an arbitrary but small 20 km of displacement along the La Trocha fault between 44 and 40 Ma and 15 km of displacement along the Cauto fault between 40 and 38 Ma, accommodating relative motion between western and central Cuba and central and eastern Cuba, respectively (based on Leroy et al., 2000; Cruz-Orosa et al., 2012a). This way, the ages of collision are younging to the southeast and the relative motions between western, central and eastern Cuba lead to a gradual but quite rapid change from NNE to E-ward relative Caribbean–North American motion.

Finally, in latest Cretaceous-Eocene time, the Cuban segment moved relative to North America. As a result, translating the Cayman Trough kinematics in terms of Caribbean-North America plate motion before final welding of the Cuban segment with North America in the early Late Eocene, requires restoration of the Cuba-North America motion. This motion is reconstructed by aligning the Caribeana rocks of Cuba with those from Guatemala around 70 Ma, i.e. 900 km SSW-wards relative to today (see Section 5.2). The direction of the motion of the Cuban segment is parallel to the Belize margin and opened the Yucatan pull-apart basin. The 50 Ma position of the Caribbean Plate shown in Figure 8a is an interpolated position between these reconstruction steps, assuming a continuous motion rate. The Cuban segment (and as a result also the Motagua-Cayman-Oriente fault system and the Caribbean plate interior) is reconstructed ~200 km SSW relative to North America at 50 Ma (Fig. 8a).

5.1.2. Caribbean-Farallon/Cocos-Nazca plate boundary evolution: the Central America Trench

The western Caribbean plate boundary is characterized by subduction of the Farallon, and subsequently, Cocos and Nazca plates in the Central America Trench. The continuous Upper Cretaceous-present record of arc volcanism in the Panama-Chocó block indicates ongoing active subduction throughout the 50-0 Ma period. The eastward motion of the Chortis Block along the margin of southwestern Mexico results in a migrating trench-trench-transform triple junction at the northwestern tip of Chortis. After passing of the Chortis Block and the consequent migration of the triple junction, the former transform boundary along the southern margin of Mexico evolved into a subduction zone, subducting Farallon/Cocos Plate below Mexico. Following Phipps Morgan et al. (2008), the triple junction has migrated since the Middle Miocene even though the nature of the plate boundaries did not change. This implies that the eastward motion of the Chortis Block must have been accommodated by intra-plate deformation. We reconstructed the post-Middle Miocene history of the Chortis Block by restoring 100 km E-W extension in the Nicaraguan Basin since 15 Ma (Phipps Morgan et al., 2008), 4° counterclockwise rotation of the fore-arc with respect to Chortis and 150 km right-lateral strike-slip motion between the Chortis Block and its western fore-arc (DeMets, 2001), following the scenario proposed by Phipps Morgan et al. (2008).

5.1.3. Eastern Caribbean plate boundary evolution: the Lesser Antilles subduction system

The eastern plate boundary of the Caribbean Plate is characterized by subduction of the Atlantic North and South American plates below the Caribbean in the Lesser Antilles subduction system. Accumulation of the Barbados Accretionary Prism since the Early Eocene indicates ongoing convergence during the 50-0 Ma period. Arc volcanics in the Lesser Antilles Arc and Aves Ridge are dated ranging from 38 to 0 Ma (Briden et al., 1979) and from 88 to 59 Ma (Neill et al., 2011) respectively, suggesting that the transition of the active arc from the Aves Ridge to the Lesser Antilles Arc took place between 59 and 38 Ma. We followed the model of subduction system evolution of Aitken et al. (2011), considering the Grenada Basin to be the fore-arc of the Aves Ridge that widened by E-W extension in the Paleocene-Middle Eocene, after which active volcanism ceased in the Aves Ridge and migrated to the Lesser Antilles Arc, separating the former fore-arc into the Grenada and Tobago Basins. We kept the island of Tobago fixed to the eastern edge of the Tobago Basin; restoring E-W Paleogene extension in the eastern Caribbean fore-arc brings Tobago closer to the southern tip of the Aves Ridge (see also Section 5.2.5).

5.1.4. Caribbean-South American plate boundary evolution

In the 50-0 Ma period, South America is slightly moving to the northwest relative to North America (according to the North America-Africa-South America plate circuit of Torsvik et al. (2012), see also Pindell and Kennan (2009) and references therein). Combining this with the reconstructed motion of the Caribbean Plate relative to North America (northeastward between 50 and 45 Ma and changing to eastward after 45 Ma) results in mainly right-lateral strike-slip motion between the Caribbean Plate and South America for the period 50-45 Ma. Since between 45 and 40 Ma, accommodation of N-S convergence along the northern Caribbean plate boundary ceased, ongoing N-S convergence between North and South America became accommodated along the Caribbean-South America plate boundary. The South American-Caribbean plate boundary was thus subjected to highly oblique convergence in this period, accommodated by oblique subduction of the Caribbean Plate below South America forming the South Caribbean Deformed Belt and the Maracaibo subduction zone, accompanied by right-lateral strike-slip faulting. The west to east younging transition in the South Caribbean Deformed Belt from back thrusting to subduction (Kroehler et al., 2011) follows the position of the Great Arc and marks the relative eastward Caribbean-South America motion. We reconstructed a total of ~250 km (below eastern Venezuela) to 850 km (below Colombia) of Caribbean Plate subduction alongside ~1000 km strike-slip motion between 50 and 0 Ma.

Together with the Caribbean plate interior, an extension of the Panama-Chocó block subducted below South America, accreting arc material to the continent, until collision of the modern Panama-Chocó block with the Northern Andes in the Late Miocene-Pliocene (Coates et al., 2004; Duque-Caro, 1990; Kennan & Pindell, 2009). As a result of tectonic escape, following the collision, the Maracaibo block of northern Colombia and
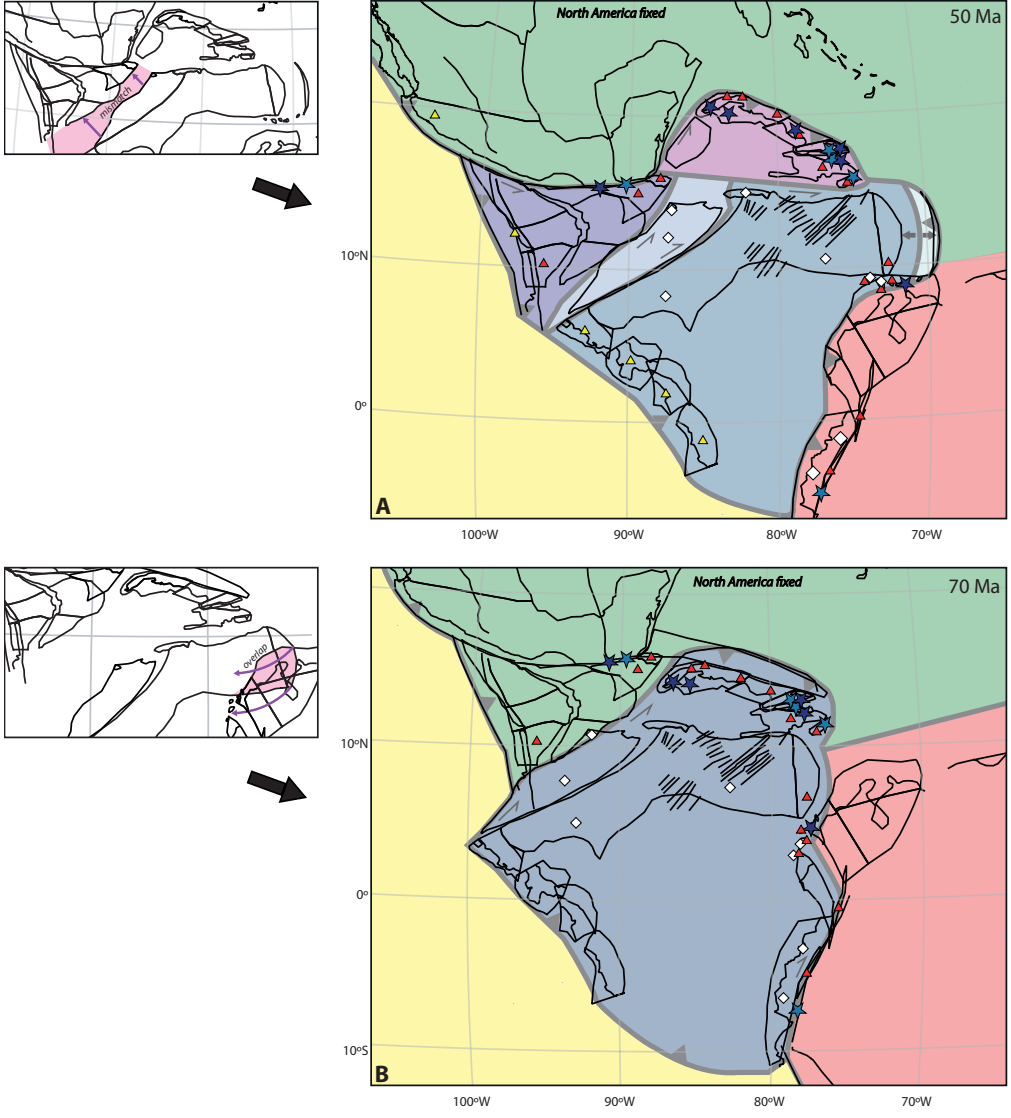
Figure 8: Snapshots of the reconstruction at selected time slices. Tectonic blocks in the same color-area move, at the time of the reconstruction snapshot, with the same velocity and direction. There is no internal deformation within a color-area. The line fragments in the Caribbean plate interior represent the magnetic anomalies identified by Ghosh et al. (1984). Insets in panels a and b indicate overlaps that were avoided by strike-slip motions in the Caribbean plate interior, and by invoking rotations of the Caribbean plate as a whole (see text for further explanation). (a) 50 Ma; (b) 70 Ma; (c) 100 Ma; (d) 135 Ma; (e) 170 Ma; (f) 200 Ma.

northwestern Venezuela has been moving to the northeast (Freymueller et al., 1993; Kellogg & Vega, 1995; Trenkamp et al., 2002). Because kinematic estimates of Ross and Scotese (1988) remain pertinent for the NW South American region in the light of data published since then, we followed their reconstruction and restored ~250 km of northeastward Maracaibo block movement relative to South America between 11 and 0 Ma. After collision, and due to ongoing convergence, the Panama Deformed Belt formed, north of the Panama-Chocó block. We reconstructed ~1000 km of NW-SE convergence between the western Panama block and the South American continent and ~250 km of NE-SW shortening across the Panama Deformed Belt, following reconstruction of the western, central and eastern Panama blocks by Montes et al. (2012).

The Late Cretaceous-Paleocene Great Arc rocks of the Leeward Antilles and the 100-90 Ma HP rocks of Isla Margarita are moving with a motion direction similar to the Caribbean Plate but with a lower velocity. This results in a 50 Ma position of the islands near the southern edge of the Aves Ridge, north of central Colombia. This is an intermediate position on their journey along the northern margin of South America between the location of formation and the modern location. Dextral shearing with the South American margin results in extension between the Leeward Antilles and Isla Margarita between 50 and 0 Ma and a more westward final position of the Leeward Antilles.

5.1.5. 50 Ma reconstruction

The 50 Ma reconstruction, following from the geological and kinematic constraints listed in Section 4, and the reconstruction choices outlined above, contains some kinematic inconsistencies, which we propose to solve as follows. Firstly, rotating the Chortis Block during its westward restoration along the Mexican margin, and reconstructing the Caribbean Plate southward prior to 38 Ma following the constraints on the Cuba-North America collision creates a gap between the Chortis Block and the interior of the Caribbean Plate at 50 Ma, corresponding to a location around the Nicaraguan Rise. This reconstructed gap between polygons would require post-50 Ma shortening of 150-200 km between the Caribbean plate interior and the Chortis Block, which is inconsistent with seismic tomographic constraints (van Benthem et al., 2013) and for which there is no geological evidence. An alternative restoration that remains consistent with the available facts requires an ~7° counterclockwise rotation of the Caribbean Plate (including the Cuban segment) at 50 Ma, around a Caribbean-North American Euler pole that is chosen such that 70-45 Ma pure strike-slip along the Belize margin transform is preserved (inset Fig. 8a). This rotation results in a slight oblique convergence between Cuba and the Bahamas platform and takes away the necessity to infer major post-50 Ma intra-Caribbean shortening. It still requires decoupling of the Caribbean plate interior from the Chortis Block, however, along a dextral strike-slip fault. We consider the Hess escarpment the most suitable candidate for such a strike-slip fault and predict ~150 km of dextral strike-slip motion on the Hess escarpment, or a structure parallel to that within ~100-200 km, between 50 and 30 Ma, during the main phase of rotation of the Chortis

Block (inset Fig. 8a). However, more strike-slip motion is required between the Chortis Block and the Caribbean plate interior, and to avoid gaps and overlaps as effectively as possible, we predict the remaining strike-slip motion to be accommodated between the Siuna-Chortis-North Nicaraguan Rise and the South Nicaraguan Rise (300 km of left-lateral motion between 50 and 38 Ma and 100 km of right-lateral motion between 38 and 32 Ma). Present-day internal deformation of the Caribbean Plate is supported by GPS data, suggesting separated western and eastern Caribbean plates (Mattioli et al., 2014). The resulting 50 Ma reconstruction is shown in Figure 8a.

5.2. 70-50 Ma
5.2.1. Caribbean-North American plate boundary evolution: transform motion and subduction in the Cuban subduction zone

The main constraint for the 70-50 Ma period is the Paleocene-Middle Eocene opening of the western Yucatan pull-apart basin (Rosencrantz, 1990), indicating transform motion parallel to the margin of Belize and convergence between the Great Arc at the leading edge of the Caribbean Plate and the Bahamas platform as recorded in the geology of the Greater Antilles. The convergence of the Great Arc of Cuba, Hispaniola, and Puerto Rico with the Bahamas platform was accommodated by subduction of the Proto-Caribbean Basin and its northern North American passive margin underneath the Caribbean Plate. Evidence for subduction is provided by Cretaceous-Eocene arc volcanism on e.g. Hispaniola and in the Yucatan basin (Abbott et al., 1999; Escuder Viruete et al., 2006, 2013; García-Casco et al., 2001, 2008a; Larue, 1991; Mitchell, 2006; Schellekens, 1991; Stanek et al., 2009). HP rocks in these serpentinite matrix mélanges range in age from 130 to 60 Ma in the Greater Antilles (Bandini et al., 2011a; García-Casco et al., 2006; Iturralde-Vinent et al., 1996; Krebs et al., 2008; Somin & Millán, 1981; Somin et al., 1992); rocks that were incorporated in the serpentinite mélanges after the Cretaceous are mainly non-metamorphic thin-skinned accreted sedimentary units with Paleocene and early to middle Eocene foreland basin units offscraped from the downgoing slab and incorporated as deformed slivers in the serpentinite mélange (Iturralde-Vinent et al., 2008; van Hinsbergen et al., 2009). The NNE-SSW trending, 450 km long western Yucatan pull-apart basin (Rosencrantz, 1990) is reconstructed as a transform plate boundary, most likely developing above a slab edge (STEP-fault sensu Govers and Wortel (2005), see van Benthem et al., 2013); this provides a minimum estimate for the amount of Greater Caribbean SSW-ward subduction since 70 Ma.

As described in Section 5.1.1, we restored the island of Jamaica and the North Nicaraguan Rise as a part of the Caribbean plate interior after 50 Ma, and restored these units adjacent to southern Yucatan and its high-pressure metamorphic southern margin, the Chuacús complex. Cooling ages of the Chuacús complex (~76-62 Ma; Ratschbacher et al., 2009 and references therein; Martens et al., 2012) and latest Campanian-Paleocene ages arc volcanism in Jamaica (McFarlane, 1977; Mitchell, 2006; Robinson, 1994) indicate the timing of collision and overthrusting of the Great Arc over the southern margin of
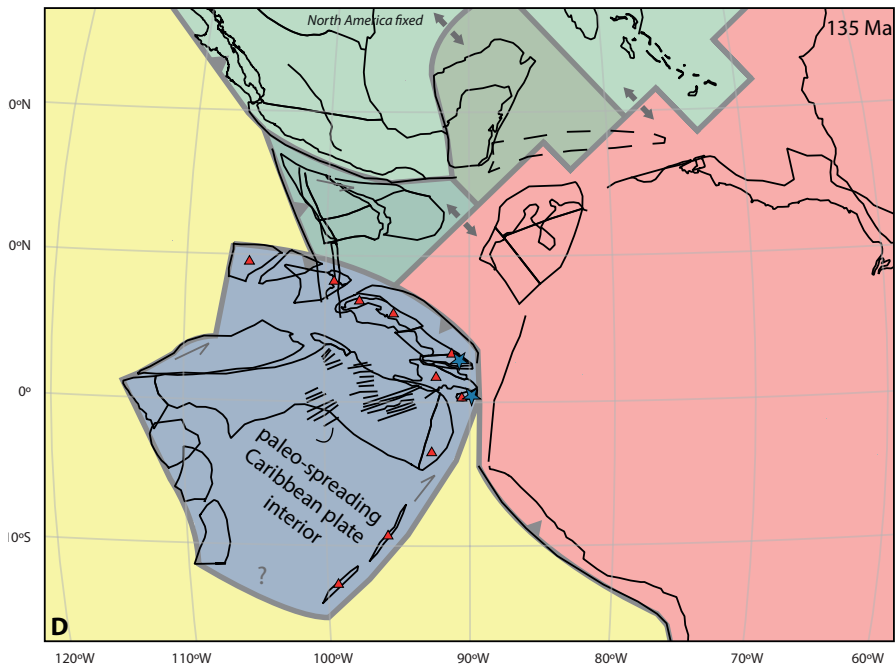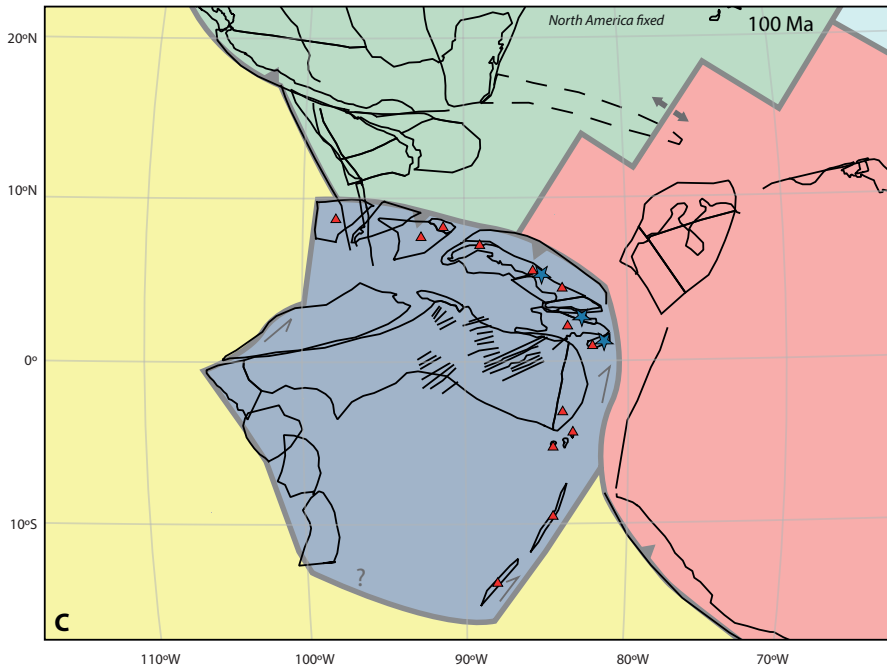
Figure 8 continued.

Yucatan. Before the inception of opening of the Cayman trench we have therefore kept the island of Jamaica and the North Nicaraguan Rise fixed relative to Yucatan between 70 and 50 Ma, as a part of the North American Plate, similar to the reconstructions of Ross and Scotese (1988) and Pindell and Kennan (2009). Restoring the Yucatan basin then aligns the Cuban and Hispaniola parts of the Great Arc with those of Jamaica and the North Nicaraguan Rise at 70 Ma. In addition, the Caribeana complexes of Cuba and Hispaniola align with their Chuacús counterpart in Guatemala. The Caribeana metamorphic terranes recorded Campanian peak metamorphism and post-70 Ma exhumation, indicating that underthrusting and accretion of Caribeana units below the leading edge of the Caribbean Plate was finalized by the latest Cretaceous (García-Casco et al., 2006, 2008a; Kantchev, 1978; Stanek et al., 2006). This is supported by the late Campanian–Danian interruption of arc volcanism in Cuba, Hispaniola and Puerto Rico (García-Casco et al., 2001, 2008a; Jolly et al., 1998; Lewis et al., 1991). As a result, the leading Great Arc (represented by Jamaica, the North Nicaraguan Rise, Cuba, Hispaniola and Puerto Rico) is reconstructed ~900 km SSW-ward relative to its modern position versus North America at 70 Ma. Latest Cretaceous-Paleocene subduction erosion of the Caribbean Plate resulted in the almost complete disappearance of the fore-arc of the Great Arc (van Hinsbergen et al., 2009); we have restored a conceptual 160 km wide fore-arc at 70 Ma, i.e., the average trench-arc distance in modern subduction zones (Gill, 1981).

After restoring the Chortis Block to the west and rotating it between 50 and 0 Ma, the boundary between the Southern Chortis terrane and the Chortis Block coincides with the boundary between Guerrero and stable western Mexico (Rogers et al., 2007). There is no indication for movement of the Chortis Block relative to North America prior to the opening of the Cayman Trough, hence we kept it fixed relative to North America between 70 and 50 Ma. With the Chortis Block and Great Arc fragments of Jamaica and the North Nicaraguan Rise being part of the North American Plate, subduction of Proto-Caribbean lithosphere below the Great Arc of the Greater Antilles implies that the plate boundary configuration between 70 and 50 Ma was different compared to the 50-0 Ma period. Between 70 and 50 Ma, the Caribbean-North American plate boundary was partly a SSW-NNE transform boundary, accommodating pure left-lateral motion (with a releasing bend creating the Yucatan basin) between Belize and western Cuba, and farther to the SW between the Chortis Block and the Caribbean plate interior (see also Section 5.2.5). To the NE, the plate boundary was a WNW-ESE striking, SSW-dipping subduction zone (Fig. 8a and b).

5.2.2. Caribbean-Farallon plate boundary evolution: the Central America Trench
The continuous upper Campanian-Neogene geological record of arc volcanism in the Panama-Chocó block (Denyer et al., 2006; Buchs et al., 2010) indicates ongoing active eastward subduction of the Farallon Plate below the Caribbean Plate throughout the 70-50 Ma period and is reconstructed as such.

5.2.3. Eastern Caribbean plate boundary evolution: the Lesser Antilles subduction system

The record of arc volcanism in the Aves Ridge (88-59 Ma; Neill et al., 2011) indicates ongoing subduction of proto-Caribbean lithosphere of the North and South American plates below the Caribbean Plate in the Lesser Antilles subduction system, which is reconstructed this way.

5.2.4. Caribbean-South American plate boundary evolution

The South American continent underwent a very minor (<100 km) eastward motion with respect to North America in the 70-50 Ma period (Pindell and Kennan, 2009; Torsvik et al., 2012). The NNE-ward motion of the Caribbean Plate inferred from the Yucatan basin predicts transpressional right-lateral motion between the Caribbean Plate and the NNE striking margin of the South American continent. This prediction is consistent with Upper Cretaceous and Paleogene dextral strike-slip recorded from the Northern Andes (Kennan and Pindell, 2009) and the Leeward Antilles area (Escalona and Mann, 2011). We reconstructed ~700 km of dextral strike-slip between 70 and 50 Ma, alongside ~500 km of convergence between the Caribbean plate interior and the South American continent, accommodated by subduction of the Caribbean Plate below South America for which evidence is provided by accreted Santonian-Paleogene 'Greater Panama' thrust slices accreted in the Northern Andes. Based on paleomagnetic studies (Burmester et al., 1996; Stearns et al., 1982), we reconstructed a 90° rotation of the Netherlands Antilles and Tobago area between 50 and 65 Ma, lining up the arc material between the Aves Ridge and arc material of the Northern Andes at 65 Ma. We followed Aitken et al. (2011) for opening of the Tobago and Grenada Basins, and fixed the island of Tobago to the eastern edge of the Tobago Basin.

5.2.5. 70 Ma reconstruction

The 70 Ma reconstruction, following from the geological and kinematic constraints listed in Section 4, and the reconstruction choices outlined above, contains some kinematic inconsistencies, which we discuss in this section. Our reconstruction demonstrates that a NNE-ward motion of the Caribbean Plate between 70 and 50 Ma relative to the America's is consistent with the geological records of all plate boundaries. The eastern margin of the Caribbean Plate, formed by the Aves ridge and its eastern fore-arc, must hence be restored sufficiently far to the west so as to move along the NW South American margin prior to ~50 Ma, and to avoid overlap between the Caribbean Plate and South America. Restoring the eastward Caribbean plate motion associated with the opening of the Cayman Trough, however, does not bring the Aves ridge sufficiently far west: subsequent reconstruction of the Yucatan margin would result in an overlap of ~300 km of the Aves Ridge and the Northern Andes and a gap of ~600 km between the Caribbean plate interior and the Siuna and Chortis blocks around 70 Ma. This would suggest that the eastern part of the Caribbean plate interior underwent ~300 km of post-70 Ma extension, and the northwestern part ~600 km of shortening, for which there is no evidence. We propose to

solve this inconsistency by inferring ~400 km of sinistral motion between the Caribbean Plate and the Chortis Block in the west, and the Cuban segment in the east prior to opening of the Cayman Trough (inset Fig. 8b). We predict the sinistral motion to be accommodated by pre-drift extension of the margins of the Cayman Trough (Mann and Burke, 1990) and by predecessors of the Oriente-Septentrional and Walton-Enriquillo-Plantain Garden fault systems south of the Cuban segment, which, as a result, is modeled as already a microplate 20 Myr prior to Cayman Trough opening. This restoration also requires the existence of a strike-slip system south of the Chortis Block, for which there is no evidence in the onshore geology. We inferred ~150 km of dextral strike-slip motion along the Hess escarpment between 50 and 30 Ma, but inferring significant transform motion along the Hess escarpment for the 70-50 Ma period would result in a major overlap between the South Nicaraguan Rise, and the Yucatan Basin and Cuba, and a gap south of the Siuna block at 70 Ma. We therefore accommodate the transform motion in this period between the South Nicaraguan Rise and the Siuna-Chortis-North Nicaraguan Rise, considering the South Nicaraguan Rise to be part of the Caribbean plate interior. Reconstructing transform motion along all plate boundaries mentioned above (in absence of evidence for major shortening or extension) requires restoring 17° counterclockwise rotation of the Caribbean Plate with respect to North America (inset Fig. 8b). The resulting 70 Ma reconstruction is shown in Figure 8b.

5.3. 100-70 Ma
5.3.1. Caribbean-North American plate boundary evolution: Proto-Caribbean Ocean subduction in the Greater Antilles subduction zone, east Cuban subduction jump, and minor transform motion

In the 100-70 Ma period, the Caribbean-North American plate boundary was characterized by subduction of Proto-Caribbean oceanic lithosphere below the Caribbean Plate, as indicated by Great Arc volcanism and HP metamorphism recorded in blocks in serpentinite-matrix mélanges (see Section 5.2.1). Prior to collision with Yucatan, Jamaica and the North Nicaraguan Rise were all part of the active Great Arc and we restored these segments as fixed to the Caribbean Plate interior before 70 Ma, aligned with the Cuban part of the Great Arc. The Siuna block contains Lower Cretaceous arc magmatic rocks, indicating that it was probably also part of the Great Arc before its Late Cretaceous collision (modeled at 85 Ma) with the Chortis Block (Venable, 1994). Prior to the collision in the Late Cretaceous, we therefore aligned the Siuna block as the westward continuation of the Great Arc and reconstructed it fixed to the Caribbean plate interior. Between the 85 Ma collision of the Siuna ophiolite terrane with the Chortis Block, and collision of the Jamaica arc with the margin of southern Yucatan around 70 Ma, we reconstructed ~550 km of transform motion between the eastern Chortis Block to the west and Jamaica and the North Nicaraguan Rise to the east, parallel to the strike of the Belize margin.

To account for the emplacement of the Mayarí-Baracoa ophiolite in East Cuba with its Campanian metamorphic sole, and the consequent blueschist facies metamorphism
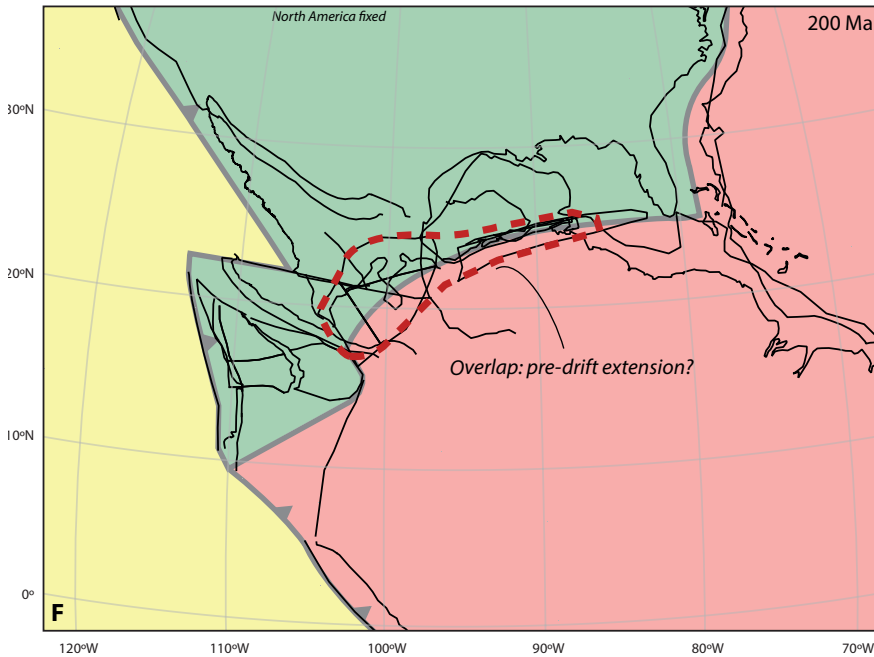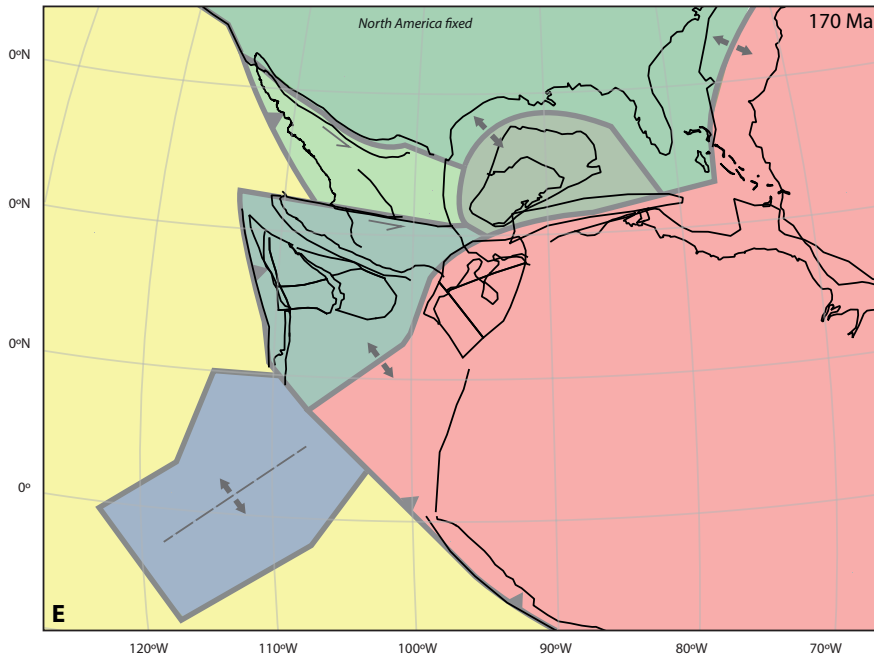
Figure 8 continued.

recorded in east Cuban Great Arc rocks, we reconstructed the opening of a narrow back-arc basin between 80 and 75 Ma, following Lázaro et al. (2013). We linked the short-lived jump of the subduction zone from below the Great Arc into the back-arc to a conceptual 75 Ma Great-Arc-Caribeana collision, and accommodated the 75-70 Ma Caribbean-North America convergence in the former back-arc. We modeled the 80-75 Ma opening by a small counterclockwise rotation of the Cuban Great Arc relative to the Caribbean plate interior and a maximum, arbitrary but small extension of ~135 km between Eastern Cuba and the Caribbean Plate. Subsequent inversion of this back-arc is modeled as a clockwise rotation of equal magnitude, and 135 km maximum convergence, sufficient to bury the Great Arc rocks to blueschist facies conditions (Fig. 9).

Easternmost Jamaica (blueschist metamorphic CLIP material) collides with the Siuna terrane at 76 Ma and consequently, ~100 km shortening is reconstructed between the South Nicaraguan Rise and easternmost Jamaica to account for subduction of CLIP material and blueschist metamorphism of the Mt. Hibernia Schist (West et al., 2014; see Fig. 9). After 72 Ma, easternmost Jamaica is kept fixed to the North Nicaraguan Rise.

In conclusion, the Caribbean-North American plate boundary in the 100-70 Ma period is a WNW-ESE subduction zone, consuming Proto-Caribbean oceanic lithosphere. Because the Chortis Block is located closer to the subduction zone than Yucatan-Caribeana, collision with Chortis preceded collision with Yucatan. This led to a transform fault sub-perpendicular to the general trend of the subduction zone, accommodating strike-slip motion between the Chortis Block and Jamaica-North Nicaraguan Rise between 85 and 70 Ma.

5.3.2. Caribbean-Farallon plate boundary evolution: origin of the Central America Trench

The oldest dated arc magmatic rocks in the Panama-Chocó block are of Campanian age (Denyer et al., 2006; Buchs et al., 2010). However, middle Turonian-Santonian and Coniacian-Santonian ages of radiolarites intercalated with arc-derived material on the Nicoya Peninsula (Bandini et al., 2008) and Santonian-Campanian boninites in the accreted Greater Panama terranes in the Northern Andes (Kennan and Pindell, 2009) suggest that the volcanic arc has been active since at least the Santonian (~85 Ma). Boninites are closely related to subduction initiation (e.g. Stern et al., 2012), and we modeled the Central American subduction zone to form only after 85 Ma. Prior to subduction initiation, there was no convergent plate boundary between the Caribbean Plate and the Farallon Plate, nor is there evidence for an ocean spreading center of Cretaceous age in Central America; the Caribbean Plate was hence either part of the Farallon Plate prior to 85 Ma, or moved relative to the Farallon Plate along a transform plate boundary.

5.3.3. Eastern Caribbean plate boundary evolution: the Lesser Antilles subduction system

The oldest reported arc magmas from the Aves Ridge (88 Ma; Neill et al., 2011), and island arc rocks on Aruba, Curaçao, La Blanquilla and Gran Roque (~58-89 Ma; van der Lelij et al., 2010; Wright & Wyld, 2011), which are geochemically very similar to those from the Aves Ridge, indicate that the Lesser Antilles subduction system has been active since at least the Coniacian. The Aves ridge is hence part of the Great Arc of the Caribbean, and the leading edge of the Caribbean Plate was somewhat irregular in shape and orientation: the Aves ridge strikes almost orthogonal to the strike of the Greater Antilles segment of the Great Arc. To have simultaneous arc volcanism in both segments, subduction must have been highly oblique below the eastern Caribbean margins between ~90 and ~60 Ma.

5.3.4. Caribbean-South American plate boundary evolution

In the 100-75 Ma period, South America moved to the southeast relative to North America, which must have been accommodated by the last stages of spreading in the Proto-Caribbean Ocean. At ~75 Ma, this motion reversed, associated with an ~5 Myr period without significant motion between the two continents (Pindell & Kennan, 2009; Torsvik et al., 2012). Major Late Cretaceous dextral faulting and shearing was reconstructed in the Northern Andes (Kennan & Pindell, 2009; Kerr et al., 1998; Trenkamp et al., 2002). In addition, convergent motion resulted in the emplacement and imbrication of slivers of ~87 Ma CLIP magmas over the South American margin in Colombia, and associated deposition of ultramafic-derived sediments in the central belt of the Northern Andes (Kennan & Pindell, 2009; Kerr et al., 1997; Vallejo et al., 2006). This requires restoration of transpression between the Caribbean Plate and South America, but quantitative kinematic data that constrain the amount of convergence and translation are not available. We reconstructed a Caribbean–South America dextral strike-slip component of ~1300 km between 100 and 70 Ma, and a convergence component of ~200 km.

HP rocks on Isla Margarita represent deep underthrusting of the margin of the South American continent. Peak metamorphism was interpreted to occur around 100-90 Ma (Maresch et al., 2009), which we adopt as the timing of final collision between the overriding Caribbean Plate with the downgoing South American continent (see also Section 5.4). Our restoration places Isla Margarita near the coast of present northern Peru during peak metamorphism, east of the southern edge of the Aves Ridge. Greenschist-facies metamorphism on Isla Margarita prevailed during exhumation, as a result of shearing during the island's journey towards its present position, north of Venezuela (Maresch et al., 2009).

Following our reconstruction philosophy, we interpret the arc rocks in the Northern Andes as part of the Great Arc of the Caribbean and test the hypothesis that the Great Arc was one, continuous island arc. Plate kinematically, this is the most simple scenario (and

therefore preferred), but we acknowledge another interpretation; the Northern Andes Arc may have been a separate subduction zone with a reversed polarity.

5.3.5. 100 Ma reconstruction

The 100 Ma position of the northern, leading edge of the Caribbean Plate is an interpolated position between the 135 Ma (see Section 5.4) and the 70 Ma positions, assuming a continuous motion rate. The Caribbean Plate is reconstructed another ~900 km SSW of its 70 Ma position relative to North America, and we restored an ~9° counterclockwise rotation between 100 and 70 Ma to reconstruct transpressional motion with South America. The resulting 100 Ma reconstruction is shown in Figure 8c. At 75 Ma, the North Nicaraguan Rise overlaps with the eastern part of the Chortis Block. Without moving the Chortis Block further west prior to 50Ma, it is not possible to avoid this overlap. Our reconstruction therefore predicts ~100 km of extension within or between the offshore portions of the Chortis Block and the North Nicaraguan Rise between 75 and 70 Ma.

Between 91 and 88 Ma, the bulk of the plateau basalts of the CLIP was been formed. Shortly after formation, the CLIP may have been twice its present size, illustrated by the size of the blue area in Figure 8b, minus the Cuban segment and the Aves Ridge. The center of the original CLIP would have been ~1000 km south of southern Hispaniola.

5.4. 135-100 Ma
5.4.1. Caribbean-North/South American plate boundary evolution: origin of the Great Arc of the Caribbean

K-Ar ages from samples of the HP metamorphic blocks in the Cuban serpentinite mélange range from ~130 to 60 Ma (Somin and Millán, 1981; Somin et al., 1992) and the oldest arc magmatic rocks have been dated at 133 Ma (Rojas-Agramonte et al., 2011), indicating that subduction of the Proto-Caribbean Ocean started in at least the Hauterivian. Pindell et al. (2012) modeled an age of 135 Ma for subduction initiation. We have adopted a 135 Ma age for initiation of subduction below the Great Arc of the Caribbean, although we note that this is a minimum age, and subduction may have started earlier. Prior to the onset of subduction and the formation of the Great Arc of the Caribbean, there was no convergent boundary between the Caribbean(/Farallon) Plate and the North and South American parts of the young Proto-Caribbean Ocean.

In the Northern Andes, sheared and accreted Lower Cretaceous island arc rocks and continental HP rocks of 120-110 Ma, found in the same tectonic belt, record the collision of the Great Arc with the South American continent (Kennan & Pindell, 2009; Nivia et al., 2006). This provides constraints on the position of the leading edge of the Caribbean Plate in the late Early Cretaceous. In the Late Jurassic-earliest Cretaceous, prior to collision, the Northern Andes formed a passive margin between the South American continent and the Proto-Caribbean Ocean (see Section 5.5) and the accreted arc rocks represent the leading
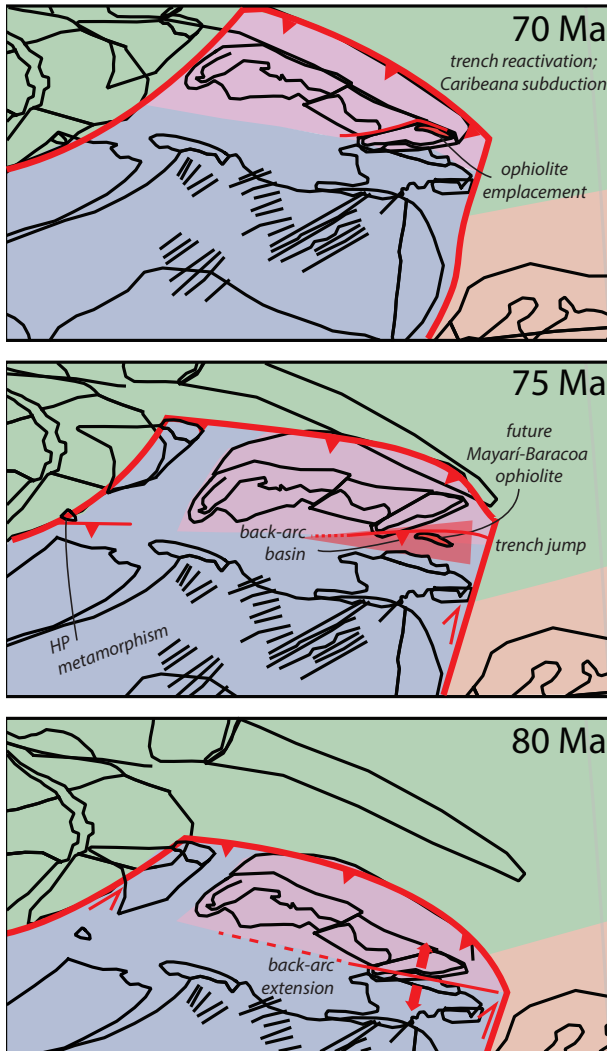
Figure 9: Reconstruction of formation and emplacement of the Mayarí–Baracoa back-arc ophiolite over the Puriol arc fragment of Eastern Cuba, as recently postulated by Lázaro et al. (2013).

edge of the Caribbean Plate. We therefore fixed the arc terranes of the Northern Andes to the Caribbean Plate prior to the ~100 Ma arc-continent collision. In the 135-100 Ma period, SE-ward motion of the South American continent relative to North America (Pindell & Kennan, 2009; Torsvik et al., 2012) must have been accommodated by ~1100 km of Proto-Caribbean Ocean spreading. The 135 Ma position of the Caribbean Plate, at the time of subduction initiation, is constrained by the relative positions of the North and South American continents. The Caribbean Plate is reconstructed to the west of the American continents, aligning the Great Arc more or less with the western margins

of the North and South American continents, but with an opposite subduction polarity (i.e. westward below the Great Arc, and eastward below the Americas). This alignment was acquired by reconstructing ~900 km of eastward motion and a 5° counterclockwise rotation of the Caribbean Plate between 135 and 100 Ma.

5.4.2. Chortis-Southern Mexico: evolution of the Motagua mélanges

HP rocks within the serpentinite mélange of the South Motagua unit (ophiolitic El Tambor complex) are dated at 124-113 Ma and 144-132 Ma (Ar-Ar cooling ages; Harlow et al., 2004; Brueckner et al., 2009) and 158-154 Ma (U-Pb zircon crystallization ages; Flores et al., 2013). This suggests Late Jurassic-earliest Cretaceous subduction of the Chortis Block below the margin of southern Mexico until collision and exhumation of the subducted continental margin between 144 and 113 Ma. We reconstructed this by giving the Chortis Block a motion similar to the motion of South America between 156 and 120 Ma, resulting in transpressional motion between the Chortis Block and southern Mexico and oblique collision around 120 Ma. This essentially means that we reconstructed a North-South America plate boundary jump from north of Chortis to its south in the Early Cretaceous.

5.4.3. 135 Ma reconstruction

The resulting 135 Ma reconstruction is shown in Figure 8d. Around 130 Ma, after full development of the eastern Caribbean subduction system and prior to collision of the Great Arc with parts of the North and South American plates, and subduction of the Caribbean plate interior below the South American continent, the Caribbean plate lithosphere and the Great Arc of the Caribbean are at their maximum sizes.

5.5. 200-135 Ma

The 143.74 ± 0.33 Ma U-Pb age of ocean floor from La Désirade Island in the Lesser Antilles (Mattinson et al., 2008), and Late Jurassic ages of sediments related to the Cuban ophiolites (Iturralde-Vinent, 1994, 1996; Iturralde-Vinent & Marí-Morales, 1988; Llanes et al., 1998) show that the oceanic crust of the Caribbean Plate formed during this time. Spreading was probably perpendicular to the orientation of the magnetic anomalies identified below the CLIP by Ghosh et al. (1984). Given the uncertainties in our reconstruction and in the imaged anomalies of Ghosh et al. (1984), the spreading responsible for these anomalies may have been sub-parallel to the NW-SE direction of spreading in the Proto-Caribbean Ocean and the early stages of opening of the Central Atlantic Ocean (Labails et al., 2010): the difference in reconstructed orientation of the anomalies and of Proto-Caribbean spreading is up to ~25°. We will discuss the likelihood of a Proto-Caribbean or Pacific origin of the Caribbean Plate lithosphere in the discussion section, by assessing the plate boundary configurations and their plate kinematic feasibility.

Because kinematic estimates of Ross and Scotese (1988) remain pertinent for southwestern Mexico, we followed their reconstruction and reconstructed southwestern Mexico westward prior to 143 Ma by motion in the Trans-Mexican volcanic belt. The reconstructed NW-ward motion of northern Mexico relative to North America along the Mojave Megashear is based on Müller et al. (2008). For opening of the Gulf of Mexico, we follow the reconstruction of Pindell and Kennan (2009), reconstructing Yucatan NW-ward prior to 130 Ma. The resulting 170 Ma reconstruction is shown in Figure 8e. Finally, a 200 Ma reconstruction is derived with a total of 300-400 km of overlap between the Northwestern Andes and Mexico. This overlap results from treating these margins and blocks as rigid, and would suggest 300-400 km of extension being accommodated by predrift extension associated with the opening of the Proto-Caribbean Ocean. Such a number is within the range of extension accommodated in modern passive margins (Torsvik et al., 2008). The 200 Ma reconstruction is shown in Figure 8f.

6. Discussion

6.1. Constraints on Jurassic plate boundaries

Between ~200 and ~135 Ma, during the break-up of Pangea, the Caribbean Plate did not exist yet as a separate plate. Africa and South America were rifting and drifting away from North America, opening the Central Atlantic and Proto-Caribbean oceans. Subduction already occurred below the Americas around and before 170 Ma (Boekhout et al., 2012; González, 2001; Kennan & Pindell, 2009; Litherland et al., 1994; Noble et al., 1997; Villagómez et al., 2008), as well as in offshore intra-oceanic subduction zones (Buchs et al., 2013; Sigloch & Mihalynuk, 2013; van der Meer et al., 2012) but little is known about exact directions of plate motion within the Panthalassa Ocean, because pre-Cretaceous plate reconstructions of this region are conceptual and not constrained by any magnetic anomaly data (Seton et al., 2012; Sigloch & Mihalynuk, 2013; van der Meer et al., 2012). The absence of arc magmatism older than 133 Ma suggests that there was no subduction zone between the future Caribbean lithosphere and the Proto-Caribbean Ocean yet before that time, although we note again that this is the minimum age of subduction initiation.

We use our reconstruction to assess whether the Caribbean lithosphere before inception of Great Arc subduction may have formed (west of the North and South American continents) due to North-South America spreading (and can be considered 'Atlantic' or 'Proto-Caribbean' in origin), or whether a Panthalassa origin is more likely. We note here that both scenarios would qualify as 'Pacific origin' in the old 'in-situ' (James, 2006) versus 'Pacific' (Pindell et al., 2006) origin debate. As described in Sections 5.4.3 and 5.5, the orientation of the magnetic anomalies identified by Ghosh et al. (1984) strike within 25° from the orientation perpendicular to spreading in the Proto-Caribbean Ocean, and the ages of formation of Caribbean oceanic crust are quite similar to spreading directions and ages that would have formed due to the Proto-Caribbean (Atlantic) spreading. It may thus be possible that the Proto-Caribbean Ocean and the Caribbean lithosphere were connected, or perhaps separated by a transform plate boundary that became inverted to

become the Great Arc subduction zone. Such a transform was conceptually termed the 'inter-American transform' by Pindell et al. (2012) and the question thus is: was the inter-American transform within Proto-Caribbean lithosphere, or between Proto-Caribbean and Panthalassa lithosphere?

Due to the similar strike of the 'inter-American transform' and the North and South American subduction zones, a Proto-Caribbean origin of Caribbean lithosphere creates some difficulties for the plate boundary configuration between 200 and 135 Ma. Figure 10a shows a conceptual, and quite complex configuration, whereby Panthalassa lithosphere is subducting below the North and South American continents, while maintaining absence of convergence between Panthalassa and Proto-Caribbean lithospheres. Alternatively, as shown in Figure 10b, a much simpler plate boundary scenario may be invoked, also consistent with the reconstructed spreading directions of the Caribbean plate interior, with a Panthalassa origin for the Caribbean Plate. This scenario is very similar to the modern Pacific-Juan de Fuca-North American-San Andreas system. This scenario may also explain the reconstructed age and paleo-spreading direction of the Caribbean lithosphere, the presence of an intra-American transform and subduction zones below the North and South American subduction zones. We stress that the scenarios of Figure 10 are conceptual, and are thought-exercises to test viability of an intra-American or Panthalassa origin of the Caribbean lithosphere; nevertheless, we note that a Panthalassa origin requires the simplest scenario.
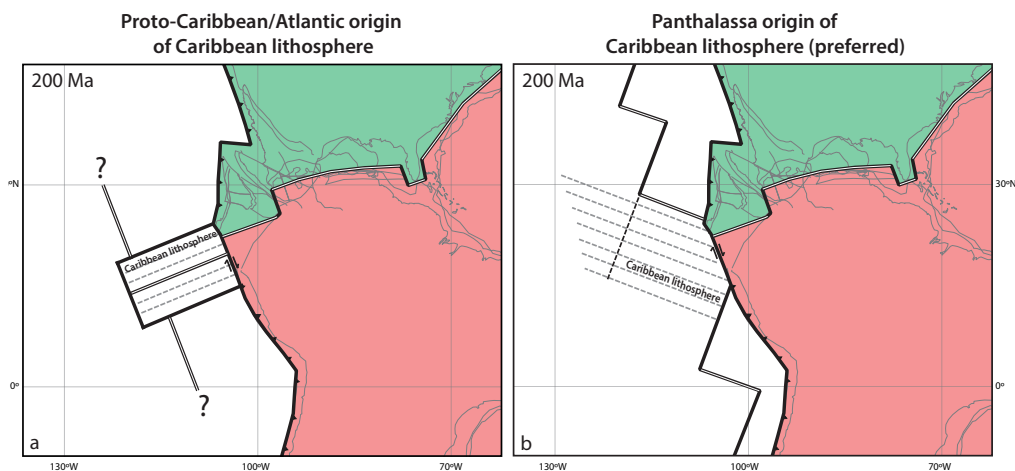
Figure 10: Conceptual plate boundary configurations at 200 Ma.

6.2. Caribbean plate origin debate

In both plate kinematic scenarios shown in Figure 10, the position of origin of the Caribbean plate is the same: west of the North and South American plates. However, this position has been subject of debate (e.g. James, 2006; Pindell et al., 2006). Here, we emphasize the two main plate kinematic arguments against the 'in-situ' model of James (2006); James (2009), where the Caribbean Plate originates between the North and South American continents as a result of Proto-Caribbean spreading), and illustrate why we are convinced that this model is in violation with geology and basic plate kinematics. For many other arguments, see e.g. Pindell and Barrett (1990), Pindell et al. (2006, 2012).

For the last 50 Myr, the motion of the Caribbean Plate relative to North America is constrained in numerous ways. We, as most authors, put faith in the oceanic spreading history of the Cayman Trough, even though the magnetic anomalies of the Trough are poor (Leroy et al., 2000). However, in conjunction with assessment of the 1000 km long west to east migrating foreland basins of northern South America (Escalona & Mann, 2011; Pindell et al., 1998; Pindell & Kennan, 2007), as well as the close match between the Cayman Trough's length and orientation and the Eocene-recent motion history of North America relative to the hotspot reference frame to which the Caribbean Plate is fixed (Pindell & Kennan, 2009, see their Fig. 25), we are confident that the Cayman Trough does in fact record most (but not all; (Mann & Burke, 1990; Sykes et al., 1982) of the Eocene-Recent displacement between the Caribbean and North American plates, which occurred in an E-W (~080°) direction relative to a stable North America.

Furthermore, the record of ongoing subduction below the Aves Ridge and Lesser Antilles Arc since at least the Late Cretaceous (Bouysse, 1988; Fox & Heezen, 1975; Neill et al., 2011; Pinet et al., 1985) and tomographic evidence of at least 1100 km of subduction (van Benthem et al., 2013; van der Hilst, 1990) indicate that there has been significant relative motion between the Caribbean Plate and the Atlantic/Proto-Caribbean Ocean, whereas the east coasts of North and South America are passive margins (i.e. no motion between the Americas and the Atlantic Ocean). This difference is direct evidence that the Caribbean Plate is a separate plate that has been moving eastwards relative to North and South America during the Cenozoic.

Another significantly different Caribbean model is the 'plateau-collision' model of Duncan (1984), Burke (1988), Kerr et al. (2003) and Hastie and Kerr (2010). This model includes a subduction polarity reversal in the Great Arc subduction zone after collision of the CLIP with the Great Arc in the Late Cretaceous. Following our reconstruction philosophy, we do not include such a polarity reversal, although this model has no kinematic problems and we acknowledge the possibility of this scenario.

6.3. Cretaceous and younger plate boundary configurations and triple junctions

Since the onset of subduction in the Panama-Costa Rica Arc, the Caribbean Plate was a separate tectonic plate, bounded on all sides by plate boundaries. Prior to Central American subduction initiation, the nature of the triple junctions at the ends of the boundary between the Farallon Plate and future Caribbean Plate remain unknown. From late Cretaceous times until the Present, the Caribbean Plate has three triple junctions: the North American-Caribbean-Farallon (A), North American-South American-Caribbean (B) and Caribbean-South American-Farallon (C) triple junctions (Fig. 11a). Since Miocene fission of the Farallon Plate into the Cocos and Nazca plates (Barckhausen et al., 2008), there was a fourth: the Cocos-Caribbean-Nazca triple junction (D), which is a stable ridge-trench-trench triple junction subducting Cocos and Nazca lithosphere in the Central American trench (Fig. 11d). We here assess the feasibility of our reconstruction by testing whether the triple junctions are consistent with the basic rules of plate tectonics.

Between ~88 and 50 Ma, the northern triple junction (North-American-Caribbean-Farallon, A) is a stable trench-transform-transform triple junction south of the Siuna block (Fig. 11a). Chortis-Siuna is part of the North American Plate. In this triple junction, the Farallon Plate subducts below the North American Plate and the Caribbean Plate has a transform motion relative to Farallon and North America. At ~50 Ma, the Chortis Block transferred to the Caribbean Plate and as a consequence, the triple junction jumped towards the western end of the Motagua fault zone and transformed into a transform-trench-trench triple junction (Fig. 11c) where Farallon subducted below the Caribbean and North American plates, and the Caribbean-North America motion is a pure transform. Subduction below Mexico initiated along the former transform upon ESE-ward motion of the triple junction relative to North America; initiation of subduction below southern Mexico must hence have been strongly diachronous, younging ESE-ward.

Between 135 Ma and the age of cessation of Proto-Caribbean spreading inferred from reconstructions of the Atlantic Ocean (~75 Ma), the eastern triple junction (North American-South American-Caribbean, B) is a stable ridge–trench–trench triple junction (Fig. 11a), at which the spreading center of the Proto-Caribbean/Central Atlantic Ocean subducted. After ~75 Ma, the Lesser Antilles subduction system continued to subduct the North and South American plates, but the relative motion between these two is very minor. The plate circuit of Torsvik et al. (2012) suggests that the North-South American plate contact was mildly transpressional. The southwestern triple junction (Caribbean-South American-Farallon, C) has undergone a similar evolution as the northwestern triple junction A. Since ~88 Ma, it has been a stable trench-transform-transform triple junction (Fig. 11a), where the Farallon Plate subducted below South America and the Caribbean Plate had a transform motion relative to Farallon and South America. Because the relative motion between the Caribbean and South American plates was accommodated along several faults and shear zones in the Northern Andes, the plate boundary is diffuse and the
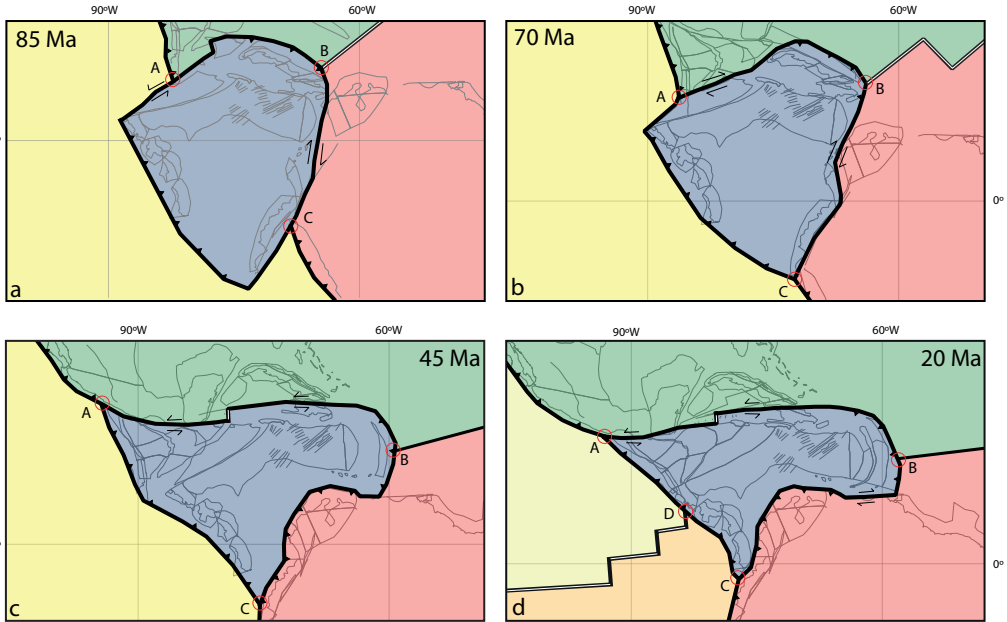
Figure 11: Plate boundary configurations at 85, 70, 45 and 20 Ma.

location of the triple junction is not precisely constrained; it may have changed positions several times during the history of dextral motion in the Northern Andes.

Around 75 Ma, the Panama-Costa Rica Arc arrived at the triple junction, transforming it into a trench–trench–transform triple junction (Fig. 11b), where the Farallon Plate subducted below the Caribbean and South American plates. The Northern Andes evolved from a passive margin that collided with the Great Arc, to a transform boundary, to an overriding plate, whereby the Caribbean Plate subducted below South America (Fig. 11c). Comparable to the transition from eastward Panthalassa subduction below Gondwana to westward subduction below Panthalassa/Caribbean lithosphere, the subduction switch seems to have been facilitated and in time separated by a stage of transform motion. Similar to the Mexican margin, renewed eastward subduction below South America was likely diachronously initiated along that transform, behind a NE-ward migrating trench-trench-transform triple junction.

6.4. Global Apparent Polar Wander Path in Caribbean coordinates

Our reconstruction may provide a reference for future paleomagnetic research in the Caribbean region. We have rotated the Global Apparent Polar Wander Path of Torsvik et al. (2012) into coordinates of three most prominent regions: the Caribbean plate interior, the Chortis Block, and the Cuban segment (Table 3). These poles may be used to

Age	A95	Chortis frame (2023)		Cuban frame (2038)		Caribbean plate interior (2007)	
		PoleLat	PoleLon	PoleLat	PoleLon	PoleLat	PoleLon
0	1.9	-88.5	353.9	-88.5	353.9	-88.5	353.9
10	1.8	-86.7	336.0	-86.4	342.2	-86.6	337.0
20	2.6	-82.3	345.4	-83.7	343.2	-84.3	337.1
30	2.6	-76.4	348.5	-82.1	338.7	-84.3	314.6
40	2.9	-65.1	355.7	-80.1	337.2	-83.2	306.0
50	2.8	-55.8	5.2	-72.2	353.3	-77.3	347.3
60	2.1	-53.5	11.6	-74.7	351.0	-73.9	2.5
70	2.5	-53.7	14.1	-79.1	334.0	-72.5	5.2
80	2.9	-54.8	12.6	-76.6	321.5	-71.0	354.7
90	2.5	-56.4	9.4	-71.7	321.4	-66.3	350.5
100	3.3	-58.1	6.4	-65.4	327.7	-59.7	352.2
110	3.3	-56.1	17.2	-64.4	345.7	-57.4	6.3
120	2.6	-54.1	15.3	-59.7	348.4	-52.6	7.6
130	2.8	-48.4	14.5	-56.7	349.4	-49.6	8.0
140	6.0	-42.7	17.6				
150	6.4	-43.5	8.2				
160	5.1	-35.9	4.3				
170	4.6	-32.3	3.2				
180	3.4	-38.4	357.5				
190	2.9	-41.6	348.9				
200	2.8	-39.5	340.0				

Table 3: Global Apparent PolarWander Path of Torsvik et al. (2012) rotated into the coordinates of the Caribbean plate interior, the Chortis Block, and the Cuban segment.

paleomagnetically test the predictions of our reconstruction, as well as serve as reference for future paleomagnetic analyses in the Caribbean region.

6.5. Caribbean motion in an absolute reference frame

Around 140 Ma, the absolute motion of the North American Plate changed from NNW to W (using the slab-fitted absolute reference frame from van der Meer et al. (2010) based on the True-Polar Wander corrected paleomagnetic reference frame of Steinberger and Torsvik (2008)). With the Farallon/Panthalassa plate(s) being anchored in the mantle by slabs below or offshore the Americas, such a change in absolute plate motion may have driven the initial E-W convergence between the Proto-Caribbean lithosphere - with passive margins attached to the American continents - and the Caribbean lithosphere, connected (probably through a transform fault) to Panthalassa lithosphere (Fig. 10). This would be an interesting case study for analyzing absolute plate motion forcing of subduction initiation. Subduction probably initiated along a transform fault (the intra-American transform; Pindell et al., 2012). The transformation of this inter-American trench-to-trench transform resulted in a continuous subduction zone from northern

North America to southern South America, but the direction of subduction in the central part, subducting the Proto-Caribbean Ocean instead of Panthalassa lithosphere, was eastwards instead of westwards. The former transform-transform-ridge triple junction between the inter-American trench and the Proto-Caribbean spreading center transformed into a trench-trench-ridge triple junction (Fig. 10, 11). Evidence for this triple junction has been found in Aptian amphibolite blocks from eastern Cuba (Blanco-Quintero et al., 2010; García-Casco et al., 2008b). After subduction initiation, the future Caribbean Plate was overriding the continuously spreading Proto-Caribbean Ocean and its spreading center.

The western Caribbean subduction system formed at 88-80 Ma (Pindell and Kennan, 2009). This implies that, if the Caribbean Plate originated as a fragment of the Farallon Plate, the Caribbean LIP (91-88 Ma) would actually be a Farallon LIP at the time of formation (Pindell and Kennan, 2009). In our reconstruction, the center of the present day CLIP was around 90 Ma located ~2000 km east of the site of the present day Galápagos hotspot in the slab-fitted mantle reference frame of van der Meer et al. (2010), and ~3000 km in the global moving hotspot reference frame of Doubrovine et al. (2012). If the CLIP represents the arrival of the Galápagos plume head below the lithosphere, this plume must have undergone significant motion relative to the mantle in a direction opposite to that of the overriding plate motion (i.e. against the mantle wind). We therefore consider it unlikely that the CLIP formed as a result of the plume-head stage of the Galápagos hotspot, but may source from a different plume event.

The North and South American plates moved WNW-ward between 100 and 70 Ma and SW-ward between ~70 and 50 Ma and resumed their WNW-ward motion at ~50 Ma (Fig. 12). The Caribbean Plate had a constant N (van der Meer et al., 2010) to NW-ward (Doubrovine et al., 2012) motion between 100 and 70 Ma. Around 70 Ma, the motion stagnated and, in particular for the last 40 Myr, the Caribbean Plate has been more or less stable relative to the mantle, particularly in longitude. It is remarkable that the relatively small Caribbean Plate may be one of the most stable plates in an absolute reference frame. The oppositely dipping subduction zones in the west and east of the Caribbean Plate likely function as an anchor keeping the subduction zones, and therefore the Caribbean Plate, relatively stable with respect to the mantle.

Since 50 Ma, the Caribbean Plate is at first order bounded by its present plate boundaries: subduction of the adjacent oceanic lithosphere in the Lesser Antilles subduction system and the Central American Trench and transform motion between the Caribbean Plate and the North and South American plates. We note that collision of the leading edge of the Caribbean Plate with Caribeana and Yucatan did not have a marked influence on relative plate motions, whereas the collision with the Bahamas platform coincided with a major change of direction of motion, onset of spreading in the Cayman Trough and the end of subduction. In particular in the slab-fitted mantle reference frame of van der Meer et
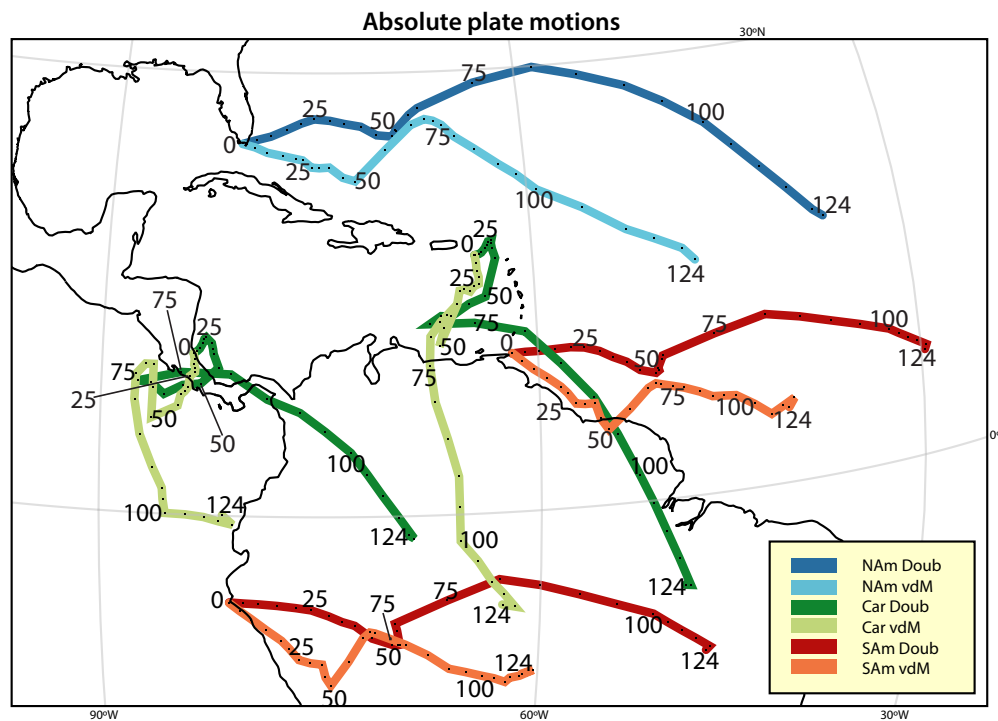
Figure 12: Absolute plate motions of the Caribbean (Car), South American (SAm) and North American (NAm) plates. Doub, global moving hotspot reference frame of Doubrovine et al. (2012); vdM, slab-fitted mantle reference frame of van der Meer et al. (2010).

al. (2010), the absolute motion of the Caribbean Plate underwent a major change at 50 Ma (Fig. 12). We therefore suggest that, as factors influencing relative plate motion, the interaction between the Caribbean Plate and the North and South American plates may be inferior to absolute plate motion and mantle anchors.

6.6. Comparing tectonic reconstructions

By comparing the amount of subduction in different subduction zones predicted by a reconstruction, different reconstructions can be quantitatively compared and tested against dimensions of relics of subduction images by seismic tomography recently estimated by van Benthem et al. (2013). Table 4 lists three of the tectonic reconstructions mentioned in the introduction. Our reconstruction predicts quite similar subduction budgets as Pindell and Kennan's (2009), except for the Nicaraguan Rise where we modeled no subduction, consistent with the absence of evidence of any slab that may be attributed to a Nicaraguan Rise subduction zone (van Benthem et al., 2013). The differences with Meschede and Frisch (1998) and Müller et al. (1999) are considerably larger. For the former, this difference is mainly the much larger amount of subduction below the Great Arc of the Caribbean in our model, and for the latter, our predicted amount of Muertos,

Nicaraguan Rise and Great Arc subduction strongly deviates. Our modeled amounts of subduction are consistent with the estimates derived from seismic tomography (van Benthem et al., 2013), although we reconstructed a somewhat larger amount of subduction below the Great Arc. The tomographic estimates are, however, based on poorly constrained slab shrinking factors associated with slabs penetrating the lower mantle.

	Tomography	Plate reconstructions			
Subduction zones	van Benthem et al (2013)	Meschede and Frisch (1998)	Müller (1999)	Pindell and Kennan (2009)	This study
Lesser Antilles	1100	1100	1100	1100	1100
Maracaibo	~1000	0-3000	1000	800	750-850
Muertos	<200	?	200 ± 94	0-150	30
Nicaraguan Rise	<200	~200	800	~300	0
Great Arc	1200-2100	1000	x	2000-3000	2200-2800

Table 4: Comparison of tectonic reconstructions on the basis of amounts of subduction. Maracaibo; subduction of the Caribbean plate below the South American continent. Modified from van Benthem et al. (2013).

7. Conclusions

This paper reviews the tectonic history of the Caribbean region and presents a quantitative, kinematically consistent reconstruction back to 200 Ma, relative to a stable North America. The reconstruction can easily be adapted to newly obtained data and may therefore form the basis of further quantitative geodynamic and kinematic research concerning the Caribbean region.

Based on our reconstruction, we conclude the following:
(1) The Caribbean Plate formed west of the North and South American continents. The direction and age of spreading in the Caribbean Plate was similar to the direction of spreading in the Proto-Caribbean Ocean, but a Panthalassa origin of the Caribbean lithosphere can be explained by a much simpler plate kinematic scenario.
(2) The Northern Andes and Mexico have accommodated 300-400 km of Early Jurassic pre-drift extension. This number is within the range of pre-drift extension accommodated in modern passive margins.
(3) During its formation, the center of the Caribbean Large Igneous Province was located 2000-3000 km east of the present-day position of the Galápagos hotspot. It is therefore not likely that the CLIP formed as the result of the Galápagos plume-head stage, but may for a separate plume event instead.
(4) Subduction initiation below the Great Arc of the Caribbean around or before 135 Ma may be the result of westward absolute plate motion of the Americas over their western subduction zones acting as anchors in the mantle; such an event would initiate E–W convergence between the future Caribbean lithosphere and the Proto-Caribbean

lithosphere between Americas and have initiated subduction along a transform fault separating these.

(5) The major Caribbean plate motion changes from NE-ward to E-ward relative to North America around 50 Ma are widely ascribed to collision of the Caribbean Plate with the Bahamas. However, we note that this change coincides with a southwestward to westward absolute plate motion change of the Americas, and may be dominated by far-field rather than local stress changes.

(6) All subduction zones surrounding the Caribbean Plate, including the Great Arc subduction zone, the Lesser Antilles Trench, the Central American trench, the South Mexican and Colombian, as well as the Maracaibo subduction zone, appear to have initiated along former transform faults. When a migrating triple junction changes a transform plate boundary into a subduction zone, subduction initiates highly diachronously. Regional subduction polarity changes are facilitated by, and intervened by phases of transform motion between plates.

3

Paleomagnetic Constraints on the Kinematic Relationship between the Guerrero terrane (Mexico) and North America since Early Cretaceous time

Colima volcano - Trans Mexican Volcanic Belt, Mexico

Abstract

The North American Cordillera has been shaped by a long history of accretion of arcs and other buoyant crustal fragments to the western margin of the North American Plate since early Mesozoic time. The southernmost accreted terrane is the Guerrero terrane of southwestern Mexico, a latest Jurassic-Cretaceous volcanic arc built on a Triassic accretionary prism. Interpretations of the origin of the Guerrero terrane vary: some authors consider it a far-travelled, exotic intra-oceanic island arc, others view it as the (par)autochthonous, extended North American continental margin. We present new paleomagnetic and U-Pb zircon data from Lower Cretaceous sedimentary rocks of the Guerrero terrane. These data show that the Guerrero terrane has a latitudinal plate motion history equal to that of the North America Plate, both before and after accretion. This confirms paleogeographic models in which the Guerrero arc successions formed on North American crust that rifted away from the Mexican mainland by ~east-west opening of a back-arc basin above an eastward dipping subduction zone. Additionally, it renders alternative paleogeographical models in which the Guerrero terrane is considered to be exotic to the North American continent unlikely. The phase of back-arc spreading resulted in the short-lived existence of an additional 'Guerrero' tectonic plate between the North American and Farallon plates, and upon closure of the back-arc basin, in the growth of the North American continent.

1. Introduction

The North American Cordillera has been shaped by a long history of accretion of arcs and other buoyant crustal fragments to the western margin of the North American Plate. Adding to the complexity of interpreting the plate tectonic provenance of these accreted terranes, the continental margin also underwent episodes of extension associated with the opening of fore- and back-arc basins, periods of shortening producing inversion of preexisting basins and fold-thrust belts, and translational deformation (moving terranes north along major strike-slip faults) (DeCelles et al., 2009; Hildebrand, 2013, 2015; Johnston, 2001; McQuarrie & Wernicke, 2005; Nokleberg, 2000; Schellart et al., 2010; Shephard et al., 2013; Sigloch & Mihalynuk, 2013; Umhoefer & Blakey, 2006; Wyld et al., 2006). Over the last decades, contrasting paleogeographic models have been proposed to explain the assembly and evolution of the Cordillera. In a first group of models, the North American Plate collided with either an offshore 'Cordilleran ribbon continent' (e.g. Hildebrand, 2013; Johnston, 2001) or a sequence of exotic archipelagos and subduction complexes (e.g. Sigloch & Mihalynuk, 2013) via westward subduction. A second group of models considers the Cordillera to have formed as the result of long-lived eastward subduction of Panthalassa/Pacific lithosphere below the North American continent (e.g. Monger & Price, 2002; Monger et al., 1982; Nokleberg, 2000; Scotese, 2004). In these models, the transfer of exotic crustal material from the subducting oceanic plates to the overriding plate plays a minor role, and deformation within the overriding North American Plate accounts for most of the formation of the Cordilleran.

From a plate tectonic perspective, terrane accretion and deformation of the North American Pacific margin was governed by the interaction between the continental North American Plate in the east, and the oceanic plates of the Panthalassa (and later, Pacific) Ocean in the west (Engebretson et al., 1985). Due to subduction and the consequent loss of oceanic spreading records, reconstructing the plate tectonic configuration of the Mesozoic northeast Pacific is prone to large uncertainties. However, marine magnetic anomalies from the northern part of the Pacific Plate are interpreted to have formed conjugate to now-subducted oceanic lithosphere of the conceptual Izanagi, Farallon and Kula plates, which were located north, east and northeast of the Pacific Plate, respectively. Relative to North America, the Farallon and Kula plates moved towards the northeast, with a larger northward motion component for Kula than for Farallon (Doubrovine & Tarduno, 2008; Seton et al., 2012; Wessel & Kroenke, 2008; Wright et al., 2016). Magnetic seafloor data cannot resolve whether the Farallon and Kula plates completely filled the northeastern Panthalassa basin, extending to the western margin of North America, or if other, smaller plates existed between the major oceanic Panthalassa plates and the continent. Reconstructing the complex plate tectonic history of the northeastern Panthalassa and the Cordillera further relies on quantitative plate motion estimates from geological observations and paleomagnetic data, providing the kinematic underpinnings for paleogeographical models.

This study focuses on the southernmost of the accreted Cordilleran terranes: the Guerrero terrane of southwestern Mexico. This terrane consists of an Upper Triassic metasedimentary basement, unconformably overlain by Middle Jurassic – Upper Cretaceous arc assemblages (Centeno-García et al., 2003, 2008; Martini et al., 2011; Talavera-Mendoza et al., 2007). The eastern boundary of the Guerrero terrane is represented by a deformed belt that includes Tithonian-Aptian, highly sheared and folded metaturbidites interbedded with uppermost Jurassic-lowermost Cretaceous rhyodacitic dykes and lava flows and Aptian intraplate-like and mid-ocean ridge basalts (Freydier et al., 1996; Martini et al., 2011, 2014; Mendoza & Suastegui, 2000; Tardy et al., 1994). The presence of mid-ocean ridge basalts indicates that during Aptian time, the Guerrero arc was located on a tectonic plate other than, and separated by a spreading ridge from, the North American Plate.

Both categories of paleogeographic models described above have been used to interpret the origin of the Guerrero terrane. On the one hand, the Guerrero terrane was interpreted as an exotic intra-oceanic island arc that accreted to mainland Mexico by closure of a large oceanic basin via westward subduction (Dickinson & Lawton, 2001; Freydier et al., 1996; Hildebrand, 2013; Lapierre et al., 1992; Sigloch & Mihalynuk, 2013; Tardy et al., 1994; Umhoefer, 2003). This interpretation predicts the presence of an additional oceanic plate and at least one subduction zone between the Guerrero terrane and the North American Plate. Depending on the paleogeographic model, the Guerrero terrane is either located on the eastern margin of the Farallon Plate (Dickinson and Lawton, 2001; Umhoefer, 2003;

Sigloch and Mihalynuk, 2013), predicting latitudinal (northward) motion of the Guerrero terrane relative to the North American Plate prior to its accretion, or in a similar position on an undefined plate within the Panthalassa Ocean (Lapierre et al., 1992; Tardy et al., 1994; Freydier et al., 1996, Hildebrand, 2013).

On the other hand, the Guerrero arc successions were interpreted to have formed on North American crust that rifted away from the Mexican mainland by opening of a back-arc basin above an eastward dipping subduction zone (Cabral-Cano et al., 2000; Centeno-García et al., 2008, 2011; Elias-Herrera et al., 2000; Fitz-Díaz et al., 2017; Martini et al., 2011). Plate tectonically, this interpretation includes ongoing eastward subduction below North America and the temporal existence of a divergent plate boundary between a small Guerrero Plate and the North American Plate. Predicted plate motion of this Guerrero Plate relative to the North American Plate was limited, and occurred more or less perpendicular to the ~N-S oriented trench and ridge, i.e., such plate motions would have been mainly longitudinal.

To determine the plate tectonic provenance of the Guerrero terrane, quantitative kinematic data are key. To this end, we constrain latitudinal plate motion of the Guerrero terrane using paleomagnetic data. High quality paleomagnetic data from the Guerrero terrane are available from the Upper Cretaceous-recent stratigraphy, but are not present for older intervals. Here, we present new paleomagnetic data and an U-Pb detrital zircon age from Lower Cretaceous sedimentary rocks of the Guerrero terrane.

2. Geological setting

The pre-Cenozoic basement of Mexico is subdivided into multiple tectonic terranes of two groups: the Proterozoic eastern terranes, which accreted to the southern part of the North American craton in late Paleozoic time (Keppie, 2004) (hereafter: 'mainland Mexico'), and the western accreted terranes that together form the Guerrero (super- or composite) terrane (Centeno-García et al., 2011; Dickinson & Lawton, 2001) (Fig. 1). The Guerrero terrane consists mostly of submarine and locally subaerial volcanic and sedimentary rocks intruded by plutons that range in age from Tithonian (Late Jurassic) to Cenomanian (Late Cretaceous) (Centeno-García et al., 2008; Martini et al., 2011; Talavera-Mendoza et al., 2007). Underlying these arc successions is the Arteaga Complex consisting of Triassic greenschist-facies metaturbidites, which were interpreted as an accretionary prism (Centeno-García et al., 1993; Centeno-García & Silva-Romo, 1997; Cuevas-Pérez, 1983; Monod & Calvet, 1991; Ranson et al., 1982; Talavera-Mendoza et al., 2007). This basement complex contains detrital zircons that returned Grenville, Pan-African and Permian U-Pb ages that match the signature of mainland Mexico and the northwestern margin of South America (Centeno-García et al., 2011). Intruding and overlying the Arteaga Complex are Middle to Upper Jurassic arc granitoids, submarine rhyolitic lavas and volcaniclastic rocks (Bissig et al., 2003; Centeno-García et al., 2003). These Jurassic arc rocks were deformed and exhumed prior to onset of the major phase of arc volcanism in the Tithonian
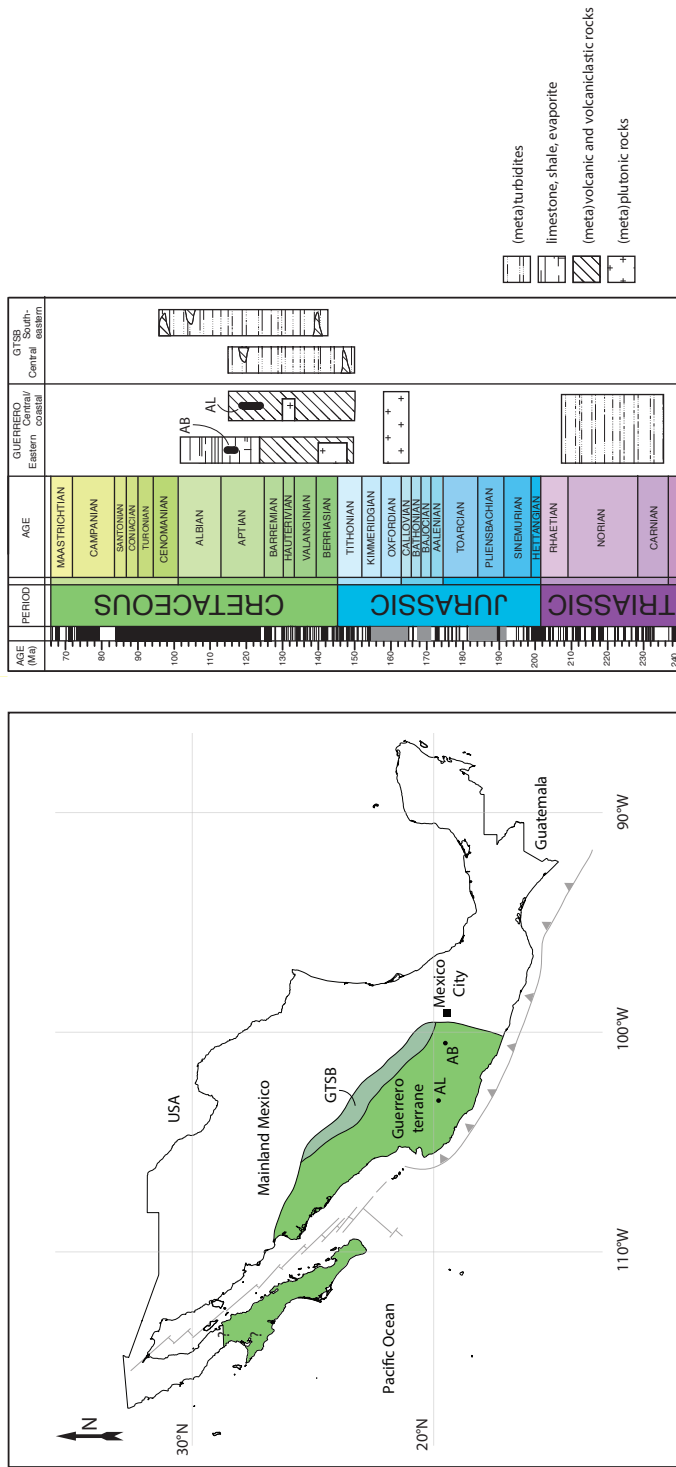
Figure 1: (A) Simplified geological map of the Guerrero terrane and the Guerrero terrane suture belt (GTSB), modified from Ortega-Flores et al. (2014), including sampling locations AL and AB. (B) Simplified stratigraphic column of the Guerrero terrane and the Guerrero terrane suture belt, modified from Centeno-García et al. (2008) and Martini et al. (2014).

(Centeno-García et al., 2003, 2008). The eastern boundary of Guerrero exposes sheared and folded metaturbidites interbedded with volcanic rocks, interpreted as remnants of an oceanic basin (the Arperos Basin) that separated the Guerrero terrane from the Mexican mainland (Freydier et al., 1996; Martini et al., 2011, 2014; Mendoza & Suastegui, 2000; Tardy et al., 1994). This deformed belt exposes Tithonian-Barremian felsic dykes and lava flows, containing Paleozoic and Precambrian inherited zircons, as well as Aptian-Cenomanian intraplate-like and mid-ocean ridge basalts (Elias-Herrera et al., 2000; Martini et al., 2011, 2014; Mortensen et al., 2008). This suggests that during the Tithonian-Barremian, the Arperos basin was floored by sediments derived from continental crust, or by continental crust itself, and oceanic crust formed since the Aptian. Accretion of the Guerrero terrane to mainland Mexico may have been diachronous, as a basaltic lava flow from the southeastern part of the Guerrero terrane suture belt, interpreted to reflect ongoing back-arc spreading, was dated at 93 Ma (Ar-Ar age, Elias-Herrera et al., 2000), whereas an undeformed sedimentary overlap assemblage on the central part of the Guerrero terrane suture belt yielded Albian paleontologic ages (Chiodi et al., 1988). After accretion, arc magmatism continued throughout western Mexico in the Sierra Madre del Sur and since the middle Miocene, in the Trans-Mexican Volcanic Belt (Ferrari et al., 2012; Morán-Zenteno et al., 2007)

3. Sampling locations

To resolve the absence of high quality paleomagnetic data from the early history of Guerrero, we extensively sampled two Lower Cretaceous sedimentary sections. In Michoacán state, near de town of Zitácuaro (locality AB, Fig. 1), we collected 133 samples from a sedimentary succession consisting of gray fine-grained sand, shale, limestone and some monomictic conglomerate containing limestone clasts. The samples were collected from fine-grained limestone intervals only. These limestone beds contain upper Aptian ammonites such as Dufrenoya sp., Huastecoceras sp., and Caseyella sp., as well as the planktonic foraminifera Globigerinelloides ferreolensis Moullade, G. aptiensis Longoria, Hedbergella trochoidea (Gandolfi), and H. roblessae (Obregón de la Parra) (C. González personal communication, 2013). This association corresponds to the upper Aptian (~119-112 Ma) Globigerinelloides ferrolensis fauna of (Premoli Silva & Verga, 2004).

In Jalisco state, near the town of Tamazula de Gordiano (locality AL, Fig. 1), we collected 168 samples of reddish andesitic sandstones and shales, at 5 sites (AL1-5) along two parallel roads ~8 km apart. These redbeds belong to the Alberca Formation, of which the age is not well constrained. Romo Ramírez et al. (2001) mapped the Alberca Formation as Valanginian-Hauterivian and interpreted it as the stratigraphically lowest volcanoclastics of the Guerrero arc succession in this region. However, Berriasian-Hauterivian and Barremian-Cenomanian ages (Cuevas (1981) and Grajales and López (1984), as cited in Centeno-García et al. (2008)) have also been reported. At site AL4, stratigraphically high in the sampled succesion, we took a sample for U-Pb detrital zircon dating to obtain a maximum depositional age.

a.

b.

c.

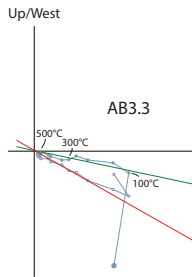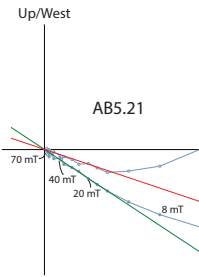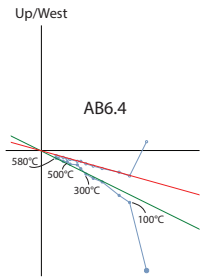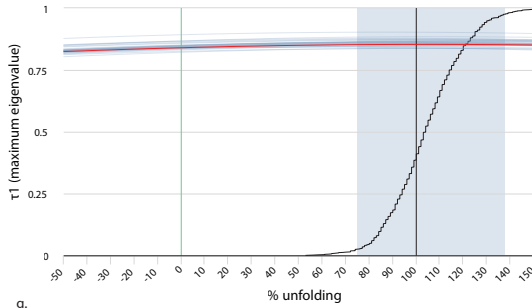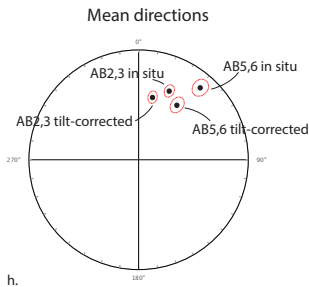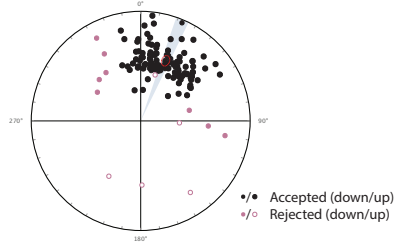
d.

e.

f.

g.

Mean directions

h.
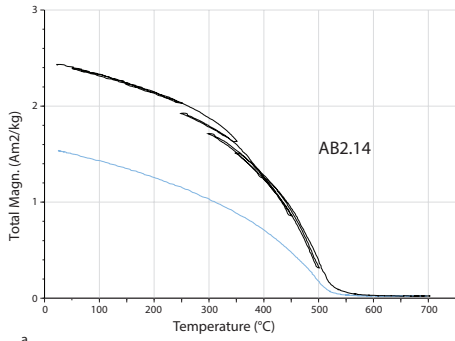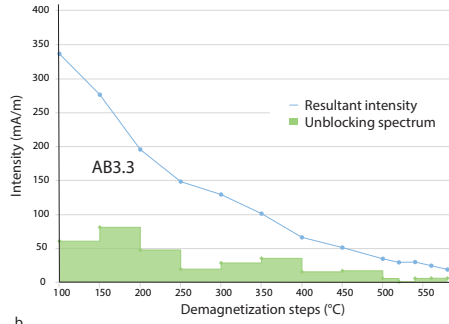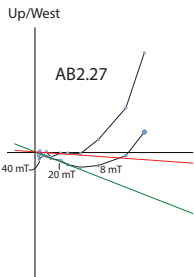
ChRM directions AB2,3,5,6
Tilt-corrected

i.

4. Methods

Paleomagnetic cores with a diameter of 2.5 cm were sampled with a gasoline-powered motor drill and their orientation was measured with a magnetic compass with an inclinometer attached. The cores were cut into samples of 2.2 cm length using a double blade circular saw. Laboratory analyses were carried out at the Paleomagnetic Laboratory Fort Hoofddijk of Utrecht University, the Netherlands. Thermomagnetic analyses to determine the nature of magnetic carriers were performed on representative samples for each site, using a horizontal translation-type Curie balance with a cycling applied magnetic field, usually 100-300 mT (Mullender et al., 1993). A number of heating-cooling cycles was applied to detect magneto-minerological alterations during heating. We used the following temperature scheme (in °C): 20-150, 50-250, 150-350, 250-400, 300-450, 350-500, 400-700. Furthermore, all 301 samples were subjected to either stepwise thermal (TH) or alternating field (AF) demagnetization and the natural remanent magnetizations were measured on a 2G DC SQUID cryogenic magnetometer. Demagnetization steps used were 4, 8, 12, 16, 20, 25, 30, 35, 40, 45, 50, 60, 70, 80, 90 and 100 mT for AF-treatment and variable temperature increments of 20-50°C up to 680°C for TH-treatment. Demagnetization diagrams were plotted on orthogonal vector diagrams (Zijderveld, 1967) and the magnetic components were determined via principal component analysis (Kirschvink, 1980). The fold test (Tauxe & Watson, 1994) and the bootstrapped coordinate reversal test (Tauxe, 2010) were used when applicable. We calculated site mean directions using (Fisher, 1953) statistics on virtual geomagnetic poles following statistical procedures described in (Deenen et al., 2011). A 45° cut-off was applied to the virtual geomagnetic poles per locality (Johnson et al., 2008). Sample interpretation and statistical analysis was conducted using the online portal Paleomagnetism.org (Koymans et al., 2016). We collected sandstone samp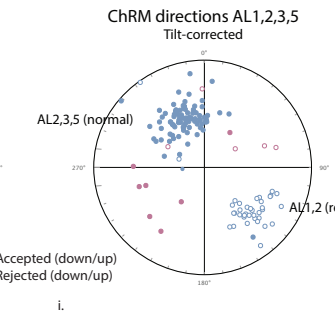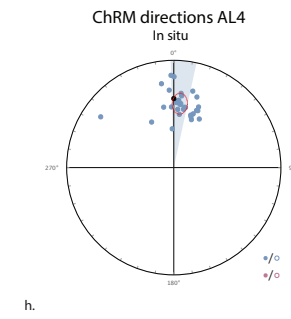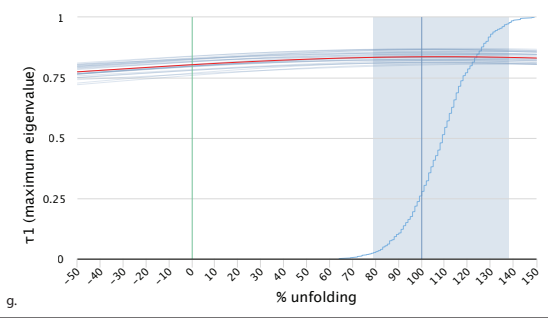le AL4DZ from site AL4 for LA-ICPMS U-Pb detrital zircon dating. The U-Pb dating analysis was performed at the Laboratorio de Estudios Isotópicos of the Centro de Geociencias of Universidad Nacional Autónoma de México, following the procedures described by (Solari et al., 2010; Solari & Tanner, 2011).

5. Results

5.1 Paleomagnetism

The thermomagnetic curves of the AB limestones are largely reversible, indicating that no alternation occurs during heating; Curie temperatures range 500-560°C, indicating that

Figure 2 (left page): Rock magnetic and paleomagnetic results from locality AB. (A) Thermomagnetic curve measured on a Curie balance. Heating in black; cooling in gray. (B) Intensity decay curve. (C–F) Orthogonal vector diagrams for in situ coordinates, where closed (open) symbols indicate declination (inclination). (G) Bootstrapped fol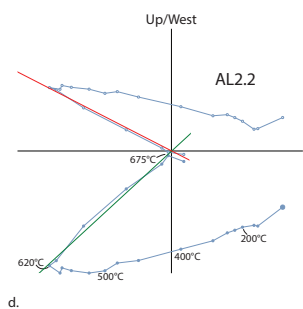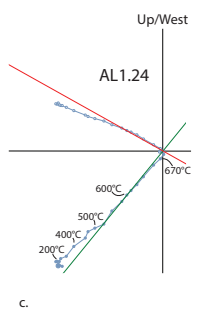d test, with cumulative distribution function (with confidence interval in light blue) based on 1000 bootstraps (average of bootstraps in red). (H) Mean directions for grouped sites AB2-AB3 and AB5-AB6 in both in situ and tilt-corrected coordinates. (I) Characteristic remanent magnetization (ChRM) values for sites AB2, AB3, AB5, and AB6 in tilt-corrected coordinates.

a.

b.

c. AL1.24

d. AL2.2

e. AL2.14

f. AL4.3

g.

h. ChRM directions AL4
In situ

i. ChRM directions AL1,2,3,5
Tilt-corrected

j. VGP positions AL1,2,3,5
Reversed directions converted to normal
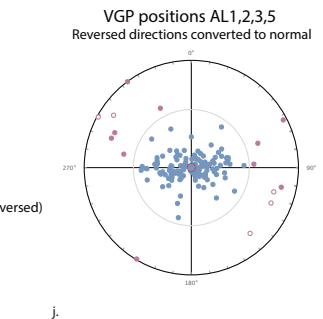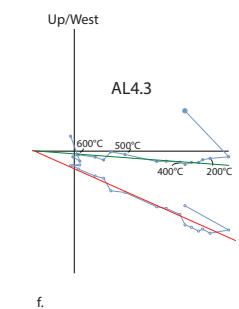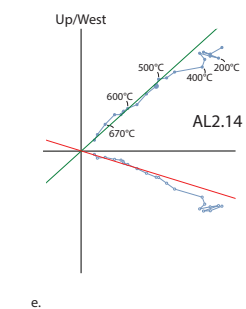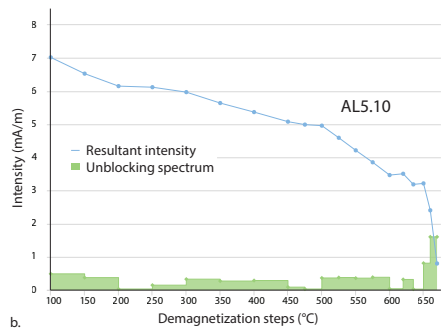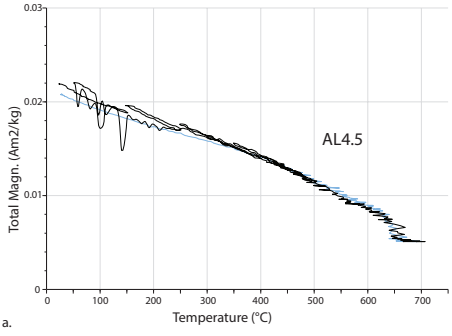
the main magnetic carrier is titanomagnetite (Fig. 2a). The intensity decay curve is in line with titanomagnetite (Fig. 2b), which is typical for a volcanic environment. We subjected samples from limestone locality AB to both TH and AF demagnetization treatments and isolated ChRMs at mid-range temperatures (~300-560°C) or ~16-40 mT (Fig. 2c-f). Initial intensities range 50-800 mA/m. All AB samples yield normal polarity directions. A slight difference in bedding orientation between AB2,3 and AB5,6 allows for a foldtest (Fig. 2g), which is positive (optimal clustering between 75-138% unfolding). However, AB2,3 and AB5,6 do not share a common true mean direction (CTMD), because declinations differ significantly between these two groups (Fig. 2h). Inclinations, however, are identical. Due to the resulting artificial elongation in the VGP position cluster, an inclination shallowing correction cannot be performed, but since limestones generally compact insignificantly, this is not problematic. The average ChRM direction (Fig. 2i) is Dec ± ΔDx = 22.5 ± 3.5°, Inc ± ΔIx = 40.5 ± 4.4°, n =117, K = 17.4, A95 = 3.2° (Fig. 2g, Table 1). There are four lines of evidence which support the primary nature of the magnetization: (1) both the in situ and bedding tilt-corrected directions differ significantly from the GAD field direction; (2) only normal directions are present, which is consistent with the late Aptian age of the section and magnetization acquisition during the Cretaceous normal superchron, (3) a fold test is positive, supporting pre-tilt magnetization acquisition; and 4) the distribution of the ChRMs satisfies the quality criteria of representing PSV (i.e. A95min= 1.8° < A95 = 3.2° < A95max = 4.1°; (Deenen et al., 2011)). The average ChRM direction results in a paleomagnetic pole at long. = 333.4º, lat. = 68.75º, A95 = 3.2º, K = 17.4.

Curie temperatures of the AL redbeds are 650-670°C (Fig. 3a), indicating that the magnetic carrier in the samples is hematite. The maximum applicable alternating field (100 mT) was not high enough to fully demagnetize these hematite-bearing redbeds, and therefore, all AL samples were measured by thermal demagnetization up to 680°C. Initial intensities range 8-80 mA/m and intensity decay curves of the demagnetizations indicate that the redbeds contain a mixture of pigmentary and detrital hematite (Fig. 3b). We interpreted a high temperature (~500-670°C) component as the characteristic remanent magnetization (ChRM) for sites 1, 2, 3 and 5 (Fig. 3c-e). Site AL4 only contains a very chaotic, or no high temperature component (Fig. 3f), and interpreting a lower temperature component (~300-550°C) yields a direction in in-situ coordinates of Dec ± ΔDx = 5.2 ± 6.7°, Inc ± ΔIx = 40.0 ± 7.1°, which is statistically indistinguishable from the local geocentric axial

Figure 3 (left page): Rock magnetic and paleomagnetic results from locality AL. (A) Thermomagnetic curve measured on a Curie balance. Heating in black; cooling in gray. (B) Intensity decay curve. (C–F) Orthogonal vector diagrams for in situ coordinates, where closed (open) symbols indicate declination (inclination). (G) Bootstrapped fold test, with cumulative distribution function (with confidence interval in light blue) based on 1000 bootstraps (average of bootstraps in red). (H) Characteristic remanent magnetization (ChRM) values from site AL4, in comparison to the geocentric axial dipole (GAD) field (gray diamond). (I) ChRM values from sites AL1, AL2, AL3, and AL5 in tilt-corrected coordinates. (J) Virtual geomagnetic pole (VGP) positions of sites AL1, AL2, AL3, and AL5.

Site(s)	N	N45(is)	N45(tc)	In-situ D	ΔD$_x$	I	ΔI$_x$	Tilt corrected D	ΔD$_x$	I	ΔI$_x$	k	a$_{95}$	K	A95min<A95<A95max
AB23	79	76	75	24.1	3.6	32.1	5.5	12.6	4.1	41.5	5.1	21.3	3.6	19.9	2.1<3.8<5.4
AB56	51	45	45	40.6	4.5	14.8	8.6	35.1	5.4	39.2	6.9	18.7	5.1	19.4	2.6<5.0<7.5
AB2356	**130**	**120**	**117**					**22.5**	**3.5**	**40.5**	**4.4**	**17.8**	**3.2**	**17.4**	**1.8<3.2<4.1**
AL1,2 (reversed)	38	35	36	124.6	3.1	-9	6	132.8	4.5	-36.5	6.1	24.3	4.9	33.7	2.9<4.2<8.6
AL2,3,5 (normal)	99	88	88	327.7	3.3	30.5	5	339.6	4	49.8	3.9	23.6	3.2	20.4	2.0<3.4<4.9
AL1235	**137**		**123**					**330.2**	**3.7**	**46.5**	**3.9**	**17.5**	**3.1**	**16.2**	**1.8<3.3<4.0**
AL4	27	26		7.7	5.3	40.1	6.7					32	5.1	35	3.3<4.9<10.5

N: number of demagnetized specimens; N45(is)/N45(tc): number of specimens that fall within the 45° cut-off in situ coordinates / after tilt correction

D: Declination, I: Inclination

Table 1: Paleomagnetic results

dipole (GAD) field direction (Dec = 0°, Inc = 36°, Fig. 3h). Therefore, we exclude this site from further analysis. Interpreted high-temperature directions from all samples from site AL1 yield reversed directions, whereas AL3 and AL5 yield normal directions. AL2 contains both normal and reversed directions, indicating the presence of a reversal within the analyzed sedimentary succession. A fold test (Fig. 3g) on the individual directions of sites AL1,2,3,5 is positive (optimal clustering with 79-138% unfolding). The clusters of reversed directions (AL1, part of AL 2) and normal directions (part of AL2 and AL 3 and 5) (Fig. 3i) do not pass the reversal test. A substantial part of the normal directions is closer to the GAD field direction, so the lack of a positive reversal test is probably best explained by an unresolved normal overprint, influencing the ChRM directions. To diminish this effect, we combine normal and reversed directions (see e.g. Scheepers & Langereis, 1993), yielding an average direction of Dec ± ΔDx = 330.2 ± 3.7°, Inc ± ΔIx = 46.5 ± 3.9°, n =123, K = 16.2, A95 = 3.3° (Fig. 3j, Table 1). Again, there are four lines of evidence which support the primary nature of the magnetization: (1) both the in situ and bedding tilt-corrected directions differ significantly from the GAD field direction showing the ChRM cannot be explained by a recent field; (2) both normal and reversed directions are present, suggesting magnetization acquisition during at least two magnetic polarity chrons, (3) a positive fold test, supporting pre-tilt magnetization acquisition; and 4) the distribution of the ChRMs satisfies the quality criteria of representing paleo-secular variation (PSV) (i.e. A95min = 1.8° < A95 = 3.3° <
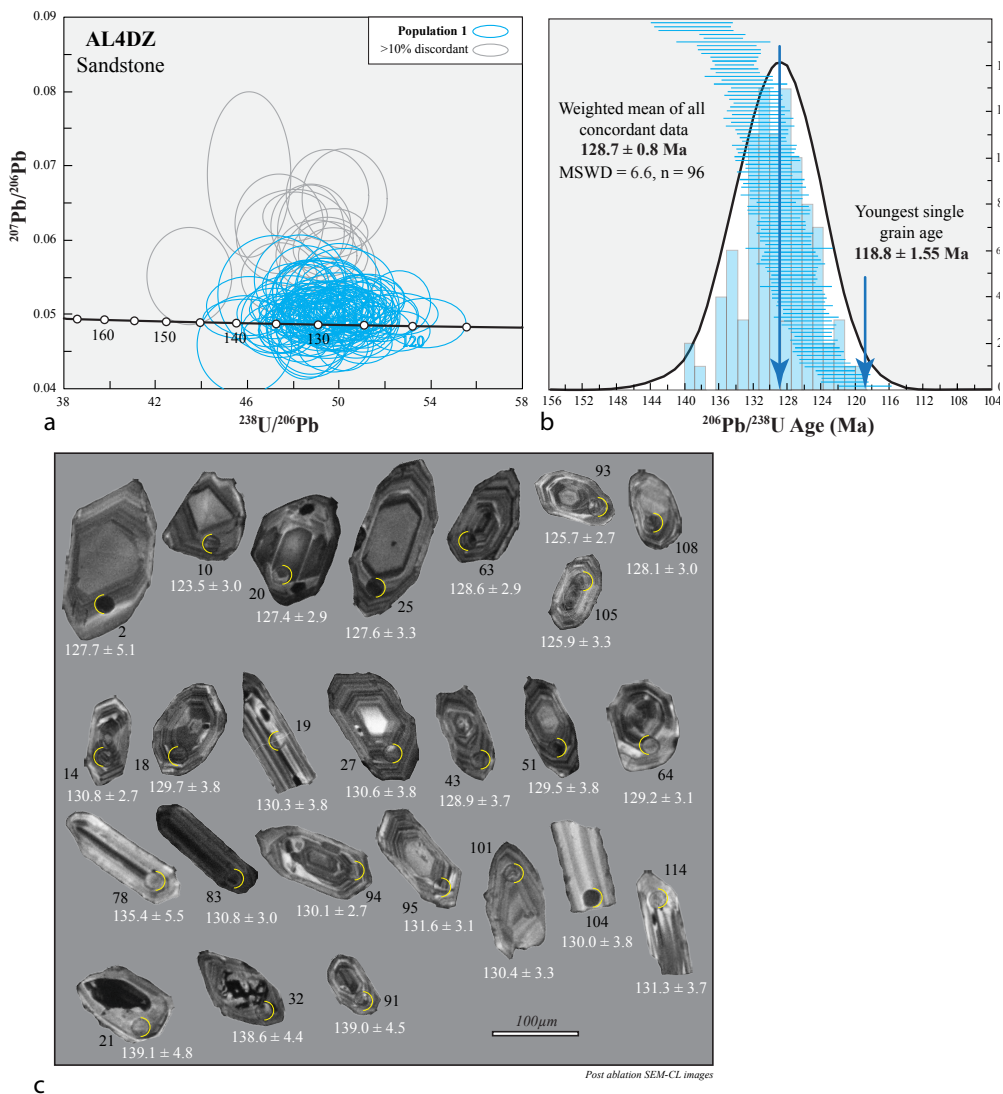
Figure 4: U-Pb age of sample AL2DZ. (A) Concordia diagram for U-Pb ratios. (B) 206Pb/238U ages. (C) Postablation scanning electron microscope (SEM) cathodoluminescence (CL) images of selected zircon crystals from this sample. MSWD— mean square weighted deviation.

A95max = 4.0°; (Deenen et al., 2011)). The cluster of VGP positions is slightly elongated (Fig. 3i), which may indicate inclination shallowing due to compaction (Tauxe and Kent, 2004). However, the elongated shape is in this case largely the result of combining AL1,2 (reversed) and AL2,3,5 (normal) with the fanning of the declinations as explained above. Furthermore, detrital hematite is expected to yield a wider range in declinations than

can be expected from secular variation, as a result of its mineral properties and way of sedimentation (Iosifidi et al., 2010; Tan et al., 2002; Tauxe & Kent, 1984). For these two reasons, application of the Tauxe and Kent (2004) inclination shallowing correction cannot be justified, as it would significantly overestimate the inclination. We note that compaction cannot be fully excluded, but argue that since the average inclination of the AB limestones (40.5 ± 4.4°) is replicated by the ~3 Myr older AL redbeds, a significant effect of inclination shallowing is highly unlikely. Inclination shallowing correction with a standard compaction factor of 0.6 (following Torsvik et al. (2012)) would increase the average inclination of the redbeds to 60.3°. This would predict a southward shift of the Guerrero terrane of ~2000 km within ~3 Myr, which would require unrealistic high tectonic speeds. We use the uncorrected average direction to calculate the paleomagnetic pole at long. = 191.81°E, lat. = 62.10°N, A95 = 3.3°, K = 16.2.

5.2 Depositional age of the Alberca Formation

Zircons from sample AL4DZ are subrounded to euhedral in shape and range in length from 80-200 μm. Some grains contain inherited cores, but in all cases, we dated the overgrown rims of the grains (Fig. 4c). Of the 111 measured zircon grains, 96 yielded concordant ages (10% cut-off, Table S1). Even though all ages fall within one group, the large dispersion (mean square weighted deviation (MSWD) = 6.6) indicates that this group is not one population (Spencer et al., 2016)(Fig. 4b). This is in line with the sedimentary nature of the rock, as single populations (associated with in-situ zircons) are expected for igneous and metamorphic rocks only (Spencer et al., 2016). To determine the maximum age of deposition, we use the youngest zircon age (youngest single grain age, following (Dickinson & Gehrels, 2009)) of 118.8 Ma ± 1.55 (1σ) (Fig. 4b). Sample AL4DZ occupies a stratigraphic high level within the sampled succession, and magnetic directions from the upper part of the succession yielded normal directions only, which is consistent with the zircon age overlapping the Cretaceous normal superchron (~125.9-83 Ma, Gradstein et al. (2012)). Lower levels (site AL1 and part of site AL2) of the sampled succession, however, yielded reversed directions and these strata must therefore pre-date the superchron, but are no older than the base of M0r (126.3 Ma, Gradstein et al., 2012). We thus conclude that the sampled succession spans at least a lowermost – mid Aptian age range (126-118 Ma).

6. Paleomagnetic database for Guerrero

We supplement our new data on the paleolatitudinal history of the Guerrero terrane with all those previously published (Fig. 5, Table S2). In general, papers presenting paleomagnetic data do not supply the original paleomagnetic directions per sample, but only site averages and their statistical parameters (N, k, α95). This is not problematic for lava sites, whereby acquisition of the natural remanent magnetization occurs geologically instantaneous upon cooling of the lava, and the recorded direction is a spot reading of the paleomagnetic field. For sedimentary or (slowly cooling) intrusive rocks, however, each individual sample cannot be considered a spot reading, and includes a certain amount of
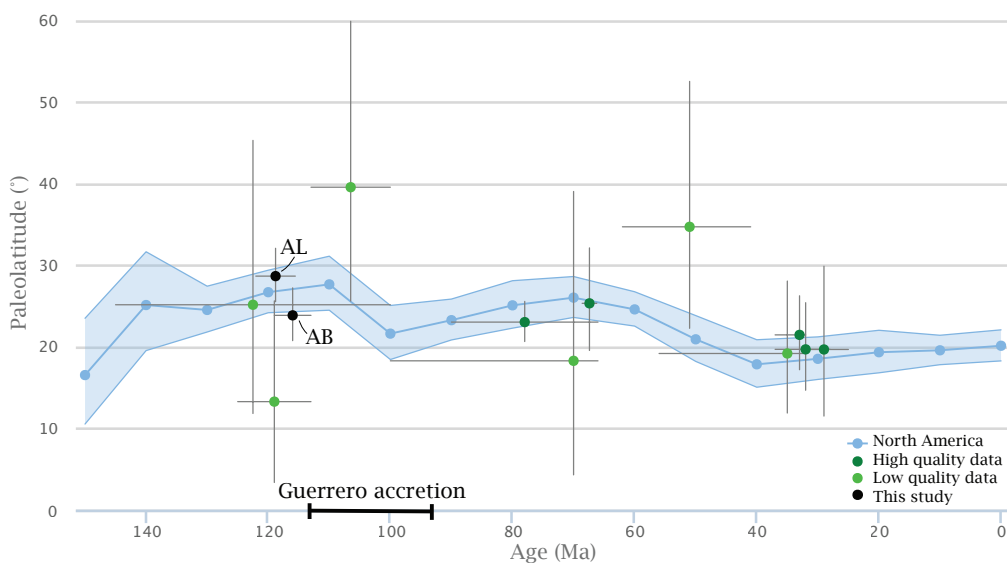
Figure 5: Overview of paleolatitudes of the Guerrero terrane, including data from Böhnel et al. (1989), Goguitchaichvili et al. (2003), Molina Garza et al. (2003), Molina Garza and Ortega Rivera (2006), Rosas- Elguera et al. (2011), Andreani et al. (2014), and this study. The data are plotted with respect to the expected paleolatitudes of the North American plate, calculated for a reference location within the Guerrero terrane (chosen at 20°N, 102°W). We used the reference values predicted by the global apparent polar wander path (GAPWaP) of Torsvik et al. (2012).

PSV. It is therefore preferred to perform statistics on the actual distribution of individual directions rather than on site averages (Deenen et al., 2011). To minimize this bias, we created parametrically sampled data sets for sites of intrusive or sedimentary rocks. For lava sites and (fast cooling) intrusive rocks with k≥50, we used site averages as single directions.

For the construction of the paleomagnetic database, we selected data according to the following quality criteria: (1) the total distribution of directions satisfies the quality criteria of representing PSV (i.e. A95min < A95 < A95max; (Deenen et al., 2011)); (2) sedimentary and intrusive rocks have n≥4, lavas have k≥50 (Biggin et al., 2008; Johnson et al., 2008), and at least 7 lava (or fast-cooling intrusive) sites could be averaged from a small area; (3) when not corrected for bedding-tilt (in their in-situ orientations), directions differ significantly from the local GAD field direction, and (4) bedding-tilt corrections are applied. Sites discarded by the original authors were not taken into account, if reasons were provided.

The database (Fig. 5) contains data sets consisting of 7-14 individual directions of the magnetic field (labeled low-quality) and data sets containing ≥20 directions (labeled high-

quality). High quality data are only available for the Late Cretaceous and younger history of the Guerrero terrane. The previously published and new poles show that paleolatitudes of the Guerrero terrane do not differ significantly from the paleolatitudinal path predicted for the North American Plate, both after collision, but notably also prior to collision (Fig. 5). In other words, motions of the Guerrero terrane in Early Cretaceous time, when it was separated from the North American Plate by a divergent plate boundary, were longitudinal only, and the Guerrero terrane did not undergo significant northward or southward motion relative to the North American Plate. Most paleomagnetic declinations indicate counterclockwise rotation, mainly concentrated in the Cretaceous, with perhaps a small rotation occurring after ~30 Ma.

7. Discussion

Paleomagnetic data from the Guerrero terrane yield a paleolatitudinal plate motion history equal to that of the North American Plate since Early Cretaceous time. This implies that, even though the Guerrero terrane must have been located on a separate 'Guerrero' Plate in Aptian time, relative plate motion between the North American Plate and the Guerrero Plate was longitudinal only. Our new data are thus consistent with paleogeographic models, based on field and petrologic data, in which the Guerrero arc successions formed on North American crust that rifted away from the Mexican mainland by opening of a back-arc basin above an eastward dipping subduction zone, as proposed by e.g. Cabral-Cano et al. (2000), Elias-Herrera et al. (2000), Martini et al. (2009, 2014) (Fig. 6). Additionally, it contradicts paleogeographical models that place the Guerrero terrane on the Farallon Plate (Dickinson and Lawton, 2001; Umhoefer, 2003; Sigloch and Mihalynuk, 2013), which would predict latitudinal motion between the Guerrero terrane and the North American Plate prior to accretion (Doubrovine & Tarduno, 2008; Seton et al., 2012; Wessel & Kroenke, 2008; Wright et al., 2016). Assessing the validity of the paleogeographical model of Hildebrand (2013, 2015) by plate kinematic data is difficult, as this model does not define tectonic plates, nor does it indicate the relative latitudinal plate motions of the Rubian ribbon continent prior to its postulated ~125 Ma collision with North America. However, Hildebrand (2013) states: "relative to North America the Rubian ribbon continent migrated south until 80-75 Ma when its relative displacement reversed to dextral". These post-collisional south and northwards shifts are not in agreement with paleomagnetic data of the Guerrero terrane. Furthermore, the mismatch between the Hildebrand-hypothesis and the large body of geological studies suggesting a North American provenance of the Guerrero terrane (e.g. Cabral-Cano et al., 2000; Centeno-García et al., 2008, 2011; Elias-Herrera et al., 2000; Fitz-Díaz et al., 2017; Martini et al., 2011) indicates either that the Guerrero terrane was not part of the Rubian ribbon continent, or that this paleogeographic model should not be considered as a plausible model for the assembly of the Mexican Cordillera.

As paleomagnetism cannot constrain paleolongitudes, the magnitude of longitudinal plate motion of the Guerrero terrane relative to North America related to the opening

and closure of the Arperos Basin remains unconstrained. During deposition of the Alberca Formation, sediments with a continental provenance did not reach the Guerrero terrane, as evidenced by the absence of any pre-Cretaceous zircons. This may give an indication of a substantial width of the Arperos Basin, although this might also be explained by the presence of significant morphological features within the basin (e.g. the spreading ridge) that prevented mixing of sediments derived from opposite sides. The presence of inherited cores within the zircon crystals suggests that the melts forming the mainly Barremian magmatic rocks intruded older crustal material. An earlier study on provenance of arc-related volcaniclastics of the Guerrero terrane (Talavera-Mendoza et al., 2007) demonstrated sediment influx through grain recycling from a variety of ultimately North and South American continental sources.

In recent years, the subduction evolution of the Cordillera received increased interest because it contains the key to interpreting the complex mantle structure below North America (e.g. Sigloch, 2011; Sigloch et al., 2008; Sigloch & Mihalynuk, 2013; van der Meer et al., 2012, 2018). Tomographic images of especially the lower mantle below North America and the eastern Pacific Ocean reveal a large number of positive wave speed anomalies that are interpreted as subducted slab remnants (Sigloch & Mihalynuk, 2013; van der Meer et al., 2012, 2018). These studies argued that some (van der Meer et al., 2012, 2018) or all (Sigloch & Mihalynuk, 2013) of these slab remnants resulted from Mesozoic intra-oceanic subduction within
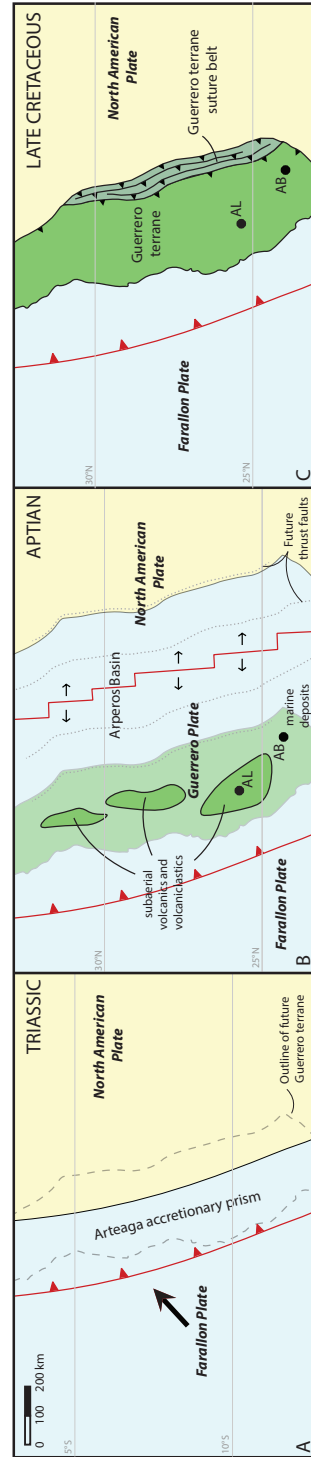
Figure 6: Mesozoic tectonic evolution of the Guerrero terrane. (A) Triassic: continental margin subduction, and development of the Arteaga accretionary prism. (B) Aptian: spreading within the Arperos Basin, formation of the Guerrero plate, and deposition of AB limestones and AL red beds. (C) Late Cretaceous: closure of the Arperos Basin, accretion of the Guerrero terrane to the Mexican mainland, and formation of the Guerrero terrane suture belt.

CHAPTER 3

115

the northeastern Panthalassa Ocean. In this context, the Guerrero terrane was correlated to either the westward subducted Mezcalera slabs (Sigloch & Mihalynuk, 2013), which correspond to the Hatteras slab of van der Meer et al. (2018), or to the equatorial Malpelo slab (van der Meer et al., 2018), both of which were interpreted to be the result of intra-oceanic subduction, suggesting an exotic nature of the Guerrero terrane. Previous field and petrologic studies, as well as our paleomagnetic analysis indicate that formation of the Guerrero terrane was instead the result of a phase of overriding plate extension within the long-lived eastward continental margin subduction system. A reinterpretation of the correlations between slabs and arcs in the Cordillera is beyond the scope of this paper, but our results ask for revision of the previous correlations between the Guerrero terrane and lower mantle slab remnants, and may provide a strong tie point for the correlation of the western North American continental margin to the mantle in Mesozoic times.

8. Conclusions

• Paleomagnetic data from the Guerrero terrane yield a paleolatitudinal plate motion history equal to that of the North American Plate since Early Cretaceous time.

• This confirms the previously developed paleogeographic model in which the Guerrero arc successions form on North American crust that rifted away from the Mexican mainland by opening of a back-arc basin above an eastward dipping subduction zone.

• It contradicts alternative paleogeographical models in which the Guerrero terrane is considered to be exotic to the North American continent.

4

220 Myr of Farallon Plate subduction below Mexico

Pelicans on the San Hipólito Formation - Vizcaíno Peninsula, Mexico

Abstract

Global tectonic reconstructions of pre-Cenozoic plate motions rely primarily on paleomagnetic and geological data from the continents, and uncertainties increase significantly with deepening geological time. In attempting to improve such deep-time plate kinematic reconstructions, restoring lost oceanic plates through the use of geological and seismic tomographical evidence for past subduction is key. The North American Cordillera holds a record of subduction of oceanic plates that composed the northeastern Panthalassa Ocean, the large oceanic realm surrounding Pangea in Mesozoic times. Here, we present new paleomagnetic data from subduction-related rock assemblages of the Vizcaíno Peninsula of Baja California, Mexico, which yield a paleolatitudinal plate motion history equal to that of the North American continent since Late Triassic time. This indicates that the basement rocks of the Vizcaíno Peninsula formed in the fore-arc of the North American Plate, adjacent to long-lived eastward-dipping Farallon subduction at the southern part of the western North American continental margin. In addition, tomographic images confirm long-lived, uninterrupted eastward subduction. We correlate episodes of overriding plate shortening and extension to flat and steep segments. By integrating paleomagnetic, geological, and tomographic evidence, we provide a first order model that reconciles absolute North American plate motion and the deformation history of Mexico with modern slab structure and Farallon subduction history since Late Triassic time.

1. Introduction

Global tectonic reconstructions of pre-Cenozoic plate motions rely primarily on paleomagnetic and geological data from the continents, as the vast majority of Mesozoic and older oceanic lithosphere has been lost to subduction. As a result, deep-time reconstructions portray the distribution of continental plates through geological time, but lack information on plate motions and -geometry in the oceanic domains. In attempting to improve such deep-time plate kinematic reconstructions, restoring lost oceanic plates is therefore key. This relies on deciphering the geological history of relics of such plates now found within orogenic belts or accretionary prisms (e.g. Domeier et al., 2017; Gürer et al., 2016; Maffione et al., 2017; Nokleberg, 2000). In parallel, the analysis of seismic tomography models of present-day mantle structure contributes to the development of paleogeographic models and tectonic reconstructions. (e.g. Domeier et al., 2017; Sigloch & Mihalynuk, 2013; van der Meer et al., 2012; Van der Voo et al., 1999a, 1999b; Wu et al., 2016). Correlations of preserved geological subduction records to imaged mantle structure suggests that the mantle holds a memory of ~250-300 Myr of subduction (Butterworth et al., 2014; Hafkenscheid et al., 2006; van der Meer et al., 2010, 2018; Van der Voo et al., 1999a; van Hinsbergen et al., 2005). Here we present a combined analysis focused on the subduction history of the Farallon Plate by using a combination of geological, paleomagnetic and tomographic evidence for deep mantle subduction below Mexico.
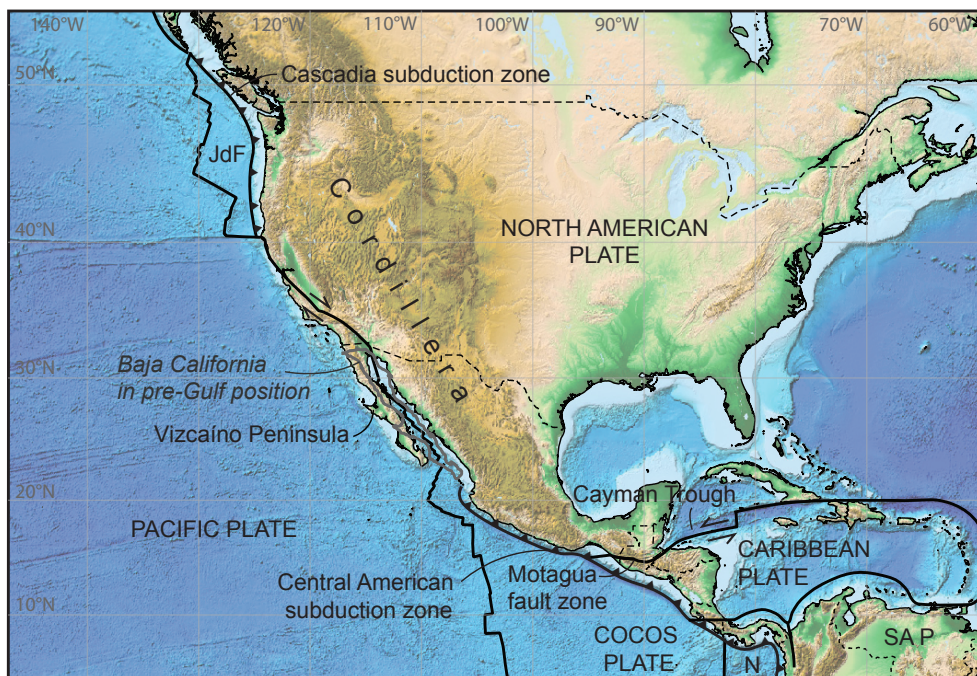
Figure 1: Tectonic map of the North American Cordillera, including the North American, South American (SA P), Caribbean, Pacific, Juan de Fuca (JdF), Cocos and Nazca (N) plates. Also including the position of Baja California prior to Gulf of California opening relative to a stable North American Plate.

The North American Cordillera comprises the intensely deformed western part of the North American continent and preserves a geological record of subduction of oceanic plates that were once underlying the northeastern paleo-Pacific or Panthalassa Ocean, such as the Farallon and Kula plates (Debiche et al., 1987; Engebretson et al., 1985). This record of subduction resulted from both overriding plate deformation (i.e. the opening and closure of fore- and back-arc basins and formation of overriding plate, Andean-style fold-thrust belts), as well as the accretion of far-travelled intra-oceanic arcs, oceanic plateaus, deep marine sediments, and ophiolites (e.g. Nokleberg, 2000). In line with the geological evidence of a complex, long-lived history of subduction, a mosaic of positive wave speed anomalies interpreted as (mainly detached) subducted slab remnants are present below North America and the present-day Pacific realm (e.g. Liu et al., 2010; Meijers et al., 2010b; Sigloch & Mihalynuk, 2013; van der Meer et al., 2012, 2018). Linking such detached slabs to surface records of subduction requires control on absolute plate motions (i.e. plate motion relative to the lower mantle) and is challenging. The best-constrained absolute plate motion frames, based on hotspots (Doubrovine et al., 2012; O'Neill et al., 2005), do not extend further back in time than ~120-130 Ma. Reference frames for earlier times are based on paleomagnetism (with or without true polar wander

correction) and have therefore no absolute paleolongitudinal control (Steinberger & Torsvik, 2008; Torsvik et al., 2012). Recent frames have attempted to provide such control using correlation of surface geology to deep mantle structure (Torsvik & Cocks, 2016; van der Meer et al., 2010), but remain subject to large uncertainties. As a consequence, correlations of seismic tomography to Mesozoic Cordilleran subduction records have led to paleogeographic interpretations that are markedly different for pre-mid-Cretaceous times, which are best summarized by scenarios with (Shephard et al., 2013; van der Meer et al., 2012) or without (Sigloch & Mihalynuk, 2013, 2017) subduction directly under the North American continental margin.

Contrary to ancient subduction and detached slabs, the establishment of a link between a mantle anomaly and a geological subduction record is straightforward for active subduction. Today, the Juan de Fuca and Cocos plates, both considered relics of the Farallon Plate, subduct eastwards below the continental margin of North America (Fig. 1). Seismic tomography shows that subduction of the Juan de Fuca Plate at the Cascadia subduction zone is associated with a short upper mantle slab that is thought to represent only the last 16-18 Myr of subduction (Obrebski et al., 2010; van der Meer et al., 2018). On the contrary, the slab connected to the Cocos Plate, subducting below Mexico and Central America, is the longest apparently continuous slab, stretching from the uppermost mantle at the Central American trench in the west towards the lowermost mantle below the Atlantic Ocean in the east (Fig. 2). This slab represents the lithosphere that was consumed at a long-lived plate boundary between the Panthalassa plate system and the Indo-Atlantic plate system, thereby providing a measure for relative plate motions between the two, as well as a starting point for the interpretation of the much more complex mantle structure surrounding this slab, related to subduction below and west of the Americas and the Caribbean region.

In Mexico, subduction-related rock assemblages are present that date back to the Triassic. Boschman et al. (2018)(Chapter 3) recently showed that Lower Cretaceous and younger records of subduction in Mexico tracked the paleolatitudinal motion of North America, and may thus be readily tied to the (deforming) North American Plate. Older records associated with subduction are exposed in the Vizcaíno-Cedros region of Baja California, but it remains unknown whether these represent far-traveled intra-oceanic subduction relics that were accreted to the North American margin, or whether these also were part of the deforming North American upper plate. If the former, they provide no constraints on the age of subduction initiation of Farallon below Mexico, if the latter, they would show sustained subduction since the Triassic. Either way, the record may provide key constraints on the longevity of subduction below Mexico.

Here, we present new paleomagnetic data from Triassic supra-subduction zone ophiolitic, as well as Jurassic arc-related sedimentary cover rocks from the Vizcaíno Peninsula of west-central Baja California, and compile previous results, to test whether these rock

units may be considered part of the (deforming) North American upper plate. We use the results to evaluate the longevity of Farallon subduction below Mexico, and we evaluate whether the deformation history of the western North American margin in combination with the shape of the Farallon-derived slab imaged in modern mantle structure may provide a novel first-order control on absolute plate motion evolution.

2. Seismic tomography below Mexico

The positive wave speed anomaly associated with subduction along the Central American trench (Fig. 2) was one of the first anomalies interpreted as deeply subducted oceanic lithosphere (Bijwaard et al., 1998; Grand et al., 1997; Jordan & Lynn, 1974). The geometry and length of the slab changes along strike with a marked transition across the sinistral Motagua fault zone in Guatemala, which forms the western part of the Caribbean - North American plate boundary. To the north, the slab is flatter, longer, and thinner (Fig. 2b), and consists of both large flat-lying and steeper segments. To the south (Fig. 2a), the slab is steeper, shorter and thicker, and flat-lying segments are largely absent. Even further north (Fig. 2c), lower mantle structure is comparable to that in Figure 2b, but no anomaly is imaged in the upper ~400 km of the mantle. This is in line with the cessation of subduction at this latitude upon arrival of the Pacific-Farallon ridge in Miocene times (Atwater, 1998; Lonsdale et al., 1992). Young, hot Farallon lithosphere that subducted
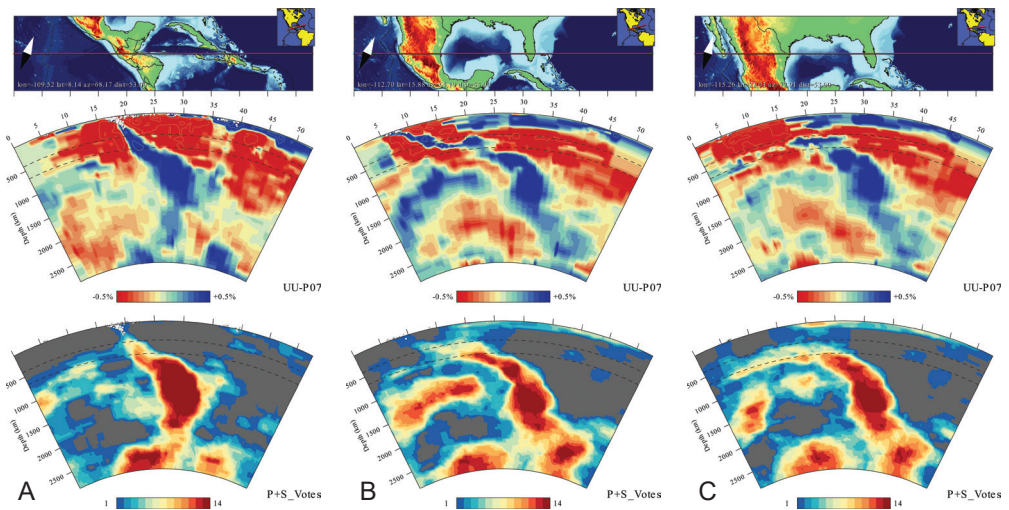
Figure 2: Seismic tomographic cross-sections along great circle segments (straight horizontal line in geographic maps) of the Cocos slab (central panels). a) Section south of the North American – Caribbean plate boundary; b) north of this boundary; c) across southern Baja California. The tomographic model is the P-wave seismic velocity model UU-P07 (Amaru, 2007). Units along the great circle arc are degrees measured from the start of the section. The lower panels show votemaps of 7 seismic P-wave velocity and 7 S-wave velocity models (Shephard et al., 2017).

just before arrival of the ridge may have been partly thermally assimilated by now, which further complicates detection with seismic tomography. The length and continuity of the slab (south of Baja California) suggests long-lived, uninterrupted eastward subduction below the North American continent, which is supported by subduction modeling (Liu, 2014). This anomaly is widely known as the Farallon slab (Bijwaard et al., 1998; Grand et al., 1997), referring to the interpreted plate that this slab contains. However, in their global compilation of slabs, (van der Meer et al., 2018) renamed it the Cocos slab, which was named as such after its geographic occurrence - the slab is currently connected to the Cocos Plate - to avoid tectonic interpretation in slab nomenclature. We will hereafter refer to this anomaly as the Cocos slab (van der Meer et al., 2018), but we note that its formation resulted from subduction of both Farallon and Cocos lithosphere. Votemaps (Shepard et al., 2017), constituting an average of 7 P-wave and 7 S-wave velocity tomography models, show general agreement on the existence of an inclined positive wave speed anomaly across the entire lower mantle (Fig. 2).

3. Geological setting
3.1. Subduction record of Mexico
Subduction below Mexico produces and produced arc volcanism in the Trans-Mexican volcanic belt and Upper Cretaceous-Cenozoic arc magmatic provinces covering much of the continental margin of western Mexico (Ferrari et al., 2007). Older, Upper Triassic - Lower Cretaceous subduction assemblages are found in the Guerrero terrane of western Mexico, and within the Alisitos arc terrane of the Baja California Peninsula (Busby et al., 1998; Campa & Coney, 1983) (Fig. 3). The Upper Cretaceous-Cenozoic arc complexes are widely interpreted as continental margin volcanism, but some regional paleogeographic and tectonic models postulated that the older, Triassic-Early Cretaceous assemblages were part of a large, allochthonous arc terrane that formed >1000 km west of, and plate kinematically independent from North America, as a result of intra-oceanic subduction within the northeastern Panthalassa realm (Hildebrand, 2013; Sigloch & Mihalynuk, 2013, 2017). Field, petrological, and sedimentological studies of the Guerrero terrane have mounted evidence, however, that the Guerrero terrane is built on North American margin rocks. The terrane became temporarily separated from North America as a result of Late Jurassic-Early Cretaceous Arperos back-arc basin opening, which was subsequently inverted to close in mid-Cretaceous time, all within the overriding plate of an eastward dipping subduction zone below North America (Cabral-Cano et al., 2000; Centeno-García, 2008, 2011, 2017; Elias-Herrera et al., 2000; Martini et al., 2011). Boschman et al. (2018) recently showed that the paleolatitudinal motion of the Guerrero terrane follows North American plate motion since Early Cretaceous time, confirming the latter hypothesis.

The Guerrero arc is built upon Triassic (Carnian-Norian) sequences of turbiditic sandstones, black shales, cherts, and conglomerates containing meter- to mountain-size lenses of basalt, gabbro, chert, and limestone (Centeno-García, 2005; Centeno-García
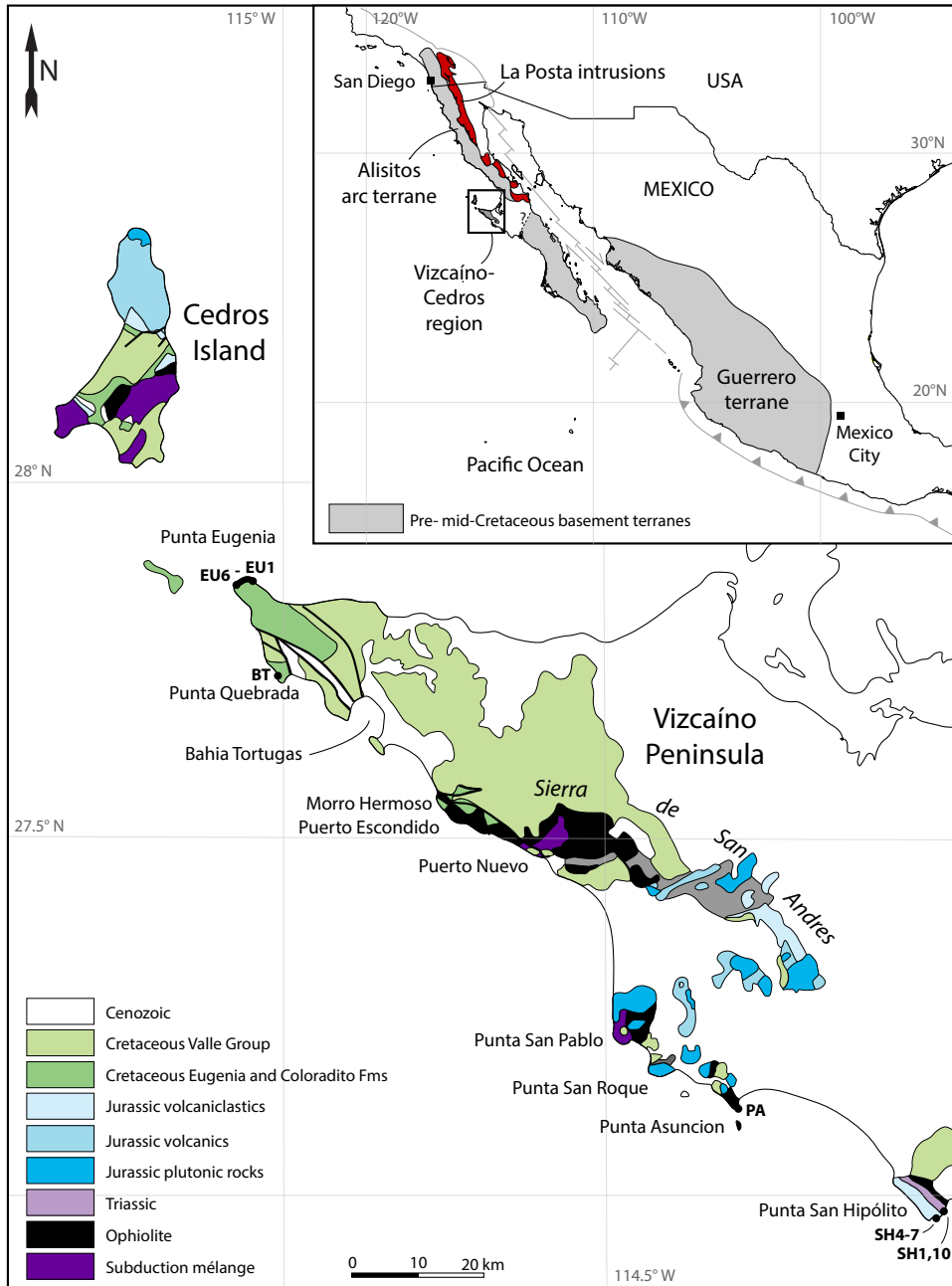
Figure 3: Geological map of the Vizcaíno Peninsula and Cedros Island, including sampling locations BT, PA, SH and EU, modified from (Kimbrough & Moore, 2003). Inset: pre- mid-Cretaceous basement terranes in western Mexico, modified from Ortega-Flores et al. (2014) and Kimbrough et al. (2006).

et al., 2003). The abundant turbiditic sandstones contain detrital zircons that yield Grenvillian (1.1 Ga), Pan-African (650-480 Ma) and Permian (260 Ma) U-Pb ages that match the signature of the Mexican continental mainland and the northwestern margin of the South American continent (Centeno-García et al., 2011). The Triassic sequences are intensely folded and, in some areas, metamorphosed to greenschist or amphibolite facies, and are interpreted as an accretionary prism structurally overlying a subduction mélange (Centeno-García, 2005; Centeno-García et al., 1993).

The Baja California Peninsula of northwestern Mexico contains subduction records of similar age. Its basement consists of a series of northwest-trending belts dominated by plutonic rocks of Cretaceous age. The peninsula became separated from the Mexican mainland and moved ~2.5° northward in late Cenozoic time during the opening of the Gulf of California, which is linked to the San Andreas transform fault system (Elders et al., 1972; Larson et al., 1968; Lonsdale, 1989; McQuarrie & Wernicke, 2005; Stock & Hodges, 1989). The peninsula consists of the Vizcaíno-Cedros region, exposing Triassic-Cretaceous subduction-related assemblages, a western belt (the Alisitos arc terrane), consisting of Lower Cretaceous volcanic, volcaniclastic and plutonic rocks, which intruded and overlie either continental margin or oceanic crust, and an eastern belt consisting of Upper Cretaceous "La Posta –type" plutons, which intruded in continental crust (Busby, 2004; Busby et al., 2006; DePaolo, 1981; Gastil et al., 1975; Gromet & Silver, 1987; Kimbrough et al., 2001, 2006, 2014; Premo et al., 2014; Schmidt et al., 2002, 2014; Silver & Chappell, 1988; Silver et al., 1979; Todd & Shaw, 1985; Wetmore et al., 2002, 2003). The boundary between the western and eastern belts is characterized by a series of west-vergent ductile thrust faults that are locally cut by the plutons of the eastern belt, from which fault activity prior to ~99 Ma was inferred (Johnson et al., 1999; Kimbrough et al., 2001). Due to the similarities between the geological history of the Alisitos and Guerrero terranes, as well as the detrital zircon ties of both arc terranes to the North American continent, these terranes are considered to be lateral equivalents. Both arcs are underlain by a basement of Triassic-Jurassic rocks, in the Guerrero area interpreted as an accretionary prism that formed at the continental margin (Centeno-García et al., 1993, 2011; Schmidt et al., 2014; Talavera-Mendoza et al., 2007). In Early Cretaceous time, the arcs terranes separated from the continent and did not receive cratonal sedimentary detritus until after their mid-Cretaceous collision with North America (Alsleben et al., 2012; Boschman et al., 2018 (Chapter 3); Busby et al., 2006; Talavera-Mendoza et al., 2007).

3.2. Geology of the Vizcaino Peninsula
The Vizcaíno-Cedros region (Fig. 3) is located along the west-central coast of Baja California ~600 km south of the USA-Mexican border and exposes subduction-related rock-units of Triassic to Cretaceous age (Busby, 2004; Kimbrough & Moore, 2003) that are the focus of this study. Upper Jurassic-Cretaceous fore-arc basin deposits of the Eugenia Formation and Valle Group are widely distributed across the Vizcaíno-Cedros region and are analogous to classic Great Valley Group fore-arc strata of California (Jones et al.,

1976). On Cedros Island, supra-subduction zone (SSZ) ophiolite and arc rocks beneath this fore-arc cover comprise a Middle Jurassic ophiolite/arc assemblage, while on the Vizcaíno Peninsula the Upper Triassic Vizcaíno ophiolite dominates the basement. As the paleomagnetic data presented here are from rocks units on the peninsula only, we limit the description of tectonic, intrusive and stratigraphic units to the Vizcaíno Peninsula.

The main topographic feature of the Vizcaíno Peninsula is the Sierra de San Andres, a ~60 km long east-southeast-trending mountainous region with elevations up to 650 m. Limited topography in the rest of the Vizcaíno Peninsula restricts most other outcrops to the coastal areas. From structurally low to high, four units are identified (1) a subduction mélange; (2) an ophiolite with overlying marine sediments; (3) a volcanic-plutonic complex; and (4) clastic sequences interpreted as fore-arc basin sediments (Barnes, 1984; Jones et al., 1976; Kimbrough, 1985; Kimbrough & Moore, 2003; Rangin et al., 1983). The structurally lowest unit of the Vizcaíno Peninsula is the Puerto Nuevo subduction assemblage: a serpentinite matrix mélange, incorporating exotic blocks of greenschist, blueschist, metagabbro, orthogneiss, amphibolite, eclogite, metabasalt and chert. The mélange is exposed in a window in the core of an antiform forming the western part of the Sierra de San Andres (Moore, 1986).

Structurally overlying is the Upper Triassic Vizcaíno ophiolite, cropping out in the northwestern part of the Sierra de San Andres and in some isolated exposures along the coast from Punta Quebrada in the north to Punta San Hipólito in the south. The most complete ophiolitic section is exposed in the Sierra de San Andres, where the ophiolite forms a west-plunging antiform and exposes serpentinized harzburgite-dunite tectonite, gabbro, dykes, sills and pillow basalts with a total estimated thickness of 3 km (Kimbrough & Moore, 2003). Other, more dismembered ophiolite sections vary from exposing gabbro, sheeted dykes and pillow lavas (Punta Asuncion) to only pillow lavas (Punta San Hipólito, Fig. 3). The ophiolite is dated by radiolaria in inter-pillow limestones at Punta Quebrada and near Morro Hermoso (Carnian to upper-middle Norian, ~237-215 Ma (Barnes, 1984)), by sphene U-Pb dating of a gabbro dyke in the northern flank of the antiform of the Sierra de San Andres (220 ± 2 Ma (Barnes & Mattison, 1981)) and by zircon U-Pb dating of a plagiogranite in the southern flank (221 ± 2 Ma, Kimbrough & Moore, 2003). Based on geochemical analysis, the Vizcaíno ophiolite is interpreted to have formed in a supra-subduction zone setting (Moore, 1983, 1985). The magmatic ophiolite section is conformably overlain by siliceous and pelagic sediments of Norian to Early Jurassic age. The cover of the Sierra de San Andres ophiolite is a 200-300 m section of vitric tuffs, tuffaceous chert, sandstone, and limestone (Barnes, 1984). These sediments are correlated with a thin sequence of pink dolomite and red chert overlying the pillows at Punta Quebrada, and with a 2400m thick sequence of green chert, limestone, breccia and sandstone at Punta San Hipólito (Barnes, 1982, 1984; Finch & Abbott, 1977).

Intruding and overlying the ophiolitic basement is an Upper Jurassic arc volcanic-plutonic complex, mainly cropping out in the southeastern part of the Sierra de San Andres and around San Pablo and San Roque. The complex contains gabbroic to granodioritic intrusions, andesite lavas, and breccia and pillow lavas, interbedded with volcaniclastic sandstone, conglomerate, and breccia (Kimbrough & Moore, 2003). K-Ar (hornblende, biotite) and U-Pb (zircon) ages from plutonic rocks range from ~160-135 Ma (Barnes, 1982, 1984; Kimbrough & Moore, 2003; Torres-Carrillo et al., 2016; Troughton, 1974). The volcanic rocks in the Sierra de San Andres have island-arc tholeiitic and boninitic geochemical affinities (Moore, 1983) and the volcaniclastic rocks are interpreted as proximal coarse-grained debris aprons deposited along a steep volcanic slope (Moore, 1984).

The sedimentary Eugenia Formation consists of Tithonian-Valanginian (Barnes, 1984) marine volcanogenic strata intercalated with local pillow lavas and major sedimentary olistostrome intervals with megablocks of Triassic chert and Paleozoic sandstone (Kimbrough & Moore, 2003). It is in depositional contact with the Vizcaíno ophiolite and its sedimentary cover (Kimbrough & Moore, 2003). A tuff within the Eugenia Formation at the northern tip of the Vizcaíno Peninsula is dated at 141.5 ± 3 Ma (Hickey, 1984), which is within the age range of the plutons of the Sierra de San Andres arc, suggesting that the strata of the Eugenia Formation are derived from the arc volcanoes of the Sierra de San Andres volcanic-plutonic complex (Barnes, 1984; Minch et al., 1976; Rangin, 1978). The Eugenia Formation is interpreted to have formed in a basin that collected active arc volcaniclastic debris as well as erosional material from exposed basement at topographic highs on the edges of the basin (Kimbrough & Moore, 2003). Detrital zircon U-Pb ages from Eugenia Formation strata document significant components of Appalachian-derived Paleozoic (480-300 Ma), Pan African (641-531 Ma), and Grenville (1335-950 Ma) grains that indicate alongstrike correlation of the Vizcaíno fore-arc to the Great Valley Group of California and indicate deposition within the same west-facing arc system (Kimbrough et al., 2014).

Overlying the Eugenia Formation are the widely exposed Aptian-Albian to Eocene, dominantly deep-marine strata of the Valle Group, interpreted as fore-arc basin turbidites (Busby-Spera & Boles, 1986; Kimbrough et al., 2001, 2006; Patterson, 1984; Smith & Busby, 1993).

Many authors have interpreted the Vizcaíno-Cedros ophiolite and arc complexes as allochthonous intra-oceanic terranes that accreted to the North American margin by Late Jurassic time, formed either above a Triassic-Jurassic westward dipping (Boles & Landis, 1984; Busby-Spera, 1988; Critelli et al., 2002; Sigloch & Mihalynuk, 2017) or eastward dipping subduction zone (Barnes, 1984; Rangin, 1978). However, based on the absence of a Triassic intra-oceanic arc, an accretionary prism or crustal suture east of the ophiolite, as well as the lack of evidence of major crustal shortening or a collision, Kimbrough and
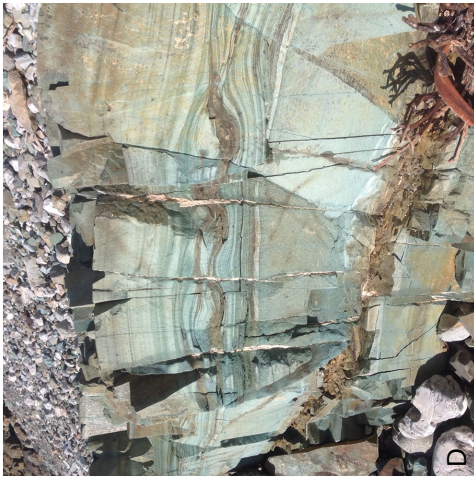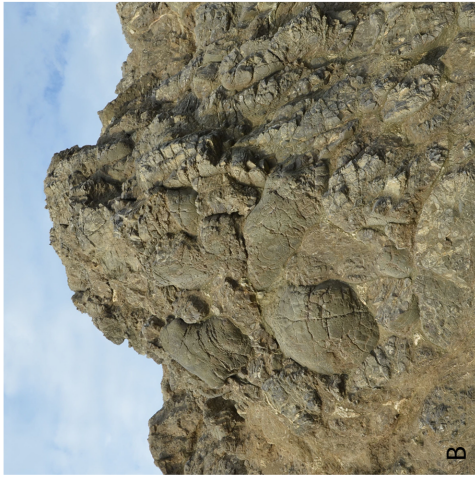
Moore (2003) instead argued that fore-arc rifting models developed for the Californian ophiolite belt to the north (Saleeby, 1981; Saleeby, 1992; Stern & Bloomer, 1992) may better explain the formation of the Vizcaíno-Cedros ophiolite and arc complexes.

4. Sampling locations and ages

We collected a total of 233 cores and 41 hand samples from four different locations. Our sampling strategy aims at sufficiently sampling paleosecular variation (PSV) per locality. Pillows from the Vizcaíno ophiolite were sampled in two locations, at Punta Asuncion (PA1-4, 44 cores from a coastal exposure of ~350 m, Fig. 4a) and at Bahia Tortugas (BT, 19 cores from a ~30 m exposure, Fig. 4b). To maximize the amount of geological time in our sample collection of the ophiolite, all samples were collected from individual pillows at least a few meters apart. Samples were collected from the center of the pillows. Interpillow limestones at Bahia Tortugas contain Norian radiolaria (Barnes, 1984). The pillows at Punta Asuncion are not dated, but there is close agreement on the age of formation of the ophiolite from different outcrop locations (Kimbrough & Moore, 2003). Therefore, we assign all ophiolitic pillows to the same Norian (221 ± 2 Ma) age interval. Paleohorizontal was determined per site by averaging multiple measurements of bedding of interpillow sediments, as well as estimates of paleohorizontal from pillow geometry.

Second, we sampled the sedimentary cover of the ophiolite at Punta San Hipólito (41 hand samples of green chert (SH1-3, SH8-11, sampled through ~150 and ~100 m of stratigraphy respectively, Fig. 4c,d) and 31 cores of fine-grained sands and cherty clays (SH4-7, 38 cores from a ~300 m exposure, Fig. 4e)). Samples were taken in stratigraphic order and per site, ~2-5 m of stratigraphic thickness was sampled. The green cherts are from the up to 245m thick lowermost member of the San Hipólito Formation, deposited directly on top of the basal pillows (Finch & Abbott, 1977). The cherts contain middle Norian radiolaria (Pessagno et al., 1979; Whalen & Pessagno, 1984). The upper 1840m of the San Hipólito Formation is occupied by the sandstone member (Finch & Abbott, 1977), of which we sampled resistant fine grained sands and cherty clays. We sampled the lowermost part of this member, which contains Lower Jurassic (upper Pliensbachian – Toarcian) radiolaria (Whalen & Pessagno, 1984).

Third, we sampled the Eugenia Formation at Punta Eugenia (EU, 139 samples, distributed over 6 sites through the succession (sampled in stratigraphic order on the site, as well as location level) with a total stratigraphic thickness of ~3 km, Fig. 4f). Per site, 5-15 m of stratigraphic thickness was sampled. Rocks at site EU6 were dated at 141.5 ± 3 Ma by U/

Figure 4 (left page): Field photographs. a) Pillow lavas at Punta Asuncion (PA1). b) Pillow lavas at Punta Quebrada, near Bahia Tortugas (BT), size of exposure on photo: ~5 m. c-d) Chert member of the San Hipólito Formation, (SH10 and SH1), stratigraphic thickness of chert beds in D: ~40 cm. e) Sandstone member of the San Hipólito Formation (SH5). f) Eugenia Formation (EU6), stratigraphic thickness of sandstone beds: ~4 m.

Pb on zircon (Hickey, 1984), the rest of the samples were collected at stratigraphically lower levels.

5. Methods

Typical paleomagnetic cores, 2.5 cm in diameter, were sampled with a gasoline-powered motor drill. Their orientation was measured with an ASC OR-2 orientation device and Brunton compass. Oriented hand samples were taken when the rock was too hard to drill in the field and for these samples 2 or 3 cores per hand sample were drilled in the laboratory using a drill press. Using a double blade circular saw, the cores were cut into samples of 2.2 cm length. Laboratory analyses were carried out at the Paleomagnetic Laboratory Fort Hoofddijk of Utrecht University, the Netherlands. To determine the nature of the magnetic carriers, thermomagnetic analyses were performed on representative samples for each locality, using a horizontal translation-type Curie Balance with cycling applied magnetic field of 100-300 or 250-300 mT (Mullender et al., 1993). In order to detect magneto-mineralogical alterations during heating, a number of heating-cooling cycles was applied. We used the following temperature scheme (in °C): 20-150, 50-250, 150-350, 250-400, 350-450, 350-500 and 400-700. All samples were subjected to either alternating field (AF) or stepwise thermal (TH) demagnetization and the natural remanent magnetizations were measured on a 2G DC SQUID cryogenic magnetometer. Demagnetization steps used were 4, 8, 12, 16, 20, 25, 30, 35, 40, 45, 50, 60, 80 mT for AF-treatment and variable temperature increments up to 600°C for TH-treatment. AF treatment demagnetization was performed on an in-house developed robotized demagnetization device (Mullender et al., 2016). We plotted demagnetization diagrams on orthogonal vector diagrams (Zijderveld, 1967) and determined the magnetic components via principal component analysis (Kirschvink, 1980). When applicable, we performed the fold test of Tauxe and Watson (1994) and to test for common means between two data sets, the bootstrapped coordinate test of Tauxe (2010). Following statistical procedures described in Deenen et al. (2011), we calculated mean directions using Fisher (1953) statistics on virtual geomagnetic poles and applied a 45° cut-off to the virtual geomagnetic poles per locality (Johnson et al., 2008). Sample interpretation and statistical analysis were operated in the online portal Paleomagnetism.org (Koymans et al., 2016). The supporting information contains all paleomagnetic results, which may be imported and viewed in the portal.

6. Paleomagnetic data compilation

We compiled all previously published paleomagnetic data from the Vizcaíno-Cedros region. Because the purpose of our study is to test the plate tectonic affinity of the Vizcaíno ophiolite and arc complexes, we restrict our data compilation to the ophiolite and the overlying sediments and arc magmatic rocks. We thus do not include paleomagnetic data from rocks in the subduction mélange on Cedros Island derived from lithosphere that subducted below the ophiolite. Papers with paleomagnetic data generally provide only site averages and their statistical parameters (N, k, α95), and not the original directions

per sample. In volcanic rocks, acquisition of the natural remanent magnetization occurs geologically instantaneously upon cooling, and therefore theoretically, all samples from a single lava flow yield the same paleomagnetic direction. Therefore, using site averages for volcanic rocks is not problematic. However, for sedimentary or slowly cooling intrusive igneous rocks, different samples from one site represent (slightly) different geological ages. Therefore, these sites include a certain amount of PSV and it is preferred to perform statistics on the actual distribution of individual directions rather than on site averages that do not take this PSV into account (Deenen et al., 2011). To allow for this, we created parametrically sampled data sets for sites of intrusive or sedimentary rocks using the online portal Paleomagnetism.org (Koymans et al., 2016). As the result of parametrical sampling, our mean directions may differ from the originally published means. However, this deviation in declination and inclination is never larger than 3°.

For the paleomagnetic database, we selected data according to the following quality criteria: (1) the total distribution of directions satisfies the quality criteria of representing PSV (i.e. A95min<A95<A95max; Deenen et al., 2011); and (2) sedimentary and intrusive igneous rocks have n≥4, lavas have k≥50 (Biggin et al., 2008; Johnson et al., 2008), and at least 7 lava sites could be averaged from a locality. Sites discarded by the original authors were not taken into account, if reasons were provided (e.g. remagnetization).

7. Paleomagnetic results
7.1. Vizcaíno Ophiolite pillow lavas: Bahia Tortugas (BT) and Punta Asuncion (PA)

Curie temperature of the BT and PA pillow lavas are close to 580° (Fig. 5a,b), indicating that the magnetic carrier in the samples is magnetite. Demagnetization diagrams reveal a minor overprint at steps up to 10 mT or 150°C, and linear decay towards the origin at temperatures up to 580°C. ChRMs were generally interpreted at high temperatures (~450-600°C) or ~25-50 mT (Fig. 5c-g). Initial intensities range from 8-2000 mA/m. When corrected for bedding tilt, directions from BT and PA are antipodal, and share a Common True Mean Direction (CTMD). Variations in bedding orientation allow for a fold test, which is positive (best fit between 53-117% unfolding, Fig. 5i). Inclinations are consistently shallow, declinations are large and there is no control on hemispheric origin or direction (clockwise or counterclockwise) of rotation. Furthermore, both normal and reversed polarities are common within the 221±2 Ma interval during which the rocks were formed (Gradstein et al., 2012). Therefore, there are two possible solutions representing paleolatitudes just north or just south of the equator, with opposite rotations. Clockwise declinations are in line with directions from SH4-7 and declinations from the San Roque pluton reported by Torres-Carrillo et al. (2016) (see below), which we therefore consider the most likely option. We reversed the polarity of PA1-4, and we combined the directions of both localities for the calculation of a single paleomagnetic pole (Fig. 5h). There are 3 lines of evidence that support the primary nature of the magnetization: (1) the fold test is positive, supporting pre-tilt magnetization acquisition; (2) the directions in both
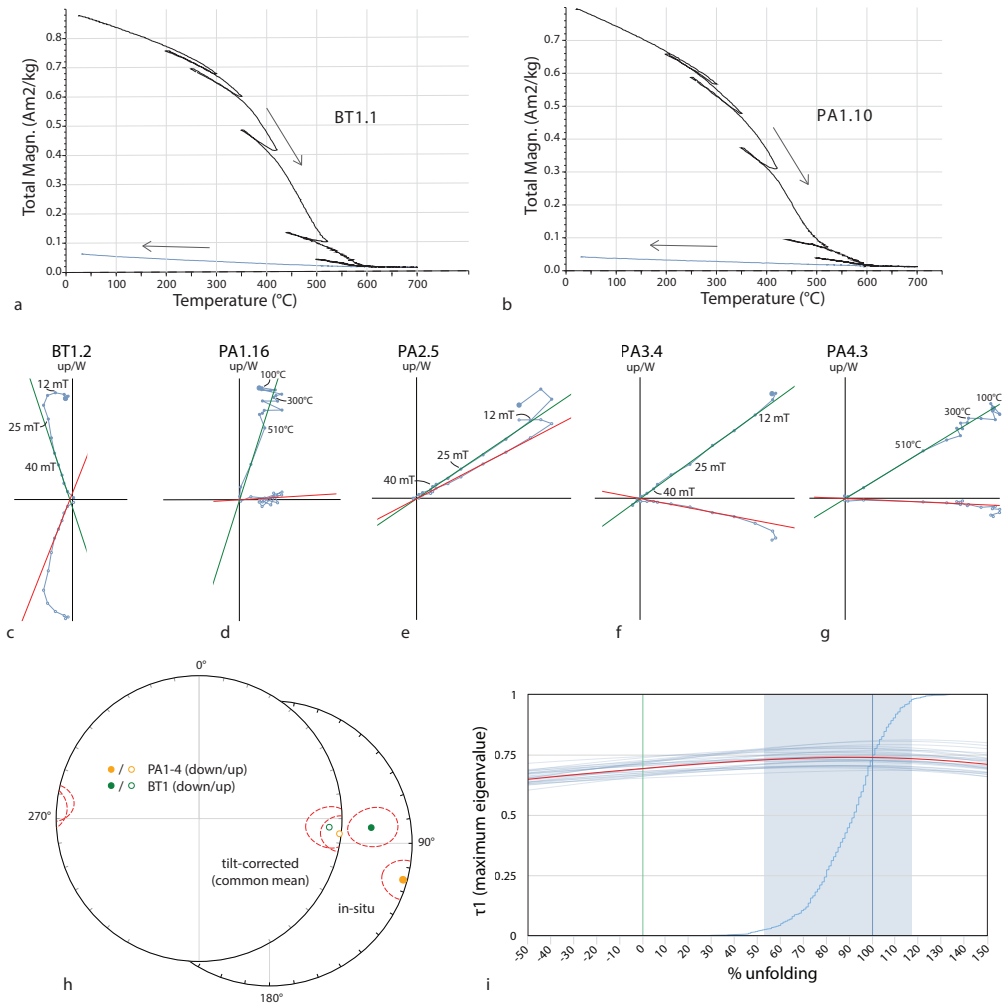
Figure 5: Rock magnetic and paleomagnetic results from localities PA and BT. a-b) Thermomagnetic curves measured on a Curie balance. Heating in black, cooling in blue; c-g) Orthogonal vector diagrams in geographic coordinates, closed (open) symbols for projection on a horizontal (vertical) plane; h) Mean directions of PA1-4 and BT, including confidence intervals (red dotted lines) in both geographic and tectonic coordinates. PA1-4 has been inverted; i) Bootstrapped fold test: cumulative distribution function (with confidence interval in light blue) based on 1000 bootstraps (average of bootstraps in red).
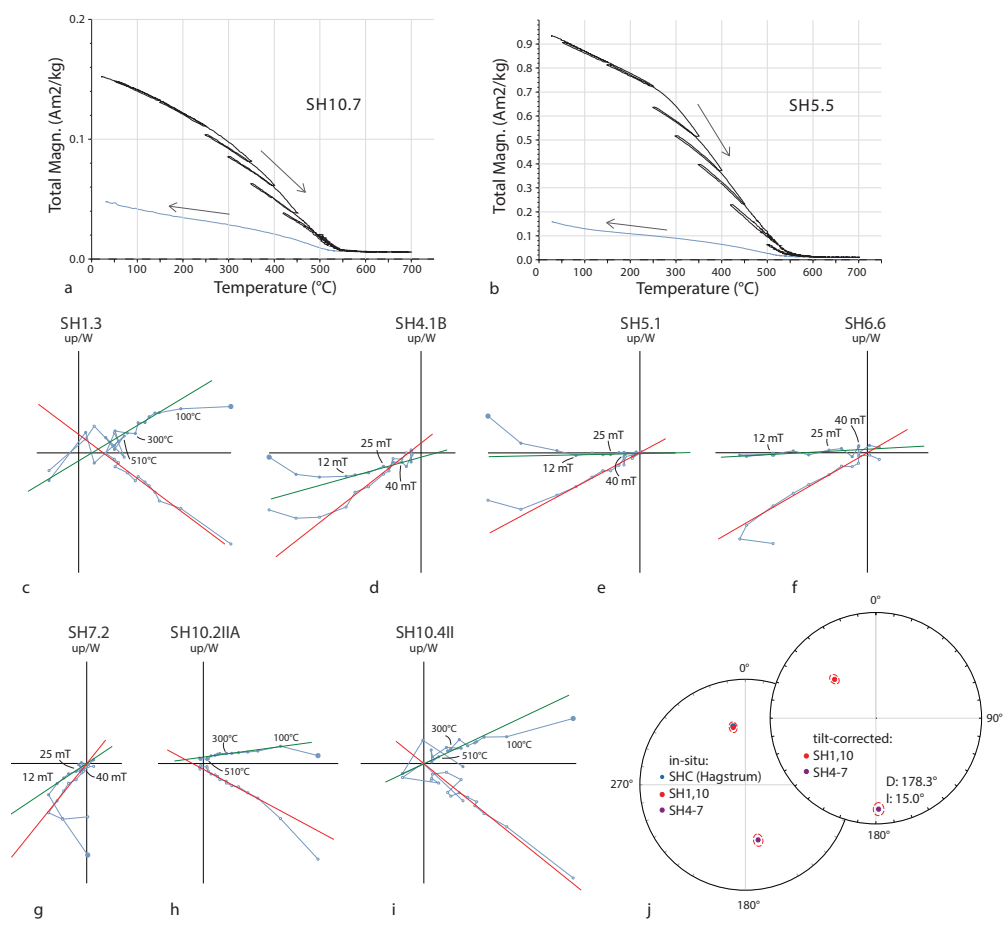
Figure 6: Rock magnetic and paleomagnetic results from locality SH. a-b) Thermomagnetic curves measured on a Curie balance. Heating in black, cooling in blue; c-i) Orthogonal vector diagrams in geographic coordinates, closed (open) symbols for projection on a horizontal (vertical) plane; j) Mean directions, including confidence intervals (red dotted lines) of SH1,10, SH4-7 and SHC of Hagstrum et al. (1985), in both geographic and tectonic coordinates.

geographic and tectonic coordinates differ significantly from the GAD field direction; and (3) the distribution of the ChRMs satisfies the quality criteria of representing PSV (i.e. A95min= 2.4 < A95 = 5.7 < A95max = 6.6; Deenen et al. (2011)). The average (tilt-corrected) ChRM direction is Dec ± ΔDx = 95.5 ± 5.7°, Inc ± ΔIx = -3.8 ± 11.4°, n =54, K = 12.4, A95 = 5.7.
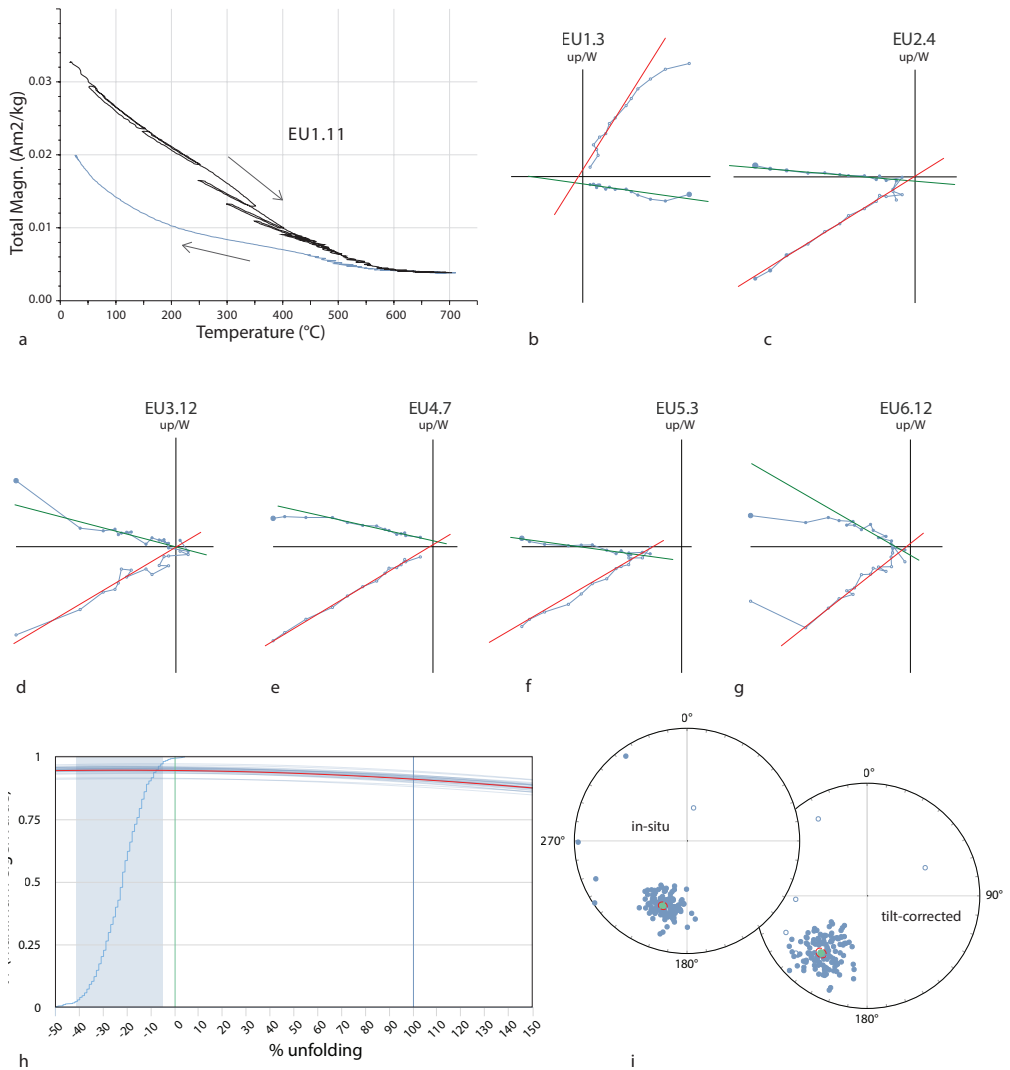
Figure 7: Rock magnetic and paleomagnetic results from locality EU. a) Thermomagnetic curve measured on a Curie balance. Heating in black, cooling in blue; b-g) Orthogonal vector diagrams in geographic coordinates, closed (open) symbols for projection on a horizontal (vertical) plane; h) Bootstrapped fold test: cumulative distribution function (with confidence interval in light blue) based on 1000 bootstraps (average of bootstraps in red); i) Directions (in blue), means (in green) and their confidence intervals (red dotted lines) of locality EU, both in geographic and tectonic coordinates.

7.2. Vizcaíno Ophiolite sedimentary sequence: San Hipólito Formation (SH)

The two sampled members of the San Hipólito Formation (the chert member (SH1,10) and the sandstone member (SH4-7)), yield very different demagnetization results. Curie

temperatures of the chert member (SH1,10) are 540-560° (Fig. 6a), indicating that the magnetic carrier is magnetite. Initial intensities were very low: 0.2-50 mA/m and ChRMs were interpreted at mid-range temperatures (180-480°C, Fig. 6c,h,i). The sampled strata did not vary significantly in bedding orientation and the demagnetization experiments yielded normal directions only. Therefore, neither the fold nor the reversal test can be performed. However, the San Hipólito chert member was also sampled by Hagstrum et al. (1985) (their sites SHC1 and SHC2; results reevaluated in Hagstrum et al. (1993)). Based on a negative fold test from the overlying limestone member, Hagstrum et al. (1993) concluded that the San Hipólito section acquired its magnetization after folding. Our chert member mean direction is statistically indistinguishable from the SHC mean direction of Hagstrum et al. (1993) in geographic coordinates (before bedding tilt-correction)(Fig. 6j). Therefore, we consider it most likely that the directions obtained from SH1,10 represent a post-tilting remagnetization. The average (in-situ) ChRM direction is Dec ± ΔDx = 348.0 ± 3.9°, Inc ± ΔIx = 43.7± 4.5°, n =36, K = 48.1, A95 = 3.5 (Fig. 6j). The inclination corresponds to a paleolatitude 25.6°N (ranging 22.2-29.2°N), which is within range of paleolatitudes of the Vizcaíno-Cedros region from the Eocene-present as predicted by the Global Apparent Polar Wander Path (GAPWaP) (Torsvik et al., 2012)(Fig. 8), suggesting that remagnetization occurred sometime during this interval.

Curie temperatures of the sandstone member (SH4-7) are close to 580°C (Fig. 6b), indicating that the magnetic carrier in the samples is magnetite. Initial intensities range from 5-550 mA/m and ChRMs were interpreted at ~150-540°C or ~16-60 mT (Fig. 6d-g). Again, no field tests were possible to determine the nature of the magnetization and both the distributions of ChRMs in both geographic and tectonic coordinates satisfy the quality criteria of representing PSV (i.e. A95min < A95 < A95max). Despite this, we consider a primary origin of the magnetic signal likely, for the following reasons. In geographic coordinates, the declinations of SH4-7 differ 180° from to the SH1,10 directions that carry a post-tilt magnetization (Fig. 6j), yet have positive inclinations, both in geographic and tectonic (tilt-corrected) coordinates, suggesting the SH4-7 directions reflect a rotated normal component rather than a reversed component. This difference cannot be explained by a post-remagnetization vertical axis rotation of SH4-7, as all San Hipólito samples are collected throughout a continuous stratigraphic succession with uniform bedding orientations. Furthermore, the strongly rotated declinations found in SH4-7 cannot be acquired during a younger remagnetization event, since that would require them to be present in SH1,10 as well. This indicates that the magnetization of SH4-7 predates the remagnetization of SH1,10 and is, in the absence of any indication of a second remagnetization event, most likely primary. The average ChRM (tilt-corrected) direction is Dec ± ΔDx = 178.3 ± 3.4°, Inc ± ΔIx = 15.0 ± 6.3°, n = 34, K = 55.9, A95 = 3.3 (Fig. 6j). We correct for inclination shallowing, typical in fine grained clastic rocks, by applying a standard compaction factor of 0.6 (Torsvik et al., 2012), which increases the average inclination from 15.0 to 24.0°, yielding a paleolatitude of 12.6°N (Fig. 8).
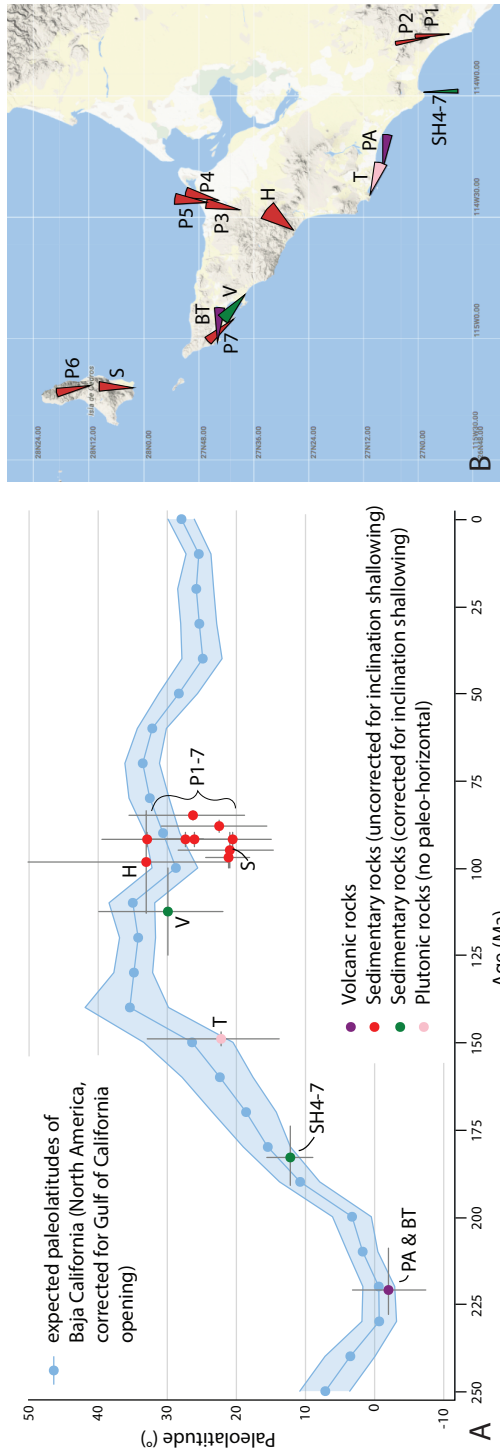
Figure 8: Paleomagnetic database of the Vizcaíno-Cedros region, including data from Hagstrum et al. (1985) (H); Patterson (1984) (P1-7); Smith and Busby (1993) (S); Torres-Carrillo et al. (2016) (T); Vaughn et al. (2005) (V) and this study (SH4-7, PA and BT). a) Paleolatitudes. The data are plotted with respect to the expected paleolatitudes of Baja California (chosen at 27.4°N, -114.4°W). We use the reference values predicted by the Global Apparent Polar Wander Path (GAPWaP) of Torsvik et al. (2012). The paleolatitudinal path of Baja California differs from North America, as we correct for Neogene Gulf of California opening following the reconstruction of McQuarrie and Wernicke (2005); b) Sampling locations and declinations with confidence parachutes (ΔDx).

				In-situ				Tilt corrected							
Localities	N	N45(is)	N45(tc)	D	ΔDx	I	ΔIx	D	ΔDx	I	ΔIx	k	a95	K	A95min<A95<A95max
EU1-6	128	127		197.8	1.6	39.2	2.1					63.5	1.6	70.3	1.7>1.5<3.9 *
SH4-7	38	34	34	167.0	4.7	45.4	5.2	178.3	3.4	15.0	6.3	33.0	4.4	55.9	2.9<3.3<8.9
SH4-7 corrected	38	34	34	167.0	4.7	45.4	5.2	178.3	3.4	24.0	6.3	33.0	4.4	55.9	
SH1,10	36	36		348.0	3.9	43.7	4.5					54.0	3.3	48.1	2.9<3.5<8.6 *
BT1	19	14	15	81.4	10.6	28.3	17.1	93.8	9.0	-9.6	17.6	11.5	11.8	19.1	4.1<9<14.0
PA1-4	44	40	39	284.7	7.7	-2.7	15.4	277.3	6.9	3.2	13.8	8.0	8.7	11.9	2.8<6.9<8.2
all pillow lavas	63	54	54	97.4	7.2	11.6	13.9	95.5	5.7	-3.8	11.4	8.1	7.2	12.4	2.4<5.7<6.6

N: number of demagnetized specimens; N45(is)/N45(tc): number of specimens that fall within the 45° cut-off in in situ coordinates / after tilt correction

D: Declination, I: Inclination

SH4-7 corrected: inclination corrected for inclination shallowing by applying compaction factor 0.6

*statistical values on in situ directions

Table 1: Paleomagnetic results

7.3 Fore-arc sedimentary sequence: Eugenia Formation (EU)

Curie temperatures of the EU sediments are 580°C (Fig. 7a), indicating that the magnetic carrier in the samples is magnetite. ChRMs were isolated at mid-range temperatures (~210-390°C) or alternating fields (~16-45 mT) (Fig. 7b-g). Initial intensities range from 2-11 mA/m. Variations in bedding orientation between the six sites allows for a fold test, which is negative (best fit between -46 and -17% unfolding, Fig. 7h). Furthermore, the A95 calculated in geographic coordinated (1.5°) falls below the A95min = 1.7°, indicating low dispersion, which suggests remagnetization. The average (in situ) ChRM direction is Dec ± ΔDx = 197.8 ± 1.6°, Inc ± ΔIx = 39.2 ± 2.1°, n =127, K = 70.3, A95 = 1.5 (Fig. 7i). Again, the associated paleolatitude (22.2°N, ranging 20.7-23.7°N) is within range of paleolatitudes of the Vizcaíno-Cedros region during the last 50 Myr as predicted by the GAPWaP (Torsvik et al., 2012)(Fig. 8).

To test whether the Vizcaíno ophiolite has moved coherently with the North American Plate, we compute the GAPWaP of Torsvik et al. (2012) in coordinates of Baja California using Euler poles for Baja California relative to North America computed from the reconstruction of McQuarrie and Wernicke (2005) following procedures described in Li et al. (2017). To compute Euler rotations for Baja California relative to North America, we have recreated the ArcGIS-based model of McQuarrie and Wernicke (2005) in GPlates plate reconstruction software. Except for two of the nine Upper Cretaceous sedimentary sites (Patterson, 1984), all previously published and new paleomagnetic data from the Vizcaíno-Cedros region yield paleolatitudes equal to the expected

paleolatitudes of Baja California when corrected for Gulf of California opening (Fig. 8a). Discordance of the two Cretaceous sites may be explained by inclination shallowing due to compaction in sedimentary rocks (Tauxe & Kent, 2004). Furthermore, declinations of >90º in Jurassic and Triassic sites suggests pre-Cretaceous clockwise vertical axis rotations (Fig. 8b), which may best be explained by local vertical axis rotations close to the oblique subduction plate boundary.

8. Discussion

8.1. 220 Myr of Farallon subduction below Mexico

SSZ zone ophiolites, such as the Vizcaíno ophiolite, are widely interpreted to form in fore-arc settings during the subduction initiation process (e.g. Stern et al., 2012; Wakabayashi et al., 2010), or shortly thereafter, during the first stage of overriding plate extension following subduction initiation (van Hinsbergen et al., 2015b). They may form both in intra-oceanic settings (e.g. Philippine Sea plate (Stern & Bloomer, 1992), or Neotethys (Dilek & Furnes, 2011; Maffione et al., 2015a, 2017; Maffione & van Hinsbergen, 2018a; Moix et al., 2008)), as well as along or close to continental margins (e.g. the Californian Coast Range Ophiolite (Metcalf & Shervais, 2008; Shervais et al., 2004; Wakabayashi, 2015), the Indus-Yarlung ophiolites of Tibet (Huang et al., 2015; Maffione et al., 2015b; Pozzi et al., 1984), or the Izmir-Ankara ophiolites of northern Turkey (Topuz et al., 2013a, 2013b)).

Our new paleomagnetic data from the Vizcaíno-Cedros region yield a paleolatitudinal plate motion history equal to that of the North American Plate since Late Triassic time. We follow the argumentation of Boschman et al. (2018) on the kinematic relationship between the Guerrero terrane and North America: latitudinal (northward) plate motion relative to the North American continent is expected for an accreted exotic terrane that formed in an intra-oceanic setting on one of the oceanic plates of the eastern Panthalassa Ocean (e.g. Farallon, Kula). A latitudinal plate motion history equal to that of the North American Plate, on the other hand, indicates that the 'accreted' terrane formed within the (deforming by fore- or back-arc spreading and subsequent shortening) upper plate. We therefore interpret that the Vizcaíno-Cedros rock assemblages formed within the North American upper plate, and were located above an eastward dipping subduction zone consuming Farallon lithosphere. Triassic fore-arc spreading created oceanic crust in the North American fore-arc, thereby widening the gap between the trench and the continental margin. As a result, the volcanic arc developed west of the continental margin, on oceanic and/or stretched accretionary prism basement. The ~220 Ma Vizcaíno supra-subduction zone ophiolite marks the (minimum age of) onset of subduction of Farallon lithosphere forming the Cocos slab, which has been subducting ever since. This inference has several first-order implications. First, it shows that the longest still-subducting slab is also the oldest, even older than previously estimated by van der Meer et al. (2018) who assigned a ~170 Ma age based on correlation to Californian geological records. Second, it shows that there has been direct interaction between the Panthalassa plate system and the
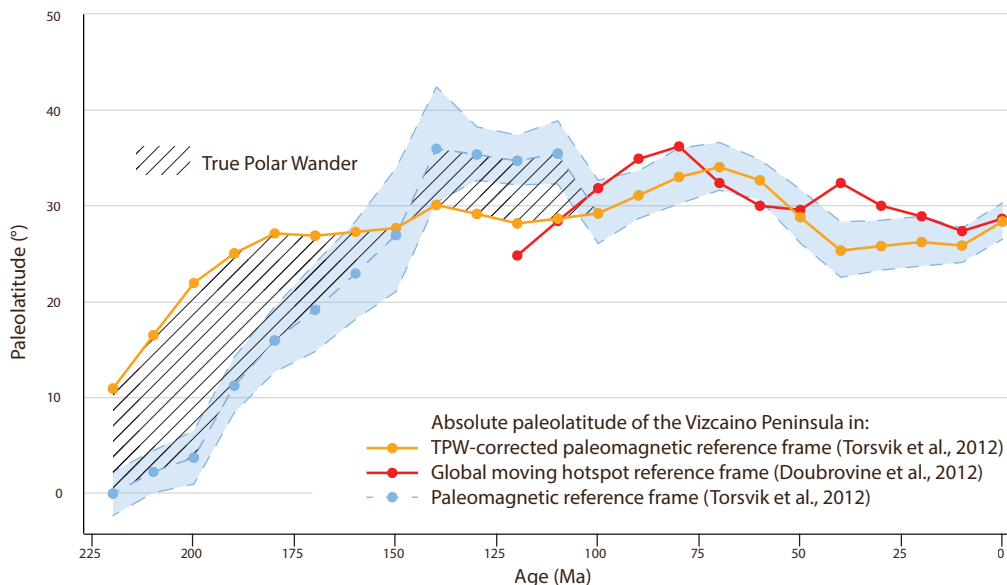
Figure 9: Absolute paleolatitudinal plate motion of the North American Plate at the latitude of the Vizcaíno Peninsula trough time, based on (1) on the global moving hotspot reference frame of Doubrovine et al. (2012) in orange; (2) the paleomagnetic reference frame corrected for TPW of Torsvik et al. (2012) in red; and (3) the paleomagnetic reference frame of Torsvik et al. (2012) in blue. Reference frames (1) and (2) represent paleolatitudinal plate motion relative to the lower mantle, whereby the difference between the red and orange lines provides an implicit measure for uncertainties in the methods and data used to establish these mantle reference frames. Shaded areas represent True Polar Wander.

Pangea-related plates since at least 220 Ma. The inferred east-dipping continental margin subduction in Mexico is consistent with the record of earliest Cordilleran magmatism along strike to the north in the southwestern United States recorded by Triassic plutons (218-213 ma) that intrude Proterozoic cratonal basement (Barth et al., 1997). Triassic magmatism in both regions was also followed by a magmatic lull before onset of voluminous Middle to Late Jurassic arc magmatism.

8.2. Paleolatitudes in a mantle reference frame
We have shown that the Mexican geological record of subduction may be correlated to (>)220 Myr of subduction below North America. However, before correlating this record to interpret the modern structure of the Cocos slab, we first need to test whether North America did not undergo major latitudinal changes relative to the mantle in this time interval. If that is the case, then the records of Mexico may (in part) belong to slab remnants located in the mantle to the north or south of the Cocos slab. Figure 8 illustrates that in a paleomagnetic reference frame (so relative to the Earth's spin axis), the North

American Plate underwent little latitudinal motion throughout the Late Cretaceous and Cenozoic, but shows a >30° northward shift during the Late Triassic and Jurassic (Fig. 8,9) followed by a ~10° southward shift in the Early Cretaceous (Torsvik et al., 2012). Other paleomagnetic reference frames (Besse & Courtillot, 2002; Kent & Irving, 2010) show a similar movement. However, to correlate North American plate kinematic history to mantle structure, these latitudes should first be converted to a mantle reference frame, thereby switching from plate motions relative to the spin axis to plate motions relative to the lower mantle, filtering out contributions of True Polar Wander (TPW) to apparent polar wander (Steinberger & Torsvik, 2008; Torsvik et al., 2012); see also (van Hinsbergen et al., 2015a). Differences between the paleomagnetic reference frames with and without correction for TPW (shaded areas in Fig. 9) represent two well-known True Polar Wander events in Cretaceous and Jurassic times (Steinberger & Torsvik, 2008; Torsvik et al., 2012). From figure 9 it follows that since 190 Ma, the Vizcaíno Peninsula (now at ~28°N) has been between 25°N and 35°N, implying that correlating the Mexican geological subduction records to mantle structure at these same latitudes is warranted. In Late Triassic-Early Jurassic time, the North American Plate moved ~15° to the north relative to the mantle (Fig. 9), which may imply that the oldest, Upper Triassic geological records of subduction (at the North American Plate) may be offset relative to deep mantle structure by such a distance, assuming that the slab did not undergo lateral dragging (Spakman et al., 2018), which may offset slabs relative to their initial position of subduction laterally by >10° (van de Lagemaat et al., 2018b). We also note that the TPW calculations of Steinberger and Torsvik (2008) and Torsvik et al. (2012) includes a mantle-fixed TPW-Euler pole that pierces through the centers of mass of the Large Low Shear wave Velocity Provinces at the core-mantle boundary. Shifting the Indo-Atlantic plate system westward relative to the mantle, e.g. through slab-fitting (van der Meer et al., 2010), thus requires recalculating TPW at each step (Torsvik et al., 2014), potentially shifting the TPW-corrected paleolatitudes. For simplicity, in the following correlation between overriding plate and subducted slab, we do not take latitudinal overriding plate motion and iterative TPW recalculation into account and use a single cross-section through the Cocos slab, noting that this may add uncertainty to the pre-190 Ma correlation.

8.3. Slab geometry and absolute plate motions

The Cocos slab anomaly contains a steep thickened segment between ~1000-1800 km and two low-angle, partially flat slab segments, one in the upper mantle and one in the uppermost lower mantle above ~1000 km. In the upper mantle and below 1800 km, the anomaly dips eastward. These geometry variations suggest episodes of subduction associated with mantle-stationary subduction alternated with episodes of westward roll-back. We now analyze the interplay between upper plate deformation as recorded in Mexican geology since the Triassic, absolute plate motions of the North American Plate, motions of the slab relative to the mantle, and development of the complex geometry of the Cocos slab. We build upon the concepts recently introduced by Schepers et al. (2017) for subduction below the Andes: we use the absolute motion of the 'slab bend' (SB in Fig.

10), i.e. the location where the subducting plate (FAR) changes from (sub-)horizontal to dipping into the mantle (M) as a measure for slab roll-back. The state of stress and related deformation in the Mexican continental margin is the result of the relative motion between the overriding plate (NAM) and the trench (T): net divergence (convergence) between the trench and the overriding plate generates overriding plate extension (shortening) (Heuret & Lallemand, 2005; Lallemand et al., 2005; Schellart, 2008a, 2008b). Subduction occurring with a mantle-stationary slab bend leads to formation of near-vertical, thickened piles of subducted material, termed 'slab walls' by Sigloch and Mihalynuk (2013). An example of a still-subducting mantle-stationary slab is the Marianas slab that subducts steeply into the lower mantle (Miller et al., 2005; van der Meer et al., 2018). When a slab rolls back, i.e., the slab bend migrates relative to the mantle in the direction of the subducting plate, slabs tend to horizontally drape the 660 km discontinuity (Faccenna et al., 2001; Funiciello et al., 2004; van der Hilst & Seno, 1993), with well-known examples in the western Mediterranean region (Faccenna et al., 2004; Spakman & Wortel, 2004), the Banda slab (Spakman & Hall, 2010), the Izu-Bonin slab (Miller et al., 2005; van der Meer et al., 2018), or the Tonga slab (Bijwaard et al., 1998; Hall & Spakman, 2002; van der Hilst, 1995). We note the paradox in slab geometry between the uppermost and mantle transition zone here: subduction with a mantle stationary slab bend and an advancing overriding plate, a situation that may generate flat slab subduction, corresponds to the formation of vertical slab walls in the mantle transition zone, whereas steep subduction (and roll-back) corresponds to slabs draping the base of the upper mantle, forming horizontal slab segments in the mantle transition zone.

Correlation of Cocos slab geometry with the geological record of the deformed western margin of Mexico may provide constraints on the timing of formation of the flat and steep segments. We define the following first-order states of overriding plate deformation: (1) Late Triassic oceanic fore-arc spreading, forming the Vizcaíno ophiolite's crust; (2) no major deformation in latest Triassic to latest Jurassic time; (3) latest Jurassic-Early Cretaceous oceanic back-arc spreading in the Arperos Basin, separating the Guerrero-Alisitos arc from North America (Cabral-Cano et al., 2000; Centeno-García et al., 2008, 2011; Elias-Herrera et al., 2000; Martini et al., 2011); (4) Early to mid-Cretaceous closure of the Arperos Basin and accretion of the Guerrero and Alisitos arcs to the North American continent, followed by the Late Cretaceous-Eocene Laramide orogeny (Bird, 1988; Coney & Reynolds, 1977; Dickinson et al., 1978; Miller et al., 1992); and (5) Late Eocene to present continental Basin and Range extension (e.g. McQuarrie & Wernicke, 2005; Wernicke, 1981). Hotspot reference frames (e.g. Doubrovine et al., 2012; O'Neill et al., 2005) indicate that North America has been undergoing absolute westward plate motion throughout the Late Cretaceous and Cenozoic. However, earlier absolute plate motions, as well as relative Farallon-North America motions are uncertain, and therefore, the amount of subducted lithosphere within each particular slab segment cannot be determined. Therefore, we focus on the timing of the style of upper plate deformation only and relate this to slab geometry.

Snapshot:

500 km

FAR   Vizcaino fore-arc basin   NAM

220 Ma   M   T
                                SB   ?
660 km

200 Ma

160 Ma
                    slab wall

                    Arperos back-arc basin
115 Ma

60 Ma   flat slab   Arperos
                              lithosphere
             slab wall

             Laramide fold thrust belt
40 Ma

             Basin and Range
0 Ma
          A
             B
               C   D
                         E
         Lower mantle and crustal   F
         deformation vertically not to scale
                              G
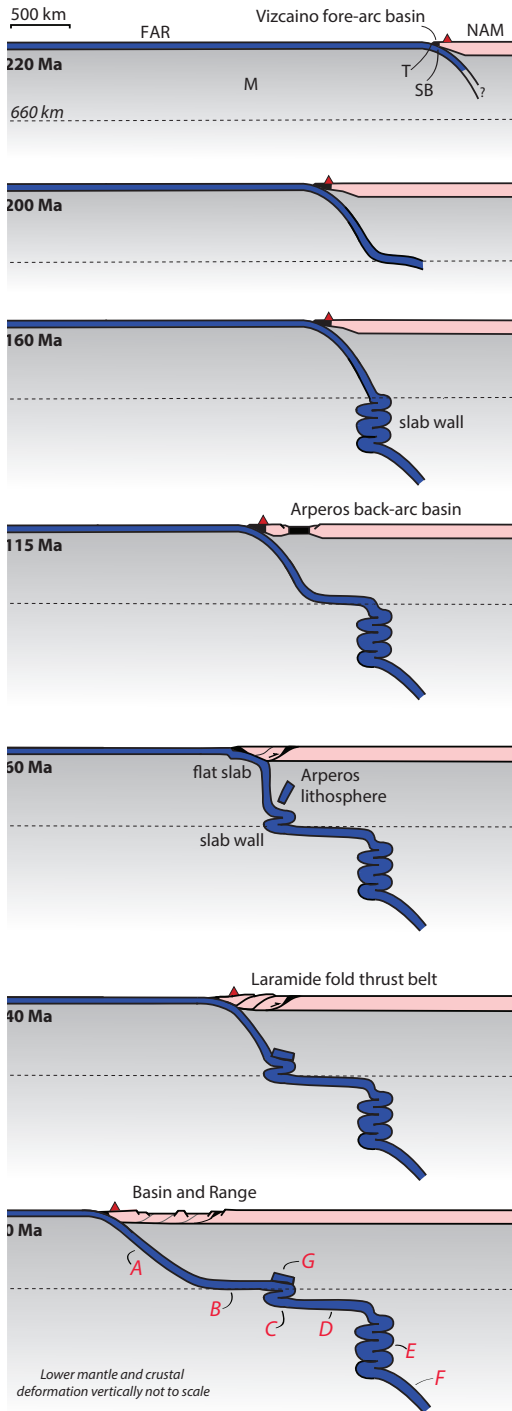
Interval:

? - 220 Ma
roll-back = trench advance > overriding plate advance:
overriding plate extension *(Vizcaino fore-arc spreading)*

overriding plate   overriding plate
extension   advance   stationary reference
SB,T   NAM   M   FAR
                              roll-back
                                    subduction rate
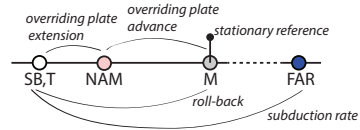
220 - 200 Ma
roll-back = trench advance = overriding plate advance

NAM, SB, T   M   FAR

200 -160 Ma
- stationary overriding plate
- stationary trench and slab bend:
slab wall formation

M, NAM, SB, T   FAR
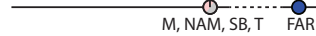
160 - 115 Ma
roll-back = trench advance > overriding plate advance:
overriding plate extension *(Arperos Basin opening)*

SB,T   NAM   M   FAR
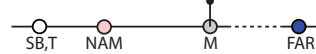
115 - 60 Ma
- mantle stationary slab bend:
slab wall formation
- overriding plate advancing > trench advance > roll-back:
overriding plate shortening and flat slab formation
(Arperos closure and Laramide shortening)

NAM   T   M, SB   FAR
overriding plate   flat slab formation
shortening
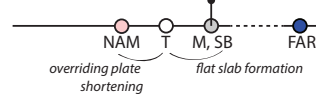
60 - 40 Ma
roll-back > overriding plate advance > trench advance:
overriding plate shortening and slab steepening
(Laramide shortening)

SB   T
     NAM   M   FAR
flat slab steepening
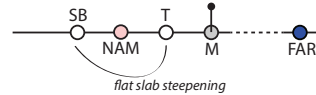
40 - 0 Ma
roll-back = trench advance > overriding plate advance:
overriding plate extension *(Basin and Range extension)*

SB, T   NAM   M   FAR

144
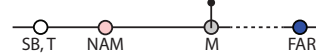
Figure 10 (left page): Left panels: cross sections illustrating the step wise evolution of Farallon Plate subduction, Cocos slab development and North American upper plate deformation relative to a stationary mantle. Horizontal and vertical scales are equal, but crustal deformation (vertically exaggerated) and depth of the lower mantle (reduced) are not to scale. Right panels: velocity diagrams per time interval illustrating trench-perpendicular motions of the overriding North American Plate (NAM), the subducting Farallon Plate (FAR), the slab bend (SB), and the trench (T), relative to the stationary sub-lithospheric mantle (M). The trench is the intersection between the subduction thrust and the seafloor; the slab bend the hinge between the horizontal and dipping parts of the subducting plate. Relative motion is represented by a distance on the line (for example, T left of NAM indicates westward motion of T relative to NAM, and hence, overriding plate extension). Relative motion between SB and T represents flat slab formation or flat slab steepening. The magnitude of Farallon Plate motion is unknown, hence the dotted line between FAR and M.

The upper part of the Cocos slab shallowly plunges down towards the base of the upper mantle which it reaches ~800 km east of the trench (Fig. 10, lower left panel: 'A'), from where it is flat-lying for another ~600 km eastwards ('B'). This suggests that the youngest episode of subduction was associated with significant roll-back, i.e. trench-perpendicular motion of the slab bend relative to the mantle. The southern part of the Cocos slab (subducting below Honduras, south of the Motagua fault zone) does not show this sub-horizontal segment (Fig. 2a). Since ~50 Ma, the northern part of the Central American land bridge, the continental Chortis block, has been displaced relative to the North American Plate by ~1100 km along the left-lateral Motagua-Cayman North American-Caribbean transform plate boundary (Boschman et al., 2014 (Chapter 2)). During these last 50 Myr, the Caribbean Plate was near-stationary relative to the mantle (Doubrovine et al., 2012), suggesting that the Mexican trench has advanced westwards over ~1100 km since 50 Ma. Additionally, part of the roll-back has been accommodated by upper plate extension since ~36 Ma, forming the Basin and Range province (McQuarrie & Wernicke, 2005). Moreover, during the final stages of the Laramide orogeny that preceded the Basin and Range extensional episode (Fig. 10, 60-40 Ma), the flat-slab that is widely interpreted to have underlain the western North American margin must have steepened due to roll-back, inducing westward motion of the slab bend relative to the trench (T) before overriding plate extension started. We thus interpret the top ~1400 km of the low-angle to flat slab segment of the Cocos slab to have formed during the waning stages of the Laramide orogeny and throughout the Basin and Range extensional episode, corresponding to subduction evolution during the last ~60 Myr (Fig. 10,11).

The first small slab wall ('C') in the mantle transition zone developed due to overriding plate advance and a mantle-stationary slab bend, resulting in closure of the Arperos Basin and subsequent Laramide flat slab formation (115-60 Ma). The slab wall connects to a second (~1000 km long) flat-lying segment in the top of the lower mantle ('D'), correlated to a phase of roll-back exceeding overriding plate advance and upper plate
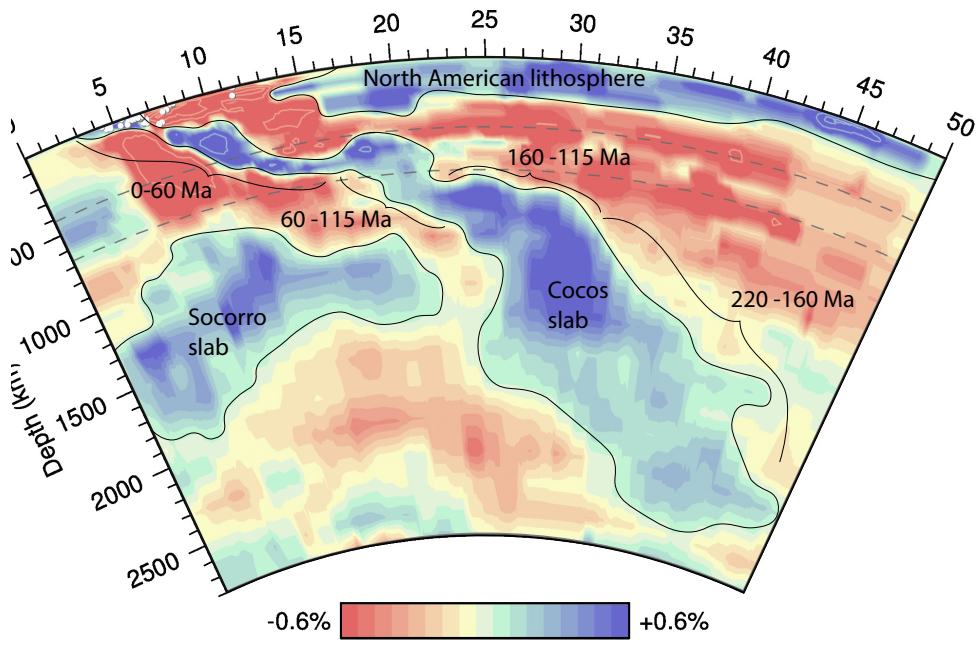
Figure 11: Interpretation of ages of subduction of the shallow-dipping and steep segments of the Cocos slab.

extension, resulting in opening of the Arperos back-arc basin (160-115 Ma). During the transition between acceleration (160-115 Ma) and slow down (115-60 Ma) of roll-back, relative motion between the slab bend (SB) and the overriding plate (NAM) reversed, but formation of the flat lying slab segment D and overriding plate shortening suggests that the North American Plate continuously moved westward relative to the mantle throughout this period (Fig. 10).

The major slab wall from ~1000-1800 km depth in the lower mantle ('E') suggests an extended period of subduction with a mantle-stationary slab bend leading to the creation of this thickened vertical pile of subducted material. Below ~1800 km the east-dipping anomaly ('F') has a somewhat thinner appearance than that of the slab wall. This may be an expression of slab stretching following the slab thickening in the slab deceleration zone above ~1500 km, which results from an increase in sinking velocity below ~1500 km, presumably related to a decrease in viscosity (van der Meer et al., 2018). We associate this deep eastward dipping portion of the slab down to the lowermost mantle with a period of relatively slow westward slab retreat starting at ~220 Ma. In the period preceding the opening of the Arperos Basin, there is no major overriding plate deformation other than the formation of the Vizcaíno ophiolite. This suggests that North America may have moved up to 1000 km westwards during the Late Triassic (220-200 Ma) and underwent no

major longitudinal motion during the Jurassic (200-160 Ma) to create the mid-mantle slab wall (Fig. 10,11).

During the Late Triassic-Early Jurassic, the North American Plate underwent absolute northward paleolatitudinal motion according to the TPW-corrected paleomagnetic reference frame (Torsvik et al., 2012)(Fig. 9), which would suggest that the oldest (Triassic) part of the Mexican record would correlate to a lower mantle slab segment further south in the mantle. We note, however, that whilst there are large slabs in the lower mantle to the north of the Cocos slab (e.g., the Hatteras slab; van der Meer et al., 2018), there are no slabs to the south that allow for an alternative correlation. We thus tentatively suggest that during the early stages of subduction, when the slab was not yet firmly anchored in the lower mantle, it may have been dragged northward relative to the surrounding and underlying mantle.

No major slab-like anomalies are found to the east of the Cocos slab, indicating that the amount of subducted oceanic lithosphere related to closure of the Arperos Basin was limited. Arperos lithosphere may have merged with the main Cocos slab anomaly, such that it became indistinguishable from subducted Farallon lithosphere ('G'). Paleomagnetic data had already shown that opening and closure of the back-arc basin was not associated with significant paleolatitudinal motion (Boschman et al., 2018 (Chapter 3)) and the absence of an identifiable slab now suggests that also paleolongitudinal motions were limited. This indicates that overriding North American plate margin extension or shortening since Triassic time was probably limited to a few hundreds of kilometers during each event. The overall history of absolute paleolongitudinal motion of North America determined here correlates well with the slab-fitted, true polar wander-corrected paleomagnetic reference frame of van der Meer et al. (2010). This frame shows little paleolongitudinal absolute motion of North America between 200-150 Ma, both preceded and followed by absolute westward motion.

8.4. Geographical continuity of the Mesozoic Mexican subduction system

Currently, subduction of the Cocos Plate continues south of the North American – Caribbean plate boundary. Tectonic reconstructions of the Caribbean region (e.g. Boschman et al., 2014 (Chapter 2); Pindell & Kennan, 2009), however, show that tectonic terranes with an oceanic basement now forming the Central American land bridge originated in an intra-Panthalassa setting, much further west compared to their present-day location. Eastward subduction at the western Caribbean plate boundary, whereby Farallon lithosphere subducted below the Caribbean Plate, is estimated to have initiated in Santonian (~85 Ma) time, but how or if this trench was connected to the Mexican continental margin trench remains uncertain. Prior to 85 Ma, Farallon-North/South America convergence was taken up by westward subduction of 'Proto-Caribbean' lithosphere below the Greater Antilles (e.g. Pindell & Kennan, 2009).

Correlations between the geology of the Vizcaíno-Cedros region and the more northern Californian Franciscan-Coast Range Ophiolite-Great Valley system are striking (Jones et al., 1976; Kimbrough, 1985; 1989; Rangin, 1978; Suppe & Armstrong, 1972). However, in contrast to the Vizcaíno ophiolite, paleomagnetic data from the Coast Range Ophiolite were interpreted to indicate northward motion of the ophiolite relative to North America (Beebe & Luyendyk, 1983; Luyendyk & Hornafius, 1982; McWilliams & Howell, 1982; Williams, 1984). Furthermore, in California, SSZ ophiolites are younger and subduction initiation is interpreted to have occurred in Jurassic time, at ~165 Ma (e.g. Wakabayashi, 2015). This ~55 Myr age difference in along-strike SSZ ophiolites at the western North American margin may be explained in different ways. Firstly, when assuming a shared tectonic history of the ophiolites despite their differences, the age difference may imply that supra-subduction fore-arc spreading at the Californian margin does not reflect subduction initiation. Recently, Guilmette et al. (2018) showed a 8-10 Myr delay between subduction initiation and upper plate extension in the Oman ophiolite, and Maffione and van Hinsbergen (2018a) argued that in the Balkan region, the East Vardar SSZ ophiolites may have formed as much as ~70 Myr after subduction initiation. However, Lu/Hf ages of Franciscan metamorphic sole garnets, argued by Guilmette et al. (2018) to record prograde mineral growth during subduction initiation, are ~169 Ma (Anczkiewicz et al., 2004). Alternatively, between ~220 and ~170-165 Ma, the trench north of Vizcaíno may have been offset westwards to an intra-oceanic setting along a transform fault. Tomographic arguments for such an intra-oceanic subduction system were shown in van der Meer et al. (2018), i.e. their Socorro slab. This slab is correlated by van der Meer et al. (2018) to Late Triassic - Early Jurassic subduction records of the Wrangellia superterrane that was located at such latitudes at the time (e.g. Enkin, 2006; Johnston, 200, 2008; Krijgsman & Tauxe, 2006), and which may have shielded the Californian margin from subduction until it moved northward towards its present-day location in the Canadian Cordillera. The latter hypothesis explains why uninterrupted Farallon subduction, resulting in the continuous, exceptionally deep Cocos slab, was restricted to the Mexican part of the Cordillera and why mantle structure further north is considerably more complex. Evidently, even though the Farallon Plate occupied the vast majority of the Mesozoic eastern Panthalassa Ocean, differences in interactions with the continental margin of Pangea resulted in significant regional variations in its subduction history.

9. Conclusions

The Vizcaíno-Cedros region of Baja California yields a paleolatitudinal plate motion history equal to that of the North American continent since Late Triassic time. This shows that the Vizcaíno-Cedros region is best interpreted as the fore-arc of the North American Plate, adjacent to a (>)220 Myr long-lived eastward dipping subduction zone of the Farallon Plate underlying the northeastern Mesozoic Panthalassa Ocean. Tomographic images of the Cocos slab confirm long-lived, uninterrupted eastward subduction. We correlate episodes of overriding plate shortening and extension to steep and flat segments of the slab and provide a first order, geology and tomography-constrained tectonic model

of dynamic Farallon Plate subduction below Mexico since the Late Triassic onset of Pangea breakup.

5

The Caribbean and Farallon plates connected: constraints from stratigraphy and paleomagnetism of the Nicoya Peninsula, Costa Rica

Sampling basalts - Nicoya Peninsula, Costa Rica

Abstract

Plate kinematic reconstructions play an essential role in our understanding of global geodynamics, but become increasingly difficult to constrain back in geological time due to the subduction of oceanic lithosphere. Here, we attempt at kinematically reconstructing the Cretaceous and older plate tectonic history of the Caribbean Plate within the Mesozoic Panthalassa (paleo-Pacific) Ocean. To this end, we present new paleomagnetic data from Jurassic and Cretaceous oceanic sedimentary and volcanic rocks of the Nicoya Peninsula and Murciélago Islands of northwestern Costa Rica. We use these data to test kinematic scenarios connecting the Caribbean Plate to the Farallon Plate as restored from Pacific spreading records. Our resulting reconstruction implies that the western Caribbean subduction zone initiated around 100 Ma, in an intra-oceanic setting, breaking up oceanic lithosphere of at least 70 Myr old.

1. Introduction

Plate kinematic reconstructions play an essential role in our understanding of global geodynamics, but become increasingly difficult to constrain back in geological time due to the subduction of oceanic lithosphere. Particularly the Panthalassa Ocean that surrounded the supercontinent Pangea, is notoriously difficult to restore (e.g. Boschman & van Hinsbergen, 2016 (Chapter 1)). Marine magnetic anomalies in the present-day seafloor of the Pacific Ocean document that the Mesozoic and early Cenozoic (north)eastern Panthalassa Basin formed from spreading between the Pacific Plate and the conceptual Farallon Plate (Engebretson et al., 1985; Wright et al., 2016). Except for the Juan de Fuca, Rivera, Cocos and Nazca plates, which are presumed present-day remnants of the Farallon Plate, the absence of anomalies conjugate to the Jurassic-early Cenozoic anomalies of the Pacific Plate indicates that the vast majority of the Farallon Plate has been lost to subduction. Reconstruction of the kinematic history of the Farallon Plate therefore relies on indirect evidence such as the spreading history of the Pacific Plate (Engebretson et al., 1985; Wright et al., 2016), geological and paleomagnetic records of the highly deformed continental margins of North and South America (Boschman et al., 2018 (Chapter 3); Johnston, 2001; Nokleberg, 2000; Tarduno & Alvarez, 1985; Tarduno et al., 1986) and interpretation of seismic tomography models that image subducted Farallon lithosphere (Grand et al., 1997; Liu et al., 2008; Liu & Stegman, 2011; Sigloch & Mihalynuk, 2013; van der Meer et al., 2010, 2012, 2018).

When restoring the Mesozoic history of the Farallon plate, the Caribbean Plate is of particular interest. This plate, currently separated from the Cocos Plate by a subduction zone, is a remnant of Panthalassa (possibly Farallon) lithosphere that, instead of subducting as happened to the north and south below the Americas, was captured between the Americas in Cretaceous time (Pindell et al., 1988). The bulk of the Caribbean Plate consists of oceanic lithosphere of unknown age covered by a thick layer of ~90 Ma oceanic plateau basalts of the Caribbean Large Igneous Province (CLIP) (Burke, 1988; Burke et al., 1978; Donnelly et al., 1973; Saunders et al., 1996; Sinton et al., 1998, 2000). During break-

up of Pangea, North and South America separated, resulting in the opening of the Proto-Caribbean Seaway that connected eastward to the Central Atlantic Ocean. Subsequent convergence between the Americas and the oceanic plates of the Panthalassa Ocean was associated with westward dipping subduction of this Proto-Caribbean lithosphere beneath the lithosphere of the future Caribbean Plate, which became progressively emplaced eastwards from within the Panthalassa Ocean to its present position between the Americas (Burke et al., 1978; Pindell, 1985). The Caribbean lithosphere became a separate plate upon initiation of the western Caribbean subduction zone. The age of this subduction initiation is debated and estimates vary from ~100 Ma (Whattam & Stern, 2015) to ~75 Ma (Buchs et al., 2010). The inferred close proximity in age of subduction initiation and extrusion of the CLIP has led several authors to suggest a causal relationship between the two phenomena, postulating that a mantle plume that generated the CLIP also induced western Caribbean subduction (Stern & Gerya, 2017; Whattam & Stern, 2015).

Kinematic reconstructions of the Caribbean Plate (e.g. Boschman et al., 2014 (Chapter 2); Burke, 1988; Burke et al., 1978; Pindell, 1985; Pindell et al., 1988; Pindell & Kennan, 2009) are based on geological records of collisions of the leading eastern edges of the Caribbean Plate with the North and South American continents since ~100 Ma and interactions between these plates along transform and subduction-dominated plate boundaries since then. Reconstructing the western margins, which were surrounded by now-subducted Panthalassa lithosphere, is more difficult, and for times prior to 100 Ma, when the Caribbean lithosphere was part of the independent Panthalassa plate system without a direct connection to the Indo-Atlantic plate system, its location and motion remains highly uncertain.

In this paper, we attempt at kinematically reconstructing the Cretaceous and older plate tectonic history of the Caribbean Plate within the Mesozoic Panthalassa Ocean. To this end, we present new paleomagnetic data from Jurassic and Cretaceous oceanic sedimentary and effusive rocks of the Nicoya Peninsula and Murciélago Islands of northwestern Costa Rica. We use these to test kinematic scenarios connecting the Caribbean Plate to the Farallon Plate as restored from Pacific spreading records, as a function of estimated ages of subduction initiation in the western Caribbean subduction zone. This establishes Mesozoic eastern Panthalassa plate motions in relation to the plate tectonic history of the continental plates making up the supercontinent Pangea.

2. Geological setting
2.1. Tectonic setting of the Nicoya Peninsula and Murciélago Islands
The Nicoya Peninsula and Murciélago Islands are currently located in the fore-arc region of the Central American subduction system, where eastward subduction below the Caribbean Plate consumes the Cocos and, south of the Panama fracture zone, the Nazca plates (Fig. 1). The modern Central American land bridge in the upper plate hosts an active volcanic arc and consists from north to south of (1) the continental Chortís block
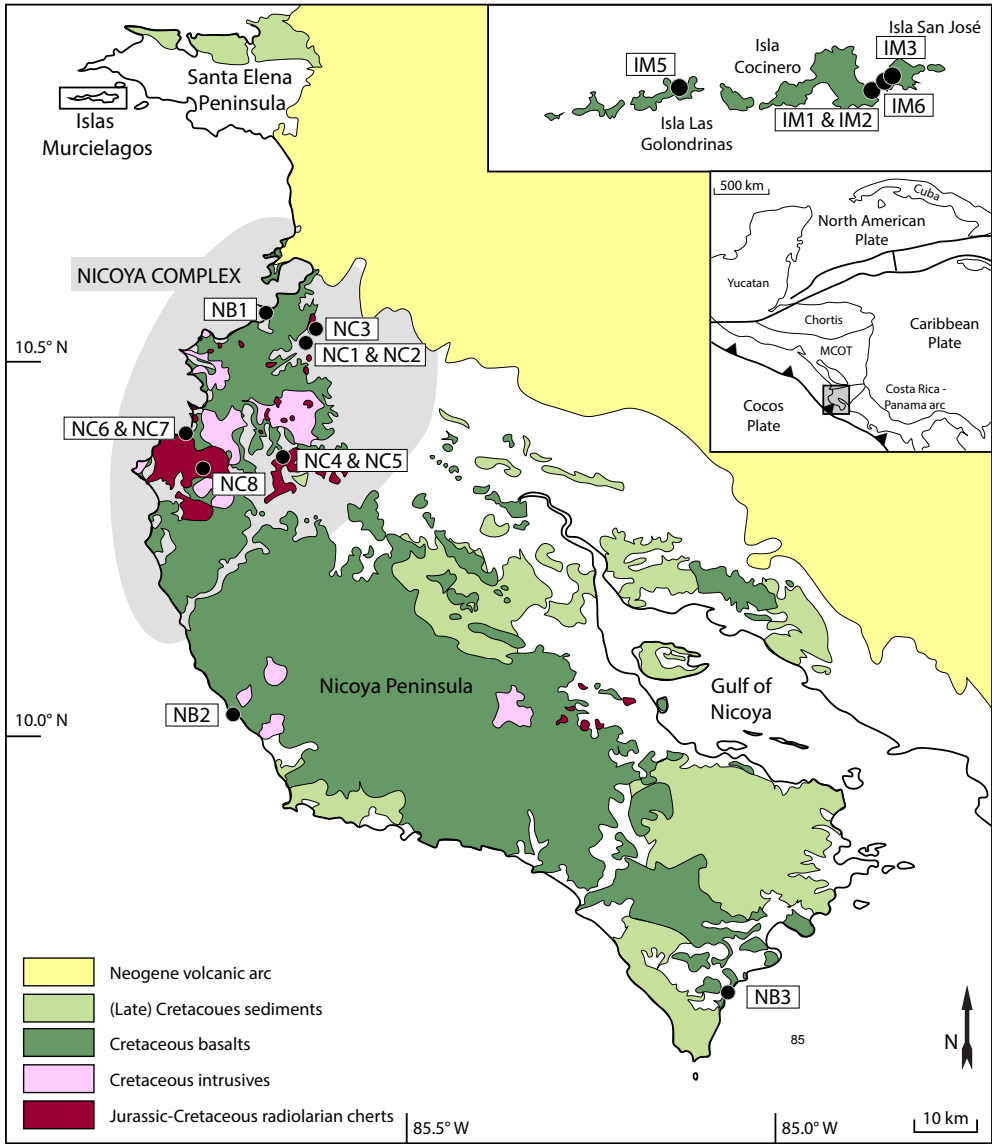
Figure 1: Geological map of the Nicoya Peninsula and the Murciélago Islands, including sampling locations, modified from Whattam et al. (2016). Inset: Caribbean region, including the basement terranes of the Central American land bridge. Nicoya is located in the boundary zone between the MCOT and the Panama-Costa Rica arc.

of southern Guatemala and northern Honduras, which is bounded in the north by the left-lateral Motagua fault zone that forms the North American – Caribbean plate boundary (Donnelly et al., 1990; Rogers et al., 2007); (2) the Siuna, or Mesquito Composite Oceanic Terrane (MCOT) containing an oceanic basement, serpentinite matrix mélanges and Mesozoic-Cenozoic arc volcanics (Baumgartner et al., 2008; Venable, 1994); and (3) the oceanic Costa Rica-Panama block, consisting of mainly CLIP and arc-related magmatic rocks (Buchs et al., 2010; Gazel et al., 2009) and connecting to the northwestern Andes, which contains the diffuse plate boundary between the Caribbean and South American plates. The Nicoya Peninsula and Murciélago Islands are located in the boundary zone between the MCOT and the Costa Rica-Panama block (Baumgartner et al., 2008)(Fig. 1). Just north of the Murciélago Islands, the Santa Elena Peninsula of northernmost Costa Rica exposes an ultramafic peridotite nappe thrusted over an oceanic accretionary complex, interpreted as the remnants of a Cretaceous paleo-trench (Baumgartner & Denyer, 2006; Escuder-Viruete & Baumgartner, 2014; Gazel et al., 2006) that may represent the Costa Rica-Panama block – MCOT plate boundary.

In the early stages, the subduction zone along the western margin of the Caribbean Plate did not connect to trenches along continental North or South America as today. Instead, it was located within the Panthalassa realm and migrated eastward relative to the Americas. In the Boschman et al. (2014) reconstruction of the Caribbean region, which serves as a basis for this study, initiation of the western Caribbean subduction zone was modeled at 85 Ma, following the 88-80 Ma estimate of Pindell and Kennan (2009). This estimate is based on the oldest, Coniacian tuffaceous, arc-derived sediments overlying the oceanic basement of the Nicoya and Santa Elena peninsulas of Costa Rica. However, other authors consider these sedimentary overlap assemblages to be unrelated to subduction in the western Caribbean subduction zone, and correlate them to either another intra-oceanic subduction zone (Baumgartner et al., 2008; Buchs et al., 2010) or subduction below the active southern margin of the North American Plate (Andjić et al., 2018). This age may thus not be representative for western Caribbean subduction initiation. Buchs et al. (2010) instead argued for 75-73 Ma proto-arc formation, based on geochemical signatures (intermediate between plateau and arc) of the oldest arc magmatic rocks in Costa Rica and Panama. Independent from implications by their geochemical signature, the presence of 75-73 Ma arc volcanic rocks in Panama and Costa Rica indicates that subduction must have been underway at least by 75 Ma, making this the minimum age limit of subduction initiation. Subduction initiation may also be older; Whattam and Stern (2015) proposed a plume-induced subduction initiation model in which ~100 Ma subduction initiation triggered by the same plume that extruded the CLIP.

2.2. Stratigraphy of the Nicoya Peninsula and Murciélago Islands
The Nicoya Peninsula exposes (1) folded ribbon-bedded radiolarian cherts of Bajocian-Bathonian, Oxfordian-Tithonian, Valanginian-Albian and Coniacian-Santonian ages (Baumgartner et al., 2008; Denyer & Baumgartner, 2006), following the Baumgartner et

al. (1995) zonation; (2) basaltic rocks, dated by 40Ar/39Ar geochronology at 139.1-132.9, 119.4-118.2, 110.6 and 94.7-89.7 Ma (Hauff et al., 2000; Hoernle et al., 2004; Madrigal et al., 2016; Sinton et al., 1997); and (3) 89.3-77.2 Ma diabases, gabbros and plagiogranites (40Ar/39Ar and U-Pb ages) (Hauff et al., 2000; Madrigal et al., 2016; Sinton et al., 1997; Whattam et al., 2016) (Fig. 1). At contacts with intrusive rocks, radiolarian cherts show chilled margins and hydrothermal leaching indicating clear cross-cutting relationships (Baumgartner et al., 2008). The bulk of the magmatic rocks fall within the narrow range (~90 Ma) of radiometric ages from basaltic rocks of the CLIP elsewhere in the Caribbean region (Alvarado et al., 1997; Hauff et al., 1997, 2000; Hoernle et al., 2004; Kerr et al., 1997; Révillon et al., 2000; Sinton et al., 1997, 1998, 2000) and all Cretaceous magmatic rocks from the Nicoya Peninsula, including the pre-90 Ma ones, yield similar geochemical signatures, reflecting mixing between MORB and intra-plate magmatism, which is interpreted as evidence for a shared plume-influenced mantle source (Hauff et al., 1997, 2000; Hoernle et al., 2004; Madrigal et al., 2016; Sinton et al., 1997).

Originally, all oceanic assemblages in northwest Costa Rica (including the Nicoya Peninsula) were termed 'Nicoya Complex' (Dengo, 1962; Kuijpers, 1980). However, in more recent studies, the use of this term is restricted to the tectonic unit cropping out in the northwestern Nicoya Peninsula only (Fig. 1)(Andjić et al., 2018; Bandini et al., 2008; Denyer & Baumgartner, 2006; Denyer & Gazel, 2009). The Nicoya Complex is covered by middle Campanian – Maastrichtian shallow water carbonate deposits (ages based on planktonic foraminifera and rudists) (Baumgartner-Mora & Denyer, 2002; Denyer et al., 2014; Pons et al., 2016). The central and southern part of the Nicoya Peninsula differs from the Nicoya Complex by the absence of Jurassic-Albian radiolarian cherts and ~139-133 Ma magmatic rocks. It is overlain by siliceous and bituminous black shales of the Loma Chumico Formation and Coniacian-Campanian pelagic to turbiditic sequences of the Sabana Grande and Nambí formations (ages based on radiolaria and 87Sr/86Sr dating on Inoceramus bivalve fossils)(Bandini et al., 2008; Flores et al., 2003b; Flores, 2006; Schmidt-Effing, 1979). The Loma Chumico Formation is dated as Albian by ammonite occurrences (Astorga, 1997; Azéma et al., 1979). However, Coniacian-upper Campanian radiolaria have also been reported (Andjić et al., 2018). In the Gulf of Nicoya region, the magmatic basement is overlain by middle Turonian-Santonian pelagic and bituminous shales and arc-related tuffaceous debris flows of the Berrugate Formation (Bandini et al., 2008; Flores et al., 2003a, 2003b).

The archipelago of the Murciélago Islands is located north of the Nicoya Peninsula, just south of the Santa Elena Peninsula (Fig. 1). These islands consist of tilted tholeiitic massive- and pillow basalts, which yielded 40Ar-39Ar ages of 109.0 ± 2 Ma and 113.43 ± 3.48 Ma (Hauff et al., 2000; Madrigal et al., 2016). Geochemically, the Murciélago Islands basalts are almost identical to the CLIP and the older basaltic suites of the Nicoya Peninsula (Escuder-Viruete et al., 2015; Madrigal et al., 2015).

2.3. Previous tectonic interpretations

Interpretations for the formation of the Nicoya Complex are broadly summarized in two categories. The first invokes that the Nicoya Complex formed as an accretionary complex, in which Large Igneous Province (LIP) and chert rocks of different ages were not deposited within each others vicinity, but were amalgamated from >1000 km of now-subducted lithosphere (e.g. Galli-Olivier, 1979; Madrigal et al., 2016). A second category of models suggests that the Nicoya complex forms a deformed, but overall coherent stratigraphy deposited on Panthalassa (Farallon) lithosphere. Deformation of the cherts would then reflect disruption and detachment from their original basement during pulses of plume-related magmatism (Denyer & Baumgartner, 2006).

Independent of any model, the presence of Bajocian-Bathonian radiolarian cherts testifies of a pre-Bajocian oceanic basement on which the oldest rock assemblages now incorporated in the Nicoya Complex formed (Denyer & Baumgartner, 2006; Denyer & Gazel, 2009; Sinton et al., 1997). The absence of coarse detrital sediments and arc-derived rocks in the Jurassic-Early Cretaceous sequence implies that this lithospheric basement was not in close proximity to a continental margin or a subduction zone throughout its early history (Andjić et al., 2018). Accretionary complexes are generally characterized by more or less coherent, trenchward younging nappes consisting of both foreland (trench-fill) sedimentation and far-travelled ocean plate stratigraphy separated by trust faults (e.g. Matsuda & Isozaki, 1991). In the Nicoya complex, no such nappes, major thrust faults or trench-fill deposits are observed (Denyer & Baumgartner, 2006) or suggested by the modern geomorphology. This forms a challenge for models that infer that the Nicoya complex consists of accreted or amalgamated fragments of ocean plate stratigraphy and plateau remnants that were originally far apart.

The Murciélago Islands basalts are by some authors associated with the Santa Elena Nappe, exposed on the Santa Elena Peninsula to the north (Denyer & Gazel, 2009; Gazel et al., 2006). However, as no contact or clear lithological relation to the Santa Elena Nappe is present and the Murciélago Islands basalts contain a geochemical signature almost identical to CLIP magmas, other authors relate the Murciélago Islands basalts to the Nicoya complex (Escuder-Viruete et al., 2015; Madrigal et al., 2015). Exclusive evidence on the tectonic relationship between the Murciélagos Islands basalts, the Santa Elena Nappe and the Nicoya complex remains absent.

3. Sampling and ages

We collected a total of 243 cores and 74 hand samples for paleomagnetic analysis, categorized in three groups: Murciélago Islands basalts (Islas Murciélagos, IM), Nicoya basalts (NB), and Nicoya cherts (NC). We obtained samples from three different islands of the Murciélago Bay; Isla Cocinero (IM1, IM2), Isla San José (IM3, IM6) and Isla Las Golondrinas (IM5). Except for IM2, where we took 7 samples from a single lava, all samples are from individual pillow basalts (9, 17, 12 and 7 samples respectively). Bedding

orientations (strike 279, dip 75N) are consistent throughout the islands and 40Ar/39Ar dating of intra-pillow glass and whole rock matrix have yielded ages of 113.43 ± 3.48 Ma (Isla Las Golondrinas, Madrigal et al., 2016) and 109.0 ± 2.0 Ma (Isla Cocinero, Hauff et al., 2000) respectively.

We sampled the Nicoya basalts at sections of pillow basalts along the western coast of the peninsula, whereby each sample represents an individual pillow. To optimize the amount of geological time within each sample set to average paleosecular variation, we collected the samples at sections of hundreds of meters thick with the spacing between samples generally 5-10 m. At locality NB1, which is located between Playa del Coco and Punta Cacique, we obtained 76 cores from a ~500 m long section. 40Ar/39Ar dating of these basalts yielded ages of 139.1 ± 1.1 (Hoernle et al., 2004) and 137.09 ± 2.48 Ma (Madrigal et al., 2016). At locality NB2, on the beach of Puerto San Juanillo, we obtained 67 samples from ~700 m of exposure. The pillow basalts are interbedded with thin layers of radiolarian chert, indicative of a significant amount of geological time within this section. 40Ar/39Ar dating yielded an age of 119.4 ± 1.1 Ma (Hoernle et al., 2004). At locality NB3, at the beach of Montezuma, we collected 46 samples from a ~ 500 m section of pillow basalts (NB3.1-3.13, 3.24-3.46) interbedded with fine grained sediments containing small grains of chert (NB3.14-3.23). Calcareous intra-pillow sediments contain late Cenomanian-Turonian (~94 Ma) foraminifera (Tournon & Alvarado, 1997).

The sampled Mn-radiolarites occur as isolated and highly tectonized exposures on the northwestern Nicoya Peninsula. We sampled sites of 7-11 hand samples in stratigraphic order, generally within 1 or 2 m of exposure. All NC exposures belong to the Nicoya Complex and were previously dated by radiolarian biostratigraphy by Denyer and Baumgartner (2006). Sites NC1 and NC2 (8 and 7 hand samples) were collected from a quarry located north of the town of Sardinal de Carrillo. This exposure is characterized by tight folds and generally steeply dipping strata (~70°). Radiolarian assemblages from this outcrop range from middle Oxfordian to early Tithonian (~155-145 Ma). Site NC3 (9 hand samples) is located 2 km further north, near the town of Santa Rita. Radiolariates from this exposure contain late Barremian to early Aptian (~123-119 Ma) radiolarian assemblages. Sites NC4 and NC5 (10 and 9 hand samples) were collected from a heavily weathered and tectonized exposure located in Oratorio de Cartagena, containing the oldest radiolarian assemblage in the Nicoya Peninsula which is Bajocian in age (~174-166 Ma). Sites NC6 and NC7 (10 and 11 hand samples) were sampled in Punta Conchal. This locality is characterized by the occurrence of late Valanginian-Hauterivian to Aptian radiolarian assemblages (~133-111 Ma). At site NC6, we sampled both west and north dipping limbs of a fold. Finally, site NC8 (10 hand samples) was sampled from a small road-cut exposure near the village of Huacas, containing late Bajocian-early Bathonian (~167-164 Ma) radiolarian assemblages.

4. Methods

We sampled typical paleomagnetic cores, 2.5 cm in diameter, with a gasoline-powered motor drill and measured their orientation with an ASR OR-2 orientation device and Brunton compass. We took orientated hand samples from the chert sites as these rocks are difficult to drill in the field, and we drilled 1 to 6 cores per hand sample in the laboratory using a drill press. The cores were cut with a double blade circular saw into samples of 2.2 cm length. Laboratory analyses were carried out at the Paleomagnetic Laboratory Fort Hoofddijk at Utrecht University in the Netherlands. Basaltic samples were subjected to either stepwise thermal (TH) or alternating field (AF) demagnetization and chert samples to TH demagnetization. Naturel remanent magnetizations (NRM) were measured on a 2G Enterprises SQUID cryogenic magnetometer. We used the following demagnetization steps: 0, 4, 8, 12, 16, 20, 25, 30, 35, 40, 45, 50, 60, 70, 80 mT for AF treatment, and 20, 100, 150, 200, 250, 300, 330, 360, 390, 420, 450, 480, 510, 540, 560, 580, 600, 620, 640, 660, 680°C or until complete demagnetization for TH treatment. AF treatment samples were preheated at 150°C to reduce effects of weathering on the NRM (van Velzen & Zijderveld, 1995) and demagnetization was performed on an in-house developed robotized demagnetization device (Mullender et al., 2016). Sample interpretation and statistical analysis were performed in the online portal paleomagnetism.org (Koymans et al., 2016), using orthogonal vector diagrams (Zijderveld, 1967) and principal component analysis (Kirschvink, 1980). We calculated site mean directions using Fisher (1953) statistics on virtual geomagnetic poles, applied a 45° cut-off to the virtual geomagnetic poles per site (Johnson et al., 2008), and calculated the N-dependent values of A95min and A95max, following statistical procedures described in (Deenen et al., 2014; Deenen et al., 2011). Fold tests (Tauxe & Watson, 1994) and bootstrapped coordinate tests (Tauxe, 2010) were performed when applicable. All paleomagnetic results are summarized in Table 1.

5. Paleomagnetic results

Demagnetization diagrams of NB1, NB2 and NB3 generally show two types of behavior. The majority (65/77 for NB1, 63/69 for NB2, 43/44 for NB3) of the samples reveal an overprint at steps up to 20 mT or 210°C and linear decay towards the origin at 40-60 mT or 580°C (e.g. NB1.18A, NB1.48A, NB1.59A, NB2.10B, NB2.27, NB2.28, NB3.28A, NB3.41A, Fig. 2). The rest of the samples, generally the weaker ones, reveal the same overprint, but subsequently scatter around the origin instead of decaying towards it (e.g. NB1.2, NB2.1A, NB3.7B, Fig. 2). The latter samples are not interpreted. Initial intensities range between 10 mA/m and 30 A/m. In all three sites, inclinations scatter around zero, so both upward and downward directed inclinations are present. All directions (within the 45° cut-off) have northwest- to southward declinations, indicating that there are no reversals recorded

Figure 2 (right page): Paleomagnetic results from localities NB1, NB2 and NB3. A-K) Orthogonal vector diagrams in geographic coordinates, closed (open) symbols for declination (inclination); L-N) ChRM directions per locality in geographic coordinates; O) Mean directions in both geographic and tectonic coordinates.
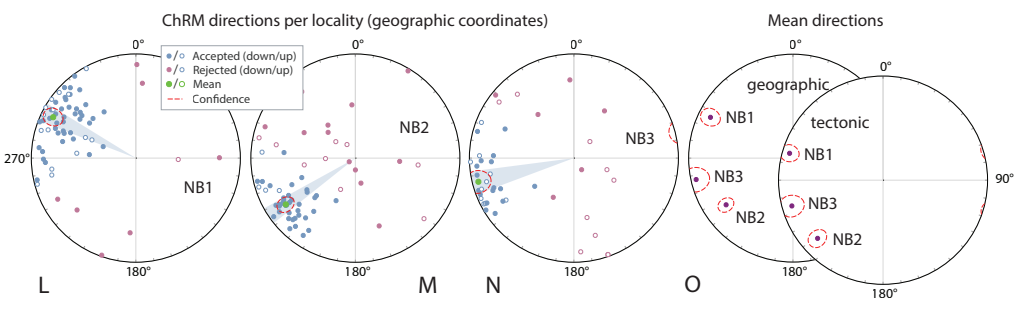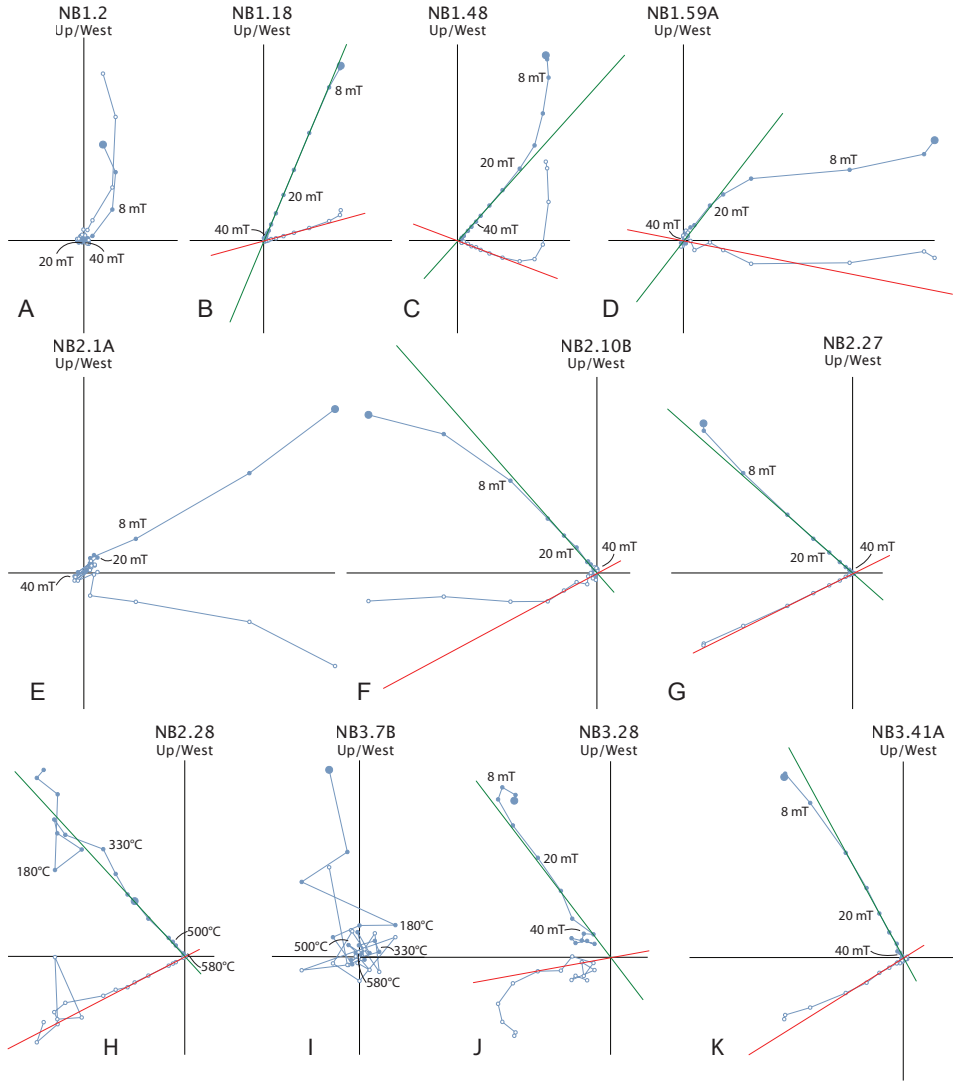
within sites NB1, NB2 and NB3. There is no sufficient variation in bedding throughout the sections to perform meaningful fold tests. The average (tilt-corrected) characteristic remanent magnetization (ChRM) directions are NB1: Dec ± ΔDx = 286.1 ± 5.0°, Inc ± ΔIx = 7.7 ± 9.9°, n =54, K = 16, A95 = 5.0; NB2: Dec ± ΔDx = 228.3 ± 5.3°, Inc ± ΔIx = 17.2 ± 9.8°, n =42, K = 18.7, A95 = 5.2 ; NB3: Dec ± ΔDx = 254.2 ± 6.5°, Inc ± ΔIx = 10.2 ± 12.7°, n =26, K = 2-.1, A95 = 6.5.

Demagnetization diagrams from IM1, IM3, IM5, and IM6 reveal a low-temperature/coercivity overprint and linear decay towards the origin at demagnetization steps up to 80 mT or 580°C. ChRM's are generally interpreted at 16-50 mT or 360-500°C (Fig. 3). Initial intensities range from 0.5-20 A/m. Similar to NB1, NB2 and NB3, inclinations scatter around zero, and all declinations (within the 45° cut-off) are westward, indicating that there are no reversals recorded within sites IM1356. The average tilt-corrected ChRM direction is Dec ± ΔDx = 291.1 ± 4.9°, Inc ± ΔIx = 3.8 ± 9.7°, n =44, K = 22.1, A95 = 4.9. For samples from IM2, most of the magnetic signal is lost within the first 4 demagnetization steps, and therefore, ChRM's can only be interpreted in low temperature/coercivity steps (330-420°C or 12-20 mT). The resulting directions are significantly different from IM1356 and the interpreted ChRM directions have a k-value of 28.9, indicating higher amounts of scatter than expected for samples from a single lava which should represent a spot reading of the magnetic field (generally k>>50, e.g. Biggin et al., 2008). For these reasons, we exclude IM2 from further analysis.

The sampled rocks from sites NB2, NB3 and IM1356 formed during the Cretaceous normal superchron, and therefore, assuming the interpreted magnetization was acquired during formation of the rocks, the polarity of these samples must be normal. As a result, a southern hemisphere origin for NB2, NB3 and IM1356 can be excluded, and the westward declinations represent counterclockwise rotations. Because demagnetization behavior and directions from NB1 are very similar to NB2 and NB3, we interpret these results to reflect counterclockwise rotations and a northern hemisphere origin as well.

There are 3 lines of evidence that support the primary nature of the magnetization of NB1, NB2, NB3 and IM1356: (1) the directions in both geographic and tectonic coordinates differ significantly from the Geocentric Axial Dipole (GAD) field direction, (2) no reversals are detected, which is consistent with the age of the rocks and magnetization acquisition during the Cretaceous normal superchron (for NB2, NB3 and IM1356); (3) the distributions of ChRM's satisfy the quality criteria of representing paleo-secular variation (PSV) (table 1).

Contrary to the sampled pillow basalt sections, the sampled cherts lack any indication of stratigraphic younging direction. Therefore, correcting for bedding tilt yields two options: a smaller correction when the sediments are considered not to be overturned (hereafter: tc1), or a larger correction assuming overturned strata (tc2).
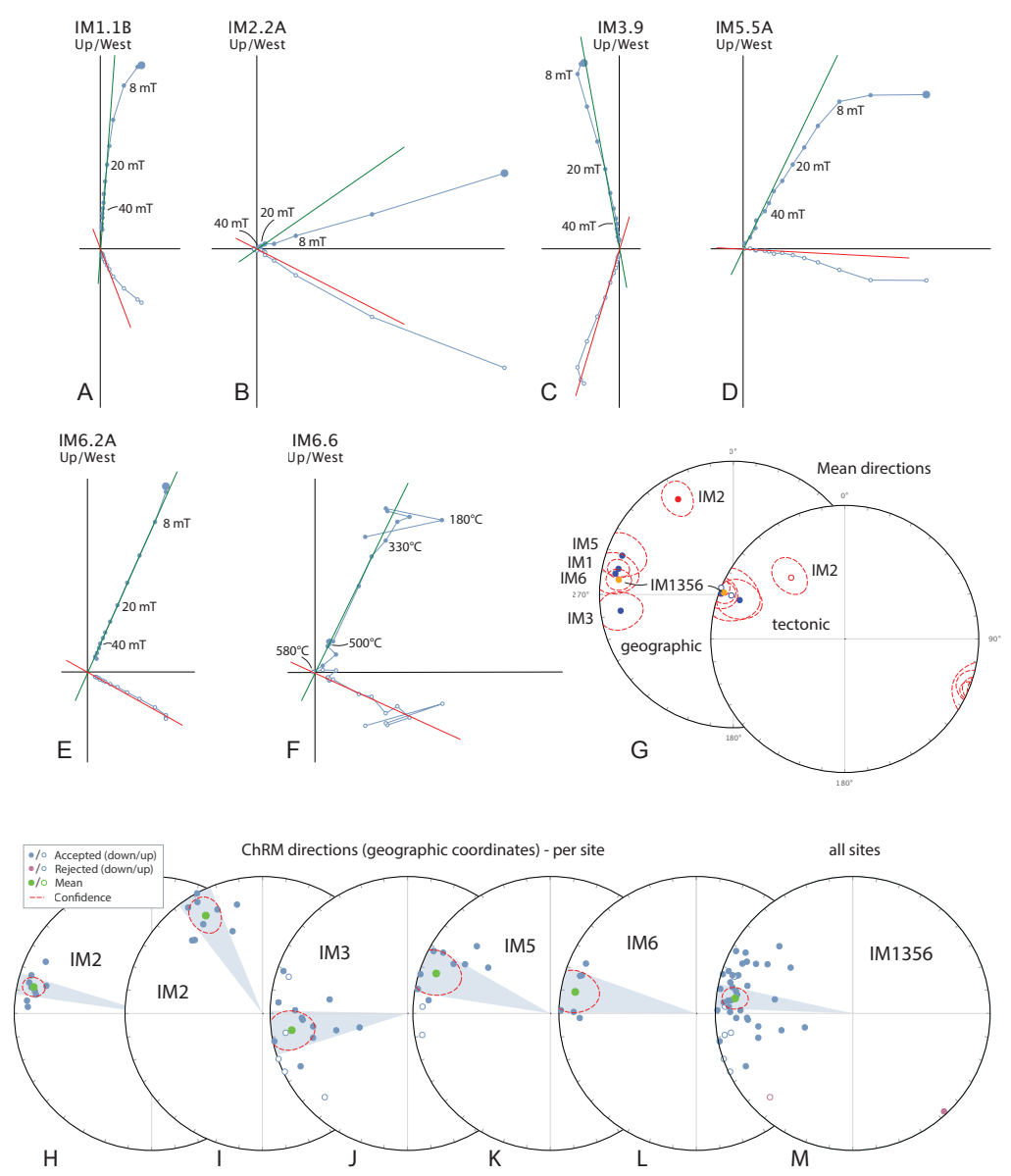
Figure 3: Paleomagnetic results from sites IM1-6. A-F) Orthogonal vector diagrams in geographic coordinates, closed (open) symbols for declination (inclination); G) Mean directions per site in both geographic and tectonic coordinates; H-L) ChRM directions per site in geographic coordinates; M) ChRM directions for sites IM1356 in geographic coordinates.

NC1 and NC2: Initial intensities range from 0.5-20 mA/m and ChRM's are interpreted between 500-680°C (Fig. 4). Directions from sites NC1 and NC2 share a common mean. A series of fold tests (indeterminate for NC1, negative (tc1, best fit between -29-24% unfolding) or indeterminate (tc2) for NC2, and negative for NC1 and NC2 combined (best fit between -20-27% (tc1) or -41-14% (tc2) unfolding, Fig. 5)) indicates that the magnetization is post-tilting and sites NC1 and NC2 are remagnetized.

NC3: Initial intensities range from 4-400 mA/m and ChRM's are generally interpreted in high temperature steps (550-680°C). Dispersion of the interpreted directions (Fig. 5) is essentially random (K=2.5), which does not allow calculation of a meaningful mean direction. We reject this site from further analysis.

NC4: Initial intensities range from 0.6-10 mA/m and ChRM's are generally interpreted between 500-620°C. Variations in bedding orientations within the site allow for a fold test, which is negative (best fit between 7-20% (tc1) or -14--5% (tc2) unfolding, Fig. 5), and the mean direction in in-situ coordinates is indistinguishable from the GAD field (inc: 20°, Fig. 5). We therefore interpret site NC4 to be recently remagnetized.

NC5: Due to the weathered nature of the rocks, many hand samples were lost during drilling in the laboratory, leaving only 9 samples available for demagnetization. Initial intensities range from 35-85 mA/m and ChRM's were generally interpreted between 360-500°C. Interpreted directions yield a near-random distribution (K=1, Fig. 5), and no meaningful site mean can be calculated. We exclude these results from further analysis.

NC6: Initial intensities range from 4-70 mA/m and ChRM's are generally interpreted between 330-580°C. Again, dispersion of the interpreted directions (Fig. 5) is too high (K=2.5) to allow for calculation of a meaningful mean direction, and we reject this site from further analysis.

NC7: Initial intensities range from 4-70 mA/m and ChRM's are generally interpreted between 330-580°C, yielding both normal and reversed directions. Both the reversal test and fold test are positive (best fit between 42-150% (tc1), tc2 is indeterminate). The absence of control on hemispheric origin, polarity or younging direction of the sampled sediments is not problematic for this site, as both tilt corrections (tc1 and tc2) yield directions with a common mean. Furthermore, both possible inclinations (2.3° or -2.3°) are within error of each other (ΔIx = 12.9). Fig. 5 and table 1 include NC7 corrected with tc1 and, in conjunction with results from NB and IM, representing counterclockwise rotations, resulting in a lower hemispheric origin (paleolatitude: -1.1°). The average tilt-corrected ChRM direction of NC7 is Dec ± ΔDx = 221.3 ± 6.5°, Inc ± ΔIx = -2.3 ± 12.9°, n =23, K = 22.8, and the distribution of ChRM's satisfies the quality criteria of representing PSV (A95min= 3.4 < A95 = 6.5 < A95max = 11.4).

NC8: Demagnetizations from NC8 show consistent linear decay towards the origin at ~620-680°C. ChRM's are interpreted between 360-680°C and initial intensities range

Figure 4 (right page): Orthogonal vector diagrams of sites NC1-8 in geographic coordinates, closed (open) symbols for declination (inclination).

165

Mean directions

geographic

ChRM directions NC12

geographic

tc1

tc2

A B C D

Foldtest NC12 (tc1)

ChRM directions NC3

K = 2.5

E F

ChRM directions NC4

GAD field

Foldtest NC4 (tc1)

G H

ChRM directions NC5

K = 1

ChRM directions NC6

K = 2.5

ChRM directions NC7

I J K
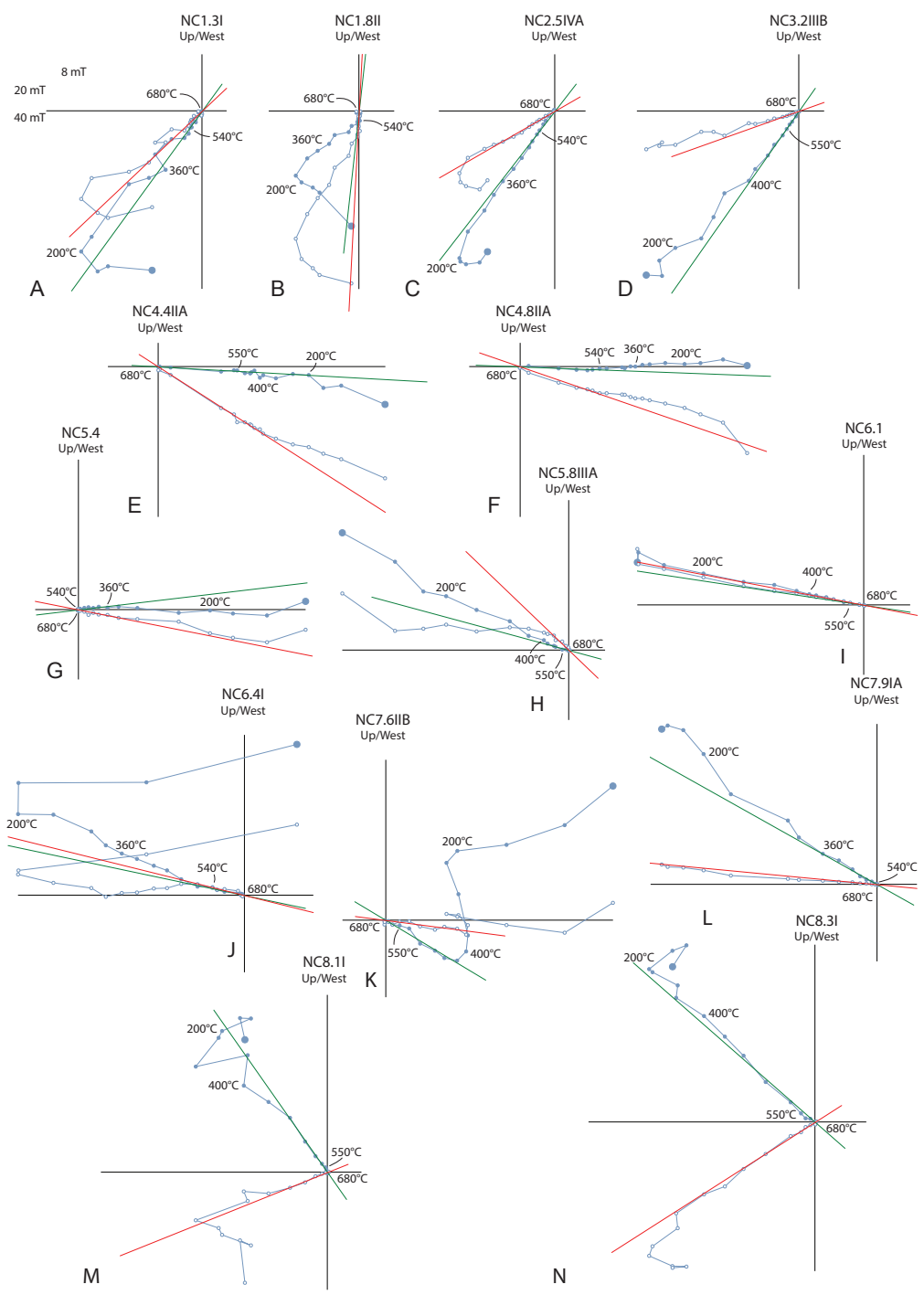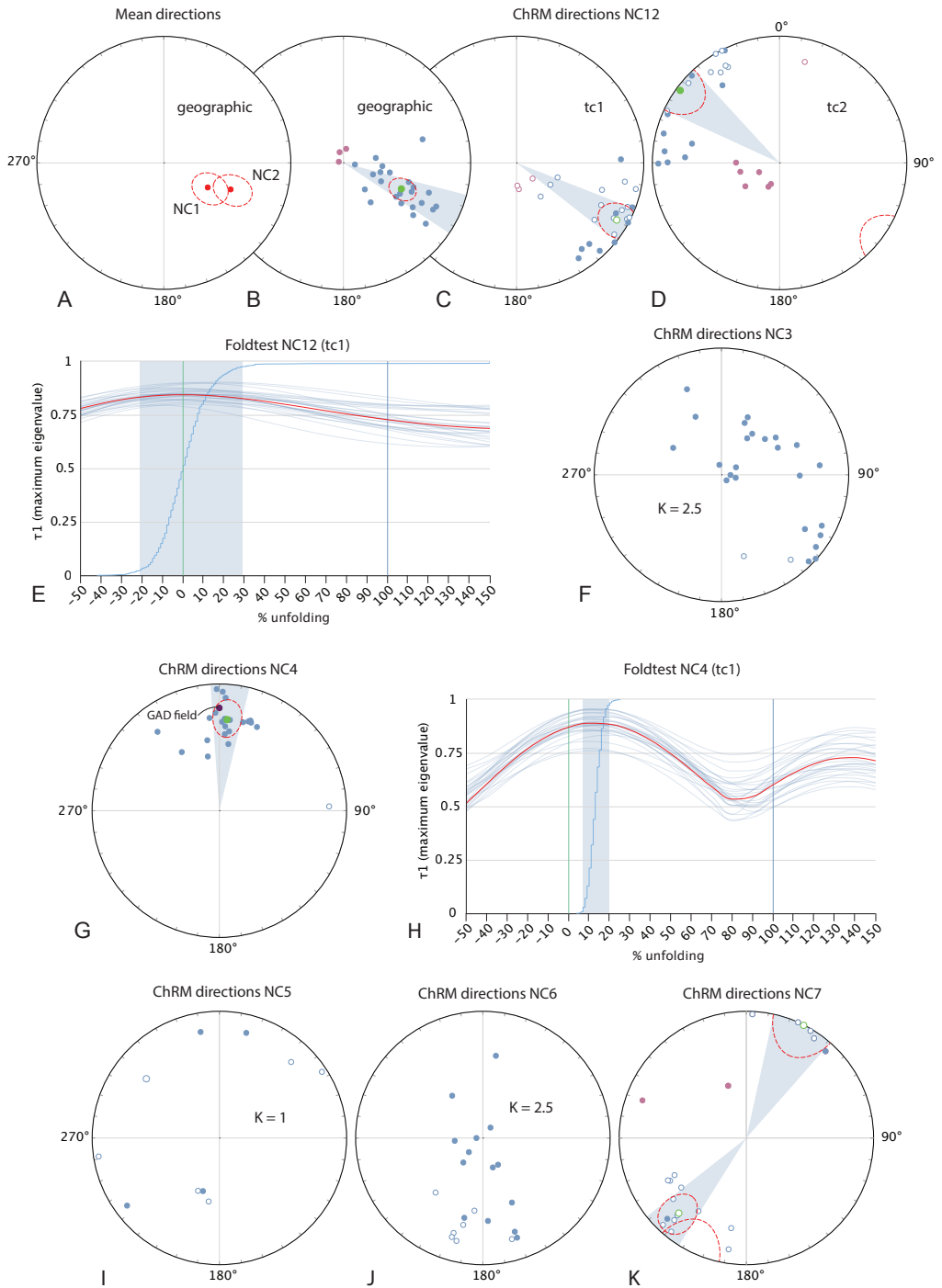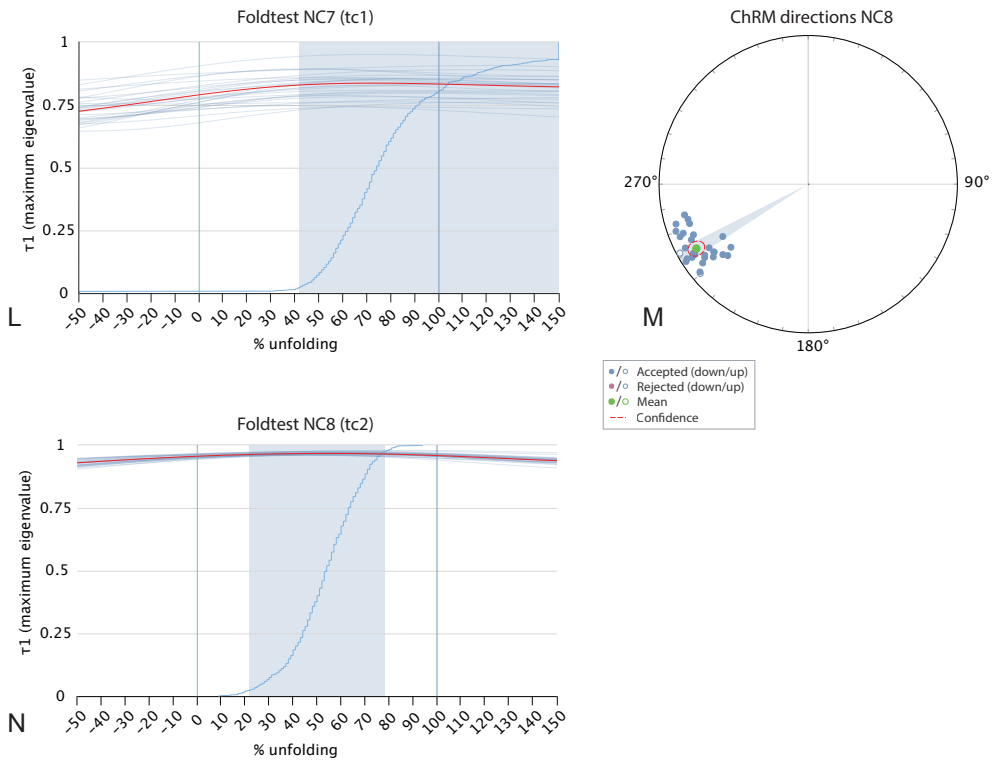
Figure 5: A) Mean directions of sites NC1 and NC2, sharing a CTMD; B-D) ChRM directions of sites NC1 and NC2 in geographic and tectonic (tc1 and tc2) coordinates; E) bootstrapped foldtest of sites NC1 and NC2: cumulative distribution function (with confidence interval in light blue) based on 1000 bootstraps (average of bootstraps in red); F) ChRM directions of site NC3; G) ChRM directions of site NC4, including the GAD field in purple; H) bootstrapped foldtest of site NC4: cumulative distribution function (with confidence interval in light blue) based on 1000 bootstraps (average of bootstraps in red); I-J) ChRM directions of sites NC5 and NC6; K) ChRM directions of site NC7 containing both normal and reversed distributions; L) bootstrapped foldtest of site NC7; M) ChRM directions of site NC8; N) bootstrapped foldtest of site NC8.

between 10-20 mA/m. Fold tests are indeterminate (tc1) or indicate that acquisition of the magnetization was syn-folding (best fit between 22-78% unfolding, tc2), and the dispersion parameter is 73.5 (in in-situ coordinates)(Fig. 5). Such a high K-value on a site of sedimentary rocks indicates that a limited amount of secular variation is recorded, which is in in line with a (rapid) remagnetization during folding.

The paleomagnetic data from successful sites indicate that the rock assemblages of the Nicoya Peninsula and Murciélago Islands formed within 10° of the equator during the

Table 1: Paleomagnetic results

Localities	Lat (°N)	Lon (°W)	Age	N	N45(is)	N45(tc)	In-situ D	ΔDx	I	ΔIx	Tilt corrected D	ΔDx	I	ΔIx	k	α95	K	λ	A95min< A95< A95max	Rejected due to
NB1	10.56755	85.69314	137.6 ± 1.8 Ma	65	56	54	296.4	5.3	12.7	10.2	286.1	5.0	7.7	9.9	10.2	6.4	16	3.9	2.4<5<6.6	
NB2	10.02701	85.73885	119.4 ± 1.1 Ma	63	41	42	236.2	4.9	21.0	8.7	228.3	5.3	17.2	9.8	13.2	6.3	18.7	8.8	2.7<5.2<7.8	
NB3	9.65157	85.06761	Cenomanian/Turonian	43	27	26	256.0	6.6	6.5	13.1	254.2	6.5	10.2	12.7	13.7	7.9	20.1	5.2	3.3<6.5<10.5	
IM1	10.85505	85.91023	109 ± 2 Ma	9	9	9	282.7	4.5	13.1	8.7	292.6	3.7	-0.1	7.4	106.9	5.0	197.0		3.7<5.0<20.5	
IM3	10.85712	85.90699	109 ± 2 Ma	17	17	15	261.8	9.5	16.0	17.8	290.4	9.8	17.5	18.1	13.1	11.0	16.5		4.1<9.7<14.9	
IM5	10.85741	85.93941	109 ± 2 Ma	11	11	11	289.4	10.5	13.0	20.0	291.0	12.2	-10.2	23.8	13.5	12.9	15.0		4.6<12.2<18.1	
IM6	10.85683	85.90814	109 ± 2 Ma	7	6	6	280.1	9.8	11.5	18.9	290.4	6.8	1.9	13.6	43.9	10.2	97.2		5.9<6.8<26.5	
IM1356	10.85524	85.91005	109 ± 2 Ma	44	42	41	277.3	5.2	14.8	9.9	291.1	4.9	3.8	9.7	14.7	6	22.1	1.9	2.7<4.9<7.9	
IM2			109 ± 2 Ma	9	9	9	330.0	14.0	18.6	14.0	318.9	10.6	-39.0	13.8	28.9	9.7	28.3		5<9.8<20.5	K too low, inconsistent with IM1356
NC1	10.52667	85.63943	middle Oxfordian-early Tithonian	9	9		119.4	16.9	57.4	12.4					2.3	10.9	16.1			* negative foldtest
NC2	10.52667	85.63943	middle Oxfordian-early Tithonian	17	17		110.3	18.4	51.5	16.8					8.9	12.7	6.3			* negative foldtest
NC3	10.54177	85.63112	late Barremian-early Aptian	26			88.7	28.4	54.9	22.8					2.9	20.3	2.5			* K too low
NC4	10.3721	85.67124	Bajocian	22			5.4	9.8	29.5	15.4					10.4	10.1	11.8			* negative foldtest, indistinguishable from GAD
NC5	10.3721	85.67124	Bajocian	9			309.2		-26.9						1.0		1.0			* K too low
NC6	10.40379	85.80329	Hauterivian-Aptian	21			186.6	28.1	38.1	37.1					2.5	28.1	2.5			* K too low
NC7	10.40379	85.80329	Hauterivian-Aptian	24	22		219.1	7.3	-11.1	14.0	221.3	6.5	-2.3	12.9	14.2	8.3	22.8	-1.1	3.4<6.5<11.4	
NC8	10.35625	85.7799	Middle Jurassic-Early Cretaceous	29			240.0	3.2	14.5	6.0					43.5	4.1	73.5			* syn-folding, K too high

N: number of interpreted demagnetized specimens; N45(is)/N45(tc): number of specimens that fall within the 45° cut-off in in situ coordinates / after tilt correction

D: Declination, I: Inclination

* statistical parameters on directions in situ coordinates

Cretaceous. The consistent southwest to northwest directed declinations demonstrate a regional counterclockwise vertical axis rotation. However, significant variations in declination between sites indicate smaller, local rotations as well (Fig. 6).

6. Discussion
6.1. Tectonic interpretation of the Nicoya Peninsula

Our study attempts to kinematically link the Caribbean Plate with the oceanic plates of the Panthalassa Ocean in Mesozoic times. To this end, the Jurassic and Cretaceous rock record of the Nicoya Peninsula and Murciélago Islands is the most promising archive to constrain such a reconstruction, but this requires that this rock record is an integral part of the lithosphere of the western Caribbean Plate. This, however, is not beyond controversy, and first requires discussion as to what extent rocks exposed on the Nicoya Peninsula and Murciélago Islands may be far-traveled, accreted exotic fragments, as recently suggested by Madrigal et al. (2016). Based on geochemistry, these authors interpreted the Cretaceous basalts exposed on the Nicoya Peninsula to represent small fragments of three separate LIPs (the ~140 Ma Nicoya I LIP and ~120 Ma Nicoya II LIP that formed at the Farallon-Pacific ridge, and ~90 Ma CLIP). The Madrigal et al. (2016) plate tectonic model hinges on the assumption that it is unlikely or impossible for oceanic plateau material spanning ~50 Myr to have been extruded on the same location on a moving oceanic plate. Madrigal et al. (2016) therefore
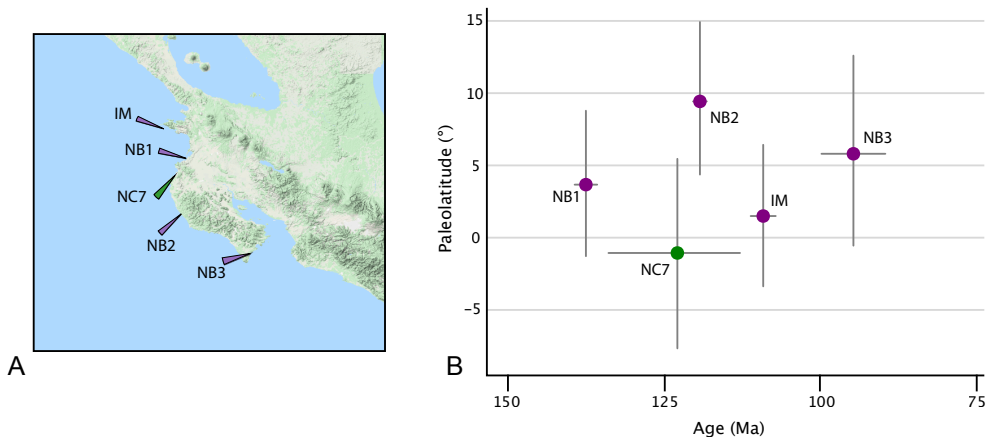
Figure 6: Paleomagnetic data from the Nicoya Peninsula and the Murciélago Islands. A) Sampling locations and declinations with confidence parachutes (ΔDx); B) paleolatitudes.

proposed that the different LIP fragments formed at the edge of the Pacific LLSVP in the central Panthalassa Ocean and were later accreted and amalgamated to form the Nicoya Complex. This scenario requires that the LIP fragments are currently separated by former subduction thrusts that consumed the hundreds of kilometers of oceanic basement that would have originally been present between the LIPs. However, no accretionary complex structures like trenchward younging nappes separated by thrust faults and foreland basin sedimentation have been documented between the different basalt exposures. Furthermore, in the Madrigal et al. (2016) model, no Bajocian or older lithosphere is present in the equatorial eastern Panthalassa Ocean to form the basement of the Nicoya Complex.

The alternative interpretation, in which the Nicoya Peninsula represents an integral part of the Farallon, and later, Caribbean Plate, implies the in-situ build-up of ~50 Myr of plume-related magmatism. As shown by Torsvik et al. (2010a), it is not uncommon for relatively small areas to contain a long history of plume-induced magmatism. Regions that have been located in proximity to the edge of an LLSVP for long periods of time (such as Southern Africa, southern Central Australia, or West Africa) contain plume-related magmatic rocks covering tens to even hundreds of Myr, and may contain large, but also small-volume plume-related volcanics. Hence, we argue that there is no direct necessity for the Nicoya basalts to represent separate LIP remnants that formed at large distances from each other, as long as Nicoya was located in close proximity to the edge of an LLSVP between ~140 and 90 Ma. We therefore choose the kinematically simpler scenario and reconstruct the Nicoya Peninsula and the Murciélago Islands as a single coherent tectonic block. We follow the interpretation of Denyer and Baumgartner (2006) and interpret the Nicoya Peninsula rock assemblages to have formed on pre-Bajocian

crust on which Bajocian and younger radiolarian cherts were deposited and multiple pulses of plume-related magmatism disrupted the original basement structures. The complex remained in this intra-plate setting until initiation of the western Caribbean subduction zone immediately to its west and arrival at the southern margin of the MCOT in Late Cretaceous time, after which it was covered by tuffaceous arc-derived sediments and shallow water carbonates (Andjić et al., 2018; Denyer & Baumgartner, 2006). In the following kinematic analysis, we test under which conditions this interpretation aligns with the available geological and paleomagnetic data.

6.2. Kinematic analysis

We develop a plate kinematic model that incorporates the Caribbean Plate into the Panthalassa plate system for the Mesozoic, prior to the initiation of the western Caribbean subduction zone. To this end, we explore connections of the Caribbean Plate to the plates reconstructed in the eastern Panthalassa Ocean at the time of subduction initiation in the western Caribbean subduction zone, and test the reconstruction against paleomagnetic data. This analysis is challenging as a result of uncertainties in (1) the post-subduction initiation reconstruction of the Caribbean Plate relative to the North and South American plates; (2) reconstruction of the Farallon Plate relative to the Pacific Plate; (3) reconstruction of the position of the Panthalassa plate system relative to the Indo-Atlantic plate system, which relies prior to 83 Ma on independent mantle reference frames for both systems each with its own uncertainties; and (4) the age of initiation of the western Caribbean subduction zone. As basis for our reconstruction, we use the GPlates (Boyden et al., 2011, gplates.org) reconstruction of the Caribbean region of Boschman et al. (2014) (updated for Chortis based on Molina Garza et al. (2017)) and add the Murciélago Islands and Nicoya Peninsula. We reconstruct a ~90° counterclockwise rotation of the Murciélago Islands following our paleomagnetic results.

The sedimentary assemblages overlying the Nicoya Peninsula are thought to record the Late Cretaceous collision with the southwestern margin of the North American Plate represented by the MCOT (Andjić et al., 2018; Baumgartner et al., 2008). In the reconstruction of Boschman et al. (2014), however, the MCOT was considered the westernmost part of the 'Great Arc of the Caribbean' and was therefore reconstructed as part of the northwestern margin the Caribbean Plate colliding with Chortis at 85 Ma, instead of the southern margin of the North American Plate. However, based on a 139.2 ± 0.4 Ma phengite cooling age of a metamorphic block from the Siuna serpentinite mélange, interpreted to record collision of the MCOT with the continental Chortis block (Baumgartner et al., 2008; Flores et al., 2015), we modify the reconstruction and consider the MCOT to be part of the North American Plate since 140 Ma. In the modified reconstruction, the Nicoya Peninsula, which represents the northwestern most part of the CLIP and (future) Caribbean Plate arrives at the southern margin of the MCOT at 88 Ma fulfilling stratigraphic constraints.

SI Age (Ma)	Mantle reference	Age lithospheric basement (Ma)	Overlap North American - Caribbean Plate	Paleomagnetic data	Proximity LLSVP (140-110 Ma)
75	VdM		✗ overlap	✓ good fit	
	O'N	✗ 154-168	✗ overlap	✓ good fit	✓ <10° pre-95 Ma
	D		✗ overlap	✓ good fit	
85	VdM	✗ 154-168	✗ overlap	✓ permitted	✓ <10° pre-100 Ma
	O'N	✓ 180-185	✗ overlap	✓ permitted	✓ <10° pre-120 Ma
	D	✓ 180-185	✗ overlap	✗ no fit	✓ <10° pre-120 Ma
90	VdM	✓ ~168	✓ <200 km overlap	✓ permitted	✓ <10° pre-105 Ma
	O'N	✓ 185-190	✗ overlap	✓ permitted	✓ <10° pre-130 Ma
	D	✓ >190	✗ overlap	✗ no fit	✓ <10° pre-130 Ma
100	VdM	✓ 168-180	✓ no overlap	✓ permitted	✓ <10° pre-112 Ma
	O'N	✓ ~190	✓ no overlap	✓ permitted	✗ >10°
	D	✓ >190	✓ no overlap	✗ no fit	✗ >10°
110	VdM	✓ ~190	✓ no overlap	✗ no fit	✓ <10° pre-130 Ma
	O'N	✓ >190	✓ no overlap	✗ no fit	✗ >10°
	D	✓ >190	✓ <200 km overlap	✗ no fit	✗ >10°

Preferred reconstruction → (100, VdM row)

Figure 7: Results of testing the 15 different reconstructions against independent data sets. For the reconstructions with subduction initiation at 75 Ma, whereby the Caribbean Plate is connected to the Farallon Plate after 83 Ma, the results of the tests 'Age lithospheric basement' and 'Proximity LLSVP' do not vary between the different mantle frames, because at 75 Ma the full reconstruction is connected through the plate circuit. The position of the Nicoya Peninsula relative to Farallon isochrons and the edge of the LLSVP does therefore not vary.

Next, we construct a Pacific-Farallon-Phoenix plate system using the isochrons of the Pacific Plate of Wright et al. (2016), and create a conjugate set of Farallon isochrons east of it, assuming symmetrical spreading, thereby constructing Pacific-Farallon plate motions. Similarly, we create Phoenix Plate isochrons conjugate to the southern (E-W oriented) Mesozoic isochrons of the Pacific Plate and construct Pacific-Phoenix plate motions. As
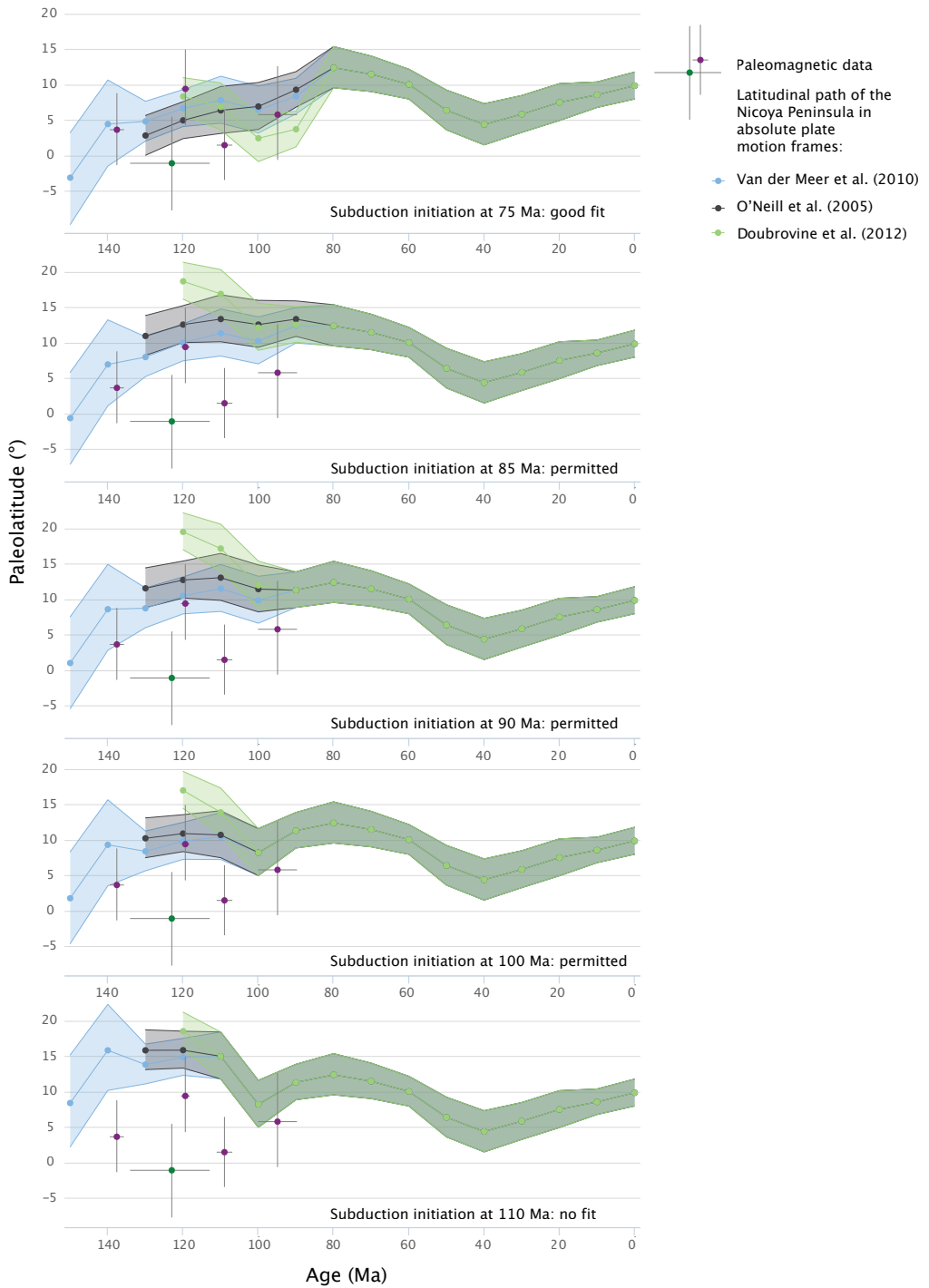
Figure 8 (left page): Paleomagnetic data compared to the expected paleolatitudes of the Nicoya Peninsula as predicted by the 15 different reconstructions, calculated for a reference location within the Nicoya Peninsula (10.1°N, 85.5°W). Reference values as predicted by the GAPWaP of Torsvik et al. (2012).

relative Farallon-Pacific and Phoenix-Pacific plate motions are now established, so is the rate and direction of spreading between the Farallon and Phoenix plates. Even though the exact geometry (i.e. location of ridge and transform segments) of the Farallon-Phoenix isochrons cannot be determined, we create hypothetical sets of isochrons for this spreading history, assuming symmetrical spreading and using minimal transform offsets.

In the next step in our analysis, we attach the Caribbean Plate to the reconstructed Farallon Plate for times prior to subduction initiation in the western Caribbean subduction zone, which marks the onset of relative Farallon-Caribbean motion and the birth of the Caribbean Plate. For times after 83 Ma, this is relatively straightforward, as the Pacific Plate was connected through Antarctica to the Indo-Atlantic plate circuit (e.g. Wright et al., 2016). For times prior to 83 Ma, this connection is absent and relative plate motions can exclusively be estimated by placing both Panthalassa and Indo-Atlantic plate systems in mantle reference frames. For the pre-83 Ma Panthalassa plate system, we use the Pacific fixed-hotspot frame of Wessel and Kroenke (2008) (145-83 Ma). For the post-83 Ma Panthalassa system and the Indo-Atlantic plate system, we use and test three different frames; the moving hotspot frames of Doubrovine et al. (2012) (124-0 Ma) and O'Neill et al. (2005) (140-0 Ma) and the slab-fitted frame of van der Meer et al. (2010) (300-0 Ma). To test the implications of different subduction initiation estimates, we attach the Caribbean Plate to the Farallon Plate at 5 different ages: 110, 100, 90, 85, and 75 Ma, resulting in a total of 15 possible reconstructions, the differences depending on the choice of mantle frame and subduction initiation age.

We then test the 15 possible reconstructions against parameters not used to build the reconstructions above. These include (a) the kinematic feasibility of Caribbean lithosphere motion relative to the North American Plate (including the MCOT and the Chortís block) for times prior to subduction initiation. In reconstructions towards the younger end of the western Caribbean subduction initiation spectrum, an overlap between the northern margin of the Caribbean Plate and the southern margin of the North American Plate is present between ~100-80 Ma, whereas reconstructions with older subduction initiation ages yield no or little overlap; (b) the age of reconstructed Farallon lithosphere at the location of the Nicoya Peninsula, which should be at least Bajocian (~170 Ma) in age given the oldest radiolarian cherts on the Nicoya Peninsula. We consider reconstructions in which the Nicoya complex is located southwest of the 168 Ma isochron (on <168 Ma crust) less plausible (Fig. 7). A good match exists between the age of the reconstructed Farallon basement underlying the reconstructed Nicoya Peninsula and the oldest radiolarian cherts now included in the Nicoya complex for all reconstructions, except for those with
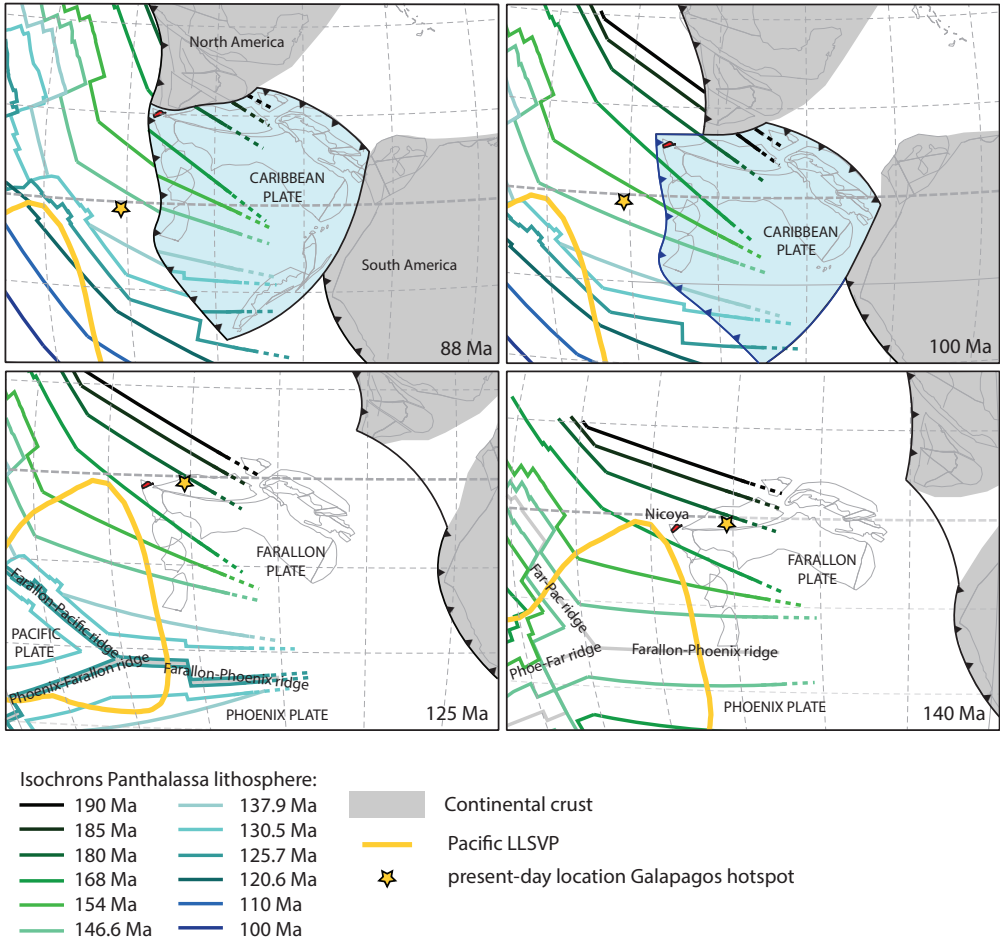
Figure 9: Reconstruction of the Caribbean region in the mantle stationary reference frame of van der Meer et al. (2010), with subduction initiation at 100 Ma. 140-125 Ma: the Nicoya Peninsula, located at the northwestern tip of the future Caribbean Plate, is close to the edge of the Pacific LLSVP. 100 Ma: subduction initiation in the western Caribbean subduction zone. 88 Ma: Nicoya is located adjacent to the southwestern margin of the North American Plate (MCOT).

a 75 Ma subduction initiation age; (c) paleomagnetic data from the Nicoya Peninsula and Murciélago Islands (Fig. 6,8); and (d) proximity of the Nicoya Peninsula to the edge of the Pacific LLSVP at the time of extrusion of plateau basalts.

For the paleomagnetic test, we use the tool on paleomagnetism.org developed by Li et al. (2017) that allows testing whether Euler-pole based tectonic reconstructions agree with paleomagnetic data. To this end, we compute Euler poles in 10 Myr steps for the Nicoya Peninsula relative to Africa for all 15 reconstructions and calculate the global apparent

polar wander path (GAPWaP) of Torsvik et al. (2012) into coordinates of the Nicoya Peninsula. In doing so, we switch from a reconstruction of plate motions relative to the lower mantle (that depends on the choice of mantle frame for the pre-83 Panthalassa plate system and the Indo-Atlantic plate system), to a reconstruction of plate motions relative to the spin axis, which enables comparison to paleomagnetic data. The paleolatitudes, declinations and inclinations are computed for a reference point within the Nicoya Peninsula (10.1°N, 85.5°W). The paleomagnetic data yields a better fit for reconstructions with younger subduction initiation ages (Fig. 8,9).

Finally, we test whether the Nicoya Peninsula is in close proximity (within 10°, as are most reconstructed LIPs (Torsvik et al., 2006)) to the edges of the Pacific LLSVP during the phases of LIP basalt extrusion (~139-133, ~120-110 and ~95-83 Ma). In all 15 reconstructions, the ~100-90 Ma position of the Nicoya Peninsula (i.e. during CLIP emplacement) is (>1000 km) east of the edge of the Pacific LLSVP, as is the present day position of the Galápagos hotspot (~850 km). For the two older pulses of LIP magmatism at ~139-133 and ~120-110 Ma, the Nicoya Peninsula restores closer to the LLSVP edges with younger western Caribbean subduction initiation ages. Taking all four tests in account, the reconstruction in the mantle reference frame of van der Meer et al. (2010) with a subduction initiation age of 100 Ma provides the optimal result (Fig. 7,9).

6.3. Implications for western Caribbean subduction initiation
Our attempt to reconstruct the Mesozoic history of the Caribbean Plate within the Panthalassa Ocean yields a reconstruction that is kinematically feasible, and is in line with paleomagnetic data. This successful reconstruction indicates that the lithosphere underlying the Caribbean Plate formed due to Farallon-Phoenix spreading prior to initiation of the western Caribbean subduction zone. Our reconstruction predicts that the Caribbean Plate is underlain by Jurassic lithosphere that increases in age towards the northeast.

This finding has important implications for the setting of formation of the western Caribbean subduction zone. Current dynamic and kinematic models widely infer that intra-oceanic subduction initiation occurs along pre-existing weakness zones at or close to active plate boundaries (transform faults and mid-ocean ridges) (Agard et al., 2007; Duretz et al., 2016; Hall et al., 2003; Leng & Gurnis, 2011; Maffione et al., 2015a; Maffione & van Hinsbergen, 2018b; Stern, 2004; Stern & Gerya, 2017; Stern et al., 2012). In our reconstruction, the western Caribbean subduction zone formed at high angles to inferred Farallon-Phoenix isochrons, and, given reconstruction uncertainties, may have formed parallel to fracture zones. However, with a subduction initiation age of ~100 Ma, the western Caribbean subduction zone formed in lithosphere that was at least 70 Myr old at that time, and was located far away from active intra-oceanic plate boundaries. Such old lithosphere is strong, cold, and therefore a surprising locus for intra-oceanic subduction initiation. In this respect, our reconstruction may provide additional support for the

proposal of Whattam and Stern (2015) for plume-induced subduction initiation (Gerya et al., 2015) in the western Caribbean region. The eruption the CLIP basalts around the Caribbean region is mostly ~90-85 Ma in age (see compilation in Whattam and Stern (2015)), somewhat younger than the best-fit subduction initiation age of 100 Ma estimated here. This may be the result of

reconstruction uncertainty, but on the other hand, numerical models have shown that the dynamic effects of plume rise on plates may precede LIP emplacement by ~10-15 Myr (van Hinsbergen et al., 2011b). We therefore concur that the Caribbean region may be an elegant test case for plume-induced subduction initiation within an old oceanic lithosphere.

7. Conclusions

We presented new paleomagnetic data from the Nicoya Peninsula and Murciélago Islands of northwestern Costa Rica, indicating that these terranes formed within 10° of the equator in Cretaceous time, and underwent counterclockwise vertical axis rotations. We developed a plate kinematic model that incorporates the Caribbean Plate into the Panthalassa plate system for Mesozoic times by connecting the Caribbean lithosphere to the Farallon Plate prior to 100 Ma subduction initiations in the western Caribbean subduction zone. This reconstruction is kinematically feasible and in line with paleomagnetic data. The western Caribbean subduction zone initiated in an intra-oceanic setting, breaking up oceanic lithosphere of at least 70 Myr old.

6

Reconstructing spreading ridge subduction within the Mesozoic Panthalassa Ocean using stratigraphic and paleomagnetic constraints from Hokkaido, Japan

Sampling the Idonappu Complex - Hokkaido, Japan

Abstract

The tectonic plates of the Panthalassa Ocean that once surrounding the supercontinent Pangea were consumed by subduction, compensating area gain during Atlantic and Indian Ocean spreading and growth of the Pacific Plate since Early Jurassic time. Tectonic reconstructions generally portray the Panthalassa Ocean as a simple four-plate system containing spreading ridges only, but the geological record of Hokkaido (Japan), includes remnants of a Jurassic intra-oceanic island arc (the Oku-Niikappu Complex). Here, we aim at reconstructing the Mesozoic intra-oceanic subduction evolution within the northwestern Panthalassa Ocean. First, we show that published marine magnetic anomaly data of the Pacific Plate record a change in Pacific-Izanagi spreading orientation between 146.6 and 137.9 Ma, coeval with Oku-Niikappu arc extinction. Second, we present an analysis of sequences of Ocean Plate Stratigraphy (OPS) exposed on both sides of the Oku-Niikappu Complex, revealing that accretion of the Oku-Niikappu Complex was paired with a major jump in age of the subducting lithosphere at the Hokkaido trench, reflecting previously subducted lithosphere. Furthermore, it reveals that at 145 Ma, the lithosphere (of Izanagi 1) that subducted in the intra-oceanic Oku-Niikappu trench (below Izanagi 2) was close to 0 Myr old, indicating that cessation of subduction was caused by ridge subduction. Upon full subduction of Izanagi 1, continued divergence between Izanagi 2 and the Pacific Plate led to renewed spreading in a slightly different orientation, resulting in differences in orientation between pre- and post-145 Ma marine magnetic anomalies. We reconstruct the Oku-Niikappu arc at ~145 Ma using Pacific magnetic anomalies to a paleolatitude of ~10°N, consistent with our new paleomagnetic data and illustrate the possible correlation between the Oku-Niikappu arc and the lower mantle Telkhinia slabs. This study illustrates the value of the concept of OPS on the development of plate kinematic reconstructions of lost oceanic plates, particularly when combined with paleomagnetic, seismic tomographic, and marine geophysical data sets.

1. Introduction

Pangea break-up resulted in the formation of the modern Atlantic and Indian oceans, which contain marine magnetic anomalies and fracture zones that allow for accurate reconstruction of the supercontinent back to early Mesozoic time (e.g. Seton et al., 2012). The gain of oceanic lithosphere associated with the break-up of Pangea led to area loss within the paleo-Pacific or Panthalassa Ocean, and together with the continuous growth of the Pacific Plate since Early Jurassic time, this led to subduction of the vast majority of the oceanic lithosphere that was underlying the Panthalassa Ocean during the Mesozoic and early Cenozoic. Tectonic reconstruction of the Panthalassa Ocean is therefore challenging, and relies on (1) marine magnetic anomalies of the Pacific Plate (Boschman & van Hinsbergen, 2016 (Chapter 1); Wright et al., 2016), (2) geological and paleomagnetic data from preserved relics of subducted plates within the circum-Pacific accretionary complexes (e.g. Ando et al., 2001; Kirschvink et al., 2015; Kodama et al., 2007; Tarduno & Alvarez, 1985) or from trapped fragments of lithosphere such as in the Caribbean Sea and Aleutian Basin (Boschman et al., 2014 (Chapter 2); Domeier et al., 2017; Vaes et al.,

Figure 1: Tectonic map of Japan and the Northeast Eurasian continent. MTL: Median Tectonic Line. Belts in Hokkaido: O: Oshima, SY: Sorachi-Yezo, H: Hidaka, T: Tokoro, N: Nemuro. Belts in southwestern Japan: MT: Mino-Tambo (Jurassic), S: Sambagawa metamorphic belt, C: Chichibu Belt, including the Paleozoic Kurosegawa Belt sandwiched between the Jurassic North and South Chichibu belts, SH: Shimanto (Late Cretaceous – Paleogene).

submitted; Chapter 5), and (3) evidence from seismic tomography revealing subducted lithosphere in the mantle (Domeier et al., 2017; Sigloch & Mihalynuk, 2017; van der Meer et al., 2012, 2018); Chapter 4). Based on marine magnetic anomaly data from the Pacific Plate alone, current global plate tectonic reconstructions generally portray the

Panthalassa Ocean as a three-plate (Izanagi-Phoenix-Farallon) system with one central ridge-ridge-ridge triple junction before, and a four-plate (Izanagi-Phoenix-Farallon-Pacific) system after Early Jurassic birth of the Pacific Plate (e.g. Scotese, 2004; Seton et al., 2012). Plate motions of the conceptual Farallon, Phoenix and Izanagi plates are derived from mirroring the marine magnetic anomalies preserved on the Pacific Plate (Boschman & van Hinsbergen, 2016 (Chapter 1); Seton et al., 2012; Chapter 5). However, subduction of the Pacific Plate along the northeast Asian margin consumed significant parts of the Pacific-Izanagi spreading record, and therefore, only a small portion (in both time and space) of the northwestern Panthalassa Ocean can be successfully reconstructed with this method. Furthermore, the simple three-plate models is inconsistent with the accretionary records in Japan and Northeast Siberia, where accreted intra-oceanic arc terranes are exposed indicating that the tectonic history of the Northwestern Panthalassa Ocean was considerably more complex. Instead, the region must have contained intra-oceanic subduction zones and more than just the Pacific and Izanagi plates (Domeier et al., 2017; Konstantinovskaia, 2001; Nokleberg, 2000; Shapiro & Solov'ev, 2009; Stone et al., 2003; Ueda & Miyashita, 2005; van der Meer et al., 2012; Vaes et al., submitted). In this study, we aim to reconstruct the Northwestern Panthalassa Ocean, relying on the Early Jurassic-mid Cretaceous Pacific-Izanagi spreading records preserved on the Pacific Plate, combined with the accretionary geological record of Hokkaido (Japan), which includes remnants of a Jurassic intra-oceanic island arc (the Oku-Niikappu Complex).

In this study, we (1) analyze marine magnetic anomalies of the Pacific Plate to reconstruct Pacific-Izanagi spreading; (2) add constraints on the age of the subducting plates through time by analyzing 'Ocean Plate Stratigraphy' (OPS) sequences on either side of the Oku-Niikappu Complex exposed on Hokkaido; (3) provide new paleomagnetic data from accreted materials of Hokkaido including the Oku-Niikappu Complex; and (4) test the resulting reconstruction of consumed oceanic lithosphere against seismic tomographic images of deep-mantle structure.

2. Geological setting
2.1. Pacific-Izanagi spreading records
The oldest part of the Pacific Plate, located in the northwestern Pacific Ocean, contains marine magnetic anomalies and fracture zones in three orientations (Fig. 2).
Pacific-Izanagi spreading records, preserved by the northeast trending 'Japanese' lineations, allow for reconstruction of the ~190-100 Ma northern part of the Izanagi Plate (Larson & Chase, 1972; Woods & Davies, 1982). In modern coordinates, the orientation of the fracture zones indicates northwestward motion of Izanagi relative to the Pacific Plate for ~190-146.6 Ma, followed by a change towards north-northwestward motion (Fig. 2). This suggests a change in spreading directions and hence, ridge orientation, sometime between 146.6 Ma and 137.9 Ma. So far this change remains tectonically unexplained.
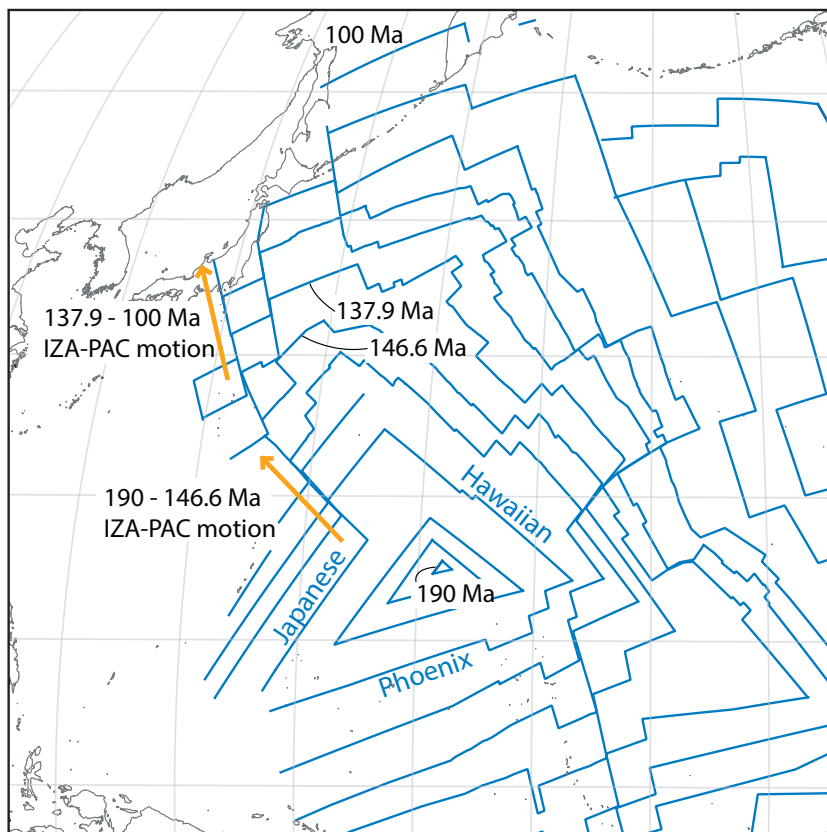
Figure 2: Isochrons (from Wright et al. (2016)) of the Pacific Plate based on marine magnetic anomalies.

The lithosphere currently subducting in the Japan-Kuril-Kamchatcha trench (Fig. 1, 2) is ~125-100 Ma, and all of the Izanagi Plate, the Pacific-Izanagi spreading ridge, and the western Pacific Plate younger than ~100 Ma have subducted. Assuming spreading rates did not change since 125 Ma, the Pacific-Izanagi ridge would have subducted sometime in the Paleogene, ~50 Ma (Seton et al., 2015).

2.2. Accretionary record of Japan

The Japanese islands contain a record of orogenesis related to ~500 Myr of subduction (Isozaki, 1996; Maruyama & Seno, 1986). Since break-up of the Neoproterozoic supercontinent Rodinia, Japan has been located on the margin between the continental China Blocks (part of Eurasia since the mid-Mesozoic) and the Panthalassa Ocean, first as a passive margin, since establishment of continental margin subduction at ~500 Ma as an active margin, and since Oligo-Miocene opening of the Sea of Japan, as an island-arc (Isozaki, 1996, 2000; Isozaki et al., 2010; Maruyama et al., 1997). During long-lived subduction, a series of overall trenchward-younging accretionary complexes formed that

contain upper plate-derived trench-fill deposits mixed with downgoing plate-derived remnants of ridges, rises, seamounts, and occasionally, the abyssal plane (Isozaki, 2000; Isozaki et al., 1990). Isozaki et al. (1990) compiled and evaluated data from all accreted oceanic materials exposed in the Paleozoic – Cenozoic accretionary complexes in Japan, and developed the concept of Ocean Plate Stratigraphy (OPS). Ideal OPS sequences consist from bottom to top of magmatic basement rocks, overlying oceanic sediments (radiolarian cherts, limestones, hemipelagic mudstones), and turbiditic trench-fill deposits, representing rocks accumulated on the ocean floor on its journey from a mid-ocean ridge to a trench. The age difference between the base and top of an ideal OPS sequence reflects the age of the oceanic crust at the time of subduction, thereby providing a valuable geological source of information on the nature and drift of lost oceanic plates. Age gaps between adjacent sequences of trench-fill deposits separate the accretionary rocks into distinct complexes, and indicate that accretion is not continuous but irregular and episodic, perhaps correlated to the timing of supply of voluminous terrigenous sediments (Isozaki et al., 1990).

The Median Tectonic Line (MTL) in southwest Japan forms an exception to the overall younging of the Japan accretionary complexes towards the trench. The MTL is a major E-W trending, northward dipping strike-slip fault, which is inferred to have accommodated >1000 km left-lateral motion during the Cretaceous (Kawamura et al., 2003; Sakashima et al., 2003). The MTL currently juxtaposes an outer (southern) zone including a Cretaceous HP-LT metamorphic belt (the Sambagawa Belt) and Paleozoic basement found sandwiched between two Jurassic accretionary complexes (the Chichibu Belt) against an inner (northern) zone consisting of Paleozoic-Jurassic accretionary complexes (Banno & Sakai, 1989; Takasu et al., 1994)(Fig. 1). The Paleozoic basement belt of the outer zone (the Kurosegawa Belt) contains clastics with a continental affinity (Aitchison et al., 1991; Hada et al., 2001). These age relationships suggest that during the Cretaceous, large-scale out-of-sequence thrusting occurred within a continental margin-derived accretionary prism burying older parts of the prism to HP-LT metamorphic conditions. Major motion across the MTL is further confirmed by fauna. Similarities in (boreal) fauna between the inner zone and east Siberia indicate that at least by Permian time, the inner zone was emplaced in its pre-Sea of Japan opening position adjacent to the Asian continent (Hayami, 1961; Kobayashi & Tamura, 1984; Sato, 1962; Tazawa, 2001). The outer zone, however, contains diverse Triassic - Jurassic faunal assemblages with a Tethyan affinity (Hallam, 1986; Hayami, 1984; Kobayashi & Tamura, 1984; Matsumoto, 1978), suggesting a major tectonic break at the MTL between terranes of different paleolatitudes.

Hokkaido is interpreted to correlate to the outer zone of southwest Japan (Ueda, 2016). The pre-Neogene basement of Hokkaido is divided into the ~N-S trending Oshima, Sorachi-Yezo, Hidaka, Tokoro and Nemuro tectonostratigraphic belts (Fig. 1), containing accretionary complexes, overlain and intruded by magmatic arc and fore-arc assemblages
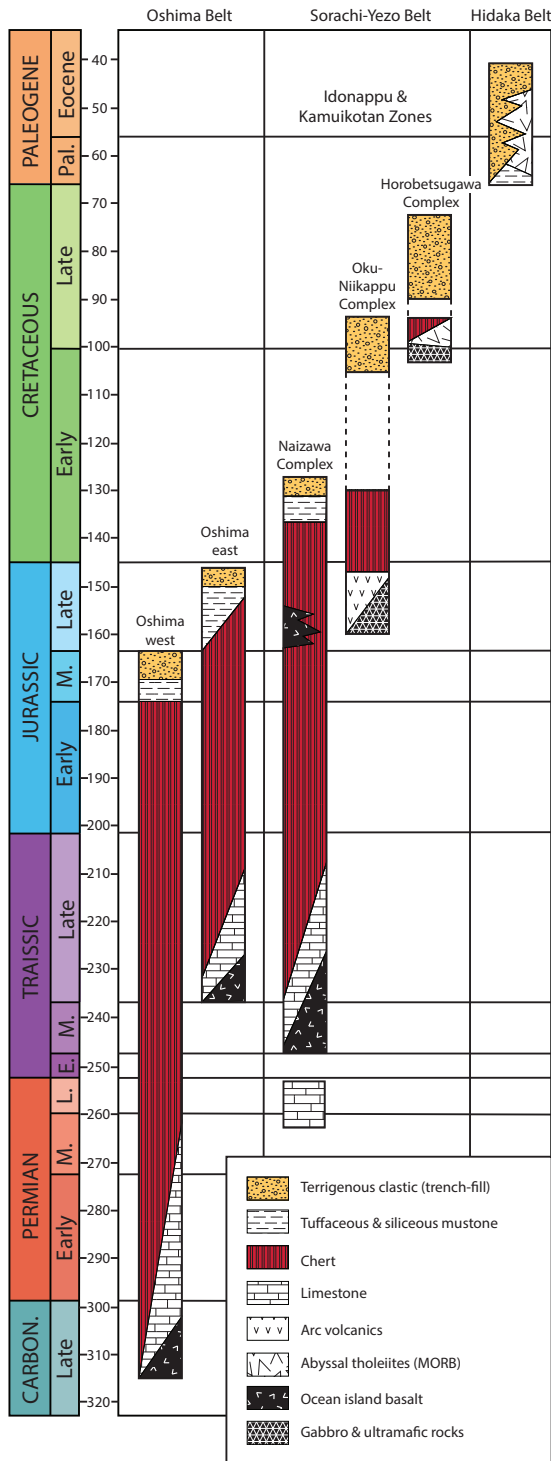
Figure 3: Simplified stratigraphic columns of the OPS sequences of the Oshima, Sorachi-Yezo and Hidaka belts. Modified from Ueda (2016).

(Kiminami, 1992; Ueda, 2016). The Jurassic-Paleogene western three belts continue into the Russian island of Sakhalin in the north and on Honshu in the south and are interpreted to have formed due to (north)westward subduction of Panthalassa lithosphere below the North China block Ueda (2016). In contrast, the Late Cretaceous-Paleogene eastern two belts (Tokoro and Nemuro) consist of thrust slices with opposite vergence and contain clastic rocks richer in basic to intermediate volcanics and only minor continent-derived silicic materials (Kiminami & Kontani, 1983). These belts correlate with an accreted intra-oceanic arc system that does not continue towards Honshu, but is exposed on eastern Sakhalin and Kamchatka (Domeier et al., 2017; Konstantinovskaia, 2001; Shapiro & Solov'ev, 2009; Vaes et al., submitted). This eastern arc-trench system was juxtaposed against western Hokkaido in Miocene time during opening of the Kuril back-arc basin (Arita et al., 1986; Kimura, 1986; Kimura & Tamaki, 1985). In this study, we focus on the subduction history between the Panthalassa plates and the North China block, and thus focus on the stratigraphy of the Oshima, Sorachi-Yezo and Hidaka belts.

The Oshima Belt consists of Middle Jurassic – lowermost Cretaceous terrigenous clastic sedimentary sequences incorporating Upper Carboniferous-Lower Jurassic pelagic chert, limestone and oceanic island basalt, overlain and intruded by Lower Cretaceous arc-related plutonic, volcanic and sedimentary rocks (Ishiga & Ishiyama, 1987; Kawamura, 1986; Minato & Rowett, 1967; Minoura & Kato, 1978; Ueda, 2016; Yoshida & Aoki, 1972). The clastic sequences are interpreted as accretionary complexes and these complexes are characterized by the occurrence of both stacked thrusts sheets of coherent OPS sequences of cherts and clastic rocks, as well as block-in-matrix mélange facies. The trench fill clastics consist of mudstones and sandstones rich in quartz and feldspars, and detrital zircon ages of ~1.8 and 2.5 Ga indicate a continental source (Kawamura et al., 2000). Kawamura et al. (2000) subdivided the Oshima accretionary complexes in an older western belt, characterized by Carboniferous-Permian limestone and chert and Middle Jurassic clastic trench-fill deposits, and a younger eastern belt containing Triassic limestone and chert and Upper Jurassic trench-fill (Fig. 3). These two belts represent the oldest two OPS sequences of Hokkaido. The lack of MORB basement (only OIB was identified) provides a minimum estimate for lithosphere age only, as the OIBs were likely deposited on older oceanic crust.

The Sorachi-Yezo Belt, located east and positioned structurally below the Oshima Belt, contains a series of Cretaceous accretionary complexes overthrust by the Jurassic Horokanai ophiolite and its conformable Sorachi and Yezo Groups sedimentary cover. The Horokanai ophiolite contains a succession of serpentinized peridotite, gabbro, amphibolite, MORB-like basalt and Upper Jurassic cherty and tuffaceous siliceous sedimentary rocks (Asahina & Komatsu, 1979; Ishizuka, 1980, 1985). The Sorachi and Yezo Groups, conformably overlying the ophiolite, comprise a coherent sequence of pillow and massive basalts (lower Sorachi Group, which is the upper basaltic section of the Horokanai ophiolite), Upper Jurassic-middle Lower Cretaceous chert, siliceous mudstone, felsic tuff and volcanic sandstone and conglomerate (upper Sorachi Group), and Lower-

Upper Cretaceous terrigenous clastic rocks (Yezo Group) (Ando, 2003; Niida & Kito, 1986; Takashima et al., 2001, 2004). These sedimentary sequences are interpreted to record fore-arc basin fill deposited on oceanic crust connected to the continental margin (Kiminami et al., 1985; Niida & Kito, 1986).

The underlying accretionary complex rocks are mainly exposed in the high-pressure, low-temperature (HP-LT) Kamuikotan and non-metamorphosed Idonnappu zones, the former interpreted as the deeper-subducted equivalent of the latter (Ueda, 2016). The metamorphic rocks of the Kamuikotan Zone are exposed as tectonic windows in the cores of anticlines and contain both coherent masses of schist and low-grade meta-clastic rocks, as well as blocks in serpentinite mélanges (Sakakibara & Ota, 1994). The Idonnappu Zone is subdivided into the western Naizawa Complex containing OIBs, Permian-lowermost Cretaceous limestones, cherts, and Lower Cretaceous trench-fill deposits (Hashimoto et al., 1975; Igo et al., 1987; Kato & Iwata, 1989; Kato et al., 1986; Kiyokawa, 1992; Sakagami & Sakai, 1979; Sakakibara et al., 1997; Ueda et al., 2001), the central Oku-Niikappu Complex, and the eastern Horobetsugawa Complex containing mid-Cretaceous MORB-basalts, chert, red pelagic mudstones, and Upper Cretaceous trench-fill deposits (Kiyokawa, 1992; Ueda et al., 2001; Ueda et al., 2000), representing three OPS sequences (Fig. 3).

The Oku-Niikappu Complex, identified by Ueda and Miyashita (2005), consists of (1) massive and foliated serpentinite; (2) a sheeted dyke complex containing andesitic, boninitic and MORB-like dykes; (3) (meta)volcanics, volcaniclastic sedimentary rocks, conglomerates (containing clasts of volcanics and serpentinite) and Lower Cretaceous (Berriasian and younger) red bedded chert; and (4) Albian-Cenomanian black mudstone and siliciclastic sandstone, partly containing meter-sized blocks of chert and (meta)volcanic rocks (Ueda, 2003; Ueda & Miyashita, 2003, 2005). Except for the MORB-like dykes, all igneous rocks from the Oku-Niikappu Complex show island arc geochemical characteristics (Ueda & Miyashita, 2005). Ueda and Miyashita (2005) interpreted the Oku-Niikappu complex as a Late Jurassic – earliest Cretaceous intra-oceanic island arc that went extinct while still in an intra-oceanic setting, was extended and partly eroded, covered by cherts in a pelagic environment, and eventually, ~45 Myr after arc extinction, by Albian-Cenomanian trench-fill deposits. In this interpretation, the andesitic dykes and pillow lavas are the oldest rocks of the complex that formed during the stages of active arc magmatism. Boninitic and MORB-like dykes are interpreted to reflect intra-arc extension, coeval with the formation of detachment faults that exhumed serpentinitized peridotite and generated the deposition of conglomerates and volcaniclastic sediments (Ueda, 2016).

The Hidaka Belt, structurally located below the Sorachi-Yezo Belt, consists of Upper Cretaceous to Paleocene-Eocene hemipelagic mudstones and Paleocene-Eocene terrigenous turbiditic sandstone, MORB-chemistry dolerite and basalt, incorporating Permian-mid-Cretaceous blocks of limestone and chert (Endo & Hashimoto, 1955;

Iwata & Tajika, 1989; Kiminami, 1990; Mariko & Kato, 1994; Miyashita & Katsushima, 1986; Miyashita & Yoshida, 1994; Tajika & Iwata, 1990; Watanabe & Iwata, 1985). These latter older rocks, as well as the Upper Cretaceous mudstones are considered to be reworked mélange blocks derived from the Idonappu Zone in the west (Tajika & Iwata, 1990). Structures in the Paleocene-Eocene mudstones and dolerites and basalts (inter-pillow mudstone, silicified baked margins of mudstones in contact with dolerites and mudstone fragments as xenoliths in the dolerites) indicate that eruption and intrusion of the magmatic rocks was syn-sedimentary (Kiminami, 1999; Mariko, 1984; Miyashita & Katsushima, 1986; Nakayama, 2003). Therefore, these magmatic rocks are interpreted to have formed due to seafloor spreading adjacent to a continent, i.e. just prior to subduction of the ridge (Miyashita & Katsushima, 1986).

3. Paleomagnetism
3.1. Sampling and ages
From a large (~100 m) riverbed exposure of block-in-matrix mélange of the Naizawa Complex of the Idonnappu zone, we sampled 5 sites (ID1-5, 72 cores) from 4 units with an internally coherent stratigraphy. These include Oxfordian-Kimmeridgian and Berriasian-Valanginian pinkish limestones and red bedded cherts of the oceanic sequence, and Valanginian – Barremian mudstones, tuffs and sandstones representing trench-fill deposits (Fig. 3,4).
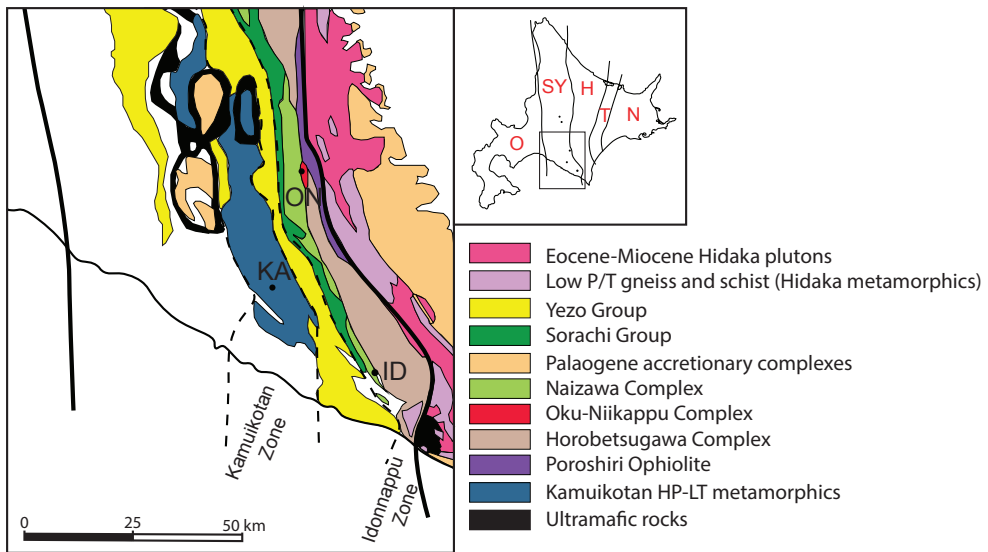
Figure 4: Geological map of the southern Hokkaido, including sampling locations ID, KA and ON. Modified from Ueda (2016).

From a continuous, internally undeformed sequence (the Iwashimizu Formation) in the Kamuikotan Zone, we sampled 8 sites (KA1-8, 62 cores and 37 hand samples) along two parallel river sections east of the Shizunai Lake. These exposures are extensively described by Hori and Sakakibara (1994) and this sequence represents the low-temperature metamorphic equivalent of the Naizawa Complex of the Idonappu zone. We sampled dolerite sills, interlayered Upper Triassic cherts, younger cherts deposited around the Triassic-Jurassic boundary, and Valanginian- Barremian green tuffaceous mudstones (Fig. 3,4) that contain ~2 Ga detrital zircons, indicating a continental source region (Ozawa, 2018).

The Oku-Niikappu Complex is a narrow (<2 km) serpentinite-bearing belt in the Idonnappu Zone exposed around the Niikappu River containing an aggregate of fault-bounded slices and blocks. We sampled 4 sites (ON1-4, 90 cores, 22 hand samples) consisting of a sequence of dykes, pillow basalts, and Berriasian overlying cherts (Fig. 3,4). These dykes are not as regular and symmetrical as typical sheeted dyke complexes formed at mid-oceanic ridges, but vary in bulk rock composition, in thickness (10 cm to 15 m) and contacts are sub-parallel (trending N-S with near-vertical dips).

3.2. Methods

We collected both hand samples (from cherts), as well as typical paleomagnetic cores (from all other rock types) using a gasoline-powered motor drill. From the hand samples we later drilled one to five cores per sample using a drill press. For hand samples, we estimated bedding planes (and perpendicular core orientations) by single measurements per sample. For cores, we averaged multiple (three to seven) bedding measurements per site. The orientation of the cores was measured with an ASR OR-2 orientation device and Brunton compass. The cores were cut into samples of 2.2 cm length, subjected to either thermal or alternating field demagnetization using successively higher temperature or field steps up to 680°C or 100 mT, and measured on a 2G DC SQUID cryogenic magnetometer. Based on the potential presence of hematite, red chert (KA1,2,6, ON3,4) and pink limestones (ID1) samples were all demagnetized thermally. Using the online portal Paleomagnetism.org (Koymans et al., 2016), we interpreted the demagnetization data plotted in Zijderveld diagrams (Zijderveld, 1967) using principle component analysis (Kirschvink, 1980), determined great circle solutions using the method of McFadden and McElhinny (1988), calculated site means using Fisher (1953) statistics following procedures described in Deenen et al. (2011), applied a 45° cut-off to the virtual geomagnetic poles per site (Johnson et al., 2008), and used the foldtest (Tauxe & Watson, 1994) and bootstrapped coordinate test (Tauxe, 2010) when applicable.

3.3. Results and tectonic interpretation

Despite the large sample set, only few samples yielded geologically meaningful paleomagnetic results. Except for ON4, all sites have been rejected or excluded from

further analysis on plate tectonic motions due to (1) high dispersions (ID1, ON1,2), a recent field overprinting the original magnetization (ID3), or directions representing ancient, but undated magnetizations that were acquired after tilting or folding (ID2,4,5, all KA sites, ON3). Paleomagnetic results and interpretations of these sites are extensively described in the Supplementary Material.

Site ON4 contains Berriasian (Ueda & Miyashita, 2005) radiolarian cherts with little variation in bedding orientation. Two components were interpreted from the demagnetization data: a medium temperature (420-560°C) or magnetite component (mt), and a high temperature (620-680°C) or hematite component (ht) (Fig. 5a-d). The mt-component is very similar to results from ON3 (Fig. 5e,f), which yielded a negative foldtest (best clustering between -42 and 3% unfolding, Fig. S8c), and is therefore interpreted to represent a magnetization that was acquired after tilting. The ht-component may represent a primary magnetic signal, although no field tests can be performed to confirm this, as no reversals were recorded and within-site variations in bedding orientation were not large enough to allow for a statistically meaningful fold test. Nonetheless, the ON4-ht component yields directions (not corrected for bedding tilt) significantly different from the GAD field and from any other direction measured in this study for which the magnetization is clearly post-folding. Furthermore, the magnetization
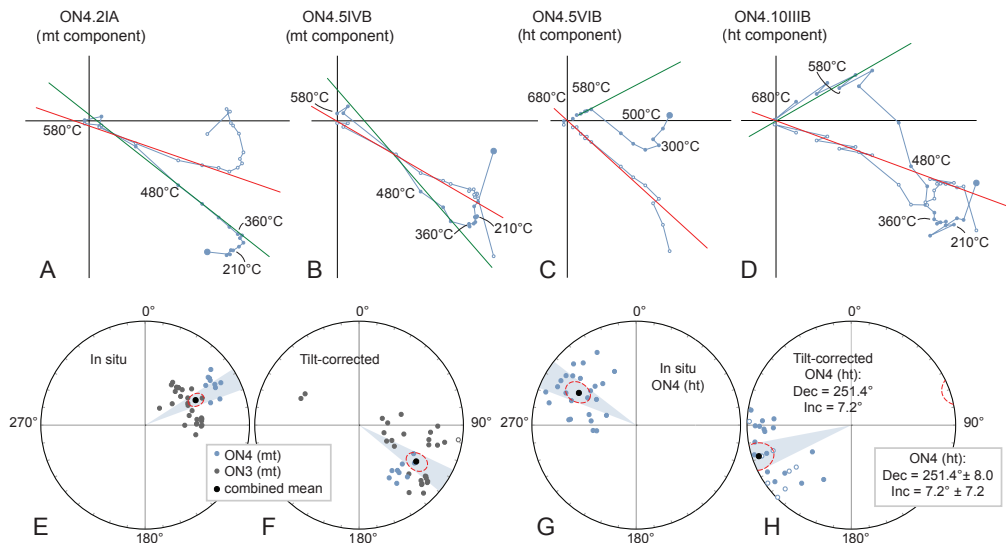
Figure 5: Paleomagnetic results. A-D) Orthogonal vector diagrams of representative samples of ON4 in geographic coordinates (not corrected for bedding tilt), closed (open) symbol for declination (inclination), up/west projection; E-H) Interpreted ChRM directions of sites ON3 (mt-component) and ON4 (mt- and ht-components).

is carried by hematite with very high (620-680°C) unblocking temperatures. For these reasons, we argue that a primary nature of this magnetization is likely and we consider the tilt-corrected ht-component of the ON4 cherts as currently the best available indicator of paleolatitude of the remnant Oku-Niikappu arc in Berriasian time. The mean direction (after tilt-correction) from ON4-ht is: Dec ± ΔDx = 251.4 ± 8.0°, Inc ± ΔIx = 7.2 ± 15.7°, n =24, K = 14.8, A95 = 8.0, Fig. 5h). This interpretation suggests that the (then just extinct) Oku-Nikkappu arc was located at equatorial latitudes (± 3.6° [-4.3°, 11.9°]) in Berriasian time, after which the remnant arc migrated northwards and accreted in the Hokkaido trench in mid-Cretaceous time.

5. Discussion: Northwest Panthalassa plate kinematic reconstruction
5.1. Izanagi reconstruction
The basis of our plate tectonic reconstruction of the western Panthalassa Ocean are Izanagi plate motions derived from Pacific-Izanagi spreading records preserved on the Pacific Plate. To this end, we used the Pacific isochrons of Wright et al. (2016) and created a conjugate set of Izanagi isochrons, assuming symmetrical spreading. We thus reconstruct ~190-100 Ma Pacific-Izanagi plate motions, which includes the pronounced change in relative plate motion direction between 146.6 and 137.9 Ma.

Next, we use the OPS sequences of the Oshima, Sorachi-Yezo and Hidaka belts, containing geological evidence for six episodes of accretion that resulted in the formation of accretionary complexes in Middle Jurassic (~165 Ma, Oshima west), Late Jurassic (~145 Ma, Oshima east), Early Cretaceous (~130 Ma, Naizawa), mid-Cretaceous (~100 Ma, Oku-Niikappu), Late Cretaceous (~80 Ma, Horobetsugawa) and Paleocene-Eocene (~50 Ma, Hidaka) times (Fig. 3). OPS sequences with MORB basement in direct contact with overlying oceanic sediments (Horobetsugawa and Hidaka) provide well-constrained ages of the subducting lithosphere during the episodes of accretion. For OPS sequences with OIB or arc magmatic basement (Oshima, Naizawa, Oku-Niikappu), the age of the base of the OPS sequence provides a minimum estimate only.

Plotting the ages of accretion versus (minimum) ages of subducting lithosphere (Fig. 6) reveals that since the Jurassic, the age of the lithosphere at the trench decreased, until the ~50 ± 10 Ma accretion of Hidaka, at which time the age of the subducting plate was equal the age of the trench fill (hence 0 Myr old). This trend indicates that throughout the Jurassic-Paleogene, a mid-ocean ridge was approaching the trench. The base of the OPS of Oshima east is younger than suggested by the overall trend, but because this age is a minimum estimate, we speculate that the underlying basement was older, at least Permian in age (Fig. 6). After accretion of Hidaka, the trend was reversed as shown by the ~125 Ma age of the Pacific Plate lithosphere currently subducting in the Japan and Kuril trenches.

Within the trend of overall decreasing age of subducting lithosphere, a vertical gap is apparent, representing the absence of an area of lithosphere in the Izanagi Plate. This gap
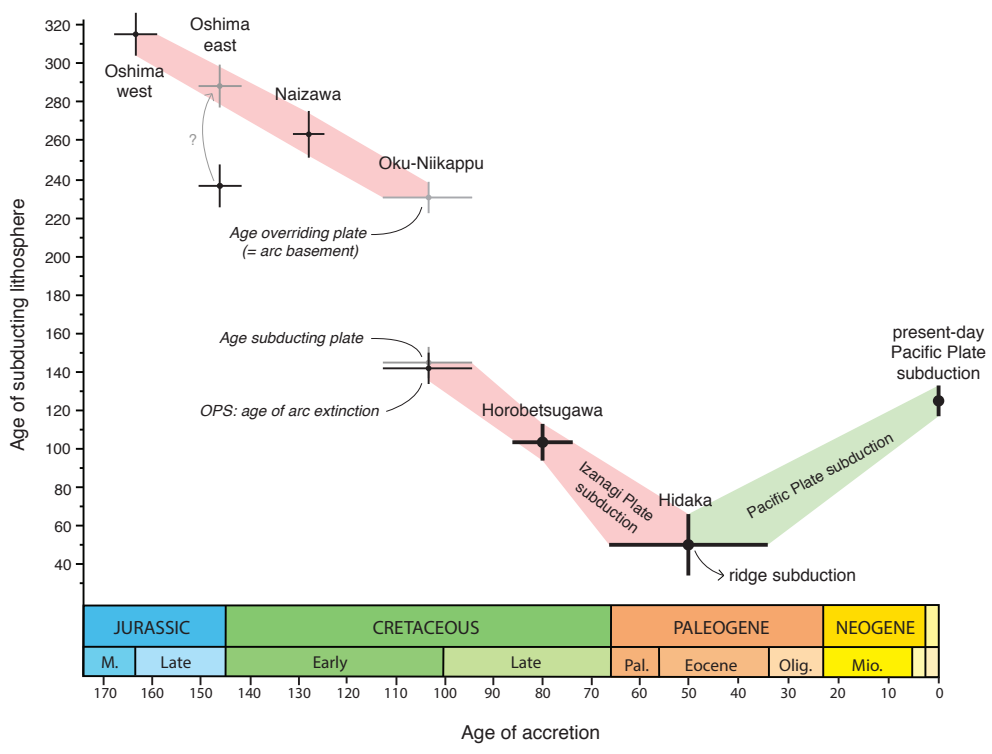
Figure 6: OPS ages versus ages of subduction in the Hokkaido trench. Thick dots and bars (Horobetsugawa, Hidaka and present-day) represent robust lithospheric ages from MORB basement; thin dots and bars are minimum estimates only. (inclination), up/west projection; E-H) Interpreted ChRM directions of sites ON3 (mt-component) and ON4 (mt- and ht-components).

coincides with accretion of the Oku-Niikappu Complex, and therefore, may readily be linked to lithosphere that subducted in the Oku-Niikappu intra-oceanic subduction zone. The age of the lithosphere on both sides of the Oku-Niikappu trench during cessation of subduction and arc extinction is not directly constrained, but based on the age of the cherts overlying the extinct arc, must be at least Berriasian (~145 Ma) in age. We extrapolate the trend defined by the two youngest (Horobetsugawa and Hidaka) OPS sequences, which contain MORB basement and thus provide robust lithospheric ages, back to the ~100 Ma arrival of the Oku-Niikappu Complex at the Hokkaido trench. This extrapolation predicts that the crust on the younger side (i.e. the formerly downgoing plate) of the inactive Oku-Niikappu arc-trench system formed ~145 ± 10 Ma. Extrapolating the trend defined by the Oshima and Naizawa complexes, on the other hand, predicts a minimum estimate of lithosphere age of the older side of the inactive trench (i.e. the former overriding plate and thus the arc basement) of ~230 ± 10 Ma. This difference suggests a major (~85 Myr)

break in lithosphere age on the Izanagi plate adjacent to the Hokkaido trench around the time of Oku-Niikappu Complex accretion – a change in slope of the trend in Figure 6 (see below) would predict a younger age for the basement of the Oku-Niikappu arc. The similarity between the age of extinction of the Oku-Niikappu arc and our estimated age of the subducting plate implies that during cessation of subduction, the subducting plate was close to 0 Ma, indicating that cessation of Oku-Niikappu subduction was caused by ridge subduction.

Cessation of the Oku-Niikappu intra-oceanic subduction zone as a result of ridge subduction opens an opportunity to explain the change in Izanagi-Pacific spreading direction between 146.6 and 137.9 Ma. During ridge subduction, a three-plate system changes into a two-plate system upon full subduction of the central plate that was spreading relative to one, and subducting below the other plate. The nature of the plate boundary between the two remaining plates depends on their relative motion, yielding three options for the resulting plate configuration: either (1) the two remaining plates converge, and subduction continues (e.g. subduction of the Izanagi-Pacific ridge below Japan was followed by subduction of the Pacific Plate (Seton et al., 2015)); (2) relative motion between the two remaining plates is parallel to the former trench, and a transform plate boundary forms (e.g. subduction of the Pacific-Farallon ridge below western North America resulted in formation of the San Andreas fault (Atwater, 1970)); or (3) the two remaining plates diverge, and the subduction plate boundary becomes inactive and a new spreading ridge forms. In all cases, the new plate boundary accommodates different rates and directions of relative plate motion compared to both plate boundaries before ridge subduction.

After Oku-Niikappu arc extinction around 145 Ma, Pacific-Izanagi spreading continued and the ridge continued to approach the Asian continental margin until the Paleogene (Fig. 6). However, around 145 Ma arc extinction, the direction of Pacific-Izanagi spreading changed (Fig. 2). Cessation of Oku-Niikappu intra-oceanic subduction upon ridge subduction was thus followed by renewed Izanagi-Pacific spreading, albeit under a slightly different angle. A plate kinematic model satisfying these observations is the following. Since initiation of intra-oceanic Oku-Niikappu subduction, the Northwest Panthalassa Ocean hosted at least three plates (Pacific (PAC), Izanagi 1 (IZA1), and Izanagi 2 (IZA2)), with an intra-oceanic subduction zone between IZA2 (in the west) and IZA1 (in the east), and a spreading ridge IZA1-PAC (Fig. 7, 8). Upon arrival of the IZA1-PAC ridge at the IZA2-IZA1 (i.e. Oku-Niikappu) trench, IZA1 was entirely subducted and the system transformed into a two-plate system containing a single spreading ridge (IZA2-PAC) (Fig. 7, 8). Because IZA2-PAC divergence was not fully parallel to IZA1-PAC divergence, a change in spreading orientation happened as recorded by the anomalies of the Pacific Plate and after full subduction of IZA1.
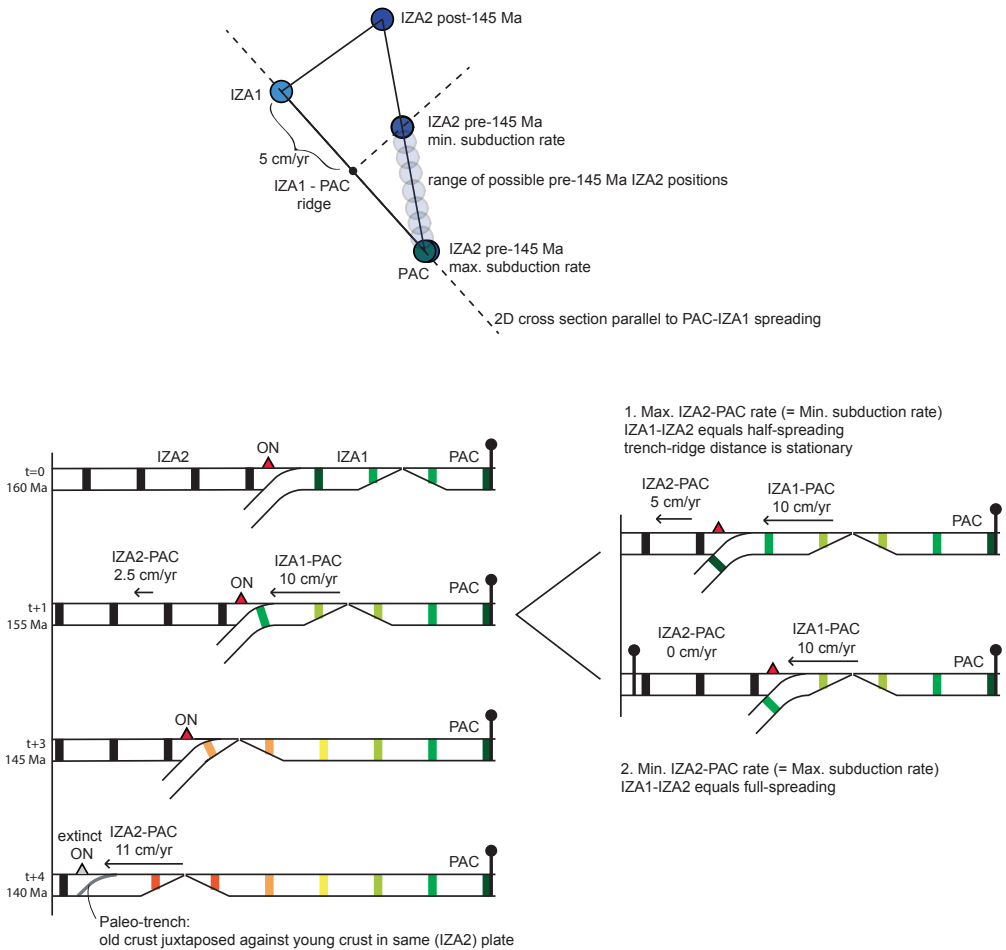
Figure 7: Upper panel: velocity diagram of PAC, IZA1 and IZA2. The orientations of the PAC-IZA1 and PAC-IZA2 lines are derived from fracture zone orientations (Fig. 2). Plate motion rates (spreading and subduction rates) described in text and illustrated in lower panels are as measured along the dashed line. Lower panels: cross sections parallel to IZA1-PAC spreading (dashed line in upper panel).

Marine magnetic anomalies provide estimates on pre-145 Ma IZA1-PAC and post-145 Ma IZA2-PAC plate motion rates. Nonetheless, the range of possible pre-145 Ma IZA1-IZA2 subduction rates (and therefore indirectly, IZA2-PAC divergence rates) can be calculated from pre-145 Ma IZA1-PAC half-spreading rates. In a 2D cross-section parallel to IZA1-PAC spreading (Fig. 7), pre-145 Ma half spreading rates were on the order of 5 cm/yr. The lower limit of subduction rates (in the same 2D cross-section) is determined by the requirement for convergence between the Oku-Niikappu trench and the PAC-IZA1

ridge. If subduction rates were lower than or equal to half spreading rates, the trench-ridge distance would increase, or be stationary, and the IZA1-PAC would not have subducted in the Oku-Niikappu trench. To accommodate trench-ridge convergence resulting in ridge subduction, subduction rates must have exceeded half-spreading rates (>5 cm/yr, Fig. 7, upper right panel). The lower limit of subduction rates, on the other hand, is constrained by the required divergence between PAC and IZA2. If subduction rates were higher than or equal to full-spreading rates, there would not be net divergence between IZA2 and PAC, and ridge subduction would not have led to renewed spreading. To accommodate net IZA2-PAC divergence, subduction rates must have been lower than full-spreading rates (<10 cm/yr, Fig. 7, lower right panel). From this, it follows that IZA2-PAC divergence rates were between 0 and 5 cm/yr (Fig. 7).

Had relative plate motion remained stationary during ridge subduction, full-spreading rates would have dropped from 10 cm/yr to anywhere between 0-5 cm/yr. However, the spacing between the post-145 Ma anomalies indicates that in fact spreading rates slightly increased (from ~10 cm/yr for 190-146.6 Ma to ~11-12 cm/yr for 137.9-110 Ma). This means that cessation of Oku-Niikappu subduction was followed by a rapid acceleration of IZA2-PAC divergence, and by inference, IZA2 subduction below the Hokkaido trench. The gap in Figure 6 is thus explained by a combination of the age contrast of lithosphere on either side of the former Oku-Niikappu trench at the time of subduction at the Hokkaido trench, and an increase in subduction rate. Although a dynamic explanation of the plate acceleration following cessation of Oku-Niikappu subduction is beyond the scope of the present paper, we note that (when placed in the Pacific fixed hotspot frame of Wessel and Kroenke (2008), see below), the Oku-Niikappu trench (and subducting slab) advanced westwards relative to the mantle. The transition at the southeastern plate boundary of IZA2 from subduction to spreading released a resisting force against westward plate motion and replaced it by a driving force (ridge push). We tentatively suggest that this transition in forcing may have driven the acceleration.

5.2. Did a major Mesozoic back-arc disappear along the Median Tectonic Line of Japan?

Further analysis of the history of subduction of the Izanagi and Pacific plates in relation to the record of accretionary events in Hokkaido requires connecting the Panthalassa plate system (containing the Pacific Plate and its conjugates) to the Indo-Atlantic plate system (containing all continents and Tethys oceans). For 83-0 Ma, relative motion between these two plate systems is based on Pacific-Antarctic spreading records. Prior to 83 Ma, however, relative motions are unconstrained, and therefore, we connect the two via the mantle by using the Pacific fixed-hotspot frame of Wessel and Kroenke (2008) for the Panthalassa plate system and the slab-fitted frame of van der Meer et al. (2010) for the Indo-Atlantic plate system (see Chapter 5). The resulting reconstruction, including the Pacific and Izanagi plates and the Northeast Asian continental margin, yields a ~2500 km wide gap between the continental margin of Northeast Asia and the remnant Oku-Niikappu arc at

its moment of accretion at the Hokkaido trench, ~100 Ma (Fig. 8d). This either implies a major error in the absolute plate motion models connecting the Panthalassa and Indo-Atlantic systems, or requires a plate tectonic explanation. As differences between (and uncertainties in) absolute reference frames probably do not exceed ~10° or ~1000 km (see Chapter 5 for an analysis of these differences for the Caribbean-Farallon connection), we advocate for the latter option.

Closing the gap to juxtapose the Oku-Niikappu Complex to the Hokkaido trench at 100 Ma requires either reconstructing the Oku-Niikappu Complex 2500 km farther to the northwest, or reconstructing the Hokkaido trench 2500 km to the southeast. The first option would imply that the Oku-Niikappu Complex was not part of the post-145 Ma IZA2 plate, but of yet another plate to the NW of Izanagi separated by another spreading ridge that accommodated 2500 km of spreading. We consider this scenario unlikely: it requires the presence of two parallel, coeval spreading ridges, a setting for which there is no modern or reconstructed equivalent. Moreover, it is not supported by the continuous age progression of OPS sequences after accretion of the Oku-Niikappu Complex at the Hokkaido trench. The second option, reconstructing the Hokkaido trench towards the southeast, infers a ~2500 km wide back-arc basin separating it from the continental North China block (Fig. 8e). In mid-Cretaceous time, the trench would then be located at 35-45°N, after which it drifted northwards to its pre-Miocene location at the Eurasian margin. Back-arc basins of this width are present in the Southwest Pacific region (Sdrolias et al., 2004; van de Lagemaat et al., 2018a), or reconstructed for the Late Cretaceous – early Cenozoic Northwest Pacific (of which the Aleutian Basin lithosphere is inferred to be a relict) (Vaes et al., submitted). Such a major basin is consistent with the faunal dichotomy across the MTL: Triassic-Jurassic Tethyan fauna from the outer zone of the Japanese accretionary complexes (to which Hokkaido belongs) suggest derivation from lower latitudes than the inner zone (Hallam, 1986; Hayami, 1984; Kobayashi & Tamura, 1984; Matsumoto, 1978). Cretaceous relative motion between the inner and outer zones is generally interpreted to be accommodated by left-lateral strike-slip motion at the MTL, whereby the outer zone migrated northwards along the continental margin of Asia (e.g. Maruyama et al., 1997; Sakashima et al., 2003; Tazawa, 2002). We postulate that in addition to strike-slip motion, the MTL accommodated convergence and represents the suture of the proposed back-arc basin. The Paleozoic Kurosegawa Belt of the outer zone of southwestern Japan and the presence of >1 Ga old zircons in trench-fill deposits of the Jurassic – Cretaceous accretionary complexes of Hokkaido indicates that the Hokkaido-outer zone system is (partly) underlain by continental crust, and sediment provenance studies indicate that it originated along the margin of South China (e.g. Ikeda et al., 2016). We thus tentatively suggest that the Hokkaido-outer zone system formed as part of the South China margin, which is consisted with the 'strike-slip models' (Ikeda et al., 2016; Maruyama et al., 1997; Sakashima et al., 2003; Tazawa, 2002), rifted away due to the opening of a back-arc basin whereby a fragment of continental crust was included in the outer margin of the back-arc, migrated northwards until oblique collision with

Figure 8: Reconstruction of IZA1, IZA2 and PAC plate motion, Oku-Niikappu subduction (A) and extinction (B), and accretion of the Oku-Niikappu remnant arc in the Hokkaido-outer zone trench separated from the Asian continent by a ~2500 km wide back-arc (E). Pacific Plate fixed to grid. Our reconstruction assumes an IZA1-IZA2 subduction rate of 7.5 cm/yr (within the permitted range of 5-10 cm/yr, see Figure 7) and extrapolates the relative post-145 Ma IZA2-PAC motion direction for earlier times, assuming that even though spreading accelerated, the orientation of relative PAC-IZA2 motion did not change during ridge subduction.

the inner zone upon full closure of the back-arc whereby the temporal presence of a second subduction zone along which the back-arc basin closed resulted in the HP-LT metamorphism in the Sambagawa belt. Such a temporal 'fringing-arc' system underlain by continental crust that rifted away from the continental margin and accreted later is not exceptional. Other examples are found in the deformed circum-Pacific continental margins of e.g. Mexico (the Guerrero arc (Boschman et al., 2018 (Chapter 3))), western Canada (the Wrangellia superterrane (Nokleberg, 2000)), and the Russian northeast (the Kolyma-Omolon terrane (Nokleberg, 2000; Stone et al., 2003)). The details of the evolution of this system in Japan remains subject for future study, whereby sediment provenance and paleomagnetic analysis, as well as increased tomographic resolution (see below) may shed further light on the tectonic evolution of the Northwest Panthalassa Ocean.

5.3. First order test against paleomagnetic and tomographic data

After converting the reconstruction as presented in Figure 8 to the paleomagnetic reference frame of Torsvik et al. (2012) (after linking the Panthalassa plate system to the Indo-Atlantic plate system by using the Wessel and Kroenke (2008) and van der Meer (2010) mantle reference frames respectively, see Chapter 5), the Oku-Niikappu arc is at 140 Ma located at ~13°N. Older absolute plate motions of the Panthalassa plate system are not constrained, but extrapolating the pre-140 Ma IZA2 latitudinal plate motion back in time would place the Oku-Niikappu arc at 9-10°N at 145 Ma. This estimate is within the range of paleolatitudes derived from ON4 (3.6° [-4.3°, 11.9°]).

Additionally, our reconstruction including subduction in an intra-oceanic, continental margin, and back-arc basin setting may be tested against mantle tomography. During subduction, slabs may migrate considerably relative to the mantle through roll-back or slab dragging (Schellart, 2017; van de Lagemaat et al., 2018a), but after slab break-off, they tend to sink near-vertically (Domeier et al., 2016) at overall lower mantle sinking rates on the order of 1-1.5 cm/yr (van der Meer et al., 2010, 2018). The top of a slab that broke off upon ~145 Ma cessation of the Oku-Niikappu subduction zone is thus expected to reside at ~1450-2100 km depth, and the bulk of the slab would be below that. Van der Meer et al. (2012) previously suggested that the Oku-Niikappu arc was associated with the Telkhinia slabs (Fig. 9b), a family of slabs below the Central Pacific ocean. The position of the reconstructed 145 Ma Oku-Niikappu arc relative to the mantle is based on the Wessel and Kroenke (2008) fixed Pacific hotspot frame, and our analysis places the Oku-Niikappu arc along the eastern margin of the equatorial part of the Telkhinia slabs (Fig. 9b).

Correlating post-50 Ma and Triassic-Early Cretaceous continental margin subduction to mantle structure is straightforward. Subduction of the Pacific Plate below Japan since ~50 Ma subduction of the Pacific-Izanagi ridge is associated with the flat-lying Manchuria slab (e.g. Chen et al., 2017; van der Hilst et al., 1991; van der Meer et al., 2018)(Fig. 9a). Furthermore, below the Manchuria slab, from the core-mantle boundary up to ~1600 km depth lies the East China slab (Fig. 9a,b), interpreted to reflect subduction from

at least Triassic to Early Cretaceous time (van der Meer et al., 2018). Between these two disconnected slabs, however, mantle structure is less conclusive, as several lower-resolution anomalies are located towards the top of the lower mantle that may either represent Izanagi Plate lithosphere that subducted prior to ridge subduction or remnants of the lithosphere of the proposed back-arc basin. Towards the east of the cross section of Figure 9, the resolution in tomography shallower than 2000 km is very low. This makes testing the back-arc hypothesis based on mantle structure beyond the state of current seismic tomography models.
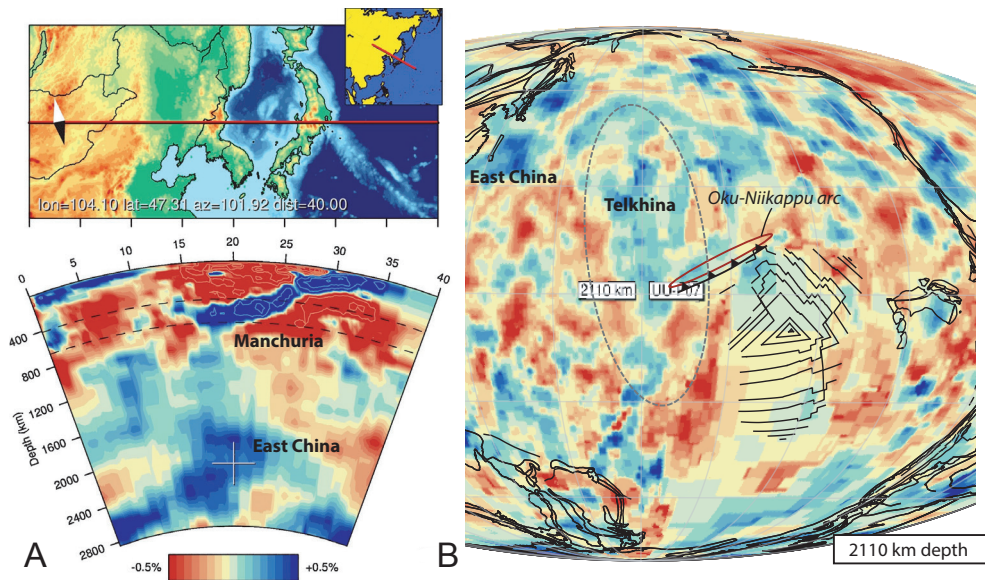
Figure 9: Seismic tomographic images from the UU-P07 model {Amaru, 2007 #341}. A) Cross-section through Japan and Northeast Asia showing the upper mantle Manchuria and lower mantle East China slab; B) Depth slice of 2110 km depth overlain by our tectonic reconstruction (at 140 Ma) including the Oku-Niikappu subduction zone. The reconstruction is placed in the mantle reference frames of van der Meer et al. (2010)(for the Indo-Atlantic plate system) and Wessel and Kroenke (2008)(for the Panthalassa plate system).

6. Conclusions

The accretionary record of Hokkaido contains a remnant intra-oceanic arc (the Oku-Niikappu Complex) that went extinct ~145 Ma and accreted ~100 Ma. We attempted at kinematic reconstruction of the Northwest Panthalassa Ocean, accommodating this evidence for intra-oceanic subduction. Marine magnetic anomalies of the Pacific Plate record a change in Izanagi-Pacific spreading orientation between 146.6 and 137.9 Ma.

Based on the series of Ocean Plate Stratigraphy sequences exposed on Hokkaido, we constrain a major age gap in the lithosphere of the Izanagi Plate that subducted at the Hokkaido trench at ~100 Ma. We ascribe this age gap to subduction in the intra-oceanic Oku-Niikappu trench. Extrapolating the ages from OPS sequences that accreted in the Hokkaido trench after 100 Ma suggests that the age of oceanic lithosphere adjacent to the Oku-Niikappu paleo-trench was similar to the age of arc extinction: ~145 Ma. Arc extinction thus likely resulted from ridge subduction. We reconstruct a three-plate (PAC, IZA1, IZA2) system, whereby arrival of the PAC-IZA1 ridge in the IZA1-IZA2 trench (associated with the Oku-Niikappu arc) was followed by renewed spreading in a slightly different direction, leading to the observed change in Izanagi-Pacific spreading orientation. In addition, we show that ridge subduction and slab break-off must was followed by an acceleration in PAC-IZA2 divergence rates. Reconstruction of the Izanagi Plate places the Oku-Niikappu arc during its extinction at ~145 Ma at ~10°N, in line with new (but sparse) paleomagnetic data from radiolarian cherts of the Oku-Niikappu Complex, and we illustrate a possible correlation with the Telkhinia slabs, which were previously linked to Oku-Niikappu subduction. Our analysis shows the value of exposures of Ocean Plate Stratigraphy in accretionary complexes in the development of plate kinematic reconstructions of lost oceanic plates. Furthermore, it illustrates how reconstructions based on these geological accretionary records may be further enhanced and validated with marine geophysical, paleomagnetic and seismic tomographic data, and illustrates how the basic rules of plate tectonics, developed over 40 years ago, still enable development of novel reconstructions of oceans almost entirely lost to subduction.

Supplementary materials

1. Additional information on sampling, methods and tectonic significance of the sampled rocks

ID - The Naizawa complex consists of depleted tholeiitic (geochemically identical to those of the lower Sorachi Group) and oceanic island basalts, Permian-Triassic limestones, Triassic- earliest Cretaceous cherts and middle Early Cretaceous hemipelagic mudstones and terrigenous clastics rocks (Hashimoto et al., 1975; Igo et al., 1987; Kato & Iwata, 1989; Kato et al., 1986; Kiyokawa, 1992; Sakagami & Sakai, 1979; Ueda, 2016; Ueda et al., 2000, 2001). The complex was interpreted by Ueda et al. (2000) to have resulted from tectonic mixing at the plate boundary contact of the upper plate ophiolite (lower Sorachi Group/ Horokonai ophiolite) and subducting seamounts. We have sampled 5 sites. ID1 (12 cores) consists of Berriasian – Valanginian pinkish limestones containing crinoids preserved in life position, indicating the younging direction of the strata. The beds dip ~40° to the northeast and are not overturned. ID2 (31 cores) contains an alternation of Valanginian – Barremian mudstones, tuffs and sandstones, interpreted as trench-fill deposits. These beds dip ~65° to the northeast. ID3 (15 hand samples) consists of Berriasian-Valanginian red bedded chert, dipping steeply (~80°) to the northeast. ID4 (31 cores) and ID5 (14 hand samples) consist of Oxfordian-Kimmeridgian reddish cherts (ID5) and gray mudstones (ID4) from the same block. These strata are folded and bedding orientations vary, but on average, they dip shallowly (~20-30°) to the northeast. In the strata of sites ID2,3,4,5, no indicators of younging direction are found, and therefore, they may be overturned. For these sites, we corrected the interpreted directions for bedding tilt in two ways: tilt-correction 1 (tc1) rotates the bedding planes to horizontal using the smallest rotation (i.e. the strata are not overturned), and tc2 uses the larger rotation (i.e. the strata are overturned).

KA - The Iwashimizu Formation contains a sequence of middle to upper Norian red siliceous shale intruded by dolerite sills, Upper Triassic – Lower Cretaceous red bedded chert (~90 m), Valanginian – Barremian greenish tuffaceous mudstone (~6 m) and post-Valanginian or Barremian black shale (~5 m) (Hori & Sakakibara, 1994), ages from radiolarian biostratigraphy). The tuffaceous mudstones contain ~2 Ga detrital zircons, indicating a continental source region (Ozawa, 2018). The Iwashimizu Formation was interpreted as an OPS sequence formed at a seamount on pre-Norian oceanic crust that reached the trench in Valanginian - Barremian time and subducted shortly thereafter. Near the base of the sequence, we sampled 3 sites (KA3,4,5) in three dolerite sills (5, 6 and 5 cores) interlayered with Upper Triassic cherts. The paleo-horizontal of these sills was estimated based on an average of multiple measurements of the bedding planes of the cherts surrounding the sills. Site KA6 consists of interlayered cherts between the sills (4 hand samples between KA3 and KA4 (KA6.1-6.4) and 12 hand samples between KA4 and KA5 (KA6.5-6.16)). Sites KA1 and KA2 (10 and 11 hand samples of red chert) are sampled further up section, around the Triassic-Jurassic boundary. Near the top of the sequence,

we sampled two sites (KA7 and KA8, 14 and 32 cores) of Valanginian - Barremian green tuffaceous mudstone. The lowermost samples of KA8 are located within 10 cm of the contact with the cherts. Strata of the entire KA section strike ENE-WSW and dip steeply (30 to 70° to the SE) and are overturned.

ON - ON1 consists of pillow basalts (45 cores, one sample per pillow, ON1.34-1.45 are from a single(?) andesitic lava). At site ON2 (55 cores), we sampled through a ~50 m section of dykes, containing approximately 27 dykes. ON3 and ON4 (12 and 10 hand samples) are sampled in red bedded chert stratigraphically overlying the pillow basalts of ON1. At the location of ON3 (base of the chert section), radiolarian biostratigraphy yielded a Berriasian age (Ueda & Miyashita, 2005). ON4 is located up section relative to ON3 and is therefore slightly younger, the basaltic rocks of ON1 are underlying the chert section and are therefore inferred to be earliest Cretaceous in age or older. We assume that the paleo-horizontal of the basalts of ON1 is the same as the average bedding orientation of ON3 and 4. The chert strata of ON3 and ON4 strike E-W and dip steeply (~80°) to the south.

Figure S1: Orthogonal vector (A-G) or equal area (H) diagrams of representative samples of sites ID1-5 in geographic coordinates (not corrected for bedding tilt), closed (open) symbol for declination (inclination), up/west projection.

2. Paleomagnetic results

ID1 – Initial intensities range from 0.3 - 8 mA/m, and demagnetization behavior is inconsistent; some samples are fully demagnetized around 580°C and contain a single magnetic component (e.g. ID1.5, Fig. S1b), others are demagnetizing up to 680°C and yield multiple components (e.g. ID1.2, Fig. S1a). None of these components yield consistent directions in more than two samples and therefore, no ChRM can be interpreted for ID1.

ID2 – Initial intensities range between 90-1200 µA/m and ChRMs are generally interpreted between 25-60 mT or 210-510°C (Fig. S1c). Variations in bedding orientation within ID2 enable a foldtest, which is negative (best clustering between -36 and 9% (tc1) or -1 and -21% (tc2) unfolding, Fig. S3a,b).
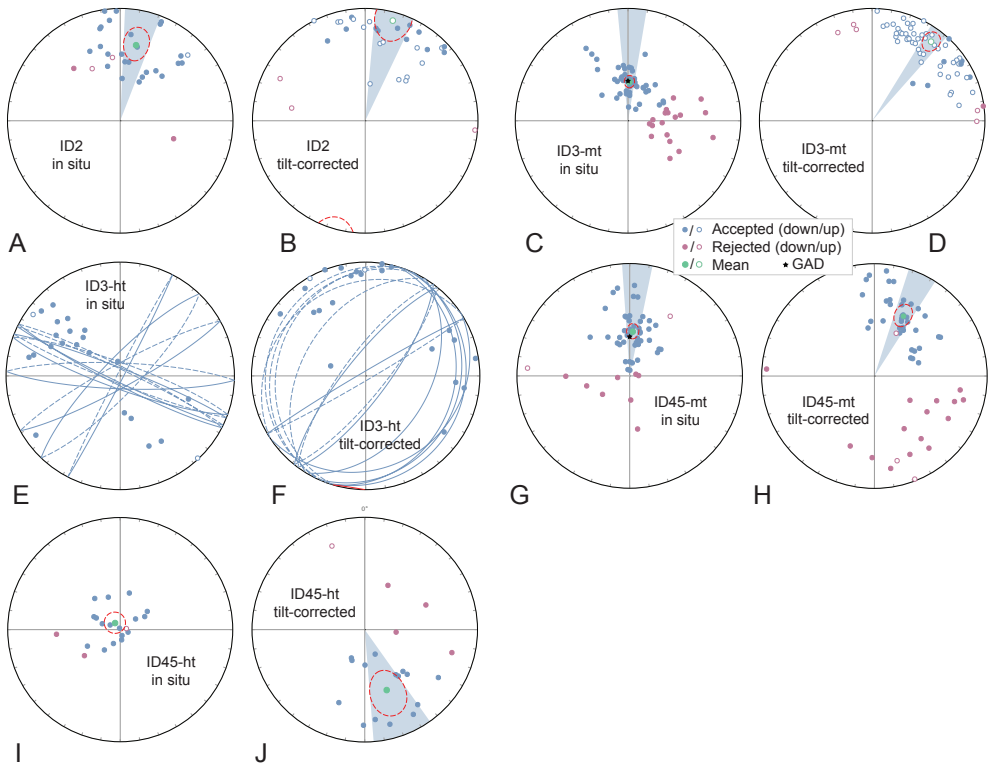
Figure S2: Interpreted directions (A-D, G-J) or directions and great circles (E-F) of sites ID2-5.

Figure S3 (right page): Bootstrapped foldtests of sites ID2-5. Cumulative distribution function (with confidence interval in light blue) based on 1000 bootstraps (25 bootstraps shown, average of bootstraps in red).
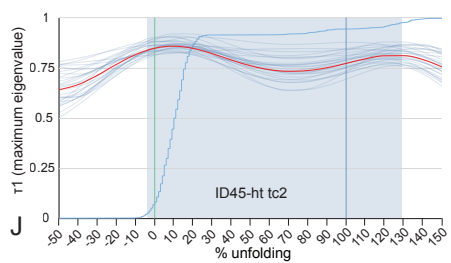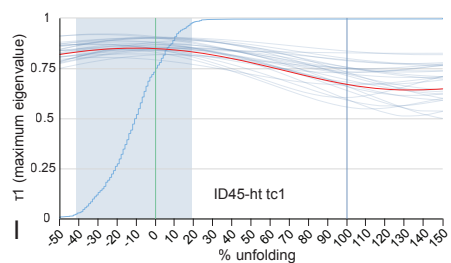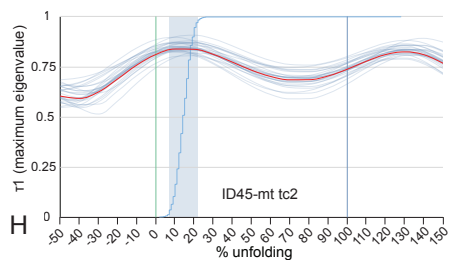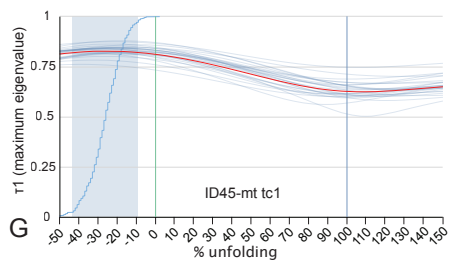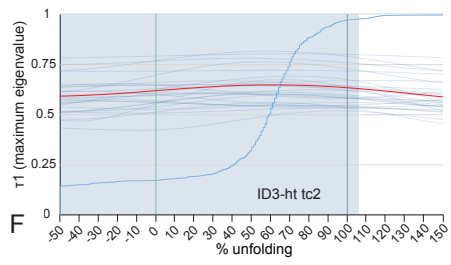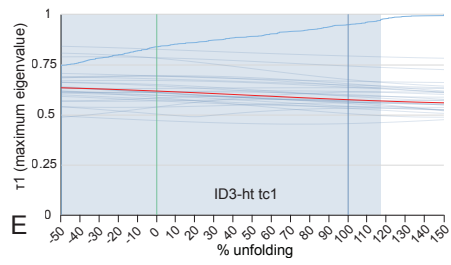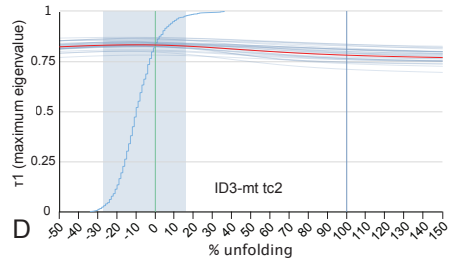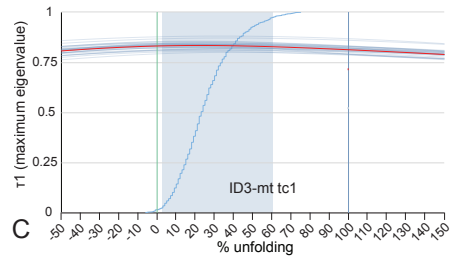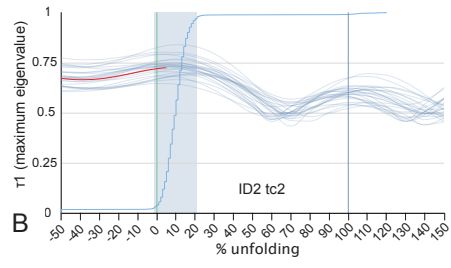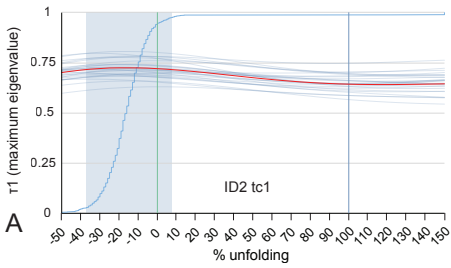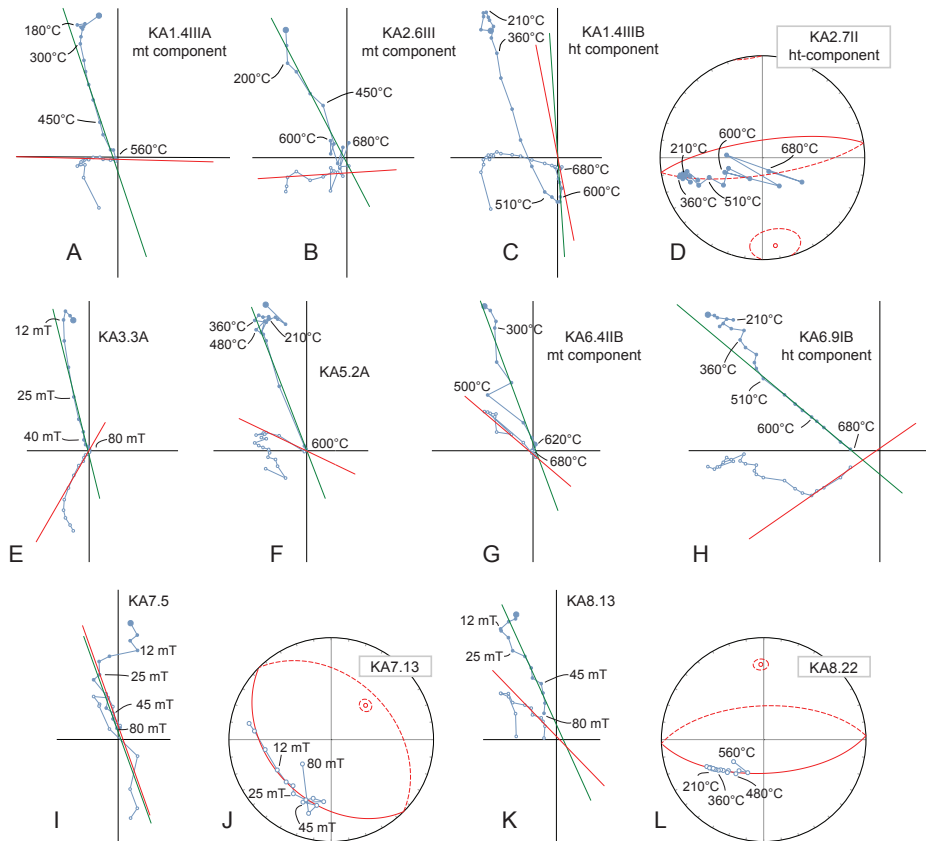
Figure S4: Orthogonal vector (A-C, E-I, K) or equal area (D, J, L) diagrams of representative samples of sites KA1-8 in geographic coordinates (not corrected for bedding tilt), closed (open) symbol for declination (inclination), up/west projection.

ID3 – Initial intensities range between 0.6-4 mA/m. A well-defined and consistent magnetic component is interpreted at medium range demagnetization steps (~200-480°C or 16-45 mT, mt-component, Fig. S1d). The dispersion of these interpreted directions is high (K= 5.5) and after a 45° cut-off (K increases to 14.7), the mean (Dec±ΔDx = 2.2° ± 7.9, Inc ±ΔIx = 61.7° ±4.8) is indistinguishable from the GAD field (Inc = 61.3°)(Fig. S2c). Furthermore, these directions yield a negative foldtest (best clustering between 2 and 60% (tc1) or -27 and 16% (tc2) unfolding)(Fig. S3c,d). A less well-defined component is interpreted in higher temperature steps (560-660°C, ht-component) with 19 directions and 14 great circles (Fig. S1e). The interpreted directions fall into two groups (with declinations around 170° and around 310°), resulting in a high dispersion (K=2.2)(Fig. S2e). Both foldtests (tc1 and tc2) are indeterminate (Fig. S3e,f). To calculate great circle
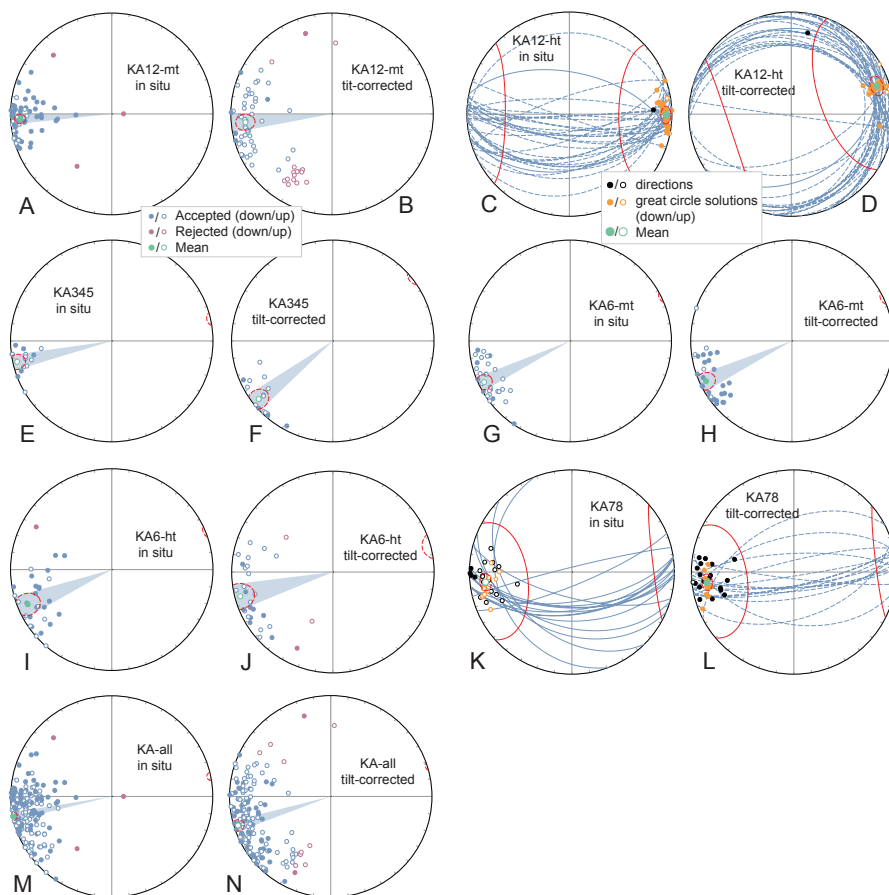
Figure S5: Interpreted directions (A-B, E-J, M-N) or directions, great circles, and great circle solutions (C-D, K-L) of sites KA1-8.

solutions, one of the two groups of directions should be excluded, because using all directions results in great circle solutions intermediate between the two groups. Due to the unambiguity of the results of this site, we exclude it from further analysis.

ID4 and ID5 – Initial intensities range from 0.2 – 230 mA/m. Similar to ID3, a very well-defined component is interpreted at medium demagnetization steps (300-580°C or 16-50 mT, mt-component)(Fig. S1f), which yields a negative foldtest (best clustering between -43 and -9% (tc1) or 7 and 22% (tc2) unfolding)(Fig. S3g,h) and is indistinguishable from the GAD field (Dec±ΔDx = 3.9° ± 7.8, Inc ±ΔIx = 57.6° ±5.7, Fig. S2g). A high temperature (ht) component (580-680°C or 40-60 mT) is interpreted with 13 directions and 7 great circles (Fig. S1g,h). These directions yield a negative (best clustering between -41 and 19% (tc1)) or indeterminate (tc2) foldtest (Fig. S3i,j).

KA1 and KA2 – Initial intensities from the KA cherts range from 200-2600 μA/m. An mt-component is interpreted in medium temperature steps (~360-560°C)(Fig. S4a,b), and an ht-component in higher temperatures (600-680°C) using 1 direction and 17 great circles for KA1 and 15 great circles for KA2 (Fig. S4c,d). All declinations within the mt-directions are westward and no reversals are recorded, but as inclinations scatter around zero, both upward and downward directed inclinations are present (Fig. S5a). The mt-directions from KA1 and KA2 share a common mean and yield a negative foldtest (best clustering between -29 and -9% unfolding, Fig. S8a). The single direction interpreted as the ht-component is directed eastward, and therefore, all great circle solutions have declinations of around 90° as well (Fig. S5c).

KA3, KA4 and KA5 – Initial intensities range from 25-1500 mA/m and ChRM's are interpreted at medium demagnetization steps (450-580°C or 25-50 mT)(Fig. S4e,f). Directions from KA4 and KA5 share a common mean. Similar to KA12-mt, all KA3,4,5 directions are westward and inclinations scatter around zero (Fig. S5e).

KA6 – Initial intensities range from 0.3-8 mA/m, and similar to KA1 and KA2, two components are interpreted: an mt-component (300-600°C)(Fig. S4g) and an
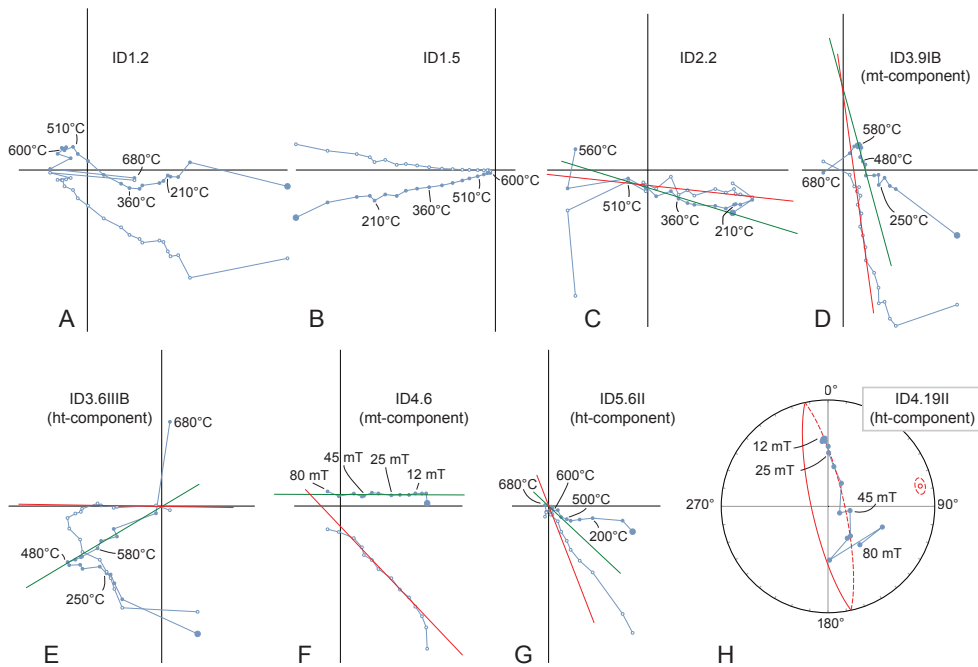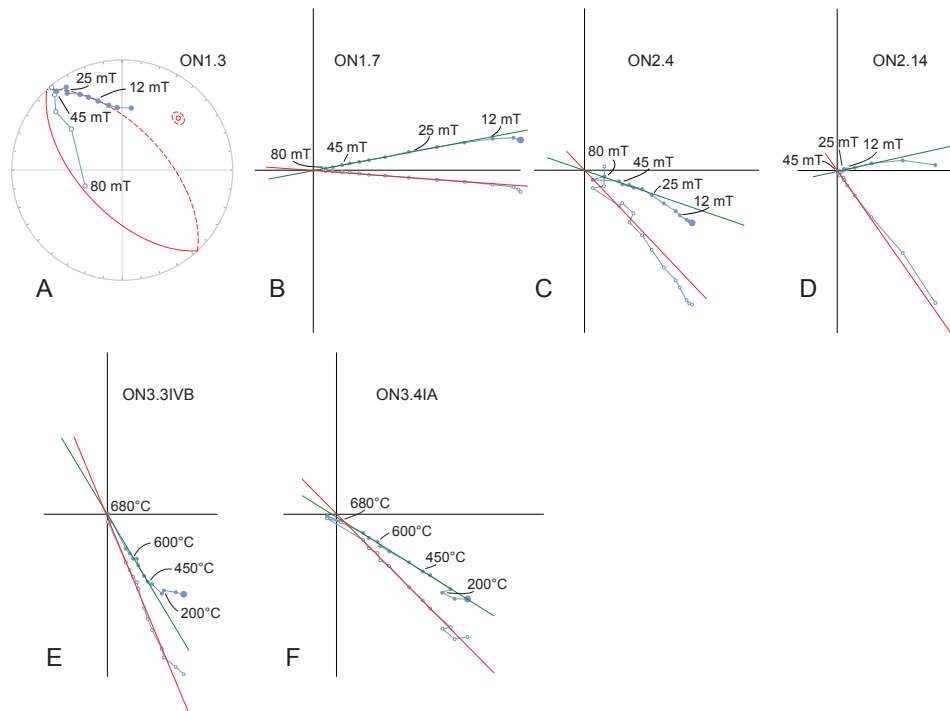

Figure S6: Orthogonal vector (B-F) or equal area (A) diagrams of representative samples of sites ON1-3 in geographic coordinates (not corrected for bedding tilt), closed (open) symbol for declination (inclination), up/west projection.

ht-component (620-680°C)(Fig. S4h). Again, for both components, directions are westward and inclinations scatter around zero (Fig. S5g,i).

KA7 and KA8 – Initial intensities range from 0.08-12 μA/m and ChRMs are interpreted as directions (21) between 330-510°C or 30-60 mT, or as great circles (15)(Fig. S4i,j,k,l).

ON1 – Initial intensities range from 17–5000 mA/m. Demagnetization behavior is variable; most samples contain single components trending towards the origin (e.g. ON1.7, Fig. S6b), but some contain overlapping components (e.g. ON1.3, Fig. S6a) that do not reach the origin. Dispersion of the interpreted directions is high (K=5.4) and especially inclinations vary substantially (between -70 and +70°, Fig. S7a), hampering calculation of a meaningful mean direction of this site.

ON2 – Initial intensities range from 2-500 mA/m. Even though demagnetizations are straightforward directions trending towards the origin (Fig. S6c,d), dispersion of the interpreted directions is essentially random (K = 1.9) and at least a third of the directions (interpreted in relatively low temperature steps, e.g. ON2.14) scatter around the GAD field (Fig. S7b).

ON3 – Initial intensities range from 0.6-7 mA/m and ChRMs are interpreted between ~450-640°C (Fig. S6e,f). A foldtest is negative (best clustering between -42 and 3% unfolding, Fig. S8c).

ON4 – Initial intensities range from 0.5-4 mA/m. Two components are interpreted: an mt-component (420-560°C) and an ht-component (620-680°C). Although ON3 and ON4-mt do not share a common mean, their directions are very similar, which we interpreted as a shared post-tilting magnetization.
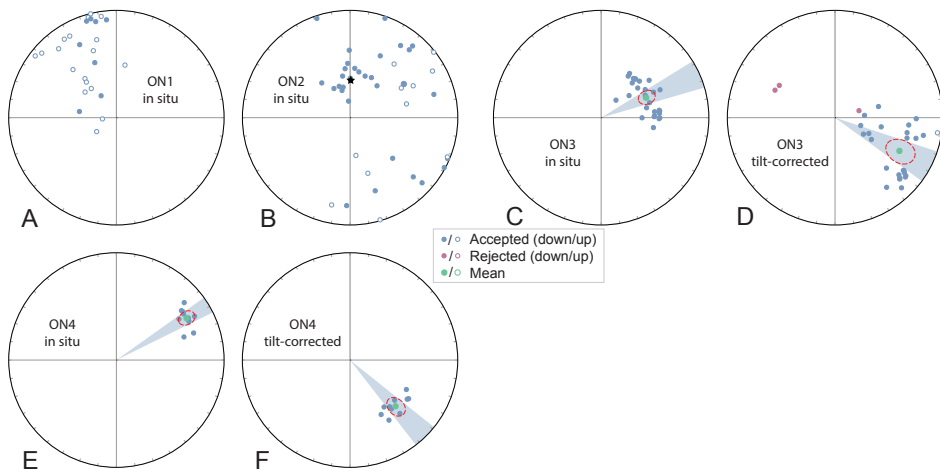
Figure S7: Interpreted directions of sites ON1-4.
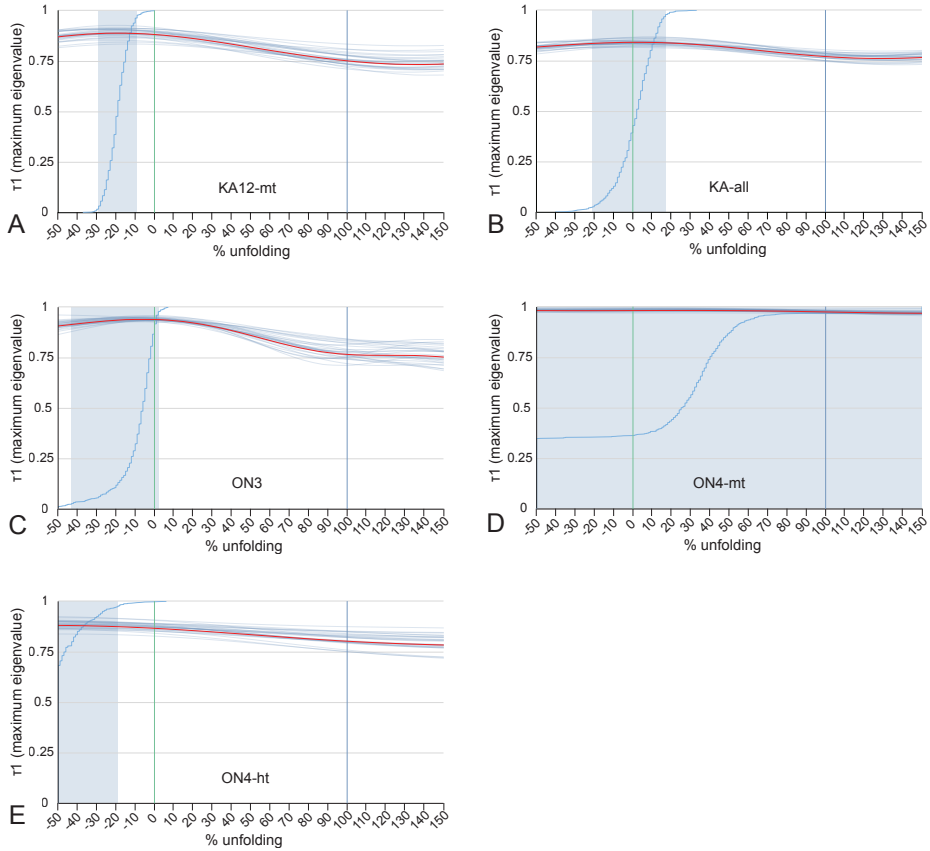
Figure S8: Bootstrapped foldtests of sites KA12, KA-all and ON3-4. Cumulative distribution function (with confidence interval in light blue) based on 1000 bootstraps (25 bootstraps shown, average of bootstraps in red).

3. Interpretation of the paleomagnetic data

ID - The paleomagnetic results from the sites in the Idonnapu Zone are random (ID1), unambiguous (ID3-ht), representing a recent overprint (ID3-mt and ID4,5-mt), or representing ancient, but undated magnetizations that were acquired after tilting or folding (ID2 and ID4,5-ht). We therefore exclude all ID sites from further analysis.

KA - Paleomagnetic directions from KA1-mt, KA2-mt, KA3, KA4, KA5, KA6-mt, KA6-ht, KA7 and KA8 are highly consistent both before and after tilt-correction, yielding declinations of ~260° and inclinations around 0°. The limited effect of correcting for bedding tilt (even though the KA section is steeply dipping) is due to the roughly ENE-WSW (~240°) strike of the section in combination with the very similar ~260° declinations. Directions from KA1-ht and KA2-ht (both before and after tilt-correction) are antipodal to the rest of the sites, and may represent reversed directions. However, as

these ht-components are derived from great circles solutions calculated based on one direction only, we consider them as less reliable. Differences in bedding tilt throughout the KA section enable a foldtest on all directions, which is negative (best clustering between -21 and 17% unfolding, Fig. S8b), indicating that the interpreted magnetization was acquired after tilting. This is in line with the remarkable consistency in magnetic directions between the sites. From a sedimentary section spanning >100 Myr that travelled through a wide range of latitudes from an open ocean setting towards a trench, the original magnetic signal would yield a much wider range of inclinations. The total mean (without tilt correction) of all KA sites is: Dec $\pm \Delta$Dx = 258.5 $\pm$ 2.4°, Inc $\pm \Delta$Ix = 0.4 $\pm$ 4.7°, n =174, K = 21.4, A95 = 2.4, Fig. S5m).

ON - Paleomagnetic results from the Oku-Niikappu complex are highly dispersed (ON1 and ON2), or represent an ancient, but undated remagnetization (ON3 and ON4-mt). Only the ht-component from site ON4 may represent a primary magnetic signal, although no field tests can be performed to confirm this. The mean direction (after tilt-correction) from ON4-ht is: Dec $\pm \Delta$Dx = 251.4 $\pm$ 8.0°, Inc $\pm \Delta$Ix = 7.2 $\pm$ 15.7°, n =24, K = 14.8, A95 = 8.0).

The remagnetized KA direction (not corrected for bedding tilt) is very similar to the ON4-ht direction (KA6-ht and KA345 share a common mean with ON4-ht). This may suggest a common tectonic history after acquisition of the magnetization, which would imply that remagnetization of the KA section happened at equatorial latitudes, after a phase of deformation and folding. This would be possible if the KA strata subducted in the equatorial trench associated with the Oku-Niikappu arc. However, this interpretation is problematic because of the presence of ~2 Ga detrital zircons in the Valanginian-Barremian tuffaceous mudstones, indicating that the KA section was in close proximity to the continental margin during deposition of these trench-fill deposits, while the Oku-Nikkappu arc was still in an open ocean setting. Furthermore, the present-day structural relationship (ON below KA) and age differences in trench-fill show show that accretion of the KA section in the Hokkaido trench (~130 Ma) occurred ~30 million years earlier than accretion of ON (~100 Ma). We therefore at this stage interpreted the agreement between KA (uncorrected for bedding tilt) and ON4-ht (corrected for bedding tilt) is be a coincidence, and the remagnetized signal of KA was acquired after deformation and folding during accretion in the Hokkaido trench, after which the KA section underwent a second phase of tilting (perhaps during exhumation or during Miocene collision with the eastern Hokkaido system) rotating the magnetic vector to shallow inclinations.

Site	Lat. (°N)	Lon. (°E)	N	N45	D	ΔD$_x$	I	ΔI$_x$	k	α95	K	A95	A95min	A95max
ID2	42.224620	142.896119	26	30	11.8	9.4	31.9	14.1	8.9	10.1	11.1	8.9	3.3	10.5
ID3-mt	42.224563	142.896189	45	63	2.2	7.9	61.7	4.8	25.3	4.3	14.7	5.7	2.6	7.5
ID3-ht			25	33	313.9	12.6	61.5	7.8	15.1	7.7	10.8	9.2	3.3	10.8
ID45-mt	42.224420	142.896013	44	54	3.9	7.8	57.6	5.7	19.0	5.1	13.3	6.1	2.6	7.6
ID45-ht			17	20	322.2	-	84.0	7.6	20.6	8.1	6.8	14.7	3.9	13.8
KA1-mt	42.427610	142.598546	36	38	265.8	3.6	6.7	7.1	28.9	4.5	45.2	3.6	2.9	8.6
KA2-mt	42.427610	142.599522	27	27	270.0	5.8	15.5	10.8	14.4	7.6	24.5	5.7	3.2	10.3
KA12-mt			62	65	266.8	3.0	10.2	5.8	21.0	4.0	38.0	3.0	2.3	6.1
KA12-ht			33	33	90.5	2.5	6.3	5.0	83.1	2.8	101.1	2.5	3.0	9.1
KA3	42.416741	142.594124	5	5	261.2	7.4	9.4	14.4	54.5	10.5	109.6	7.3	6.3	29.7
KA4	42.416741	142.594124	6	6	258.0	6.2	-15.5	11.6	52.1	9.4	120.7	6.1	5.9	26.5
KA5	42.416741	142.594124	5	5	253.4	8.7	-5.9	17.2	61.0	9.9	79.0	8.7	6.3	29.7
KA345			16	16	257.5	4.5	-4.7	9.0	29.3	6.9	68.0	4.5	4.0	14.3
KA6-mt	42.416740	142.594120	30	30	244.4	4.4	-6.3	8.8	24.4	5.4	36.1	4.4	3.1	9.6
KA6-ht			28	29	247.5	6.9	11.2	13.4	10.0	9.1	16.6	6.9	3.2	10.0
KA7	42.416502	142.590248	3	3	264.7	35.1	-31.4	53.2	13.4	35.0	14.7	33.4	7.7	41.0
KA8	42.416502	142.591225	18	18	265.6	4.2	-13.3	8.0	39.8	5.5	70.7	4.1	3.8	13.3
KA78			37	37	263.3	3.1	-16.3	5.7	39.4	3.8	60.6	3.1	2.8	8.4
ON1	42.674133	142.670783	22	26	334.8	9.5	-16.1	17.7	6.7	13.0	11.9	9.4	3.5	11.7
ON2	42.675297	142.680870	22	41	9.0	12.2	49.1	12.0	9.3	10.8	9.7	10.5	3.5	11.7
ON3	42.674091	142.671721	28	28	66.0	7.8	52.2	6.9	30.9	5.0	18.5	6.5	3.2	10.0
ON4-mt	42.673689	142.673946	10	10	59.1	4.6	25.1	7.8	100.5	4.8	115.8	4.5	4.8	19.2
ON4-ht			25	25	299.4	8.4	37.0	11.5	13.7	8.1	14.5	7.9	3.3	10.8

N45: number of samples after 45° cut-off

Table S1: Paleomagnetic results

7

Reconstructing lost plates of the Panthalassa Ocean

Folded radiolarian chert beds - Cedros Island, Mexico

Abstract

The Panthalassa Ocean, covering approximately half of the globe during the culmination of Pangea, was underlain be multiple tectonic plates that have been lost to subduction. Here, we aim to reconstruct Panthalassa plate motions and plate boundaries for times in which all but paleomagnetic data is unavailable. We present new and review published paleomagnetic data from Ocean Plate Stratigraphy materials of the accretionary complexes of Cedros Island (Mexico), the Santa Elena Peninsula (Costa Rica), the North Island of New Zealand, and Japan, which provide paleolatitudinal constraints on the Farallon, Phoenix and Izanagi plates respectively. We start with a global reconstruction of the Indo-Atlantic plate system in which we incorporate reconstructions of complex plate boundary deformation of the circum-Panthalassa trenches, developed in previous chapters or in other studies. Next, we add a marine magnetic anomaly-based 'Panthalassa plate system' including the Pacific Plate and its conjugates, their relative spreading histories, ages, and plate boundaries. For 83-140 Ma, we use two independent mantle frames to connect the Panthalassa plate system to the Indo-Atlantic plate system via the mantle, and test the feasibility of this approach with paleomagnetic data. For times prior to 140 Ma, we reconstruct the Panthalassa plates such that divergence is maintained between Izanagi, Farallon and Phoenix (for 140-190 Ma, following marine magnetic anomaly data), convergence is maintained with Japan, Mexico and New Zealand, and paleomagnetic constraints are met. The reconstruction approach developed in this chapter illustrates that in absence of marine magnetic anomaly data and mantle reference frames, deep-time plate circuits of supercontinents and superoceans may be reconstructed using OPS sequences, paleomagnetism, and constraints on the nature of circum-oceanic plate boundaries.

1. Introduction

Compared to continental lithosphere, which was generated through many cycles of partial melting and subsequent fractional crystallization of mantle and crustal material since the early days of the Earth, oceanic lithosphere has a limited lifespan on the Earth's surface, because contrary to continental crust, it becomes denser than the sub-lithospheric mantle upon cooling (Vlaar & Wortel, 1976). Due to the continuous generation of new oceanic lithosphere at mid-ocean ridges and the consumption of older oceanic lithosphere in subduction zones, oceanic lithosphere is virtually all renewed every ~200 Myr. This implies that the lithosphere that was underlying ancestral oceans, such as the Paleo- and Neo-Tethys Oceans separating Gondwana and Laurasia or the Panthalassa Ocean surrounding Pangea in late Paleozoic – early Mesozoic times, has (almost) all been lost to subduction. As a result, deep-time plate tectonic reconstructions rely primarily on geological, paleontological and paleomagnetic data from the continents. Such reconstructions portray the distribution of continents through geological time from which plates hosting these may be inferred, but lack information on plate motions and -geometry in the oceanic domains. In attempting to improve such deep-time plate kinematic reconstructions, restoring lost oceanic plates, even though highly challenging, is therefore key.

The Panthalassa Ocean, covering approximately half of the globe during the culmination of Pangea, decreased in size since then due to area gain in the Atlantic and Indian oceans breaking up the supercontinent. The present day descendant of the Panthalassa, the Pacific Ocean, is mainly occupied by the Pacific Plate, which originated in Jurassic time (Larson & Chase, 1972; Larson & Pitman, 1972). The overall area loss of the Panthalassa Ocean, combined with the continuous growth of the Pacific Plate led the surrounding oceanic plates that were underlying the Panthalassa Ocean in Mesozoic and older times to be lost to subduction. However, even though these Panthalassa plates are no longer at the surface of the Earth, their formation and demise left an imprint on the Earth and their plate motions may be reconstructed from indirect sources of data. First, marine magnetic anomalies and fracture zones preserved on the Pacific Plate provide constraints on plate motions of plates conjugate to the Pacific (the conceptual Izanagi, Farallon and Phoenix plates) back to ~190 Ma (Engebretson et al., 1985)(Chapters 1,5,6). Second, the preservation of fragments of captured lithosphere withheld from subduction (e.g. in the Caribbean Sea and the Aleutian Basin), as well as remnants of oceanic ridges, rises, seamounts, and intra-oceanic arcs, scraped off the downgoing plates during subduction and presently exposed in circum-Pacific accretionary complexes, enables the collection of geological and paleomagnetic data from the rock record representative of the former Panthalassa plates (Chapters 2,5,6). Third, seismic tomographic images revealing the presence of subducted lithosphere in the lower mantle may be correlated to geological records of either intra-oceanic or continental margin subduction, thereby constraining the position of these subduction zones relative to the mantle (van der Meer et al., 2012, 2018; Chapters 1,4,6).

So far, this thesis has used newly collected and previously published geological and paleomagnetic data from the circum-Pacific accretionary margins and lower mantle tomography to develop reconstructions of segments of the Panthalassa Ocean back to 190 Ma. Since 190 Ma, which marks the birth of the Pacific Plate, a 'Panthalassa plate system' may be constructed, containing the Pacific, Farallon, Phoenix, and Izanagi plates, their relative motions, plate boundaries, and lithospheric ages. Prior to 190 Ma, however, the presence of the Izanagi Plate in the northwest, the Farallon Plate in the northeast, and the Phoenix Plate in the south of the Panthalassa Ocean may be inferred, but plate boundary geometry and orientations are unknown. Therefore, no constraints are available on the extent of the plates, let alone on the spatial distribution of lithospheric ages. Prior to 190 Ma, reconstruction relies fully on geological accretionary records. In this chapter, we aim to reconstruct Panthalassa plates and plate motions for times prior to 190 Ma, and illustrate the methodological reconstruction steps required to do so. The methods described in this paper are not limited to the Panthalassa Ocean, but may in principle be applied to other ancient oceans, such as those surrounding and forming within previous supercontinents such as Rodina and Nuna, as long as associated accretionary complexes are identified exposing off-scraped remnants of the former oceanic plates (Isozaki, 2014).
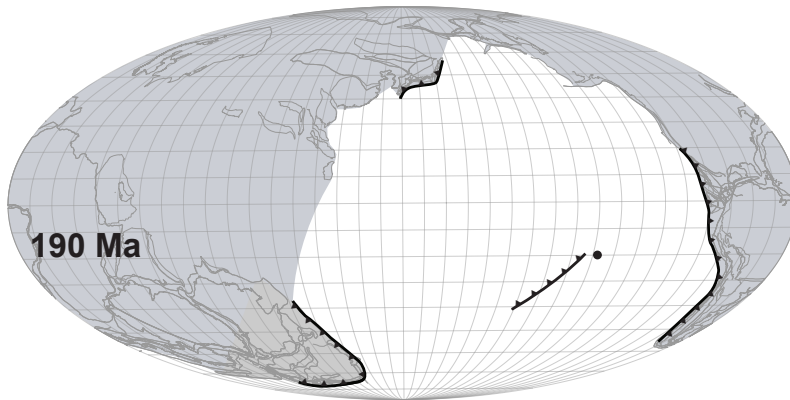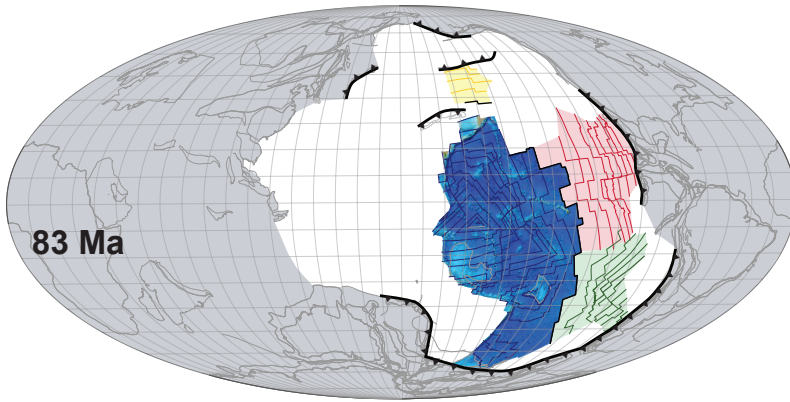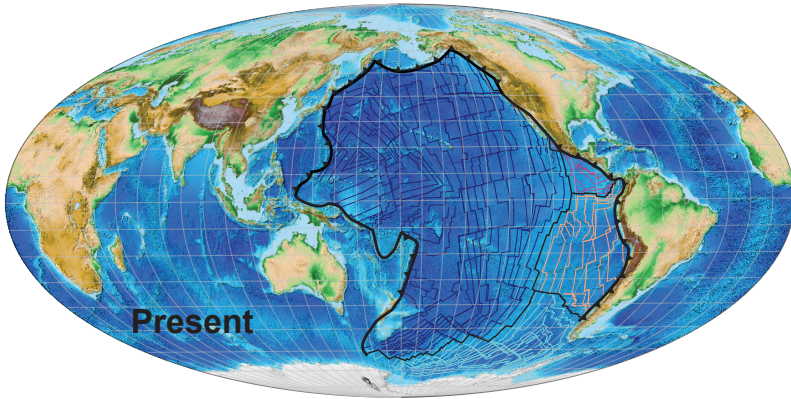
Figure 1: Reconstructed and unreconstructed (in white) areas of the Panthalassa domain. Fragments of circum-Panthalassa trenches included based on Chapters 2-6, Schepers et al. (2017), van de Lagemaat et al. (2018b), and Vaes et al. (submitted).

2. Determining the boundaries of the unreconstructed Panthalassa domain

At the basis of reconstructing the Panthalassa Ocean lie relative plate motions of the Panthalassa plate system derived from spreading records preserved in the modern plates of the Pacific Ocean. Unlike the symmetrical and complete set of anomalies in the Atlantic Ocean representing its full tectonic history, the spreading records of the Pacific document only a fraction of the total of oceanic crust formation and past plate motions in the Panthalassa Ocean. By going backwards in geological time and restoring past plate motions from these spreading records, first, the modern Juan de Fuca, Cocos, Nazca, Antarctic and Pacific Plates become smaller as the young history of oceanic lithosphere formation is reversed (e.g. Wright et al., 2016). At 83 Ma, only the central part of the Pacific Plate is left and all other modern plates have disappeared. The unreconstructed area, increasing backwards in time (Fig. 1), represents the extent of subducted lithosphere. Some parts of this are straightforwardly reconstructed by mirroring marine magnetic anomalies preserved on the Pacific Plate assuming symmetric spreading parallel to transform faults, thereby creating the conceptual Farallon, Phoenix, and Izanagi plates (Engebretson et al., 1985; Chapters 5, 6), but these constrained areas too decrease in size. At 190 Ma (Fig. 1) the Panthalassa Ocean is completely 'empty' except for the intra-oceanic Oku-Niikappu subduction zone (Chapter 6) and a point representing the birthplace of the Pacific Plate (Chapter 1).

The extent of the unreconstructed area (white in Figure 1) through time is on the one hand determined by the spreading records of the Pacific, and on the other hand, by the location of the subduction systems surrounding the Panthalassa Ocean. Reconstructing the supercontinent Pangea closes the Atlantic and Indian oceans, resulting in, from a Panthalassian perspective, the retreat of the surrounding subduction zones and an increase in 'white space'. Furthermore, subduction zones are often associated with extensional or compressional overriding plate deformation resulting in the formation of fore- or back-arc basins (e.g. the Japan Sea) or fold-thrust belts (e.g. the Andes). Long-lived subduction systems may even have experienced sequences of alternating overriding plate shortening and extension (e.g. Laramide shortening followed by Basin and Range extension in the western North American Plate, Chapter 4). Reconstructions of such overriding plate deformation have been developed particularly for Late Cretaceous and younger times, many of which as part, or as side projects of this thesis (Northwest Pacific: Vaes et al. submitted, Southwest Pacific: van de Lagemaat et al. (2018a), Scotia Sea: van Hinsbergen et al., submitted, Andes: Schepers et al. (2017), Caribbean: Chapters 2; Molina Garza et al. (2017), or by other authors (e.g. North American Cordillera: Johnston (2001); McQuarrie and Wernicke (2005), Southeast Asia: Advokaat et al. (2018); Hall (2002)). These reconstructions provide constraints on the location of the trenches through time, thereby constraining the outer extent of the white space.

3. Reconstructing plate motions from paleomagnetic data of accretionary complex rocks

The extent of the white space indicates that thousands of kilometers of Panthalassa lithosphere subducted in the circum-Panthalassa trenches. Of the geological records of the circum-pacific belts that remained after those thousands of kilometers of subduction, however, the vast majority reflects relatively minor plate motion of the overriding plate relative to the trench, causing the overriding plate to deform. The thousands of kilometers of plate motion of the downgoing plate relative to the trench, on the other hand, generally leaves no or very little trace. Nevertheless, the scarce materials that were scraped off during subduction, accreted to the overriding plate and are now exposed in the accretionary complexes around the Pacific, provide unique and essential information for the reconstruction of subducted plates. Such accreted materials consist of fragments or entire sequences of 'Ocean Plate Stratigraphy' (OPS), a concept developed by the Japanese micropaleontologist Yukio Isozaki (Isozaki, 2014; Isozaki et al., 1990). OPS sequences ideally consist from bottom to top of magmatic basement (MORB, arc, plateau or seamount), cherts or limestones, hemipelagic sediments, and tuffaceous and turbiditic deposits, representing rocks of an oceanic plate accumulated during its journey from the open ocean to a trench. OPS materials are typically exposed in accretionary complexes or tectonic mélanges. In Chapter 6, we analyzed the sequence of accretionary complexes exposed on Hokkaido containing evidence for at least six accretion events throughout the Jurassic – Paleogene (Ueda, 2016), and presented paleomagnetic data from OPS rocks to quantify their paleolatitude during sedimentation. In this chapter, we present new and previously published paleomagnetic data from Permian to Cretaceous OPS materials that accreted in Jurassic to Cretaceous times, and are now exposed in accretionary complexes on Cedros Island (Baja California, Mexico), the Santa Elena Peninsula (Costa Rica), the North Island of New Zealand, and Honshu (Japan), as well as from the Pacific Plate itself. For these regions, we restore Cenozoic overriding plate deformation and reconstruct the position of the trenches back towards their pre-Cenozoic location by including reconstructions of the Caribbean and Mexican margins, the Southwest Pacific and the Northwest Pacific, based on Chapters 2 and 5, Chapters 3 and 4, van de Lagemaat et al. (2018a), and Chapter 6 and Vaes et al. (submitted), respectively. Furthermore, the pre-36 Ma position of Baja California relative to the North American continent is based on the Basin and Range reconstruction of McQuarrie and Wernicke (2005) and motions of the China blocks relative to Eurasia are based the reconstruction of Domeier and Torsvik (2014).

3.1. Setting, previous work, and sampling of circum-Pacific OPS sequences
3.1.1. Mexico
On Cedros Island (Fig. 2), a blueschist-bearing serpentinite-matrix mélange is exposed that contains ~1-50 m scale blocks of (meta-) basalt, chert, limestone, and up to upper Lower Cretaceous turbiditic sediments (Rangin, 1978; Sedlock, 1988). This mélange is part of an assemblage of Mesozoic subduction-related rocks, including a Triassic (220 Ma)
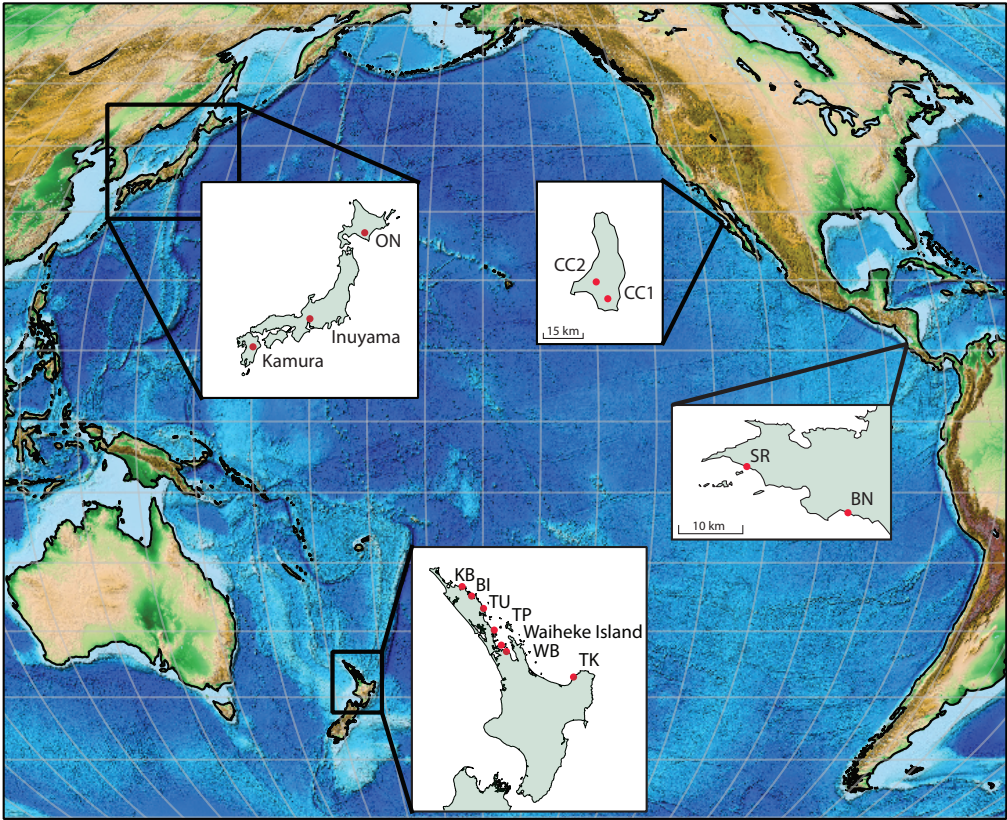
Figure 2: Sampling location from Kodama et al. (2007)(Waiheke Island), Kirschvink et al. (2015) (Kamura), Shibuya and Sasajima (1989)(Inuyama), Ando et al. (2001)(Inuyama), Oda and Suzuki (2000) (Inuyama), and this study.

supra-subduction zone (SSZ) ophiolite, Jurassic arc magmatic rocks, and Cretaceous fore-arc deposits exposed throughout the Vizcaíno-Cedros region of central Baja California (e.g. Kimbrough & Moore, 2003). In Chapter 4, we presented paleomagnetic data from the Triassic SSZ ophiolite and Jurassic overlying sediments indicating that the Vizcaíno-Cedros region has a paleolatitudinal plate motion history equal to that of the North American Plate, which we interpreted as evidence that these assemblages formed as part of the deforming margin of the overriding plate.

From a continuous section of pillow basalts, ~40 m of red radiolarian ribbon cherts and ~250 m of thin-bedded turbidites, exposed within the mélange on southeastern Cedros Island, pillow basalts and cherts were sampled by Hagstrum and Sedlock (1990). Based on radiolarian biostratigraphy, the cherts were shown to represent a long, condensed stratigraphic section spanning from the Upper Triassic to the Lower Cretaceous (Sedlock & Isozaki, 1990). Initially, Hagstrum and Sedlock (1990) concluded that these rocks were

remagnetized, and that no original magnetic signal was present. However, later reanalysis of the cherts samples (Hagstrum & Sedlock, 1992) yielded a stable high-temperature (600-680ºC) component in 13 of the total of 101 samples, including antipodal normal and reversed polarities, which was interpreted as the primary magnetization. The directions from these 13 samples suggest deposition of the cherts at equatorial latitudes (2 ± 3º).

From the lower (Upper Triassic) part of the chert section sampled by Hagstrum and Sedlock (1990), we collected another 89 hand samples (CC1, Fig. 2), with the aim of (in) validating the results from the 13 samples with a larger dataset, as well as determining inclination shallowing due to compaction through the Elongation/Inclination (E/I) method of Tauxe and Kent (2004), which requires a large (>100 directions) dataset. Furthermore, we collected 16 hand samples from a block of green chert exposed on southern central Cedros Island (CC2, Fig. 2), containing ~5 m of stratigraphy (samples were collected from ~1.5 m of stratigraphy). Coauthor Hayato Ueda retrieved Upper Triassic radiolaria from samples of CC2.

At the time of accretion (~105 Ma) of these two chert sequences, the Cedros Island trench was located at 32º N. In Chapter 5, we have shown that since at least 220 Ma, the Farallon Plate was continuously subducting below the western margin of Mexico. We thus interpreted the Cedros cherts to be derived from the Farallon Plate, and use the differences in latitude between the time of their deposition and their accretion as a measure of Farallon Plate motion.

3.1.2. Costa Rica

The Santa Elena Peninsula of northwestern Costa Rica exposes a peridotite nappe, intruded by ~121 Ma diabase dykes, overthrusting the Santa Rosa accretionary complex (SRAC). The SRAC contains sheared peridotites and megabreccias, an isolated block of layered gabbros, and volcano-sedimentary successions interpreted as the remnants of a seamount (Bandini et al., 2011b; Baumgartner & Denyer, 2006; Buchs et al., 2013; Denyer & Gazel, 2009; Escuder-Viruete & Baumgartner, 2014; Gazel et al., 2006; Madrigal et al., 2015; Tournon, 1994). The layered gabbros, exposed at Bahia Nancite (BN, Fig. 2) have been dated at 124 ± 4.1 Ma (40Ar-39Ar age), and based on similarities in incompatible element characteristics with nearby pillow basalts (of the Murciélagos Islands, Chapter 5) and dykes, were interpreted to be generated in a subduction zone environment (Hauff et al., 2000). The Murciélagos Island pillow basalts, however, have later been interpreted to have a Large Igneous Province-related origin (e.g. Madrigal et al., 2015).

The seamount complex (SR, Fig. 2) contains fault-bounded sequences of ~190-180 Ma red bedded cherts, ~175 Ma alkaline basalt sills and massive basalts, and ~110 Ma cherts, tuffaceous mudstones, turbiditic sediments, and polymict breccias (Bandini et al., 2011b; Baumgartner & Denyer, 2006; Buchs et al., 2013; Tournon, 1994). In the latter ~110 Ma rocks, the cherts (at the base) grade into muddy-sandy turbidites whereby amounts of

tuffaceous material increase and are topped by polymict breccias (Bandini et al., 2011b; Baumgartner & Denyer, 2006; Buchs et al., 2013). This sequence is interpreted as (the transition to) trench-fill deposits, and radiolarians from the pelagic to hemipelagic facies dating the onset of distal detrital sedimentation yielded a late early Albian to early middle Albian age (~110 Ma) (Bandini et al., 2011b). From the top of this sequence, De Wever (1985) obtained a (less precise) Barremian-Cenomanian age. Buchs et al. (2013) used the Albian (110 Ma) age of the chert at the base of the trench-fill sequence to interpret the seamount to have accreted at 110 Ma, but we argue that a considerable amount of time (and plate motion) must have passed between the deposition of the cherts and the breccias, and interpret the age of accretion to be ~100 Ma, consistent with the younger end of the age spectrum for the top of the chert-to-breccia sequence.

We collected 46 oriented hand samples from the ~190-180 Ma cherts (sites SR1,3,4,10,11), 30 hand samples from ~175 Ma basalt sills (sites SR5-9), and 20 hand samples from the ~110 Ma cherts (site SR2). Additionally, we collected 36 hand samples from the layered gabbros exposed at Bahia Nancite (site BN). Estimates of magmatic foliation in these gabbros were collected as a best (but uncertain) measure for the paleohorizontal.

The tectonic and magmatic origin of the Bahia Nancite gabbros and the Santa Elena ophiolite remain uncertain (see Madrigal et al. (2015) for an overview), but the position of the peridotite nappe in the hanging wall overthrusting the SRAC, which contains open-ocean derived material, indicates that the peridotite nappe must have been located at the westernmost boundary of the North American Plate, adjacent to a trench. We interpret the Santa Elena Peninsula to be adjacent to the southwesternmost part of the North American trench below which the Farallon subducted (Chapter 5), that was separated from the North American continent by a back-arc basin in latest Jurassic-mid Cretaceous times (Chapter 3,4), and interpret the SR seamount rocks and the BN gabbros to de derived from the Farallon Plate. At the time of accretion (100 Ma), the Santa Elena Peninsula was located at 11° N.

3.1.3. New Zealand

The Waipapa terrane, an accretionary complex exposed in a northwest-southeast trending belt on the North Island of New Zealand, consists of abundant Upper Jurassic volcaniclastic sandstones and minor pillow basalts, Permian-Lower Jurassic cherts, limestones and mudstones (Adams et al., 2007; Adams et al., 2009, 2012; Kear & Mortimer, 2003; Mortimer et al., 2014; Spörli & Grant-Mackie, 1976; Sporli et al., 1989). The Waipapa terrane is part of New Zealand's Eastern Province, comprising volcanic arc, ocean floor, fore-arc, and accretionary complex terranes, interpreted as an intra-Panthalassa trench-arc system separated from Gondwana-derived units in western New Zealand by the Median Batholith, which represents a long-lived Gondwana margin arc (Mortimer, 2004). Paleomagnetic studies on basement rocks from New Zealand have concluded widespread remagnetization, which probably occurred in Late Cretaceous

time (e.g. Haston & Luyendyk, 1991; Kodama et al., 2007; Oliver, 1994; van de Lagemaat et al., 2018b). Nonetheless, paleomagnetic analysis on Lower Jurassic sediments and volcanics of the Murihiku fore-arc terrane yielded potentially primary results (Grindley et al., 1980; van de Lagemaat et al., 2018b). Neither study presented ideal data (the first study involved volcanic rocks with an uncertain paleohorizontal, the second a very small dataset), but estimates of paleolatitude are consistent (66°S and 62.1 ± 12°S). However, due to proximity to the South Pole, this paleolatitude does not provide conclusive constraints on the tectonic origin of the Eastern Province. During the Early Jurassic, New Zealand's Gondwana margin was located at ~75°S. A latitude of ~65°S for the Eastern Province trench-arc system may indicate either proximity to the northeast Australian margin, proximity to the Antarctic Peninsula, or a far-offshore intra-oceanic origin on opposite side (the Panthalassa side) of the South Pole (see Figure 11 in van de Lagemaat et al. (2018b)). Sediment provenance links the Eastern Province to northeast Australia (Adams et al., 2007) and Triassic plant fossils from the Murihiku terrane and nearby coastal regions of Gondwana are similar (Retallack, 1987), indicating that a far-offshore origin is unlikely. We interpret the Eastern Province (including the Waipapa accretionary complex terrane) to be an intra-oceanic (fringing) arc system separated from the northeastern Australian continental margin by a small back-arc basin. All tectonostratigraphic terranes were sutured and remained in their present configuration since the end of the Early Cretaceous (Howell, 1980).

From various locations within the Waipapa terrane along the north coast of the North Island, we collected a total of 101 hand samples from 11 blocks of chert (sites TK, WB, TP, TU, BI1-5, KB1,2, Fig. 2). Hand samples were typically collected from ~2 m of stratigraphy. Only the cherts from site WB1 were previously dated, yielding a radiolarian biostratigraphy age of Late Triassic - Early Jurassic (Sporli et al., 1989). The chert blocks from the Bay of Islands (BI1-5) are from a large (~200 m) coastal exposure including pillow basalts. We assume that the Waipapa terrane encompasses a single disrupted OPS, and these cherts are therefore interpreted to represent the oldest (Permian) segment of the stratigraphy of the Waipapa terrane.

Furthermore, Kodama et al. (2007), presenting results from an extensive paleomagnetic sampling campaign on pre-Neogene rocks, demonstrated that the remanent magnetization from a single Lower Triassic chert layer from Waiheke Island (Fig. 2) may be interpreted as primary. The directions from this chert layer indicate deposition at a relatively low paleolatitude (33.6°), far north of the intra-oceanic Eastern Province margin. We interpret the Waipapa accreted materials to be derived from the Phoenix Plate, accreted in latest Jurassic (150 Ma) time.

3.1.4. Japan
The basement of the Japanese Islands consists of a series of Paleozoic-Paleogene accretionary complex belts, divided into an inner and outer zone separated by the Median

Tectonic Line (MTL) (Isozaki, 1996, 2000; Isozaki et al., 2010; Maruyama et al., 1997). Cretaceous strike-slip motion (and potentially, opening and closure of a back-arc basin, Chapter 6) along the Median Tectonic Line (MTL) juxtaposed the two zones, from which Paleozoic - Jurassic faunal differences (e.g. Hallam, 1986; Hayami, 1984; Kobayashi & Tamura, 1984; Matsumoto, 1978; Tazawa, 2001; Tazawa, 2002) suggest a major tectonic break between terranes of different paleolatitudes. For the pre-Cretaceous position of the inner and outer zones, we follow reconstructions from e.g. Ikeda et al. (2016), Maruyama et al. (1997), Sakashima et al. (2003), Tazawa (2002), in which the inner zone is formed at the margin of the North China block and the outer zone at the South China block.

The Inuyama region of the inner zone of central Japan (Fig. 2), located within the Jurassic Mino-Tamba accretionary complex belt, contains the type locality of OPS (Isozaki, 2014; Isozaki et al., 1990; Matsuda & Isozaki, 1991), including a >80 m continuous section of cherts spanning the Lower Triassic to Lower Jurassic. This chert sequence was dated by high-resolution conodont and radiolaria studies, and was instrumental in demonstrating the extremely low sedimentation rates of radiolarian cherts, of 1-4 mm/kyr (Isozaki, 2014; Matsuda & Isozaki, 1982; Yao et al., 1980). Paleomagnetic studies on the Inuyama cherts have been conducted by Shibuya and Sasajima (1986), Oda and Suzuki (2000), and Ando et al. (2001). All studies presented data from folded chert beds that yielded positive fold tests, thereby strengthening the conclusion that these cherts contain primary magnetizations, and indicate low-latitude depositional environments (Table 1, Fig. 3).
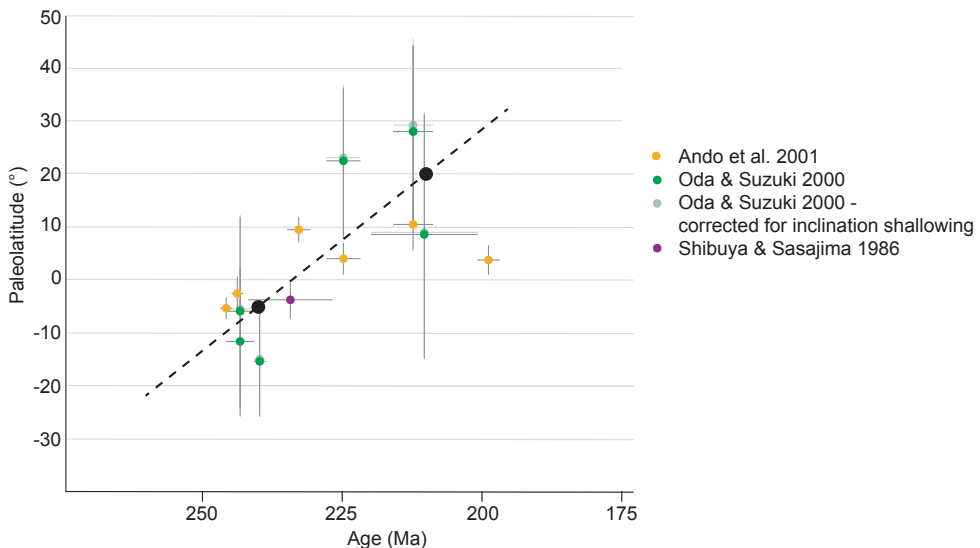
Figure 3: Compilation of paleolatitudes derived from paleomagnetic data from the Inuyama cherts. The black dashed line represents the inferred paleolatitudinal motion of the Inuyama OPS (5° S at 240 Ma, 20° N at 215 Ma) used in the reconstruction.

In the Kamura region of the outer zone of southwestern Japan, located in the Jurassic accretionary complex of the Chichibu belt, Permian-Triassic limestones are exposed that are interpreted to be formed in the atoll of a mid-oceanic seamount (Isozaki & Ota, 2001; Kasuya et al., 2012; Kirschvink et al., 2015; Ota & Isozaki, 2006; Sano & Nakashima, 1997)(Fig. 2). Kirschvink et al. (2015) presented paleomagnetic data from these limestones, yielding a paleolatitude of 12.2º S for the Permian, whereby the southern hemispheric origin is concluded based on correlation of the polarity pattern with the magnetostratigraphic timescale.

In addition, in Chapter 6, we presented paleomagnetic data from Berriasian cherts of the Oku-Niikappu Complex, a remnant intra-oceanic arc that went extinct in latest Jurassic to earliest Cretaceous time and is currently exposed in a mid-Cretaceous accretionary complex within the Sorachi-Yezo Belt of Hokkaido (Ueda & Miyashita, 2005) (Fig. 2). These cherts yielded a paleolatitude of 3.6º [-4.3º, 11.9º]. We interpret the Inuyama cherts, Kamura limestones, and Oku-Niikappu cherts to be derived from the Izanagi Plate and incorporated in the Japanese accretionary complexes at 150 Ma, 160 Ma and 100 Ma respectively (Table 2).

3.1.5. The Pacific Plate
Paleomagnetic data from the Pacific Plate itself has recently been presented by Fu and Kent (2018). These authors analyzed samples from a sequence of red radiolarian cherts, mudstones and basalts obtained from ODP Site 801B, dated by radiolarian biostratigraphy to be middle Bathonian-late Valanginian in age (~167-133 Ma, (Matsuoka, 1992, 1995), and yielding southern hemispheric paleolatitudes between 0-20º for 6 ages (Table 1,2). Furthermore, based on consistent near-north declinations, Fu and Kent (2018) concluded that no resolvable vertical axis rotation occurred to the Pacific Plate since the middle Jurassic.

3.2. Methods
Anticipating the extreme durability of radiolarian cherts, we collected hand samples, from which we drilled typical 25 mm diameter paleomagnetic cores in the paleomagnetic laboratory Fort Hoofddijk (Utrecht University, the Netherlands) using a drill press. Hand samples yielded between 1 and 6 cores, which were subsequently cut into samples of max. 22 mm length. We determined core orientations by measuring planes on the hand samples in the field (generally bedding planes, with the exception of SR5-9), and drilling perpendicular to those planes. Based on the red color of the cherts that may indicate the presence of hematite, most red cherts were subjected to thermal demagnetization only; other lithologies (black/gray cherts, basalts) were subjected to both thermal and alternating field demagnetization up to 680º or 100 mT. The samples were measured on a 2G DC SQUID cryogenic magnetometer. Interpretation of the demagnetizations (plotted in Zijderveld (1967) diagrams) and statistical analysis (following procedure described in Deenen et al. (2011) was performed using the online portal Paleomagnetism.org

(Koymans et al., 2016). We used the principle component analysis of Kirschvink (1980) to interpret demagnetization diagrams, determined great circle solutions using the method of McFadden and McElhinny (1988), calculated site mean directions using Fisher (1953) statistics applied on VGP's, calculated declination and inclination errors ΔD_x and ΔI_x following (Butler, 1992), and applied 45° cut-offs per site (Johnson et al., 2008). For sites in which the stratigraphic younging direction was not determined (all New Zealand sites and Cedros site CC2), we corrected the interpreted directions for both the normal facing (<90° tilting) and overturned (>90° tilting) option. When applicable, we used the fold test of Tauxe and Watson (1994) and to test for common true mean directions, the bootstrapped coordinate test of Tauxe (2010).

3.3. New paleomagnetic results

3.3.1. Mexico

Demagnetization of the Upper Triassic cherts of site CC1 (N=131) unfortunately did not yield the stable high temperature (600-680° C) component demonstrated by Hagstrum and Sedlock (1992), except for in a single sample (CC1.82, Fig. 4a). However, in 47 samples, we were able to determine great circles encompassing the transition between a medium (300-600°C) and the high (>600°C) temperature component (Fig. 4b,c). Using the direction from CC1.82, we calculated great circle solutions for the planes, resulting in a mean direction of D ± ΔDx = 193.6 ± 3.7°, I ± ΔIx = -20.0 ± 6.6° (Fig. 4d,e), which corresponds to a paleolatitude of 10.3° [6.8°, 14.1°]. Although similar, this result is not statistically indistinguishable from 2 ± 3° as determined by Hagstrum and Sedlock (1992), which may be due to the fact that these authors sampled through a larger section of stratigraphy, thereby sampling through more geological time.

From CC2, we interpreted Characteristic Remanent Magnetizations (ChRMs) in the range of 450-550°C or 16-60 mT (Fig. 4g,h), yielding a mean direction of D ± ΔDx = 189.4 ± 7.0°, I ± ΔIx = -10.0 ± 13.6° after correcting for bedding tilt (Fig. 4j), which corresponds to a paleolatitude of 5° [-1.8°, 12.3°]. Stratigraphic younging directions are not determined, but when assuming overturned strata in the chert block, the degree of clustering and the mean inclination is unchanged, albeit positive (I ± ΔIx = 10.0 ± 13.8°). Within site variations in bedding orientations are too small to allow for a fold test.

3.3.2. Costa Rica

Demagnetization behavior of the ~190-180 Ma red cherts collected at sites SR1,3,4,10,11 shows that Curie temperatures are generally around 580-600°C (Zijderveld diagrams in Figure S1), indicating that, somewhat surprisingly, most of these samples do not contain hematite. 21 out of the total of 105 measured samples do contain a high temperature component carried by hematite, which is best preserved in SR11. We interpreted a medium-temperature component (~430-580°C or ~25-60 mT) in all sites (Fig. 5a,b), and a high temperature component (540-680°C) in site SR11 (Fig. 5g,h). The total of medium-temperature component directions yielded a negative foldtest (best clustering between -7
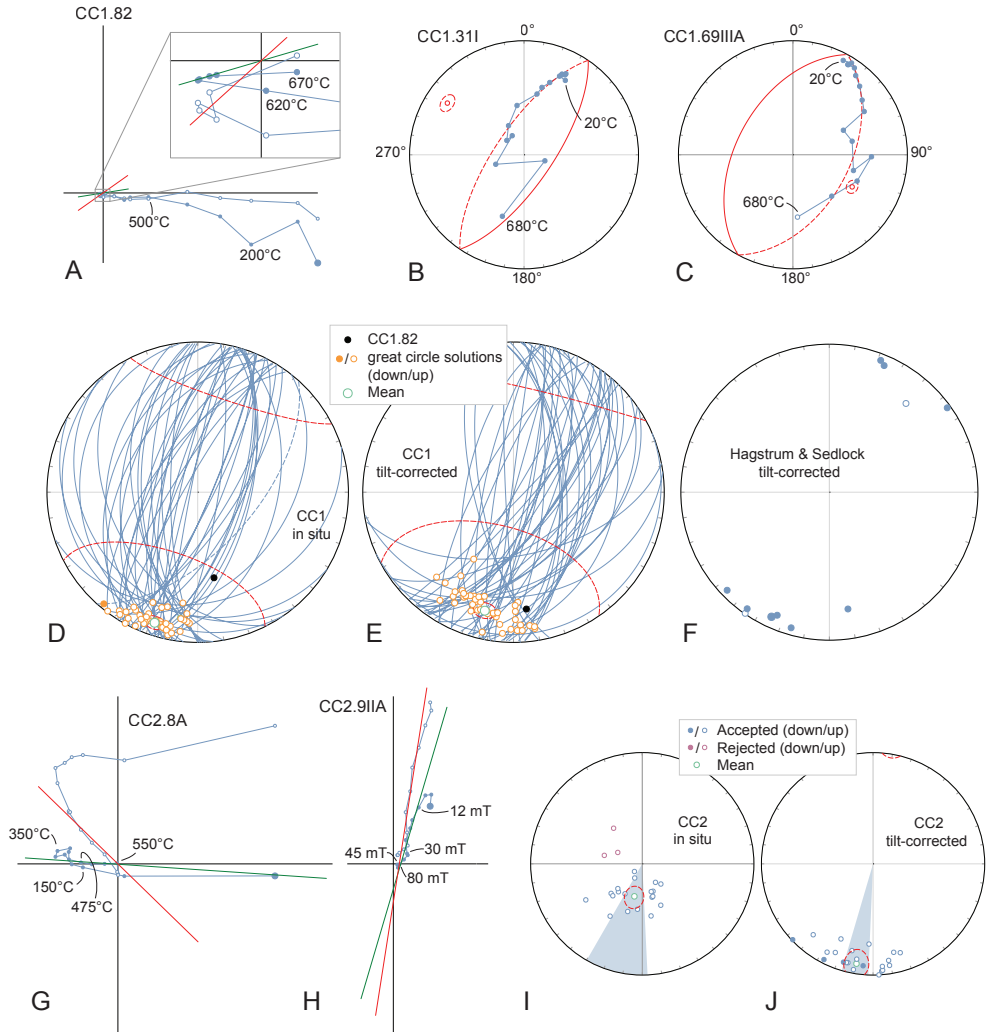
Figure 4: Orthogonal vector (A, G, H) and equal area (B, C) diagrams of representative samples of sites CC1 and CC2 in geographic coordinates (not corrected for bedding tilt), closed (open) symbol for declination (inclination), up/west projection; D-E) Great circles and great circle solutions of CC1; F) Interpreted directions of CC1 from Hagstrum and Sedlock (1992); I-J) interpreted directions from CC2.

and 20% unfolding, Fig. S3), indicating that this component reflects a remagnetization. A foldtest on the set of SR11-ht (high-temperature) directions is indeterminate (Fig. S3). If primary, the mean direction of SR11-ht (N=7, Dec ± ΔDx = 350.4 ± 11.0°, Inc ± ΔIx = -11.3 ± 21.3°, corrected for bedding tilt) indicates a depositional latitude of 5.7° [-5°, 17.7°].

ChRMs from sites SR5-9 were interpreted at 16-45 mT or 360-520°C. Site SR9 was excluded from further analysis due to a high dispersion (K=2.0 before 45° cut-off). The paleohorizontal of these bedding-parallel sills was determined from bedding measurements of the surrounding chert layers; variations in these measurements are too small to allow for a fold test. SR6 and SR7 yielded both normal and reversed directions, but a reversal test is negative. Directions (before tilt correction) are very similar to directions from SR1,3,4,10,11 (Fig. 5), and we therefore interpret these samples to record the same remagnetization.

Demagnetization behavior of the ~110 Ma red cherts collected at site SR2 is similar to that of sites SR1,3,4,10,11; ChRMs are interpreted at 20-50 mT or 300-500°C. Correcting for bedding tilt yields an enigmatic result. The bulk of the directions cluster significantly better after tilt correction, but the number of outliers is increased (Fig. 5c,d). We hypothesize that this pattern is the result of partial remagnetization, and that the tight cluster (Fig. 5d) represents a pre-folding magnetization. The mean (D ± ΔDx = 45.7 ± 4.3°, I ± ΔIx = 24.9 ± 7.3°, would indicate deposition at a latitude of 13.0° [9.0°, 17.5°].
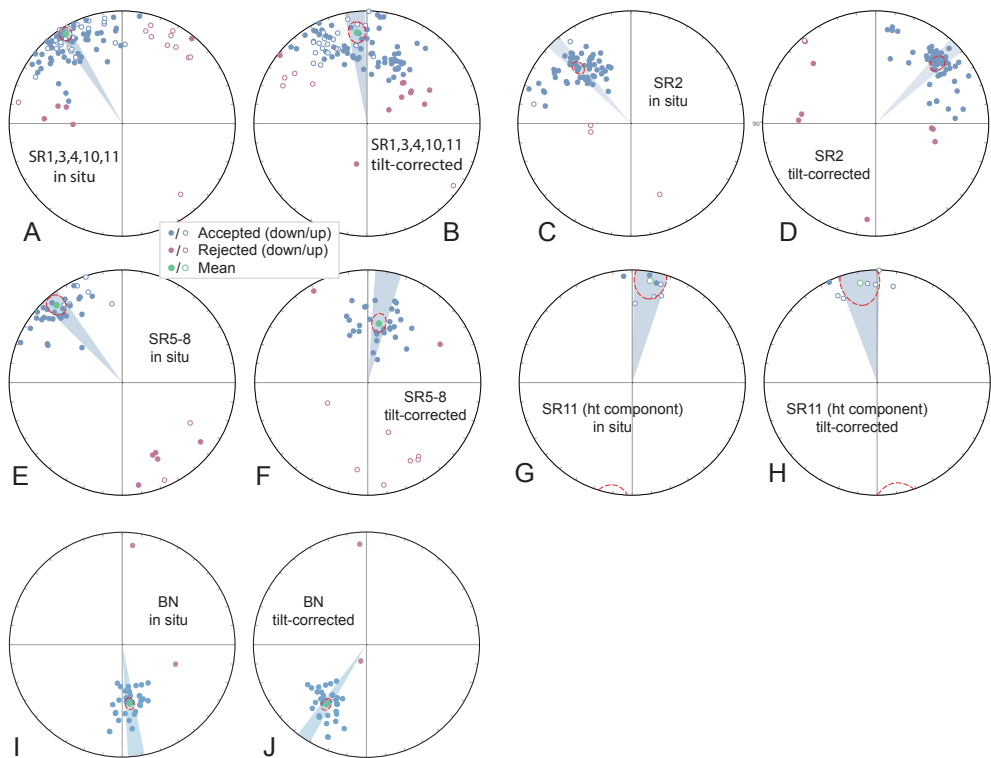
Figure 5: Interpreted directions from localities SR and BN (Costa Rica).

ChRMs from the BN gabbros are generally interpreted between 390-560° or 35-70 mT. The mean (tilt corrected) ChRM direction is D ± ΔDx = 213.8 ± 3.6°, I ± ΔIx = 36.6 ± 5.0° (Fig. 5j), indicating a latitude of formation of 20.4° [17.1°, 23.9°].

3.3.3. New Zealand

From the total of ten blocks of chert, six blocks (TK, TU, TP, WB, KB1,2, BI4) yielded mean directions (not corrected for bedding tilt) similar to the Late Cretaceous remagnetization direction documented by e.g. van de Lagemaat et al. (2018) (Fig. 6a). Four blocks (BI1,2,3,5) yielded different results (Fig. 6a,b), indicating the possibility of a primary magnetization. In BI3 only, variations in bedding were sufficient to allow for a statistically meaningful fold test, which is negative (best clustering between -17 and 17% unfolding, Fig. S3). The mean ChRM directions (corrected for bedding tilt) from BI1, BI2 and BI5 are D ± ΔDx = 19.2 ± 13.1°, I ± ΔIx = 23.9 ± 22.4°, D ± ΔDx = 165.3 ± 13.0°, I ± ΔIx = -27.3 ± 21.1°, and D ± ΔDx = 320.4 ± 9.7°, I ± ΔIx = 14.0 ± 18.4° (Fig. 6h,j,l), corresponding to paleolatitudes of 12.5° [0.8°, 27.6°], 14.5° [3.1°, 29.4°], and 7.1° [-2.2°, 17.6°], respectively. When correcting for bedding assuming overturned strata, ChRM directions cluster significantly less for all three sites.
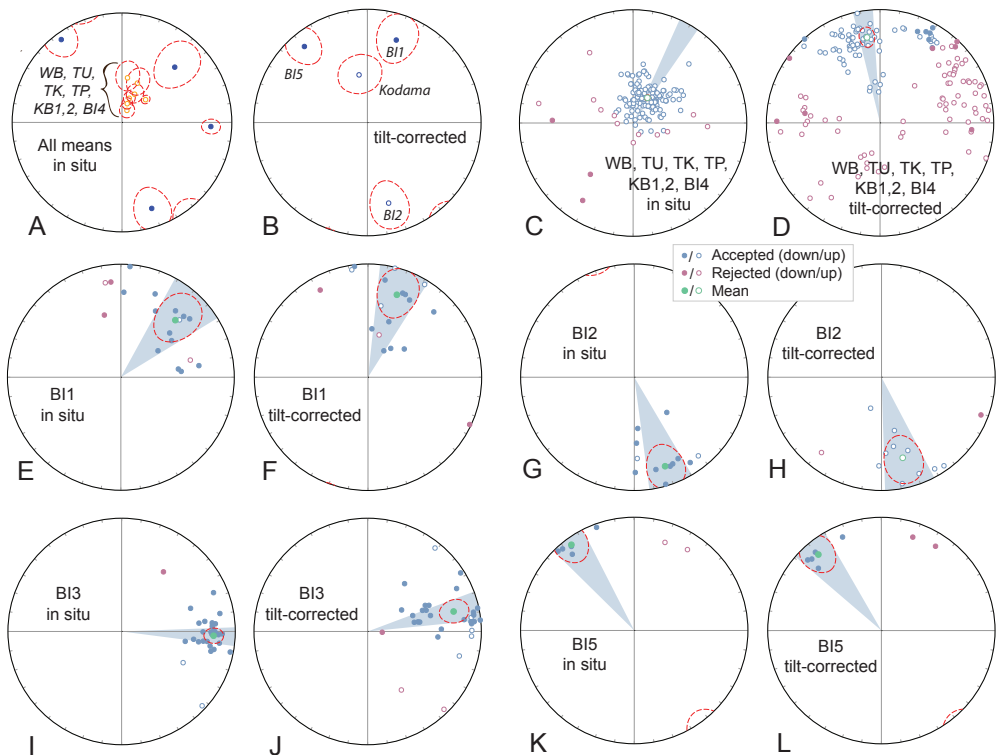
Figure 6: Interpreted directions from sites in New Zealand, including results from Kodama et al. (2007).

3.4. Potential inclination error

Radiolarian chert is suitable for obtaining depositional latitudes with paleomagnetism, because it preserves well-developed bedding planes necessary to restore the paleomagnetic vector to its original direction, can be dated with biostratigraphy, and generally contains sufficient magnetic carrier minerals. A disadvantage of using chert, however, is that little is known about its compaction behavior. Compaction of sediments after deposition has been shown to significantly alter the inclination of primary magnetizations, which may lead to significant underestimation of paleolatitude (e.g Collombat et al., 1993; Kent & Tauxe, 2005; Krijgsman & Tauxe, 2006; Torsvik & Van der Voo, 2002). Two methods have been developed to account for inclination shallowing: the magnetic fabric method of Jackson et al. (1991) and Kodama (2009), and the E/I method of Tauxe and Kent (2004). Alternatively, the inclination of detrital sedimentary rocks may be corrected using an assumed compaction factor (f), commonly 0.6 (e.g. Torsvik et al., 2012). It is unclear, however, what flattening factor is appropriate for radiolarian cherts.

We aimed at determining inclination shallowing due to compaction in cherts by the E/I method of Tauxe and Kent (2004) and collected large sampling sets at Cedros Island (CC1) and from the San Hipólito section of the Vizcaíno Peninsula (Sites SH1-3, SH8-11, Chapter 5). Unfortunately, interpreted directions from the first 36 samples from the San Hipólito cherts (SH1, 10) yielded a negative fold test (we refrained from measuring the additional samples) and the results from CC1 (great circle solutions only) presented in this chapter are not suitable for the E/I method.

Previous estimates on inclination shallowing in cherts vary. Huang et al. (2015) collected large paleomagnetic data sets from two sections of Lower Cretaceous (~130-120 Ma) radiolarian cherts and one section of time-equivalent sandstones that unconformably overlie ophiolites in the Indus-Yarlung suture zone of Tibet. They demonstrated through detrital zircon analysis that these sandstones were derived from the Tibetan plateau, which in Early Cretaceous time was located at a latitude of ~15°N (Ma et al., 2014; van Hinsbergen et al., 2018; Yang et al., 2015). Inclination of the sandstones and cherts were similar, and correcting for inclination shallowing in the sandstones by both the E/I as well as the magnetic fabric method yielded a corrected paleolatitude estimate of ~16°N consistent with the latitude of the Tibetan plateau (Huang et al., 2015). Correcting the inclinations of the cherts to match the sandstone paleolatitude would require a flattening factor for the cherts of ~0.7-0.8. Furthermore, Iijima et al. (1989) estimated compaction in chert from central Honshu to be 60-80%, based on the bending of sedimentary laminae around a fragment of silicified wood.

On the other hand, the preservation of unflattened radiolaria suggests that compaction in cherts is generally rather minor. Oda and Suzuki (2000) applied the relationship between

Table 1 (right page): Parameters from all new and compiled paleomagnetic data.

Region	Site	Authors*	Lat. (°N)	Lon. (°E)	Age	N	N45	D	ΔD_x	I	ΔI_x	k	α_{95}	K	A_{95min}< A_{95}< A_{95max}	λ
Mexico	CC1		28.055831	-115.227354	Late Triassic	48	48	198.2	2.8	-9.3	5.4	38.4	3.4	56.4	2.6<3.6<7.2	-10.3
	CC1	Hagstrum & Sedlock 1990	28.055831	-115.227354	Late Triassic-Early Cretaceous	10	48	193.6	3.7	-20	6.6	26.7	4.1	33.5		2.7
	CC2		28.114172	-115.275147	Late Triassic	22	19	208.8	11.2	5.5	22.3	16.3	12.3	19.5		
								193.6	16.3	-65.4	8.3	21.1	7.5	10.4		
							22	189.4	7	-10	13.6	17.1	7.7	20.9	3.5<7<11.7	-5
Costa Rica	SR1,3,4,10,11		10.881325	-85.879024	~190-180 Ma	93	79	329.2	3.5	6.1	7	13.3	4.5	21.4		
	SR11-ht		10.881325	-85.879024	~190-180 Ma	7	7	9.9	8.8	-9.1	17.3	20.8	13.5	47.9		
	SR5-8		10.881389	-85.878912	~175 Ma	37	30	350.4	11	-11.3	21.3	25.7	12.1	31.2	5.5<11<24.1	-5.7
								319.5	5.6	10.8	10.9	14.6	7.1	23.1		
	SR2		10.878507	-85.874661	~110 Ma	62	59	316.7	3.9	32.8	5.7	20	4.2	26.5		
	BN		10.815429	-85.733133	124 ± 4.1 Ma	36	53	45.7	4.3	24.9	7.3	22.1	4.3	22.9		
							34	172.8	4.3	46.3	4.6	41.7	3.9	42.6	2.5<4.2<6.7	13
							34	213.8	3.6	36.6	5	41.7	3.9	53.3	2.9<3.4<8.9	20.4
New Zealand	WB		-36.932241	175.19215		18	16	16.7	13.3	-71.3	4.8	73	4.3	25.8		
	TU		-35.618648	174.540604		15	14	22.1	34.7	-80.4	5.7	49.8	5.7	15.2		
	TP		-36.379692	174.83118		15	14	22.1	34.7	-80.4	5.7	49.8	5.7	15.2		
	TK		-37.736264	177.672451		54	52	45.9	6.9	-65.6	3.5	37.8	3.3	19.3		
	KB1		-34.997889	173.802669		14	11	7	14.9	-56.3	11.4	22.9	9.8	15.7		
	KB2		-34.997889	173.802669		13	11	24	15.6	-67	7.3	50.6	6.5	21.7		
	BI1		-35.250401	174.132982		18	14	43.6	14.9	30.9	22.9	7.2	15.9	8.7		
	BI2		-35.250401	174.132982	Permian	12	15	19.2	13.1	23.9	22.4	6.1	16.9	9.9	4.1<12.8<14.9	12.5
							12	161	11.4	18	21	8.8	15.5	15.7		
	BI3		-35.254136	174.132507	Permian	31	12	165.3	13	-27.3	21.1	11.3	15	15.8	4.8<12.5<19.2	-14.5
							30	92.7	4.8	20.1	8.6	20.1	6	32.1		
	BI4		-35.254136	174.132507	Permian	7	7	21.4	15	-58.4	10.6	55	8.2	28		
	BI5		-35.257472	174.132507	Permian	7	5	323.9	9.2	7	18.1	60.5	9.9	70.6		
							5	320.4	9.7	14	18.4	55.6	10.3	63.9	6.3<9.6<29.7	7.1
	Waiheke Island	Kodama et al. 2007	-38.6	174.9	Early Triassic	21		323		-1			17			
								349		-53						-33.6
Japan	ON4	Shibuya & Sasajima 1986	42.673689	142.673946	Berriasian	25	25	299.4	8.4	37	11.5	13.7	8.1	14.5	3.4<8<11.1	3.6
							24	251.4	8	7.2	15.7	9.7	10	14.8		0.7 ± 3.4
	Inuyama - CI	Ando et al. 2001	35.4	137	middle Triassic	12	12	270.9		1.4						
								252.8		-13.5	6.8	126.8	2.3			-2.7
	Inuyama - C2	Ando et al. 2001	35.4	137	middle Anisian	32		81		-5.4						
								48		46.9		26.8	4.4			5.5
	Inuyama - N1	Ando et al. 2001	35.4	137	upper Anisian	41		176.5		10.9						
								339.4		23.7		4.8	26.1			9.3
	Inuyama - N3	Ando et al. 2001	35.4	137	middle Carnian	36		163.9		18.2						
								218.7		35.8		6.4	23.4			3.9
	Inuyama - KI	Ando et al. 2001	35.4	137	lower Norian	23		352.2		7.7						
								320.8		20		7.1	53.6			10.3
	Inuyama - K4	Ando et al. 2001	35.4	137	upper Norian	9		185.5		72.9						
								234.2		-7.2		5.5	43.7			-3.6
	Inuyama - UN1	Oda & Suzuki 2000	35.4	137	lowermost Jurassic	17		-124.8		-17.8		2.7	39.2			
								154.7		12		3.2	34.3			6.7 ± 17.8**
	Inuyama - UN2	Oda & Suzuki 2000	35.4	137	Anisian	9		-39.3		-9.7		9.8	20.3			
								-88.8		46.6		9.9	20.2			29.5 ± 17.4**
	Inuyama - KA1	Oda & Suzuki 2000	35.4	137	upper Norian	7		-35.1		8.2		4.2	26.8			
								111.9		22.6		4.5	25.9			11.8 ± 14.6**
	Inuyama - KA2	Oda & Suzuki 2000	35.4	137	lower Norian	10		-9.3		16.8		4.8	26.1			
								82.4		39.4		8.1	19.3			23.5 ± 14.2**
	Inuyama - KA3	Oda & Suzuki 2000	35.4	137	upper Norian-Rhaetian	9		4.4		-13.8		2.5	48.5			
								132.7		16.5		2.9	43.3			9 ± 23.3**
	Inuyama - KA5	Oda & Suzuki 2000	35.4	137	lower Ladinian	7		-32		17		8.8	19.8			
								94.5		29.4		12.5	16.3			16.9 ± 10.2**
	Kamura	Kirschvink et al. 2015	32.8	131.3	Upper Permian	150		149.6		-66.6		12.33	3.4			
								327.5		-23.4		13.99	3.2			-12.2 ± 1.8
Pacific Plate	OPD Site 801B	Fu & Kent 2018	18.64199	156.35966	Upper Valanginian - Lower Hauterivian	3										-12.7 ± 1.8
					Upper Tithonian - Lower Valanginian	11										-7.7 ± 1.8
					Lower Tithonian - Middle Tithonian	10										-2.7 ± 1.3
					Kimmeridgian	9										-10.4 ± 3.8
					middle Bathonian- Upper Callovian	10										-4.5 ± 1.6
					167 ± 1.4 Ma	11										-4.4 ± 2.0

N45: number of samples after 45° cut-off
Bold numbers are corrected for bedding tilt
* When other than this study
** Palaeolatitudes based on inclinations corrected for inclination shallowing

ARM anisotropy and inclination shallowing of Jackson et al. (1991) to IRM anisotropy, and concluded that this correction method changed their obtained inclinations by a maximum of 2° only (corresponding to flattening factors of 0.9-1.0)(Fig. 3). Ando et al. (2001) used the argument of undeformed microfossils in their samples to argue for little effect of compaction.

Due to the lack of control on the amount of compaction in cherts and the absence of data to apply a correction method, we use uncorrected values of inclination, which correspond to minimum estimates of depositional paleolatitudes. As a result of the non-linear relationship between inclination and latitude, the effect of compaction on inclination is largest around ~50° N/S and considerably smaller around the poles and the equator. The results from New Zealand may therefore be subject to a larger inclination error compared to all other (low inclination) results, for which the error should be minor. To give an estimate of the possible error, Table 2 includes paleolatitudes corrected for inclination shallowing using a flattening factor of 0.7, inferred from the study of Huang et al. (2015).

3.5. Hemispheric origin

Based on a correlation with the global magnetostratigraphic timescale, Kirschvink et al. (2015) and Ando et al. (2001) argued for a southern hemispheric origin of the Permian Kamura limestones and Anisian cherts of the Inuyama region of Japan. For all other obtained paleolatitudes from OPS materials, however, hemispheric origin is unknown. In our reconstruction, we generally assume minimum plate motions, implying that we assume a northern hemisphere origin for the post-Anisian rocks accreted in Japan (Fig. 3), and a southern hemisphere origin for the rocks accreted in New Zealand. For a discussion on hemispheric origin of the rocks accreted in Costa Rica and Mexico, see below.

3.6. Summary of paleomagnetic results

The paleomagnetic data presented in this chapter (summarized in Table 1) are by no means ideal. Positive fold tests on the results from the Inuyama cherts and the presence of both normal and reversed directions in the Kamura limestones, the Waiheke Island cherts, and the CC1 cherts indicate that these magnetizations are likely primary. For all other results however, we assume a primary nature of the magnetization based on (1) the statistical difference between the mean interpreted directions and the present day field or any other known remagnetized direction from the area; and (2) the absence of positive evidence for remagnetization. Furthermore, A95 values from all our new sites that have been interpreted as potentially primary fall within the A95min-A95max window (Table 1), indicating that the distribution of ChRM's satisfies the statistical criteria of representing paleo-secular variation (Deenen et al., 2011).

4. Reconstruction: relative plate motions, mantle reference frames, and the use of paleomagnetic data

4.1. 0-140 Ma

Modern global plate kinematic reconstructions consist of mathematical descriptions of relative plate motions of the major plates based on marine magnetic anomaly and fracture zone data, supplemented by motions of smaller tectonic terranes, generally based on estimates of crustal deformation derived from the geological record. For 0-83 Ma, relative plate motions of the Pacific Plate and its conjugates (the Panthalassa plate system) are linked to the Indo-Atlantic plate system through marine spreading records of the Antarctic-Pacific ridge, thereby enabling the reconstruction of relative plate motions of almost all major plates on Earth. Prior to 83 Ma, however, no ridge was present connecting the Panthalassa and Indo-Atlantic plate systems, and consequently, relative plate motions of the two systems cannot be constrained from marine geophysical data. Alternatively, both systems may be placed in mantle reference frames, thereby connecting the two via the lower mantle. Absolute plate motion frames for the Indo-Atlantic plate system are for example the moving hotspot reference frames of Torsvik et al. (2008)(0-130 Ma), O'Neill et al. (2005)(0-130 Ma) and Doubrovine et al. (2012)(0-124 Ma) or the slab-fitted frame of van der Meer et al. (2010) (0-300 Ma). Wessel and Kroenke (2008) computed absolute plate motions

	Location	Site	Age (Ma)	λ	λ |uncertainty|	ISC λ ff0.7	Age in Trench (Ma)	Reconstructed at
83-140 Ma	Costa Rica	SR2	110	±13	[9.0,17.5]	18.3	100	13
	Costa Rica	BN	124.4	±20.4	[17.1, 23.9]		100	12.5
	Pacific Plate	OPD Site 801B	135	-12.7	[-10.9, -14.5]	17.8	-	-1
140-190 Ma	Pacific Plate	OPD Site 801B	141.9	-7.7	[-5.9, -9.5]	10.9	-	-1
	Japan	ON4	145	±3.6	[-4.3, 11.9]	5.1	100	10
	Pacific Plate	OPD Site 801B	149.4	-2.7	[-1.4, -4]	3.9	-	-4
	Pacific Plate	OPD Site 801B	154.7	-10.4	[-6.6, -14.2]	14.7	-	-6
	Pacific Plate	OPD Site 801B	161.1	-4.5	[-2.9, -10.6]	6.4	-	-7
	Pacific Plate	OPD Site 801B	167.7	-4.4	[-2.4, -6.4]		-	-8
	Costa Rica	SR11-ht	190	-5.7	[-17.7, +5]	8.1	100	-17.5
190-260 Ma	Japan	Inuyama cherts	215	20		27.5	170	20
	Mexico	CC1/CC2	220	±7.5	[14.8, 4.3]	10.7	105	-13.5
	Japan	Inuyama cherts	240	-5		7.1	170	-5
	New Zealand	Waiheke Island	250	-33.6	[-51.2, -20]	43.5	150	-33.6
	New Zealand	BI1/BI2/BI5	260	-11.4	[-0.6, -24.9]	16.1	150	-22
	Japan	Kamura	260	-12.2	[-14, -10.4]		160	-12.2

Table 2: Estimates on age, paleolatitude and accretion age of OPS materials. λ: paleolatitude, ISC λ ff0.7: Inclination shallowing corrected paleolatitude using a flattening factor of 0.7.

of the Pacific Plate from hotspot tracks back to 144 Ma, assuming hotspot fixity. Later studies, however, have shown changes in inter-hotspot distances (Konrad et al., 2018; Wessel & Kroenke, 2009). Nonetheless, for pre-Late Cretaceous times, the Wessel and Kroenke (2008) frame provides the only available constraint on absolute plate motions of the Panthalassa plate system. In Chapter 5, we showed that linking the two plate systems by using the Wessel and Kroenke (2008) and van der Meer (2010) frames yield a kinematically feasible reconstruction of the Caribbean – Farallon connection. The validity of this approach may be further tested with post-140 Ma paleomagnetic data of the Pacific Plate (Fu & Kent, 2018) and from Costa Rica (SR2 and BN). To do so, we take the following steps: for 83-140 Ma, we determine Euler rotations of the Pacific Plate relative to the Indo-Atlantic plate system (represented by its base, Africa) assuming motion according to the Wessel and Kroenke (2008) frame for the Panthalassa plate system and the van der Meer et al. (2010) frame for the Indo-Atlantic plate system and place the resulting combined reconstruction in the paleomagnetic reference frame of Torsvik et al. (2012). Next, we add marking points representing the SR2 and BN rocks that are located at the Cedros and Santa Elena trenches at the age of their accretion (105 and 100 Ma), and move with the Farallon Plates before these times (following van Hinsbergen and Schmid (2012)). The 83-140 Ma reconstruction is fully consistent with the paleolatitudinal estimate from SR2 (110 Ma), and within 10° from those of BN (124 Ma) and the ODP site (135 Ma). The latter two estimates are relatively uncertain due to a potential primary dip of the layered gabbros at site BN and the small number of samples (N=3) used in the calculation of the 135 Ma paleolatitude of the Pacific Plate.

4.2. 140-190 Ma
Prior to 140 Ma, control on absolute plate motions of the Panthalassa system from hotspots is lost (Fig. 7). In Chapter 1, we have shown how the birth of the Pacific Plate may be explained by cessation of an intra-oceanic subduction system between the Farallon and Izanagi plates, and suggested that the location of the early Pacific Plate may be inferred from fitting the ~190 Ma Izanagi-Farallon-Phoenix triple junction on a lower mantle slab remnant. This opened the possibility of slab fitting the triple junction. We showed that fitting the triple junction on either of two previously identified slabs (the Telkhinia and Trans-Americas slabs) results in 190-140 Ma plate motions of the Pacific Plate within the range of elsewhere reconstructed absolute plate motion velocities (Zahirovic et al., 2015). However, we also noted that further discrimination between the different slab-fitting scenarios relies on assessment of the relative motions between the Panthalassa plates and the surrounding continents. Development of the Panthalassa plate system (in Chapters 4, 5 and 6 of this thesis) now allows for assessment of these relative motions.

The geological records of Mexico, New Zealand, and Japan contain evidence of subduction since at least 220 Ma, 260 Ma, and 500 Ma, respectively (Chapters 3, 4 and 6; Mortimer, 2004). Although these geological records (arc volcanics, accretionary complexes, fore-arc
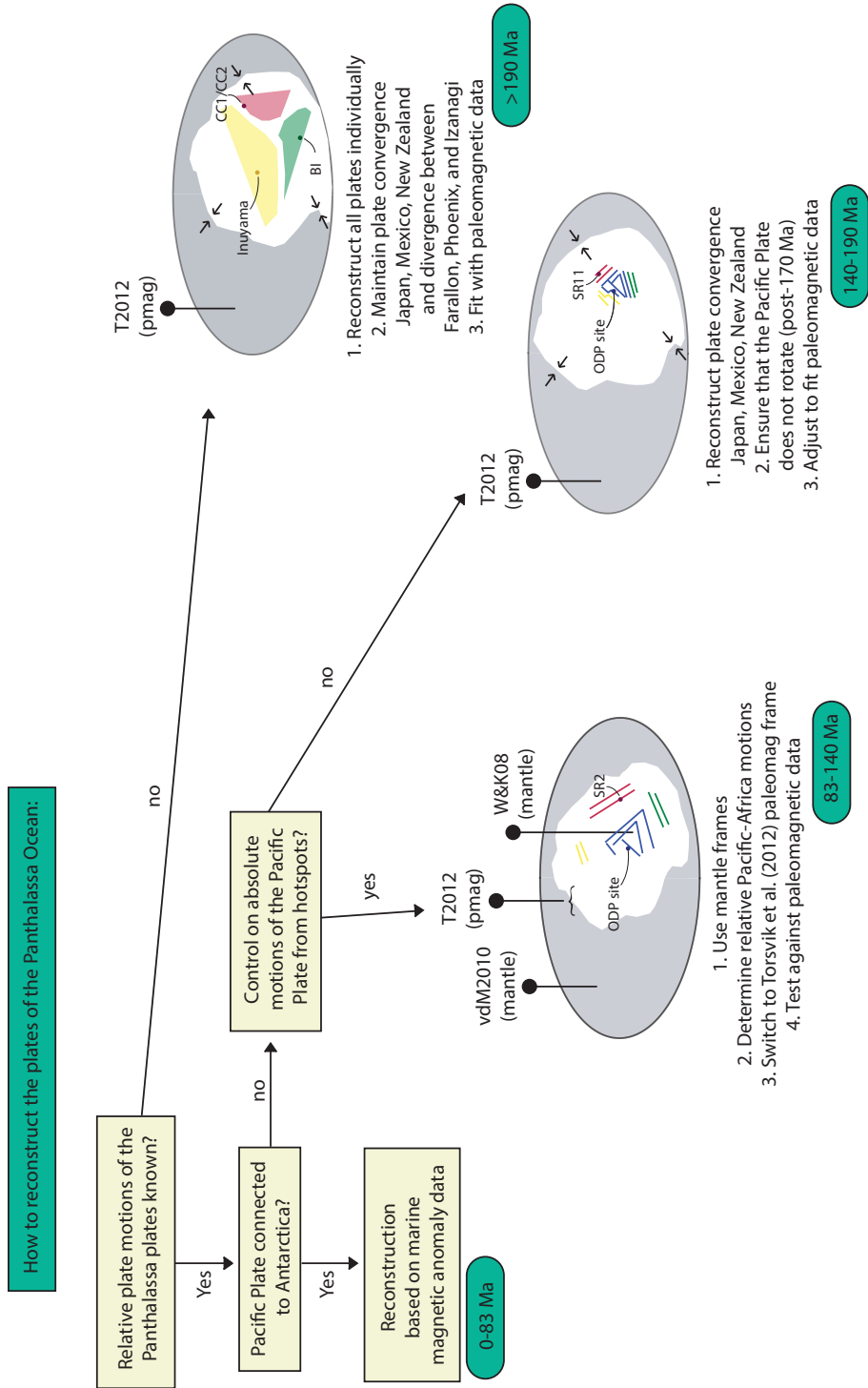
Figure 7: Flowchart illustrating the adopted reconstruction approach to reconstruct the plates of the Panthalassa Ocean and link the tectonic history of those plates to the global plate circuit.

237

sequences etc.) are not continuous but rather episodic and temporal interruptions in subduction, trench migration, or subduction jumps cannot be excluded, they do testify of hundreds of million years of overall plate convergence between the Panthalassa and Indo-Atlantic plate systems. Furthermore, the continuous Cocos slab reaching into the lowermost mantle does indicate that subduction below the Mexican margin was uninterrupted since probably 220 Ma (Chapter 4). However, fitting the 190 Ma Izanagi-Farallon-Phoenix triple junction on the Trans-Americas slab (the preferred scenario in Chapter 1) yields divergence between Farallon and North America (placed in the van der Meer et al. (2010) slab-fitted mantle reference frame) between 190-140 Ma. Similarly, fitting the triple junction on the Telkhinia slab yields phases of divergence between the Izanagi Plate and Japan. This implies that either fit violates the evidence for subduction on the northeastern and -western margins of the Panthalassa Ocean, and that the 190 Ma absolute location of the Izanagi-Farallon-Phoenix triple junction was most likely located somewhere between the Trans-Americas and the Telkhinia slab. This region is associated with very low-resolution mantle tomography (Fig. 4 in Chapter 1), and slabs may exist within this domain, but cannot be used for a slab-fitting approach. Instead, we determine 140-190 Ma plate motions of the Panthalassa plate system based on the inferred convergence between Izanagi and Japan, Farallon and Mexico, and Phoenix and New Zealand, and on paleomagnetic data from the Pacific Plate, SR11 and ON4. We add marking points for the SR11 and ON4 cherts on the Farallon and Izanagi plates. We reconstruct the Panthalassa plate system (incorporating subduction in the intra-oceanic Oku-Niikappu trench as reconstructed in Chapter 6) back to 190 Ma (by moving the Pacific Plate, which is the base of the plate system) such that (1) preceding (120-140 Ma) convergence directions between Farallon and Mexico/Costa Rica and Izanagi and Japan are maintained as much as possible, and (2) there is no significant vertical axis rotation of the Pacific Plate (Fu & Kent, 2018). Next, we adjust the reconstruction to place the marking points of the ODP site and SR11 within the uncertainty limit of the obtained paleolatitudes (Fig. 7). For SR11, there are two hemispheric options. Placing SR11 at the northern hemisphere would place the ODP site (from which southern hemispheric latitudes are obtained) at the northern hemisphere as well, and furthermore, would result in southeastward motion of the Farallon Plate relative to North America (sub-parallel to the continental margin). This southward component is not the result of actual absolute southward motion of the Farallon Plate, but is due to North America moving south more rapidly than Farallon in this time period. To comply with convergence (and hence, relative northeastward motion of Farallon) and a southern hemispheric origin of the OPD site sediments, we place SR11 at the southern hemisphere, requiring a much smaller adjustment to the reconstruction of the previous step, and yielding a reconstruction without major relative plate motion changes. Upholding the relative plate motions of the Panthalassa plate system from marine magnetic anomaly data, it is not possible to reconstruct the plate system such that all paleomagnetic sites fall within the uncertainty margins of the paleolatitudes. However, misfits are no larger than a few (<5) degrees (Table 2).
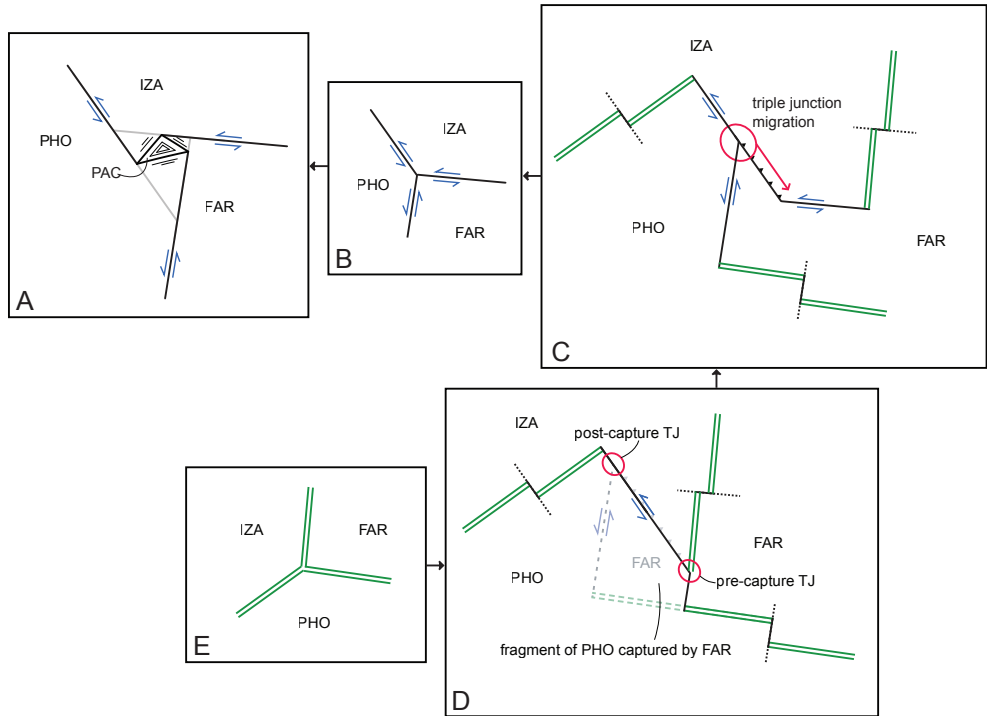
Figure 8: Schematic representation of ~190 M tectonic events that led to the birth of the Pacific Plate.

4.3. 190-260 Ma

Reconstructing pre-190 Ma motions of the Izanagi, Farallon and Phoenix plates, or any older ocean, requires a different approach, as there is no control on relative plate motions through marine geophysical data. As a consequence, a 'plate system' is no longer available, and the plates can only be reconstructed individually. In Chapter 1, we discussed how the birth of the Pacific Plate followed upon reorganization at an unstable triple junction that was generated upon cessation of a subduction zone between the Farallon and Izanagi plates. Even though no data are available that recorded the ~190 Ma events, simple rules of plate kinematics (Cox & Hart, 1986) allow us to hypothesize the situation that preceded the plate reorganization. The orientation of the pre-190 Ma Farallon-Izanagi subduction segment (Fig. 8c) is not straightforwardly explained in a Farallon-Izanagi spreading context, but instead, is equal to the orientation of Izanagi-Phoenix transforms. We therefore suggest that initiation of the subduction that culminated in the birth of the Pacific plate may have followed upon capture of a fragment of Phoenix lithosphere by the Farallon Plate (Fig. 8d). Plate capture may have been preceded by reorganization of the original Izanagi-Farallon-Phoenix ridge-ridge-ridge triple junction into a ridge-transform-transform or ridge-ridge-transform triple junction, a feature that is not
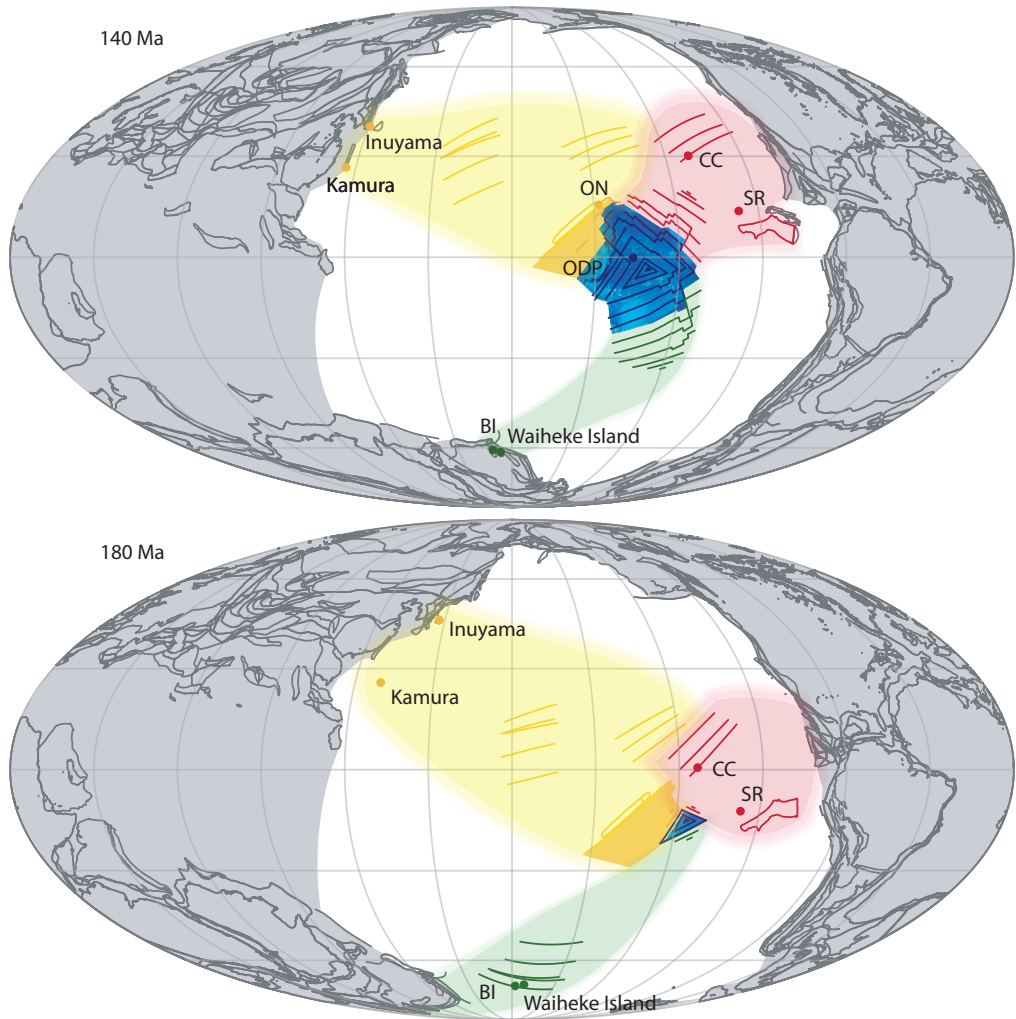
Figure 9: Reconstruction of the Izanagi (IZA1 and IZA2), Farallon and Phoenix plates of the Panthalassa Ocean. Reconstruction of North/South America and Africa from Torsvik et al. (2012); Europe/Asia from Müller et al. (2016) and Domeier and Torsvik (2014).

uncommon in RRR triple junctions (Kleinrock & Morgan, 1988; Viso et al., 2005). The duration of subduction depends on the length of the transform segment along which the triple junction migrated from the moment of plate capture until formation of the unstable transform-transform-transform triple junction (Fig. 8b), and may have been in the order of only a few to ten million years. Before that time, we assume that the Izanagi, Farallon and Phoenix plates were joined in a long-lived stable RRR triple junction (Fig. 8e).
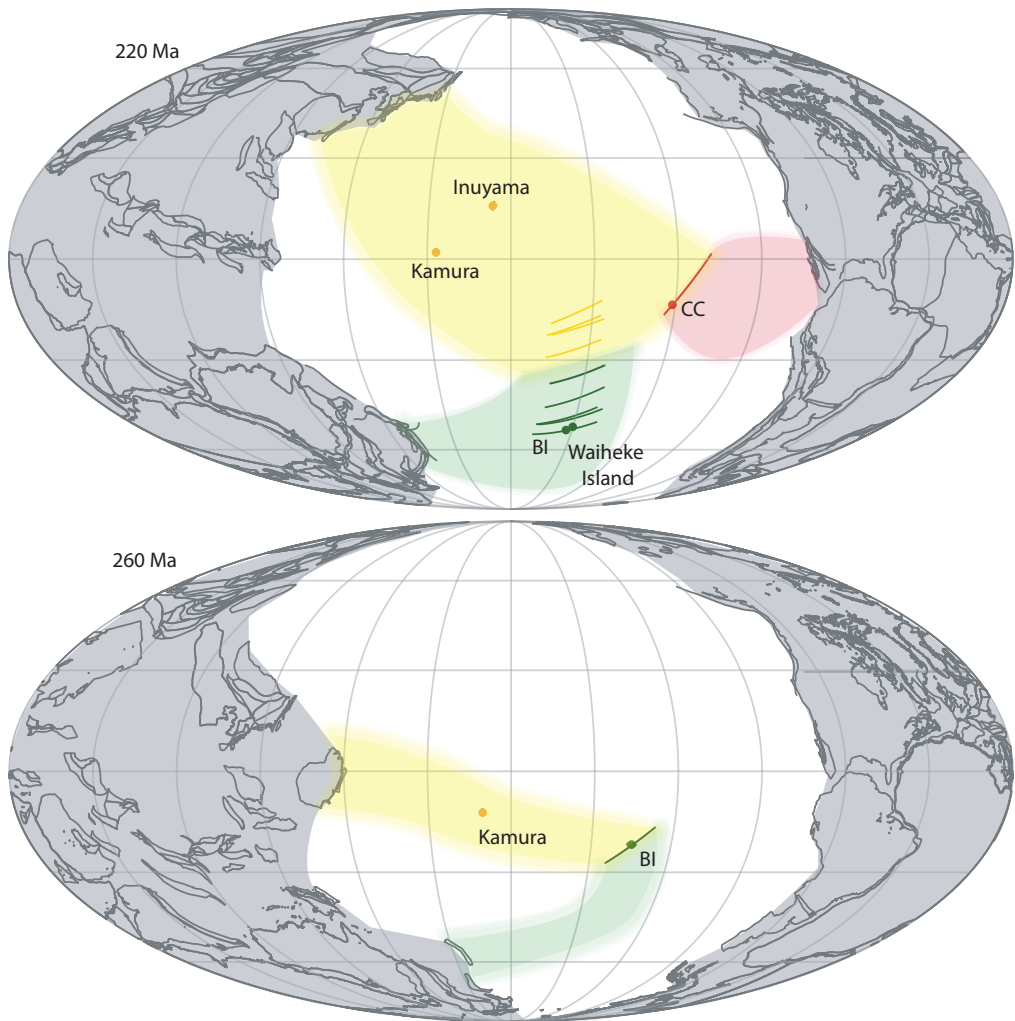
Figure 9 continued.

To reconstruct pre-190 Ma plate motions, we add additional marking points: the BI1/BI2/BI5 and Waiheke Island cherts from New Zealand, the 215 Ma and 240 Ma Inuyama cherts, the Kamura limestones from Japan, and the CC1/CC2 cherts from Mexico. Next, we reconstruct Farallon, Izanagi and Phoenix plate by plate, whereby we accommodate (1) the paleomagnetic data; (2) minimal relative plate motion changes; (3) continuous convergence between Izanagi and Japan, Farallon and Mexico/Costa Rica, and Phoenix and New Zealand; and (4) continuous divergence between Izanagi, Farallon and Phoenix. Restricted by the age of the oldest rocks from which paleolatitudes are obtained, the Farallon Plate is reconstructed back to 220 Ma; the Izanagi and Phoenix plates to 260

Ma. The Late Triassic CC1 cherts now located at Cedros Island are in outcrop in direct contact with pillow basalts and are therefore interpreted to be deposited immediately upon formation of the magmatic basement. In other words, at 220 Ma, the CC1 cherts were located adjacent to a Farallon ridge. At 190 Ma, CC1/CC2 is located north of the Izanagi-Farallon-Phoenix triple junction, and we therefore infer that this ridge was the Farallon-Izanagi ridge. We reconstruct a segment of this ridge by creating artificial 10 Myr interval isochrons since 220 Ma. Similarly, the Permian Bay of Island cherts from New Zealand are associated with pillow basalts. BI1/BI2/BI5 is at 190 Ma located west of the Izanagi-Farallon-Phoenix triple junction, and we infer those cherts to be deposited near the Phoenix-Izanagi ridge. We reconstruct a fragment of this ridge since 260 Ma. The other sites (the Inuyama cherts, Kamura limestones, and Waiheke Islands cherts) are not directly associated with basement rocks and are thus deposited in an intra-plate setting.

5. Discussion

5.1. Exchanges between the Indo-Atlantic and Panthalassa plate systems

Reconstructing the tectonic evolution of the margins of Japan, New Zealand and Mexico illustrates that these circum-Panthalassa trenches have not been stable continental-margin trenches throughout their entire history, but instead, that these margins have been subject to significant overriding plate deformation, including the opening and closure of back-arc basins. When a back-arc basin develops a mature spreading ridge, an additional plate is created and the formerly continental margin arc becomes a 'fringing arc'. Upon opening, this additional plate is still part of the Indo-Atlantic plate system, as it connects to the overriding plate with a spreading center and is separated from the Panthalassa plate system by the subduction zone. Upon subsequent closure of the back-arc basin, however, a temporal second subduction zone is generated, which separates the plate that hosts the fringing arc from the Indo-Antlantic plate system. Whereas relative plate motion through a spreading ridge is limited in direction by the orientation of the ridge, relative plate motions over a subduction zone are completely 'free' and plate motions of the fringing arc-plate are now thus fully independent from the overriding plate. Reconstructions of the fringing arcs from Japan en New Zealand (the Hokkaido-outer zone system and the Eastern Province) indicate that prior to accretion resulting in their modern configurations, these arcs underwent margin-parallel plate motion in line with the latitudinal motion of the Izanagi and Phoenix plates. The Hokkaido-outer zone system of Japan was rifted off the continental margin of South China and accreted further north, the Eastern Province of New Zealand was rifted off the continental margin of northeastern Australia and accreted further south. A similar tectonic scenario is reconstructed for the Wrangellia terrane of the northern North American Cordillera that moved north with the Farallon (or Kula) Plate (e.g. Scotese, 2004)). The Guerrero terrane of Mexico forms an exception to this trend; it has a latitudinal plate motion history equal to that of the North American Plate. We interpret this as indication that the Arperos back-arc basin (behind the Guerrero arc) was a relatively small basin, thereby not allowing major latitudinal plate motions upon closure.

Pacific - Africa

83.0	47.5	-61.0	68.4
90.0	48.9	-64.5	70.9
95.0	48.0	-64.4	74.7
100.0	48.3	-62.8	79.3
106.2	47.0	-62.3	85.5
110.0	46.7	-62.2	88.5
120.0	48.0	-59.4	95.1
130.0	49.6	-59.4	101.9
140.0	50.5	-59.8	109.9
150.0	53.2	-59.6	113.6
160.0	53.4	-63.0	117.5
170.0	53.9	-66.7	118.6
180.0	54.9	-71.0	121.0
190.0	55.8	-76.1	121.0

Farallon - Pacific

83	39.4446	38.7475	87.7423
100	40.225	43.384	68.3205
110	36.6404	39.8589	58.6827
120.6	34.5129	41.9779	46.8523
125.7	32.8439	42.0058	41.2868
130.5	32.0612	43.0875	35.8133
137.9	37.7757	63.2591	28.7745
146.6	37.7444	63.1022	23.7231
154	37.759	61.1671	18.904
168	37.1554	62.9053	10.376
180	34.8767	61.6925	3.9973
185	34.3939	61.7605	1.4758
190	0	0	0

Farallon - Africa

190	39.4446	38.7475	87.7423
200	74.9094	33.9383	126.745
210	-56.5174	102.344	-135.934
220	-51.8945	93.1434	-145.34

Phoenix - Pacific

83	42.0772	-94.4693	85.6399
90	34.856	-88.9396	74.8044
100	25.4597	-89.6326	67.2492
110	18.5447	-88.4392	57.206
120.6	15.3108	-97.372	52.2892
125.7	16.0672	-100.4202	47.9047
130.5	16.0228	-99.8703	41.7283
137.9	15.1097	-97.971	33.0244
146.6	16.2333	-105.2665	25.6301
154	13.1725	-105.6315	18.76
168	11.7098	-104.85	11.2791
180	11.4846	-104.8964	5.5717
185	10.4121	-104.9377	2.3569
190	0	0	0

Phoenix - Africa

190	55.8195	-76.0988	121.035
230	-62.0514	80.7874	-113.716
250	-61.9234	75.8978	-112.32
260	66.5155	-119.998	113.365

Izanagi 1 - Pacific

83	40.3463	-118.692	-95.7468
100	41.7875	-121.2788	-84.2393
110	42.728	-129.5726	-78.5873
120.6	43.8562	-131.4884	-69.0458
125.7	44.4921	-135.2895	-64.2488
130.5	45.5546	-136.716	-58.216
137.9	47.3307	-136.2292	-49.1018
146.6	47.9656	-96.7309	-36.4024
149	47.7801	-95.5329	-33.2081
154	47.9139	-93.4008	-30.4856
160	49.7333	-103.8211	-25.8344
168	50.5538	-114.2768	-20.0267
180	-47.0227	23.2941	7.9206
185	-49.2665	89.64	3.2341
190	0	0	0

Izanagi 2 - Pacific

137	35.7145	-153.983	-30.7567
145	32.6792	-159.2135	-27.204
155	32.165	-162.6416	-25.3016
165	31.4752	-166.3509	-23.4805
175	30.6073	-170.8524	-21.7616
185	29.4888	-175.8454	-20.1764
190	28.9317	-178.124	-19.2357

Izanagi 2 - Africa

190	60.6838	-57.6036	116.185
215	-54.5388	98.2467	-141.821
240	-39.9199	84.0361	-155.988
260	-44.7228	86.1954	-165.959

Table 3: Euler rotations (age, lat, lon., angle) of the Pacific, Izanagi (Izanagi 1 and Izanagi 2, see Chapter 6), Phoenix, and Farallon plates. Pacific plate rotations (the base of the Panthalassa plate system are relative to Africa (the base of the Indo-Atlantic plate system). 83-140 Ma rotations are derived from combining the van der Meer et al. (2010) mantle reference frame for the Indo-Atlantic plate system and the Wessel and Kroenke (2008) mantle reference frame for the Panthalassa plate system.

5.2 Limitations on deriving plate motions from paleomagnetic data

In the reconstruction presented in this chapter, the reconstructed plates are at all times within 10° of the paleomagnetically determined paleolatitudes. Compilations of paleomagnetic data from the Indo-Atlantic plate system, however, illustrate that individual paleomagnetic poles scatter considerably around Apparent Polar Wander Paths (e.g. Torsvik et al., 2008; Torsvik et al., 2012)). Tectonic reconstruction of large plates from paleomagnetic data thus improves from larger datasets including multiple poles per time period, which may then be averaged.

Paleomagnetic data and plate motions derived from them record a combined signal of (1) plate motion relative to the sub-lithospheric mantle, and (2) rotation of the crust and mantle combined relative to the spin axis (True Polar Wander, TPW). TPW is shown to be especially large during the Triassic – Early Cretaceous (e.g. Kent & Irving, 2010; Mattei et al., 2014; Meijers et al., 2010a; Muttoni et al., 2005). The paleomagnetic reference frame used in this study (Torsvik et al., 2012) is based on hundreds of paleomagnetic poles, from which a running mean path is calculated using a 20 Myr sliding window. This approach results in smoothing of the Global Apparent Polar Wander Path (GAPWaP), which may lead to an underestimation of both the rate and magnitude of TPW events. This potential underestimation may induce a mismatch between our approach and the data.

5.3. Perspectives on further improvements in reconstructing lost oceans

In 4 years of sampling geological records of ancient subduction around the Pacific, we collected a total of 1532 samples (core and hand) from remnants of overriding plates (arc magmatic and sedimentary rocks, SSZ ophiolites, fore-arc sequences etc.) and 674 samples from downgoing plate-derived rocks. From those, 629 (41%) and 106 (16%) yielded paleomagnetic directions that we interpreted as (potentially) primary. Despite being labor intensive and high risk, this thesis illustrates that reconstructing lost oceanic plates from paleomagnetic data of OPS rocks is possible, and that attempting to do so is worthwhile. The pre-190 Ma reconstruction of the Panthalassa Ocean developed in this final chapter is associated with considerable uncertainties emerging from uncertainties in paleomagnetic data, plate geometry, plate rotations and longitudinal plate motion rates, but it does comply with all currently available geological, paleomagnetic, tomographic and marine geophysical data of the Pacific and Mexico, Costa Rica, New Zealand and Japan.

Further development of the Panthalassa reconstruction depends on the development of kinematic reconstructions of the remaining segments of the Panthalassian trenches (particularly the North American Cordillera, far-eastern Russia, and Southeast Asia), and subsequently, on the incorporation of newly collected or published paleomagnetic data from OPS rocks from accretionary complexes along these trenches (e.g. Cretaceous limestones from the Franciscan complex (Tarduno et al., 1986)). Plate rotations (or a lack thereof) of the Izanagi, Farallon and Phoenix plates can be determined when paleomagnetic data are available from age-equivalent OPS rocks derived from accretionary

complexes far apart (e.g. for Farallon, from Mexico and from accretionary complexes of the Canadian Cordillera). Additionally, when paleomagnetic data become available from (sediments directly overlying) MORB basement, more and more ridge segments can be reconstructed, thereby gradually generating a picture of the geometry of the Panthalassa plates.

Finally, a way of falsifying the assumptions underlying our approach would have been to arrive at paleolatitude evolution from circum-Pacfific OPS materials that requires unrealistically high plate convergence rates. Instead, we show that paleomagnetic data require that the Panthalassa Ocean hosted at least three major tectonic plates since the Triassic, and that these moved at 'normal' plate tectonic rates, whereby the mismatch between predicted and measured paleomagnetic data, between reconstructed trenches and tomographically imaged slabs, and between LIPS and LLSVP edges, is not larger than 10-15°. This suggests that the developed approach is promising and may be used to improve reconstructions of the major oceans within and surrounding older supercontinents – although for pre-Phanerozoic oceans, dating OPS materials will add yet another challenge to overcome.

6. Conclusions
We presented a quantitative kinematic reconstruction of subducted plates of the Panthalassa Ocean, based on (1) relative plate motions derived from marine magnetic anomaly an fracture zone data; (2) absolute plate motions from hotspot tracks; and (3) paleomagnetic data from OPS materials of the circum-Pacific accretionary complexes and the Pacific Plate. We showed that determining relative plate motions between the Panthalassa and Indo-Atlantic plate system through the use of two independent mantle reference frames is in line with paleomagnetic data. Furthermore, in absence of absolute plate motion control, we reconstructed plate motions of the Izanagi, Farallon and Phoenix plates such that divergence between the three major oceanic plates is maintained, convergence with the continental margins of Japan, Mexico and New Zealand is maintained, and paleomagnetic constraints are met. The reconstruction approach developed in this chapter illustrates that in absence of marine magnetic anomaly data and mantle reference frames, deep-time plate circuits of supercontinents and superoceans may be reconstructed using OPS sequences, paleomagnetism, and constraints on the nature of circum-oceanic plate boundaries.

Supplementary materials
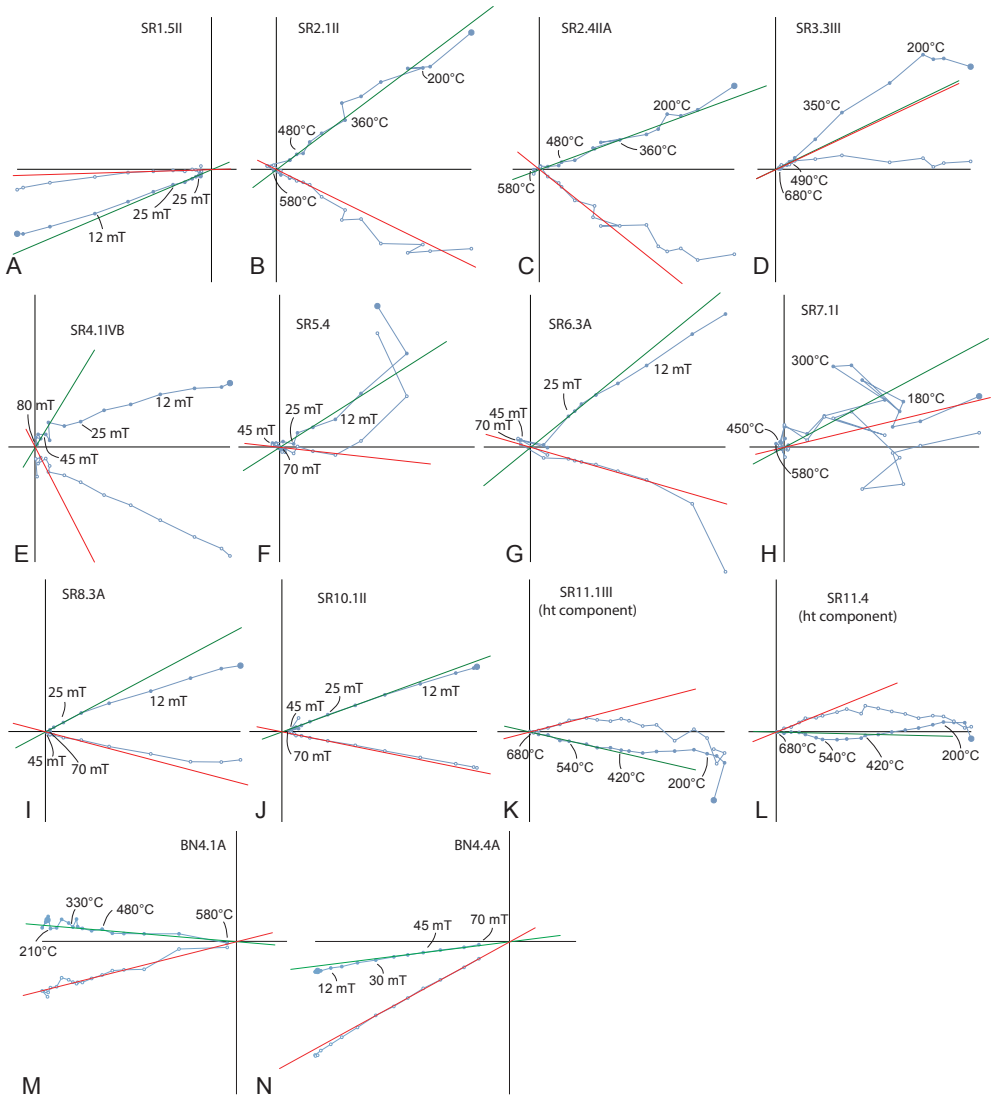
Figure S1: Orthogonal vector diagrams of representative samples of localities SR and BN (Costa Rica) in geographic coordinates (not corrected for bedding tilt), closed (open) symbol for declination (inclination), up/west projection.
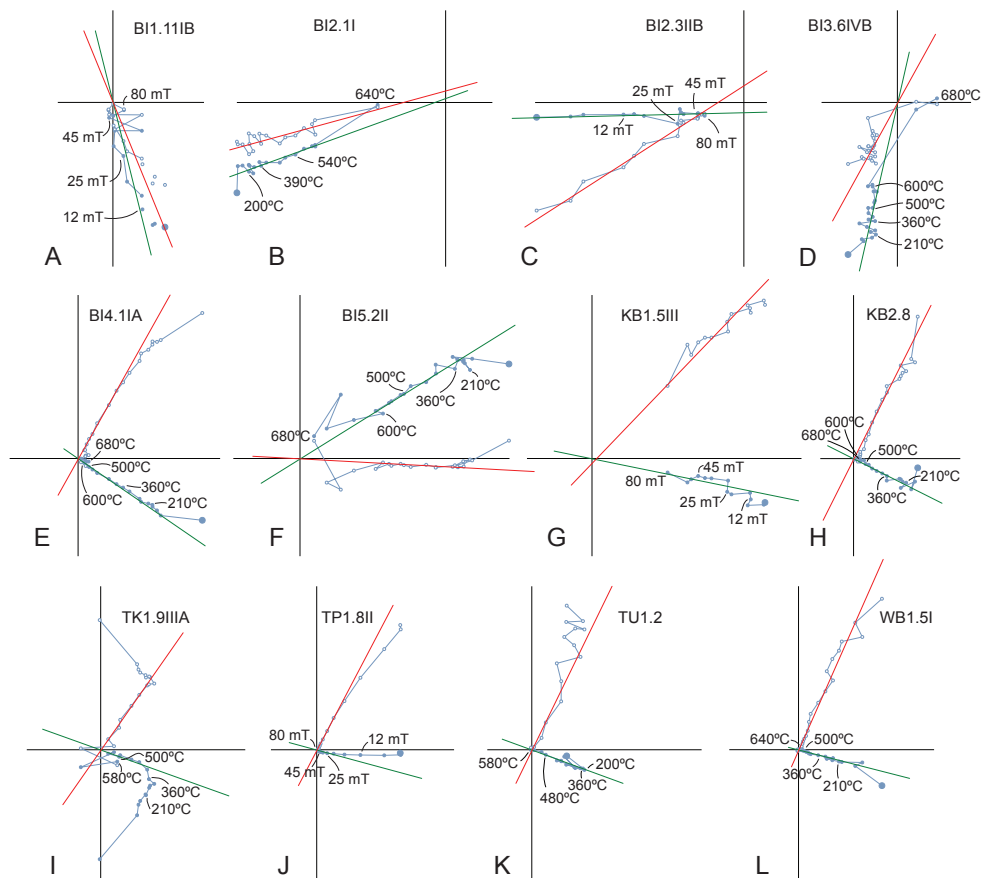
Figure S2: Orthogonal vector diagrams of representative from New Zealand in geographic coordinates (not corrected for bedding tilt), closed (open) symbol for declination (inclination), up/west projection.
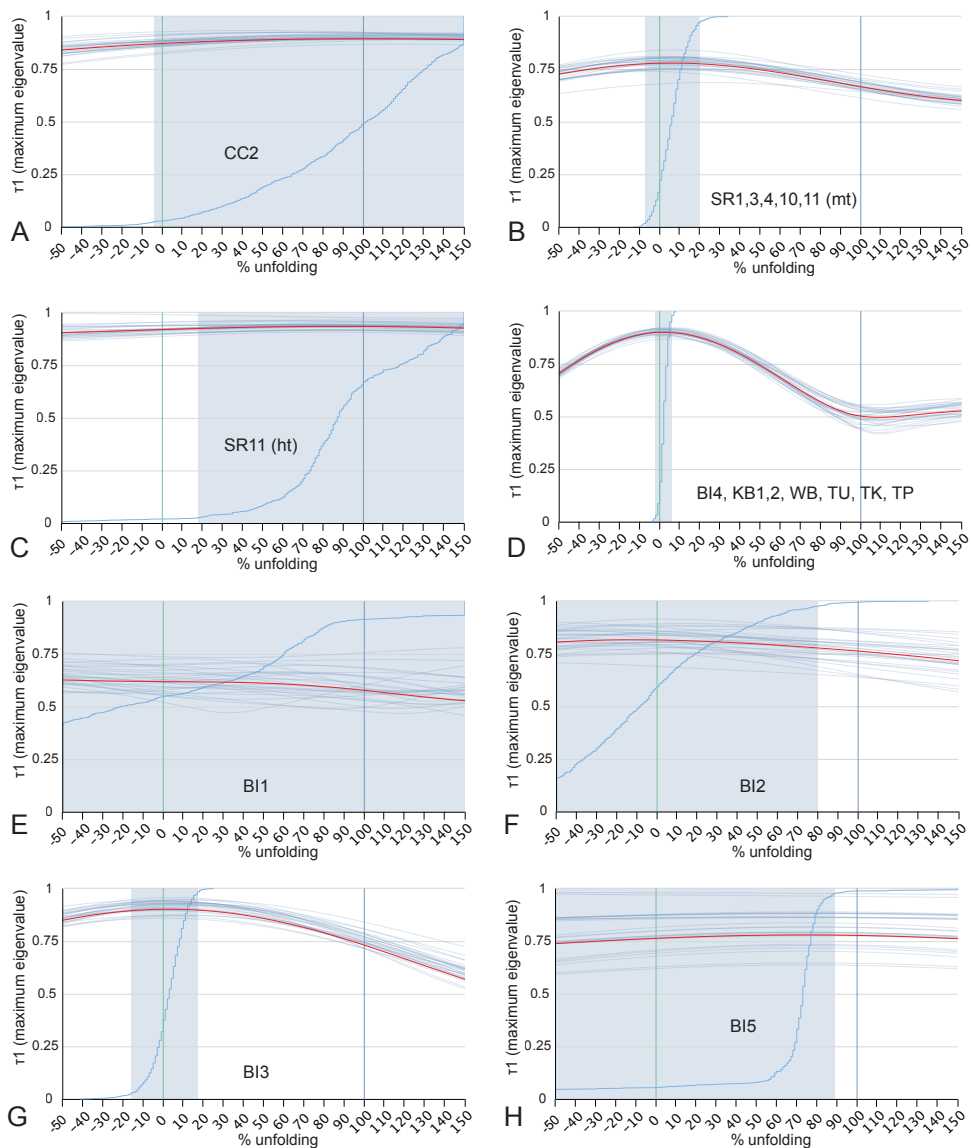
Figure S3: Bootstrapped fold tests on directions from sites from Cedros Island (CC2), Costa Rica (SR1,3,4,10,11 and SR11-ht), and New Zealand. Cumulative distribution function (with confidence interval in light blue) based on 1000 bootstraps (average of bootstraps in red).

CONCLUSIONS

View from the Punta Prieta Ridge - Cedros Island, Mexico

The aim of this thesis was to develop new, systematic reconstruction approaches for data-informed, quantitative plate kinematic reconstructions of former ocean basins whose lithosphere has (almost) entirely been lost to subduction. The main conclusions of this thesis, per chapter, are as follows:

(1) Applying basic plate tectonic theory and the set of rules, techniques and methods of analysis that come with it is as relevant today as it was 40 years ago, and enables the development of a kinematically feasible reconstruction of events that led to the birth of the Pacific Plate.

(2) Reconstructing complex plate boundary zone deformation following a reconstruction protocol and including quantitative geological data alone results in transparent, reproducible reconstructions that may be used as an independent platform in studies involving more qualitative datasets such as magmatic petrology or paleontology.

(3) Paleomagnetic data, particularly when combined with sediment provenance information are successful in discriminating between truly intra-oceanic and fringing arc systems.

(4) Integrating slab geometry with overriding plate deformation yields estimates of absolute plate motion of the overriding plate, downgoing plate, and trench, and improves reconstruction of long-lived dynamic continental margins subduction zones.

(5) In absence of a direct connection through passive margins, estimating a global plate circuit from independent mantle reference frames yields results within ~10° consistent with paleomagnetic data and LIP-LLSVP fits.

(6) The concept of Ocean Plate Stratigraphy (Isozaki et al., 1990) is invaluable in the reconstruction of lost oceanic plates and especially combined with marine magnetic anomaly, paleomagnetic, and tomographic data, allows detailed reconstruction of intra-oceanic subduction evolution.

(7) In absence of marine magnetic anomaly data and mantle reference frames, deep-time plate circuits of supercontinents and superoceans may be reconstructed using OPS sequences, paleomagnetism, and constraints on the nature of circum-oceanic plate boundaries.

References

Abbott, R. N., Bandy, B. R., Jackson, T. A., & Scott, P. W. (2003). Blueschist-Greenschist Transition in the Mt. Hibernia Schist, Union Hill, Parish of St. Thomas, Jamaica. International Geology Review, 45(1), 1-15.

Abbott, R. N., Jackson, T. A., & Mcsween Jr, H. Y. (1996). Metamorphic conditions in the Westphalia Schists of the Blue Mountain Inlier, Jamaica: tectonic implications. International Geology Review, 38(12), 1143-1154.

Abbott, R. N., Jackson, T. A., & Scott, P. W. (1999). The Serpentinization of Peridotite from Cedar Valley, Jamaica. International Geology Review, 41(9), 836-844.

Adams, C. J., Campbell, H. J., & Griffin, W. L. (2007). Provenance comparisons of Permian to Jurassic tectonostratigraphic terranes in New Zealand: perspectives from detrital zircon age patterns. Geological Magazine, 144(04).

Adams, C. J., Mortimer, N., Campbell, H. J., & Griffin, W. L. (2009). Age and isotopic characterisation of metasedimentary rocks from the Torlesse Supergroup and Waipapa Group in the central North Island, New Zealand. New Zealand Journal of Geology and Geophysics, 52(2), 149-170.

Adams, C. J., Mortimer, N., Campbell, H. J., & Griffin, W. L. (2012). Detrital zircon geochronology and sandstone provenance of basement Waipapa Terrane (Triassic–Cretaceous) and Cretaceous cover rocks (Northland Allochthon and Houhora Complex) in northern North Island, New Zealand. Geological Magazine, 150(01), 89-109.

Advokaat, E. L., Marshall, N. T., Li, S., Spakman, W., Krijgsman, W., & van Hinsbergen, D. J. (2018). Cenozoic rotation history of Borneo and Sundaland, SE Asia revealed by paleomagnetism, seismic tomography, and kinematic reconstruction. Tectonics, 37(8), 2486-2512.

Agard, P., Jolivet, L., Vrielynck, B., Burov, E., & Monie, P. (2007). Plate acceleration: the obduction trigger? Earth and Planetary Science Letters, 258(3-4), 428-441.

Aitchison, J., C., Hada, S., & Yoshikura, S. (1991). Kurosegawa terrane: disrupted remnants of a low latitude Paleozoic terrane accreted to SW Japan. Journal of Southeast Asian Earth Sciences, 6(2), 83-92.

Aitken, T., Mann, P., Escalona, A., & Christeson, G. L. (2011). Evolution of the Grenada and Tobago basins and implications for arc migration. Marine and Petroleum Geology, 28(1), 235-258.

Alsleben, H., Wetmore, P. H., Gehrels, G., & Paterson, S. (2012). Detrital zircon ages in Palaeozoic and Mesozoic basement assemblages of the Peninsular Ranges batholith, Baja California, Mexico: constraints for depositional ages and provenance. International Geology Review, 54(1), 93-110.

Alvarado, G. E., Denyer, P., & Sinton, C. W. (1997). The 89 Ma Tortugal komatiitic suite, Costa Rica: implications for a common geological origin of the Caribbean and Eastern Pacific region from a mantle plume. Geology, 25(5), 439-442.

Amaru, M. (2007). Global travel time tomography with 3-D reference models. PhD Thesis, Utrecht University, (274)

Anczkiewicz, R., Platt, J. P., Thirlwall, M. F., & Wakabayashi, J. (2004). Franciscan subduction off to a slow start: evidence from high-precision Lu–Hf garnet ages on high grade-blocks. Earth and Planetary Science Letters, 225(1-2), 147-161.

Andjić, G., Baumgartner, P. O., & Baumgartner-Mora, C. (2018). Rapid vertical motions and formation of volcanic arc gaps: Plateau collision recorded in the forearc geological evolution (Costa Rica margin). Basin Research.

Ando, A., Kodama, K., & Kojima, S. (2001). Low-latitude and Southern Hemisphere origin of Anisian (Triassic) bedded chert in the Inuyama area, Mino terrane, central Japan. Journal of Geophysical Research: Solid Earth, 106(B2), 1973-1986.

Ando, H. (2003). Stratigraphic correlation of Upper Cretaceous to Paleocene forearc basin sediments in Northeast Japan: cyclic sedimentation and basin evolution. Journal of Asian Earth Sciences, 21(8), 921-935.

Andó, J., Harangi, S., Szakmány, B., & Dosztály, L. (1996). Petrología de la asociación ofiolítica de Holguín. Ofiolitas y arcos volcánicos de Cuba. Miami, USA, IGCP Project, 364, 154-176.

Arden, D. D. (1975). Geology of Jamaica and the Nicaragua rise. In The Gulf of Mexico and the Caribbean (pp. 617-661): Springer.

Arita, K., Toyoshima, T., Owada, M., Miyashita, S., & Jolivet, L. (1986). Tectonic movement of the Hidaka metamorphic belt, Hokkaido, Japan. Geology and Tectonics of Hokkaido.

Asahina, T., & Komatsu, M. (1979). The Horokanai ophiolitic complex in the Kamuikotan tectonic belt, Hokkaido, Japan. Jour. Geol. Soc. Japan, 85, 317-330.

Astorga, A. (1997). El puente-istmo de América Central y la evolución de la Placa Caribe (con énfasis en el Mesozoico). Profil, 12, 1-201.

Atwater, T. (1970). Implications of plate tectonics for the Cenozoic tectonic evolution of western North America. Geological Society of America Bulletin, 81(12), 3513-3536.

Atwater, T. M. (1998). Plate tectonic history of southern California with emphasis on the western Transverse Ranges and northern Channel Islands.

Authemayou, C., Brocard, G., Teyssier, C., Simon-Labric, T., Guttiérrez, A., Chiquín, E. N., & Morán, S. (2011). The Caribbean-North America-Cocos Triple Junction and the dynamics of the Polochic-Motagua fault systems: Pull-up and zipper models. Tectonics, 30(3), n/a-n/a.

Azéma, J., Tournon, J., & Sornay, J. (1979). Presencia de amonites del Albiano Superior en las formaciones del Complejo de Nicoya. El yacimiento de Loma Chumico, provincia de Guanacaste, Costa Rica. Informe Semestral del Instituto Geográfico Nacional, 2, 71-76.

Bandini, A. N., Baumgartner, P. O., Flores, K., Dumitrica, P., Hochard, C., Stampfli, G. M., & Jackett, S.-J. (2011a). Aalenian to Cenomanian Radiolaria of the Bermeja Complex (Puerto Rico) and Pacific origin of radiolarites on the Caribbean Plate. Swiss Journal of Geosciences, 104(3), 367-408.

Bandini, A. N., Baumgartner, P. O., Flores, K., Dumitrica, P., & Jackett, S. J. (2011b). Early Jurassic to Early Late Cretaceous Radiolarians from the Santa Rosa Accretionary Complex (Northwestern Costa Rica). Ofioliti, 36(1), 1-35.

Bandini, A. N., Flores, K., Baumgartner, P. O., Jackett, S. J., & Denyer, P. (2008). Late Cretaceous and Paleogene Radiolaria from the Nicoya Peninsula, Costa Rica: a tectonostratigraphic application. Stratigraphy, 5(1), 3-21.

Banno, S., & Sakai, C. (1989). Geology and metamorphic evolution of the Sanbagawa metamorphic belt, Japan. Geological Society, London, Special Publications, 43(1), 519-532.

Barckhausen, U., Ranero, C. R., Cande, S. C., Engels, M., & Weinrebe, W. (2008). Birth of an intraoceanic spreading center. Geology, 36(10).

Barnes, D., A. (1984). Volcanic arc derived, Mesozoic sedimentary rocks, Vizcaino Peninsula, Baja California Sur, Mexico. In V. A. J. Frizzell (Ed.), Geology of the Baja California Peninsula (Vol. Pacific Section S.E.P.M. 39, pp. 119-130).

Barnes, D., & Mattison, J. (1981). Late Triassic/Early Cretaceous age of eugeosynclinal terranes, Western Vizcaíno Peninsula, Baja California Sur, México. Geol. Soc. Amer., Abstr. with Progr. Cord. Section, 13.

Barnes, D. A. (1982). Basin analysis of volcanic arc-derived, Jura-Cretaceous sedimentary rocks, VizcaÌno peninsula, Baja California Sur, Mexico. PhD Thesis, University of California, Santa Barbara,

Barth, A. P., Tosdal, R., Wooden, J., & Howard, K. (1997). Triassic plutonism in southern California: Southward younging of arc initiation along a truncated continental margin. Tectonics, 16(2), 290-304.

Baumgartner, P. O., & Denyer, P. (2006). Evidence for middle Cretaceous accretion at Santa Elena Peninsula (Santa Rosa Accretionary Complex), Costa Rica. Geologica Acta, 4(1-2), 179-191.

Baumgartner, P. O., Flores, K., Bandini, A. N., Girault, F., & Cruz, D. (2008). Upper Triassic to Cretaceous radiolaria from Nicaragua and Northern Costa Rica - The Mesquito Composite Oceanic Terrane. Ofioliti, 33(1), 1-19.

Baumgartner, P. O., O'Dogherty, L., Goričan, Š., Urquhart, E., Pillevuit, A., & De Wever, P. (1995). Middle Jurassic to Lower Cretaceous radiolaria of Tethys: occurrences, systematics, biochronology. International Association of Radiolarian Paleontologists, INTERRAD Jurassic-Cretaceous Working Group, 37-685.

Baumgartner-Mora, C., & Denyer, P. (2002). Campanian-Maastrichtian limestone with larger foraminifera from Peña Bruja Rock (Santa Elena Península). Revista Geológica de América Central, 26, 85-89.

Bayona, G., Cardona, A., Jaramillo, C., Mora, A., Montes, C., Valencia, V., et al. (2012). Early Paleogene magmatism in the northern Andes: Insights on the effects of Oceanic Plateau–continent convergence. Earth and Planetary Science Letters, 331, 97-111.

Beccaluva, L. (1995). The northwestern border of the Caribbean plate in Guatemala: new geological and petrological data on the Motagua ophiolitic belt. Ofioliti, 20, 1-15.

Beebe, W., & Luyendyk, B. (1983). Preliminary paleomagnetic results from the Llanada remnant of the Coast Range ophiolite. San Benito County, California: Eos (Transactions, American Geophysical Union), 64, 686.

Benthem, S., Govers, R., & Wortel, R. (2014). What drives microplate motion and deformation in the northeastern Caribbean plate boundary region? Tectonics, 33(5), 850-873.

Besse, J., & Courtillot, V. (2002). Apparent and true polar wander and the geometry of the geomagnetic field over the last 200 Myr. Journal of Geophysical Research: Solid Earth, 107(B11).

Biggin, A. J., van Hinsbergen, D. J. J., Langereis, C. G., Straathof, G. B., & Deenen, M. H. L. (2008). Geomagnetic secular variation in the Cretaceous Normal Superchron and in the Jurassic. Physics of the Earth and Planetary Interiors, 169(1-4), 3-19.

Bijwaard, H., Spakman, W., & Engdahl, E. R. (1998). Closing the gap between regional and global travel time tomography. Journal of Geophysical Research: Solid Earth, 103(B12), 30055-30078.

Bird, D. E., Hall, S. A., Casey, J. F., & Millegan, P. S. (1993). Interpretation of magnetic anomalies over the Grenada Basin. Tectonics, 12(5), 1267-1279.

Bird, D. E., Hall, S. A., Casey, J. F., & Millegan, P. S. (1999). Tectonic evolution of the Grenada Basin. In Sedimentary Basins of the World (Vol. 4, pp. 389-416): Elsevier.

Bird, P. (1988). Formation of the Rocky Mountains, western United States: A continuum computer model. Science, 239(4847), 1501-1507.

Bissig, T., Mortensen, J. K., & Hall, B. V. (2003). The volcano-sedimentary setting of the Kuroko type VHMS district of Cuale, Jalisco, Mexico. Geological Society of America Abstracts with Programs, 35(4), 61.

Blanco-Quintero, I. F., García-Casco, A., Rojas-Agramonte, Y., Rodríguez-Vega, A., Lázaro, C., & Iturralde-Vinent, M. A. (2010). Metamorphic evolution of subducted hot oceanic crust (La Corea Melange, Cuba). American Journal of Science, 310(9), 889-915.

Boekhout, F., Spikings, R., Sempere, T., Chiaradia, M., Ulianov, A., & Schaltegger, U. (2012). Mesozoic arc magmatism along the southern Peruvian margin during Gondwana breakup and dispersal. Lithos, 146, 48-64.

Boiteau, A., Michard, A., & Saliot, P. (1972). Métamorphisme de haute pression dans le complexe ophiolitique du Purial (Oriente, Cuba). Comptes Rendus de l'Académie des Sciences Paris, 274, 2137-2140.

Boles, J. R., & Landis, C. A. (1984). Jurassic sedimentary mélange and associated facies, Baja California, Mexico. Geological Society of America Bulletin, 95(5).

Borrero, C., Pardo, A., Jaramillo, C. M., Osorio, J. A., Cardona, A., Flores, A., et al. (2012). Tectonostratigraphy of the Cenozoic Tumaco forearc basin (Colombian Pacific) and its relationship with the northern Andes orogenic build up. Journal of South American Earth Sciences, 39, 75-92.

Boschman, L. M., Garza, R. S. M., Langereis, C. G., & van Hinsbergen, D. J. (2018). Paleomagnetic constraints on the kinematic relationship between the Guerrero terrane (Mexico) and North America since Early Cretaceous time. Geological Society of America Bulletin, 130(7-8), 1131-1142.

Boschman, L. M., & van Hinsbergen, D. J. J. (2016). On the enigmatic birth of the Pacific Plate within the Panthalassa Ocean. Science Advances, 2(7).

Boschman, L. M., van Hinsbergen, D. J. J., Torsvik, T. H., Spakman, W., & Pindell, J. L. (2014). Kinematic reconstruction of the Caribbean region since the Early Jurassic. Earth-Science Reviews, 138, 102-136.

Bouysse, P. (1988). Opening of the Grenada Back-Arc Basin and Evolution of the Caribbean Plate during the Mesozoic and Early Paleogene. Tectonophysics, 149(1-2), 121-143.

Bowland, C. L. (1993). Depositional history of the western Colombian Basin, Caribbean Sea, revealed by seismic stratigraphy. Geological Society of America Bulletin, 105(10), 1321-1345.

Boyden, J., Müller, R. D., Gurnis, M., Torsvik, T., Clark, J. A., Turner, M., et al. (2011). Next-generation plate-tectonic reconstructions using GPlates. In Geoinformatics: Cyberinfrastructure for the Solid Earth Sciences (pp. 95-114). Cambridge Cambridge University Press.

Bralower, T. J., & Iturralde-Vinent, M. A. (1997). Micropaleontological dating of the collision between the North American Plate and the Greater Antilles Arc in western Cuba. Palaios, 133-150.

Briden, J., Rex, D., Faller, A., & Tomblin, J. (1979). K-Ar geochronology and palaeomagnetism of volcanic rocks in the Lesser Antilles island arc. Philosophical Transactions of the Royal Society of London A, 291(1383), 485-528.

Brueckner, H. K., Avé Lallemant, H. G., Sisson, V. B., Harlow, G. E., Hemming, S. R., Martens, U., et al. (2009). Metamorphic reworking of a high pressure–low temperature mélange along the Motagua

fault, Guatemala: A record of Neocomian and Maastrichtian transpressional tectonics. Earth and Planetary Science Letters, 284(1-2), 228-235.

Buchs, D. M., Arculus, R. J., Baumgartner, P. O., Baumgartner-Mora, C., & Ulianov, A. (2010). Late Cretaceous arc development on the SW margin of the Caribbean Plate: Insights from the Golfito, Costa Rica, and Azuero, Panama, complexes. Geochemistry, Geophysics, Geosystems, 11(7), Q07S24.

Buchs, D. M., Pilet, S., Cosca, M., Flores, K. E., Bandini, A. N., & Baumgartner, P. O. (2013). Low-volume intraplate volcanism in the Early/Middle Jurassic Pacific basin documented by accreted sequences in Costa Rica. Geochemistry, Geophysics, Geosystems, 14(5), 1552-1568.

Burkart, B. (1983). Neogene North-American Caribbean Plate Boundary across Northern Central-America - Offset Along the Polochic Fault. Tectonophysics, 99(2-4), 251-270.

Burkart, B. (1994). Northern Central America. In S. Donovan & T. Jackson (Eds.), Caribbean Geology: An Introduction (pp. 265-284). Jamaica: University of the West Indies Publisher's Association.

Burke, K. (1988). Tectonic evolution of the Caribbean. Annual Review of Earth and Planetary Sciences, 16(1), 201-230.

Burke, K., Fox, P. J., & Şengör, A. M. C. (1978). Buoyant ocean floor and the evolution of the Caribbean. Journal of Geophysical Research, 83(B8).

Burmester, R. F., Beck, M. E., Speed, R. C., & Snoke, A. W. (1996). A preliminary paleomagnetic pole for mid-Cretaceous rocks from Tobago: Further evidence for large clockwise rotations in the Caribbean South American plate boundary zone. Earth and Planetary Science Letters, 139(1-2), 79-90.

Busby, C. J. (2004). Continental growth at convergent margins facing large ocean basins: a case study from Mesozoic convergent-margin basins of Baja California, Mexico. Tectonophysics, 392(1-4), 241-277.

Busby, C. J., Adams, B. F., Mattinson, J., & Deoreo, S. (2006). View of an intact oceanic arc, from surficial to mesozonal levels: Cretaceous Alisitos arc, Baja California. Journal of Volcanology and Geothermal Research, 149(1), 1-46.

Busby, C. J., Smith, D., Morris, W., & Fackler-Adams, B. (1998). Evolutionary model for convergent margins facing large ocean basins: Mesozoic Baja California, Mexico. Geology, 26(3), 227-230.

Busby-Spera, C. J. (1988). Evolution of a Middle Jurassic Back-Arc Basin, Cedros Island, Baja California - Evidence from a Marine Volcaniclastic Apron. Geological Society of America Bulletin, 100(2), 218-233.

Busby-Spera, C. J., & Boles, J. R. (1986). Evolution of subsidence styles in forearc basin: example from Cretaceous of southern Vizcaino Peninsula, Baja California, Mexico. American Association of Petroleum Geologists Bulletin, 70(8604187).

Bush, V., & Shcherbakova, I. (1986). New data on the deep tectonics of Cuba. Geotectonics, 20(3), 192-203.

Bustamante, A., Juliani, C., Hall, C., & Essene, E. (2011). 40Ar/39Ar ages from blueschists of the Jambaló region, Central Cordillera of Colombia: implications on the styles of accretion in the Northern Andes. Geologica Acta, 9(3).

Butler, R. F. (1992). Paleomagnetism: magnetic domains to geologic terranes (Vol. 319): Blackwell Scientific Publications Boston.

Butterworth, N., Talsma, A., Müller, R., Seton, M., Bunge, H.-P., Schuberth, B., et al. (2014). Geological, tomographic, kinematic and geodynamic constraints on the dynamics of sinking slabs. Journal of Geodynamics, 73, 1-13.

Byrne, D., Suarez, G., & McCann, W. (1985). Muertos Trough subduction—Microplate tectonics in the northern Caribbean? Nature, 317(6036), 420.

Cabral-Cano, E., Lang, H. R., & Harrison, C. G. A. (2000). Stratigraphic assessment of the Arcelia-Teloloapan area, southern Mexico: implications for southern Mexico's post-Neocomian tectonic evolution. Journal of South American Earth Sciences, 13(4-5), 443-457.

Calais, E., Béthoux, N., & Lépinay, B. M. (1992). From transcurrent faulting to frontal subduction: A seismotectonic study of the northern Caribbean plate boundary from Cuba to Puerto Rico. Tectonics, 11(1), 114-123.

Calais, E., & De Lépinay, B. M. (1995). Strike-slip tectonic processes in the northern Caribbean between Cuba and Hispaniola (Windward Passage). Marine Geophysical Researches, 17(1), 63-95.

Campa, M. F., & Coney, P. J. (1983). Tectono-stratigraphic terranes and mineral resource distributions in Mexico. Canadian Journal of Earth Sciences, 20(6), 1040-1051.

Cardona, A., Montes, C., Ayala, C., Bustamante, C., Hoyos, N., Montenegro, O., et al. (2012). From arc-continent collision to continuous convergence, clues from Paleogene conglomerates along the southern Caribbean–South America plate boundary. Tectonophysics, 580, 58-87.

Cardona, A., Valencia, V., Bayona, G., Duque, J., Ducea, M., Gehrels, G., et al. (2011). Early-subduction-related orogeny in the northern Andes: Turonian to Eocene magmatic and provenance record in the Santa Marta Massif and Rancheria Basin, northern Colombia. Terra Nova, 23(1), 26-34.

Carr, M. J., Feigenson, M. D., Patino, L. C., & Walker, J. A. (2004). Volcanism and Geochemistry in Central America: Progress and Problems. In J. Eiler (Ed.), Inside the Subduction Factory. Washington, D. C: American Geophysical Union.

Case, J. E., MacDonald, W. D., & Fox, P. J. (1990). Caribbean crustal provinces; seismic and gravity evidence. In C. A. Dengo & J. Case (Eds.), The Geology of North America, Vo.l H, The Caribbean Region (A decade of North American Geology). (pp. 15-36). Boulder, Colorado: Geological Society of America.

CAYTROUGH. (1979). Geological and geophysical investigations of the Mid-Cayman Rise spreading centre: initial results and observations. In M. Talwani (Ed.), Deep Drilling Results in the Atlantic Ocean: Oceanic Crust, Maurice Ewing Series (Vol. 2, AGU, pp. 66-93). Washington.

Centeno-García, E. (2005). Review of Upper Paleozoic and Lower Mesozoic stratigraphy and depositional environments of central and west Mexico: Constraints on terrane analysis and paleogeography. Geological Society of America Special Papers, 393, 233-258.

Centeno-García, E. (2017). Mesozoic tectono-magmatic evolution of Mexico: An overview. Ore Geology Reviews, 81, 1035-1052.

Centeno-García, E., Busby, C., Busby, M., & Gehrels, G. (2011). Evolution of the Guerrero composite terrane along the Mexican margin, from extensional fringing arc to contractional continental arc. Geological Society of America Bulletin, 123(9-10), 1776-1797.

Centeno-García, E., Corona-Chávez, P., Talavera-Mendoza, O., & Iriondo, A. (2003). Geologic and tectonic evolution of the western Guerrero terrane—A transect from Puerto Vallarta to Zihuatanejo, Mexico. Paper presented at the Geologic transects across Cordilleran Mexico, guidebook for the field

trips of the 99th Geological Society of America Cordilleran section annual meeting, Puerto Vallarta, Jalisco, Mexico.

Centeno-García, E., Guerrero-Suastegui, M., & Talavera-Mendoza, O. (2008). The Guerrero Composite Terrane of western Mexico: Collision and subsequent rifting in a supra-subduction zone. In Special Paper 436: Formation and Applications of the Sedimentary Record in Arc Collision Zones (pp. 279-308).

Centeno-García, E., Ruíz, J., Coney, P. J., Patchett, P. J., & Ortega-Gutiérrez, F. (1993). Guerrero terrane of Mexico: Its role in the Southern, Cordillera from new geochemical data. Geology, 21(5), 419-422.

Centeno-García, E., & Silva-Romo, G. (1997). Petrogenesis and tectonic evolution of central Mexico during Triassic-Jurassic time. Revista Mexicana de Ciencias Geológicas, 14(2), 244-260.

Chen, C., Zhao, D., Tian, Y., Wu, S., Hasegawa, A., Lei, J., et al. (2017). Mantle transition zone, stagnant slab and intraplate volcanism in Northeast Asia. Geophysical Journal International, 209(1), 68-85.

Chiodi, M., Monod, O., Busnardo, R., Gaspard, D., Sánchez, A., & Yta, M. (1988). Une discordance ante albienne datée par une fauned'Ammonites et de Brachiopodes de type téthysien au Mexique central. Geobios, 21(2), 125-135.

Christeson, G. L., Mann, P., Escalona, A., & Aitken, T. J. (2008). Crustal structure of the Caribbean–northeastern South America arc-continent collision zone. Journal of Geophysical Research, 113(B8).

Coates, A. G., Collins, L. S., Aubry, M. P., & Berggren, W. A. (2004). The Geology of the Darien, Panama, and the late Miocene-Pliocene collision of the Panama arc with northwestern South America. Geological Society of America Bulletin, 116(11-12), 1327-1344.

Collombat, H., Rochette, P., & Kent, D. V. (1993). Detection and correction of inclination shallowing in deep-sea sediments using the anisotropy of anhysteretic remanence. Bulletin de la Société Géologique de France, 164(1), 103-111.

Coney, P. J., & Reynolds, S. J. (1977). Cordilleran benioff zones. Nature, 270(5636), 403.

Conrad, C. P., Steinberger, B., & Torsvik, T. H. (2013). Stability of active mantle upwelling revealed by net characteristics of plate tectonics. Nature, 498(7455), 479-482.

Cortés, M., & Angelier, J. (2005). Current states of stress in the northern Andes as indicated by focal mechanisms of earthquakes. Tectonophysics, 403(1-4), 29-58.

Cox, A., & Hart, R. B. (1986). Plate Tectonics - How it works. Palo Alto, CA: Blackwell Scientific Publications.

Cribb, J., Jimenez, J., Lewis, J., & Sutter, J. (1989). 40Ar/39Ar ages from Loma de Cabrera batholith: implications for timing of tectonic events in northern Hispaniola. Paper presented at the Geological Society of American Abstracts with Programs.

Critelli, S., Marsaglia, K. M., & Busby, C. J. (2002). Tectonic history of a Jurassic backarc-basin sequence (the Gran Cañon Formation, Cedros Island, Mexico), based on compositional modes of tuffaceous deposits. Geological Society of America Bulletin, 114(5), 515-527.

Cruz-Orosa, I., Sàbat, F., Ramos, E., Rivero, L., & Vázquez-Taset, Y. M. (2012a). Structural evolution of the La Trocha fault zone: Oblique collision and strike-slip basins in the Cuban Orogen. Tectonics, 31(5).

Cruz-Orosa, I., Sàbat, F., Ramos, E., & Vázquez-Taset, Y. M. (2012b). Synorogenic basins of central Cuba and collision between the Caribbean and North American plates. International Geology Review, 54(8), 876-906.

Cuevas-Pérez, E. (1983). The geological evolution of the Mesozoic in the State of Zacatecas Mexico. Zentralblatt für Geologie und Palaeontologie, Teil I: Allgemeine, Angewandte: Regionale und Historische Geologie(1), 190-201.

De Wever, P. (1985). Découverte de materiel océanique du Lias-Dogger inférieur dans la peninsula de Santa Elena (Costa Rica, Amerique Centrale). Comptes Rendus de l'Academie des Sciences de Paris Serie II, 15, 759-764.

de Zoeten, R., & Mann, P. (1991). Structural geology and Cenozoic tectonic history of the central Cordillera Septentrional, Dominican Republic. In Geologic and tectonic development of the North America-Caribbean plate boundary in Hispaniola (Vol. 262, pp. 265-279): Geological Society of America.

Debiche, M. G., Cox, A., & Engebretson, D. C. (1987). The motion of allochthonous terranes across the North Pacific basin (Vol. 207): Geological Society of America.

DeCelles, P. G., Ducea, M. N., Kapp, P., & Zandt, G. (2009). Cyclicity in Cordilleran orogenic systems. Nature Geoscience, 2(4), 251-257.

Deenen, M. H. L., Langereis, C. G., van Hinsbergen, D. J., & Biggin, A. J. (2014). Erratum: Geomagnetic secular variation and the statistics of palaeomagnetic directions. Geophysical Journal International, 197(1), 643-643.

Deenen, M. H. L., Langereis, C. G., van Hinsbergen, D. J. J., & Biggin, A. J. (2011). Geomagnetic secular variation and the statistics of palaeomagnetic directions. Geophysical Journal International, 186(2), 509-520.

DeMets, C. (2001). A new estimate for present-day Cocos-Caribbean plate motion: Implications for slip along the Central American volcanic arc. Geophysical Research Letters.

DeMets, C., Mattioli, G., Jansma, P., Rogers, R. D., Tenorio, C., & Turner, H. L. (2007). Present motion and deformation of the Caribbean plate: Constraints from new GPS geodetic measurements from Honduras and Nicaragua. In Special Paper 428: Geologic and Tectonic Development of the Caribbean Plate Boundary in Northern Central America (pp. 21-36).

DeMets, C., & Wiggins-Grandison, M. (2007). Deformation of Jamaica and motion of the Gonâve microplate from GPS and seismic data. Geophysical Journal International, 168(1), 362-378.

Dengo, G. (1962). Estudio geológico de la región de Guanacaste, Costa Rica: Instituto Geográfico de Costa Rica.

Dengo, G. (1969). Problems of tectonic relations between Central America and the Caribbean. Gulf Coast Association of Geological Societies Transactions, 19, 311-320.

Dengo, G. (1985). Mid America: Tectonic setting for the Pacific margin from southern México to northwestern Colombia. In The ocean basins and margins (pp. 123-180): Springer.

Denyer, P., Aguilar, T., & Montero, W. (2014). Cartografía geológica de la península de Nicoya, Costa Rica: estratigrafía y tectónica: Editorial UCR.

Denyer, P., & Baumgartner, P. O. (2006). Emplacement of Jurassic-Lower Cretaceous radiolarites of the Nicoya Complex (Costa Rica). Geologica Acta, 4(1-2), 203-218.

Denyer, P., Baumgartner, P. O., & Gazel, E. (2006). Characterization and tectonic implications of Mesozoic-Cenozoic oceanic assemblages of Costa Rica and Western Panama. Geologica Acta, 4(1-2), 219-235.

Denyer, P., & Gazel, E. (2009). The Costa Rican Jurassic to Miocene oceanic complexes: Origin, tectonics and relations. Journal of South American Earth Sciences, 28(4), 429-442.

DePaolo, D. J. (1981). A neodymium and strontium isotopic study of the Mesozoic calc-alkaline granitic batholiths of the Sierra Nevada and Peninsular Ranges, California. Journal of Geophysical Research: Solid Earth, 86(B11), 10470-10488.

Dercourt, J., et al., Zonenshain, L., Ricou, L.-E., Kazmin, V., Le Pichon, X., et al. (1986). Geological evolution of the Tethys belt from the Atlantic to the Pamirs since the Lias. Tectonophysics, 123(1-4), 241-315.

Dewey, J., Helman, M., Knott, S., Turco, E., & Hutton, D. (1989). Kinematics of the western Mediterranean. Geological Society, London, Special Publications, 45(1), 265-283.

Díaz, C., Furrazola Bermúdez, G., & Iturralde-Vinent, M. (1997). Estratigrafía de la zona de Remedios. Estudios sobre Geología de Cuba: La Habana, Cuba, Centro Nacional de Información Geológica, 221-242.

Dickinson, W. R., & Coney, P. J. (1980). Plate tectonic constraints on the origin of the Gulf of Mexico. Paper presented at the The origin of the Gulf of Mexico and the early opening of the central North Atlantic Ocean. Department of Geology, Louisiana State University and Louisiana Geological Survey, Proceedings of Symposium.

Dickinson, W. R., & Gehrels, G. E. (2009). Use of U–Pb ages of detrital zircons to infer maximum depositional ages of strata: A test against a Colorado Plateau Mesozoic database. Earth and Planetary Science Letters, 288(1-2), 115-125.

Dickinson, W. R., & Lawton, T. F. (2001). Carboniferous to Cretaceous assembly and fragmentation of Mexico. Geological Society of America Bulletin, 113(9), 1142-1160.

Dickinson, W. R., Snyder, W. S., & Matthews, V. (1978). Plate tectonics of the Laramide orogeny (Vol. 3): Matthews.

Dilek, Y., & Furnes, H. (2011). Ophiolite genesis and global tectonics: Geochemical and tectonic fingerprinting of ancient oceanic lithosphere. Geological Society of America Bulletin, 123(3-4), 387-411.

Dillon, W. P., Edgar, N. T., Scanlon, K. M., & Coleman, D. F. (1996). A review of the tectonic problems of the strike-slip northern boundary of the Caribbean plate and examination by GLORIA. Geology of the United States' Seafloor: The View From GLORIA, 135-164.

Dolan, J., Mann, P., de Zoeten, R., Heubeck, C., Shiroma, J., & Monechi, S. (1991). Sedimentologic, stratigraphic, and tectonic synthesis of Eocene-Miocene sedimentary basins, Hispaniola and Puerto Rico. In Geologic and tectonic development of the North America-Caribbean plate boundary in Hispaniola (pp. 217-264).

Dolan, J. F., Mullins, H. T., Wald, D. J., & Mann, P. (1998). Active tectonics of the north-central Caribbean: Oblique collision, strain partitioning, and opposing subducted slabs. Geological Society of America Special Papers, 1-62.

Domeier, M., Doubrovine, P. V., Torsvik, T. H., Spakman, W., & Bull, A. L. (2016). Global correlation of lower mantle structure and past subduction. Geophysical Research Letters, 43(10), 4945-4953.

Domeier, M., Shephard, G. E., Jakob, J., Gaina, C., Doubrovine, P. V., & Torsvik, T. H. (2017). Intraoceanic subduction spanned the Pacific in the Late Cretaceous–Paleocene. Science Advances, 3(11).

Domeier, M., & Torsvik, T. H. (2014). Plate tectonics in the late Paleozoic. Geoscience Frontiers, 5(3), 303-350.

Donnelly, T. W., Horne, G. S., Finch, R. C., & López-Ramos, E. (1990). Northern Central America; the Maya and chortis blocks. The Geology of North America, 11, 37-76.

Donnelly, T. W., Melson, W., Kay, R., & Rogers, J. W. (1973). Basalts and dolerites of Late Cretaceous age from the Central Caribbean. In Initial Reports of the Deep Sea Drilling Project. (pp. 1137). Washington, DC: US Government Printing Office.

Donovan, S. (1994). Trinidad. In Caribbean Geology: An Introduction (pp. 209-228). Kingston, Jamaica: University of theWest Indies Publishers' Association.

Doubrovine, P. V., Steinberger, B., & Torsvik, T. H. (2012). Absolute plate motions in a reference frame defined by moving hot spots in the Pacific, Atlantic, and Indian oceans. Journal of Geophysical Research: Solid Earth, 117(B9).

Doubrovine, P. V., & Tarduno, J. A. (2008). A revised kinematic model for the relative motion between Pacific oceanic plates and North America since the Late Cretaceous. Journal of Geophysical Research, 113(B12).

Draper, G., & Barros, J. (1994). Cuba. In S. K. Donovan & T. A. Jackson (Eds.), Caribbean Geology: An Introduction (pp. 65-86). Kingston, Jamaica: University of the West Indies Publishers' Association.

Draper, G., & Lewis, J. (1991). Geologic map of the central Dominican Republic (1: 150,000). Geological and Tectonic Development of the North American-Caribbean Plate Boundary in Hispaniola. Geological Society America Special Paper, 262.

Draper, G., & Nagle, F. (1991). Geology, structure, and tectonic development of the Rio San Juan Complex, northern Dominican Republic. Geologic and tectonic development of the North America-Caribbean plate boundary in Hispaniola. Geological Society of America Special Paper, 262, 77-95.

Ducloz, C., & Vuagnat, M. (1962). A propos de l'age des serpentinites de Cuba. In Archives des Sciences. 15. Socièté de Physique et d'Histoire Naturelle, Geneve, pp. 309–332.

Duncan, R. (1984). Plate-tectonic evolution of the Caribbean region in the mantle reference frame. The Caribbean-South American plate boundary and regional tectonics.

Duque-Caro, H. (1990). The Choco Block in the northwestern corner of South America: structural, tectonostratigraphic, and paleogeographic implications. Journal of South American Earth Sciences, 3(1), 71-84.

Duretz, T., Agard, P., Yamato, P., Ducassou, C., Burov, E. B., & Gerya, T. V. (2016). Thermo-mechanical modeling of the obduction process based on the Oman ophiolite case. Gondwana Research, 32, 1-10.

Egbue, O., & Kellogg, J. (2010). Pleistocene to Present North Andean "escape". Tectonophysics, 489(1-4), 248-257.

Elders, W. A., Rex, R. W., Robinson, P. T., Biehler, S., & Meidav, T. (1972). Crustal Spreading in Southern California: The Imperial Valley and the Gulf of California formed by the rifting apart of a continental plate. Science, 178(4056), 15-24.

Elias-Herrera, M., Sanchez-Zavala, J. L., & Macias-Romo, C. (2000). Geologic and geochronologic data from the Guerrero terrane in the Tejupilco area, southern Mexico: new constraints on its tectonic interpretation. Journal of South American Earth Sciences, 13(4-5), 355-375.

Endo, R., & Hashimoto, W. (1955). Unquestionably Paleozoic (Permian) fossils found in Hokkaido, Japan. Proceedings of the Japan Academy, 31(10), 704-708.

Engebretson, D. C., Cox, A., & Gordon, R. G. (1985). Relative Motions Between Oceanic and Continental Plates in the Pacific Basin. Geological Society of America Special Papers, 206.

Enkin, R. J. (2006). Paleomagnetism and the case for Baja British Columbia. Paleogeography of the North American Cordillera: evidence for and against large-scale displacements. Edited by JW Haggart, RJ Enkin, and JWH Monger. Geological Association of Canada, Special Paper, 46, 233-253.

Escalona, A., & Mann, P. (2011). Tectonics, basin subsidence mechanisms, and paleogeography of the Caribbean-South American plate boundary zone. Marine and Petroleum Geology, 28(1), 8-39.

Escuder Viruete, J., Díaz de Neira, A., Hernáiz Huerta, P. P., Monthel, J., Senz, J. G., Joubert, M., et al. (2006). Magmatic relationships and ages of Caribbean Island arc tholeiites, boninites and related felsic rocks, Dominican Republic. Lithos, 90(3-4), 161-186.

Escuder-Viruete, J., & Baumgartner, P. O. (2014). Structural evolution and deformation kinematics of a subduction-related serpentinite-matrix mélange, Santa Elena peninsula, northwest Costa Rica. Journal of Structural Geology, 66, 356-381.

Escuder-Viruete, J., Baumgartner, P. O., & Castillo-Carrión, M. (2015). Compositional diversity in peridotites as result of a multi-process history: The Pacific-derived Santa Elena ophiolite, northwest Costa Rica. Lithos, 231, 16-34.

Escuder-Viruete, J., Friedman, R., Castillo-Carrión, M., Jabites, J., & Pérez-Estaún, A. (2011a). Origin and significance of the ophiolitic high-P mélanges in the northern Caribbean convergent margin: Insights from the geochemistry and large-scale structure of the Río San Juan metamorphic complex. Lithos, 127(3-4), 483-504.

Escuder-Viruete, J., Pérez-Estaún, A., Booth-Rea, G., & Valverde-Vaquero, P. (2011b). Tectonometamorphic evolution of the Samaná complex, northern Hispaniola: implications for the burial and exhumation of high-pressure rocks in a collisional accretionary wedge. Lithos, 125(1-2), 190-210.

Escuder-Viruete, J., Pérez-Estaún, A., Gabites, J., & Suárez-Rodríguez, Á. (2011c). Structural development of a high-pressure collisional accretionary wedge: the Samaná complex, northern Hispaniola. Journal of Structural Geology, 33(5), 928-950.

Escuder-Viruete, J., Valverde-Vaquero, P., Rojas-Agramonte, Y., Jabites, J., & Pérez-Estaún, A. (2013). From intra-oceanic subduction to arc accretion and arc-continent collision: Insights from the structural evolution of the Río San Juan metamorphic complex, northern Hispaniola. Journal of Structural Geology, 46, 34-56.

Faccenna, C., Funiciello, F., Giardini, D., & Lucente, P. (2001). Episodic back-arc extension during restricted mantle convection in the Central Mediterranean. Earth and Planetary Science Letters, 187(1-2), 105-116.

Faccenna, C., Piromallo, C., Crespo-Blanc, A., Jolivet, L., & Rossetti, F. (2004). Lateral slab deformation and the origin of the western Mediterranean arcs. Tectonics, 23(1), n/a-n/a.

Farris, D. W., Jaramillo, C., Bayona, G., Restrepo-Moreno, S. A., Montes, C., Cardona, A., et al. (2011). Fracturing of the Panamanian Isthmus during initial collision with South America. Geology, 39(11), 1007-1010.

Feigenson, M. D., Carr, M. J., Maharaj, S. V., Juliano, S., & Bolge, L. L. (2004). Lead isotope composition of Central American volcanoes: Influence of the Galapagos plume. Geochemistry, Geophysics, Geosystems, 5(6).

Ferrari, L., Orozco-Esquivel, T., Manea, V., & Manea, M. (2012). The dynamic history of the Trans-Mexican Volcanic Belt and the Mexico subduction zone. Tectonophysics, 522-523, 122-149.

Ferrari, L., Valencia-Moreno, M., & Bryan, S. (2007). Magmatism and tectonics of the Sierra Madre Occidental and its relation with the evolution of the western margin of North America. In Special Paper 422: Geology of México: Celebrating the Centenary of the Geological Society of México (pp. 1-39).

Finch, J. W., & Abbott, P. L. (1977). Petrology of a Triassic Marine Section, Vizcaino Peninsula, Baja California Sur, Mexico. Sedimentary Geology, 19(4), 253-273.

Finch, R. C., & Ritchie, A. W. (1991). The Guayape Fault System, Honduras, Central-America. Journal of South American Earth Sciences, 4(1-2), 43-60.

Fisher, R. (1953). Dispersion on a Sphere. Proceedings of the Royal Society A: Mathematical, Physical and Engineering Sciences, 217(1130), 295-305.

Fitz-Díaz, E., Lawton, T. F., Juárez-Arriaga, E., & Chávez-Cabello, G. (2017). The Cretaceous-Paleogene Mexican orogen: Structure, basin development, magmatism and tectonics. Earth-Science Reviews.

Flores, K., Denyer, P., & Aguilar, T. (2003a). Nueva propuesta estratigráfica: Geología de la hoja Abangares Guanacaste, Costa Rica. Revista Geológica de América Central(29), 127-136.

Flores, K., Denyer, P., & Aguilar, T. (2003b). Nueva propuesta estratigráfica: Geología de las hojas Matambú y Talolinga, Guanacaste, Costa Rica. Revista Geológica de América Central, 28, 131-138.

Flores, K. E. (2006). Jurassic-Late Cretaceous oceanic crustal terranes and arc-derived sediments south Chortis Block (NE Nicaragua to NW Costa Rica) - Preliminary results of two key areas: Nicoya Peninsula and Siuna District. (DEA Thesis), Université de Lausanne, (107 p.)

Flores, K. E., Martens, U. C., Harlow, G. E., Brueckner, H. K., & Pearson, N. J. (2013). Jadeitite formed during subduction: In situ zircon geochronology constraints from two different tectonic events within the Guatemala Suture Zone. Earth and Planetary Science Letters, 371-372, 67-81.

Flores, K. E., Skora, S., Martin, C., Harlow, G. E., Rodríguez, D., & Baumgartner, P. O. (2015). Metamorphic history of riebeckite-and aegirine-augite-bearing high-pressure–low-temperature blocks within the Siuna Serpentinite Mélange, northeastern Nicaragua. International Geology Review, 57(5-8), 943-977.

Fonseca, E., González, R., Delgado, R., & Savieleva, G. (1989). Presencia de efusivos ofiolíticos y de boninitas en las provincias de La Habana y Matanzas. Boletín Técnico, Geología, 1, 1-9.

Fonseca, E., Zelepugin, V., & Heredia, M. (1985). Structure of the ophiolite association of Cuba. Geotectonics, 19(4), 321-329.

Fox, P. J., & Heezen, B. C. (1975). Geology of the Caribbean crust. In The Gulf of Mexico and the Caribbean (pp. 421-466): Springer.

French, S. W., & Romanowicz, B. A. (2014). Whole-mantle radially anisotropic shear velocity structure from spectral-element waveform tomography. Geophysical Journal International, 199(3), 1303-1327.

Frey, M., Saunders, J., & Schwander, H. (1988). The mineralogy and metamorphic geology of low-grade metasediments, Northern Range, Trinidad. Journal of the Geological Society, 145(4), 563-575.

Freydier, C., Martinez, J., Lapierre, H., Tardy, M., & Coulon, C. (1996). The Early Cretaceous Arperos oceanic basin (western Mexico). Geochemical evidence for an aseismic ridge formed near a spreading center. Tectonophysics, 259, 343-367.

Freymueller, J. T., Kellogg, J. N., & Vega, V. (1993). Plate motions in the North Andean region. Journal of Geophysical Research: Solid Earth, 98(B12), 21853-21863.

Fu, R. R., & Kent, D. V. (2018). Anomalous Late Jurassic motion of the Pacific Plate with implications for true polar wander. Earth and Planetary Science Letters, 490, 20-30.

Funiciello, F., Faccenna, C., & Giardini, D. (2004). Role of lateral mantle flow in the evolution of subduction systems: insights from laboratory experiments. Geophysical Journal International, 157(3), 1393-1406.

Gaina, C., Torsvik, T. H., van Hinsbergen, D. J. J., Medvedev, S., Werner, S. C., & Labails, C. (2013). The African Plate: A history of oceanic crust accretion and subduction since the Jurassic. Tectonophysics, 604, 4-25.

Galli-Olivier, C. (1979). Ophiolite and Island-Arc Volcanism in Costa-Rica. Geological Society of America Bulletin, 90(5), 444-452.

García-Casco, A., Iturralde-Vinent, M. A., & Pindell, J. (2008a). Latest Cretaceous collision/accretion between the Caribbean Plate and Caribeana: origin of metamorphic terranes in the Greater Antilles. International Geology Review, 50(9), 781-809.

García-Casco, A., Lázaro, C., Rojas-Agramonte, Y., Kröner, A., Torres-Roldán, R. L., Núñez, K., et al. (2008b). Partial Melting and Counterclockwise P–T Path of Subducted Oceanic Crust (Sierra del Convento Mélange, Cuba). Journal of Petrology, 49(1), 129-161.

García-Casco, A., Torres-Roldan, R. L., Iturralde-Vinent, M. A., Millan, G., Cambra, K. N., Lazaro, C., & Vega, A. R. (2006). High pressure metamorphism of ophiolites in Cuba. Geologica Acta, 4(1-2), 63-88.

García-Casco, A., Torres-Roldan, R. L., Millan, G., Monie, P., & Haissen, F. (2001). High-grade metamorphism and hydrous melting of metapelites in the Pinos terrane (W Cuba): Evidence for crustal thickening and extension in the northern Caribbean collisional belt. Journal of Metamorphic Geology, 19(6), 699-715.

García-Casco, A., Torres-Roldán, R., Millán, G., Monié, P., & Schneider, J. (2002). Oscillatory zoning in eclogitic garnet and amphibole, Northern Serpentinite Melange, Cuba: a record of tectonic instability during subduction? Journal of Metamorphic Geology, 20(6), 581-598.

Gardner, T. W., Fisher, D. M., Morell, K. D., & Cupper, M. L. (2013). Upper-plate deformation in response to flat slab subduction inboard of the aseismic Cocos Ridge, Osa Peninsula, Costa Rica. Lithosphere, 5(3), 247-264.

Gastil, R. G., Phillips, R. P., & Allison, E. C. (1975). Reconnaissance geology of the state of Baja California. Geological Society of America Memoirs, 140, 1-201.

Gazel, E., Carr, M. J., Hoernle, K., Feigenson, M. D., Szymanski, D., Hauff, F., & van den Bogaard, P. (2009). Galapagos-OIB signature in southern Central America: Mantle refertilization by arc-hot spot interaction. Geochemistry, Geophysics, Geosystems, 10(2), Q02S11.

Gazel, E., Denyer, P., & Baumgartner, P. O. (2006). Magmatic and geotectonic significance of Santa Elena Peninsula, Costa Rica. Geologica Acta, 4(1-2), 193-202.

Gerya, T. V., Stern, R. J., Baes, M., Sobolev, S. V., & Whattam, S. A. (2015). Plate tectonics on the Earth triggered by plume-induced subduction initiation. Nature, 527(7577), 221.

Ghosh, N., Hall, S., & Casey, J. (1984). Seafloor spreading magnetic anomalies in the Venezuelan Basin. Geological Society of America, Memoir 162, 65-80.

Gill, J. B. (2012). Orogenic andesites and plate tectonics (Vol. 16): Springer Science & Business Media.

Giunta, G., Beccaluva, L., Coltorti, M., Mortellaro, D., Siena, F., & Cultrupia, D. (2002a). The peri-Caribbean ophiolites: structure, tectono-magmatic significance and geodynamic implications. Caribbean Journal of Earth Science, 36, 1-20.

Giunta, G., Beccaluva, L., Coltorti, M., Siena, F., & Vaccaro, C. (2002b). The southern margin of the Caribbean Plate in Venezuela: tectono-magmatic setting of the ophiolitic units and kinematic evolution. Lithos, 63(1-2), 19-40.

González, H. (2001). Mapa geologico del departamento de Antioquia y memoria explicitiva (Scale 1: 400000). Instituto Colombiano de Minería y Geología, Bogotá. In.

Gordon, M. B., Mann, P., Caceres, D., & Flores, R. (1997). Cenozoic tectonic history of the North America Caribbean plate boundary zone in western Cuba. Journal of Geophysical Research-Solid Earth, 102(B5), 10055-10082.

Gordon, R. G., & Jurdy, D. M. (1986). Cenozoic global plate motions. Journal of Geophysical Research: Solid Earth, 91(B12), 12389-12406.

Govers, R., & Wortel, M. J. R. (2005). Lithosphere tearing at STEP faults: response to edges of subduction zones. Earth and Planetary Science Letters, 236(1-2), 505-523.

Gradstein, F. M., Ogg, J. G., Schmitz, M., & Ogg, G. (2012). The Geologic Time Scale 2012: Elsevier.

Gradstein, F. M., Ogg, J. G., Smith, A. G., Agterberg, F. P., Bleeker, W., Cooper, R. A., et al. (2004). A Geologic Time Scale 2004. Cambridge: Cambridge University Press, UK.

Grand, S. P., van der Hilst, R. D., & Widiyantoro, S. (1997). Global Seismic Tomography: A Snapshot of Convection in the Earth. GSA Today, 7(4), 1-7.

Grindley, G., Oliver, P., & Sukroo, J. (1980). Lower Mesozoic position of southern New Zealand determined from paleomagnetism of the Glenham Porphyry, Murihiku Terrane, eastern Southland. Gondwana Five, Wellington, New Zealand, 319-326.

Gromet, P., & Silver, L. T. (1987). REE variations across the Peninsular Ranges batholith: Implications for batholithic petrogenesis and crustal growth in magmatic arcs. Journal of Petrology, 28(1), 75-125.

Guilmette, C., Smit, M. A., van Hinsbergen, D. J., Gürer, D., Corfu, F., Charette, B., et al. (2018). Forced subduction initiation recorded in the sole and crust of the Semail Ophiolite of Oman. Nature Geoscience, 1.

Gürer, D., Hinsbergen, D. J., Matenco, L., Corfu, F., & Cascella, A. (2016). Kinematics of a former oceanic plate of the Neotethys revealed by deformation in the Ulukışla basin (Turkey). Tectonics, 35(10), 2385-2416.

Guzmán-Speziale, M. (2010). Beyond the Motagua and Polochic faults: Active strike-slip faulting along the western North America–Caribbean plate boundary zone. Tectonophysics, 496(1-4), 17-27.

Hada, S., Ishii, K.-i., Landis, C., Aitchison, J., & Yoshikura, S. (2001). Kurosegawa Terrane in Southwest Japan: disrupted remnants of a Gondwana-derived terrane. Gondwana Research, 4(1), 27-38.

Hafkenscheid, E., Wortel, M., & Spakman, W. (2006). Subduction history of the Tethyan region derived from seismic tomography and tectonic reconstructions. Journal of Geophysical Research: Solid Earth, 111(B8).

Hagstrum, J. T., Martínez, M. L., & York, D. (1993). Paleomagnetic and 40Ar/39Ar evidence for remagnetization of Mesozoic oceanic rocks on the Vizcaino Peninsula, Baja California Sur, Mexico. Geophysical Research Letters, 20(17), 1831-1834.

Hagstrum, J. T., McWillams, M., Howell, D. G., & Grommé, S. (1985). Mesozoic paleomagnetism and northward translation of the Baja California Peninsula. Geological Society of America Bulletin, 96, 1077-1090.

Hagstrum, J. T., & Sedlock, R. L. (1990). Remagnetization and northward translation of Mesozoic red chert from Cedros Island and the San Benito Islands, Baja California, Mexico. Geological Society of America Bulletin, 102, 983-991.

Hagstrum, J. T., & Sedlock, R. L. (1992). Paleomagnetism of Mesozoic Red Chert from Cedros Island and the San-Benito Islands, Baja-California, Mexico Revisited. Geophysical Research Letters, 19(3), 329-332.

Hall, C. E., Gurnis, M., Sdrolias, M., Lavier, L. L., & Müller, R. D. (2003). Catastrophic initiation of subduction following forced convergence across fracture zones. Earth and Planetary Science Letters, 212(1-2), 15-30.

Hall, R. (2002). Cenozoic geological and plate tectonic evolution of SE Asia and the SW Pacific: computer-based reconstructions, model and animations. Journal of Asian Earth Sciences, 20(4), 353-431.

Hall, R., & Spakman, W. (2002). Subducted slabs beneath the eastern Indonesia–Tonga region: insights from tomography. Earth and Planetary Science Letters, 201(2), 321-336.

Hallam, A. (1986). Evidence of displaced terranes from Permian to Jurassic faunas around the Pacific margins. Journal of the Geological Society, 143(1), 209-216.

Harlow, G. E., Hemming, S. R., Avé Lallemant, H. G., Sisson, V. B., & Sorensen, S. S. (2004). Two high-pressure–low-temperature serpentinite-matrix mélange belts, Motagua fault zone, Guatemala: A record of Aptian and Maastrichtian collisions. Geology, 32(1).

Hashimoto, W., Koike, T., & Hasegawa, T. (1975). First confirmation of the Permian System in the central part of Hokkaido. Proceedings of the Japan Academy, 51(1), 34-37.

Hastie, A. R., & Kerr, A. C. (2010). Mantle plume or slab window?: Physical and geochemical constraints on the origin of the Caribbean oceanic plateau. Earth-Science Reviews, 98(3-4), 283-293.

Hastie, A. R., Mitchell, S. F., Treloar, P. J., Kerr, A. C., Neill, I., & Barfod, D. N. (2013). Geochemical components in a Cretaceous island arc: The Th/La–(Ce/Ce*)Nd diagram and implications for subduction initiation in the inter-American region. Lithos, 162-163, 57-69.

Haston, R. B., & Luyendyk, B. P. (1991). Paleomagnetic Results from the Waipapa Terrane, Northland Peninsula, North Island, New-Zealand - Tectonic Implications from Widespread Remagnetizations. Tectonics, 10(5), 986-994.

Hatten, C., Schooler, O., Giedt, N., & Meyerhoff, A. (1958). Geology of central Cuba, eastern Las Villas and western Camagüey provinces: La Habana. Cuba, Archivo del Servicio Geológico Nacional. unpubl. report.

Hatten, C. W., Somin, M., Millan, G., Renne, P., Kistler, R., & Mattinson, J. (1988). Tectonostratigraphic units of central Cuba. Paper presented at the Transactions of the 11th Caribbean Geological Conference, Barbados.

Hauff, F., Hoernle, K., Schmincke, H. U., & Werner, R. (1997). A Mid Cretaceous origin for the Galapagos hotspot: Volcanological, petrological and geochemical evidence from Costa Rican oceanic crustal segments. Geologische Rundschau, 86(1), 141-155.

Hauff, F., Hoernle, K., van den Bogaard, P., Alvarado, G., & Garbe-Schönberg, D. (2000). Age and geochemistry of basaltic complexes in western Costa Rica: Contributions to the geotectonic evolution of Central America. Geochemistry, Geophysics, Geosystems, 1(5).

Hayami, I. (1961). On the Jurassic pelecypod faunas in Japan. Journal of the Faculty of Science University of Tokyo, 2, 13, 243-343.

Hayami, I. (1984). Jurassic marine bivalve faunas and biogeography in Southeast Asia. Geology and palaeontology of southeast Asia, 25, 229-237.

Hayes, G. P., Briggs, R. W., Sladen, A., Fielding, E. J., Prentice, C., Hudnut, K., et al. (2010). Complex rupture during the 12 January 2010 Haiti earthquake. Nature Geoscience, 3(11), 800-805.

He, H., Pan, Y., Tauxe, L., Qin, H., & Zhu, R. (2008). Toward age determination of the M0r (Barremian–Aptian boundary) of the Early Cretaceous. Physics of the Earth and Planetary Interiors, 169(1-4), 41-48.

He, Y., & Wen, L. (2009). Structural features and shear-velocity structure of the "Pacific Anomaly". Journal of Geophysical Research, 114(B2).

Heuret, A., & Lallemand, S. (2005). Plate motions, slab dynamics and back-arc deformation. Physics of the Earth and Planetary Interiors, 149(1-2), 31-51.

Hickey, J. J. (1984). Stratigraphy and composition of a Jura-Cretaceous volcanic arc apron, Punta Eugenia, Baja California Sur, Mexico. In V. A. J. Frizzell (Ed.), Geology of the Baja California peninsula (Vol. 39, pp. 149-160). Field Trip Guidebook, Pacific Section: Society of Economic Paleontologists and Miner- alogists Pacific Section.

Hilde, T. W. C., Uyeda, S., & Kroenke, L. (1977). Evolution of the western Pacific and its margin. Tectonophysics, 38, 145-165.

Hildebrand, R. S. (2013). Mesozoic assembly of the North American Cordillera. The Geological Society of America, Special Paper 495.

Hildebrand, R. S. (2015). Dismemberment and northward migration of the Cordilleran orogen: Baja-BC resolved. GSA Today, 4-11.

Hill, R. I. (1993). Mantle plumes and continental tectonics. Lithos, 30(3-4), 193-206.

Hippolyte, J.-C., Mann, P., & Grindlay, N. R. (2005). Geologic evidence for the prolongation of active normal faults of the Mona rift into northwestern Puerto Rico. Active tectonics and seismic hazards of Puerto Rico, the Virgin Islands and Offshore areas, Geological Society of America Special Paper, 385, 161-171.

Hoernle, K., Hauff, F., & Bogaard, P. v. d. (2004). 70 m.y. history (139–69 Ma) for the Caribbean large igneous province. Geology, 32(8).

Hoernle, K., van den Bogaard, P., Werner, R., Lissinna, B., Hauff, F., Alvarado, G., & Garbe-Schönberg, D. (2002). Missing history (16–71 Ma) of the Galápagos hotspot: Implications for the tectonic and biological evolution of the Americas. Geology, 30(9).

Holcombe, T. L., Vogt, P. R., Matthews, J. E., & Murchison, R. R. (1973). Evidence for sea-floor spreading in the Cayman Trough. Earth and Planetary Science Letters, 20, 357-372.

Hori, R. S., & Sakakibara, M. (1994). A chert-clastic sequence spanning the late Triassic-early Cretaceous Period of the Kamuikotan Complex in the Shizunai area, south-central Hokkaido, Japan. Journal of the Geological Society of Japan, 100(8), 575-583.

Howell, D. G. (1980). Mesozoic accretion of exotic terranes along the New Zealand segment of Gondwanaland. Geology, 8, 487-491.

Huang, W., Van Hinsbergen, D. J., Maffione, M., Orme, D. A., Dupont-Nivet, G., Guilmette, C., et al. (2015). Lower Cretaceous Xigaze ophiolites formed in the Gangdese forearc: Evidence from paleomagnetism, sediment provenance, and stratigraphy. Earth and Planetary Science Letters, 415, 142-153.

Hutko, A. R., Lay, T., Garnero, E. J., & Revenaugh, J. (2006). Seismic detection of folded, subducted lithosphere at the core-mantle boundary. Nature, 441(7091), 333-336.

Igo, H., Sashida, K., & Ueno, H. (1987). Early Cretaceous radiolarians from the Esashi Mountains, northern Hokkaido. Annual report of the Institute of Geoscience, the University of Tsukuba, 13, 105-109.

Iijima, A., Kakuwa, Y., & Matsuda, H. (1989). Silicified wood from the Adoyama chert, Kuzuh, Central Honshu, and its bearing on compaction and depositional environment of radiolarian bedded chert. In Siliceous deposits of the Tethys and Pacific Regions (pp. 151-168): Springer.

Ikeda, T., Harada, T., Kouchi, Y., Morita, S., Yokogawa, M., Yamamoto, K., & Otoh, S. (2016). Provenance analysis based on detrital-zircon-age spectra of the Lower Cretaceous formations in the Ryoseki–Monobe area, Outer Zone of Southwest Japan. Memoir of the Fukui Prefectural Dinosaur Museum, 15, 33-84.

Iosifidi, A. G., Mac Niocaill, C., Khramov, A. N., Dekkers, M. J., & Popov, V. V. (2010). Palaeogeographic implications of differential inclination shallowing in permo-carboniferous sediments from the donets basin, Ukraine. Tectonophysics, 490(3-4), 229-240.

Ishiga, H., & Ishiyama, D. (1987). Jurassic accretionary complex in Kaminokuni terrane, southwestern Hokkaido, Japan. Mining Geology, 37(206), 381-394.

Ishizuka, H. (1985). Prograde metamorphism of the Horokanai ophiolite in the Kamuikotan Zone, Hokkaido, Japan. Journal of Petrology, 26(2), 391-417.

Ishizuka, H. t. (1980). Geology of the Horokanai ophiolite, Kamuikotan belt, Hokkaido. Journal of the Geological Society of Japan, 86, 119-134.

Isozaki, Y. (1996). Anatomy and genesis of a subduction-related orogen: A new view of geotectonic subdivision and evolution of the Japanese Islands. Island Arc, 5(3), 289-320.

Isozaki, Y. (2000). The Japanese Islands: Its origin, evolution, and future. Science Journal Kagaku, 70, 133-145.

Isozaki, Y. (2014). Memories of Pre-Jurassic Lost Oceans: How To Retrieve Them From Extant Lands. Geoscience Canada, 41(3).

Isozaki, Y., Aoki, K., Nakama, T., & Yanai, S. (2010). New insight into a subduction-related orogen: A reappraisal of the geotectonic framework and evolution of the Japanese Islands. Gondwana Research, 18(1), 82-105.

Isozaki, Y., Maruyama, S., & Furuoka, F. (1990). Accreted Oceanic Materials in Japan. Tectonophysics, 181(1-4), 179-205.

Isozaki, Y., & Ota, A. (2001). Middle-Upper Permian (Maokouan-Wuchiapingian) boundary in mid-oceanic paleo-atoll limestone of Kamura and Akasaka, Japan. Proceedings of the Japan Academy, Series B, 77(6), 104-109.

Iturralde-Vinent, M. (1988). Consideraciones generales sobre el magmatismo de margen continental de Cuba. Revista Tecnológica, 18(4), 17-24.

Iturralde-Vinent, M. (1994). Cuban geology: a new plate-tectonic synthesis. Journal of Petroleum Geology, 17(1), 39-69.

Iturralde-Vinent, M. (1996). Cuban ophiolites and volcanic arcs. In M. Iturralde-Vinent (Ed.), IGCP Project 364, Special Contribution 1.

Iturralde-Vinent, M. (1997). Introducción a la geología de Cuba. In G. Furrazola Bermúdez & K. Núñez Cambra (Eds.), Estudios sobre geologia de Cuba (pp. 35-68). La Habana, Cuba: Instituto de Geología y Paleontología.

Iturralde-Vinent, M. (1998). Synopsis of the geological constitution of Cuba. Acta Geologica Hispanica, 33(1/4), 9-56.

Iturralde-Vinent, M., & Marí-Morales, T. (1988). Toleitas del Tithoniano de la Sierra de Camaján, Camagüey: Posible datación de la corteza oceánica. Revista Tecnológica, 18, 25-32.

Iturralde-Vinent, M., Millán, G., Korkas, L., Nagy, E., & Pajón, J. (1996). Geological interpretation of the Cuban K-Ar data base. In M. Iturralde-Vinent (Ed.), Cuban ophiolites and volcanic arcs, IGCP Project 364 (pp. 48-69).

Iturralde-Vinent, M., Otero, C. D., García-Casco, A., & van Hinsbergen, D. (2008). Paleogene Foredeep Basin Deposits of North-Central Cuba: A Record of Arc-Continent Collision between the Caribbean and North American Plates. International Geology Review, 50(10), 863-884.

Iturralde-Vinent, M. A. (2006). Meso-Cenozoic Caribbean Paleogeography: Implications for the Historical Biogeography of the Region. International Geology Review, 48(9), 791-827.

Iwata, K., & Tajika, J. (1989). Jurassic and Cretaceous radiolarians from the pre-Tertiary system in the Hidaka Belt, Maruseppu region, Northeast Hokkaido. Journal of the Faculty of Science, Hokkaido University. Series 4, Geology and mineralogy, 22(3), 453-466.

Jackson, M. J., Banerjee, S. K., Marvin, J. A., Lu, R., & Gruber, W. (1991). Detrital remanence, inclination errors, and anhysteretic remanence anisotropy: quantitative model and experimental results. Geophysical Journal International, 104(1), 95-103.

James, K. H. (2006). Arguments for and against the Pacific origin of the Caribbean Plate: discussion, finding for an inter-American origin. Geologica Acta, 4(1-2), 279-302.

James, K. H. (2009). In situ origin of the Caribbean: discussion of data. Geological Society, London, Special Publications, 328(1), 77-125.

Jansma, P., Lopez, A., Mattioli, G., DeMets, C., Dixon, T., Mann, P., & Calais, E. (2000). Microplate tectonics in the northeastern Caribbean as constrained by Global Positioning (GPS) geodesy. Tectonics, 19(6), 1021-1037.

John, T., Scherer, E. E., Schenk, V., Herms, P., Halama, R., & Garbe-Schönberg, D. (2010). Subducted seamounts in an eclogite-facies ophiolite sequence: the Andean Raspas Complex, SW Ecuador. Contributions to Mineralogy and Petrology, 159(2), 265-284.

Johnson, C. L., Constable, C. G., Tauxe, L., Barendregt, R., Brown, L. L., Coe, R. S., et al. (2008). Recent investigations of the 0-5 Ma geomagnetic field recorded by lava flows. Geochemistry, Geophysics, Geosystems, 9(4), Q04032.

Johnson, S. E., Tate, M. C., & Mark Fanning, C. (1999). New geologic mapping and SHRIMP U-Pb zircon data in the Peninsular Ranges batholith, Baja California, Mexico: Evidence for a suture? Geology, 27(8).

Johnston, S. T. (2001). The Great Alaskan Terrane Wreck: reconciliation of paleomagnetic and geological data in the northern Cordillera. Earth and Planetary Science Letters, 193(3-4), 259-272.

Johnston, S. T. (2008). The cordilleran ribbon continent of North America. Annu. Rev. Earth Planet. Sci., 36, 495-530.

Jolly, W. T., Lidiak, E. G., & Dickin, A. P. (2008). The case for persistent southwest-dipping Cretaceous convergence in the northeast Antilles: Geochemistry, melting models, and tectonic implications. Geological Society of America Bulletin, 120(7-8), 1036-1052.

Jolly, W. T., Lidiak, E. G., Schellekens, J. H., & Santos, H. (1998). Volcanism, tectonics, and stratigraphic correlations in Puerto Rico. Geological Society of America Special Paper, 322, 1-34.

Jones, D. L., Blake Jr, M., & Rangin, C. (1976). The four Jurassic belts of northern California and their significance to the geology of the southern California borderland. In D. G. Howell (Ed.), Aspects of the geologic history of the California continental borderland (Vol. Pacific Section Miscellaneous Publication 24, pp. 343-362): American Association of Petroleum Geologists.

Jordan, T. H., & Lynn, W. S. (1974). A velocity anomaly in the lower mantle. Journal of Geophysical Research, 79(17), 2679-2685.

Joyce, J. (1983). The lithology and structure of the eclogite and glaucophanite-bearing rocks of the Samana Peninsula, Dominican Republic. Paper presented at the Transaction of the 9th Caribbean Geological Conference, Santo Domingo, Dominican Republic.

Kaneshima, S., & Helffrich, G. (2010). Small scale heterogeneity in the mid-lower mantle beneath the circum-Pacific area. Physics of the Earth and Planetary Interiors, 183(1-2), 91-103.

Kantchev, I. (1978). Informe geológico de la provincia Las Villas-Resultados de las investigaciones geológicas a escala 1: 250.000 durante el período 1969-1975. Report is available at the Oficina Nacional de Recursos Minerales, Ministerio de Industria Básica, La Habana, Cuba,(unpublished).

Kasuya, A., Isozaki, Y., & Igo, H. (2012). Constraining paleo-latitude of a biogeographic boundary in mid-Panthalassa: Fusuline province shift on the Late Guadalupian (Permian) migrating seamount. Gondwana Research, 21(2-3), 611-623.

Kato, Y., & Iwata, K. (1989). Radiolarian biostratigraphic study of the pre-Tertiary system around the Kamikawa Basin, central Hokkaido, Japan. Journal of the Faculty of Science, Hokkaido University. Series 4, Geology and mineralogy, 22(3), 425-452.

Kato, Y., Iwata, K., Uozumi, S., & Nakamura, K. (1986). Re-examination on the pre-Tertiary System distributed in the Toma-Kaimei district of central Hokkaido. Journal of the Geological Society of Japan, 92(3), 239-242.

Kawamura, M. (1986). Constitution and occurrences of the Paleozoic and Mesozoic formations in SW Hokkaido, northern Japan. Geology and Tectonics of Hokkaido, 17-32.

Kawamura, M., Yasuda, N., Watanabe, T., Fanning, M., & Terada, T. (2000). Composition and provenance of the Jurassic quartzofeldspathic sandstones of the Oshima Accretionary Belt, SW Hokkaido, Japan. Memoirs of the Geological Society of Japan, 57, 63-72.

Kawamura, T., Onishi, M., Kurashimo, E., Ikawa, T., & Ito, T. (2003). Deep seismic reflection experiment using a dense receiver and sparse shot technique for imaging the deep structure of the Median Tectonic Line (MTL) in east Shikoku, Japan. Earth, planets and space, 55(9), 549-557.

Kear, D., & Mortimer, N. (2003). Waipa Supergroup, New Zealand: A proposal. Journal of the Royal Society of New Zealand, 33(1), 149-163.

Kellogg, J. N., & Vega, V. (1995). Tectonic development of Panama, Costa Rica, and the Colombian Andes: constraints from global positioning system geodetic studies and gravity. Geological Society of America Special Papers, 295, 75-90.

Kennan, L., & Pindell, J. L. (2009). Dextral shear, terrane accretion and basin formation in the Northern Andes: best explained by interaction with a Pacific-derived Caribbean Plate? Geological Society, London, Special Publications, 328(1), 487-531.

Kent, D. V., & Irving, E. (2010). Influence of inclination error in sedimentary rocks on the Triassic and Jurassic apparent pole wander path for North America and implications for Cordilleran tectonics. Journal of Geophysical Research, 115(B10).

Kent, D. V., & Tauxe, L. (2005). Corrected Late Triassic latitudes for continents adjacent to the North Atlantic. Science, 307(5707), 240-244.

Keppie, J. D. (2004). Terranes of Mexico revisited: A 1.3 billion year odyssey. International Geology Review, 46(9), 765-794.

Kerr, A. C., Iturralde-Vinent, M. A., Saunders, A. D., Babbs, T. L., & Tarney, J. (1999). A new plate tectonic model of the Caribbean: Implications from a geochemical reconnaissance of Cuban Mesozoic volcanic rocks. Geological Society of America Bulletin, 111(11), 1581-1599.

Kerr, A. C., Marriner, G. F., Tarney, J., Nivia, A., Saunders, A. D., Thirlwall, M. F., & Sinton, C. W. (1997). Cretaceous basaltic terranes in western Colombia: Elemental, chronological and Sr-Nd isotopic constraints on petrogenesis. Journal of Petrology, 38(6), 677-702.

Kerr, A. C., Tarney, J., Nivia, A., Marriner, G. F., & Saunders, A. D. (1998). The internal structure of oceanic plateaus: Inferences from obducted Cretaceous terranes in western Colombia and the Caribbean. Tectonophysics, 292(3-4), 173-188.

Kerr, A. C., White, R. V., Thompson, P. M., Tarney, J., & Saunders, A. D. (2003). No oceanic plateau—no Caribbean plate? The seminal role of an oceanic plateau in Caribbean plate evolution. In C. Bartolini, R. T. Buffler, & J. F. Blickwede (Eds.), The Circum-Gulf of Mexico and the Caribbean; Hydrocarbon Habitats, Basin Formation, and Plate Tectonics. (Vol. Memoir 79, pp. 126-168): American Association of Petroleum Geologists.

Kesler, S. E., Russell, N., Polanco, J., McCurdy, K., & Cumming, G. L. (1991). Geology and geochemistry of the Early Cretaceous Los Ranchos Formation, central Dominican Republic. Geological Society of America Special Paper, 262, 187-201.

Khudoley, K. (1967). Principal features of Cuban geology. AAPG Bulletin, 51(5), 668-677.

Kimbrough, D. L. (1985). Tectonostratigraphic Terranes of the Vizcaino Peninsula and Cedros and San Benito Islands, Baja California, Mexico. In Tectonostratigrahic Terranes of the Circum-Pacific Region (Vol. Earth Science Series, pp. 285-298).

Kimbrough, D. L. (1989). Franciscan Complex rocks on Cedros Island, Baja California Sur, Mexico: Radiolarian biostratigraphic ages from a chert mélange block and petrographic observations on metasandstone.

Kimbrough, D. L., Abbott, P. L., Balch, D. C., Bartling, S. H., Grove, M., Mahoney, J. B., & Donohue, R. F. (2014). Upper Jurassic Peñasquitos Formation—Forearc basin western wall rock of the Peninsular Ranges batholith. In Peninsular Ranges Batholith, Baja California and Southern California (pp. 625-643).

Kimbrough, D. L., Abbott, P. L., Grove, M., Smith, D. P., Mahoney, J. B., Moore, T. E., & Gehrels, G. (2006). Contrasting cratonal provinces for Upper Cretaceous Valle Group quartzite clasts, Baja California.

Kimbrough, D. L., & Moore, T. E. (2003). Ophiolite and volcanic arc assemblages on the Vizcaino Peninsula and Cedros Island, Baja California Sur, Mexico: Mesozoic for ear c lithosphere of the Cordilleran magmatic arc. Tectonic evolution of northwestern Mexico and the southwestern USA, 374, 43.

Kimbrough, D. L., Smith, D. P., Mahoney, J. B., Moore, T. E., Grove, M., Gastil, R. G., et al. (2001). Forearc-basin sedimentary response to rapid Late Cretaceous batholith emplacement in the Peninsular Ranges of southern and Baja California. Geology, 29(6).

Kiminami, K. (1990). Discovery of Paleogene radiolarians from the Hidaka Supergroup and its significance with special reference to ridge subduction. Journal of Geological Society of Japan, 96, 323-326.

Kiminami, K. (1992). Cretaceous-Paleogene arc-trench systems in Hokkaido, Paleozoic and Mesozoic terranes: basement of the Japanese Island arcs. 29th IGC field trip guidebook, 1, 1-43.

Kiminami, K. (1999). Occurrence and significance of in-situ basaltic rocks from the Rurochi Formation in the Hidaka Supergroup, northern Hokkaido, Japan. Memoirs of the Geological Society of Japan, 52, 103-112.

Kiminami, K., & Kontani, Y. (1983). Mesozoic arc-trench systems in Hokkaido, Japan. In M. Hashimoto & S. Uyeda (Eds.), Accretion Tectonics in the Circum-Pacific Regions (pp. 107-122). Tokyo: Terrapub.

Kiminami, K., Kontani, Y., & Miyashita, S. (1985). Lower Cretaceous strata covering the abyssal tholeiite (the Hidaka Western Greenstone Belt) in the Chiroro area, central Hokkaido, Japan. Jour. Geol. Soc. Japan, 91(1), 27-42.

Kimura, G. (1986). Oblique subduction and collision: Forearc tectonics of the Kuril arc. Geology, 14(5), 404-407.

Kimura, G., & Tamaki, K. (1985). Tectonic framework of the Kuril arc since its initiation. Formation of active ocean margins, 641-676.

Kirschvink, J. L. (1980). The least-squares line and plane and the analysis of palaeomagnetic data. Geophysical Journal International, 62, 699-718.

Kirschvink, J. L., Isozaki, Y., Shibuya, H., Otofuji, Y.-i., Raub, T. D., Hilburn, I. A., et al. (2015). Challenging the sensitivity limits of paleomagnetism: magnetostratigraphy of weakly magnetized Guadalupian–Lopingian (Permian) limestone from Kyushu, Japan. Palaeogeography, Palaeoclimatology, Palaeoecology, 418, 75-89.

Kito, T., Rost, S., Thomas, C., & Garnero, E. J. (2007). New insights into theP- andS-wave velocity structure of the D discontinuity beneath the Cocos plate. Geophysical Journal International, 169(2), 631-645.

Kiyokawa, S. (1992). Geology of the Idonnappu belt, central Hokkaido, Japan: Evolution of a Cretaceous accretionary complex. Tectonics, 11(6), 1180-1206.

Kleinrock, M. C., & Morgan, J. P. (1988). Triple junction reorganization. Journal of Geophysical Research, 93(B4).

Klitgord, K. D., & Schouten, H. (1986). Plate kinematics of the Central Atlantic. The geology of North America. Vol. M. The Western North Atlantic Region (A decade of North American Geology). (Geological Society of America, Boulder, Colorado), Ch. 22, 50 pp. .

Knipper, A., & Cabrera, R. (1974). Tectnica y geología histórica de la zona de articulaciónentre el mio- y eugeosinclinal y del cinturon de hiperbasitas. In Contribución a la Geología de Cuba (pp. 15-77). Instituto de Geología, La Habana: Academia de Ciencias de Cuba.

Kobayashi, D., LaFemina, P., Geirsson, H., Chichaco, E., Abrego, A. A., Mora, H., & Camacho, E. (2014). Kinematics of the western Caribbean: Collision of the Cocos Ridge and upper plate deformation. Geochemistry, Geophysics, Geosystems, 15(5), 1671-1683.

Kobayashi, T., & Tamura, M. (1984). The Triassic bivalvia of Malaysia, Thailand and adjacent areas. Geology and palaeontology of southeast Asia, 25, 201-228.

Kodama, K. (2009). Simplification of the anisotropy-based inclination correction technique for magnetite-and haematite-bearing rocks: a case study for the Carboniferous Glenshaw and Mauch Chunk Formations, North America. Geophysical Journal International, 176(2), 467-477.

Kodama, K., Fukuoka, M., Aita, Y., Sakai, T., Hori, R., Takemura, A., et al. (2007). Paleomagnetic results from Arrow Rocks in the framework of paleomagnetism in pre-Neogene rocks from New Zealand. The Oceanic Permian/Triassic Boundary Sequence at Arrow Rocks (Oruatemanu), Northland, New Zealand: Lower Hutt, New Zealand, Geological and Nuclear Science Monograph, 24, 177-196.

Konrad, K., Koppers, A. A., Steinberger, B., Finlayson, V. A., Konter, J. G., & Jackson, M. G. (2018). On the relative motions of long-lived Pacific mantle plumes. Nature Communications, 9(1), 854.

Konstantinovskaia, E. (2001). Arc–continent collision and subduction reversal in the Cenozoic evolution of the Northwest Pacific: an example from Kamchatka (NE Russia). Tectonophysics, 333(1-2), 75-94.

Koymans, M. R., Langereis, C. G., Pastor-Galán, D., & van Hinsbergen, D. J. J. (2016). Paleomagnetism. org: An online multi-platform open source environment for paleomagnetic data analysis. Computers & Geosciences, 93, 127-137.

Krebs, M., Maresch, W. V., Schertl, H. P., Münker, C., Baumann, A., Draper, G., et al. (2008). The dynamics of intra-oceanic subduction zones: A direct comparison between fossil petrological evidence (Rio San Juan Complex, Dominican Republic) and numerical simulation. Lithos, 103(1-2), 106-137.

Krebs, M., Schertl, H. P., Maresch, W. V., & Draper, G. (2011). Mass flow in serpentinite-hosted subduction channels: P–T–t path patterns of metamorphic blocks in the Rio San Juan mélange (Dominican Republic). Journal of Asian Earth Sciences, 42(4), 569-595.

Krijgsman, W., & Tauxe, L. (2006). E/I corrected paleolatitudes for the sedimentary rocks of the Baja British Columbia hypothesis. Earth and Planetary Science Letters, 242(1-2), 205-216.

Kroehler, M. E., Mann, P., Escalona, A., & Christeson, G. L. (2011). Late Cretaceous-Miocene diachronous onset of back thrusting along the South Caribbean deformed belt and its importance for understanding processes of arc collision and crustal growth. Tectonics, 30(6).

Kuijpers, E. P. (1980). The geologic history of the Nicoya Ophiolite Complex, Costa-Rica, and its geotectonic significance. Tectonophysics, 68(3-4), 233-255.

Labails, C., Olivet, J.-L., Aslanian, D., & Roest, W. R. (2010). An alternative early opening scenario for the Central Atlantic Ocean. Earth and Planetary Science Letters, 297(3-4), 355-368.

LaFemina, P., Dixon, T. H., Govers, R., Norabuena, E., Turner, H., Saballos, A., et al. (2009). Fore-arc motion and Cocos Ridge collision in Central America. Geochemistry, Geophysics, Geosystems, 10(5).

Lallemand, S., Heuret, A., & Boutelier, D. (2005). On the relationships between slab dip, back-arc stress, upper plate absolute motion, and crustal nature in subduction zones. Geochemistry, Geophysics, Geosystems, 6(9).

Laó-Dávila, D. A., Llerandi-Román, P. A., & Anderson, T. H. (2012). Cretaceous-Paleogene thrust emplacement of serpentinite in southwestern Puerto Rico. Geological Society of America Bulletin, 124(7-8), 1169-1190.

Lapierre, H., Ortiz, L. E., Abouchami, W., Monod, O., Coulon, C., & Zimmerman, J.-L. (1992). A crustal section of an intra-oceanic island arc: The Late Jurassic-Early Cretaceous Guanajuato magmatic sequence, central Mexico. Earth and Planetary Science Letters, 108, 61-77.

Larson, R. L., & Chase, C., G. (1972). Late Mesozoic Evolution of the Western Pacific Ocean. Geological Society of America Bulletin, 83, 3627-3644.

Larson, R. L., Menard, H., & Smith, S. (1968). Gulf of California: A result of ocean-floor spreading and transform faulting. Science, 161(3843), 781-784.

Larson, R. L., & Pitman, W. C. (1972). World-Wide Correlation of Mesozoic Magnetic Anomalies, and Its Implications. Geological Society of America Bulletin, 83, 3645-3662.

Larue, D. K. (1991). The Toa-Baja Drilling Project, Puerto-Rico - Scientific Drilling into a Non-Volcanic Island-Arc Massif. Geophysical Research Letters, 18(3), 489-492.

Lázaro, C., Blanco-Quintero, I. F., Rojas-Agramonte, Y., Proenza, J. A., Núñez-Cambra, K., & García-Casco, A. (2013). First description of a metamorphic sole related to ophiolite obduction in the northern Caribbean: Geochemistry and petrology of the Güira de Jauco Amphibolite complex (eastern Cuba) and tectonic implications. Lithos, 179, 193-210.

Lázaro, C., García-Casco, A., Rojas Agramonte, Y., Kröner, A., Neubauer, F., & Iturralde-Vinent, M. (2009). Fifty-five-million-year history of oceanic subduction and exhumation at the northern edge of the Caribbean plate (Sierra del Convento mélange, Cuba). Journal of Metamorphic Geology, 27(1), 19-40.

Leng, W., & Gurnis, M. (2011). Dynamics of subduction initiation with different evolutionary pathways. Geochemistry, Geophysics, Geosystems, 12(12).

Leroy, S., Mauffret, A., Patriat, P., & de Lepinay, B. M. (2000). An alternative interpretation of the Cayman trough evolution from a reidentification of magnetic anomalies. Geophysical Journal International, 141(3), 539-557.

Lewis, J., Amarante, A., Bloise, G., Jimenez, J., & Donminguez, H. (1991). Lithology and stratigraphy of upper Cretaceous volcanic, and volcanoclastic rocks of Tireo Group, Dominican Republic, and correlations with the Massif du Nord in Haiti. Geologic and tectonic development of the North America-Caribbean plate boundary in Hispaniola, Geological Society of America Special Paper. 262, 143–163.

Lewis, J., Draper, G., Espaillat, J., Proenza, J., & Jiménez, J. (2006). Ophiolite-related ultramafic rocks (serpentinites) in the Caribbean region: a review of their occurrence, composition, origin, emplacement and Ni-laterite soil formation. Geologica Acta: an international earth science journal, 4(1), 237-264.

Lewis, J. F., & Draper, G. (1990). Geology and tectonic evolution of the northern Caribbean margin. In C. A. Dengo & J. E. Case (Eds.), The Geology of North America, Vol. H, The Caribbean Region (pp. 77-140). Boulder, Colorado: Geological Society of America.

Lewis, J. F., Mattietti, G. K., Perfit, M., & Kamenov, G. (2011). Geochemistry and petrology of three granitoid rock cores from the Nicaraguan Rise, Caribbean Sea: implications for its composition, structure and tectonic evolution. Geologica Acta, 9(3-4), 467-479.

Li, S., Advokaat, E. L., van Hinsbergen, D. J., Koymans, M., Deng, C., & Zhu, R. (2017). Paleomagnetic constraints on the Mesozoic-Cenozoic paleolatitudinal and rotational history of Indochina and South China: Review and updated kinematic reconstruction. Earth-Science Reviews, 171, 58-77.

Lissinna, B., Hoernle, K., Hauff, F., van den Bogaard, P., & Sadofsky, S. (2006). The Panamanian island arc and Galápagos hotspot: A case study for the long-term evolution of arc/hotspot interaction.

Litherland, M., Aspden, J. A., & Jemielita, R. A. (1994). The metamorphic belts of Ecuador. British Geological Survey, overseas Memoir., 11.

Liu, L. (2014). Constraining Cretaceous subduction polarity in eastern Pacific from seismic tomography and geodynamic modeling. Geophysical Research Letters, 41(22), 8029-8036.

Liu, L., Gurnis, M., Seton, M., Saleeby, J., Müller, R. D., & Jackson, J. M. (2010). The role of oceanic plateau subduction in the Laramide orogeny. Nature Geoscience, 3(5), 353-357.

Liu, L., Spasojevic, S., & Gurnis, M. (2008). Reconstructing Farallon plate subduction beneath North America back to the Late Cretaceous. Science, 322(5903), 934-938.

Liu, L., & Stegman, D. R. (2011). Segmentation of the Farallon slab. Earth and Planetary Science Letters, 311(1-2), 1-10.

Llanes, A., García, D. E., & Meyerhoff, D. H. (1998). Hallazgo de fauna jurásica (Tithoniano) enofiolitas de Cuba central. Geología i Minería, Memórias, 2, 241-244.

Lonsdale, P. (1989). Geology and tectonic history of the Gulf of California. The eastern Pacific Ocean and Hawaii: Boulder, Colorado, Geological Society of America, Geology of North America, v. N, 499-521.

Lonsdale, P., Blum, N., & Puchelt, H. (1992). The Rrr Triple Junction at the Southern End of the Pacific-Cocos East Pacific Rise. Earth and Planetary Science Letters, 109(1-2), 73-85.

Lu, C., & Grand, S. P. (2016). The effect of subducting slabs in global shear wave tomography. Geophysical Journal International, 205(2), 1074-1085.

Luyendyk, B., & Hornafius, J. (1982). Paleolatitude of the Point Sal ophiolite. Paper presented at the Geological Society of America Abstracts with Programs.

Ma, Y., Yang, T., Yang, Z., Zhang, S., Wu, H., Li, H., et al. (2014). Paleomagnetism and U-Pb zircon geochronology of Lower Cretaceous lava flows from the western Lhasa terrane: New constraints on the India-Asia collision process and intracontinental deformation within Asia. Journal of Geophysical Research: Solid Earth, 119(10), 7404-7424.

MacDonald, K. C., & Holcombe, T. L. (1978). Inversion of magnetic anomalies and sea-floor spreading in the Cayman Trough. Earth and Planetary Science Letters, 40(407-414).

MacDonald, W., Estrada, J., Sierra, G., & González, H. (1996). Late Cenozoic tectonics and paleomagnetism of North Cauca Basin intrusions, Colombian Andes: dual rotation modes. Tectonophysics, 261(4), 277-289.

MacDonald, W. D. (1980). Anomalous paleomagnetic directions in Late Tertiary andesitic intrusions of the Cauca depression, Colombian Andes. Tectonophysics, 68(3-4), 339-348.

MacGillavry, H. J. (1937). Geology of the province of Camaguey, Cuba: with revisional studies in rudist paleontology (mainly based upon collections from Cuba).

Madrigal, P., Gazel, E., Denyer, P., Smith, I., Jicha, B., Flores, K. E., et al. (2015). A melt-focusing zone in the lithospheric mantle preserved in the Santa Elena Ophiolite, Costa Rica. Lithos, 230, 189-205.

Madrigal, P., Gazel, E., Flores, K. E., Bizimis, M., & Jicha, B. (2016). Record of massive upwellings from the Pacific large low shear velocity province. Nature Communications, 7, 13309.

Maffione, M., Hinsbergen, D. J., Gelder, G. I., Goes, F. C., & Morris, A. (2017). Kinematics of Late Cretaceous subduction initiation in the Neo-Tethys Ocean reconstructed from ophiolites of Turkey, Cyprus, and Syria. Journal of Geophysical Research: Solid Earth, 122(5), 3953-3976.

Maffione, M., Thieulot, C., van Hinsbergen, D. J. J., Morris, A., Plümper, O., & Spakman, W. (2015a). Dynamics of intraoceanic subduction initiation: 1. Oceanic detachment fault inversion and the formation of supra-subduction zone ophiolites. Geochemistry, Geophysics, Geosystems, 16(6), 1753-1770.

Maffione, M., & van Hinsbergen, D. J. (2018a). Reconstructing Plate Boundaries in the Jurassic Neo-Tethys From the East and West Vardar Ophiolites (Greece and Serbia). Tectonics, 37(3), 858-887.

Maffione, M., & van Hinsbergen, D. J. (2018b). Reconstructing Plate Boundaries in the Jurassic Neo-Tethys From the East and West Vardar Ophiolites (Greece and Serbia). Tectonics.

Maffione, M., Van Hinsbergen, D. J., Koornneef, L. M., Guilmette, C., Hodges, K., Borneman, N., et al. (2015b). Forearc hyperextension dismembered the south Tibetan ophiolites. Geology, 43(6), 475-478.

Mann, P. (1997). Model for the formation of large, transtensional basins in zones of tectonic escape. Geology, 25(3).

Mann, P., & Burke, K. (1984a). Cenozoic rift formation in the northern Caribbean. Geology, 12(12).

Mann, P., & Burke, K. (1984b). Neotectonics of the Caribbean. reviews of Geophysics and Space Physics, 22(4), 309-362.

Mann, P., & Burke, K. (1990). Transverse intra-arc rifting: Palaeogene Wagwater Belt, Jamaica. Marine and Petroleum Geology, 7, 410-427.

Mann, P., Burke, K., & Matumoto, T. (1984). Neotectonics of Hispaniola - Plate Motion, Sedimentation, and Seismicity at a Restraining Bend. Earth and Planetary Science Letters, 70(2), 311-324.

Mann, P., Calais, E., Ruegg, J.-C., DeMets, C., Jansma, P. E., & Mattioli, G. S. (2002). Oblique collision in the northeastern Caribbean from GPS measurements and geological observations. Tectonics, 21(6), 7-1-7-26.

Mann, P., Demets, C., & Wiggins-Grandison, M. (2007). Toward a better understanding of the Late Neogene strike-slip restraining bend in Jamaica: geodetic, geological, and seismic constraints. Geological Society, London, Special Publications, 290(1), 239-253.

Mann, P., Draper, G., & Lewis, J. F. (1991). An overview of the geologic and tectonic development of Hispaniola. In Geologic and tectonic development of the North America-Caribbean plate boundary in Hispaniola (pp. 1-28).

Mann, P., Prentice, C. S., Hippolyte, J.-C., Grindlay, N. R., Abrams, L. J., & Laó-Dávila, D. (2005). Reconnaissance study of Late Quaternary faulting along Cerro Goden fault zone, western Puerto Rico. Active Tectonics and Seismic Hazards of Puerto Rico, the Virgin Islands, and Offshore Areas, 385, 115-138.

Mann, P., Taylor, F., Edwards, R. L., & Ku, T.-L. (1995). Actively evolving microplate formation by oblique collision and sideways motion along strike-slip faults: An example from the northeastern Caribbean plate margin. Tectonophysics, 246(1-3), 1-69.

Marchesi, C., Garrido, C. J., Bosch, D., Proenza, J. A., Gervilla, F., Monie, P., & Rodriguez-Vega, A. (2007). Geochemistry of Cretaceous Magmatism in Eastern Cuba: Recycling of North American Continental Sediments and Implications for Subduction Polarity in the Greater Antilles Paleo-arc. Journal of Petrology, 48(9), 1813-1840.

Maresch, W. (1975). The geology of northeastern Margarita Island, Venezuela: A contribution to the study of Caribbean plate margins. Geologische Rundschau, 64(1), 846-883.

Maresch, W. V., Kluge, R., Baumann, A., Pindell, J. L., Krückhans-Lueder, G., & Stanek, K. (2009). The occurrence and timing of high-pressure metamorphism on Margarita Island, Venezuela: a constraint on Caribbean-South America interaction. Geological Society, London, Special Publications, 328(1), 705-741.

Mariko, T. (1984). Sub-sea hydrothermal alteration of basalt, diabase and sedimentary rocks in the Shimokawa copper mining area, Hokkaido, Japan. Mining Geology, 34(187), 307-321.

Mariko, T., & Kato, Y. (1994). Host Rock Geochemistry and Tectonic Setting of Some Volcanogenic Massive Sulfide Deposits in Japan. Shigen-Chishitsu, 44(247), 353-367.

Markey, R. (Cartographer). (1995). Mapa Geológica de Honduras, Hoja de Moroceli (Geologic Map of Honduras, Morocelli sheet): Tegucigalpa, Honduras, Instituto Geográfico Nacional, escala 1:50,000.

Martens, U. C., Brueckner, H. K., Mattinson, C. G., Liou, J. G., & Wooden, J. L. (2012). Timing of eclogite-facies metamorphism of the Chuacús complex, Central Guatemala: Record of Late Cretaceous continental subduction of North America's sialic basement. Lithos, 146-147, 1-10.

Martini, M., Ferrari, L., Lopez-Martinez, M., Cerca-Martinez, M., Valencia, V. A., & Serrano-Duran, L. (2009). Cretaceous-Eocene magmatism and Laramide deformation in southwestern Mexico: No role for terrane accretion. Geological Society of America Memoirs, 204(0), 151-182.

Martini, M., Mori, L., Solari, L., & Centeno-García, E. (2011). Sandstone Provenance of the Arperos Basin (Sierra de Guanajuato, Central Mexico): Late Jurassic–Early Cretaceous Back-Arc Spreading as the Foundation of the Guerrero Terrane. The Journal of Geology, 119(6), 597-617.

Martini, M., Solari, L., & López-Martínez, M. (2014). Correlating the Arperos Basin from Guanajuato, central Mexico, to Santo Tomás, southern Mexico: Implications for the paleogeography and origin of the Guerrero terrane. Geosphere, 10(6), 1385-1401.

Maruyama, S., Isozaki, Y., Kimura, G., & Terabayashi, M. (1997). Paleogeographic maps of the Japanese Islands: plate tectonic synthesis from 750 Ma to the present. Island Arc, 6(1), 121-142.

Maruyama, S., & Seno, T. (1986). Orogeny and relative plate motions: example of the Japanese Islands. Tectonophysics, 127(3-4), 305-329.

Masaferro, J. L., Bulnes, M., Poblet, J., & Eberli, G. P. (2002). Episodic folding inferred from syntectonic carbonate sedimentation: the Santaren anticline, Bahamas foreland. Sedimentary Geology, 146(1-2), 11-24.

Matsuda, T., & Isozaki, Y. (1982). Radiolarians around the Triassic-Jurassic boundary from the bedded chert in the Kamiaso area, Southwest Japan. Appendix:" Anisian" radiolarians. News of Osaka Micropaleont., Special Volume, 5, 93-101.

Matsuda, T., & Isozaki, Y. (1991). Well-Documented Travel History of Mesozoic Pelagic Chert in Japan - from Remote Ocean to Subduction Zone. Tectonics, 10(2), 475-499.

Matsumoto, T. (1978). Japan and adjoining areas. Mesozoic A, 79-144.

Matsuoka, A. (1992). Jurassic and Early Cretaceous radiolarians from ODP Leg 129, Sites 800 and 801, western Pacific ocean. Proceedings of the Ocean Drilling Program, Scientific results, College Station, TX, USA, 1992, 129, 203-220.

Matsuoka, A. (1995). Jurassic and Lower Cretaceous radiolarian zonation in Japan and in the western Pacific. Island Arc, 4(2), 140-153.

Mattei, M., Muttoni, G., & Cifelli, F. (2014). A record of the Jurassic massive plate shift from the Garedu Formation of central Iran. Geology, 42(6), 555-558.

Mattinson, J. M., Pessagno, E. A., Montgomery, H., & Hopson, C. A. (2008). Late Jurassic age of oceanic basement at La Désirade Island, Lesser Antilles arc. In Special Paper 438: Ophiolites, Arcs, and Batholiths: A Tribute to Cliff Hopson (pp. 175-190).

Mattioli, G., Miller, J., DeMets, C., & Jansma, P. (2014). Rigidity and definition of Caribbean plate motion from COCONet and campaign GPS observations. Paper presented at the EGU General Assembly Conference Abstracts.

Mauffret, A., & Leroy, S. (1997). Seismic stratigraphy and structure of the Caribbean igneous province. Tectonophysics, 283(1-4), 61-104.

Maurrasse, F., Husler, J., Georges, G., Schmitt, R., & Damond, P. (1979). Upraised Caribbean sea floor below acoustic reflector B" at the Southern Peninsula of Haiti. Geol. Mijnbouw, 8, 71-83.

Maya-Sánchez, M. (2001). Distribución, Facies y Edad de las Rocas Metamórficas en Colombia, Memoria Explicitiva: Mapa metamorfico de Colombia. Instituto Colombiano de Minería y Geología, Bogotá.

Maya-Sánchez, M., & Vásquez-Arroyave, E. (2001). Mapa metamorfico de Colombia (Scale 1: 2 000 000). In: Instituto Colombiano de Minería y Geología, Bogota.

McCann, W. R., & Sykes, L. R. (1984). Subduction of aseismic ridges beneath the Caribbean plate: Implications for the tectonics and seismic potential of the northeastern Caribbean. Journal of Geophysical Research: Solid Earth, 89(B6), 4493-4519.

McCourt, W., Aspden, J., & Brook, M. (1984). New geological and geochronological data from the Colombian Andes: continental growth by multiple accretion. Journal of the Geological Society, 141(5), 831-845.

McFadden, P. L., & McElhinny, M. W. (1988). The combined analysis of remagnetization circles and direct observations in palaeomagnetism. Earth and Planetary Science Letters, 87, 161-172.

McFarlane, N. (1977). Geological map of Jamaica–1: 250,000. Ministry of Mining and Natural Resources: Kingston.

McKenzie, D. P., & Morgan, W. J. (1969). Evolution of triple junctions. Nature, 224, 125-133.

McQuarrie, N., & Wernicke, B. P. (2005). An animated tectonic reconstruction of southwestern North America since 36 Ma. Geosphere, 1(3).

McWilliams, M., & Howell, D. (1982). Exotic terranes of western California. Nature, 297(5863), 215-217.

Meijers, M. J., Langereis, C. G., van Hinsbergen, D. J., Kaymakcı, N., Stephenson, R. A., & Altıner, D. (2010a). Jurassic–Cretaceous low paleolatitudes from the circum-Black Sea region (Crimea and Pontides) due to True Polar Wander. Earth and Planetary Science Letters, 296(3-4), 210-226.

Meijers, M. J. M., Hamers, M. F., van Hinsbergen, D. J. J., van der Meer, D. G., Kitchka, A., Langereis, C. G., & Stephenson, R. A. (2010b). New late Paleozoic paleopoles from the Donbas Foldbelt (Ukraine): Implications for the Pangea A vs. B controversy. Earth and Planetary Science Letters, 297(1-2), 18-33.

Menard, H. W. (1978). Fragmentation of the Farallon Plate by pivoting subduction. Journal of Geology, 86, 99-110.

Mendoza, O. T., & Suastegui, M. G. (2000). Geochemistry and isotopic composition of the Guerrero Terrane (western Mexico): implications for the tectono-magmatic evolution of southwestern North America during the Late Mesozoic. Journal of South American Earth Sciences, 13(4-5), 297-324.

Meschede, M., & Frisch, W. (1998). A plate-tectonic model for the Mesozoic and Early Cenozoic history of the Caribbean plate. Tectonophysics, 296(3-4), 269-291.

Metcalf, R. V., & Shervais, J. W. (2008). Suprasubduction-zone ophiolites: Is there really an ophiolite conundrum? Geological Society of America Special Papers, 438, 191-222.

Meyerhoff, A., & Hatten, C. (1968). Diapiric structures in central Cuba. AAPG Memoir., 8, 315–357.

Meyerhoff, A., & Hatten, C. (1974). Bahamas salient of North America: tectonic framework, stratigraphy, and petroleum potential. AAPG Bulletin, 58(6), 1201-1239.

Millán, G. (1996). Metamorfitas de la asociación ofiolítica de Cuba. In Ofiolitas y arcos volcánicos de Cuba, IGCP project 364 (pp. 131-146).

Millán, G. (1997). Geología del macizo metamórfico del Escambray. Estudios sobre Geología de Cuba. La Habana, Cuba, Centro Nacional de Información Geológica, 271-288.

Millán, G., & Somin, M. L. (1985). Contribución al conocimiento geológico de las metamorfitas del Escambray y del Purial: Academia de Ciencias de Cuba.

Miller, D., Nilsen, T., & Bilodeau, W. (1992). Late Cretaceous to early Eocene geologic evolution of the US Cordillera. The Geology of North America, 3, 205-260.

Miller, M. S., Gorbatov, A., & Kennett, B. (2005). Heterogeneity within the subducting Pacific slab beneath the Izu–Bonin–Mariana arc: Evidence from tomography using 3D ray tracing inversion techniques. Earth and Planetary Science Letters, 235(1-2), 331-342.

Millward, D., Marriner, G., & Saunders, A. (1984). Cretaceous tholeiitic volcanic rocks from the Western Cordillera of Colombia. Journal of the Geological Society, 141(5), 847-860.

Minato, M., & Rowett, C. (1967). New Paleozoic fossils from southern Hokkaido, Japan. Journal of the Faculty of Science, Hokkaido University. Series 4, Geology and mineralogy, 13(4), 321-332.

Minch, J. C., Gastil, G., Fink, W., Robinson, J., & James, A. H. (1976). Geology of the Vizcaino Peninsula.

Minoura, N., & Kato, M. (1978). Permian Calcareous Algae Found in the Matsumae Group, Matsumae Peninsula, Southwestern Hokkaido. Journal of the Faculty of Science, Hokkaido University. Series 4, Geology and mineralogy, 18(3), 377-383.

Mitchell, S. F. (2006). Timing and implications of Late Cretaceous tectonic and sedimentary events in Jamaica. Geologica Acta, 4(1-2), 171-178.

Miyashita, S., & Katsushima, T. (1986). The Tomuraushi greenstone complex of the central Hidaka zone: Contemporaneous occurrence of abyssal tholeiite and terrigenous sediments. Journal of the Geological Society of Japan, 92(8), 535-557.

Miyashita, S., & Yoshida, A. (1994). Geology and petrology of the Shimokawa ophiolite (Hokkaido, Japan): ophiolite possibly generated near RTT triple junction. Paper presented at the Circum Pacific Ophiolite, Proc. 29th IGC Ophiolite Symposium, Part D, VSP Pub., Netherlands.

Moix, P., Beccaletto, L., Kozur, H. W., Hochard, C., Rosselet, F., & Stampfli, G. M. (2008). A new classification of the Turkish terranes and sutures and its implication for the paleotectonic history of the region. Tectonophysics, 451(1), 7-39.

Molina Garza, R. S., van Hinsbergen, D. J., Boschman, L. M., Rogers, R. D., & Ganerød, M. (2017). Large-scale rotations of the Chortis Block (Honduras) at the southern termination of the Laramide flat slab. Tectonophysics, doi: 10.1016/j.tecto.2017.11.026

Molina Garza, R. S., van Hinsbergen, D. J., Rogers, R. D., Ganerød, M., & Dekkers, M. J. (2012). The Padre Miguel Ignimbrite Suite, central Honduras: paleomagnetism, geochronology, and tectonic implications. Tectonophysics, 574, 144-157.

Molnar, P., & Sykes, L. R. (1969). Tectonics of the Caribbean and Middle America regions from focal mechanisms and seismicity. Geological Society of America Bulletin, 80(9), 1639-1684.

Monger, J., & Price, R. (2002). The Canadian Cordillera: geology and tectonic evolution. CSEG Recorder, 27(2), 17-36.

Monger, J. W. H., Price, R. A., & Tempelman-Kluit, D. J. (1982). Tectonic accretion and the origin of the two major metamorphic and plutonic welts in the Canadian Cordillera. Geology, 10(2), 70-75.

Monod, O., & Calvet, P. (1991). Structural and stratigraphic reinterpretation of the Triassic units near Zacatecas, Zac., Central Mexico: Evidence of a Laramide nappe pile. Zentralblatt für Geologie und Palaeontologie, Teil I: Allgemeine, Angewandte: Regionale und Historische Geologie(1), 1533-1544.

Montes, C., Bayona, G., Cardona, A., Buchs, D. M., Silva, C., Morón, S., et al. (2012). Arc-continent collision and orocline formation: Closing of the Central American seaway. Journal of Geophysical Research: Solid Earth, 117(B4).

Montes, C., Guzman, G., Bayona, G., Cardona, A., Valencia, V., & Jaramillo, C. (2010). Clockwise rotation of the Santa Marta massif and simultaneous Paleogene to Neogene deformation of the Plato-San Jorge and Cesar-Ranchería basins. Journal of South American Earth Sciences, 29(4), 832-848.

Moore, T. E. (1983). Geology, petrology, and tectonic significance of the Mesozoic paleooceanic terranes of the Vizcaíno peninsula, Baja California Sur, Mexico. PhD Thesis, Stanford University, Stanford, California.

Moore, T. E. (1984). Sedimentary facies and composition of Jurassic volcaniclastic turbidites at Cerro El Calvario, Vizcaino Peninsula, Baja California Sur, Mexico. In V. A. J. Frizzell (Ed.), Geology of the Baja California Peninsula (Vol. 39, pp. 131-147): Pacifc Section S.E.P.M.

Moore, T. E. (1985). Stratigraphic and tectonic significance of the Mesozoic tectonostratigraphic terranes of the Vizcaíno peninsula, Baja California Sur, Mexico. In D. G. Howell (Ed.), Tectonostratigraphic terranes of the circum-Pacific region (pp. 315-329). Houston, Texas: Circum-Pacific Council for Energy and Mineral Resources.

Moore, T. E. (1986). Petrology and tectonic implications of the blueschist-bearing Puerto Nuevo melange complex, Vizcaino Peninsula, Baja California Sur, Mexico Geological Society of America Memoirs, 164, 43-58.

Morán-Zenteno, D. J., Cerca, M., & Keppie, J. D. (2007). The Cenozoic tectonic and magmatic evolution of southwestern México: Advances and problems of interpretation. In Special Paper 422: Geology of México: Celebrating the Centenary of the Geological Society of México (pp. 71-91).

Mortensen, J. K., Hall, B. V., Bissig, T., Friedman, R. M., Danielson, T., Oliver, J., et al. (2008). Age and paleotectonic setting of volcanogenic massive sulfide deposits in the Guerrero terrane of central Mexico: Constraints from U-Pb age and Pb isotope studies. Economic Geology, 103(1), 117-140.

Mortimer, N. (2004). New Zealand's Geological Foundations. Gondwana Research, 7(1), 261-272.

Mortimer, N., Rattenbury, M. S., King, P. R., Bland, K. J., Barrell, D. J. A., Bache, F., et al. (2014). High-level stratigraphic scheme for New Zealand rocks. New Zealand Journal of Geology and Geophysics, 57(4), 402-419.

Mullender, T. A., Frederichs, T., Hilgenfeldt, C., de Groot, L. V., Fabian, K., & Dekkers, M. J. (2016). Automated paleomagnetic and rock magnetic data acquisition with an in-line horizontal "2G" system. Geochemistry, Geophysics, Geosystems, 17(9), 3546-3559.

Mullender, T. A. T., Vanvelzen, A. J., & Dekkers, M. J. (1993). Continuous Drift Correction and Separate Identification of Ferrimagnetic and Paramagnetic Contributions in Thermomagnetic Runs. Geophysical Journal International, 114(3), 663-672.

Müller, R. D., Royer, J.-Y., Cande, S. C., Roest, W. R., & Maschenkov, S. (1999). New constraints on the Late Cretaceous/Tertiary plate tectonic evolution of the Caribbean. In Sedimentary Basins of the World (Vol. 4, pp. 33-59): Elsevier.

Müller, R. D., Sdrolias, M., Gaina, C., & Roest, W. R. (2008a). Age, spreading rates, and spreading asymmetry of the world's ocean crust. Geochemistry, Geophysics, Geosystems, 9(4).

Müller, R. D., Sdrolias, M., Gaina, C., Steinberger, B., & Heine, C. (2008b). Long-term sea-level fluctuations driven by ocean basin dynamics. Science, 319(5868), 1357-1362.

Müller, R. D., Seton, M., Zahirovic, S., Williams, S. E., Matthews, K. J., Wright, N. M., et al. (2016). Ocean basin evolution and global-scale plate reorganization events since Pangea breakup. Annual Review of Earth and Planetary Sciences, 44, 107-138.

Muttoni, G., Erba, E., Kent, D. V., & Bachtadse, V. (2005). Mesozoic Alpine facies deposition as a result of past latitudinal plate motion. Nature, 434(7029), 59.

Nakayama, K. (2003). Internal structure of the Shimokawa greenstone-argillaceous sediment complex. Reconstruction of the paleo-sedimented spreading center. Shigen-Chishitsu, 53(1), 81-94.

Neill, I., Gibbs, J. A., Hastie, A. R., & Kerr, A. C. (2010). Origin of the volcanic complexes of La Désirade, Lesser Antilles: Implications for tectonic reconstruction of the Late Jurassic to Cretaceous Pacific-proto Caribbean margin. Lithos, 120(3-4), 407-420.

Neill, I., Kerr, A. C., Chamberlain, K. R., Schmitt, A. K., Urbani, F., Hastie, A. R., et al. (2014). Vestiges of the proto-Caribbean seaway: origin of the San Souci Volcanic Group, Trinidad. Tectonophysics, 626, 170-185.

Neill, I., Kerr, A. C., Hastie, A. R., Pindell, J. L., & Millar, I. L. (2013). The Albian–Turonian Island Arc Rocks of Tobago, West Indies: Geochemistry, Petrogenesis, and Caribbean Plate Tectonics. Journal of Petrology, 54(8), 1607-1639.

Neill, I., Kerr, A. C., Hastie, A. R., Pindell, J. L., Millar, I. L., & Atkinson, N. (2012). Age and Petrogenesis of the Lower Cretaceous North Coast Schist of Tobago, a Fragment of the Proto–Greater Antilles Inter-American Arc System. The Journal of Geology, 120(4), 367-384.

Neill, I., Kerr, A. C., Hastie, A. R., Stanek, K. P., & Millar, I. L. (2011). Origin of the Aves Ridge and Dutch-Venezuelan Antilles: interaction of the Cretaceous 'Great Arc' and Caribbean-Colombian Oceanic Plateau? Journal of the Geological Society, 168(2), 333-348.

Niida, K., & Kito, N. (1986). Cretaceous arc-trench systems in Hokkaido. Monograph of the Association of Geological Collaboration, Japan, 31, 379-402.

Nivia, A., Marriner, G. F., Kerr, A. C., & Tarney, J. (2006). The Quebradagrande Complex: A Lower Cretaceous ensialic marginal basin in the Central Cordillera of the Colombian Andes. Journal of South American Earth Sciences, 21(4), 423-436.

Noble, S. R., Aspden, J. A., & Jemielita, R. (1997). Northern Andean crustal evolution: New U-Pb geochronological constraints from Ecuador. Geological Society of America Bulletin, 109(7), 789-798.

Nokleberg, W. J. (2000). Phanerozoic Tectonic Evolution of the Circum-North Pacific. Denver: U.S. Dept. of the Interior, U.S. Geological Survey.

O'Neill, C., Müller, D., & Steinberger, B. (2005). On the uncertainties in hot spot reconstructions and the significance of moving hot spot reference frames. Geochemistry, Geophysics, Geosystems, 6(4), Q04003.

Obrebski, M., Allen, R. M., Xue, M., & Hung, S. H. (2010). Slab-plume interaction beneath the Pacific Northwest. Geophysical Research Letters, 37(14).

Oda, H., & Suzuki, H. (2000). Paleomagnetism of Triassic and Jurassic red bedded chert of the Inuyama area, central Japan. Journal of Geophysical Research: Solid Earth, 105(B11), 25743-25767.

Oliver, P. (1994). The tectonic significance of paleomagnetic results from the Triassic and Jurassic Murihiku sedimentary rocks of the Kawhia region, North Island, New Zealand. Paper presented at the Evolution of the Tasman Sea basin: proceedings of the Tasman Sea conference. Rotterdam: Balkema.

Ortega-Gutiérrez, F., Solari, L. A., Ortega-Obregón, C., Elías-Herrera, M., Martens, U., Morán-Icál, S., et al. (2007). The Maya-Chortís Boundary: A Tectonostratigraphic Approach. International Geology Review, 49(11), 996-1024.

Ortega-Obregon, C., Solari, L. A., Keppie, J. D., Ortega-Gutierrez, F., Sole, J., & Moran-Ical, S. (2008). Middle-Late Ordovician magmatism and Late Cretaceous collision in the southern Maya block, Rabinal-Salama area, central Guatemala: Implications for North America-Caribbean plate tectonics. Geological Society of America Bulletin, 120(5-6), 556-570.

Ozawa, M. (2018) Eruption and accretion process of oceanic volcanoes in the Iwashimizu complex, Shizunami and Mitsuishi area, Hokkaido, Japan. MSc Thesis, Niigata University

Ota, A., & Isozaki, Y. (2006). Fusuline biotic turnover across the Guadalupian–Lopingian (Middle–Upper Permian) boundary in mid-oceanic carbonate buildups: biostratigraphy of accreted limestone in Japan. Journal of Asian Earth Sciences, 26(3-4), 353-368.

Pardo, G. (1975). Geology of Cuba. In A. E. M. Nairn & F. G. Stehi (Eds.), The Ocean Basins and Margins (pp. 553-615). New York: Plenum Press.

Patriat, P., & Courtillot, V. (1984). On the Stability of Triple Junctions and Its Relation to Episodicity in Spreading. Tectonics, 3(3), 317-332.

Patterson, D. L. (1984). Paleomagnetism of the Valle Formation and the Late Cretaceous paleogeography of the Vizcaino Basin, Baja California, Mexico. In V. A. J. Frizzell (Ed.), Geology of the Baja California Peninsula (Vol. Pacific Section S.E.P.M. 39, pp. 173-182).

Pennington, W. D. (1981). Subduction of the eastern Panama Basin and seismotectonics of northwestern South America. Journal of Geophysical Research: Solid Earth, 86(B11), 10753-10770.

Perfit, M. R., & Heezen, B. C. (1978). The geology and evolution of the Cayman Trench. Geological Society of America Bulletin, 89(8), 1155-1174.

Pessagno, E. A., Finch, W., & Abbott, P. L. (1979). Upper Triassic Radiolaria from the San Hipolito Formation, Baja California. Micropaleontology, 160-197.

Phipps Morgan, J., Ranero, C. R., & Vannucchi, P. (2008). Intra-arc extension in Central America: Links between plate motions, tectonics, volcanism, and geochemistry. Earth and Planetary Science Letters, 272(1-2), 365-371.

Pindell, J. L. (1985). Alleghenian Reconstruction and Subsequent Evolution of the Gulf of Mexico, Bahamas, and Proto-Caribbean. Tectonics, 4(1), 1-39.

Pindell, J. L., & Barrett, S. F. (1990). Geologic evolution of the Caribbean region: a plate-tectonic perspective. Vol. H, The Caribbean Region(Geological Society of America), 405-432.

Pindell, J. L., Cande, S. C., Pitman, W. C., Rowley, D. B., Dewey, J. F., Labrecque, J., & Haxby, W. (1988). A Plate-Kinematic Framework for Models of Caribbean Evolution. Tectonophysics, 155(1-4), 121-138.

Pindell, J. L., Higgs, R., & Dewey, J. F. (1998). Cenozoic palinspastic reconstruction, paleogeographic evolution and hydrocarbon setting of the northern margin of South America. SEPM Special Publication, 58, 45-85.

Pindell, J. L., & Kennan, L. (2007). Cenozoic Caribbean-South American tectonic interaction: A case for prism-prism collision in eastern Venezuela, Trinidad and Barbados. In L. Kennan, J. L. Pindell, & N. Rosen (Eds.), Proceedings, 27th GCSSEPM Bob F. Perkins Research Conference (pp. 458–553). Houston.

Pindell, J. L., & Kennan, L. (2009). Tectonic evolution of the Gulf of Mexico, Caribbean and northern South America in the mantle reference frame: an update. Geological Society, London, Special Publications, 328(1), 1.1-55.

Pindell, J. L., Kennan, L., Maresch, W. V., Stanek, K.-P., Draper, G., & Higgs, R. (2005). Plate-kinematics and crustal dynamics of circum-Caribbean arc-continent interactions: Tectonic controls on basin development in Proto-Caribbean margins. In Special Paper 394: Caribbean-South American plate interactions, Venezuela (pp. 7-52).

Pindell, J. L., Kennan, L., Stanek, K. P., Maresch, W. V., & Draper, G. (2006). Foundations of Gulf of Mexico and Caribbean evolution: eight controversies resolved. Geologica Acta, 4(1-2), 303-341.

Pindell, J. L., Maresch, W. V., Martens, U., & Stanek, K. (2012). The Greater Antillean Arc: Early Cretaceous origin and proposed relationship to Central American subduction mélanges: implications for models of Caribbean evolution. International Geology Review, 54(2), 131-143.

Pinet, B., Lajat, D., Le Quellec, P., & Bouysse, P. (1985). Structure of Aves Ridge and Grenada Basin from multichannel seismic data. Paper presented at the Géodynamique des caraïbes. Symposium.

Pons, J. M., Vicens, E., & Schmidt-Effing, R. (2016). Campanian rudists (Hippuritida, Bivalvia) from Costa Rica (Central America). Journal of Paleontology, 90(2), 211-238.

Pozzi, J., Westphal, M., Girardeau, J., Besse, J., Zhou, Y. X., Chen, X. Y., & Xing, L. S. (1984). Paleomagnetism of the Xigaze ophiolite and flysch (Yarlung Zangbo suture zone, southern Tibet): latitude and direction of spreading. Earth and Planetary Science Letters, 70(2), 383-394.

Premo, W. R., Morton, D. M., Wooden, J. L., & Fanning, C. M. (2014). U-Pb zircon geochronology of plutonism in the northern Peninsular Ranges batholith, southern California: Implications for the Late Cretaceous tectonic evolution of southern California. In Peninsular Ranges Batholith, Baja California and Southern California (pp. 145-180).

Premoli Silva, I., & Verga, D. (2004). Practical manual of Cretaceous planktonic foraminifera. International school on planktonic foraminifera, 3rd course: Cretaceous. Universities of Perugia and Milan, Tiporafia Pontefelcino, Perugia (Italy), 283.

Prentice, C. S., Mann, P., Crone, A. J., Gold, R. D., Hudnut, K. W., Briggs, R. W., et al. (2010). Seismic hazard of the Enriquillo–Plantain Garden fault in Haiti inferred from palaeoseismology. Nature Geoscience, 3(11), 789-793.

Pszczkowski, A., & Myczyski, R. (2003). Stratigraphic constraints on the Late Jurassic–Cretaceous paleotectonic interpretations of the Placetas belt in Cuba. In C. Bartolini, R. T. Buffler, & J. Blickwede (Eds.), The Circum-Gulf of Mexico and the Caribbean: Hydrocarbon Habitats, Basin Formation, and Plate Tectonics. AAPG Memoir 79 (pp. 545-581).

Ranero, C. R., von Huene, R., Flueh, E., Duarte, M., Baca, D., & McIntosh, K. (2000). A cross section of the convergent Pacific margin of Nicaragua. Tectonics, 19(2), 335-357.

Rangin, C. (1978). Speculative model of Mesozoic geodynamics, central Baja California to northeastern Sonora (Mexico). In Mesozoic Paleogeography of the Western United States: Pacific Section S.E.P.M.

Rangin, C., Girard, D., & Maury, R. (1983). Geodynamic significance of Late Triassic to Early Cretaceous volcanic sequences of Vizcaino Peninsula and Cedlros Island, Baja California, Mexico. Geology, 11, 552-556.

Ranson, W. A., Fernández, L. A., Simmons Jr, W. B., & de la Vega, S. E. (1982). Petrology of the metamorphic rocks of Zacatecas, Zac., Mexico. Boletín de la Sociedad Geológica Mexicana, 37-59.

Ratschbacher, L., Franz, L., Min, M., Bachmann, R., Martens, U., Stanek, K., et al. (2009). The North American-Caribbean Plate boundary in Mexico-Guatemala-Honduras. Geological Society, London, Special Publications, 328(1), 219-293.

Reid, J. A., Plumley, P. W., & Schellekens, J. (1991). Paleomagnetic evidence for late Miocene counterclockwise rotation of north coast carbonate sequence, Puerto Rico. Geophysical Research Letters, 18(3), 565-568.

Renne, P. R., Mattinson, J. M., Hatten, C. W., Somin, M., Onstott, T. C., Millán, G., & Linares, E. (1989). 40 Ar/39 Ar and U-Pb evidence for Late Proterozoic (Grenville-age) continental crust in North-Central Cuba and regional tectonic implications. Precambrian Research, 42(3), 325-341.

Renne, P. R., Scott, G. R., Doppelhammer, S. K., Cala, E. L., & Hargraves, R. B. (1991). Discordant mid-Cretaceous paleomagnetic pole from the Zaza Terrane of central Cuba. Geophysical Research Letters, 18(3), 455-458.

Restrepo-Pace, P. (1992). Petrotectonic characterization of the central Andean terrane, Colombia. Journal of South American Earth Sciences, 5(1), 97-116.

Restrepo-Pace, P. A., Ruiz, J., Gehrels, G., & Cosca, M. (1997). Geochronology and Nd isotopic data of Grenville-age rocks in the Colombian Andes: new constraints for Late Proterozoic-Early Paleozoic paleocontinental reconstructions of the Americas. Earth and Planetary Science Letters, 150(3-4), 427-441.

Retallack, G. (1987). Triassic vegetation and geography of the New Zealand portion of the Gondwana supercontinent. Monograph by the American Geophysical Union, Washington, District of Columbia, USA.

Révillon, S., Hallot, E., Arndt, N., Chauvel, C., & Duncan, R. (2000). A complex history for the Caribbean Plateau: petrology, geochemistry, and geochronology of the Beata Ridge, South Hispaniola. The Journal of Geology, 108(6), 641-661.

Ritsema, J., Deuss, A., van Heijst, H. J., & Woodhouse, J. H. (2011). S40RTS: a degree-40 shear-velocity model for the mantle from new Rayleigh wave dispersion, teleseismic traveltime and normal-mode splitting function measurements. Geophysical Journal International, 184(3), 1223-1236.

Robinson, E. (1994). Jamaica. In S. Donovan & T. Jackson (Eds.), Caribbean Geology: An Introduction (pp. 111-128). Kingston, Jamaica: University of the West Indies Publishers' Association.

Rockwell, T., Gath, E., González, T., Madden, C., Verdugo, D., Lippincott, C., et al. (2010). Neotectonics and paleoseismology of the Limón and Pedro Miguel faults in Panamá: Earthquake hazard to the Panamá Canal. Bulletin of the Seismological Society of America, 100(6), 3097-3129.

Rogers, R. D., Mann, P., & Emmet, P. A. (2007). Tectonic terranes of the Chortis block based on integration of regional aeromagnetic and geologic data. In Special Paper 428: Geologic and Tectonic Development of the Caribbean Plate Boundary in Northern Central America (pp. 65-88).

Rojas-Agramonte, Y., Kroner, A., García-Casco, A., Kemp, T., Hegner, E., Perez, M., et al. (2010). Zircon ages, Sr-Nd-Hf isotopic compositions, and geochemistry of granitoids associated with the northern ophiolite melange of Central Cuba: Tectonic implication for Late Cretaceous magmatism in the Northwestern Caribbean. American Journal of Science, 310(10), 1453-1479.

Rojas-Agramonte, Y., Kröner, A., García-Casco, A., Somin, M., Iturralde-Vinent, M., Mattinson, J. M., et al. (2011). Timing and Evolution of Cretaceous Island Arc Magmatism in Central Cuba: Implications for the History of Arc Systems in the Northwestern Caribbean. The Journal of Geology, 119(6), 619-640.

Rojas-Agramonte, Y., Neubauer, F., Garcia-Delgado, D. E., Handler, R., Friedl, G., & Delgado-Damas, R. (2008). Tectonic evolution of the Sierra Maestra Mountains, SE Cuba, during Tertiary times: From arc-continent collision to transform motion. Journal of South American Earth Sciences, 26(2), 125-151.

Rojas-Agramonte, Y., Neubauer, F., Handler, R., Garcia-Delgado, D. E., Friedl, G., & Delgado-Damas, R. (2005). Variation of palaeostress patterns along the Oriente transform wrench corridor, Cuba: significance for Neogene–Quaternary tectonics of the Caribbean realm. Tectonophysics, 396(3-4), 161-180.

Rosencrantz, E. (1990). Structure and tectonics of the Yucatan Basin, Caribbean Sea, as determined from seismic reflection studies. Tectonics, 9(5), 1037-1059.

Rosencrantz, E., Ross, M. I., & Sclater, J. G. (1988). Age and spreading history of the Cayman Trough as determined from depth, heat flow, and magnetic anomalies. Journal of Geophysical Research: Solid Earth, 93(B3), 2141-2157.

Rosencrantz, E., & Sclater, J. G. (1986). Depth and Age in the Cayman Trough. Earth and Planetary Science Letters, 79(1-2), 133-144.

Ross, M. I., & Scotese, C. R. (1988). A Hierarchical Tectonic Model of the Gulf of Mexico and Caribbean Region. Tectonophysics, 155(1-4), 139-168.

Sakagami, S., & Sakai, A. (1979). Triassic bryozoans from the Hidaka Group in Hokkaido, Japan. Paper presented at the Trans. Proc. Palaeontol. Soc. Japan.

Sakakibara, M., Hori, R., Ikeda, M., & Umeki, M. (1997). Petrologic characteristics and geologic age of green rocks including chert xenoliths in the Pippu area, central Hokkaido, Japan. Journal of the Geological Society of Japan, 103, 953-961.

Sakakibara, M., & Ota, T. (1994). Metamorphic evolution of the Kamuikotan high-pressure and low-temperature metamorphic rocks in central Hokkaido, Japan. Journal of Geophysical Research: Solid Earth, 99(B11), 22221-22235.

Sakashima, T., Terada, K., Takeshita, T., & Sano, Y. (2003). Large-scale displacement along the Median Tectonic Line, Japan: evidence from SHRIMP zircon U–Pb dating of granites and gneisses from the South Kitakami and paleo-Ryoke belts. Journal of Asian Earth Sciences, 21(9), 1019-1039.

Saleeby, J. (1981). Ocean floor accretion and volcanoplutonic arc evolution of the Mesozoic Sierra Nevada.

Saleeby, J. (1992). Petrotectonic and paleogeographic settings of US Cordilleran ophiolites. The Cordilleran Orogen: Conterminous US: Boulder, Colorado, The Geology of North America, 3, 653-682.

Sano, H., & Nakashima, K. (1997). Lowermost Triassic (Griesbachian) microbial bindstone-cementstone facies, southwest Japan. Facies, 36(1), 1-24.

Sato, T. (1962). Études biostratigraphiques des ammonites du Jurassique du Japon. Mémoires de la Societé géologique de France NS, 94, 1-122.

Saunders, A. D., Tarney, J., Kerr, A. C., & Kent, R. W. (1996). The formation and fate of large oceanic igneous provinces. Lithos, 37(2-3), 81-95.

Saunders, J. B. (1974). Trinidad. Geological Society, London, Special Publications, 4(1), 671-682.

Scheepers, P., & Langereis, C. (1993). Analysis of NRM directions from the Rossello composite: implications for tectonic rotations of the Caltanissetta basin, Sicily. Earth and Planetary Science Letters, 119(3), 243-258.

Schellart, W. (2017). A geodynamic model of subduction evolution and slab detachment to explain Australian plate acceleration and deceleration during the latest Cretaceous–early Cenozoic. Lithosphere, 9(6), 976-986.

Schellart, W. P. (2008a). Overriding plate shortening and extension above subduction zones: A parametric study to explain formation of the Andes Mountains. Geological Society of America Bulletin, 120(11-12), 1441-1454.

Schellart, W. P. (2008b). Subduction zone trench migration: Slab driven or overriding-plate-driven? Physics of the Earth and Planetary Interiors, 170(1-2), 73-88.

Schellart, W. P., Stegman, D. R., Farrington, R. J., Freeman, J., & Moresi, L. (2010). Cenozoic tectonics of western North America controlled by evolving width of Farallon slab. Science, 329(5989), 316-319.

Schellekens, J. H. (1991). Late Jurassic to Eocene geochemichal evolution of volcanic rocks in Puerto Rico. Geophysical Research Letters, 18(3), 553-556.

Schepers, G., van Hinsbergen, D. J. J., Spakman, W., Kosters, M. E., Boschman, L. M., & McQuarrie, N. (2017). South-American plate advance and forced Andean trench retreat as drivers for transient flat subduction episodes. Nature Communications, 8, 15249.

Schmidt, K. L., Wetmore, P. H., Alsleben, H., & Paterson, S. R. (2014). Mesozoic tectonic evolution of the southern Peninsular Ranges batholith, Baja California, Mexico: Long-lived history of a collisional segment in the Mesozoic Cordilleran arc. In Peninsular Ranges Batholith, Baja California and Southern California (pp. 645-668).

Schmidt, K. L., Wetmore, P. H., Johnson, S., & Paterson, S. (2002). Controls on orogenesis along an ocean-continent margin transition in the Jura-Cretaceous Peninsular Ranges batholith. Geological Society of America Special Paper, 49-72.

Schmidt-Effing, R. (1979). Alter und Genese des Nicoya-Komplexes, einer ozeanischen Paläokruste (Oberjura bis Eozän) im südlichen Zentralamerika. Geologische Rundschau, 68(2), 457-494.

Schneider, J., Bosch, D., Monié, P., Guillot, S., García-Casco, A., Lardeaux, J. M., et al. (2004). Origin and evolution of the Escambray Massif (Central Cuba): an example of HP/LT rocks exhumed during intraoceanic subduction. Journal of Metamorphic Geology, 22(3), 227-247.

Scotese, C. R. (2004). A continental drift flipbook. The Journal of Geology, 112(6), 729-741.

Sdrolias, M., Müller, R. D., Mauffret, A., & Bernardel, G. (2004). Enigmatic formation of the Norfolk Basin, SW Pacific: A plume influence on back-arc extension. Geochemistry, Geophysics, Geosystems, 5(6).

Sedlock, R. L. (1988). Tectonic setting of blueschist and island-arc terranes of west-central Baja California, Mexico. Geology, 16(7).

Sedlock, R. L., & Isozaki, Y. (1990). Lithology and Biostratigraphy of Franciscan-Like Chert and Associated Rocks in West-Central Baja-California, Mexico. Geological Society of America Bulletin, 102(7), 852-864.

Sen, G., Hickey-Vargas, R., Waggoner, D. G., & Maurrasse, F. (1988). Geochemistry of basalts from the Dumisseau Formation, southern Haiti: implications for the origin of the Caribbean Sea crust. Earth and Planetary Science Letters, 87(4), 423-437.

Seton, M., Flament, N., Whittaker, J., Muller, R. D., Gurnis, M., & Bower, D. J. (2015). Ridge subduction sparked reorganization of the Pacific plate-mantle system 60-50 million years ago. Geophysical Research Letters, 42(6), 1732-1740.

Seton, M., Müller, R. D., Zahirovic, S., Gaina, C., Torsvik, T., Shephard, G., et al. (2012). Global continental and ocean basin reconstructions since 200Ma. Earth-Science Reviews, 113(3-4), 212-270.

Shapiro, M., & Solov'ev, A. (2009). Formation of the Olyutorsky–Kamchatka foldbelt: A kinematic model. Russian Geology and Geophysics, 50(8), 668-681.

Sharp, W., & Snoke, A. (1988). Tobago, West Indies: Geochronological study of a fragment of a composite Mesozoic oceanic island arc. Paper presented at the Geological Society of America Abstracts with Programs.

Shephard, G. E., Müller, R. D., & Seton, M. (2013). The tectonic evolution of the Arctic since Pangea breakup: Integrating constraints from surface geology and geophysics with mantle structure. Earth-Science Reviews, 124, 148-183.

Shervais, J. W., Kimbrough, D. L., Renne, P., Hanan, B. B., Murchey, B., Snow, C. A., et al. (2004). Multi-Stage Origin of the Coast Range Ophiolite, California: Implications for the Life Cycle of Supra-Subduction Zone Ophiolites. International Geology Review, 46(4), 289-315.

Shibuya, H., & Sasajima, S. (1986). Paleomagnetism of red cherts: a case study in the Inuyama area, central Japan. Journal of Geophysical Research: Solid Earth, 91(B14), 14105-14116.

Sigloch, K. (2011). Mantle provinces under North America from multifrequency P wave tomography. Geochemistry, Geophysics, Geosystems, 12(2).

Sigloch, K., McQuarrie, N., & Nolet, G. (2008). Two-stage subduction history under North America inferred from multiple-frequency tomography. Nature Geoscience, 1(7), 458-462.

Sigloch, K., & Mihalynuk, M. G. (2013). Intra-oceanic subduction shaped the assembly of Cordilleran North America. Nature, 496(7443), 50-56.

Sigloch, K., & Mihalynuk, M. G. (2017). Mantle and geological evidence for a Late Jurassic–Cretaceous suture spanning North America. Geological Society of America Bulletin, 129(11-12), 1489-1520.

Silver, L., & Chappell, B. (1988). The Peninsular Ranges Batholith: an insight into the evolution of the Cordilleran batholiths of southwestern North America. Earth and Environmental Science Transactions of The Royal Society of Edinburgh, 79(2-3), 105-121.

Silver, L., Taylor, H., & Chappell, B. (1979). Some petrological, geochemical and geochronological observations of the Peninsular Ranges batholith near the international border of the USA and Mexico. Paper presented at the Mesozoic Crystalline Rocks: Geological Society of America, Annual Meeting, Guidebook.

Sinton, C. W., Duncan, R. A., & Denyer, P. (1997). Nicoya Peninsula, Costa Rica: A single suite of Caribbean oceanic plateau magmas. Journal of Geophysical Research: Solid Earth, 102(B7), 15507-15520.

Sinton, C. W., Duncan, R. A., Storey, M., Lewis, J., & Estrada, J. J. (1998). An oceanic flood basalt province within the Caribbean plate. Earth and Planetary Science Letters, 155(3-4), 221-235.

Sinton, C. W., Sigurdsson, H., & Duncan, R. A. (2000). Geochronology and petrology of the igneous basement at the Lower Nicaraguan Rise, Site 1001. In Proceedings of the Ocean Drilling Program, 165 Scientific Results.

Smith, D. P., & Busby, C. J. (1993). Shallow magnetic inclinations in the Cretaceous Valle Group, Baja California: remagnetization, compaction, or terrane translation? Tectonics, 12(5), 1258-1266.

Snoke, A., Yule, J., Rowe, D., Wadge, G., & Sharp, W. (1990). Stratigraphic and structural relationships on Tobago, West Indies, and some tectonic implications. Paper presented at the Transactions of the 12th Caribbean Geological Conferences (St. Croix, US Virgin Islands, 1989). South Miami, FL, Miami Geol. Soc.

Snoke, A. W., & Noble, P. J. (2001). Ammonite-radiolarian assemblage, Tobago Volcanic Group, Tobago, West Indies—Implications for the evolution of the Great Arc of the Caribbean. Geological Society of America Bulletin, 113(2), 256-264.

Snoke, A. W., Rowe, D. W., Yule, J. D., & Wadge, G. (2001a). Geologic Map of Tobago, West Indies: Geological Society of America.

Snoke, A. W., Rowe, D. W., Yule, J. D., & Wadge, G. (2001b). Petrologic and structural history of Tobago, West Indies: a fragment of the accreted Mesozoic oceanic arc of the southern Caribbean. Geological Society of America Special Paper 354.

Solari, L. A., García-Casco, A., Martens, U., Lee, J. K. W., & Ortega-Rivera, A. (2013). Late Cretaceous subduction of the continental basement of the Maya block (Rabinal Granite, central Guatemala): Tectonic implications for the geodynamic evolution of Central America. Geological Society of America Bulletin, 125(3-4), 625-639.

Solari, L. A., Gómez-Tuena, A., Bernal, J. P., Pérez-Arvizu, O., & Tanner, M. (2010). U-Pb Zircon Geochronology with an Integrated LA-ICP-MS Microanalytical Workstation: Achievements in Precision and Accuracy. Geostandards and Geoanalytical Research, 34(1), 5-18.

Solari, L. A., & Tanner, M. (2011). UPb.age, a fast data reduction script for LA-ICP-MS U-Pb geochronology. Revista Mexicana de Ciencias Geológicas, 28(1), 83-91.

Solari, L. A., Tuena, A. G., Gutiérrez, F. O., & Obregón, C. O. (2011). The Chuacús Metamorphic Complex, central Guatemala: geochronological and geochemical constraints on its Paleozoic-Mesozoic evolution. Geologica Acta: an international earth science journal, 9(3), 329-350.

Somin, M., & Millán, G. (1981). Geology of the metamorphic complexes of Cuba. Nauka: Moscow [in Russian].

Somin, M. L., Arakelyants, M. M., & Kolesnikov, E. M. (1992). Age and Tectonic Significance of High-Pressure Metamorphic Rocks of Cuba. International Geology Review, 34(2), 105-118.

Spakman, W., Chertova, M. V., van den Berg, A., & van Hinsbergen, D. J. (2018). Puzzling features of western Mediterranean tectonics explained by slab dragging. Nature Geoscience, 11(3), 211.

Spakman, W., & Hall, R. (2010). Surface deformation and slab–mantle interaction during Banda arc subduction rollback. Nature Geoscience, 3(8), 562.

Spakman, W., & Wortel, R. (2004). A tomographic view on western Mediterranean geodynamics. In The TRANSMED atlas. The Mediterranean region from crust to mantle (pp. 31-52): Springer.

Speed, R. (1985). Cenozoic collision of the Lesser Antilles arc and continental South America and the origin of the El Pilar fault. Tectonics, 4(1), 41-69.

Speed, R. C., & Larue, D. K. (1982). Barbados: Architecture and implications for accretion. Journal of Geophysical Research, 87(B5).

Spencer, C. J., Kirkland, C. L., & Taylor, R. J. M. (2016). Strategies towards statistically robust interpretations of in situ U–Pb zircon geochronology. Geoscience Frontiers, 7(4), 581-589.

Spörli, K., & Grant-Mackie, J. (1976). Upper Jurassic fossils from the Waipapa Group of Tawharanui Peninsula, North Auckland, New Zealand. New Zealand Journal of Geology and Geophysics, 19(1), 21-34.

Sporli, K. B., Aita, Y., & Gibson, G. W. (1989). Juxtaposition of Tethyan and Non-Tethyan Mesozoic Radiolarian Faunas in Melanges, Waipapa Terrane, North-Island, New-Zealand. Geology, 17(8), 753-756.

Stampfli, G. M., & Borel, G. D. (2002). A plate tectonic model for the Paleozoic and Mesozoic constrained by dynamic plate boundaries and restored synthetic oceanic isochrons. Earth and Planetary Science Letters, 196(1-2), 17-33.

Stanek, K. P., Maresch, W., Grafe, F., Grevel, C., & Baumann, A. (2006). Structure, tectonics and metamorphic development of the Sancti Spiritus Dome (eastern Escambray massif, Central Cuba). Geologica Acta: an international earth science journal, 4(1-2), 151-170.

Stanek, K. P., Maresch, W. V., & Pindell, J. L. (2009). The geotectonic story of the northwestern branch of the Caribbean Arc: implications from structural and geochronological data of Cuba. Geological Society, London, Special Publications, 328(1), 361-398.

Stearns, C., Mauk, F. J., & Van der Voo, R. (1982). Late Cretaceous-Early Tertiary paleomagnetism of Aruba and Bonaire (Netherlands Leeward Antilles). Journal of Geophysical Research: Solid Earth, 87(B2), 1127-1141.

Steinberger, B., & Torsvik, T. H. (2008). Absolute plate motions and true polar wander in the absence of hotspot tracks. Nature, 452(7187), 620-623.

Stern, R. J. (2004). Subduction initiation: spontaneous and induced. Earth and Planetary Science Letters, 226(3-4), 275-292.

Stern, R. J., & Bloomer, S. H. (1992). Subduction Zone Infancy - Examples from the Eocene Izu-Bonin-Mariana and Jurassic California Arcs. Geological Society of America Bulletin, 104(12), 1621-1636.

Stern, R. J., & Gerya, T. (2017). Subduction initiation in nature and models: A review. Tectonophysics.

Stern, R. J., Reagan, M., Ishizuka, O., Ohara, Y., & Whattam, S. (2012). To understand subduction initiation, study forearc crust: To understand forearc crust, study ophiolites. Lithosphere, 4(6), 469-483.

Stock, J. M., & Hodges, K. V. (1989). Pre-Pliocene extension around te Gulf of California and the transfer of Baja California to the Pacific Plate. Tectonics, 8(1), 99-115.

Stone, D. B., Minyuk, P., & Kolosev, E. (2003). New paleomagnetic paleolatitudes for the Omulevka terrane of northeast Russia: a comparison with the Omolon terrane and the eastern Siberian platform. Tectonophysics, 377(1-2), 55-82.

Suppe, J., & Armstrong, R. L. (1972). Potassium-argon dating of Franciscan metamorphic rocks. American Journal of Science, 272(3), 217-233.

Sykes, L. R., McCann, W. R., & Kafka, A. L. (1982). Motion of Caribbean plate during last 7 million years and implications for earlier Cenozoic movements. Journal of Geophysical Research: Solid Earth, 87(B13), 10656-10676.

Taboada, A., Rivera, L. A., Fuenzalida, A., Cisternas, A., Philip, H., Bijwaard, H., et al. (2000). Geodynamics of the northern Andes: Subductions and intracontinental deformation (Colombia). Tectonics, 19(5), 787-813.

Tait, J., Rojas-Agramonte, Y., García-Delgado, D., Kröner, A., & Pérez-Aragón, R. (2009). Palaeomagnetism of the central Cuban Cretaceous Arc sequences and geodynamic implications. Tectonophysics, 470(3-4), 284-297.

Tajika, J., & Iwata, K. (1990). Paleogene melange of the northern Hidaka belt--geology and radiolarian age of the Kamiokoppe formation. Journal of the Hokkai-Gakuen University, 66, 35-55.

Takashima, R., Kawabe, F., Nishi, H., Moriya, K., Wani, R., & Ando, H. (2004). Geology and stratigraphy of forearc basin sediments in Hokkaido, Japan: Cretaceous environmental events on the north-west Pacific margin. Cretaceous Research, 25(3), 365-390.

Takashima, R., Yoshida, T., & Nishi, H. (2001). Stratigraphy and sedimentary environments of the Sorachi and Yezo Groups in the Yubari-Ashibetsu area, Hokkaido, Japan. Journal of the Geological Society of Japan, 107(6), 359-378.

Takasu, A., Wallis, S., Banno, S., & Dallmeyer, R. (1994). Evolution of the Sambagawa metamorphic belt, Japan. Lithos, 33(1-3), 119-133.

Talavera-Mendoza, O., Ruiz, J., Gehrels, G. E., Valencia, V. A., & Centeno-García, E. (2007). Detrital zircon U/Pb geochronology of southern Guerrero and western Mixteca arc successions (southern Mexico): New insights for the tectonic evolution of southwestern North America during the late Mesozoic. Geological Society of America Bulletin, 119(9-10), 1052-1065.

Tan, X. D., Kodama, K. P., & Fang, D. J. (2002). Laboratory depositional and compaction-caused inclination errors carried by haematite and their implications in identifying inclination error of natural remanence in red beds. Geophysical Journal International, 151(2), 475-486.

Tarduno, J. A., & Alvarez, W. (1985). Paleolatitudes of Franciscan Limestones. Geology, 13(10), 741-741.

Tarduno, J. A., McWilliams, M., Sliter, W. V., Cook, H. E., Blake, M. C., Jr., & Premoli-Silva, I. (1986). Southern hemisphere origin of the cretaceous laytonville limestone of california. Science, 231(4744), 1425-1428.

Tardy, M., Lapierre, H., Freydier, C., Coulon, C., Gill, J.-B., Mercier de Lépinay, B., et al. (1994). The Guerrero suspect terrane (western Mexico) and coeval arc terranes (the Greater Antilles and the Western Cordillera of Colombia): a late Mesozoic intra-oceanic arc accreted to cratonal America during the Cretaceous. Tectonophysics, 230, 49-73.

Tauxe, L. (2010). Essentials of paleomagnetism: University of California Press.

Tauxe, L., & Kent, D. V. (1984). Properties of a detrital remanence carried by haematite from study of modern river deposits and laboratory redeposition experiments. Geophysical Journal International, 77, 543-561.

Tauxe, L., & Kent, D. V. (2004). A simplified statistical model for the geomagnetic field and the detection of shallow bias in paleomagnetic inclinations: was the ancient magnetic field dipolar? Timescales of the Paleomagnetic field, 101-115.

Tauxe, L., & Watson, G. S. (1994). The Fold Test - an Eigen Analysis Approach. Earth and Planetary Science Letters, 122(3-4), 331-341.

Tazawa, J.-i. (2001). Middle Permian brachiopod faunas of Japan and South Primorye, Far East Russia: their palaeobiogeographic and tectonic implications. Geosciences Journal, 5(1), 19.

Tazawa, J. I. (2002). Late Paleozoic brachiopod faunas of the South Kitakami Belt, northeast Japan, and their paleobiogeographic and tectonic implications. Island Arc, 11(4), 287-301.

ten Brink, U. S., Marshak, S., & Bruña, J.-L. G. (2009). Bivergent thrust wedges surrounding oceanic island arcs: Insight from observations and sandbox models of the northeastern Caribbean plate. Geological Society of America Bulletin, 121(11-12), 1522-1536.

Thomas, C., Garnero, E. J., & Lay, T. (2004). High-resolution imaging of lowermost mantle structure under the Cocos plate. Journal of Geophysical Research: Solid Earth, 109(B8).

Thompson, P., Kempton, P., White, R., Saunders, A., Kerr, A. C., Tarney, J., & Pringle, M. (2004). Elemental, Hf–Nd isotopic and geochronological constraints on an island arc sequence associated with the Cretaceous Caribbean plateau: Bonaire, Dutch Antilles. Lithos, 74(1), 91-116.

Todd, V., & Shaw, S. (1985). S-type granitoids and an IS line in the Peninsular Ranges batholith, southern California. Geology, 13(4), 231-233.

Tomblin, J. F. (1975). The Lesser Antilles and Aves Ridge. In The Gulf of Mexico and the Caribbean (pp. 467-500): Springer.

Tominaga, M., Tivey, M. A., & Sager, W. W. (2015). Nature of the Jurassic Magnetic Quiet Zone. Geophysical Research Letters, 42(20), 8367-8372.

Topuz, G., Çelık, Ö. F., Şengör, A. C., Altintaş, İ. E., Zack, T., Rolland, Y., & Barth, M. (2013a). Jurassic ophiolite formation and emplacement as backstop to a subduction-accretion complex in northeast Turkey, the Refahıye ophiolite, and relation to the Balkan ophiolites. American Journal of Science, 313(10), 1054-1087.

Topuz, G., Göçmengil, G., Rolland, Y., Çelik, Ö. F., Zack, T., & Schmitt, A. K. (2013b). Jurassic accretionary complex and ophiolite from northeast Turkey: No evidence for the Cimmerian continental ribbon. Geology, 41(2), 255-258.

Torres-Carrillo, X. G., Delgado-Argote, L. A., Böhnel, H., Molina-Garza, R. S., & Weber, B. (2016). Palaeomagnetic assessment of plutons from the southern Peninsular Ranges batholith and the Jurassic Vizcaíno igneous suites, Baja California, México. International Geology Review, 58(4), 489-509.

Torsvik, T. H., Burke, K., Steinberger, B., Webb, S. J., & Ashwal, L. D. (2010a). Diamonds sampled by plumes from the core-mantle boundary. Nature, 466(7304), 352-355.

Torsvik, T. H., & Cocks, L. R. M. (2016). Earth history and palaeogeography: Cambridge University Press.

Torsvik, T. H., Müller, R. D., Van der Voo, R., Steinberger, B., & Gaina, C. (2008). Global plate motion frames: Toward a unified model. Reviews of Geophysics, 46(3).

Torsvik, T. H., Rousse, S., Labails, C., & Smethurst, M. A. (2009). A new scheme for the opening of the South Atlantic Ocean and the dissection of an Aptian salt basin. Geophysical Journal International, 177(3), 1315-1333.

Torsvik, T. H., Smethurst, M. A., Burke, K., & Steinberger, B. (2006). Large igneous provinces generated from the margins of the large low-velocity provinces in the deep mantle. Geophysical Journal International, 167(3), 1447-1460.

Torsvik, T. H., Steinberger, B., Gurnis, M., & Gaina, C. (2010b). Plate tectonics and net lithosphere rotation over the past 150 My. Earth and Planetary Science Letters, 291(1-4), 106-112.

Torsvik, T. H., & Van der Voo, R. (2002). Refining Gondwana and Pangea palaeogeography: estimates of Phanerozoic non-dipole (octupole) fields. Geophysical Journal International, 151(3), 771-794.

Torsvik, T. H., van der Voo, R., Doubrovine, P. V., Burke, K., Steinberger, B., Ashwal, L. D., et al. (2014). Deep mantle structure as a reference frame for movements in and on the Earth. Proc Natl Acad Sci U S A, 111(24), 8735-8740.

Torsvik, T. H., Van der Voo, R., Preeden, U., Mac Niocaill, C., Steinberger, B., Doubrovine, P. V., et al. (2012). Phanerozoic polar wander, palaeogeography and dynamics. Earth-Science Reviews, 114(3-4), 325-368.

Tournon, J. (1994). The Santa Elena Peninsula: an ophiolitic nappe and a sedimentary volcanic relative autochthonous. Profil, 7, 87-96.

Tournon, J., & Alvarado, G. (1997). Mapa geológico de Costa Rica: Escala 1: 500000. Editorial Tecnológica de Costa Rica.

Trenkamp, R., Kellogg, J. N., Freymueller, J. T., & Mora, H. P. (2002). Wide plate margin deformation, southern Central America and northwestern South America, CASA GPS observations. Journal of South American Earth Sciences, 15(2), 157-171.

Troughton, G. H. (1974). Stratigraphy of the Vizcaíno Peninsula near Asunción Bay, Territorio de Baja California, Mexico. MSc Thesis, San Diego State Univeristy

Ueda, H. (2003). Accretionary complex of remnant-arc origin: Greenstone-conglomerate-chert succession in the Oku-Niikappu area of the Idonnappu Zone, Hokkaido, Japan. The Journal of the Geological Society of Japan, 109(9), XVII-XVIII.

Ueda, H. (2016). Hokkaido. In T. Moreno, S. Wallis, T. Kojima, & W. Gibbons (Eds.), The Geology of Japan (pp. 201-221). London: Geological Society.

Ueda, H., Kawamura, M., & Iwata, K. (2001). Tectonic evolution of Cretaceous accretionary complex in the Idonnappu Zone, Urakawa area, central Hokkaido, Northern Japan: with reference to radiolarian ages and thermal structure. Journal of the Geological Society of Japan, 107, 81-98.

Ueda, H., Kawamura, M., & Niida, K. (2000). Accretion and tectonic erosion processes revealed by the mode of occurrence and geochemistry of greenstones in the Cretaceous accretionary complexes of the Idonnappu Zone, southern central Hokkaido, Japan. Island Arc, 9(2), 237-257.

Ueda, H., & Miyashita, S. (2003). Discovery of sheeted dikes in the Cretaceous accretionary complex of the Idonnappu Zone, Hokkaido, Japan. The Journal of the Geological Society of Japan, 109(9), 559-562.

Ueda, H., & Miyashita, S. (2005). Tectonic accretion of a subducted intraoceanic remnant arc in Cretaceous Hokkaido, Japan, and implications for evolution of the Pacific northwest. Island Arc, 14(4), 582-598.

Umhoefer, P. (2003). A model for the North America Cordillera in the Early Cretaceous: Tectonic escape related to arc collision of the Guerrero terrane and a change in North America plate motion. In Special Paper 374: Tectonic evolution of northwestern Mexico and the Southwestern USA (pp. 117-134).

Umhoefer, P., & Blakey, R. C. (2006). Moderate (1600 km) northward translation of Baja British Columbia from southern California: An attempt at reconciliation of paleomagnetism and geology. In J. W. Haggart, R. J. Enkin, & J. W. H. Monger (Eds.), Paleogeography of the North American Cordillera: Evidence For and Against Large-Scale Displacements (Vol. Special Paper 46, pp. 307-329): Geological Association of Canada.

Vaes, B., van Hinsbergen, D.J.J., Boschman, L.M., (2018). Kinematic reconstruction of intra-oceanic subduction and back-arc opening in the NW Pacific Ocean and Aleutian Basin: clues to causes of Cretaceous and Eocene plate reorganizations, Tectonics, accepted pending revision.

Vallejo, C., Spikings, R. A., Luzieux, L., Winkler, W., Chew, D., & Page, L. (2006). The early interaction between the Caribbean Plateau and the NW South American Plate. Terra Nova, 18(4), 264-269.

van Benthem, S., Govers, R., Spakman, W., & Wortel, R. (2013). Tectonic evolution and mantle structure of the Caribbean. Journal of Geophysical Research: Solid Earth, 118(6), 3019-3036.

van de Lagemaat, S. H., van Hinsbergen, D. J., Boschman, L. M., Kamp, P. J., & Spakman, W. (2018a). Southwest Pacific absolute plate kinematic reconstruction reveals major Cenozoic Tonga-Kermadec slab dragging. Tectonics, doi: 10.1029/2017TC004901

van de Lagemaat, S. H. A., Boschman, L. M., Kamp, P. J. J., Langereis, C. G., & van Hinsbergen, D. J. J. (2018b). Post-remagnetisation vertical axis rotation and tilting of the Murihiku Terrane (North Island, New Zealand). New Zealand Journal of Geology and Geophysics, 61(1), 9-25.

van der Hilst, R., Engdahl, R., Spakman, W., & Nolet, G. (1991). Tomographic imaging of subducted lithosphere below northwest Pacific island arcs. Nature, 353(6339), 37.

van der Hilst, R., & Seno, T. (1993). Effects of relative plate motion on the deep structure and penetration depth of slabs below the Izu-Bonin and Mariana island arcs. Earth and Planetary Science Letters, 120(3-4), 395-407.

van der Hilst, R. D. (1990). Tomography with P, PP, and pP delay-time data and the three-dimensional mantle structure below the Caribbean region. PhD Thesis, Utrecht University.

van der Hilst, R. D. (1995). Complex morphology of subducted lithosphere in the mantle beneath the Tonga trench. Nature, 374(6518), 154.

van der Hilst, R. D., de Hoop, M. V., Wang, P., Shim, S. H., Ma, P., & Tenorio, L. (2007). Seismostratigraphy and thermal structure of Earth's core-mantle boundary region. Science, 315(5820), 1813-1817.

van der Lelij, R., Spikings, R. A., Kerr, A. C., Kounov, A., Cosca, M., Chew, D., & Villagomez, D. (2010). Thermochronology and tectonics of the Leeward Antilles: Evolution of the southern Caribbean Plate boundary zone. Tectonics, 29(6).

van der Meer, D. G., Spakman, W., van Hinsbergen, D. J. J., Amaru, M. L., & Torsvik, T. H. (2010). Towards absolute plate motions constrained by lower-mantle slab remnants. Nature Geoscience, 3(1), 36-40.

van der Meer, D. G., Torsvik, T. H., Spakman, W., van Hinsbergen, D. J. J., & Amaru, M. L. (2012). Intra-Panthalassa Ocean subduction zones revealed by fossil arcs and mantle structure. Nature Geoscience, 5(3), 215-219.

van der Meer, D. G., van Hinsbergen, D. J., & Spakman, W. (2018). Atlas of the Underworld: Slab remnants in the mantle, their sinking history, and a new outlook on lower mantle viscosity. Tectonophysics.

Van der Voo, R., Spakman, W., & Bijwaard, H. (1999a). Mesozoic subducted slabs under Siberia. Nature, 397(6716), 246.

Van der Voo, R., Spakman, W., & Bijwaard, H. (1999b). Tethyan subducted slabs under India. Earth and Planetary Science Letters, 171(1), 7-20.

Van Fossen, M. C., & Channell, J. E. (1988). Paleomagnetism of Late Cretaceous and Eocene limestones and chalks from Haiti: tectonic interpretations. Tectonics, 7(3), 601-612.

van Hinsbergen, D. J., Iturralde-Vinent, M. A., van Geffen, P. W., García-Casco, A., & van Benthem, S. (2009). Structure of the accretionary prism, and the evolution of the Paleogene northern Caribbean subduction zone in the region of Camagüey, Cuba. Journal of Structural Geology, 31(10), 1130-1144.

van Hinsbergen, D. J., Vissers, R. L., & Spakman, W. (2014). Origin and consequences of western Mediterranean subduction, rollback, and slab segmentation. Tectonics, 33(4), 393-419.

van Hinsbergen, D. J. J. (2010). A key extensional metamorphic complex reviewed and restored: The Menderes Massif of western Turkey. Earth-Science Reviews, 102(1-2), 60-76.

van Hinsbergen, D. J. J., de Groot, L. V., van Schaik, S. J., Spakman, W., Bijl, P. K., Sluijs, A., et al. (2015a). A Paleolatitude Calculator for Paleoclimate Studies. PLoS One, 10(6), e0126946.

van Hinsbergen, D. J. J., Hafkenscheid, E., Spakman, W., Meulenkamp, J. E., & Wortel, R. (2005). Nappe stacking resulting from subduction of oceanic and continental lithosphere below Greece. Geology, 33(4).

van Hinsbergen, D. J. J., Kapp, P., Dupont-Nivet, G., Lippert, P. C., DeCelles, P. G., & Torsvik, T. H. (2011a). Restoration of Cenozoic deformation in Asia and the size of Greater India. Tectonics, 30(5).

van Hinsbergen, D. J. J., Lippert, P. C., Li, S., Huang, W., Advokaat, E. L., & Spakman, W. (2018). Reconstructing Greater India: Paleogeographic, kinematic, and geodynamic perspectives. Tectonophysics.

van Hinsbergen, D. J. J., Peters, K., Maffione, M., Spakman, W., Guilmette, C., Thieulot, C., et al. (2015b). Dynamics of intraoceanic subduction initiation: 2. Suprasubduction zone ophiolite formation and

metamorphic sole exhumation in context of absolute plate motions. Geochemistry, Geophysics, Geosystems, 16(6), 1771-1785.

van Hinsbergen, D. J. J., & Schmid, S. M. (2012). Map view restoration of Aegean-West Anatolian accretion and extension since the Eocene. Tectonics, 31(5), n/a-n/a.

van Hinsbergen, D. J. J., Steinberger, B., Doubrovine, P. V., & Gassmöller, R. (2011b). Acceleration and deceleration of India-Asia convergence since the Cretaceous: Roles of mantle plumes and continental collision. Journal of Geophysical Research: Solid Earth, 116(B6).

Van Hinsbergen, D.J.J., Kosters, M.E., Boschman, L.M., Bijl, P.K., and Spakman, W. (2018). Eocene absolute South American plate motion change triggered opening of Drake Passage, Earth and Planetary Science Letters, in review.

van Velzen, A. J., & Zijderveld, J. (1995). Effects of weathering on single-domain magnetite in Early Pliocene marine marls. Geophysical Journal International, 121(1), 267-278.

Vargas, C. A., & Mann, P. (2013). Tearing and breaking off of subducted slabs as the result of collision of the Panama Arc-Indenter with northwestern South America. Bulletin of the Seismological Society of America, 103(3), 2025-2046.

Venable, M. E. (1994). A geologic, tectonic and metallogenic evaluation of the Siuna terrane. PhD Thesis, The University of Arizona,

Vila, J.-M., Boisson, D., Butterlin, J., Feinberg, H., & Pubellier, M. (1987). Le complexe chaotique fini-éocène de Chouchou (Massif du Nord d'Haïti): un enregistrement du début des décrochements senestres nord-caraïbes. Comptes rendus de l'Académie des sciences. Série 2, Mécanique, Physique, Chimie, Sciences de l'univers, Sciences de la Terre, 304(1), 39-42.

Villagómez, D., Spikings, R., Magna, T., Kammer, A., Winkler, W., & Beltrán, A. (2011). Geochronology, geochemistry and tectonic evolution of the Western and Central cordilleras of Colombia. Lithos, 125(3), 875-896.

Villagómez, D., Spikings, R., Seward, D., Magna, T., Winkler, W., & Kammer, A. (2008). Thermotectonic history of the Northern Andes. Paper presented at the 7th International Symposium on Andean Geodynamics (ISAG 2008, Nice), Extended Abstracts.

Viso, R., Larson, R., & Pockalny, R. (2005). Tectonic evolution of the Pacific–Phoenix–Farallon triple junction in the South Pacific Ocean. Earth and Planetary Science Letters, 233(1-2), 179-194.

Vlaar, N., & Wortel, M. (1976). Lithospheric aging, instability and subduction. Tectonophysics, 32(3-4), 331-351.

Von Huene, R., Aubouin, J., Azema, J., Blackinton, G., Carter, J. A., Coulbourn, W. T., et al. (1980). Leg 67: The Deep Sea Drilling Project Mid-America Trench transect off Guatemala. Geological Society of America Bulletin, 91(7).

Wadge, G., Draper, G., & Lewis, J. F. (1984). Ophiolites of the northern Caribbean: A reappraisal of their roles in the evolution of the Caribbean plate boundary. Geological Society, London, Special Publications, 13(1), 367-380.

Wakabayashi, J. (2015). Anatomy of a subduction complex: architecture of the Franciscan Complex, California, at multiple length and time scales. International Geology Review, 57(5-8), 669-746.

Wakabayashi, J., Ghatak, A., & Basu, A. R. (2010). Suprasubduction-zone ophiolite generation, emplacement, and initiation of subduction: A perspective from geochemistry, metamorphism, geochronology, and regional geology. Geological Society of America Bulletin, 122(9-10), 1548-1568.

Watanabe, Y., & Iwata, K. (1985). Discovery of Paleogene radiolarians from the Yuyanbetsu Formation, Central Hokkaido, and its geological significance. Chikyu Kagaku, 39(6), 446-452a.

Wegener, A. (1915). Die Entstehung der Kontinente und Ozeane. Hamburgischen Universität: Braunscheig, F., Vieweg & sohn.

Wegner, W., Worner, G., Harmon, R. S., & Jicha, B. R. (2010). Magmatic history and evolution of the Central American Land Bridge in Panama since Cretaceous times. Geological Society of America Bulletin, 123(3-4), 703-724.

Wernicke, B. (1981). Low-angle normal faults in the Basin and Range Province: nappe tectonics in an extending orogen. Nature, 291(5817), 645.

Wessel, P., & Kroenke, L. W. (2008). Pacific absolute plate motion since 145 Ma: An assessment of the fixed hot spot hypothesis. Journal of Geophysical Research, 113(B6).

Wessel, P., & Kroenke, L. W. (2009). Observations of geometry and ages constrain relative motion of Hawaii and Louisville plumes. Earth and Planetary Science Letters, 284(3-4), 467-472.

West, D. P., Abbott, R. N., Bandy, B. R., & Kunk, M. J. (2014). Protolith provenance and thermotectonic history of metamorphic rocks in eastern Jamaica: Evolution of a transform plate boundary. Geological Society of America Bulletin, 126(3-4), 600-614.

Wetmore, P. H., Herzig, C., Alsleben, H., Sutherland, M., Schmidt, K. L., Schultz, P. W., & Paterson, S. R. (2003). Mesozoic tectonic evolution of the Peninsular Ranges of southern and Baja California. Geological Society of America Special Paper, 93-116.

Wetmore, P. H., Schmidt, K. L., Paterson, S. R., & Herzig, C. (2002). Tectonic implications for the along-strike variation of the Peninsular Ranges batholith, southern and Baja California. Geology, 30(3), 247-250.

Whalen, P. A., & Pessagno, E. A. (1984). Lower Jurassic radiolaria, San Hipolito Formation, Vizcaino Peninsula, Baja California Sur. In V. A. J. Frizzell (Ed.), Geology of the Baja California peninsula (Vol. 39, pp. 53-66): Society of Economic Paleontologists and Mineralogists, Pacific Section.

Whattam, S. A., Gazel, E., Yi, K., & Denyer, P. (2016). Origin of plagiogranites in oceanic complexes: A case study of the Nicoya and Santa Elena terranes, Costa Rica. Lithos, 262, 75-87.

Whattam, S. A., & Stern, R. J. (2015). Late Cretaceous plume-induced subduction initiation along the southern margin of the Caribbean and NW South America: The first documented example with implications for the onset of plate tectonics. Gondwana Research, 27(1), 38-63.

White, R., Tarney, J., Kerr, A., Saunders, A., Kempton, P., Pringle, M., & Klaver, G. T. (1999). Modification of an oceanic plateau, Aruba, Dutch Caribbean: implications for the generation of continental crust. Lithos, 46(1), 43-68.

Williams, K. M. (1984). Remnants of an apparent eastwest-trending Middle Jurassic subduction and spreading-center system along the west margin of North America: Stanford University Publications. Geological Sciences, 18, 208-211.

Wilson, H. (1974). Cretaceous sedimentation and orogeny in nuclear Central America. AAPG Bulletin, 58(7), 1348-1396.

Wilson, J. T. (1966). Are the structures of the Caribbean and Scotia arc regions analogous to ice rafting? Earth and Planetary Science Letters, 1(5), 335-338.

Woods, M. T., & Davies, G. F. (1982). Late Cretaceous Genesis of the Kula Plate. Earth and Planetary Science Letters, 58(2), 161-166.

Wright, J. E., & Wyld, S. J. (2011). Late Cretaceous subduction initiation on the eastern margin of the Caribbean-Colombian Oceanic Plateau: One Great Arc of the Caribbean (?). Geosphere, 7(2), 468-493.

Wright, N. M., Seton, M., Williams, S. E., & Müller, R. D. (2016). The Late Cretaceous to recent tectonic history of the Pacific Ocean basin. Earth-Science Reviews, 154, 138-173.

Wu, J., Suppe, J., Lu, R., & Kanda, R. (2016). Philippine Sea and East Asian plate tectonics since 52 Ma constrained by new subducted slab reconstruction methods. Journal of Geophysical Research: Solid Earth, 121(6), 4670-4741.

Wyld, S. J., Umhoefer, P., & Wright, J. E. (2006). Reconstructing northern Cordilleran terranes along known Cretaceous and Cenozoic strike-slip faults: Implications for the Baja British Columbia hypothesis and other models. In J. W. Haggart, R. J. Enkin, & J. W. H. Monger (Eds.), Paleogeography of the North American Cordillera: Evidence For and Against Large-Scale Displacements (Vol. 46, pp. 277-298): Geological Association of Canada, Special Paper.

Yang, T., Ma, Y., Zhang, S., Bian, W., Yang, Z., Wu, H., et al. (2015). New insights into the India–Asia collision process from Cretaceous paleomagnetic and geochronologic results in the Lhasa terrane. Gondwana Research, 28(2), 625-641.

Yao, A., Matsuda, T., & Isozaki, Y. (1980). Triassic and Jurassic radiolarians from the Inuyama area, central Japan. Jouranl of Geoscience Osaka City University, 23(4).

Yoshida, T., & Aoki, C. (1972). Paleozoic formation in the Matsumae Peninsula, Hokkaido, and the occurrence of conodonts from the southern part of the Oshima Peninsula, Hokkaido. Bulletin of the Geological Survey of Japan, 23(11), 635-646.

Zahirovic, S., Müller, R. D., Seton, M., & Flament, N. (2015). Tectonic speed limits from plate kinematic reconstructions. Earth and Planetary Science Letters, 418, 40-52.

Zhong, S., Zhang, N., Li, Z.-X., & Roberts, J. H. (2007). Supercontinent cycles, true polar wander, and very long-wavelength mantle convection. Earth and Planetary Science Letters, 261(3-4), 551-564.

Zijderveld, J. D. A. (1967). A.C. Demagnetization of rocks: Analysis of results. In D. W. Collinson, K. M. Crees, & S. K. Runcorn (Eds.), Methods in Paleomagnetism (pp. 254-286): Elsevier.

Samenvatting in het Nederlands

Tijdens het Perm (ongeveer 300 tot 250 miljoen jaar geleden) lagen alle continenten op aarde tegen elkaar aan en vormden één gigantische woestijnachtige landmassa, het supercontinent Pangea. De andere helft van de aarde was bedekt met water: de Panthalassa Oceaan. Pangea en Panthalassa werden voor het eerst beschreven in 1915 door de Duitse meteoroloog Alfred Wegener, en hij gebruikte het Oudgrieks voor de naamgeving van deze supercontinent en -oceaan: pan betekent alle of geheel, gaia betekent aarde, thalassa betekent zee. Tijdens het Trias (ongeveer 250 tot 200 miljoen jaar geleden) begon Pangea uit elkaar te vallen, wat resulteerde in het ontstaan van de Atlantische en Indische Oceaan, en het kleiner worden van de Panthalassa Oceaan. Ondanks de afname in oppervlak is het restant van de Panthalassa, de Grote Oceaan, vandaag de dag nog steeds de grootste watermassa op aarde. In dit proefschrift heb ik een poging gedaan tot het maken van een tektonische reconstructie van de Panthalassa Oceaan. Om uit te leggen hoe ik dit gedaan heb en waarom de tektonische geschiedenis van een oceaan die niet meer bestaat relevant is, begin ik bij het begin:

De aarde bestaat uit drie delen: de korst, de mantel en de kern, welke voornamelijk van elkaar te onderscheiden zijn door verschillen in chemische samenstelling en dichtheid. Van de buitenste laag, de korst, bestaan er twee varianten: oceanische korst en continentale korst. Continentale korst is dikker (gemiddeld 30-40 km), ligt hoger (verder verwijderd van de kern van de aarde), en heeft een lagere dichtheid (gemiddeld 2800 kg/m^3) dan oceanische korst (5-10 km dik, dieper, 3100 kg/m^3). De korst is opgedeeld in tektonische platen, die kunnen bestaan uit enkel oceanische korst, enkel continentale korst, of een combinatie. Een oceaan of zee (de watermassa) beslaat hierdoor over het algemeen niet hetzelfde deel van het aardoppervlak als een oceanische plaat. Zo beslaat de Atlantische Oceaan delen van de Noord- en Zuid-Amerikaanse, Euraziatische, Afrikaanse en Antarctische plaat, en ligt op de Afrikaanse plaat een deel van zowel de Atlantische als de Indische Oceaan. Ook van de Panthalassa Oceaan wordt gedacht dat hij meerdere oceanische platen besloeg, waarvan de configuratie (de grootte van de platen en de locatie van de plaatgrenzen) door de geologische tijd aan verandering onderhevig was.

Continentale korst heeft niet alleen een lagere dichtheid dan oceanische korst, maar ook dan de onderliggende mantel, waardoor hij als het ware blijft drijven. De dichtheid van oceanische korst, daarentegen, neemt toe met een toenemende ouderdom, en kan hoger worden dan de dichtheid van de onderliggende mantel. In een situatie waarbij twee tektonische platen naar elkaar toe bewegen zal de oude oceanische korst daarom onder de andere (continentale of ook oceanische) plaat schuiven en daarmee de mantel in verdwijnen, een proces genaamd subductie (Fig. 1). Het subduceren van oceanische korst wordt in balans gehouden door de productie van nieuwe oceanische korst langs mid-oceanische ruggen. Waar twee oceanische platen uit elkaar drijven, smelt de onderliggende mantel, waarna dit gesmolten mantelgesteente de ruimte opvult van de

twee divergerende platen, weer stolt, en daarbij nieuwe oceanische korst maakt. Deze twee processen, het maken van nieuwe oceanische korst en subductie van oude oceanische korst, zijn de twee belangrijkste processen in de plaattektoniek, en zorgen ervoor dat continenten (die vast zitten aan oceanische korst) over het aardoppervlak schuiven. Ook resulteren deze twee processen erin dat oceanische korst een gelimiteerde levensduur op het oppervlak van de aarde heeft: het merendeel van de oceanische korst van vandaag de dag is niet ouder dan 100 miljoen jaar. Dit in tegenstelling tot continentale korst: door hun lage dichtheid zullen continenten nooit de mantel in verdwijnen en sommige delen continentale korst zijn dan ook miljarden jaren oud.

Tektonische reconstructies spelen een belangrijke rol in vele takken van de wetenschap. Ze vormen de basis voor studies in bijvoorbeeld klimaat, oceanografie, evolutie en biodiversiteit, geodynamica (de studie naar de drijvende krachten achter alle processen op en in de aarde), en spelen een cruciale rol in de zoektocht naar grondstoffen (fossiele brandstoffen, ertsen, etc.). Om een voorbeeld te geven: zonder een goede tektonische reconstructie is het niet te bepalen of plantenfossielen met een Triasouderdom, gevonden op Antarctica, aangeven dat het wereldwijd een heel stuk warmer was in het Trias, óf, dat de globale temperatuur vergelijkbaar was met het heden en er planten groeiden op Antarctica omdat het continent op 60 graden zuiderbreedte lag, ver weg van de Zuidpool.

Het maken van tektonische reconstructies van de relatief jonge geschiedenis van de aarde (de laatste 200 miljoen jaar) is relatief eenvoudig. De ontstaansgeschiedenis van de Atlantische en Indische Oceaan ligt vastgelegd in het ouderdomspatroon van de zeebodem, en dit patroon kan gebruikt worden om de oceanen te sluiten, waarmee plaatbewegingen gereconstrueerd worden. De absentie van oudere oceanische korst maakt dat het reconstrueren van plaatbewegingen verder terug in de tijd aanmerkelijk lastiger is. Zulke reconstructies kunnen alleen gebaseerd worden op data van de continenten (fossielen, de locatie van gebergteketens, paleomagnetisme, etc.), wat ervoor zorgt dat in zulke reconstructies de oceanische domeinen ingevuld zijn met conceptuele platen, of zelfs worden leeg gelaten. In dit proefschrift probeer ik de Panthalassa Oceaan te voorzien van platen, plaatgrenzen, en hun evolutie door de tijd heen.

Het begin van het maken van deze reconstructie is het definiëren van de grenzen van de Panthalassa Oceaan, en het bepalen van de locatie van deze grenzen door de tijd heen. De grenzen zijn de subductiezones, eerst rondom Pangea, en later langs de randen van Noord-Amerika, Zuid-Amerika, Antarctica, Australië, en Eurazië, waarin de platen van de Panthalassa Oceaan gesubduceerd zijn. Deze subductiezones hebben echter niet altijd op dezelfde plek gelegen. Deformatie aan de randen van de bovenliggende platen in de subductie-systemen, bijvoorbeeld het ontstaan van het Andesgebergte of het opengaan van de Japanse Zee, zorgt ervoor dat zo'n subductie-plaatgrens zich in de richting van het continent (in het geval van de Andes) of richting de Panthalassa (in het geval van de Japanse Zee) beweegt. De afgelopen 5 jaar, sinds ik met mijn masteronderzoek begon, heb

ik mij samen met collega's en studenten bezig gehouden met het reconstrueren van dit soort deformatie langs de randen van de Panthalassa Oceaan. We hebben reconstructies ontwikkeld van Mexico en het Caribisch gebied (hoofdstuk 2,3 en 4 van dit proefschrift), de Andes, de Scotia Zee, het gebied in het zuidwesten van de Grote Oceaan (van Nieuw-Zeeland tot Antarctica en van Fiji tot Australië), en het noordwesten van de Grote Oceaan (van Japan tot de Beringstraat). Hiermee zijn in deze gebieden de grenzen van de Panthalassa Oceaan door de tijd heen vastgelegd, en werd het mogelijk de volgende stap te zetten.

Stap twee is het gebruiken van de beschikbare data van de oceanische platen van de huidige Grote Oceaan die nog níet gesubduceerd zijn. Het oudste deel van de Pacifische plaat, die vandaag de dag het merendeel van de Grote Oceaan beslaat, is een driehoekig stuk korst van Juraouderdom dat zich ten oosten van de Marianetrog bevindt (Fig. 2). Het middelpunt van deze driehoek is ongeveer 190 miljoen jaar oud, en hoe verder naar de randen van deze driehoek, hoe jonger de korst wordt. De jongste korst van de Grote Oceaan wordt op dit moment gevormd aan weerszijden van Oost-Pacifische rug; de plaatgrens tussen de Pacifische plaat in het westen, en de Cocos- en Nazcaplaat in het oosten. Deze ouderdomsverdeling geeft een heleboel informatie over de geschiedenis van de platen van de Panthalassa Oceaan. Mid-oceanische ruggen creëren een symmetrisch patroon van nieuwe korst direct langs de rug, en steeds ouder wordende korst verder van de rug vandaan. Dit patroon kan gebruikt worden om het ontstaan van oceanische korst terug te draaien en daarmee de plaatbewegingen te reconstrueren. Het volledige
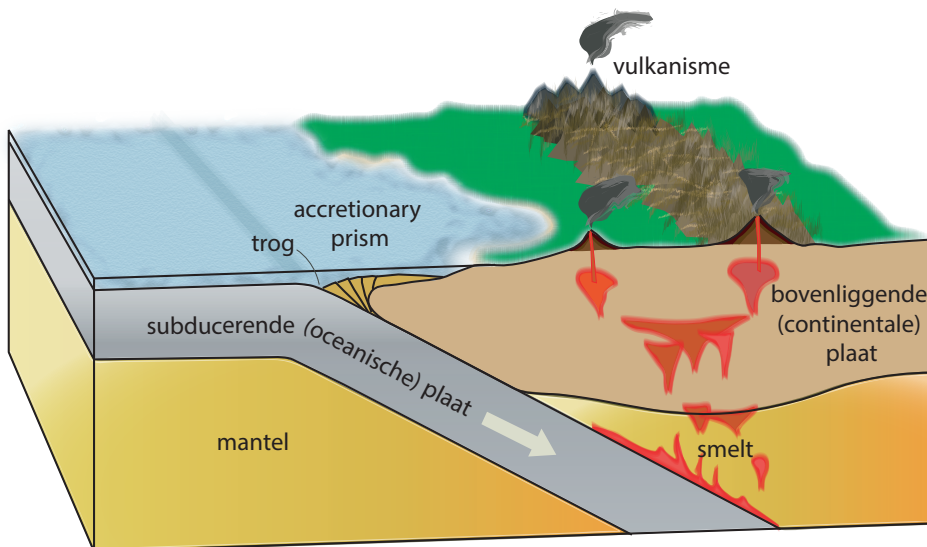
Figuur 1: Schematische doorsnede van een subductiezone
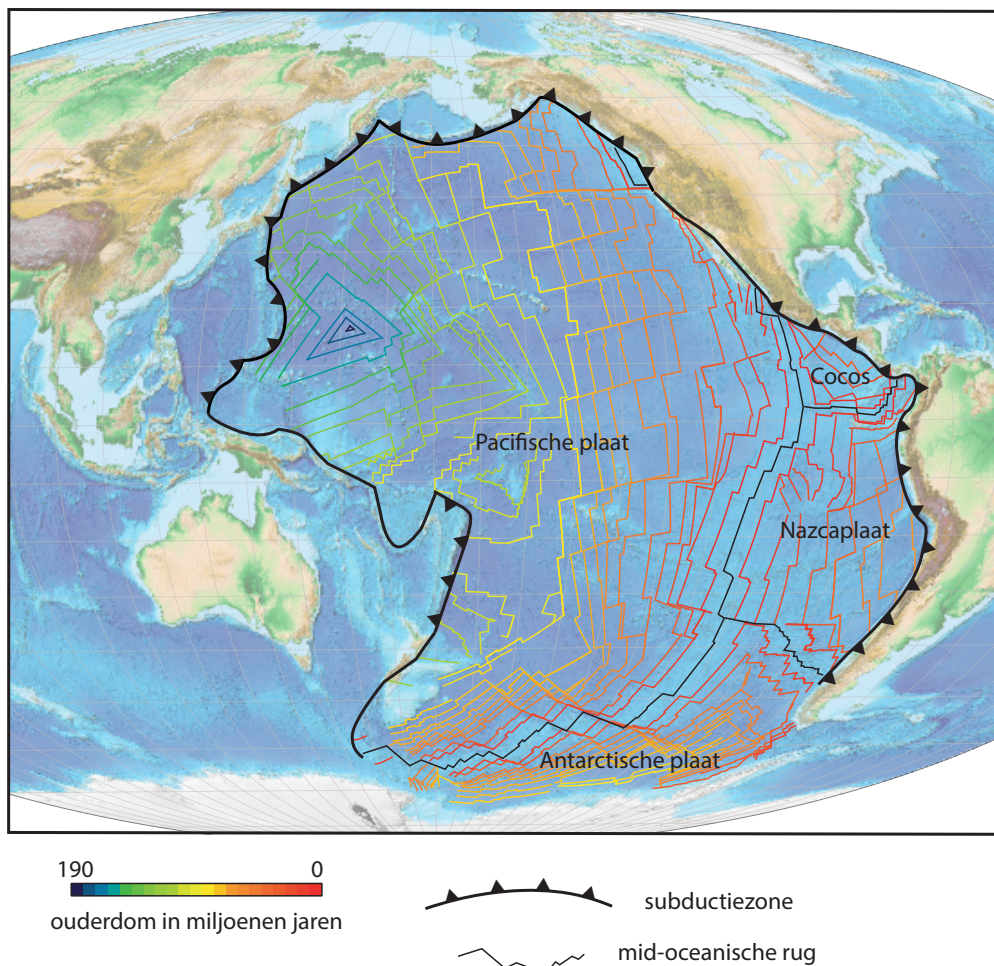
Figuur 2: Ouderdomspatroon van de zeebodem van de Grote Oceaan.

ouderdomspatroon van alle platen van de Grote Oceaan (Fig. 2) maakt het mogelijk om plaatbewegingen te reconstrueren tot terug in het Jura. Wel wordt de beschikbare informatie steeds beperkter en ontstaan er als het ware steeds meer lege plekken die niet ingevuld kunnen worden (zie figuur 1 in hoofdstuk 7). Deze lege plekken representeren de korst die door de geologische tijd heen gesubduceerd is in de subductiezones rondom de Panthalassa Oceaan.

De laatste stap die ik in dit proefschrift gezet heb, is het opvullen van delen van deze lege plekken. Een subductiezone bestaat uit een plaatcontact tussen de bovenliggende en de subducerende plaat, waar een trog ontstaat. De diepte van deze trog wordt bepaald door de hoeveelheid sediment die in de omgeving aanwezig is; soms is sediment bijna geheel

afwezig en kan een uitzonderlijke diepe trog ontstaan (bijvoorbeeld de 11 km diepe Marianetrog), soms is er zó veel sediment aanwezig dat de trog geheel wordt opgevuld en zelfs boven zeeniveau uitkomt en eilandjes vormt (bijvoorbeeld Barbados). Het sediment dat in een trog terecht komt vormt een *accretionary prism* (Fig. 1) en is een mix van (grotendeels) materiaal van de bovenliggende plaat én (in veel mindere mate) van de subducerende plaat. Het materiaal van de subducerende plaat, wat afgeschraapt wordt tijdens subductie en daarmee 'gered' wordt van verdwijnen in de mantel, is van groot belang in het maken van tektonische reconstructies van platen die er niet meer zijn.

Langs de randen van de huidige Grote Oceaan zijn op meerdere plekken uitstekend bewaarde accretionary prisms te vinden, die materiaal van de verdwenen platen van de Panthalassa Oceaan bevatten. In dit promotieonderzoek heb ik een aantal van deze plekken opgezocht, en heb veldwerk gedaan in Mexico (het Baja California schiereiland), Costa Rica (de Santa Elena en Nicoya schiereilanden), Japan (Hokkaido) en Nieuw-Zeeland (het Noordereiland). Ik ben in deze veldgebieden in samenwerking met Mexicaanse, Costa Ricaanse, Japanse en Nieuw-Zeelandse geologen, op zoek gegaan naar afgeschraapte restanten van gesubduceerde platen en heb duizenden monsters genomen om vervolgens in het lab in Utrecht met behulp van paleomagnetisme uit te zoeken wat de plek van herkomst is van deze stenen. De techniek paleomagnetisme maakt gebruik van het aardmagneetveld en van het feit dat sommige stenen (zwak) magnetisch zijn. Stenen die magnetische mineralen bevatten (bijvoorbeeld magnetiet of hematiet) hebben een intern magneetveld en op het moment dat zo'n steen gevormd wordt (bijvoorbeeld op het moment dat lava stolt), wordt het interne magneetveld opgelijnd met het veel sterkere magneetveld van de aarde. Verplaatst zo'n steen zich vervolgens over het aardoppervlak (omdat de plaat waar hij deel van uitmaakt beweegt), dan zal de richting van het interne magneetveld in de steen op den duur afwijken van het magneetveld van de aarde en niet meer naar de pool wijzen. De magnetische vector in een gesteentemonster kan ontleed worden in twee componenten: de inclinatie (de hoek met het aardoppervlak, die afhankelijk is van de breedtegraad (latitude)) en de declinatie (de hoek met het noorden). Door deze twee componenten te meten in gesteentemonsters en ze te vergelijken met het huidige magneetveld op de plek waarop ze gemonsterd zijn, kunnen dus latitudinale plaatbewegingen en verticale-as rotaties gereconstrueerd worden. Met behulp van de paleomagnetische data uit de bovengenoemde veldwerkgebieden heb ik latitudinale plaatbewegingen weten te reconstrueren van drie platen die de zuidelijke, noordwestelijke, en noordoostelijke Panthalassa Oceaan beslagen hebben en gesubduceerd zijn in subductiezones langs de kust van respectievelijk Nieuw-Zeeland, Costa Rica en Mexico, en Japan.

Naast de vergaarde data van afgeschraapt materiaal van gesubduceerde platen speelt het Caribisch gebied een grote rol in dit onderzoek. De Caribische plaat is een stuk oceaankorst dat ooit onderdeel was van de Panthalassa Oceaan, maar in tegenstelling tot de korst die in het noorden en zuiden aangrenzend was, niet gesubduceerd is onder

de Noord- en Zuid-Amerikaanse platen. In plaats daarvan werd dit stuk korst gevangen *tussen* de Noord- en Zuid-Amerikaanse platen, en daarmee dus, op een veel grotere schaal, net als de afschraapsels 'gered' is van subductie. Hierdoor is de Caribische plaat een uniek Panthalassa-restant waarvan de plaatbewegingen te reconstrueren zijn, en is daarmee een waardevolle bron van informatie over de tektonische geschiedenis van de oostelijke Panthalassa Oceaan in het Jura.

Met dit proefschrift is de reconstructie van de Panthalassa Oceaan geenszins af, ik heb maar een heel klein deel van de beschikbare data weten te verzamelen. Wel is dit proefschrift een mijlpaal in de zin dat ik heb laten zien dat het kán: het is mogelijk om - gebaseerd op data - bewegingen van platen te reconstrueren die er niet meer zijn. De methode die beschreven is in dit proefschrift is niet alleen relevant voor de Panthalassa Oceaan, maar kan toegepast worden op elke oude verdwenen oceaan, zolang er maar stenen achter gebleven zijn op het aardoppervlak tijdens subductie. Ik hoop dan ook dat in de komende jaren meer mensen enthousiast hun boor in oude accretionary prisms zetten, en onze kennis over de geschiedenis van de oceanen van de oude aarde met sprongen vooruit zal gaan.

Acknowledgements

This thesis would not have come together without the help of many. First and foremost: Douwe, I could not have hoped for a better PhD supervisor. It is great to work with you, not only because you do cutting-edge science, but especially because you have created an atmosphere that inspires the people around you to set their bars high and make the absolute most of their possibilities, and in the meantime making reaching those goals feel easy, and a ton of fun. Thank you for designing projects (twice!) that inspired me, that lived up to my ambitions and passed my pickiness, and that I was eager to dive into. Thank you for your mentorship, and for giving me many incredible opportunities to develop myself as a scientist and make a name for myself in the scientific community.

Wim, thank you for your valuable comments on manuscripts, your advice, and especially, for creating such a good vibe in our group. You have made me feel and appreciated and cared for from the first day.

Cor, thank you for the many afternoons we spent together with the intention of interpreting data, but often being side-tracked and doing other things. I have learned a lot from you, especially on topics I didn't know I wanted to know things about.

Lennart, thank you for your endless willingness to help and to explain the ins and outs of lab equipment and the more technical aspects of paleomagnetism to me. It was great to know that you were always available for help and support.

Hayato Ueda, Kennet Flores, Dave Kimbrough, Peter Kamp and Roberto Molina Garza, thank you all so much for your hospitality and for introducing me to the geology of your 'geological backyards' in Japan, Costa Rica, Mexico and New Zealand. These fieldtrips, and therefore, this research, could not have succeeded without your generous help.

A number of MSc and BSc students worked with me in the lab and joined me in the field. Special thanks to Suzanna van de Lagemaat, Erik van der Wiel, Yvette Mellink and Alex Mols for making these field trips more fun, and for processing enormous amounts of samples in the lab.

And then there's so many others that brought these years to life: Kalijn - I really enjoyed sharing an office with you, Annemarieke - that Iceland field trip was awesome (cold! but awesome), Jan, Dan, Karin – such good Aliaga memories, Pete, Nienke, Cedric, Menno, Eldert, Bram, the rest of the Aliaga-staff, everybody else in our group and at the fort; thanks for the good times.

Annique, Janneke, Janja, Geertje, Anouk and Marily, it's wonderful to have you in my life. Thank you for all the adventures, inspiration, friendship and support. It seems that the

borders between us don't separate us, but instead only provide good excuses for a holiday now and then. I hope that many many years from now, we'll still enjoy each other's company, as well as that of mountains, rocks, and a beer on a terrace at some exotic or foreign location (or Utrecht!). Let's start with Zürich sometime soon.

And last but not least, Jorad, I'm so grateful to be able to share science with you. Thank you for enduring my absence of mind every now and then when I couldn't let the plates go, for listening to my endless ramblings about paleomag, reference frames, true polar wander, and slabs (and genuinely understanding what I'd be talking about!), and for thinking along and asking the right questions to get me out of problems I wasn't able to solve myself. If you ever become fed up with plants, I'm sure you've picked up enough on geology and tectonics by now to make a career switch. Lastly, thank you for letting me drag you out of your comfort zone once more by taking you with me to Zürich.

Curriculum Vitae

23 October 1989   **Born in Hoofddorp, The Netherlands**

2001 - 2007   **Secondary school**
                    Atheneum college Hageveld, Heemstede

2007 - 2010   **BSc Earth Sciences**
                    Utrecht University

2010 - 2013   **MSc Geology (cum laude)**
                    Utrecht University

2013 - 2014   **Junior Teacher Earth Sciences**
                    Utrecht University

2014 - 2018   **PhD Candidate**
                    Utrecht University

2019 - ...   **Postdoctoral researcher**
                    ETH Zürich, Switserland

Bibliography

Thesis chapters:

Boschman, L.M. and van Hinsbergen, D.J.J., 2016. On the enigmatic birth of the Pacific Plate within the Panthalassa Ocean, *Science Advances*, Vol. 2, no. 7, e1600022

Boschman, L.M., van Hinsbergen, D.J.J., Torsvik, T.H., Spakman, W., and Pindell, J.L., 2014, Kinematic reconstruction of the Caribbean region since the Early Jurassic, *Earth-Science Reviews* 138, p. 102-136

Boschman, L.M., Molina Garza, R.S., Langereis, C.G., van Hinsbergen, D.J.J., 2018. Paleomagnetic constraints on the kinematic relationship between the Guerrero terrane (Mexico) and North America since Early Cretaceous time, *GSA Bulletin*, 130 (7-8), 1131-1142

Boschman, L.M., van Hinsbergen, D.J.J., Kimbrough, D.L., Langereis, C.G., Spakman, W., 2018. The dynamic history of 220 million years of subduction below Mexico: a correlation between slab geometry and overriding plate deformation based on geology, paleomagnetism and seismic tomography, *Geochemistry, Geophysics, Geosystems*, DOI: 10.1029/2018GC007739.

Boschman, L.M., Flores, K., van der Wiel, E., Langereis, C.G., van Hinsbergen, D.J.J., The Caribbean and Farallon plates connected: constraints from stratigraphy and paleomagnetism of the Nicoya Peninsula, Costa Rica, *Journal of Geophysical Research - Solid Earth*, accepted pending revision.

Other publications not included in this thesis:

Schepers, G., van Hinsbergen, D.J.J., Kosters, M.E., Boschman, L.M., McQuarrie, N., and Spakman, W., 2017. South American plate advance and forced trench retreat as drivers for transient Andean flat subduction episodes, *Nature Communications* 8, 15249.

Van de Lagemaat, S.H.A., Boschman, L.M., Kamp, P.J.J., Langereis, C.R., and van Hinsbergen, D.J.J., 2018. Vertical axis rotation and tilting after remagnetization of the Murihiku Terrane (North Island, New Zealand), *New Zealand Journal of Geology and Geophysics* 61(1), p.9-25,

Molina Garza, R.S., van Hinsbergen, D.J.J., Boschman, L.M., Rogers, R., and Ganerød, M., 2018. Large-scale rotations of the Chortis Block (Honduras) at the southern termination of the Laramide flat slab, *Tectonophysics*, doi: 10.1016/j.tecto.2017.11.026

Van de Lagemaat, S.H.A., van Hinsbergen, D.J.J., Boschman, L.M., Kamp, P.J.J., and Spakman, W., 2018. Southwest Pacific absolute plate kinematic reconstruction reveals major mid- to Late Cenozoic Tonga-Kermadec slab dragging, *Tectonics*, doi: 10.1029/2017TC004901

Vaes, B., van Hinsbergen, D.J.J., Boschman, L.M., 2018. Kinematic reconstruction of intra-oceanic subduction and back-arc opening in the NW Pacific Ocean and Aleutian Basin: clues to causes of Cretaceous and Eocene plate reorganizations, *Tectonics*, accepted pending revision.